NASA CP-002

THE STRUCTURE AND CONTENT OF THE GALAXY AND GALACTIC GAMMA RAYS

A symposium sponsored by
Goddard Space Flight Center,
Greenbelt, Maryland
June 2-4, 1976

NASA Conference Publications (CP Series) contain compilations of scientific and technical papers or transcripts arising from conferences, workshops, symposia, seminars and other professional meetings that NASA elects to publish.

The text of these proceedings was reproduced from author-supplied manuscripts. Each paper was reviewed for adherence to format, use of the International System of Units, and basic grammatical accuracy.

NASA CP-002

THE STRUCTURE AND CONTENT OF THE GALAXY AND GALACTIC GAMMA RAYS

Edited by
Carl E. Fichtel and Floyd W. Stecker

A symposium sponsored by
Goddard Space Flight Center,
Greenbelt, Maryland
June 2-4, 1976

Scientific and Technical Information Office 1977
NATIONAL AERONAUTICS AND SPACE ADMINISTRATION
Washington, D.C.

For sale by the National Technical Information Service
Springfield, Virginia 22161
Price: $ 10.75

PREFACE

An International Symposium on "The Structure and Content of the Galaxy and Galactic Gamma-Rays" was held at NASA/Goddard Space Flight Center in Greenbelt, Maryland, June 2 through 4, 1976. It was the third international γ-ray symposium; the first was held at Goddard Space Flight Center in April 1973 (*Gamma Ray Astrophysics,* ed. F. W. Stecker and J. I. Trombka, NASA SP-339, U.S. Government Printing Office, Washington, D.C.), and the second was held in May 1974 at the European Space Agency conference facility in Frascati (*The Context and Status of Gamma Ray Astronomy*, ed. B. G. Taylor, ESRO SP-106, ESTEC Reprod. Serv., Noordwijk). Since the previous symposia were held, γ-ray astronomy has developed from the discovery phase into the exploratory phase experimentally and blossomed in a remarkable way theoretically. The results of SAS-2 have become available in nearly final form, COS-B has been launched, and new results have become available at both very high and low energies. These results have provided the stimulus for several new theoretical concepts, many of which are just now being developed. Most prominent among these new results are the new observations of γ-rays from the galaxy. The time appeared to be ripe to tie these observations into the mainstream of galactic astronomy and explore the relationship of galactic γ-ray astrophysics to other fields of galactic astronomy. Thus, although the recent γ-ray results presented play a very important role in the symposium, relevant observations from many disciplines, including radio, infrared, optical, and ultraviolet astronomy, are also included. All these results are then considered together in the theoretical papers on galactic sources. The synoptic approach to the problem of galactic structure is evolved here with the new γ-ray and CO observations playing a prominent role.

The symposium consisted primarily of invited talks and their associated discussion; however, it was supplemented by three short sessions of contributed papers on very recent results. These proceedings include the full text of all invited papers and titles and references to the shorter contributed papers. Much new and previously unpublished material is included such as: (1) the first reported results from the COS-B γ-ray satellite presented by our European colleagues, (2) new SAS-2 results on γ-ray pulsars, Cygnus X-3, and new maps of the diffuse flux, (3) very recent data from CO surveys of the galaxy, (4) new results on the galactic distribution of pulsars, and (5) new theoretical work on galactic γ-ray emission. The following highlights from the symposium will serve as an overview and introduction.

The first speakers at the conference summarized the experimental status of γ-ray astronomy. David Thompson and Robert Hartman presented the results from the second Small Astronomy Satellite, SAS-2, showing sky contour where data are available and the galactic longitude and latitude distributions of $>$ 100-MeV γ-rays. Evidence for pulsed γ-radiation from four radio pulsars (PSR 0531+21, PSR 0833-45, PSR 1818-04, and PSR 1747-46) is reported.

These results are particularly significant in that only one radio pulsar has been seen at optical and X-ray wavelengths. In addition, several general features in the γ-ray data are correlated with galactic structural features, such as Gould's Belt, and peaks along the galactic plane at about 315°, 330° to 335°, 340° to 345°, 0°, 25°, and 35°, corresponding to the galactic center and possibly to tangential directions of galactic arms. The γ-rays seen by SAS-2 from the direction of Cygnus are determined to have a periodicity of 4.8 hours, matching the frequency and phase of the X-ray source, Cyg X-3.

A description of the COS-B γ-ray instrument, which was launched on August 9, 1975, was given by Boudewijn Swanenburg, and preliminary results were presented by Jacques Paul, Hans Mayer-Hasselwander, and Rosolino Buccheri. These results include latitude and longitude distributions of γ-rays from parts of the galactic plane and a confirmation of a strong γ-ray source near galactic coordinates 195°, +5°. The temporal analysis of data from PSR 0531+21 shows excellent correlation between the X-ray and γ-ray light curves, and the analysis of PSR 0833-45 indicates that the γ-ray pulses are narrow and that γ-rays with energy in excess of 10^9 eV are coming from PSR 0833-45.

These talks were followed by a discussion of low-energy γ-ray astronomy by Gerald Share, who noted that the galactic γ-ray energy spectrum below 30 MeV shows a predicted steepening characteristic of bremsstrahlung radiation. Jonathan Grindlay then summarized the results in very high-energy γ-ray astronomy ($E \geqslant 10^{12}$ eV), and noted that there now appear to be at least two sources emitting γ-rays at these energies.

Peter Sturrock and Hakki Ögelman both presented papers on the general subject of pulsars. Sturrock suggested that a cascade process resulting from electron-positron pair creation in the pulsar magnetic field may be the cause of the pulsed γ-radiation, whereas the radio and optical emission from the Crab pulsar is best understood as coherent curvature radiation. Ögelman suggests that theory and observation indicate that pulsars radiate predominantly the 10^6 to 10^9 eV energy range. Further studies of γ-rays from pulsars will clearly be important in understanding the nature of the energy-loss process associated with these objects.

Three different papers on observations of the interstellar matter, covering a range of wavelengths from radio to ultraviolet, were presented. Butler Burton and Nicholas Scoville both presented radio measurements of the 2.6-mm CO line, which is excited primarily by collisions of CO with H_2 molecules in dense clouds. These studies indicate that molecular hydrogen clouds in the galaxy are concentrated between galactic radii of 4 and 8 kiloparsecs (kpc), in contrast to the atomic hydrogen, which is relatively uniform in distribution at radii from 4 to 14 kpc. The CO measurements also show that H_2 clouds are more tightly confined to the galactic plane than atomic hydrogen gas. Edward Jenkins of Princeton University noted that direct ultraviolet measurements of the molecular hydrogen in the local region of the galaxy give a value of the molecular hydrogen density a factor of 4 lower than that predicted at a galactic radius of 10 kpc, although the results do not necessarily conflict because of various selection effects and nonuniformities in the large-scale distribution of interstellar gas.

William Roberts discussed the density wave theory of galactic structure and showed that, using this theory, one can account for the apparently striking separation of atomic and molecular hydrogen as a result of: (1) stronger compression of gas in the inner galaxy, and (2) an increase of the frequency at which the interstellar gas is periodically compressed. Both these effects could be caused by the spiral density wave pattern in the galaxy.

Turning to the nonthermal galactic radiation, generally assumed to be synchrotron radiation from cosmic-ray electrons in the galactic magnetic fields, John Baldwin noted that the nonthermal radiation extends to several kiloparsecs above the galactic plane, implying a much broader distribution of the cosmic-ray electrons than of matter in the galaxy. This is also indicated in studies of other spiral galaxies.

The pulsar distribution within the galaxy was discussed by John Seiradakis, who showed that, within the present very limited statistics, the radial distribution of pulsars is generally correlated with that of other young (Population I) galactic objects.

Both Giovanni Fazio and Jean-Loup Puget discussed the significance of the local clouds of dust and H_2 and noted that future infrared and γ-ray observations could help reveal their nature. Puget concluded that the γ-ray observations indicate that the cosmic-ray density inside and outside these clouds is similar.

Two papers involving rather different subjects included predictions of γ-ray spectral lines. Richard Lingenfelter described the γ-ray lines emitted by the excited heavy nuclei produced by interactions of cosmic rays with interstellar matter. He predicts that the 4.4-MeV carbon line would be the most intense and that the emission lines from the carbon in dust grains would be quite narrow. David Arnett described the possibility of studying the results of nucleosynthesis in supernovae by examining the γ-ray lines emitted by the end products. He noted that the time interval after the explosion before the supernova envelope becomes transparent to γ-rays is much longer than had been estimated earlier. As a consequence, the observed flux levels would be less than previously predicted.

Eugene Parker then presented a theoretical discussion of cosmic-ray propagation and galactic containment, in which he noted that the cosmic rays, the magnetic field, and the interstellar gas affect each other, so that the problem of the propagation and containment of cosmic rays in the galaxy is inseparable from the dynamical theory of the disk. He explained that the cosmic rays below about 10^{16} eV/nucleon are tied to the lines of force. The cosmic rays are not free to escape individually from the surface of the galaxy. This view forces the conclusion that, if cosmic rays escape from the galaxy, it must be as a consequence of collective cosmic-ray pressure inflating the field and pushing it outward from the galactic plane.

The last two papers, by Donald Kniffen and Floyd Stecker, discussed the role that γ-ray astronomy can play in determining the large-scale galactic structure. Kniffen noted that, since γ-ray production is proportional to the product of the cosmic-ray and matter densities and since they have a high penetrating power, the γ-rays are particularly valuable in searching for spiral structure for which there is an indication in the γ-ray data. He presented models of γ-ray production based on current estimates of the interstellar atomic and molecular hydrogen-gas densities which give good fits to the observed galactic γ-ray longitude distribution. Although a constant or universal cosmic-ray model appears to be ruled out by this work, the large uncertainties in the interstellar gas densities weaken this conclusion.

Stecker argued that galactic γ-ray emission and deduced cosmic-ray distribution are correlated with the molecular cloud distribution in the galaxy. The cosmic-ray distribution in the galactic disk, he deduces, appears to follow the supernova remnant and pulsar distributions in the galaxy, favoring a galactic origin for most cosmic rays. He also discussed the relationship between cosmic rays and other components of the galaxy and the galactic contribution to the high-latitude background γ-ray flux. He noted that the galactic cosmic-ray gradient implied by the γ-ray results provides a new argument against containment of cosmic rays in a large halo region.

The conference ended with a panel discussion in which it was noted that, after almost two decades of strenuous effort in developing instruments of sufficient sophistication and sensitivity, there have been significant advancements in γ-ray astronomy in the last few years. Not only the general level of the galactic radiation has been established, but also its broad features. With improved angular resolution and much greater sensitivity, γ-ray astronomy, together with astronomy at other wavelengths, holds great promise for the study of our own galaxy and others. At the same time, contributions from discrete objects will be distinguished more clearly so that the study of pulsars, molecular clouds, globular clusters, and supernovae may be greatly expanded.

Some of what will be learned when the large γ-ray telescopes of the future are flown is predictable. However, each time a new region of the spectrum has been viewed in astronomy or the study of a wavelength region has been extended by an order of magnitude in sensitivity, many unexpected results have emerged, leading to a major expansion of our knowledge. Not only should this also be true of γ-ray astronomy, but it should be even more likely for several reasons: (1) γ-ray astronomy, by its very nature, relates directly to the highest energy processes, (2) it will not be troubled by absorption effects because of the high penetrating power of γ-rays, and (3) because γ-ray astronomy is just reaching the exploratory phase, relatively less is as yet known.

We believe that the contents of this lengthy volume speak for themselves in representing a significant advance in our knowledge of the structure and nature of the galaxy. They represent a presentation and a theoretical synthesis of observations over the entire range of the electromagnetic spectrum from the radio to the γ-ray range, possible here for the first time. We feel that they also show the success of the concept of holding such an interdisciplinary symposium in benefiting all of the participants as well as the general scientific community.

C. E. Fichtel
F. W. Stecker
NASA/Goddard Space Flight Center
Greenbelt, Maryland

ACKNOWLEDGMENTS

We should like first of all to thank the other members of the organizing committee, Drs. Carol Crannell, Frank Jones, Donald Kniffen, David Thompson, and Jacob Trombka, for their long hours and invaluable aid in coordinating and carrying out the many facets of work involved in undertaking an international symposium.

We also wish to thank the many authors who have contributed solid, thoughtful manuscripts to these proceedings and who gave excellent presentations at the Symposium. We particularly appreciate the time and effort extended by the authors in preparing this material under a severely short time schedule so that these proceedings would be available to the astrophysics community in a time comparable to that for publication of a journal article.

We also thank Drs. John F. Clark, George F. Pieper, John Brandt, Frank McDonald, and Theodore G. Northrop for their support, which enabled us to hold the Symposium at the Goddard Space Flight Center.

Most special thanks go to Rose Ramberg for her untiring work in handling most of the administrative work and also to Evelyn Peters, Barbara Shavatt, Barbara Dallas, Nancy Gaffney, Bonnie Slaughter, Brenda Lueders, and Carlynn Thompson for help in making the conference run smoothly.

C. E. Fichtel
F. W. Stecker

CONTENTS

CONTENTS (Continued)

CONTENTS (Continued)

OPENING REMARKS

John F. Clark
*Director**
NASA/Goddard Space Flight Center
Greenbelt, Maryland 20771

It gives me great pleasure to welcome you to Goddard Space Flight Center to participate in our second international Gamma-Ray Symposium. We are all happy to see that so many distinguished members of the international scientific community are with us today.

There has been a deep interest in γ-ray astronomy at Goddard since shortly after Goddard was formed—not only because it was realized that the space age permitted this new astronomical window to be opened, but also because of the great significance of γ-ray astronomy which arises from its very direct relationship to the largest transfers of energy occurring in astrophysical processes.

At the time of the first international γ-ray symposium held here at Goddard just over 3 years ago, shortly after the launch of SAS-2, I expressed the hope that it would be the first of many fruitful international γ-ray symposia. That hope has become a reality. In the following year, our colleagues at the European Space Agency held a symposium at Frascati in preparation for COS-B, the first results from which we will hear about this morning. ESA has also planned a symposium in the near future which, we are certain, will also be very successful.

The progress in γ-ray astronomy over the last 3 years has been very encouraging. The first fairly definitive results are now beginning to emerge particularly in regard to the galactic plane, and, as they do, great interest is evolving in the interrelationship between galactic structure, cosmic-ray origin, the cosmic-ray distribution in the galaxy, and γ-rays. Point sources are also beginning to emerge with one of the great surprises being the identification of several γ-ray pulsars with their radio counterparts. We are, of course, pleased at the active role that Goddard has been playing in both the observational and theoretical aspects of this work.

Our meeting this week will be of a somewhat different nature than the first symposium. It will address itself primarily to a particular task, namely that of determining the relationship of the new galactic γ-ray results to the overall problem of the structure, content, and dynamics of the galaxy. To this end, distinguished colleagues from other scientific disciplines

*Dr. Clark retired as Director of the Goddard Space Flight Center on July 1, 1976.

of observational and theoretical astronomy and astrophysics have been invited to report and review recent advances in these fields which also bear on these problems. We are confident that the interaction of knowledgeable scientists in these various fields will greatly further progress in determining the nature of our galaxy and its contents, through both dialogue and inspiration. Periods of free discussion and a panel discussion have been planned to further that dialogue.

The recent NASA report on the "Outlook for Space" to the year 2000 lists many questions which it is hoped that both NASA and the world space community will help to answer, and γ-ray astronomy should be prominently involved in the solution of these problems. To this end, this symposium, together with the one sponsored by ESLAB in the spring of next year should act as a strong catalyst to stimulate even further continued strong research in this very important scientific field.

On that note for the future, I would once again like to thank you all for coming, welcome you to Goddard, and wish you the greatest success in your present work.

SAS-2 GALACTIC GAMMA-RAY RESULTS–I. DIFFUSE EMISSION

D. J. Thompson, C. E. Fichtel, R. C. Hartman,
D. A. Kniffen, G. F. Bignami,* and R. C. Lamb**
Laboratory for High Energy Astrophysics
NASA/Goddard Space Flight Center
Greenbelt, Maryland 20771

H. Ögelman, M. E. Özel, and T. Tümer
Physics Department
Middle East Technical University, Ankara, Turkey

ABSTRACT

Continuing analysis of the data from the SAS-2 high energy γ-ray experiment has produced an improved picture of the sky at photon energies above 35 MeV. On a large scale, the diffuse emission from the galactic plane is the dominant feature observed by SAS-2. This galactic plane emission is most intense between galactic longitudes 310° and 45°, corresponding to a region within 7 kpc of the galactic center. Within the high-intensity region, SAS-2 observes peaks around galactic longitudes 315°, 330°, 345°, 0°, and 35°. These peaks appear to be correlated with galactic features and components such as molecular hydrogen, atomic hydrogen, magnetic fields, cosmic-ray concentrations, and photon fields.

INTRODUCTION

Because high-energy γ-rays can be produced by a variety of mechanisms, observations of galactic γ-radiation can provide information about many different galactic components. Gamma-rays originating from neutral pions produced in collisions between cosmic-ray nucleons and interstellar matter, for example, are related directly to the product of the cosmic-ray and matter densities. Bremsstrahlung γ-rays represent a probe of the cosmic-ray electron and interstellar matter distributions, while inverse Compton γ-rays relate the cosmic-ray electrons to the photon fields in the galaxy. By combining the γ-ray measurements with other observations related to these galactic components, it may be possible to

*NAS-NRC Postdoctoral Research Associate 1973-75.
**On faculty leave from Iowa State University during 1975-76.

obtain a more complete picture of the galaxy than would be possible with any single set of observations alone. In simplest terms, then, the goal of this paper will be to present the Small Astronomy Satellite-2 (SAS-2) results in their current form and to attempt to indicate how these γ-ray observations may be related to other constituents of the galaxy.

EXPERIMENTAL

The SAS-2 experiment, the calibration procedure, and the methods of data analysis have all been described by Derdeyn et al. (1972) and Fichtel et al. (1975). The detector is a digitized, wire-grid spark chamber which uses as a triggering telescope an anticoincidence scintillator dome, a set of scintillators, and a set of Cerenkov detectors. The energy threshold is somewhat less than 30 MeV, photon energies can be measured up to approximately 200 MeV, and an integral intensity can be obtained above 200 MeV. The two-dimensional angular resolution for γ-ray energies above 100 MeV is between 3° and 4°, depending on the incident spectrum.

Results from most of the SAS-2 observations along the galactic plane have been published previously (Fichtel et al., 1975). Since the time that these results were compiled, however, a number of changes have taken place to give improvements in the results:

- New orbit-attitude solutions have been obtained for portions of the data. These solutions have provided greater accuracy for portions of the data already analyzed and have permitted the analysis of additional data for which no orbit-attitude information was previously available.
- Some additional telemetry data became available.
- A slightly different method of computing arrival directions for individual γ-rays was incorporated into the data-analysis system.
- Some inconsistencies in data analysis procedures between different observing periods were removed.

Two important features of these improvements should be emphasized. First, none of the adjustments changes any of the large-scale features of the results. At most, these modifications enhance the statistics for certain regions of the SAS-2 exposure and slightly alter the small-scale picture of the γ-ray sky. Second, at present, not all of these changes have been included in the SAS-2 data base. Work is continuing on incorporating these changes. The reader is cautioned that the SAS-2 results presented here are not in final form, although the regions around the galactic center and the galactic anticenter have been updated.

RESULTS OF LARGE-SCALE SAS-2 OBSERVATIONS

One of the most graphic ways of viewing the γ-ray sky is shown in the map of γ-ray flux contours in figure 1. A description of the construction of this map will indicate its values and limitations. The entire celestial sphere is divided into 20,736 bins of equal solid angle.

Figure 1. Contour map of γ-ray intensities observed by SAS-2 at energies above 100 MeV. The dashed line shows the limits of the SAS-2 exposure. In units of 10^{-4} photons cm^{-2} s^{-1} sr^{-1}, the contours are 5.1, 4.0, 3.0, 2.1, 1.3, and 0.7. The highest and lowest contours are darker than the others.

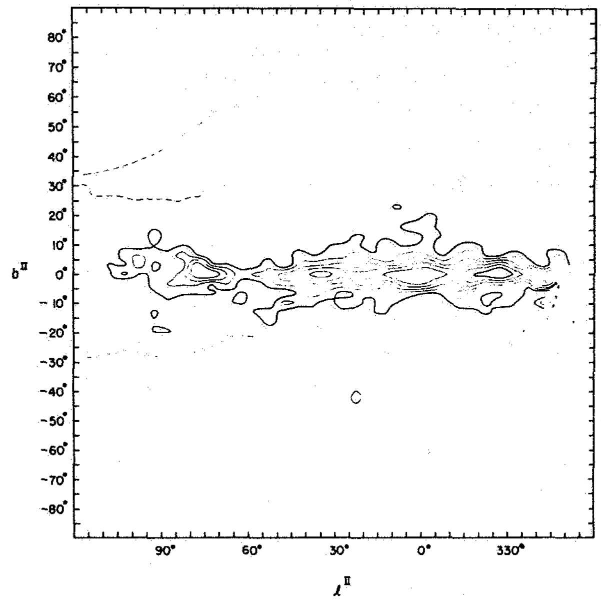

The bins are separated by 2.5° in galactic longitude throughout the sky. The latitude bins have widths adjusted to maintain the equal solid angle. At the galactic equator, the bins have a latitude width of about 0.7°. For each bin, the number of detected photons within the bin is divided by an exposure parameter (the sensitivity of the observations at that bin) to yield a γ-ray intensity. The intensities obtained in this way are smoothed by combining bins, and contours of equal intensity are then drawn, using the centroids of the bins to represent the bin positions. Because of this smoothing procedure, this sky map is most useful for examining large-scale features. Any single feature observed in this plot has a positional uncertainty of ±2°.

As can be seen in figure 1, the SAS-2 observations used for this plot cover about one-half of the galactic plane in longitude and a range of galactic latitudes from well below the plane to the north galactic pole. The lowest γ-ray intensity contour lies at a value about three times greater than the diffuse flux observations by SAS-2 (Fichtel et al., 1975). Only γ-rays with measured energies greater than 100 MeV were used. Clearly, at this intensity level, the only significant features in the γ-ray sky are those associated with our own galaxy.

In terms of γ-ray emission, the galactic plane can be roughly divided into two regions. The section of the plane between galactic longitudes 310°and 45°, surrounding the galactic center, is an intense ridge. The entire range stands out above all other parts of the γ-ray sky, but prominent peaks and valleys are visible within the region. The remainder of the galactic plane resembles the section in figure 1 between 45°and 120° longitude. The plane stands out clearly above the diffuse background, but at a significantly lower level than the central region.

Within the intense central region of the plane, four peaks are visible on the contour plot, centered on longitudes 315°, 330°, 0°, and 35°. The single most intense region observed by SAS-2 is the section of the plane around 330°. On a finer resolution scale, what appears as an elongated peak in figure 1 is actually two separate intense peaks, one centered on 330° and the other centered on 345°. In terms of galactic structure, the entire intense region encompasses the part of the galaxy within about 7 kpc of the galactic center. The discussion of how these observations may be related to other components of the galaxy will be postponed until the following section, "Discussion."

The parts of figure 1 away from the central ridge also show some features, the most prominent of which appears at galactic longitudes centered on 75° to 80°. Although this excess is not as intense as any of the peaks around the galactic center, it does stand out from the parts of the plane on either side. Other apparent features between 50° and 120° are all of low statistical significance, as is the small region at galactic latitude -35°. By contrast, the excess extending from the galactic plane up to latitudes about +15° above the galactic center lies in a region of high exposure by SAS-2 and may very well be significant.

Figure 2 shows the SAS-2 data above 100 MeV summed as a function of galactic latitude for the regions around the galactic center and the galactic anticenter. As in figure 1, the dominance of the galactic emission over the diffuse radiation is clear, even for the anticenter region where the plane is relatively weaker. In the center region, the data has been largely updated with the changes discussed in the "Experimental" section. The principal features of these results are the same as those discussed by Fichtel et al. (1975). The latitude distribution in the center longitude range is broader than would be expected from the detector resolution alone. Two components, a narrow one with the detector resolution and a broader one with a gaussian 1 σ of 6° to 7° are needed to give a good fit to the data. The resolution-limited component represents at least one-half the total radiation. This narrow component must originate either from localized sources or from features with a width comparable to the galactic disk thickness at a distance greater than 2 kpc. The broader component could originate either from the nearby galactic disk or from a more distant component with a greater thickness. In the anticenter direction, the observed γ-radiation has a distribution significantly broader than the detector resolution, suggesting that most of this radiation originates in nearby regions, as would be expected from the position of the solar system in the galaxy.

One additional aspect of the latitude distribution deserves mention. In the galactic center region, the intensity is somewhat higher on the positive side of the plane than on the negative side. In the anticenter region, the intensity is higher on the negative side of the plane than on the positive side. These excesses are also visible in figure 1 and the anticenter flux contour plot of Hartman et al. (1976). Although these regions of greater intensity are difficult to localize, their general position suggests an identification with the local distribution of stars and gas known as Gould's Belt.

Figure 2. Distribution of γ-rays with measured energies greater than 100 MeV as a function of galactic latitude. Data from the center cover $330° < \ell^{II} < 30°$. Data from the anticenter exclude the Crab, Vela, and (195, +5) sources. The diffuse background is shown as a dashed line.

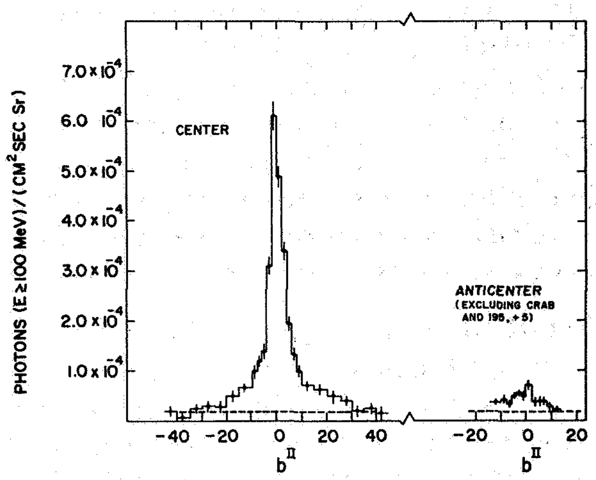

The distribution of high-energy γ-ray emission as a function of galactic longitude is one of the most useful observations for relating γ-ray results to galactic structure. Figure 3 shows the SAS-2 data summed between $-10° < b^{II} < +10°$ in longitude bins 2.5° wide. Two important considerations concerning this data are: First, the 2.5° bin size is smaller than the SAS-2 resolution for γ-ray energies above 100 MeV. Even a point source will appear with finite width on this plot. Second, not all the data shown here have been updated with the changes discussed in the "Experimental" section, particularly in regions away from the galactic center. Even though these changes are not expected to alter any large-scale features, any individual point may show a noticeable adjustment in the final analysis. In short, no single bin on this present longitude plot should be taken by itself as decisive.

Figure 3 emphasizes many features of the galactic plane which were visible in figures 1 and 2: (1) the dominance of the plane itself above the diffuse background, (2) the strong contrast between the galactic center region and the rest of the galactic plane, and (3) the non-uniformity of the high-intensity region around the galactic center. In the part of the plane away from the galactic center, four peaks above the general plane emission can be seen. Those associated with the Crab (Kniffen et al., 1974) and the Vela supernova remnant (Thompson et al., 1975) have been discussed in detail previously. The regions around longitudes 75° and 195° have not been definitely identified with known sources (Fichtel et al., 1975), but available evidence points to their being localized rather than extended sources (Kniffen et al., 1975; Hartman et al., 1976).

In the region of strong γ-ray emission between 310° and 45°, five peaks stand out. These peaks are centered on longitudes 315°, 330°, 345°, 0°, and 35°. From figure 1, all of the peaks could be seen to lie on the galactic plane itself, within uncertainties. Because the peak near 315° lies relatively close to the limit of the SAS-2 exposure, its overall significance is the smallest of the five. The peaks at 330° and 345° are sufficiently narrow to be consistent with

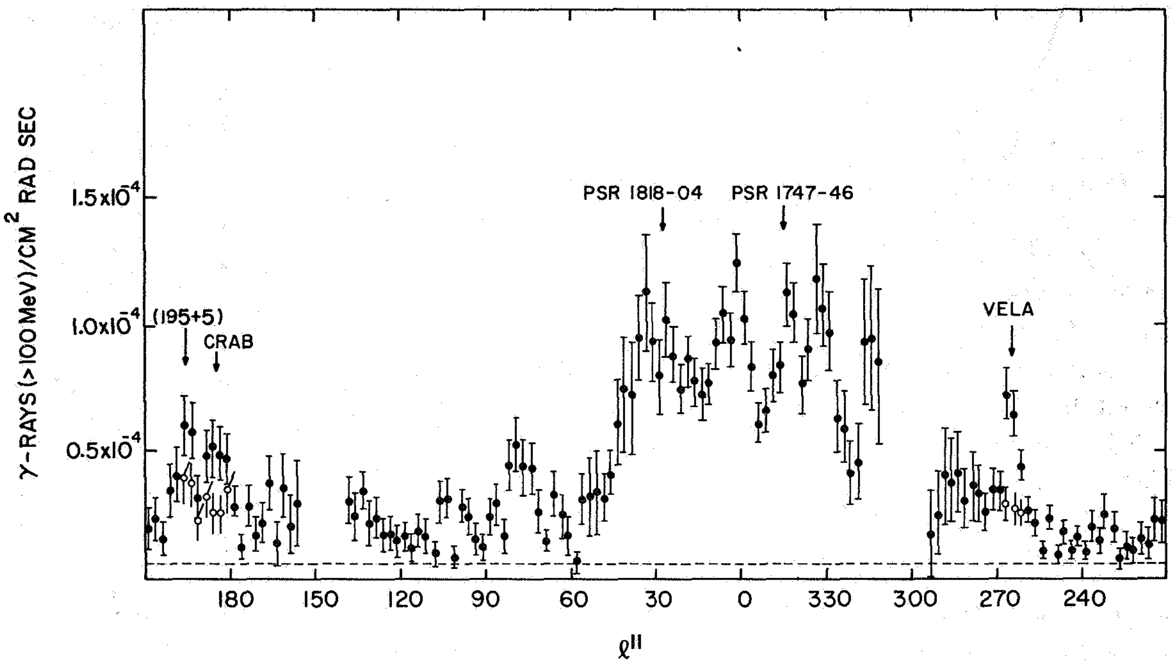

Figure 3. Distribution of high-energy (> 100 MeV) γ-rays along the galactic plane. The SAS-2 data are summed from $b^{II} = -10°$ to $b^{II} = +10°$. The diffuse background is shown as a dashed line. Arrows mark the locations of localized sources. The open circles give the estimated galactic emission with localized sources subtracted. Error bars shown are statistical only. An additional uncertainty of about 10 percent should be attached to the overall normalization.

the detector resolution, implying that they must be distant large-scale features or intense localized sources. The fact that these peaks lie in a direction not far from the galactic center suggests a large-scale rather than discrete origin for two reasons. First, the inner section of the galaxy is the region most likely to contain cosmic rays and matter which produce diffuse galactic γ-rays. Second, unless a discrete source were extremely intense, it would have to be relatively nearby in order to be seen against the general galactic background. This effect is illustrated by the locations of two candidate γ-ray pulsars in the general region around the center (PSR 1747-46 and PSR 1818-04; Ögelman et al., 1976). Although these are identified γ-ray sources, they contribute less than 10 percent of the intensity in any one bin in figure 3. The enhancement in the longitude distribution around the 0° direction itself appears to be slightly broader than the detector resolution. Although this effect may not be statistically significant, it suggests the possibility of an extended source in the galactic center direction.

DISCUSSION

Any attempt to interpret the galactic γ-ray emission in terms of a model faces the difficulty that the galactic components which produce γ-rays (cosmic rays, interstellar matter, and magnetic fields) are interrelated. Many different approaches to the problem can therefore be considered. Bignami et al. (1975) have used the spiral pattern deduced from 21-cm data in the galaxy as the basis for the matter and cosmic-ray distributions. Stecker et al. (1975) started with the distribution of molecular hydrogen in the galaxy estimated from 2.6-mm carbon-monoxide emission. Fuchs et al. (1975) developed a model based on the magnetic field configuration in the galaxy. Paul et al. (1975) used radio measurements of the synchrotron radiation to estimate cosmic-ray and matter distribution. Cowsik and Voges (1975) studied the possible inverse Compton component of the radiation by using a model for the starlight distribution in the galaxy. All of these models have had some success in interpreting either part or all of the SAS-2 γ-ray observations. Instead of reviewing such models in detail or proposing a new model, this discussion will attempt to show how the γ-ray results themselves motivated the various approaches.

One of the key questions in studying the galactic emission is the production mechanism for the γ-radiation. The available data (Samimi et al., 1974; Fichtel et al., 1975; Sood et al., 1975) suggest that the dominant source of high-energy ($>$ 100 MeV) γ-rays is neutral pion decay, and the dominant source of medium energy ($<$ 50 MeV) γ-rays has a spectrum like that expected from inverse Compton scattering or electron bremsstrahlung. The high-energy radiation then reflects the product of the matter density and the nucleonic cosmic-ray density along a given line of sight. In order to calculate the medium-energy component, knowledge is needed of the cosmic-ray electron density, the matter density, and the photon density as a function of position in the galaxy. Some information is also needed about the degree of association or coupling between the various components. No single aspect of this problem can be considered to be definitively understood at present, and one of the special advantages of γ-ray astronomy lies in its unique ability to probe the galactic cosmic-ray distributions in conjunction with other galactic components.

In studying the spatial distribution of the observed γ-radiation, as summarized in figures 1, 2, and 3, the most important features are: (1) the broad relatively flat excess around the galactic center and the contrast between this excess and the anticenter regions; (2) the specific nonuniformities within the high-intensity central sector; and (3) the resolution-limited and broader components of the latitude distribution in the galactic center region. Each of these features contains important information about the distribution in the galaxy of the components responsible for the γ-radiation.

The center-to-anticenter intensity ratio does not appear to be explainable strictly in terms of the galactic interstellar matter distribution. The neutral hydrogen distribution as measured by 21-cm radio observations shows far less contrast than the γ-ray observations. The 2.6-mm observations of CO, considered to be a tracer of molecular hydrogen, do show a strong contrast as a function of galactic radius, but the peak of this distribution lies at a radius between 4 and 6 kpc from the galactic center. Such a distribution alone could not account for the high-intensity ridge extending from 310° to 45° (Stecker et al., 1975). The failure of the galactic matter distributions to explain the γ-ray distribution is a strong argument that the cosmic rays which interact with the matter are themselves not uniform in the galaxy—an argument which supports the galactic origin for the bulk of the cosmic rays.

If it is assumed that the expansive pressures of the kinetic motion of the gas, the cosmic rays, and the magnetic fields in the galaxy can only be contained by the mass of the gas, then some degree of correlation would be expected between the matter density, the magnetic field and the cosmic-ray density, at least on a large scale (Bignami et al., 1975). This approach suggests that the synchrotron emission from cosmic-ray electrons interacting with the magnetic fields might show some of the same features as the γ-ray emission originating from cosmic-ray nucleons interacting with interstellar matter (Paul et al., 1974). A comparison of figure 1 with the 150-MHz map of Landecker and Wielebinski (1970), reproduced in figure 4, shows that this is indeed the case. In particular, the synchrotron measurements show the same strong center-to-anticenter contrast as seen in the SAS-2 results. On a galaxy-wide scale, then, these radio measurements seem to support the concept of coupling between the matter density, the magnetic field, and the cosmic-ray density.

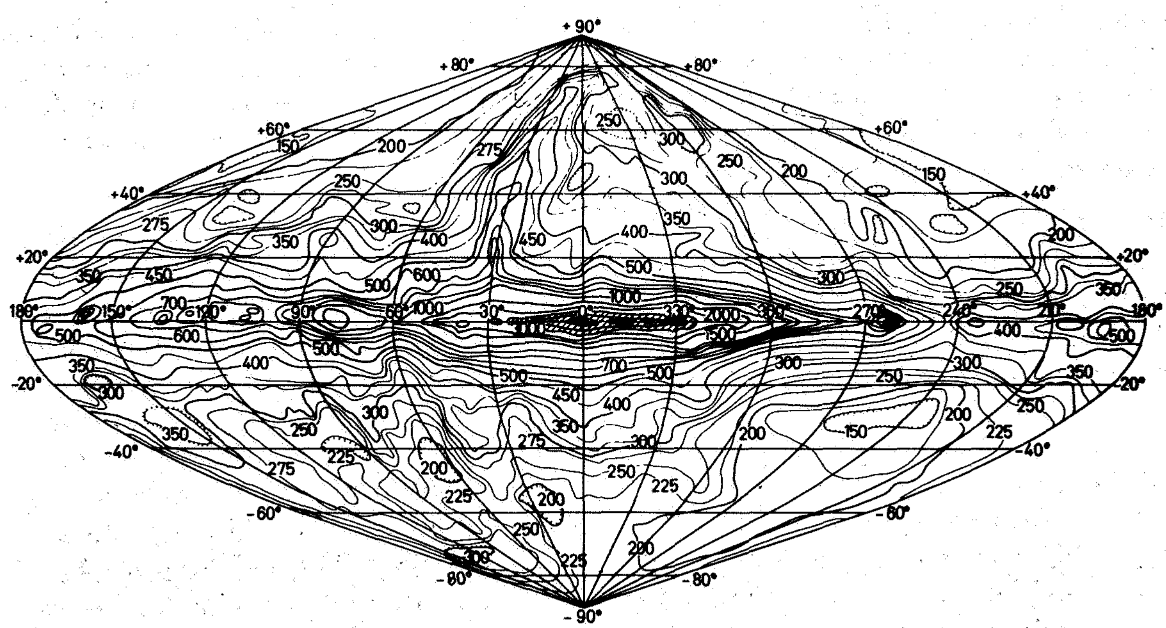

Figure 4. Map of 150-MHz brightness temperatures in galactic coordinates (Landecker and Wielebinski, 1970).

The five strong peaks in the γ-ray data surrounding the galactic center offer additional clues to the origin of this high-energy radiation. Under the general assumption that ours is a spiral galaxy (although the pitch angle of the spiral may be small in some regions), a peak in the γ-ray data implies a long line of sight through a region of high emissivity, such as along a spiral feature. For example, the direction of the 35° peak, would be tangent to a galactic arm at a radius of about 6 kpc. This direction is roughly coincident with the observed peak in the molecular hydrogen distribution and with one of the arms which has been observed in 21-cm neutral hydrogen measurements. The fact that this is the only strong peak observed between the galactic center and 45° longitude is a strong motivation for considering the molecular hydrogen as the principal source of the γ-radiation.

Because relatively little is known about conditions at the center of the galaxy, the somewhat broadened peak close to the galactic center may have several origins. Radio observations indicate that neutral and molecular hydrogen are not particularly abundant over the general galactic center region. If this γ-ray peak is attributed to cosmic-ray/matter interactions, either the cosmic-ray intensity would have to be much higher in the galactic center than in other parts of the galaxy or the matter would have to be in some unseen form, such as ionized gas. The fact that the galactic center is a strong source of radio, infrared, and X-ray emission suggests the possibility of discrete source contributions, although the intensity appears rather large to be explained by any one γ-ray source at such a large distance. Another possibility is an inverse Compton contribution resulting from an increase in the cosmic-ray electron density and the starlight density toward the galactic center. Such a component would be strongly peaked toward 0° longitude, as shown, for example, by Cowsik and Voges (1975). The central peak in the SAS-2 longitude distribution could also be made up of several components. Until more is learned about the galactic center region, it will be difficult to determine whether this γ-ray excess has an origin similar to the other peaks in the data or whether it represents a unique γ-ray source.

The three peaks observed between 310° and the galactic center direction all coincide with spiral arm features in the Simonson (1976) picture of the galaxy, based on 21-cm measurements and the density wave theory. Because the observed densities of neutral hydrogen in these arms are not extremely high, a strong correlation between the cosmic-ray density and the matter density in this region would be necessary in order to explain the results solely in terms of these features (Bignami et al., 1976). In the absence of any CO measurements of this region of the sky to indicate where molecular hydrogen might be concentrated, one possibility would be to assume some sort of symmetry with the opposite side of the galactic center. The molecular hydrogen might then be found at the position of the 330° feature. Some other explanation would then be needed for the other two peaks in this region. An alternate possibility, suggested by Fichtel et al. (1976), is that the molecular hydrogen densities are high, as observed around the 35° direction, but that the cosmic rays are more strongly coupled to the diffuse neutral hydrogen than to the high-density clouds of molecular hydrogen. One additional observation which might tend to support such a concept is the 150-MHz sky map (Landecker and Wielebinski, 1970), which shows the 310° to 45°-segment of the galactic plane to be an intense source of synchrotron radiation, with an additionally intense ridge between 330°and 0° longitude. As mentioned before, this radio observation would suggest a strong coupling between the cosmic-ray electrons and the magnetic field, with an implied coupling to the distributed matter in the same region.

Finally, the two-component nature of the observed γ-ray latitude distribution is a somewhat unexplored subject. The most likely explanation of the broad component of the latitude distribution toward the galactic center is that this radiation is originating from regions close enough to the solar system that the galactic disk itself appears broader than the detector resolution, and the resolution-limited component originates from more distant parts of the galactic plane. A small contribution to the broad component could come from an extension of the cosmic-ray disk above the disk defined by interstellar matter, although Bignami et al. (1975) have shown that a broader cosmic-ray disk would have little effect. Another small contributor to the broad-latitude component could be inverse Compton γ-rays produced by cosmic-ray electrons and starlight or 3°K radiation, because both stars and cosmic-ray electrons are thought to extend above the interstellar gas disk. Additional work on the SAS-2 data, studying only the broad-latitude component, may reveal additional information about the nature and origin of this radiation.

In summary, the SAS-2 results have shown that high-energy γ-rays are an excellent tracer of the components and structure of the galaxy. The γ-ray evidence for a galactic origin of cosmic rays is strong, and the combination of γ-ray data with measurements at other wavelengths provides useful information about the dynamic processes coupling the matter, magnetic fields, and cosmic rays in the galaxy. As more γ-ray data and more data from other sources become available, some of the prospects and possibilities which have been raised by SAS-2 should become a greatly improved picture of our galaxy.

REFERENCES

Bignami, G. F., C. E. Fichtel, D. A. Kniffen, and D. J. Thompson, 1975, *Ap. J.*, **199**, p. 54.

Cowsik, R., and W. Voges, 1975 (Proc. 14th Intl. Cosmic Ray Conf., No. 1, Munich), p. 74.

Derdeyn, S. M., C. H. Ehrmann, C. E. Fichtel, D. A. Kniffen, and R. W. Ross, 1972, *Nucl. Instr. and Methods* **98**, p. 557.

Dodds, D., A. W. Strong, and A. W. Wolfendale, 1974, *Nature*, **250**, p. 716.

Fichtel, C. E., R. C. Hartman, D. A. Kniffen, D. J. Thompson, G. F. Bignami, H. Ögelman, M. E. Özel, and T. Tümer, 1975, *Ap. J.* **198**, p. 163.

Fichtel, C. E., D. A. Kniffen, D. J. Thompson, G. F. Bignami, and C. Y. Cheung, 1976, *Ap. J.*, in press.

Fuchs, B., R. Schlickeiser, and K. O. Thielheim, 1975 (Proc. 14th Intl. Cosmic Ray Conf. No. 1, Munich) p. 83.

Hartman, R. C., C. E. Fichtel, D. A. Kniffen, D. J. Thompson, G. F. Bignami, R. C. Lamb, H. Ögelman, M. E. Özel, and T. Tümer, 1976 (Proc. Goddard Gamma-Ray Symposium (this conference)).

Kniffen, D. A., R. C. Hartman, D. J. Thompson, G. F. Bignami, C. E. Fichtel, H. Ögelman, and T. Tümer, 1974, *Nature*, **251**, p. 397.

Kniffen, D. A., G. F. Bignami, C. E. Fichtel, R. C. Hartman, H. Ögelman, D. J. Thompson, M. E. Özel, and T. Tümer, 1975 (Proc. 14th Intl. Cosmic Ray Conf., No. 1, Munich), p. 100.

Landecker, T. L. and R. Wielebinski, 1970, *Australian J. Phys. Astrophys.*, Supplement 16.

Ögelman, H. B., C. E. Fichtel, D. A. Kniffen, and D. J. Thompson, 1976, *Ap. J.*, in press.

Paul, J., M. Cassé, and C. J. Cesarsky, 1974 (Proc. 9th ESLAB Symposium, ESRO SP-106), p. 246.

Paul, J., M. Cassé, and C. J. Cesarsky, 1975 (Proc. 14th Intl. Cosmic Ray Conf., No. 1, Munich), p. 59.

Samimi, J., G. H. Share, and R. L. Kinzer, 1974, (Proc. 9th ESLAB Symposium, ESRO *SP-106*), p. 211.

Simonson, S. C., III, 1976, *Astron. and Astrophys.*, **46**, p. 261.

Sood, R. K., K. Bennett, P. G. Clayton, and G. K. Rochester, 1975 (Proc. 14th Intl. Cosmic Ray Conf., No. 1, Munich), p. 35.

Stecker, F. W., P. M. Solomon, N. Z. Scoville, and C. E. Ryter, 1975, *Ap. J.* **201**, p. 90.

Thompson, D. J., C. E. Fichtel, D. A. Kniffen, and H. B. Ögelman, 1975, *Ap. J. Letters*, **200**, p. L79.

SAS-2 GALACTIC GAMMA-RAY RESULTS—II. LOCALIZED SOURCES

R. C. Hartman, C. E. Fichtel, D. A. Kniffen, R. C. Lamb,* D. J. Thompson, and G. F. Bignami**

Laboratory for High Energy Astrophysics
NASA/Goddard Space Flight Center
Greenbelt, Maryland 20771

H. Ögelman, M. Özel, and T. Tümer

Middle East Technical University, Ankara, Turkey

ABSTRACT

Gamma-ray emission has been detected from the radio pulsars PSR 1818-04 and PSR 1747-46, in addition to the previously reported γ-ray emission from the Crab and Vela pulsars. Since the Crab pulsar is the only one observed in the optical and X-ray bands, these γ-ray observations suggest a uniquely γ-ray phenomenon occurring in a fraction of the radio pulsars. Using distance estimates of Taylor and Manchester (1975), we find that PSR 1818-04 has a γ-ray luminosity comparable to that of the Crab pulsar, whereas the luminosities of PSR 1747-46 and the Vela pulsar are approximately an order of magnitude lower. This survey of SAS-2 data for pulsar correlations has also yielded upper limits to γ-ray luminosity for 71 other radio pulsars. For five of the closest pulsars, upper limits for γ-ray luminosity are found to be at least three orders of magnitude lower than that of the Crab pulsar.

The γ-ray enhancement around galactic coordinates $\ell^{II} = 195°$, $b^{II} = +5°$ is probably not associated with the recently discovered Milky Way satellite galaxy (Simonson, 1975), because its position seems to be incompatible, and its intensity appears to be unreasonably high. The enhancement near the galactic plane in the Cygnus region, although consistent with the location of a galactic spiral-arm feature, is sufficiently well-localized to be compatible with a point-like source.

---

*On faculty leave from Iowa State University during 1975-76.
**NAS-NRC Postdoctoral Research Associate, 1973-75.

INTRODUCTION

Three years ago, at the time of the Denver Cosmic Ray Conference, there was only one confirmed γ-ray point-source observation of high statistical weight, the Crab Nebula. Some results from balloon-borne experiments indicated excesses of three or even four standard-deviation significance; however, with the exception of observations of the Crab pulsar, none of those results were convincingly confirmed.

At the present time, analysis of the SAS-2 data is nearing completion. In addition to the general galactic-plane emission discussed in the previous paper, the SAS-2 γ-ray telescope also recorded a number of localized regions of enhanced γ-ray emission, all within about 10° of the galactic plane.

RESULTS

In the general direction of the galactic anticenter, two enhancements are seen in the SAS-2 data above the background, about 12° apart. This region has recently been reanalyzed, as discussed in the previous paper, with the result shown in figure 1. The two enhancements are clearly separated. One of them is obviously associated with the Crab Nebula, because a large portion of its emission is pulsed at the period of the Crab pulsar. In deriving a total intensity for the Crab source, some uncertainty is encountered in estimating the diffuse background to be subtracted. A recent reanalysis yields a total intensity above 100 MeV of $(3.7 \pm 0.8) \times 10^{-6}$ cm^{-2} s^{-1}, in agreement with the preliminary SAS-2 result (Kniffen et al., 1974). Figure 2 shows the result of folding individual event times at the predicted radio pulsar period. The γ-ray emission is found to be strongly pulsed, with structure and phase similar to those of radio, optical, and X-ray bands. The pulsed intensity is $(2.9 \pm 0.5) \times 10^{-6}$ cm^{-2} s^{-1} above 100 MeV. Thus, the pulsed emission accounts for most, if not all, of the enhancement seen in the Crab region. The spectrum of the Crab γ-rays is consistent with a power-law extrapolation from X-ray energies for both the pulsed and the total intensities.

The strongest source observed by SAS-2 is associated with the Vela supernova remnant. The surprising discovery (Thompson et al., 1975) is that a major part of the Vela γ-ray flux is pulsed at the radio period, although no pulsation is observed in the optical range and no confirmed observation of pulsation has been made in the X-ray range. Still more intriguing are the facts that the γ-radiation is double-pulsed and that neither pulse is in the phase with the single radio pulse. Figure 3 shows the dramatic difference in the pulsed behavior of the Crab and Vela pulsars in the radio, optical, X-ray and γ-ray energy ranges. Although the Vela pulsar is a brighter γ-ray source than the Crab as seen from the Earth, the γ-ray luminosity of the Crab pulsar is about eight times that of the Vela pulsar above 100 MeV. In contrast, the luminosity ratio L_{CRAB}/L_{VELA} in the X-ray region is at least 80 (Fritz et al., 1971; Harnden and Gorenstein, 1973) at 1 keV, and may be 1000 or more in the 1.5- to 10-keV band (Rappaport et al., 1974).

The energy spectrum of the Vela source is essentially the same as that of the galactic plane, within the detector ability to see a difference. Furthermore, the pulsed fraction is independent

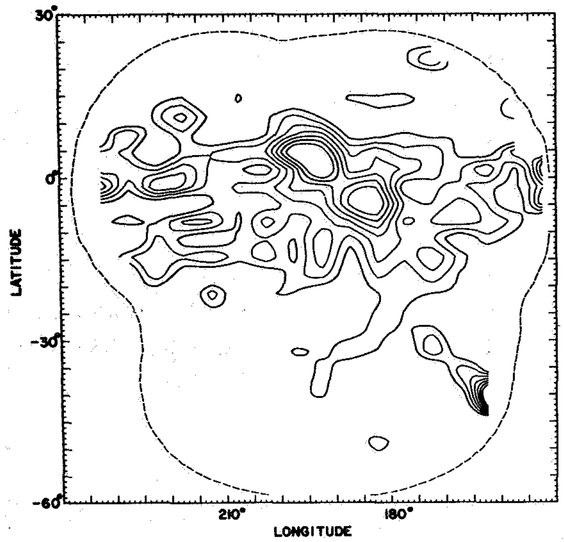

Figure 1. Contour plot of the intensity of γ-rays with energy > 35 MeV from the galactic anticenter region. The contour lines represent 75, 66, 57, 48, 39, 30, and 21 percent of the maximum value, 4.25×10^{-4} cm^{-2} sr^{-1} s^{-1}.

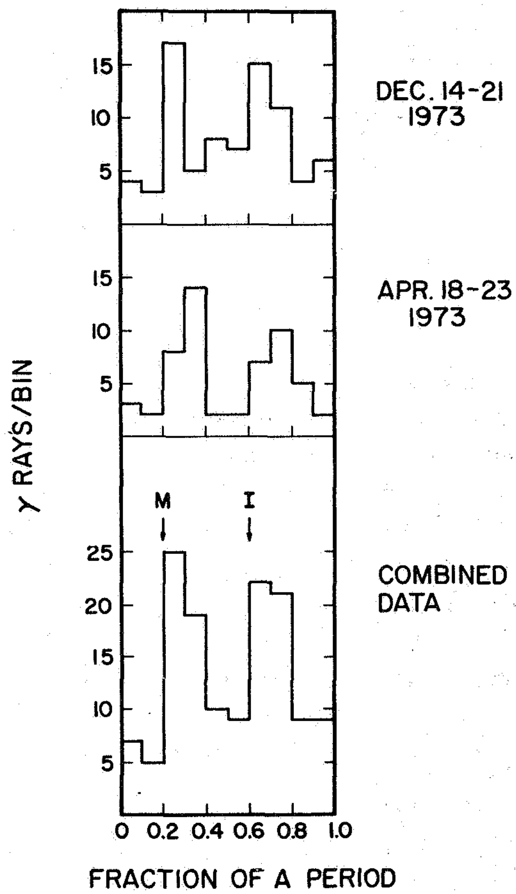

Figure 2. Phase plot for γ-rays (E > 35 MeV) from the Crab Pulsar (NP0531+21). The arrows marked M and I indicate the positions of the main radio pulse and the interpulse.

of energy, again within the detector limitations. For all energies combined, the pulsed fraction is 70 +14/-12 percent. The total flux above 35 MeV is $(15.1 \pm 2.4) \times 10^{-6}$ cm^{-2} s^{-1}, and above 100 MeV, $(6.3 \pm 1.1) \times 10^{-6}$ cm^{-2} s^{-1}.

Thompson (1975) has proposed a model for the Vela pulsar in which the radio emission originates near the polar surface of a neutron star which has its magnetic dipole axis roughly perpendicular to its spin axis. The γ-ray emission then arises from synchrotron radiation in the region where the polar-field lines reach the speed-of-light cylinder. In each case, the photons are emitted roughly along the magnetic-field lines, and the spiral shape of the field lines produces the observed 13-ms delay between the radio pulse and the γ-ray pulse. The double-pulsed γ-ray structure is explained by assuming that the γ-rays are emitted in a broader cone than the radio emission, and that γ-ray emission is observed from both magnetic poles, but radio emission is observed from only one pole. Obviously, this picture does not apply to the Crab pulsar. Its different phase structure and spectrum indicate that a different mechanism is probably responsible for its γ-ray emission.

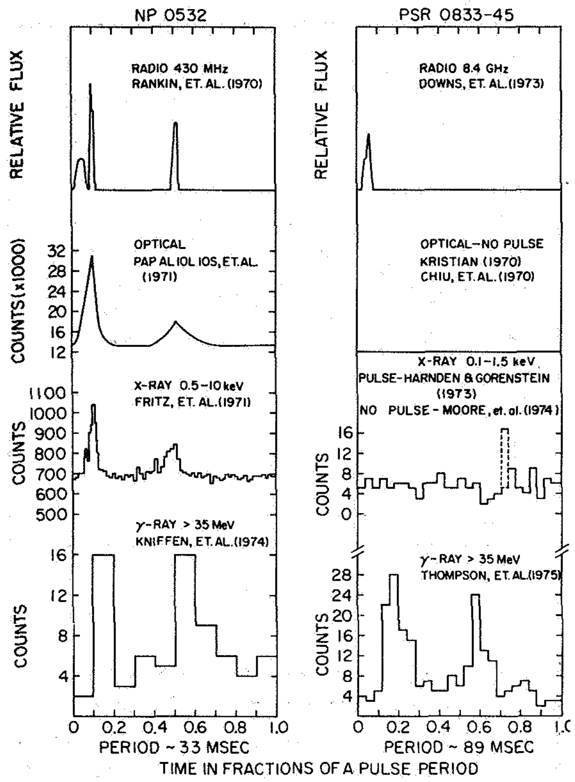

Figure 3. Comparison of Crab and Vela pulsar phase plots in radio, optical, X-ray and γ-ray bands.

The observation of γ-rays from the Vela pulsar, which is not seen in the optical or X-ray regions, suggests that other radio pulsars might be observable at γ-ray energies. Of the 147 known radio pulsars, 134 were within the region of the sky observed by SAS-2. For 59 of these, however, the period and period derivative were not known with sufficient accuracy to give adequate phase information during the SAS-2 observations. This leaves 75 pulsars available for study, two of which have already been discussed—the Crab and Vela pulsars. For the remaining 73, a search has been made for γ-ray pulsation at the predicted radio periods. In two cases, phase distributions were obtained which are relatively improbable. The phase plot for PSR 1818-04, with a period of about 0.6 s, is shown in figure 4. The position of the radio pulse is shown by the arrow marked "R."

The chance that a distribution like this might occur randomly in one of the 73 pulsars is about 0.3 percent. The contour plot shown in figure 5 indicates an enhancement, not significant by itself, in the appropriate region for this pulsar. The pulsed flux above 35 MeV found for PSR 1818-04 is $(2.0 \pm 0.5) \times 10^{-6}$ cm^{-2} s^{-1}.

The phase plot in figure 6 is for γ-rays from the region around the pulsar 1747-46, which has a period of 0.742 s. There is a chance probability of about 0.6 percent of seeing it in one of 73 distributions. Because PSR 1747 lies 10° south of the galactic plane at a galactic longitude of 345°, it is feasible to look for an enhancement in the total γ-ray flux from that

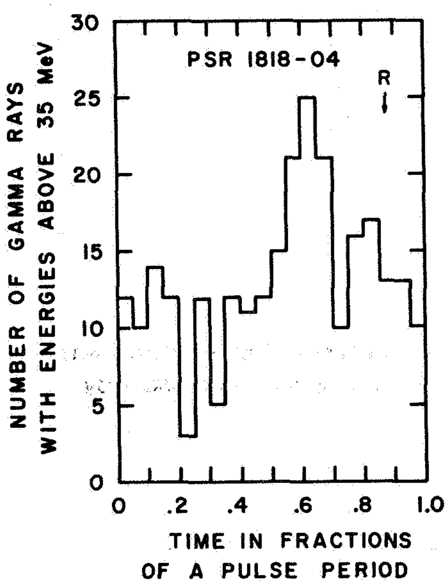

Figure 4. Phase plot for γ-rays ($E > 35$ MeV) from PSR 1818-04. The arrow marked "R" is the position of the observed radio pulse.

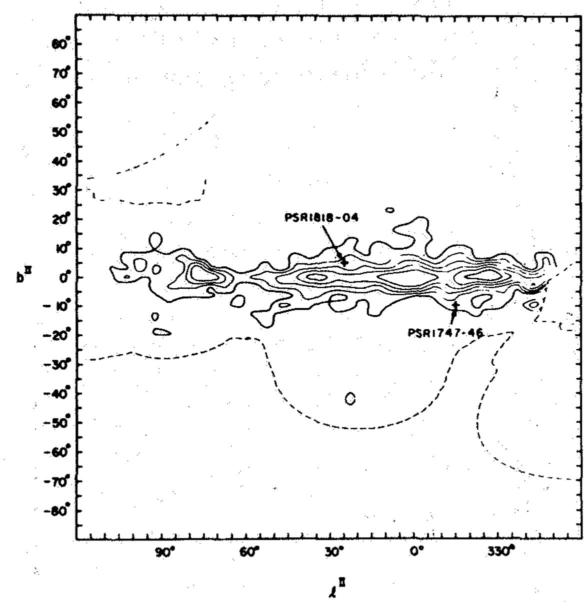

Figure 5. Contour plot of the intensity of γ-rays with energy > 100 MeV for galactic longitudes between 270° and 90°. The contour lines represent 81, 63, 47, 33, 21 and 11 percent of the maximum, which is 6.3×10^{-4} cm^{-2} sr^{-1} s^{-1}.

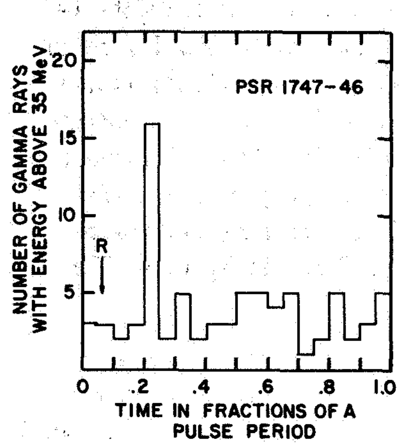

Figure 6. Phase plot for γ-rays ($E > 35$ MeV) from PSR 1747-46. The arrow marked "R" indicates the position of the observed radio pulse.

region. The contour plot in figure 5 shows a bump in the proper region; a more careful analysis, using a band of latitudes from -6° to -14° to estimate background, yields a 3σ positive result. This independent evidence enhances the significance of the pulsed result.

The total flux obtained for PSR 1747-06 is $(1.6\pm0.6) \times 10^{-6}$ cm^{-2} s^{-1} above 100 MeV. For pulsed flux above 100 MeV, we find a value of $(6.5\pm3.3) \times 10^{-7}$ cm^{-2} s^{-1}, based on only six events. Above 35 MeV, the pulsed flux is $(2.40\pm0.7) \times 10^{-6}$ cm^{-2} s^{-1}. We note that the delay between the radio pulse and the γ-ray pulse is 115 ± 20 ms, or 0.16 ± 0.03 of a pulse period. This delay is very close to that between the radio pulse and the closer of the two γ-ray pulses for the Vela pulsar of 0.15 ± 0.02 period.

Thus, we now have strong evidence of four radio γ-ray pulsars, only one of which (the youngest) is detectable at optical and X-ray energies. Several obvious questions immediately come to mind. For instance, what fraction of the energy lost by the pulsar goes into γ-radiation? If we know the period and its derivative and assume a moment of inertia of 10^{45} g cm^2, we can estimate the pulsar's rotational energy loss rate from

$$\frac{dE_R}{dt} = I \Omega \dot{\Omega} = \frac{4 \pi^2 I \dot{P}}{P^3}$$

where Ω, $\dot{\Omega}$, P, and $\dot{P}$ are the angular frequency and period and their time derivatives, and I is the moment of inertia.

For the γ-rays, we assume a radiating cone of 1 sr and a typical energy of 100 MeV, with the result shown in figure 7. We see that the Crab and Vela pulsars are apparently radiating only 10^{-3} to 10^{-2} of their energy in γ-rays. Pulsars PSR 1747 and PSR 1818, however, seem to be radiating a major fraction of their energy in this range. The apparent excess of the γ-ray luminosity over the energy loss rate for PSR 1818 is attributable to large uncertainties in both the pulsar moment of inertia and the width of the γ-ray emission cone.

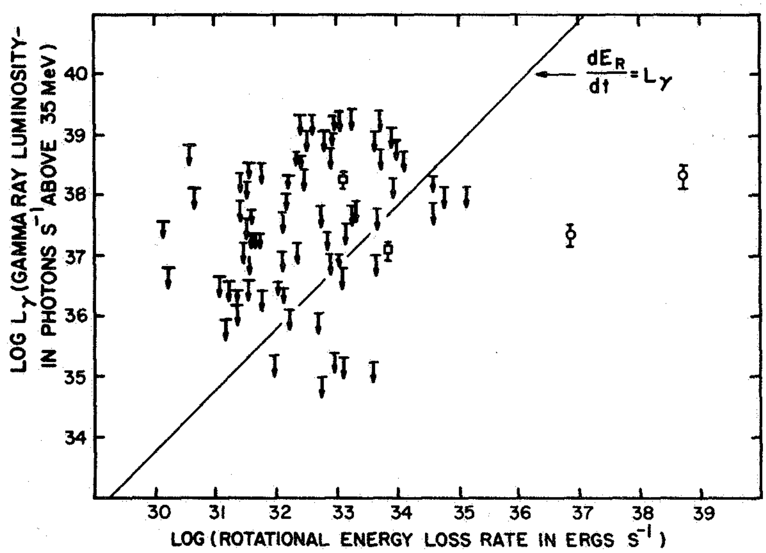

Figure 7. Observed γ-ray luminosities and upper limits as a function of pulsar rotational energy loss rates, from Taylor and Manchester (1975). Open circles are the Crab (Kniffen et al., 1974) and Vela pulsar (Thompson et al., 1975) observations. The open boxes are for PSR 1747-46 and PSR 1818-04. Distance estimates from Taylor and Manchester (1975) were used in calculating luminosities. Error bars reflect only γ-ray flux uncertainties. The line indicates the condition in which all pulsar rotational energy loss appears in the form of γ-rays.

We can also compare the pulsar luminosities and upper limits with apparent ages, $P/2\dot{P}$, as shown in figure 8. No simple relationship is obvious between γ-ray luminosity and apparent age; however, it is worthwhile to note that all four of the pulsars for which γ-ray pulsations have been observed show ages less than about 10^6 years, whereas most of the pulsars included in the study have ages greater than 10^6 years. This suggests, although not conclusively, that γ-ray luminosity decreases rapidly for pulsars older than 10^6 years, as is the case for radio luminosity.

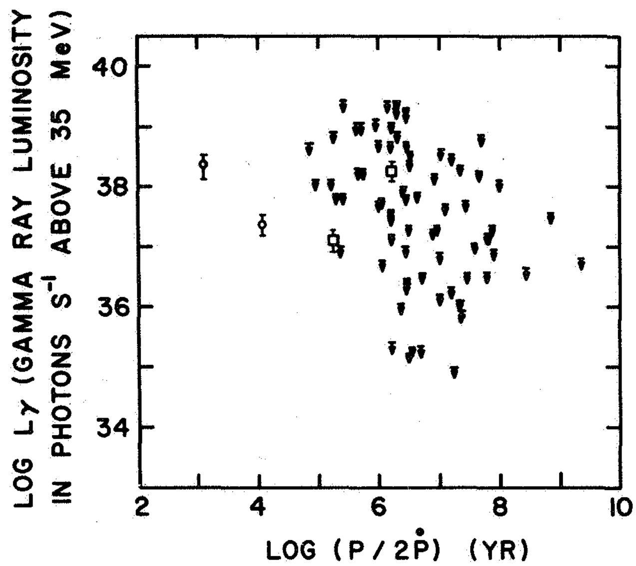

Figure 8. Observed γ-ray luminosities and upper limits as a function of apparent age, $P/2\dot{P}$. See caption for figure 7.

If γ-ray emission is a fairly general property of pulsars, as now seems possible, it is natural to ask what portion of the γ-ray luminosity of the galaxy is attributable to pulsars. Because no γ-ray pulsars are presently seen with ages greater than about 10^6 years, we use that figure as the pulsar γ-ray lifetime. If pulsars are created in the galaxy at the rate of one every 100 years and each radiates for 10^6 years a γ-ray luminosity of 10^{37} photons s^{-1} above 35 MeV, we find a contribution of 10^{41} s^{-1}, or about 5 percent of the luminosity of the galaxy due to cosmic-ray interactions.

One region of enhanced γ-ray intensity has been observed with SAS-2 which has not been clearly identified with any known object. In the region of the galactic anticenter, there is a major flux enhancement centered at approximate galactic coordinates $\ell^{II} = 195°$, $b^{II} = +5°$. This source has an intensity comparable to that of the Crab for energies above 100 MeV. However, it appears on the basis of limited statistics to have a somewhat flatter spectrum, because it stands out most prominently as a localized source for energies above 100 MeV. Lamb et al. (1975) have investigated the possibility that this source might be associated with the recently discovered (Simonson, 1975) satellite galaxy near the Milky Way. They concluded that the association is unlikely for two reasons: (1) the position obtained for the γ-ray source is at least five standard deviations from the position given by Simonson (1975); and (2) from Simonson's (1975) estimates of the distance and mass of the new galaxy, it appears that its cosmic-ray density would have to be nearly two orders of magnitude greater than is observed locally if its emission is assumed to be due to cosmic-ray interactions. Similar conclusions have been reached by Cesarsky et al. (1976) and Bignami et al. (1976). Several supernova remnants are known in the same general direction as that of the unidentified γ-ray enhancement, but the closest, IC 443, is more than 4°, or at least 5σ, from the γ-ray source.

Very recently, we have found evidence for possible periodicity in this source, with a period of about 1 minute. This possibility was first noticed by examining the time intervals between individual γ-rays from the source. Figure 9 lists all pairs of events near $\ell^{II} = 195°$, $b^{II} = +5°$ which occurred during single SAS-2 orbits during 1 week of observation. (The SAS-2 telescope was recording celestial γ-rays for about 60 percent of each 95-minute orbit.) It was noted that the shorter intervals all appear to be approximate multiples of the shortest interval, 57.7 seconds. By assigning integer factors of multiplication, a better value of the hypothetical period was found, as shown in figure 9. The probability that this indication of periodicity is a chance regularity is estimated to be 1 or 2 percent. A folding search of the three observing intervals, each 1-week long, showed evidence for periodicity, but the intervals showed slightly different periods, consistent with a period increasing at a rate of 2.2×10^{-9}. Figure 10 shows the resulting phase plot. In view of the number of trials used and the added degree of freedom in assuming a nonzero $\dot{P}$, we feel that the evidence for this periodicity is not statistically compelling, but must await confirmation. However, this unidentified object, which presently appears to be a uniquely γ-ray phenomenon, is certainly one of the important experimental problems in γ-ray astronomy.

The final source we will mention is in the Cygnus region, near the galactic plane at a galactic longitude of about 77°. It has been pointed out previously that this enhancement, which is clearly seen in the contour map of figure 5, is in about the same position as the local spiral arm seen in 21-cm radio measurements, and therefore might be a galactic-arm feature rather than a point source. Reanalysis of the 2 weeks of observation indicates, however, that the enhancement is compatible with a point-like source and is considerably narrower in longitude than the calculated width of about 15° for a galactic-arm feature in this direction (e.g., Bignami et al., 1975). If a galactic-arm feature is 200-pc thick normal to the galactic plane and is 1 to 2 kpc away, its observed latitude extent would be 5° to 10°, which is also probably incompatible with the observations.

The observed position is consistent with that of Cygnus X-3, a prominent X-ray source modulated with a 4.8-hour period. The period and phase of the X-ray modulation are known precisely enough to make a fold of the SAS-2 data at this period meaningful. However, this period is almost exactly three times the orbital period of the SAS-2 satellite, and care is required in order to avoid a possible spurious indication of periodicity. Figure 11 shows the result of folding the SAS-2 data at the known X-ray period of 4.8 hours. The bottom part of the figure includes all data from the week of observation, $\sim$ 90 percent of which are

CLOSE PAIRS FROM DEC. 14-21, 1972 DATA

PAIR NO.	Δt (SEC)	ASSUMED MULTIPLE M	Δt/M (SEC)	CALCULATED MULTIPLE
1	756.7	13	58.2	12.94
2	652.8	11	59.3	11.16
3	1271.5	22	57.8	21.74
4	57.7	1	57.8	0.99
5	177.2	3	59.1	3.03
6	347.1	6	57.9	5.93
7	133.4	2	66.7	2.28
8	300.1	5	60.1	5.13
9	519.2	9	57.7	8.88
10	1568.2	27	58.1	26.81
11	122.4	2	61.2	2.09
12	939.8	16	58.7	16.06
TOTAL	6846.1	117	58.5	

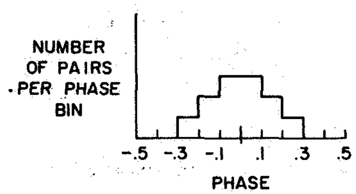

PROBABILITY OF ALL 12 PAIRS IN 0.6 PHASE PLOT = 2.2×10^{-3}

Figure 9. Time intervals between pairs of γ-ray events from near $\ell^{II} = 195°$, $b^{II} = +5°$ which occurred within single SAS-2 orbits (45-minute intervals).

γ-rays not associated with the Cygnus X-3 region. The small modulation seen in this data is the direct result of the nearness of the orbital period to one-third of the folding period. In the upper part of figure 11, only those γ-ray events near Cygnus X-3 are shown. There is clear indication of a 4.8-hour modulation in these γ-rays with a minimum near the minimum predicted from the X-ray data. The probability of finding this behavior by a random fluctuation of a uniform time distribution is about 0.1 percent.

The SAS-2 observations have also produced upper limits on γ-ray fluxes from a number of interesting astrophysical objects. In general, for objects away from the galactic plane, these limits are around 10^{-6} cm^{-2} s^{-1} for γ-rays above 100 MeV. Objects in this group include Cen A, Cas A, Tycho SNR, M87, M31, Sco X-1, Cyg X-1, Cyg X-2, LMC, SMC, and Jupiter. We note that our upper limit on Cen A does not contradict the Compton-synchrotron model recently proposed by Grindlay (1975) for that object.

SUMMARY

SAS-2 has provided evidence for γ-ray emission from four radio pulsars (the Crab and Vela pulsars, PSR 1747-46 and PSR 1818-04). Three of the four have not been observed to pulse at optical or X-ray energies. We have made a tentative identification of Cygnus X-3 as a γ-ray source, with intensity modulated at the 4.8-hour period observed in X-rays. Finally, a strong γ-ray source seen near the galactic anticenter has not been identified with any known object.

Past experience in astrophysics has shown that each time a new frequency band has been investigated, totally new and unexpected objects and processes have been discovered. Gamma-ray astronomy is apparently beginning to demonstrate this principle again.

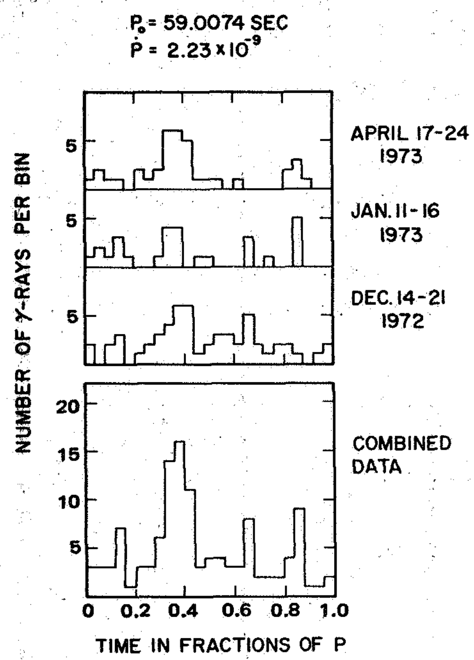

Figure 10. Phase plot for the γ-ray source at ℓ^{II} = 195°, b^{II} = +5°, assuming a period increasing with the indicated $\dot{P}$.

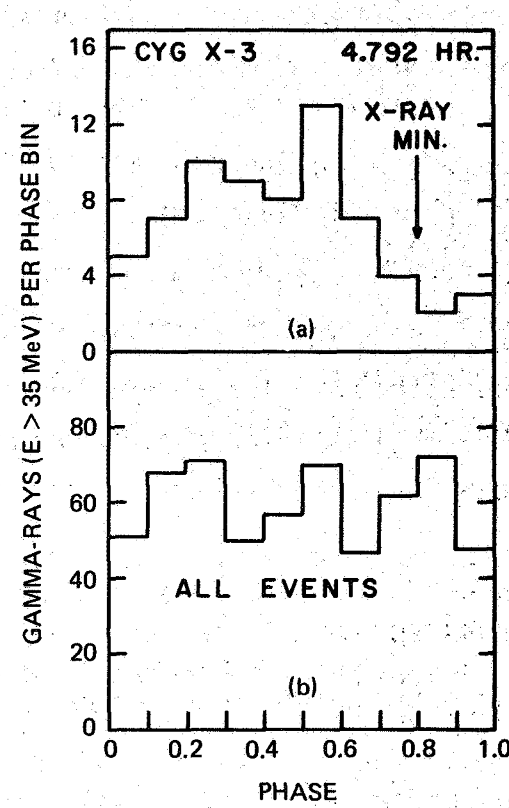

Figure 11. (a) Phase plot for γ-rays from the region around Cygnus X-3, folded at the 4.792-hour period observed in X-rays from Cygnus X-3; (b) Phase plot for all γ-rays observed during the same observation interval. The small modulation at three times the Cygnus X-3 frequency is due to the fact that the SAS-2 orbital period was almost exactly one-third of the Cygnus X-3 period. A distribution similar to this would be expected in figure 11 (a) if no 4.792-hour modulation is present.

REFERENCES

Bignami, G. F., C. E. Fichtel, D. A. Kniffen, and D. J. Thompson, 1975, *Ap. J.*, **199**, p. 54.

Bignami, G. F., T. Maccaro, and C. Paizis, 1976, *Astron and Ap.*, in press.

Cesarsky, C. J., M. Cassé, and J. Paul, 1976, *Astron and Ap.*, **48**, p. 481.

Fritz, G., J. F. Meekins, G. A. Chubb, H. Friedman, and R. C. Henry, 1971, *Ap. J.*, **164**, p. L55.

Grindlay, J. E., 1975, *Ap. J.*, **199**, p. 49.

Harnden, F. R., Jr., and P. Gorenstein, 1973, *Nature*, **241**, p. 107.

Kniffen, D. A., R. C. Hartman, D. J. Thompson, G. F. Bignami, C. E. Fichtel, H. Ögelman, and T. Tümer, 1974, *Nature*, **251**, p. 397.

Lamb, R. C., D. J. Thompson, and C. E. Fichtel, 1975, NASA TM X-71047, 1975.

Rappaport, S., H. Bradt, R. Doxsey, A. Levine, and G. Spada, 1974, *Nature*, **251**, p. 471.

Simonson, S. C., III, 1975, *Ap. J. Letters*, **201**, p. L103.

Taylor, J. H., and R. N. Manchester, 1975, *Astron. J.*, **80**, p. 794.

Thompson, D. J., C. E. Fichtel, D. A. Kniffen and H. B. Ögelman, 1975, *Ap. J.*, **200**, p. L79.

Thompson, D. J., 1975, *Ap. J.*, **201**, p. L117.

PRELIMINARY RESULTS FROM THE EUROPEAN SPACE AGENCY'S COS-B SATELLITE FOR GAMMA-RAY ASTRONOMY

THE CARAVANE COLLABORATION

K. Bennett, J. J. Burger, G. G. Lichti, B. G. Taylor, and R. D. Wills
Space Science Department, European Space Research and Technology Centre
Noordwijk, The Netherlands

G. F. Bignami and G. Boella
Laboratorio di Fisica Cosmica e Tecnologie Relative del CNR
Istituto di Scienze Fisiche dell'Università di Milano, Italy

R. Buccheri, A. Cuccia, and L. Scarsi
Istituto Fisica, Università di Palermo, Italy

W. Hermsen, J. Higdon, and B. N. Swanenburg
Cosmic-Ray Working Group, Hugens Laboratorium, Leiden, The Netherlands

G. Kanbach and H. A. Mayer-Hasselwander
Max Planck Institut für Physik und Astrophysik,
Istitut für Extraterrestrische Physik, Garching bei München, Germany

L. Koch, J. Masnou, J. A. Paul, and P. G. Shukla
Service d'Electronique Physique, Centre d'Etudes Nucléaires de Saclay
Gif-sur-Yvette, France

FOREWORD

The idea of a European mission for γ-ray astronomy was first considered about 10 years ago when an ESRO feasibility study was undertaken. Five University and Research Institutes–Max Planck Institut, Garching; Cosmic-Ray Working Group, Leiden; Istituto di Scienze Fisische, University of Milan; Centre d'Etudes Nucleaires, Saclay; and the Physical Laboratory, University of Southampton–forming the Caravane Collaboration, then developed the mission requirements and instrument characteristics. In May 1969, the Caravane Collaboration approached ESRO with a letter of intent, proposing that they produce the experiment for the proposed COS-B satellite, and, in July 1969, the ESRO council formally approved the inclusion of COS-B in the organization's scientific program.

Many scientists were already involved at this stage, but it is appropriate here that particular mention be made of the senior members of the collaboration responsible for bringing the idea of a γ-ray mission to life:

H. C. van de Hulst, G. W. Hutchinson, J. Labeyrie, R. Lüst,
G. P. Occhialini, C. Occhialini-Dilworth, and K. Pinkau.

In 1970, the Southampton group had to withdraw from the collaboration, and the remaining members invited the Space Science Department of ESTEC, lead by Dr. E. A. Trendelenburg, to join the collaboration. At about the same time, the University of Palermo joined the Milan group for the provision of the X-ray detector.

During the course of the next 5 years, many scientists who were no longer directly involved made vital contributions to the COS-B program, namely:

R. D. Andresen, I. Arens, P. Coffaro, M. Gorisse,
E. Pfeffermann, A. Scheepmaker, G. Sironi, and W. H. Voges

Supporting the scientists were the engineers, technicians, and programmers of the institutes without whom the project could not have continued, including:

R. Duc, N. Heinecke, T. Hydra, P. Keirle, G. Kettenring,
E. Leimann, P. Mussio, R. Roger, and F. Soroka.

The authors cannot do better than to quote the words of H. C. van de Hulst, the chairman of the COS-B Steering Committee, in an article written prior to the launch of the satellite in August 1975:

> ". . . . I wish to thank each member of the Collaboration for his contribution, members whose unrelenting input and caution in safeguarding the technical and scientific quality of the experiment are the best guarantee of ultimate success."

COS-B has now achieved 10 months of life in orbit and is repaying all the time and effort expended over almost the last decade.

THE COS-B EXPERIMENT AND MISSION

The Caravane Collaboration

ABSTRACT

The COS-B satellite carries a single experiment, capable of detecting γ-rays with energies greater than 30 MeV. Its objectives are to study the spatial, energy, and time characteristics of high-energy radiation of galactic and extragalactic origin. The capability to search for γ-ray pulsations is enhanced by the inclusion in the payload of a proportional counter sensitive to X-rays of 2 to 12 keV.

The experiment has been calibrated using particle accelerators. The results of these measurements are presented, and the performance of the system in orbit is discussed.

INTRODUCTION

The European Space Agency's satellite, COS-B, was launched from NASA's Western Test Range on August 9, 1975. Its mission is to study in detail the sources of extraterrestrial γ-radiation of energy above about 30 MeV. The principal objectives of this study are:

- To investigate the spatial structure and energy spectrum of γ-ray emission from the galactic plane.
- To examine known or postulated localized sources of γ-radiation, to determine the energy spectrum of sufficiently strong sources and to search for time variations (long- and short-term) in their intensities.
- To measure the flux and energy spectrum of the diffuse radiation from high galactic latitudes.

Two further objectives, defined during the development stages of the program, are a study of the long-term variability of X-ray sources (Boella et al., 1974a) and a high time-resolution study of cosmic γ-ray bursts (Boella et al., 1975).

COS-B carries a single large experiment, which was designed, constructed, and tested under the responsibility of a collaboration of research laboratories known as the Caravane Collaboration. Members of this collaboration are:

- Max Planck Institut für Physik und Astrophysik, Institut für Extraterrestrische Physik, Garching-bei-München

- Service d'Electronique Physique, Centre d'Etudes Nucléaires de Saclay
- Cosmic-Ray Working Group, Huygens Laboratory, Leiden
- Laboratorio di Fisica Cosmica e Tecnologie Relative, Istituto di Scienze Fisische dell'Università di Milano
- Istituto Fisica, Università di Palermo
- Space Science Department, ESA, Noordwijk

The definition of the observation program and the analysis of the data are also collaborative activities.

INSTRUMENTATION

The experiment has been described in detail by Bignami et al., (1975). A sectional view of the central detector is shown in figure 1. It features a 240- by 240-mm^2 16-gap, wire-matrix spark chamber (SC) with magnetic-core readout. Interleaved between the gaps are 12 tungsten plates giving a total thickness of 0.5-radiation length for the conversion of incident photons to electron pairs. The top gap and the bottom three gaps have no tungsten immediately above them.

The chamber is triggered by a coincidence pulse from a three-element telescope. The field of view of the telescope is defined by the 30-mm-thick plexiglas directional Cherenkov counter C (Andresen et al., 1974b) and the 10-mm-thick plastic scintillation counter B2, each of which is divided into four quadrants. The 4-mm-thick plastic scintillator B1 (Andresen et al., 1974a) above counter C provides a measurement of the number of particles leaving the bottom of the spark chamber. The 10-mm-thick plastic-scintillator guard counter A, surrounding the spark chamber and upper part of the telescope, is placed in anticoincidence to reject triggers due to incident-charged particles.

Beneath the telescope is the energy calorimeter, consisting of a caesium-iodide scintillator E, 4.7-radiation length thick, to absorb the secondary particles produced by the incident photons and a plastic scintillator D to provide information on high-energy events for which this absorption is incomplete.

Alongside the γ-ray detector is mounted a proportional counter, sensitive to X-rays in the 2- to 12-keV energy range, to provide synchronization for possible pulsations of γ-ray emission from sources known to pulsate at X-ray wavelengths (Boella et al., 1974b). The relative times of arrival of individual X-ray photons are recorded with a precision of 0.2 ms.

THE SATELLITE AND ITS ORBIT

COS-B is configured as a cylinder, 1.40-m diameter and 1.13-m long, with the main experiment package occupying the central region as shown in the cutaway view of figure 2.

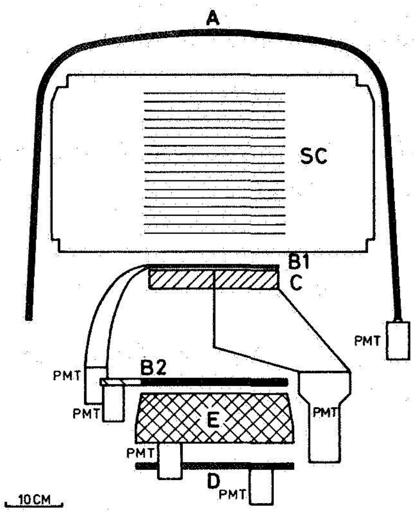

Figure 1. Sectional view of the COS-B experiment. Units are identified in the text.

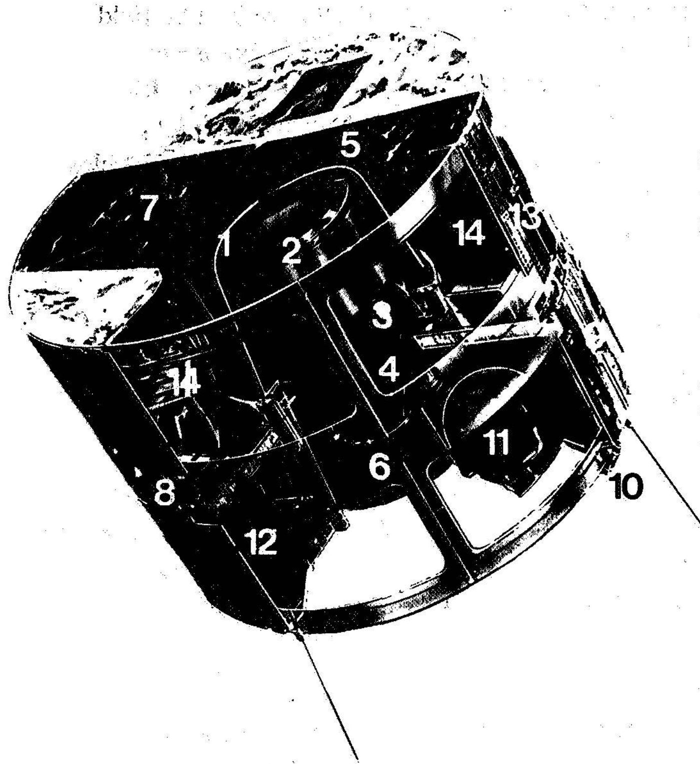

Figure 2. Cutaway view of the COS-B satellite. Subsystems are: (1) anticoincidence counter, (2) spark chamber, (3) triggering telescope, (4) energy calorimeter, (5) pulsar synchronizer, (6) structure, (7) superinsulation, (8) Sun and Earth-albedo sensors (attitude measurement), (9) spin thruster, (10) precession thruster (attitude control), (11) nitrogen tank (attitude control), (12) neon tank (spark-chamber gas flushing), (13) solar-cell array, and (14) electronics.

The pulsar synchronizer is mounted on the equatorial equipment platform with its optical axis parallel to that of the main experiment. All experiment electronics units and spacecraft subsystems are mounted above or below this platform in order to minimize the amount of material in the field of view and to reduce the probability of the experiment being triggered by background induced by charged-particle interactions in these units. The total mass at launch was 278 kg of which the experiment units comprise 118 kg.

The satellite is spin-stabilized at approximately 10 rpm about its axis of symmetry, which coincides with the optical axis of the γ-ray detector. A nitrogen-gas attitude-control system is used to point the experiment in the desired direction. Sun and Earth sensors provide data from which the attitude can be reconstituted with a precision of better than 0.5°.

The initial elements of the COS-B orbit and their latest available values are given in table 1. The eccentric orbit was preferred over a low orbit because the loss of observation time due to Earth occultation is much less. The orbital plane is inclined at 90° to the Earth's equator with the argument of perigee in the fourth quadrant, which ensures that, for most of the operational part of the orbit, the satellite is in sight of one of the ESTRACK ground stations. This provides for a high data recovery without the use of an on-board tape recorder. Regions of the celestial sphere which are close to the direction of the line of apsides are

Table 1
COS-B Orbital Parameters

Date (Y, M, D)		1975-08-08	1976-03-30
Orbit number		1	154
Altitude of perigee	(km)	346	2624
Altitude of apogee	(km)	99103	96828
Semimajor axis	(km)	56103	56104
Eccentricity		0.880	0.840
Inclination	(deg.)	90.15	93.08
Right ascension of ascending node	(deg.)	43.72	42.43
Argument of perigee	(deg.)	344.68	325.19
Period	(h, m)	36-44	36-44

difficult or impossible to observe due to the entry of the Earth into the field of view or because the Earth-aspect angle is outside the range of operation of the albedo sensors for most of the orbit. The right ascension of the ascending node was chosen so that these regions contained only target directions of lowest scientific interest.

The position of the satellite at any time may be reconstituted from tracking data with a precision of 75 km. This is compatible with the 250-μs relative accuracy of the on-board clock and, allowing for uncertainties in the propagation delay, permits the determination of the absolute Universal times of γ-ray or X-ray events in either the satellite or the solar-barycentric frame of reference with an uncertainty of better than 1 ms.

OBSERVATION PROGRAM AND ORBITAL OPERATIONS

Routine experiment operations began on August 17, 1975, when the satellite was directed towards its first target, the Crab Nebula, with the instrument axis pointing at pulsar NP 0532. Table 2 shows the subsequent program of observations, and the relative sky coverage achieved so far is as shown in figure 3. At the present time, the satellite is pointed towards Virgo, midway between 3C273 and M87. It is intended that in the next 6 months the observations of Vela and the anticenter will be repeated, and as many as possible of the parts of the galactic disk not yet studied will be observed. A study of either the Large or the Small Magellanic Cloud is also foreseen.

Table 2
COS-B Observation Program

Beginning of Observation		Target	Galactic Coordinates (deg.)	
			l^{II}	b^{II}
Orbit 6	1975-08-17	NP0532	185	-6
26	1975-09-17	GX5-1	5	-1
48	1975-10-20	Vela X	264	-3
60	1975-11-08	Vela X-1	263	4
73	1975-11-28	Cygnus	74	0
90	1975-12-24	Cen X-3	292	0
110	1976-01-23	Cen A	309	19
130	1976-02-23	Cir X-1	322	0
150	1976-03-24	3U 1832-05	26	1
170	1976-04-24	Aquila	45	0
190	1976-05-24	Virgo	286	69

Scheduling of observations is constrained by limitations on solar-aspect angle, attitude-sensor coverage, and entry of the Earth into the field of view, but takes account of scientific priorities and, where possible, the known plans of other satellite, balloon, or ground-based astronomy experiments. The standard period of 1 month for each observation was chosen to provide good statistics and is also the minimum necessary to achieve the full capability of the attitude-reconstitution software.

The experiment is only operated outside the radiation belts (i.e., about 80 percent of the time). Occasionally, the observation is reduced due to automatic switchoff caused by fluctuations of the boundary of the radiation belts or by solar-flare events. About 45 minutes per orbit are devoted to calibration of the detectors, using either cosmic-ray protons or an In-Flight-Test system with electronic stimulation and light-emitting diodes. During alternate orbits, a calibration of the pulsar synchronizer is made using an Am^{241} Sr target source.

The satellite carries a gas-flushing system to permit emptying and refilling the spark chamber. This has been used at 6- to 8-week intervals to forestall progressive deterioration of spark-chamber performance due to poisoning of the gas. At this rate of usage, the supply of gas carried is more than sufficient for the nominal 2-year lifetime.

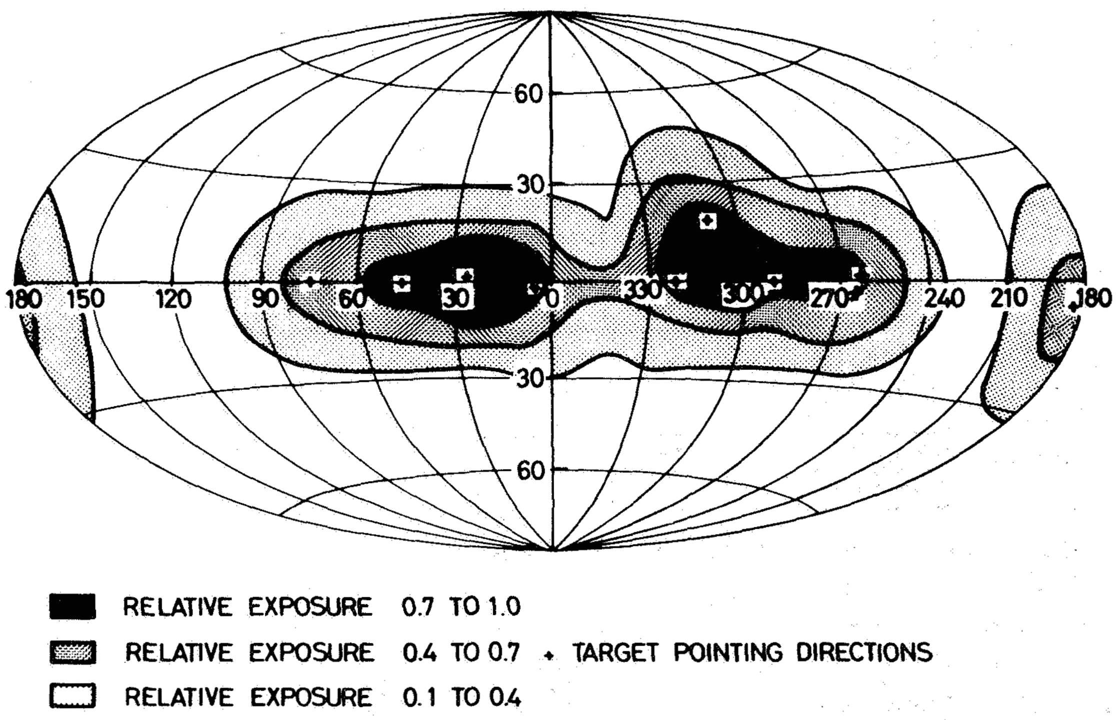

Figure 3. Relative sky coverage between August 17, 1975, and May 23, 1976 (galactic coordinates).

Data are received by the ESTRACK ground stations at Redu, Belgium, and Fairbanks, Alaska. The subsequent paths of data processing are summarized in figure 4. The recorded data are dispatched at regular intervals to the European Space Operations Centre (ESOC), Darmstadt, where they form the basis of the final data processing. In addition, data recorded at Redu can be transmitted to the Operations Centre in ESOC, either in real time or, by playing back the tape, at the end of a pass. Real-time data are used for monitoring the correct functioning of spacecraft and experiment subsystems, especially during telecommanding operations.

From the data played back to ESOC, a fraction, averaging about 20 percent of all data acquired, is made available to the experimenters' "Fast Routine Facility." In this facility, the Collaboration has set up programs for a preliminary analysis of this sample of data, using predicted orbit, attitude, and time information provided by ESOC. This permits a thorough check of the performance of the experiment, providing the possibility of a fast feedback to keep the equipment in the optimum operational mode. In addition, preliminary scientific conclusions can be reached (Bennett et al., 1976), which can be taken into account in planning the future observation program well in advance of the analysis of the final data.

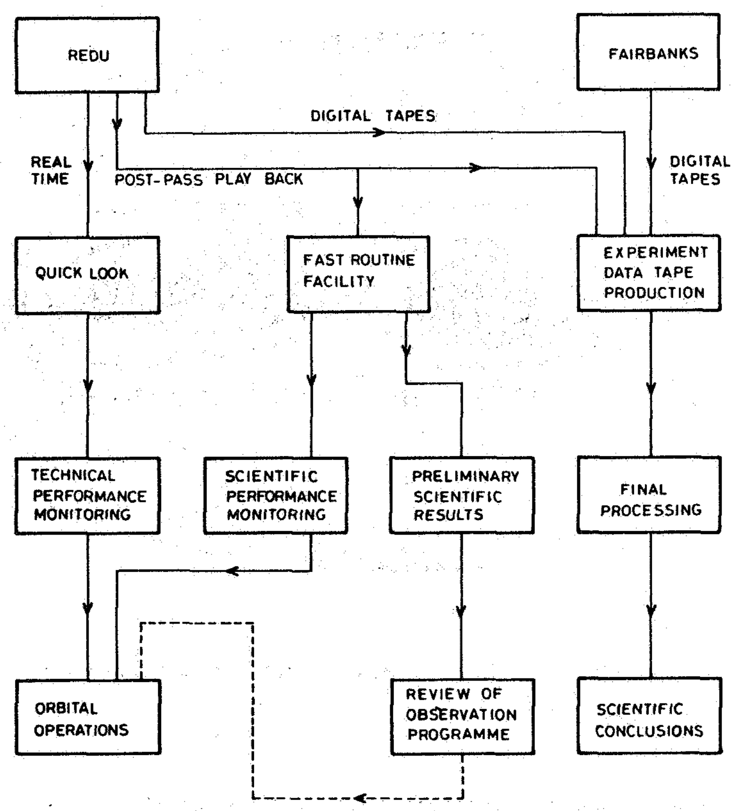

Figure 4. Overall flow chart of data processing.

CALIBRATION AND IN-FLIGHT PERFORMANCE

The characteristics of the experiment were determined before launch by exposing the instrument to beams of γ-rays and charged particles at particle accelerators. The data acquired were analyzed, using the same computer programs that are used for flight-data analysis. An automatic spark-chamber picture-analysis program classifies the events and assigns the addresses of set cores to electron tracks from which the directions of incidence of the γ-ray photons are reconstructed. Analysis of the data from proton and electron exposures showed that acceptance of only events in which an electron pair is recognized in both projections (class 22 events) gives a high confidence that little background is included, but does imply rejecting some genuine γ-rays. For many purposes, where the signal can be identified by another criterion (e.g., spatial localization or time pulsation), events showing a pair in only one projection (class 2 events) may also be used.

Both the engineering model and the flight model were calibrated in tagged photon beams with energies between 20 MeV and 6 GeV at DESY, Hamburg (Christ et al., 1974). Measurements were made at a selection of photon energies and directions of incidence (Bennett et al., 1974), and the results were smoothed and interpolated to provide the sensitivities used in the analysis of the flight data. The effective area of the engineering model for recognition of γ-rays as class 2 or class 22 events is shown in figure 5. The efficiency for class 22 only events is about 30 percent lower. The data from the calibration of the flight model are currently being analyzed. First indications are that the results are not much different from those of the engineering model.

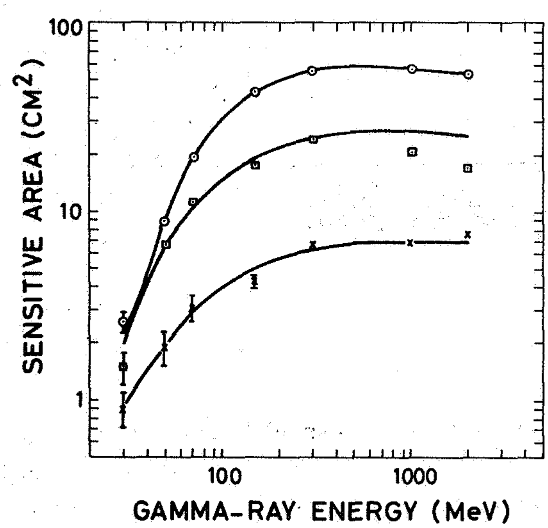

Figure 5. Effective sensitive area of the engineering model for detecting and recognizing γ-rays. Measurements are shown by circles (0°), squares (15°), crosses (30° incidence), and the solid lines represent the interpolations used in the analysis of flight data.

The angular resolution has been characterized by the half-angle of a cone, centered on the observed source direction, within which 68 percent of the reconstituted directions lie. This parameter is shown in figure 6 for the engineering model. Observation of the point source in Vela, which will be presented in a following paper, confirms that the flight model is similar to the engineering model, at least at the higher energies.

An important characteristic of the experiment is its capability to measure γ-ray energy over a wide dynamic range. The energy can be derived from measurements of track length in the spark chamber and from the energy loss as measured by the counter pulse heights. The method is still being optimized, using data from the accelerator calibration of the flight model. For incidence parallel to the axis, an energy resolution of about 50 percent (FWHM) is achievable in the energy range 70 to 500 MeV.

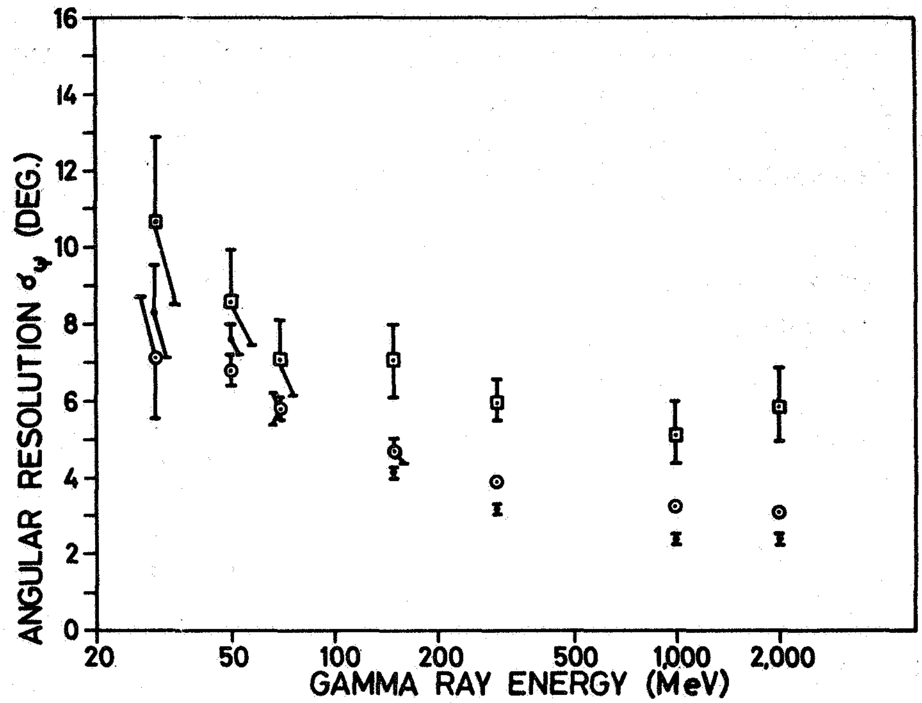

Figure 6. Angular resolution of the engineering model as a function of energy for selected events incident parallel to the axis (closed circles) and at 15° (open circles and 30° (squares) to the axis.

The charged-particle environment in the eccentric orbit required special care to be taken in suppressing background triggers. From the accelerator tests and a balloon flight, it was concluded that the expected trigger rate would be compatible with the telemetry capability. This prediction proved to be justified, with trigger rates between 0.15 and 0.25 s^{-1} (depending on the triggering mode). The majority of residual background triggers can be rejected from the data by very simple criteria on the spark-chamber pictures. Although the automatic spark-chamber analysis program has been very highly refined, there are still occasions when the track assignment or event classification can be improved upon by human intervention. A system is available which uses a minicomputer with interactive display to permit such intervention, and it is intended to use it to monitor the performance of the automatic analysis and to apply corrections where necessary to those events that have been automatically selected as the best candidates for γ-ray events.

The performance of the complete system (hardware plus software) can be expected to vary with time, especially due to aging of the spark-chamber gas. A check on this has been made by dividing the first two observation periods into shorter intervals of time and measuring for each the counting rates of selected γ-rays in different energy intervals. This has shown that, over a period of a month, the total efficiency does not vary by more than about 10 percent. Day-to-day monitoring of spark-chamber performance is possible using the real-time display facilities in the Control Center. A display of the first γ-ray event seen on this system is shown in figure 7.

In the accompanying papers, results are presented that are based on analysis using the calibration data and analysis methods described above. For the following reasons, these results are preliminary:

- The calibration used may not reflect exactly the performance of the flight unit
- The automatic analysis without human correction leaves a nonnegligible background
- Not all data acquired for the observations discussed have been received.

As a result, absolute values should be treated with caution. None of the conclusions derived are affected by these limitations. However, at present, the combined effect of the quoted uncertainties prohibits the drawing of conclusions on energy spectra in most cases.

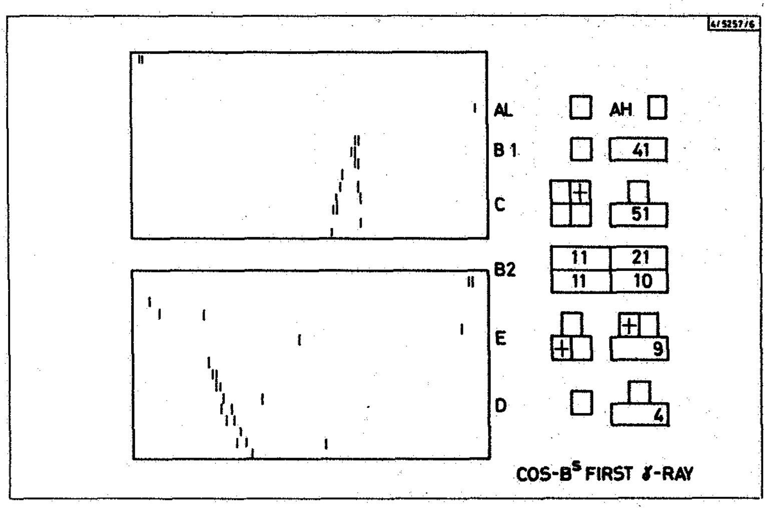

Figure 7. Real-time display of spark-chamber "picture" for the first event accepted as a γ-ray event. (This display has only half the resolution of the spark chamber.)

REFERENCES

Andresen, R. D., I. Arens, B. G. Taylor, and R. D. Wills, 1974a, *Nucl. Inst. and Meths.*, **115**, p. 531.

Andresen, R. D., I. Arens, B. G. Taylor, and R. D. Wills, 1974b, *Nucl. Inst. and Meths.*, **120**, p. 85.

Bennett, K., J. J. Burger, M. Gorisse, H. A. Mayer-Hasselwander, J. A. Paul, E. Pfeffermann, P. G. Shukla, R. Stiglitz, B. N. Swanenburg, B. G. Taylor, and R. D. Wills, 1974, (Proc. 9th ESLAB Symposium (Frascati), ESRO SP-106), p. 323.

Bennett, K., G. F. Bignami, G. Boella, R. Buccheri, M. Gorisse, W. Hermsen, K. Kanbach, G. G. Lichti, H. A. Mayer-Hasselwander, J. A. Paul, L. Scarsi, B. N. Swanenburg, B. G. Taylor, and R. D. Wills, 1976, to be published in *Astron. and Astrophysics*.

Bignami, G. F., G. Boella, J. J. Burger, P. Keirle, H. A. Mayer-Hasselwander, J. A. Paul, E. Pfeffermann, L. Scarsi, B. N. Swanenburg, B. G. Taylor, W. Voges, and R. D. Wills, 1975, *Space Sci. Instr.*, **1**, p. 245.

Boella, G., R. Buccheri, P. Coffaro, D. Molteni, and L. Scarsi, 1974a, (Proc. 9th ESLAB Symposium (Frascati), ESRO SP-106), p. 345.

Boella, G., R. Buccheri, J. J. Burger, P. Coffaro, and J. Paul, (Proc. 9th ESLA Symposium (Frascati), ESRO SP-106), p. 353.

Boella, G., M. Gorisse, J. A. Paul, B. G. Taylor, and R. D. Wills, 1975, *Space Sci. Inst.*, 1, p. 269.

Christ, H., F. Peters, G. F. Bignami, J. J. Burger, W. Hermsen, J. A. Paul, E. Pfeffermann, B. G. Taylor, W. H. Voges, and R. D. Wills, 1974, *Nucl. Inst. and Meths.*, **116**, p. 477.

COS-B OBSERVATIONS OF THE HIGH-ENERGY GAMMA RADIATION FROM THE GALACTIC DISK

The Caravane Collaboration

ABSTRACT

During the first months of operation, COS-B has observed galactic high-energy γ-rays from the galactic disk. In the galactic center and Vela regions, the disk emission distribution has been measured. From these data, the existence of a local (< 1 kpc) and a distant (> 3 kpc) emitting region is apparent in the general direction of the inner galaxy.

INTRODUCTION

During the first 3 months of operation, the COS-B experiment has observed approximately one-fourth of the galactic disk, including the galactic-center region, the galactic anticenter, and the Vela region. A completely automatic analysis of the events recorded during these observations reveals a galactic γ-ray emission from the three regions. In the anticenter and Vela regions, localized sources of γ-ray emission are present. The study of these discrete γ-ray sources is described in an accompanying paper.

The presence of localized sources complicates the observation of the diffuse galactic emission, especially in the anticenter region, where the contribution of the galactic background cannot be resolved from the discrete sources at present. The reduction of the effective sensitive area for photons incident at large angles limits the significance of the events recorded at the edges of the observation zones. For this presentation, our survey of the galactic emission is then restricted to the Vela region ($244° < \ell^{II} < 284°$) and to the galactic center region ($350° < \ell^{II} < 20°$).

The exact nature of the origin of the high-energy γ-rays from the galaxy is still questionable in spite of the large number of interpretations of the SAS-2 data. (For a review, see, for instance, Paul et al., 1976.) Most of these interpretations indicate that the galactic γ-rays originate in the galactic disk and especially in the interstellar gas layer—the scale height of the galactic disk, the observed width of the galactic emission, and the angular resolution of the γ-ray detector provide limits to the distance of the emitting regions. For example, an emitting region located in a disk $\sim$ 200 pc thick would appear to be about 4° wide if its distance from the Sun is 3 kpc. It has been suggested (Fichtel et al., 1975) that towards the galactic center (within ±30° longitude) the high-energy γ-ray emission (> 100 MeV) is represented by the sum of a wide contribution from the nearby Sagittarius arm and a narrow component coming from distant regions. At other galactic longitudes, only a wide component has been observed. A high-resolution observation of the galactic γ-ray emission ($>$ 15 MeV) indicates that a dominant part of the γ-radiation emitted from the direction of the galactic center may be confined to a $\sim 3°$ wide band lying along the galactic equator (Samimi, et al., 1974) suggesting a source location more distant than 4 kpc.

High-resolution observations can be achieved by the COS-B experiment if high-energy events are selected. For example, the angular resolution of the experiment is about 3° for photons of 300 MeV (Bennett et al., 1974). With such a resolution, a line emission as thin as 4° may be resolved. The long exposure time achieved during our galactic-disk survey enables us to take advantage of the better angular resolution at high energy.

For the purpose of this paper, only those γ-ray events are considered for which the tracks of the electron pair are separately identified in two projections. Applying this selection assures that the instrumental background can be neglected with respect to the galactic emission. However, the detection efficiency is not accurately known at present, so that the quoted intensities should be considered to be preliminary.

OBSERVATIONS

Figure 1 shows the latitude profile of the galactic emission in the galactic longitude interval $244° < \ell^{II} < 284°$ for the energy ranges 70 to 2000 MeV and 300 to 2000 MeV. The contribution of the Vela source has been excluded from both distributions by ignoring a circular region centered at the position of the Vela pulsar and with a radius equal to 9° (range 70 to 2000 MeV) or 6° (range 300 to 2000 MeV).

The better angular resolution in the 300- to 2000-MeV range does not reveal more structure. The observed distribution width of about 20° suggests that at $\ell^{II} \approx 270°$, the galactic high-energy γ-rays originate in regions less than 1 kpc distant.

Figure 2 shows the latitude profile of the galactic emission in the galactic longitude interval $350° < \ell^{II} < 20°$ for the energy ranges 70 to 2000 MeV and 300 to 2000 MeV. The difference between the two profiles is consistent with the variation of angular resolution with energy. The data imply the existence of a wide component and a narrow one. The measured thickness of the narrow component ($< 4°$ above 300 MeV) is compatible with a thin-line emission. The wide component is reminiscent of the disk profile in the Vela region. This result suggests that most of the γ-rays recorded in the latitude intervals $-10° < b^{II} < -2°$ and $2° < b^{II} < 10°$ originate in close-by regions ($\leqslant 1$ kpc), whereas a large fraction of those observed in the range $-2° < b^{II} < 2°$ come from distant regions, at least > 3 kpc if one assumes that the scale height of the emitting region is 100 pc. A more quantitative analysis is required to resolve the possible contribution from intermediate distances.

The sensitivity of our survey permits the investigation of the galactic structure in more detail. Figure 3 shows the longitude distributions of the two components separately. The longitude

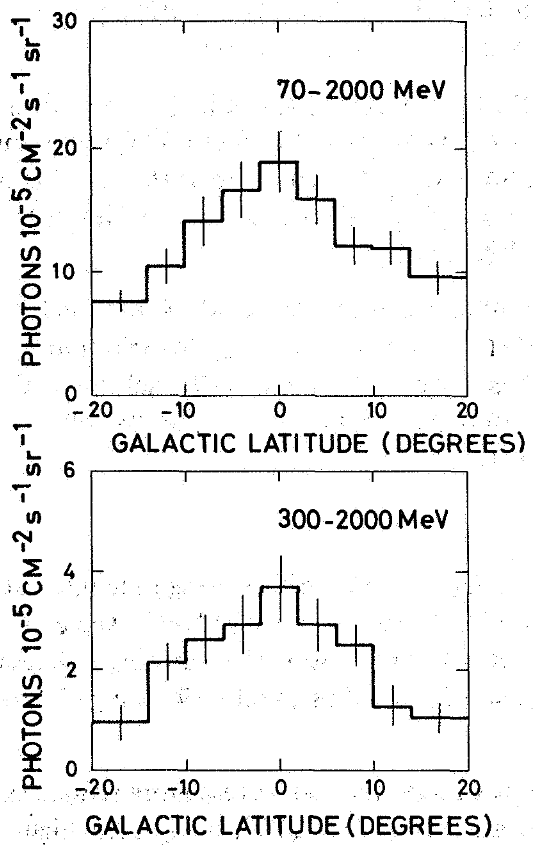

Figure 1. Latitude profile of the γ-ray emission summed from $244° < \ell^{II} < 284°$, excluding the contribution of the Vela source. The error bars reflect only the statistical uncertainties.

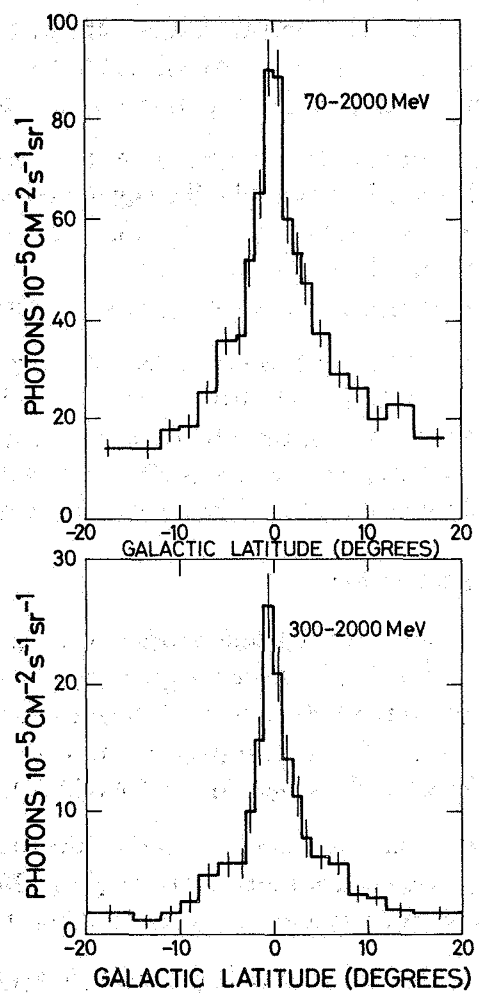

Figure 2. Latitude profile of the γ-ray emission summed from $\ell^{II} = 350°$ to $\ell^{II} = 20°$.

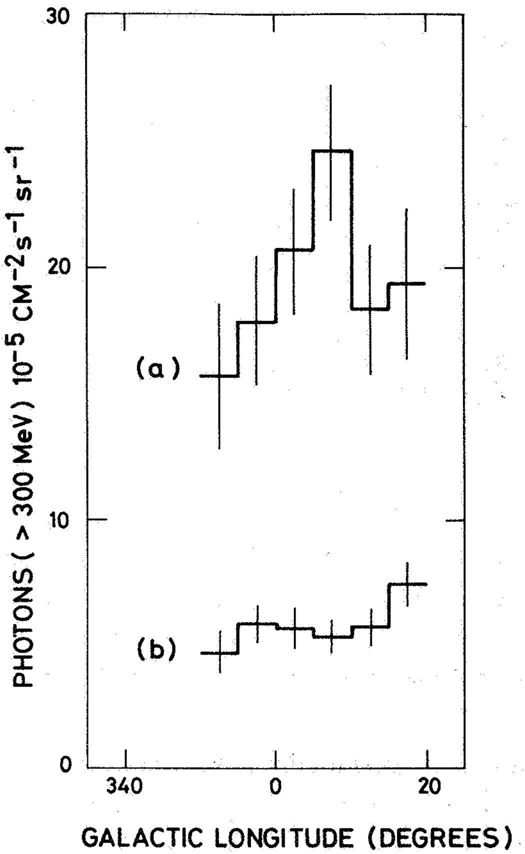

Figure 3. Longitude profile of the γ-ray emission in the energy range 300 to 2000 MeV summed from $-2° < b^{II} < 2°$ (curve a) and from $-10° < b^{II} < -2°$ and $2° < b^{II} < 10°$ (curve b).

distribution of the close-by component (curve b) is reminiscent of the distribution of the predicted contribution from the interstellar medium within 1 kpc of the Sun as deduced from interstellar reddening by Puget et al. (1975).

The distribution of the distant component (curve a) reaches a maximum for $5° < \ell^{II} < 10°$. Although this may be taken as a hint of some structure in the inner region of the galaxy, the data definitely exclude a peaking of this high-energy radiation at $\ell^{II} = 0$.

CONCLUSION

In spite of the rather incomplete survey of the galactic disk presented here, the following conclusions are derived:

1. most of the galactic high-energy γ-rays originate from either: (a) close-by regions whose latitude-profile widths are compatible with a distance $\leqslant$ 1 kpc, or (b) distant regions compatible with a thin-line source indicating a distance $>$ 3 kpc.
2. Such distant regions are not observed at $\ell^{II} \sim 270°$, indicating that the contribution of the outer galaxy is very weak.

REFERENCES

Bennett, K., J. J. Burger, M. Gorisse, H. A. Mayer-Hasselwander, J. A. Paul, E. Pfeffermann, P. G. Shukla, R. Stiglitz, B. N. Swanenburg, B. G. Taylor, and R. D. Wills, 1974, (Proc. 9th ESLAB Symposium (Frascati), ESRO SP-106), p. 323.

Fichtel, C. E., R. C. Hartman, D. A. Kniffen, D. J. Thompson, G. F. Bignami, H. Ögelman, M. F. Özel, and T. Tümer, 1975, *Ap. J.*, **198**, p. 163.

Paul, J., M. Cassé, and C. J. Cesarsky, 1976, *Ap. J.*, **207**, p. 62.

Puget, J. L., C. Ryter, G. Serra, and G. Bignami, 1975, (Proc. 14th Intl. Cosmic Ray Conf. No. 1, Munich), p. 52.

Samimi, J., G. H. Share, and R. L. Kinzer, 1974, (Proc. 9th ESLAB Symposium, ESRO SP-106), p. 211.

COS-B OBSERVATIONS OF LOCALIZED SOURCES OF GAMMA-RAY EMISSION

The Caravane Collaboration

ABSTRACT

In October 1975, the high-energy γ-ray flux from the Vela pulsar was measured by COS-B to be 1.6 to 2.1 times higher than the flux measured by SAS-2 in 1973.

The existence is confirmed of a second region of enhanced radiation in the galactic anticenter in addition to that from the Crab pulsar.

INTRODUCTION

COS-B data from the first three observation periods—galactic anticenter, galactic center, and Vela region—have been analyzed by the automatic processing sequence. This comprises spark-chamber picture recognition and classification and derivation of the direction of incidence and energy for each event recognized as a γ-ray. Intensity sky maps were produced for selected event classes and energy ranges.

Because only the purely automatic picture-recognition process is used for the present analysis, there remains a residual background in these sky maps. Although for the gamma classes 2 and 22 used for this analysis the background is higher than for class 22 alone, the possibility to use the calibration data already available for class 2 and 22 makes it preferable to use these data.

In figure 1, the data from the first three observation periods for γ-rays of energy greater than 100 MeV are plotted as line fluxes derived by integrating intensities from -10° to +10° galactic latitude. The error bars indicate statistical errors. The striking feature is the high peak observed in the Vela region.

VELA

Figure 2 shows a latitude profile across the galactic plane integrated over 22° of longitude centered on the Vela pulsar. To make use of the better angular resolution, the 300- to 2000-MeV energy band is used for this latitude profile. In this profile, it is seen that the peak coincides within 0.5 degree with the position of the Vela radio pulsar (PSR 0833 45) at $b^{II} = -2.8°$. The width of the peak is consistent with that expected from the angular resolution as determined from the calibration for this energy range. It is therefore evident that

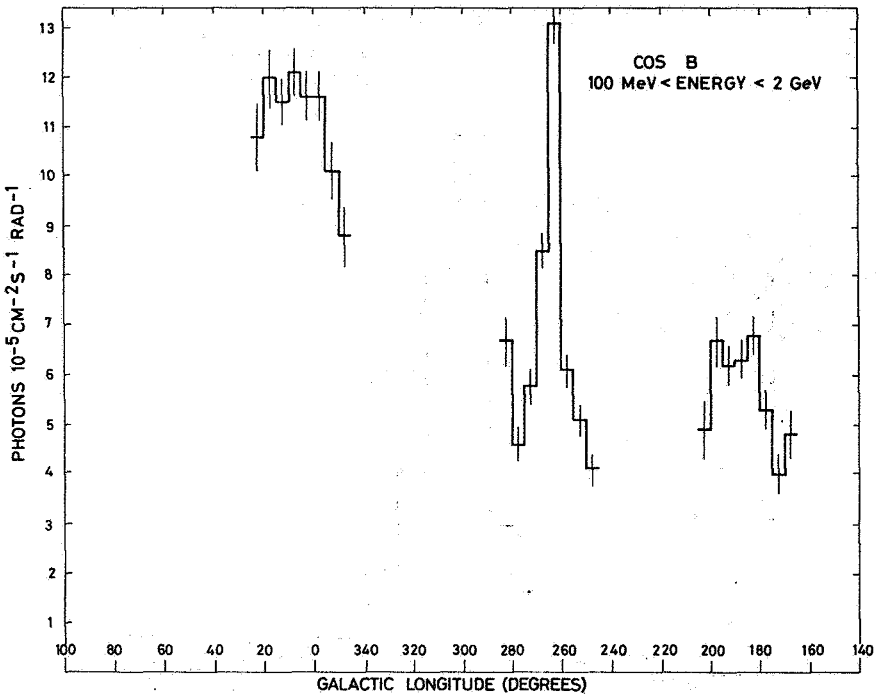

Figure 1. Observed flux for three observation periods integrated over the latitude range -10 to +10° for the energy range 100 MeV to 2 GeV, derived by automatic analysis without background subtraction. Statistical errors are indicated.

most of the source flux is emitted from a source much less extended than the supernova remnant which has a diameter of 5°. Final evidence for the identification of this γ-ray point source with the radio pulsar will be provided in a following paper on pulsation analysis.

It is worthwhile to remark that the Vela observation period was divided into two parts, one with the experiment axis pointed to the Vela pulsar (ℓ^{II} = 264°, b^{II} = -3°) and the other with the axis directed to the binary system 3U0900-40, (ℓ^{II} = 263°, b^{II} = +4°). Analysis of these two periods gave consistent results and prove the correctness of the applied analysis procedure concerning the reconstitution of arrival directions.

Longitude scans for different latitude intervals are presented in figure 3 for energy greater than 100 MeV. These clearly indicate the source contribution above the galactic disk and background. In order to separate the intensity of the Vela point source from the underlying galactic disk and background components, a maximum and minimum background level in each scan has been assigned and the excess flux above these levels has been attributed to the point source leading to the flux values given in table 1. Comparing these limits with the measurement of SAS-2 (Thompson et al., 1975), we find that our values are 1.6 to 2.1 times higher.

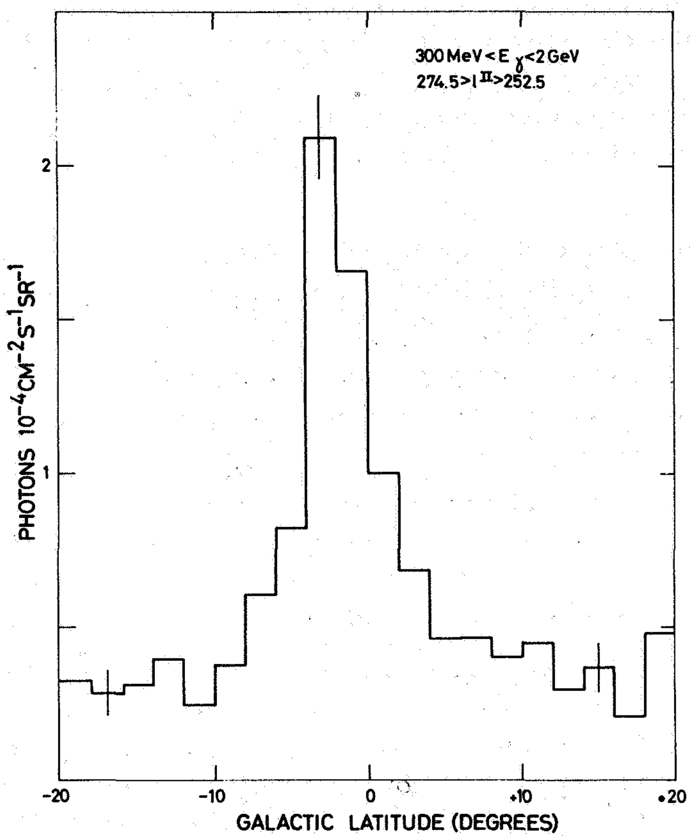

Figure 2. Latitude profile in the Vela region for the energy range 300 MeV to 2 GeV. (Analysis and errors as for figure 1.)

Table 1
Flux of Vela Source

Energy Range	COS-B 100 to 2000 MeV	SAS-2 >100 MeV
Flux upper limit (cm^{-2} s^{-1})	1.3×10^{-5}	$(6.3 \pm 1.1) \times 10^{-6}$
Flux lower limit (cm^{-2} s^{-1})	1.0×10^{-5}	

This factor is too large to be accounted for by error in the COS-B calibration or analysis. This is supported by a comparison of the COS-B measurement of the narrow-line component from the galactic center region with the flux derived from the measurements of SAS-2; the COS-B flux comes out about 15 percent lower than the SAS-2 figure.

It is interesting to note that a glitch in the pulsar period took place about 1 month prior to the COS-B observation (Manchester et al., 1976); the previous glitch occurred about 1.5 years before the SAS-2 observation. The increased rotational energy loss after the glitch cannot simply explain the increased γ-ray luminosity. If the two phenomena are related, the γ-ray emission, absorption, or beaming process must be extremely sensitive to changes in rotational parameters.

No change in intensity (greater than 20 percent) is apparent in the 39 days of observation. A second observation is scheduled for August 1976 with the aim of gaining insight into the long-term behavior of the Vela luminosity.

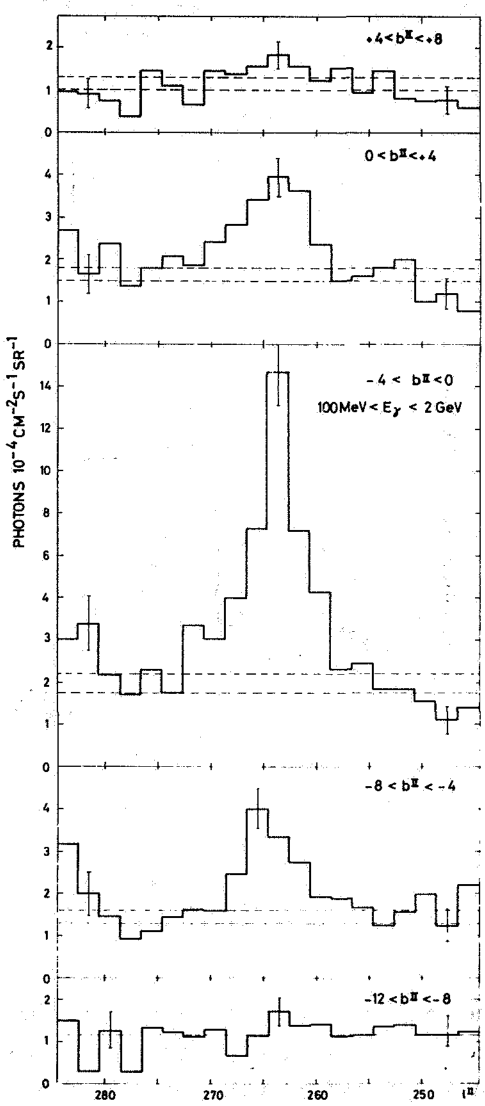

Figure 3. Longitude scans for the Vela region in five latitude bands for the energy range 100 MeV to 2 GeV. (Analysis and errors as for figure 1.)

THE GALACTIC ANTICENTER REGION

In figure 1, the COS-B data show a relatively weak and wider peak in the anticenter, as compared with the Vela region. From the detailed sky map, it was seen that this enhancement has broad maxima centered at two positions, one being $\ell^{II} = 185°$, $b^{II} = -6°$, the Crab Pulsar, and the other being the location $\ell^{II} = 195°$, $b^{II} = +5°$ for which enhanced radiation has been already reported by Kniffen et al. (1975). More detailed longitude and latitude profiles centered at each of the two positions are given in figures 4 and 5.

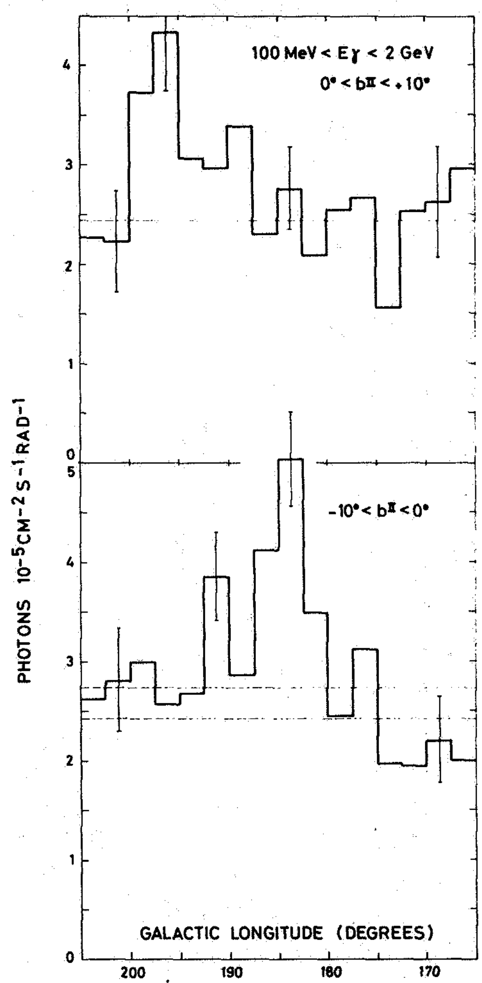

Figure 4. Integrated fluxes in two latitude bands in the anticenter region for the energy range 100 MeV to 2 GeV. (Analysis and errors as for figure 1.)

Figure 4 shows longitude profiles, one north and the other south of the galactic equator, integrated over 10° of latitude. The profiles show similar asymmetric peaks. In figure 5, latitude profiles are shown; we again find distrinct asymmetric peaks with maxima at the location of Crab and at $b^{II} = 5°$. The larger statistical errors in the latter region are due to the reduced sensitivity since this region is about 14° from the experiment axis.

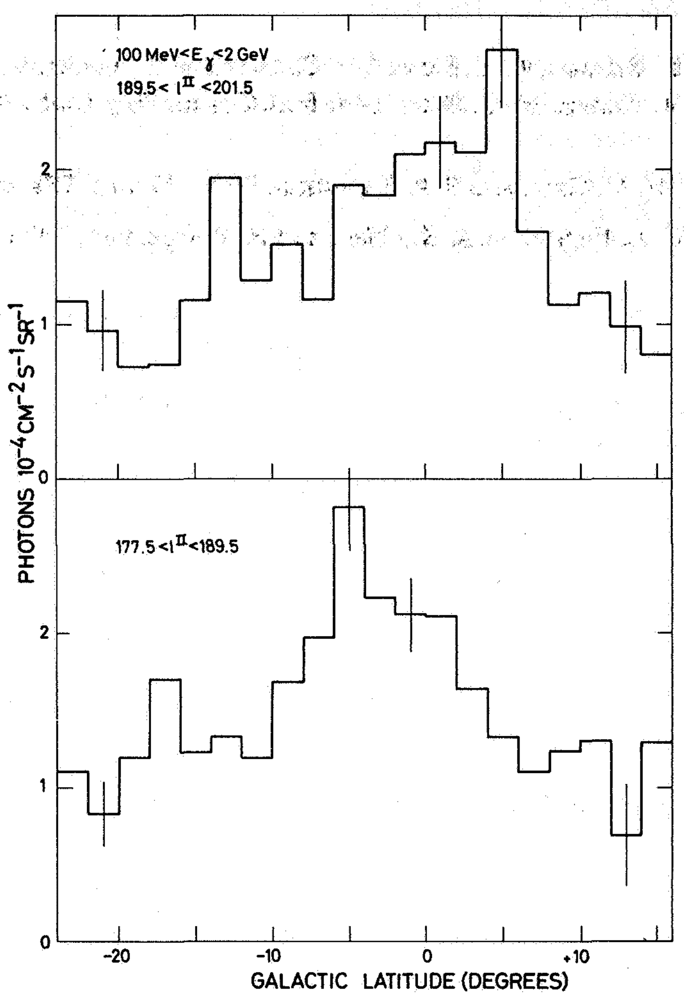

Figure 5. Latitude profiles for the anticenter region centered on the longitudes ℓ^{II} = 185° and ℓ^{II} = 195°. (Analysis and errors as for figure 1.)

Using a method similar to that for the Vela source, the magnitude of the enhancement from the region $-10° < b^{II} < 0°$ and $177.5° < \ell^{II} < 192.5°$ (Crab) is found to be $(3.0 \pm 0.5) \times 10^{-6}$ cm^{-2} s^{-1}. The flux determined for the region $0° < b^{II} < 10°$ and $187.5° < \ell^{II} < 202.5°$ is 2.2×10^{-6} cm^{-2} s^{-1} with similar uncertainties.

The statistical uncertainties in the present data do not allow a detailed investigation of the structure of the emission region. The peak at ℓ^{II} = 195°, b^{II} = 5° is consistent with a point source, but an extended object cannot be ruled out.

It is planned to look in this region again with COS-B in October 1976 with the optical axis nearer to the region ℓ^{II} = 195°, b^{II} = 5°. These data may help to resolve the uncertain nature of the emission in this complex region of the sky.

REFERENCES

Kniffen, D. A., G. F. Bignami, C. E. Fichtel, R. C. Hartman, H. Ögelman, D. J. Thompson, M. E. Özel, and T. Tümer, 1975, (Proc. 14th Intl. Cosmic Ray Conf., No. 1, Munich), p. 100.

Manchester, R. N., W. M. Goss, and P. A. Hamilton, 1976, *Nature*, **259**, p. 291.

Thompson, D. J., C. E. Fichtel, D. A. Kniffen, and H. B. Ögelman, 1975, *Ap. J. Letters*, 200, p. L79.

THE TIME STRUCTURE OF THE GAMMA-RAY EMISSION FROM THE CRAB AND VELA PULSARS

The Caravane Collaboration

ABSTRACT

High-resolution data on the pulsed γ-ray emission from the Crab and Vela pulsars are presented. The light curves of these two pulsars at γ-ray energies show striking similarities.

The measured pulsed intensity from Vela at energies greater than 50 MeV was found to be $\sim 1.3 \times 10^{-5}$ cm^{-2} s^{-1}. The energy spectrum is not consistent with a power law.

INTRODUCTION

The objective of studying the short-period temporal behavior of possible γ-ray emission from sources known to have time structure at longer wavelengths was included when the COS-B mission was defined. At that time, some 50 radio pulsars were known and one, NP 0532, the Crab puslar, had been observed to emit pulsed radiation in X-rays and possibly γ-rays (Vasseur et al., 1971; and Leray et al., 1972). The number of radio pulsars now known is about 150, and two, possibly four, γ-ray pulsars have been detected (Browning et al., 1971; Albats et al., 1972; McBreen et al., 1973; Albats et al., 1974; Thompson et al., 1975; and Ögelman et al., 1976).

Apart from the intrinsic interest in the temporal properties per se, the detection and correlation of a characteristic time structure can be decisive for the identification of weak γ-ray point sources buried in, for example, the galactic plane.

The low intensity of γ-rays above 30 MeV requires long observation times ($\sim 10^6$ s) to provide sufficient statistics to extract temporal patterns from the background. Under these conditions, a phase analysis down to 1 ms or less with the solar barycentric system as reference frame, would require a stability of the on-board clock and a knowledge of the satellite orbital elements beyond the expected scope of the COS-B program. Hence, a small X-ray detector, referred to as the pulsar synchronizer (PS), with an effective area of 80 cm^2 sensitive to X-rays in the interval 2 to 12 KeV was included in the payload (Boella et al., 1974). The arrival times of the X- and γ-quanta at the satellite would be determined by sampling the spacecraft clock to 0.2-ms increments. This detector would provide a convenient counting rate capability so that the period and phase of X-ray pulsars of intensity down to 0.1 of the pulsed emission from the Crab could be obtained in the satellite reference frame in intervals of about 1 hour, within which Doppler effects due to the motion of the Earth and satellite could be neglected. With this information, the search for pulsations in the γ-ray emission could be undertaken.

In fact, it has been possible to determine the satellite position to better than 20 km, a factor ~ 4 better than expected, and the on-board clock has achieved a stability of 1 in 10^9 over 3 hours, ten times better than specified. The on-board time can be related to UTC to better than 1 ms. Thus, COS-B is able to perform a γ-ray phase analysis both by synchronizing with the X-ray data from the pulsar synchronizer in the satellite reference frame and by using the solar-system barycenter as a reference frame.

DESCRIPTION OF PROCEDURES USED FOR PULSAR ANALYSIS

The following block-diagram outlines the phase analysis by the synchronization method:

Subdivide the entire observation in time intervals, Δt_i, small enough to neglect Doppler effect.

↓

Check the statistical confidence of the X-ray data sample collected during each interval, Δt_i.

↓

Phase-analyze the X-ray arrival times with variable value of the source period, P, for each Δt_i.

↓

Select, for each Δt_i, the value, P_i, corresponding to the maximum χ^2 phase distribution.

↓

Obtain $P_x(t)$ and $\phi_x(t)$ from P_i.

↓

Phase γ-ray arrival times using $P_x(t)$ and $\phi_x(t)$.

The validity of the method was checked by a study in which the experimental conditions of COS-B were simulated. That part of the X-ray analysis relative to the extraction of the pulsating pattern in each of the synchronization intervals, Δt_i, has been tested on experimental and Monte Carlo simulated data in order to check the confidence of the algorithm used (Boella et al., 1974).

For the Solar-System Barycenter analysis, the two steps were: (a) transformation of photon arrival times at the barycenter, using the ephemeris (kindly supplied by Lincoln Laboratories through the courtesy of Dr. Henry Helmken (SAO)) and the position of the satellite, and (b) computation of residual phases at the barycenter. In the case of NP 0532, the solar-barycentric period and phase have been derived from the X-ray analysis through the synchronization method. For PSR 0833, a "period model" has been used as obtained from radio observations by Manchester et al. (1976) and Reichley and Downs (private communication). Absolute radio phase values are not yet available for comparison.

NP 0532 OBSERVATIONS

COS-B observed NP 0532, the Crab Nebula, and the region of the galactic anticenter from August 17 to September 17, 1975. The X-ray light curve is shown in figure 1 for the entire observation period, excluding intervals when the data were disturbed. The pulsed fraction of X-ray emission in the range 2 to 12 keV, accounting for the instrumental background, is 8.5 percent, which is compatible with the results of Ducros et al., (1970).

Figure 2 shows, superimposed on the X-ray light curve, the γ-ray light curve derived by the synchronization method for class 2 and 22 events for energies $\geqslant$ 50 MeV and for reconstituted directions within an acceptance cone of half-angle $\theta_{max} = 6°$ centered on the pointing direction, for all intervals when both X-ray and γ-ray data were available simultaneously ($\sim$ 50 percent of the operational time). The very strong similarity of the X- and γ-ray light-curves is evident.

Figure 3 shows the γ-ray light curve derived by the solar-barycentric analysis for class 2 and 22 events with energies $\geqslant$ 50 MeV and within $\theta_{max} = 8°$. This analysis used radio data supplied by Rankin (private communication) and updated by phase information obtained from the PS. All available γ-ray data over the completed observation period have been used. The separation of the two peaks is 13.5 ms, and the main- and interpulse have 1.5-ms and 3.0-ms widths at half-height, respectively. The lower limit for the pulsed fraction for $E_\gamma \geqslant 50$ MeV derived from figure 3 is $\sim$ 35 percent, with the background level taken as the average of bins 47 to 66. It must be noted that the unpulsed fraction includes any continuous component from the source, a contribution from the general γ-ray emission from the anticenter region and instrumental background.

So far, only 36 hours of X-ray data have been analyzed by this method. The X-ray light-curve obtained is superimposed on the γ-ray light-curve in figure 3. The overall similarity of figures 2 and 3 gives confidence for the application of the barycentric analysis for pulsars not exhibiting temporal structure observable by the PS.

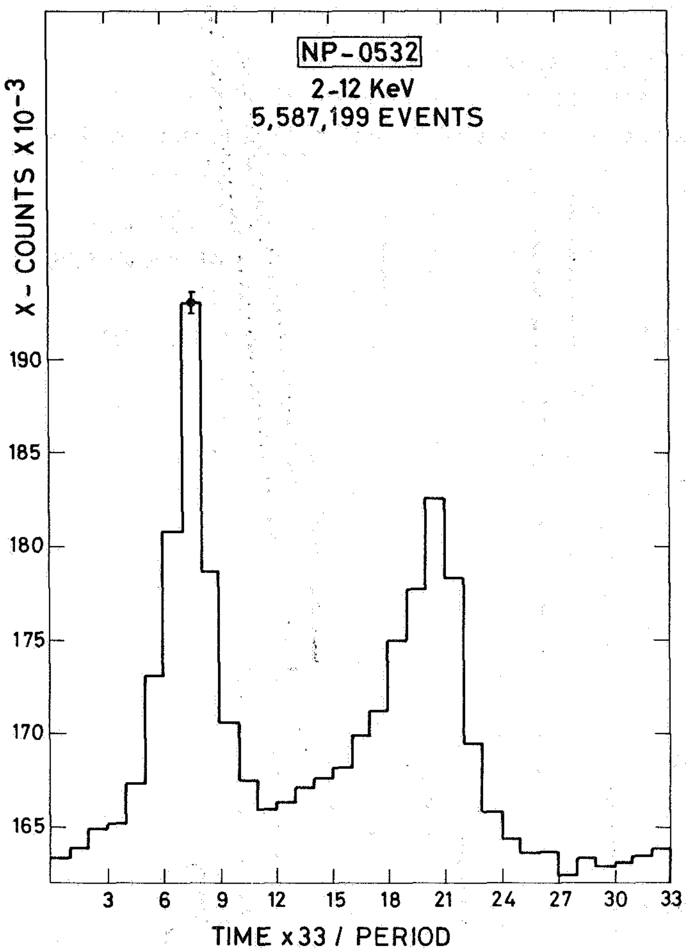

Figure 1. X-ray light curve of the Crab pulsar, NP 0532, obtained for the period August 17 to September 17, 1975. The pulsar period of 33.1 ms is divided into bins of ~ 1 ms.

PSR 0833-45 OBSERVATIONS

COS-B observed the neighborhood of the Vela supernova remnant, with the experiment axis directed to PSR 0833-45 from October 20 to November 8 and to 3U0900-40 from November 8 to November 28, 1975. Because the pulsar emits little or no pulsed X-radiation (Rappaport et al., 1974), the synchronization method cannot be applied and γ-ray light curves can be obtained only through the barycentric method. The barycentric analysis has been carried out separately for the two periods, based on the radio data. Only the first period has been analyzed in detail.

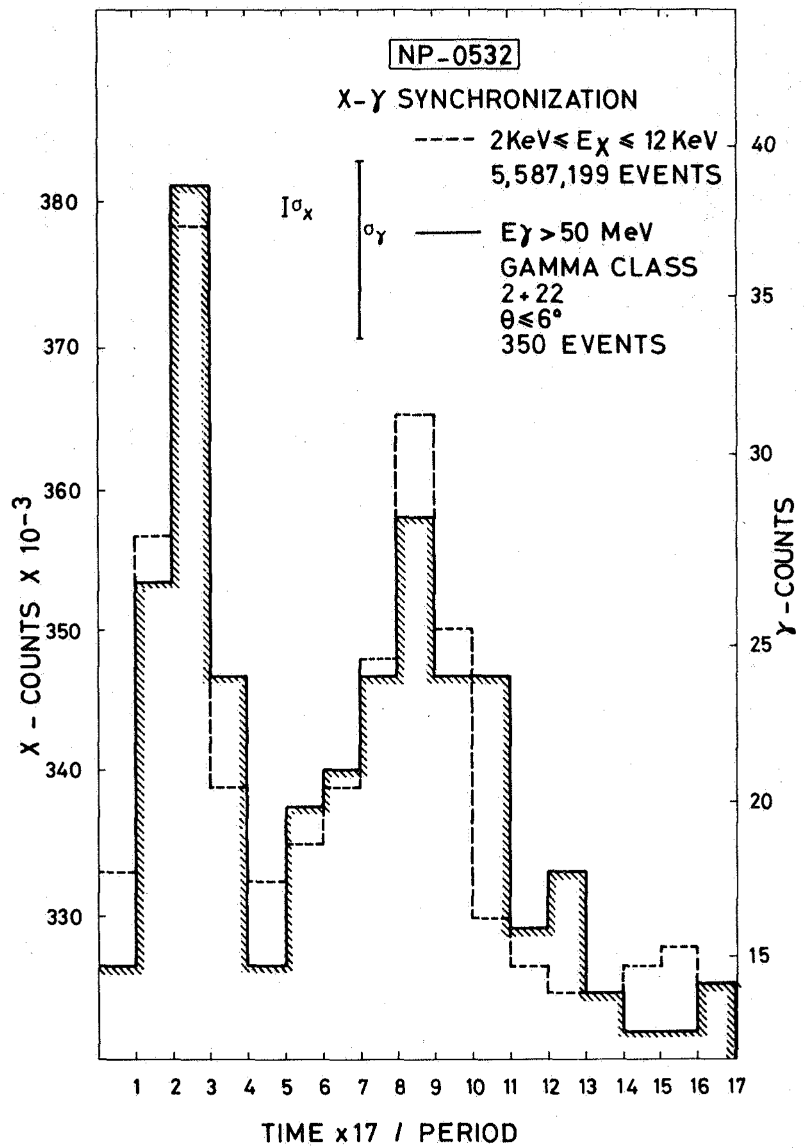

Figure 2. Gamma-ray light curve of NP 0532, obtained by the synchronization method, compared with the X-ray light curve. The pulsar period is divided into bins of ~ 2 ms.

Figure 4 is an example of the γ-ray light curve for class 2 and 22 events of $E_\gamma > 50$ MeV and for $\theta_{max} = 7°$. This result clearly establishes details of the pulsed γ-ray emission. The separation of the two peaks is 38 ms, and the main- and interpulse have 3-ms and 6-ms widths at half-height, respectively. These widths are in contrast with the measurements of Thompson et al., (1975), who report widths of 14 ms.

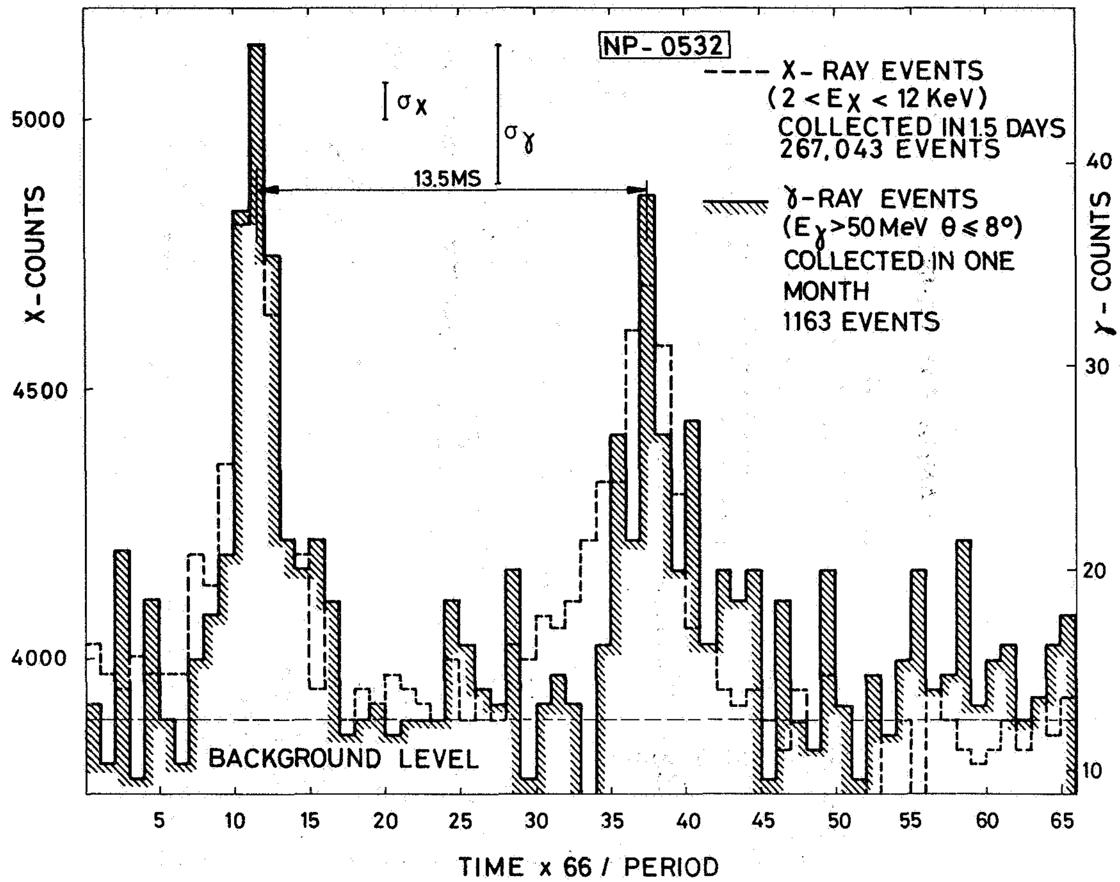

Figure 3. Gamma-ray light curve of NP 0532, obtained by solar-system barycentric analysis, compared with the X-ray light curve. The pulsar period is divided into bins of ~ 0.5 ms.

A series of light-curves for various selections on energy and arrival direction has been produced. From these, figure 5 has been derived, which shows the number of γ-rays above the background (average of bins 67 to 90) in the phase plot as a function of Θ_{max} for five energy intervals. The number of pulsed γ-rays reaches a maximum at higher acceptance angles as the energy is decreased, consistent with the variation of angular resolution with energy. The curves through the data points have been fitted qualitatively. The asymptotic value of the number of pulsed events for each energy has been taken, and, correcting for the energy dependence of the sensitivity of the instrument, the integral energy spectrum shown in figure 6 was obtained. Over the energy range from 50 to 1000 MeV, the spectrum is not consistent with a power law. The pulsed flux above 50 MeV is 1.3×10^{-5} cm^{-2} s^{-1}, and, above 100 MeV, is 1.0×10^{-5} cm^{-2} s^{-1}.

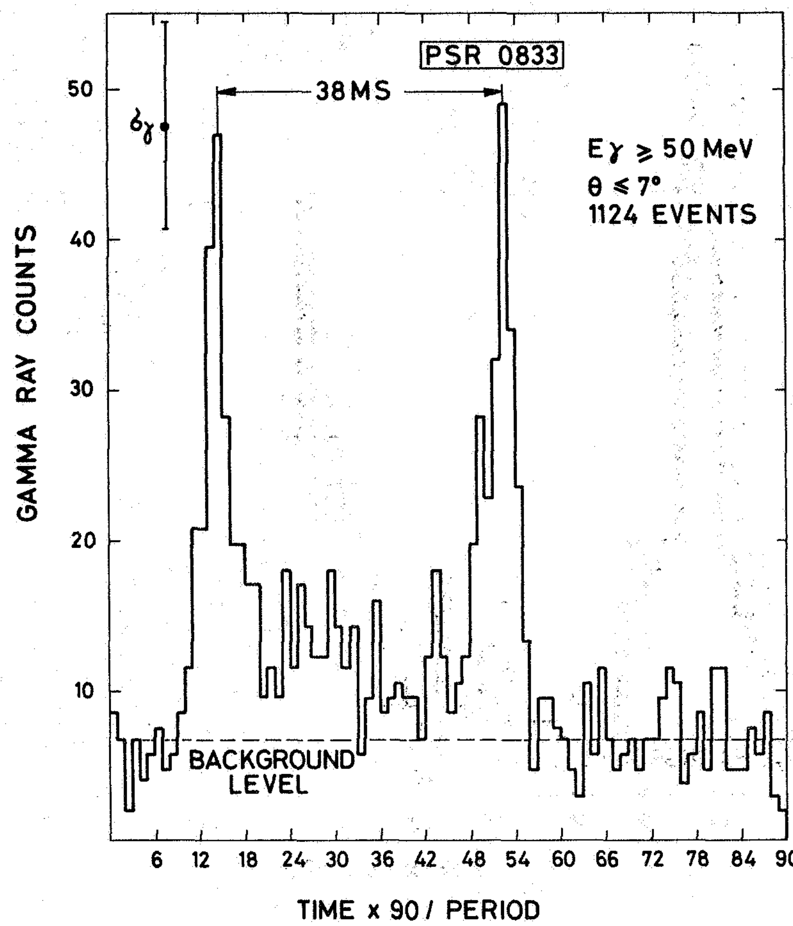

Figure 4. Gamma-ray light curve of PSR 0833, obtained through solar-system barycentric analysis, for the period October 20 to November 8, 1975. The pulsar period of 89.2 ms is divided into bins ~ 1 ms.

The pulsed fraction of γ-rays for above 50 MeV and above 500 MeV as a function of acceptance angle is plotted in figure 7. The diagram shows that the lower limit of the pulsed fraction is approximately 85 percent. The unpulsed fraction contains any nonvarying component from the pulsar, the supernova remnant, the galactic plane, and the instrumental background. Given this pulsed fraction, the pulsed flux is consistent with the total flux quoted in the previous paper.

Comparing these measurements with those of Thompson et al. (1975), we conclude that the pulsed luminosity has increased significantly (by about a factor of 2). It is uncertain whether the apparent change in pulse widths is related to this change in luminosity.

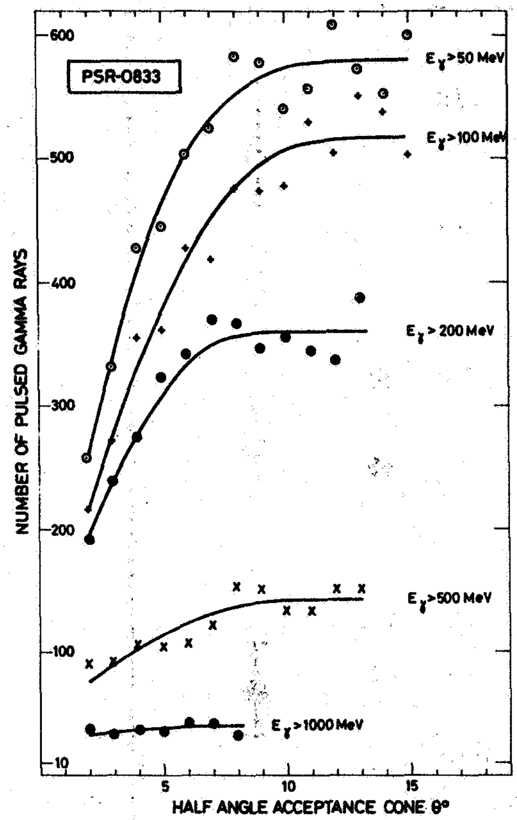

Figure 5. The number of pulsed γ-rays (i.e., those in the light-curve peaks above the background level), shown as a function of the half-angle of the acceptance cone for reconstituted γ-ray arrival directions centered on PSR 0833, for five energy intervals.

COMPARISON OF NP 0532 AND PSR 0833-45

Figure 8 shows the γ-ray light curves for $E_\gamma \geqslant 50$ MeV and $E_\gamma \geqslant 200$ MeV derived by solar barycentric analysis for the complete observation period of NP 0532 and for the second period (November 8 through 28, 1975) on PSR 0833-45. For both pulsars, the structure is dominated by two narrow pulses separated by 0.42 of the period. This structure is practically the same for the two energies shown.

In the light of the extreme difference of these two pulsars at longer wavelengths and their striking similarity at γ-ray energies, it is tempting to suggest that the pulsar process manifests itself directly in the γ-ray emission and that the radiation at lower energies reflects more complicated processes.

ACKNOWLEDGMENTS

The success of this mission owes much to the dedicated efforts of the COS-B Project Staff lead by Mr. G. Altmann at ESTEC, Noordwijk, The Netherlands, and the operations and data processing staffs at ESOC, Darmstadt, Federal Republic of Germany. For their efforts

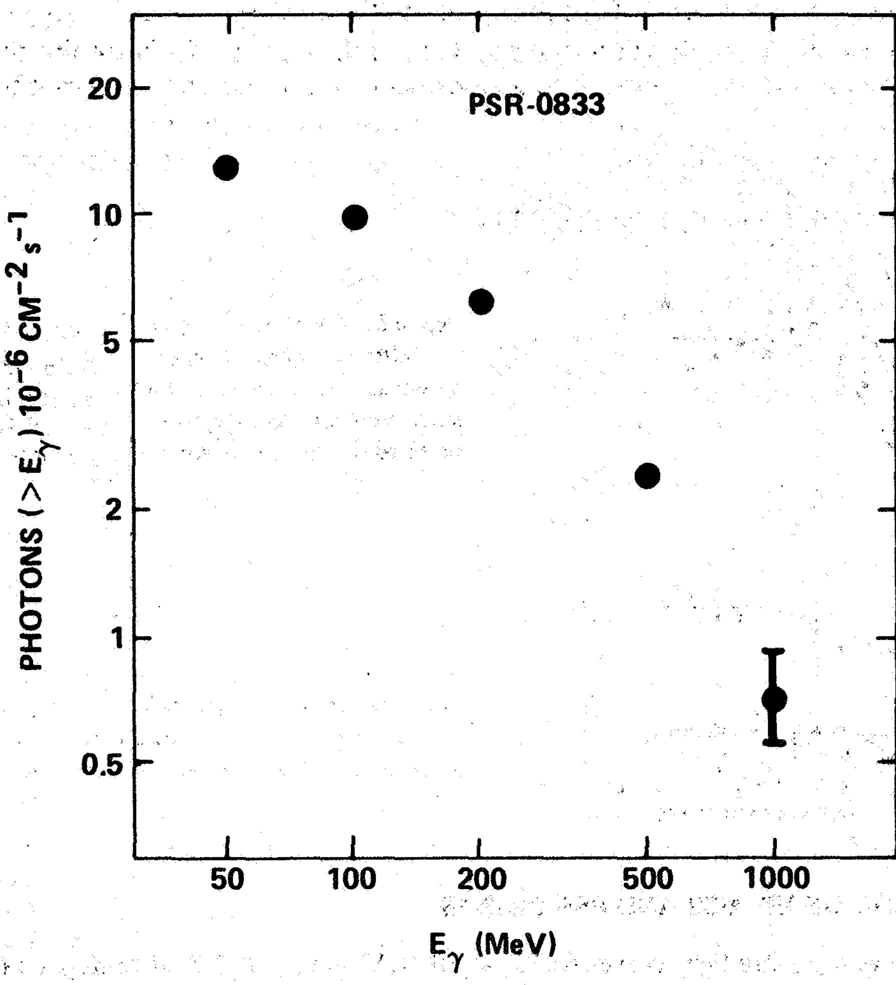

Figure 6. The integral energy spectrum for the pulsed component of the γ-ray emission from PSR 0833. The statistical error at 1 GeV (40 counts) is indicated. The data have not been corrected for the finite energy resolution, which may result in uncertainties ~ 20 percent in energy assignment. The intensity for $E_\gamma \geq 50$ MeV is 1.3×10^{-5} photons cm^{-2} s^{-1}.

in the provision of the experiment hardware, the individual institutes of the Collaboration are indebted to the engineers of their contractors, namely: Dr. W. Brunner of M.B.B. and Dr. E. Hübner of Siemens (Spark Chamber); Messrs. W. Drtil and R. Zobl of A.E.G.–Telefunken (Triggering Telescope); Messrs. E. H. Stogsdill, P. Christon, and R. McConaughey of Ball Brothers Research Corporation (Energy Calorimeter); and Messrs. A. Bonanni and A. Jacopini of Laben (Experiment Electronics and Pulsar Synchronizer).

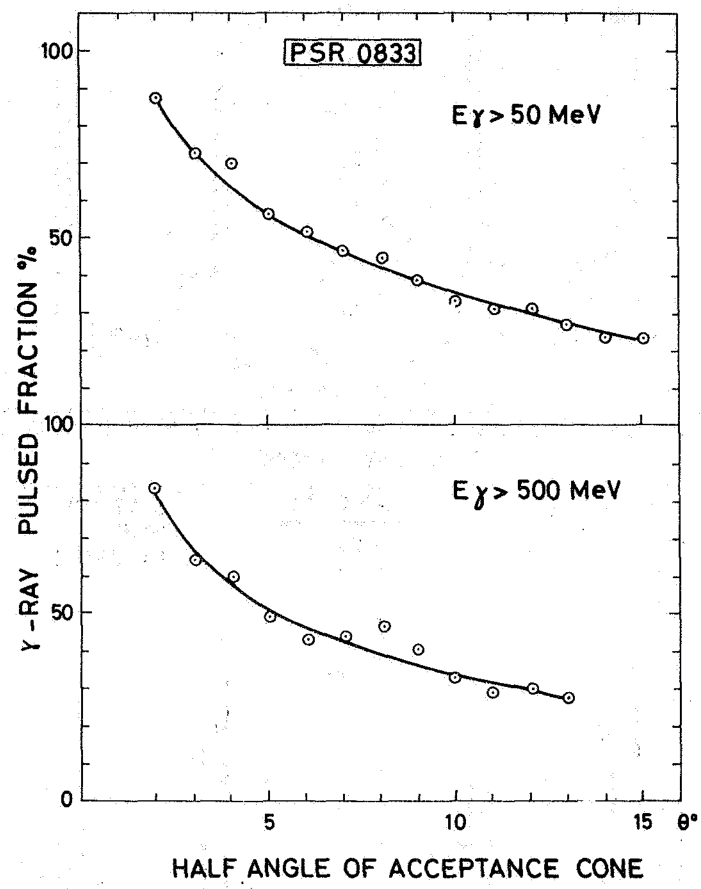

Figure 7. The pulsed fraction of γ-rays recorded as a function of the half-angle of the acceptance cone for reconstituted γ-ray arrival directions centered on PSR 0833 for $E_\gamma > 50$ and > 500 MeV. The lower limit to the pulsed fraction is ~ 85 percent.

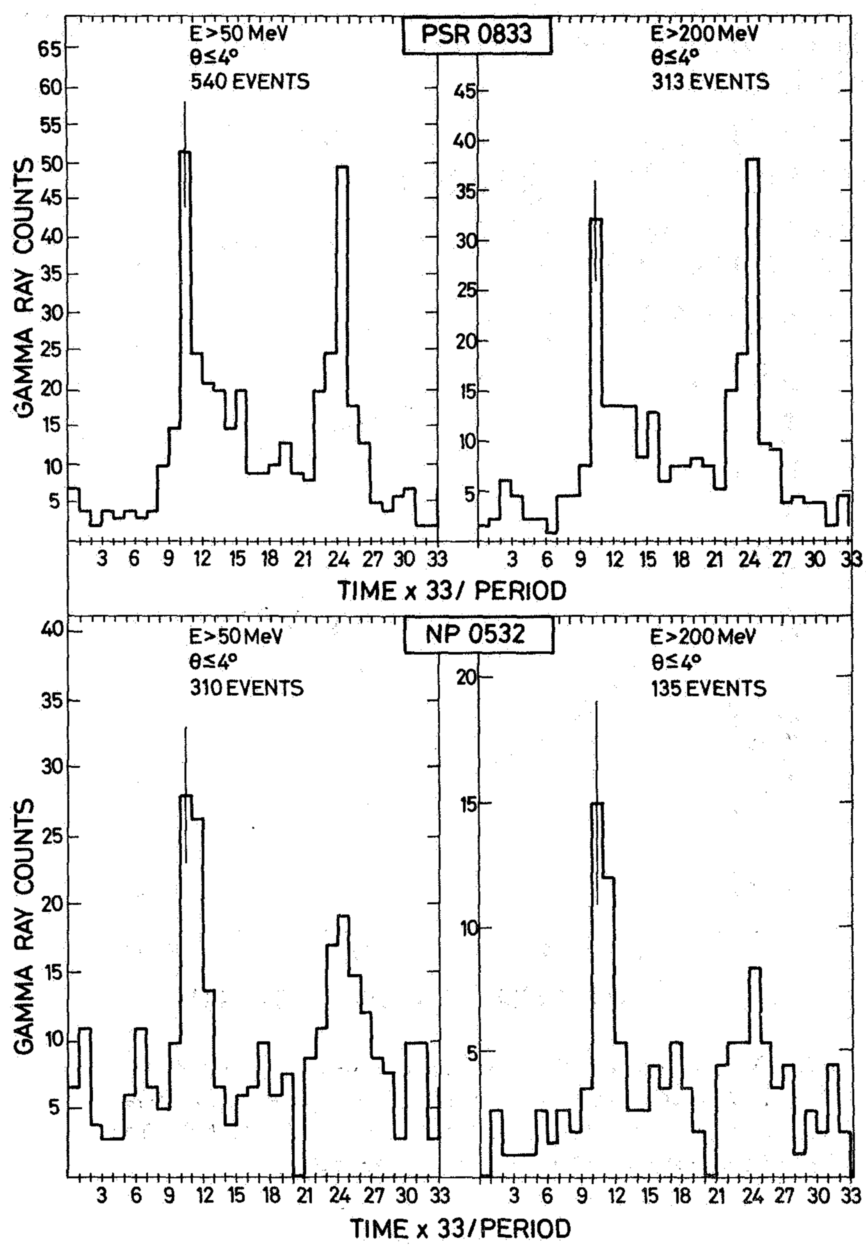

Figure 8. The γ-ray light-curves of PSR 0833 (November 8 through 28, 1975) and NP 0532 (August 17 to September 17, 1975) compared at $E_{\gamma} > 50$ and 200 MeV, with the periods of both pulsars divided into 33 time bins.

REFERENCES

Albats, P., G. M. Frye Jr., A. D. Zych, O. B. Mace, V. D. Hopper, and J. A. Thomas, 1972, *Nature*, **240**, p. 221.

Albats, P., G. M. Frye, Jr., G. B. Thomson, V. D. Hopper, O. B. Mace, J. A. Thomas, and J. A. Staib, 1974, *Nature*, **251**, p. 400.

Boella, G., R. Buccheri, J. J. Burger, P. Coffaro, and J. Paul, (Proc. 9th ESLAB Symposium (Frascati) ESRO SP-106, 1974), p. 353.

Browning, R., D. Ramsden, and P. J. Wright, 1971, *Nature Phys. Sci.*, **232**, p. 99.

Ducros, G., R. Ducros, R. Rocchia, and A. Tarrius, 1970, *Nature*, **227**, p. 153.

Leray, J. P., J. Vasseur, J. Paul, B. Parlier, M. Forichon, B. Agrinier, G. Boella, L. Maraschi, A. Treves, R. Buccheri, A. Cuccia, and L. Scarsi, 1972, *Astron. and Astrophys.*. **216**, p. 443.

Manchester, R. N., W. H. Goss, and P. A. Hamilton, 1976, *Nature*, **259**, p. 291.

McBreen, B., S. E. Ball, M. Campbell, K. Greisen, and D. Koch, 1973, *Ap. J.*, **184**, p. 571.

Ögelman, H., C. E. Fichtel, D. A. Kniffen, and D. J. Thompson, 1976, preprint.

Rappaport, S., H. Bradt, R. Doxsey, A. Levine, and G. Spada, 1974, *Nature*, **251**, p. 471.

Thompson, D. J., C. E. Fichtel, D. A. Kniffen, and H. B. Ögelman, 1975, *Ap. J. Letters*, **200**, p. L79.

Vasseur, J., J. Paul, B. Parlier, J. P. Leray, M. Forichon, B. Agrinier, G. Boella, L. Maraschi, A. Treves, R. Buccheri, A. Cuccia, and L. Scarsi, 1971, *Nature Phys. Sci.*, **203**, p. 46.

LOW- AND MEDIUM-ENERGY GALACTIC GAMMA-RAY OBSERVATIONS

G. H. Share
E. O. Hulburt Center for Space Research
U.S. Naval Research Laboratory Washington, D.C. 20375

ABSTRACT

Observation of 0.2- to 100-MeV-diffuse γ-radiation emitted from the galaxy can provide information on the intensities of 5- to 50-MeV/nucleon cosmic-rays and $\gtrsim$ 50-MeV electrons in interstellar space. Recent measurements of γ-rays emitted from the galactic center region provide evidence for a diffuse continuum between 10 and 100 MeV, which is dominant over the π°-decay emission generated in high-energy nuclear collisions. The intensities of the recently reported nuclear-line γ-rays, also observed in the direction of the galactic center, require the presence of intense fluxes of low-energy cosmic-rays in the inner galaxy if the γ-ray are produced on a galactic scale. Current detection techniques for 0.1- to 100-MeV γ-ray measurements are summarized, and their capabilities for measuring the diffuse galactic emission are evaluated. Significant improvement in our knowledge of low- and medium-energy galactic γ-radiation can be expected within the next few years.

INTRODUCTION

In this Symposium, we are primarily interested in large-scale features of our galaxy, such as the spatial distribution of interstellar matter and energetic particles. Diffuse γ-radiation emitted from the galaxy provides us with information which either supplements or is not obtainable from the more traditional disciplines of astronomy.

Observations of galactic γ-radiation in the 100-MeV energy region from SAS-2 and COS-B have been summarized earlier in these Proceedings. These high-energy photons are generated in the interactions of particles with kinetic energies of $\gtrsim$ 500 MeV. Although discrete γ-ray sources, such as the Crab Nebula and the Vela pulsar, contribute to the enhanced emission from along the galactic plane, it is likely that most of this radiation is produced in interactions of high-energy cosmic-ray protons and alpha particles with interstellar matter. These interactions produce the characteristic π°-decay γ-ray spectrum which peaks near 70 MeV, and above which energy more than 80 percent of the emission occurs. For this reason, $>$ 100-MeV γ-rays can provide information on the fluxes of GeV cosmic-ray nuclei and on the densities of interstellar gas in regions of the galaxy distant from Earth.

In this paper, the status of the observations of lower-energy ($E < 100$ MeV) galactic γ-radiation is summarized. In like manner, these low- and medium-energy γ-rays provide us with information on the fluxes of two other components of the galactic cosmic radiation, electrons with energies $\gtrsim 50$ MeV and nuclei with energies between 5 and 50 MeV/nucleon. The electrons can generate continuum γ-radiation from bremsstrahlung interactions on interstellar gas or from "inverse" Compton scattering on interstellar starlight. The low-energy nuclei produce nuclear-line emission in inelastic collisions with interstellar gas.

The next section discusses the low- and medium-energy γ-ray observations which have been made in the general vicinity of the galactic center ($|b^{II}| < 10°$; $-30° \lesssim \ell^{II} < +30°$), where the intensity is expected to be greatest. Future investigations will aim at achieving better sensitivities so that low- and medium-energy γ-ray emission can be mapped from other extended regions of the galaxy as well. The last section treats the detection techniques that will be in use in the next few years and the anticipated improvements in the measurements.

OBSERVATIONAL STATUS

Detection Techniques

Before presenting the observations which have been made to date, it will be helpful to first describe the instruments used. Although the SAS-2 multiplate spark chamber (Fichtel et al., 1975a) is most sensitive at energies above 100 MeV, it responds to photons down to ~ 35 MeV. At these energies, the angular resolution is considerably degraded, but some spectral information on diffuse galactic emission is available.

An experiment which provides both good angular resolution ($\lesssim 2°$) and good energy resolution (±15 percent) in the 15- to 100-MeV range is the emulsion wide-gap spark-chamber array which Bob Kinzer, Carl Noggle, Nat Seeman, and I developed at NRL (Share et al., 1974). A drawing of the configuration flown during a 1971 exposure to the galactic center region is shown in figure 1. Gamma-rays convert in the stack of nuclear emulsions (E) producing electron pairs which are detected by a counter telescope consisting of a proportional counter (P) and two plastic scintillation counters (B). The plastic scintillation counters (A) reject charged cosmic radiation. Use of a combination absorption/Cerenkov counter (C) limits detectable γ-ray energies to < 200 MeV. The trajectories of the electron pairs are photographed in a wide-gap spark chamber, permitting the tracks to be located in the emulsion where precise measurements can be made near the point at which the γ-rays converted.

The third instrument, shown in figure 2, was developed at the Smithsonian Astrophysical Observatory (Helmken and Hoffman, 1970) and was flown in 1971. It consists of a telescope arrangement using plastic scintillators and a gas Cerenkov counter. Although it has excellent background rejection properties and is sensitive down to ~ 15 MeV, it has rather poor angular resolution ($\sim 25°$) and provides no spectral information.

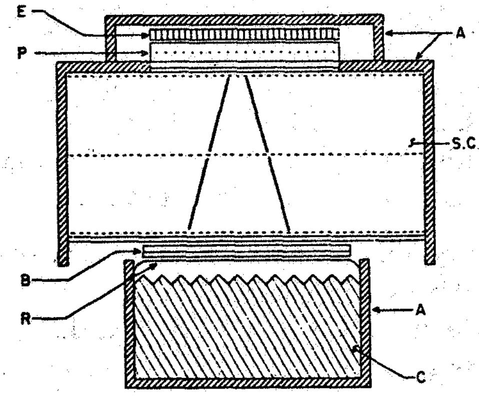

Figure 1. NRL Emulsion Spark-Chamber Telescope ($\gtrsim$ 15 MeV).

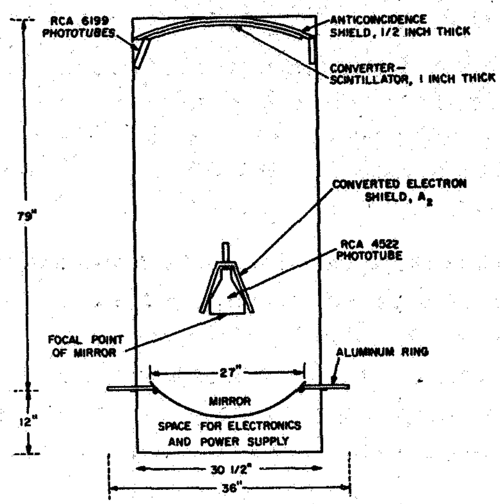

Figure 2. SAO Cerenkov Telescope ($\gtrsim$ 15 MeV).

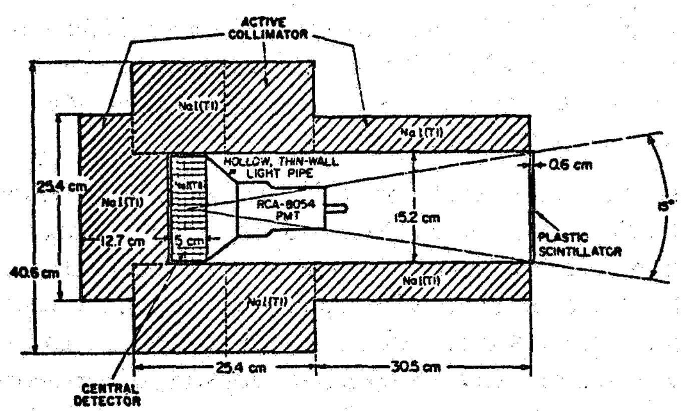

Figure 3. Rice Actively Shielded Scintillator (0.1 to 10 MeV).

The fourth instrument is shown in figure 3 and was designed at Rice University to detect γ-rays of much lower energy, from ~ 50 keV to ~ 10 MeV (Walraven et al., 1975). It consists of a 5-cm thick NaI crystal, with a sensitive area of ~180 cm^2, which is shielded by other NaI crystals and collimated to an aperture of ~ 13° FWHM.

Summary of the Observations

Much of the data from these experiments relating to galactic observations have already been published. What I have attempted to do is to combine these results with some theoretical studies in order to appraise the status of our knowledge of the 0.1- to 100-MeV diffuse emission from the galactic plane. The summary takes the form of the differential spectrum, shown in figure 4, of the radiation emitted from the direction of the galactic center ($|b^{II}| < 10°$; $-30° < \ell^{II} < 30°$). From the shape of the spectrum, especially at energies < 100 MeV, we can determine the relative contributions that processes such as high-energy proton interactions and electron bremsstrahlung make to the total γ-ray flux. This determination is critical to the interpretation of the longitude distribution of galactic γ-rays which is discussed later in the Symposium by Floyd Stecker and Donald Kniffen.

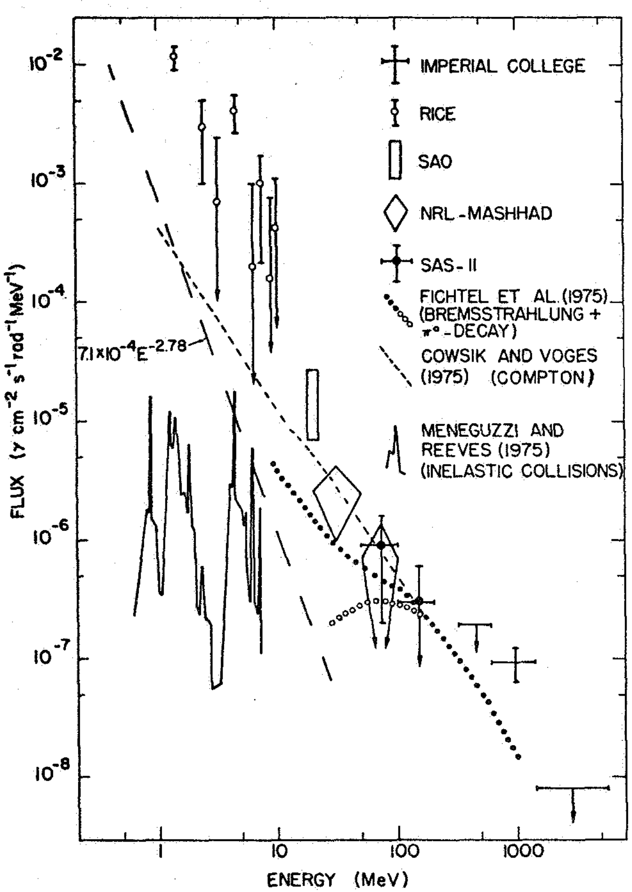

Figure 4. Differential measurements of galactic γ-ray emission ($|b^{II}| < 10°$; $|\ell^{II}| < 30°$) compared with calculations.

Shown at high energies are the data obtained by the group at Imperial College, London (Sood et al., 1975). The measurement between 600 and 1400 MeV was ~ 4σ over background in the latitude interval $|b^{II}| < 4°$; and the other points were 2σ upper limits. Recent extended balloon-borne exposures with this same experiment promise significant improvement in these high-energy measurements (G. K. Rochester, 1976, private communication). In addition, forthcoming results from COS-B should provide good quality spectral data up to ~ 2 GeV (Bennett et al., 1974).

The data from SAS-2 have been adapted from the integral spectrum given by Fichtel et al. (1975a). Caution must be taken in using such a subtraction procedure; the large errors shown reflect this uncertainty. As suggested by Cowsik and Voges (1975), a "direct" differential representation of the SAS-2 galactic energy data, similar to that given for the diffuse cosmic background in the same paper, is desirable.

The points designated as NRL-Mashhad have been derived from an analysis of data obtained during a 1971 exposure with the emulsion spark-chamber system shown in figure 1 (Share et al., 1974; Samimi et al., 1974). The emulsion analysis, which has been performed recently at the Ferdowsi University, Mashhad, Iran, is almost completed. The spectral data shown in figure 1 were obtained in collaboration with Robert Kinzer and Jalal Samimi and have not been presented before in this form. They have been derived using only γ-ray events < 100 MeV for which both members of the electron pair were energetic enough to leave the stack of emulsions and to be recorded in the spark chamber. Final results from a complete analysis will be presented in a forthcoming publication. The differential intensities were found by subtracting the contribution of atmospheric background (determined from data taken at $|b^{II}| > 6°$) from the γ-ray spectrum observed within $\pm 3°$ of the galactic equator for longitudes $-30° \lesssim \ell^{II} \lesssim 30°$. The limited statistics in both the galactic and background spectra yield large errors after subtraction.

Because of the important energy range over which it was made, data obtained using the SAO Čerenkov telescope have been included, even though only an integral measurement was made. The conversion to a differential intensity yields a large uncertainty which is reflected in the errors given.

Before discussing the low-energy data, it is well to reflect on the measurements above 10 MeV. Various systematic uncertainties, such as exposures to differing sections of the galactic plane near the galactic center, are present, in addition to the statistical uncertainties shown. With this in mind, the agreement between experiments is reasonable. Shown for comparison are the calculated differential spectra of galactic γ-rays produced by electron bremsstrahlung and Compton collisions and by cosmic-ray interactions on interstellar matter. The bremsstrahlung and $\pi°$-decay intensities are from the calculations of Fichtel et al. (1975b) for a galactic longitude of 335°. The $\pi°$ intensity dominates over bremsstrahlung for energies above 100 MeV. However, as suggested by Ramaty and Westergaard (1976), the bremsstrahlung contribution could be significantly greater if the cosmic-ray electrons are stopped before they can escape from the galaxy (closed galaxy model). The Compton spectrum shown was calculated by Cowsik and Voges (1975) and indicates that the Compton process dominates the galactic γ-ray emission even at energies above 100 MeV. However, other estimates of the Compton source strength are significantly lower (Shukla and Paul, 1976; and Dodds et al., 1975).

In their present fragmentary form, the data provide an indication of the dominant production mechanisms for γ-rays < 100 MeV. The NRL-Mashhad observations, taken together with those from SAS-2, are consistent with a continuum produced primarily by electron bremsstrahlung or Compton collisions.

The data plotted below 10 MeV from the Rice observations (Haymes et al., 1975) were obtained during an exposure centered on the hard X-ray source, GX 1 + 4. Continuum emission up to ~ 800 keV was observed from this region of the galactic plane; it is likely that much, if not all, of it is emitted from the hard X-ray source. However, for purposes of comparison, I have chosen to plot the extrapolation of this continuum spectrum ($dN/dE = 7.1 \times 10^{-4} E^{-2.78}$) to higher energies assuming that the γ-rays are emitted from a diffuse source along the plane. There is some evidence in the Rice data for such diffuse emission. A brief exposure to the longitude range from 339° to 352° along the plane during a background portion of the flight also showed an enhancement over background measurements taken at higher latitudes.

In addition, the continuum intensity measured in an earlier Rice experiment (Johnson and Haymes, 1973) was about a factor of 2 larger than the current measurement; this is consistent with a diffuse interpretation because of the larger aperture of the earlier experiment.

Some of the higher-energy data points observed by the Rice group above 1 MeV are also plotted, assuming a diffuse origin, in order to indicate the level of sensitivity of the current measurements in this energy range. Most of the data points > 800 keV are consistent with zero; however, evidence was found for features which can be attributed to nuclear-line emission. This evidence is illustrated in figure 5, which is taken from Haymes et al. (1975). The features at ~ 0.5 and ~ 4.5 MeV can be attributed to positron annihilation and emission from the excited state of ^{12}C, respectively, whereas the broad enhancement from 1.2 to 2 MeV could be due to a combination of lines from ^{56}Fe, ^{24}Mg, ^{20}Ne, and ^{29}Si. If confirmed, these line features represent the first observation of nuclear γ-rays emitted from outside our solar system.

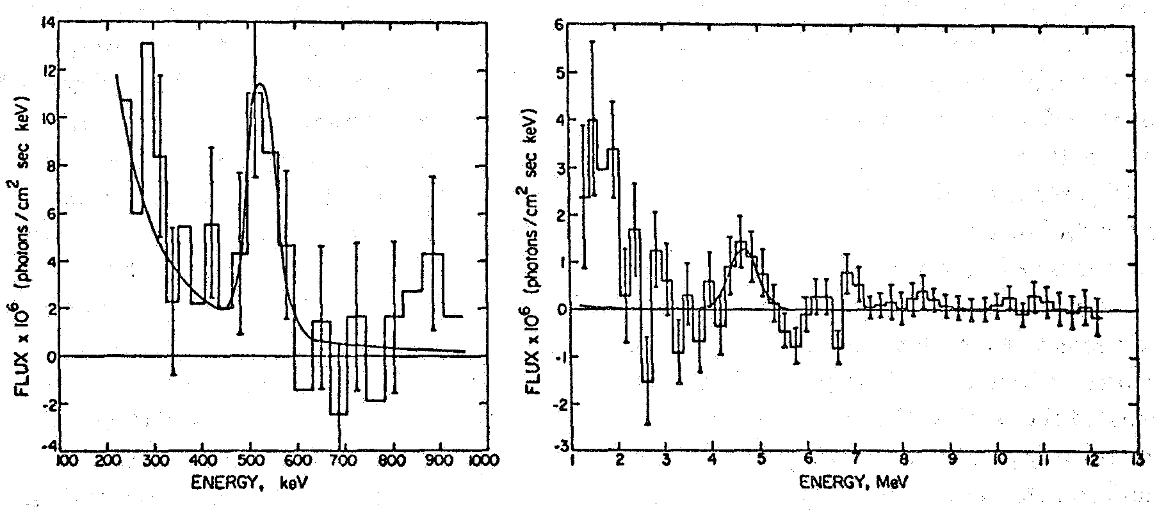

Figure 5. Spectral data obtained by Haymes et al. (1975), giving evidence for nuclear-line features emitted from the galactic center region.

Returning to figure 4, we can compare the intensity of these features, assuming a diffuse origin from the galactic plane, with recent calculations by Meneguzzi and Reeves (1975; see also Rygg and Fishman, 1973). I've plotted their results for an assumed E^{-3} differential spectrum in kinetic energy for cosmic-ray nuclei in the 5- to 50-MeV/nucleon range by normalizing to their calculated π°-decay γ-ray intensity. Although the expected features agree with the observations, the calculated intensity is about two orders of magnitude below the observations, requiring either that the cosmic-ray intensities are significantly higher or that the features come from localized sources such as supernova remnants.

A detailed discussion of galactic nuclear-line features is found in Richard Lingenfelter's paper in these Proceedings. It is of importance to note in figure 4 that both narrow and broad features are expected. The broad features arise from Doppler broadening of γ-rays emitted from heavy cosmic-ray nuclei excited in collisions with ambient hydrogen gas. With this in mind, I wish to question the interpretation by Fishman and Clayton (1972) of a possible line feature at $\sim$478 keV, observed by Johnson and Haymes (1973), as being produced by excited ^{7}Li in the cosmic radiation. Any feature produced in this way would be severely broadened and would not show evidence for a narrow-line profile. Even the narrow features, arising from cosmic-ray proton excitation of nuclei in the ambient gas, may show significant broadening (e.g., $\sim$ 80-keV FWHM in the 4.43-MeV line of ^{12}C).

FUTURE OBSERVATIONS

There is considerable activity at present devoted to the development of suitable instrumentation for observing low- and medium-energy γ-radiation. For the purpose of observing diffuse emission from the galactic plane, an optimum instrument would be one having a reasonably broad field of view ($\sim$ 25°-FWHM) and an angular resolution of about 1°. This not only would enable the galactic diffuse emission to be resolved simultaneously from the background, but would also permit variations of the diffuse emission to be mapped and resolved from any point sources. Energy resolution in the > 10-MeV range is not critical; a resolution of $\sim$ 25-percent FWHM should be adequate to distinguish the various processes contributing to the diffuse emission. Below 10 MeV, better energy resolution is critical in order to identify and distinguish the lines which may be emitted. In the near future, it is perhaps not essential to attain the excellent resolution ($\sim$ 2.5-keV FWHM) characteristic of germanium detectors. High-sensitivity crystal detectors with moderate energy resolution ($\sim$ 3 to 8-percent) can perform a large part of the pioneering activity in this field. (This is especially true because many of the nuclear lines are expected to be significantly Doppler-broadened.) Future detection systems will probably employ arrays of large-volume ($\sim$ 150 cm^3), intrinsic germanium detectors capable of achieving both high sensitivity and excellent energy resolution.

It is clear from the results obtained from SAS-1, SAS-2, and COS-B that long-term observations are important for making high-sensitivity measurements and for detecting transient phenomena which can complicate measurements of a diffuse intensity. It is probably more important for the observations > 10 MeV to be performed above any overlying atmosphere than it is for observations < 10 MeV. This is true because the intrinsic background of the high-energy detectors is much lower than the background produced in the overlying atmosphere as viewed from high-altitude balloons. The reverse is true for energies < 10 MeV. In fact, there are significant advantages that balloon-borne low-energy γ-ray detectors have, for example, a stable background environment which is free from the high-intensity radiation fields that most satellites periodically encounter.

The prospects for long-duration balloon observations are growing. In the past, most flights have been limited to durations of $\sim$ 8 hours, except for the semiannual wind turnaround periods, when durations of 40 hours have been achieved. Recent innovations (such as transatlantic balloon flights such as the one launched last year from Sicily) offer flight durations of 5 to 7 days. Even longer durations of up to 2 to 3 months will be possible with the successful development of large superpressure balloons expected within the next 1 or 2 years.

With these general considerations in mind, I wish to summarize the current status of instrument development in the low- and medium-energy γ-ray domain and also of the sensitivities for detecting diffuse galactic emission that can be achieved in the next few years. Table 1 lists the types of instruments that are currently in operation, or being planned, which are known to me. Within each category, there may be one or more variations developed by different groups. My purpose here is not to provide an all-inclusive listing, but one which is just representative. Typical properties of currently used detectors are also given in table 1.

The Rice detector shown in figure 3 falls into the first category of actively shielded and collimated crystals. Another example of this type is the UCSD-MIT detector (Matteson et al., 1974) which will be launched on board the HEAO-A satellite in the spring of 1977. This instrument is shown in figure 6. It consists of a cluster of detectors with different apertures and energy ranges of operation. The most sensitive element for detecting the diffuse galactic γ-ray emission is the central detector with its 40° field of view. The four point-source detectors (20° aperture) will be helpful in distinguishing discrete sources. The block of CsI shown in figure 6 is used as a shutter, primarily for measurements of the diffuse cosmic background.

A second type of shielded scintillator is also listed in table 1. This type has a large aperture and uses an occulter to identify point sources of radiation; it is therefore not designed for observation of extended sources. Groups at Toulouse (Mandrou et al., 1975) and the University of New Hampshire (Chupp, 1975, private communication) are currently employing this technique.

High-energy resolution germanium detectors make up the next group. Significant progress is being made in the utilization of large-volume detectors such as the instrument developed at Toulouse (Vedrenne 1976, private communication) which employs a 140-cm^3 diode. This instrument will be flown within the next year from Brazil to study the nuclear-line emission from the galactic center region. Shown in figure 7 is the array of four 40-cm^3 Ge (Li) detectors developed for balloon observations by the Jet Propulsion Laboratories (Jacobson et al., 1975). The detectors are actively shielded and collimated by cylindrical crystals of CsI. This configuration is similar to the one being developed for the HEAO-C satellite, which has four 60-cm^3 diodes (Hicks and Jacobson, 1974). This will not be the first germanium detector to be placed in orbit. The group at Lockheed flew two 50-cm^3 Ge(Li) detectors on a polar-orbiting satellite in 1972 (Nakano et al., 1974). Other laboratories with experiments using germanium include the Goddard Space Flight Center (Cline, 1976, private communication) and a Sandia-Bell Labs collaboration (Leventhal, 1976, private communication).

Table 1
Typical Properties of Low- and Medium-Energy γ-Ray Detectors

Detector	Energy Range (MeV)	Area (cm^2)	Aperture (°FWHM)	Efficiency (percent)	Resolution (FWHM)	
					Energy	Angle
Actively shielded and collimated inorganic scintillators	~0.1 to 10	100 to 300	10 to 30	~50 @ 1 MeV ~20 @ 5 MeV	~ 60 keV @ 0.7 MeV ~180 keV @ 5 MeV	10 to 30°
Actively shielded inorganic scintillators with shutter/occulter	~0.1 to 10	100 to 300	~80	~50 @ 1 MeV ~20 @ 5 MeV	~ 60 keV @ 0.7 MeV ~180 keV @ 5 MeV	~20°
Actively shielded germanium detectors	~0.1 to 10	40 to 50	20 to 60	~12 @ 1 MeV ~ 5 @ 5 MeV	2.5 keV @ 1 MeV	20 to 60°
Semiactively shielded Compton detector	0.5 to 20	500	~2	~12 @ 1 MeV ~ 5 @ 5 MeV ~ 3 @ 10 MeV	~150 keV @ 1 MeV	~2°
Double Compton telescope	0.5 to 20	4000 to 10,000	70 to 100	2-3 @ 1 MeV 3-5 @ 5 MeV 2-3 @ 10 MeV	14 to 40 percent	15 to 30°
Large-area low-mass multiplate chambers	$\gtrsim 5$	500 to 10,000	~60	2 @ 10 MeV 10 @ 100 MeV	~100 percent	10 to 20° @ 20 MeV ~3° @ 100 MeV
Heavy-gas wide-gap spark chamber (conceptual)	$\gtrsim 5$	~3000	~60	0.5 @ 10 MeV 2 @ 100 MeV	~ 50 percent	~4° @ 10 MeV ~2° @ 20 MeV
Emulsion spark chamber	$\gtrsim 15$	650	~60	2 @ 20 MeV 15 @ 100 MeV	~ 30 percent	~2° @ 20 MeV ~1° @ 100 MeV

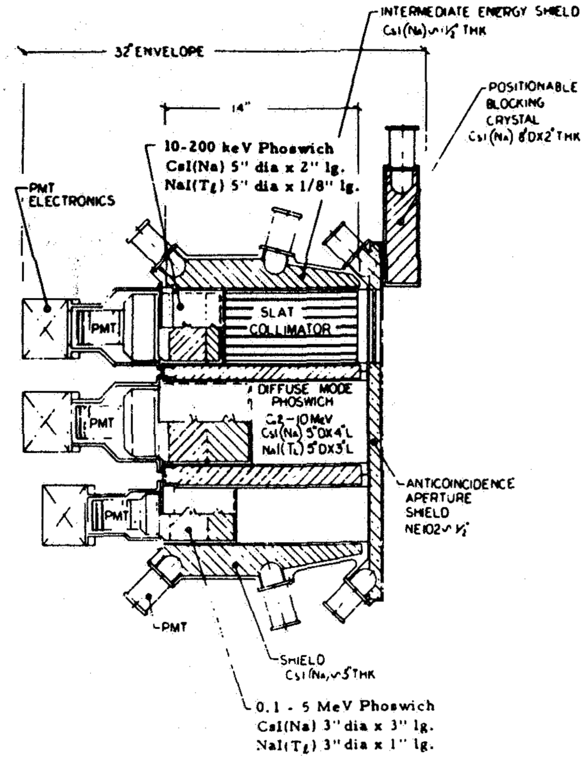

Figure 6. The γ-ray detector on HEAO-A.

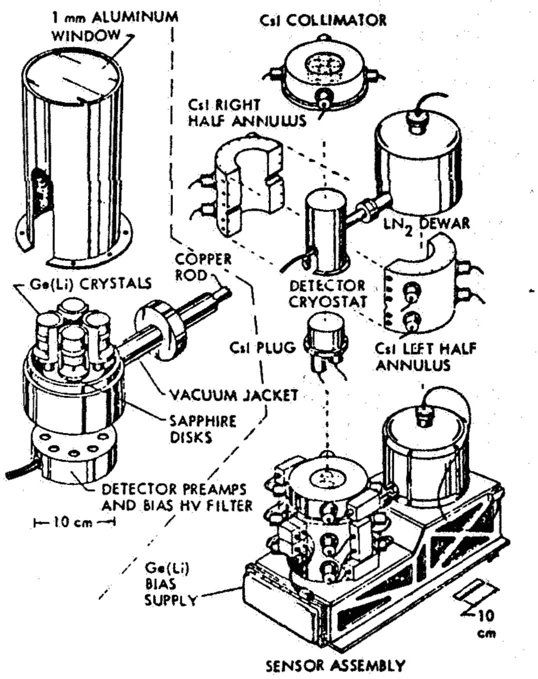

Figure 7. The JPL balloon-borne germanium array.

The next two types of instruments operate in a higher energy range. Both make use of the Compton effect for detecting incident γ-radiation, but they are significantly different in their concept and operation. Shown in figure 8 is the semiactively shielded Compton detector built in a collaboration between Milan and Southampton (Maccagni et al., 1975). An $\sim 2°$ field of view is provided by the lead-slats and lead-scintillator shielding. This type of shielding represents significant cost savings over inorganic crystals, but its background rejection still needs to be demonstrated under flight conditions. The narrow field of view primarily limits this system to observation of point sources.

The double Compton telescopes developed independently at Munich (Schönfelder et al., 1973) and at the University of California at Riverside (Herzo et al., 1975) represent the first attempts to develop an imaging system in this difficult energy domain. The Riverside system utilizes several tanks of liquid scintillator which also make it a sensitive detector for solar neutrons. A modified and significantly enlarged Compton telescope is currently being constructed at Munich (Graml et al., 1975). It is shown in figure 9 and consists of 16 separate detecting elements in each plane. The use of NaI in the bottom plane greatly improves the instrument's energy resolution and sensitivity.

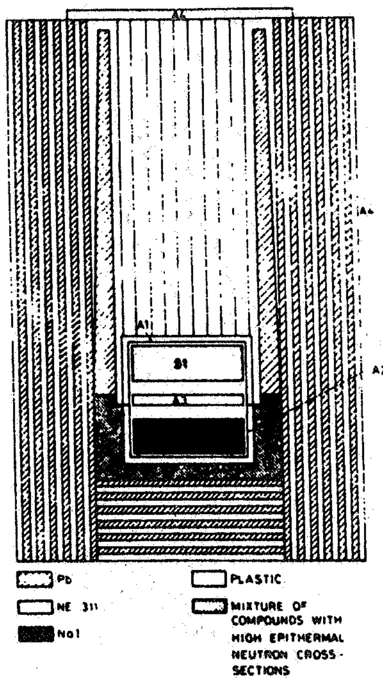

Figure 8. The Southampton/ Milan shielded Compton detector.

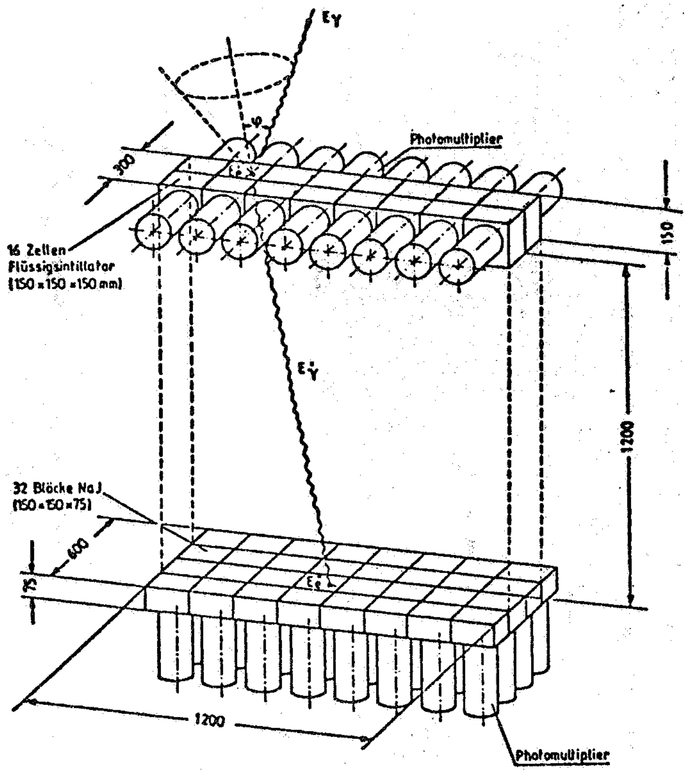

Figure 9. The large-area Compton telescope designed at the Max Planck Institute.

The last three detectors listed in table 1 are all imaging systems designed for higher γ-ray energies. The large-area low-mass multiplate chambers are basically the same as the systems designed for photons > 50 MeV, except for the emphasis on reducing the scattering of the pair-produced electrons, primarily by incorporating thinner converting plates. The instrument shown in figure 10, which was designed at the Moscow Engineering Physics Institute (Galper et al., 1975), illustrates some of the characteristics of this low-mass design. The conversion plates are a factor of ~4 thinner than those used in COS-B. In addition, thin-window proportional counters (designated by C) are used as triggering elements. The angular resolution attainable with this instrument should be about a factor of 2 better than that achieved by COS-B, based on the reduction of scattering material; it is therefore difficult to understand how a resolution of 3° at 17 MeV can be achieved as claimed by the authors. Other instruments for investigating this same energy domain, but having considerably larger sensitive areas, have been developed by the Case-Western Melbourne collaboration (Jenkins, et al., 1974), by the Saclay-Toulouse collaboration (Bonfand et al., 1975), and by the group at the Goddard Space Flight Center (D. Kniffen, 1975, private communication).

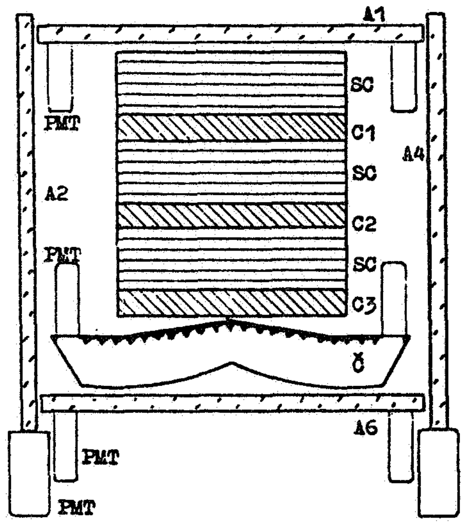

Figure 10. Diagram of the low-mass γ-ray telescope developed at the Moscow Engineering Physics Institute.

The next type of instrument is only conceptual (Kinzer et al., 1970; see also Kniffen, 1971) but, if developed, it should provide a significant improvement in angular resolution in its energy range without having the difficulties inherent in the emulsion spark-chamber design listed last in table 1. In this concept, the γ-rays convert in a heavy noble gas (e.g., xenon) of a wide-gap spark chamber. This permits measurements to be made on the directions of pair electrons before they are scattered appreciably. The limiting feature of this instrument is its low conversion efficiency and high operating voltage. Perhaps, though, with the age of the Space Shuttle near, it may be worth further appraisal.

I've already discussed the operation of the emulsion wide-gap spark-chamber array developed at NRL. (See figure 1.) A modified instrument, with sensitivity extending to ~1 GeV (Samimi et al., 1974), was recently flown and obtained 10 hours of exposure to the galactic center region. From this exposure, ~500 galactic γ-rays will be mapped at a resolution of 1 to 2°. The analysis which is proceeding at NRL and the Ferdowsi University at Mashhad, Iran, is arduous; but, as is evident from table 1, no other operating system can approach this angular resolution in the 10- to 100-MeV range. This resolution is also critical for identifying any point sources which contribute to the diffuse galactic emission.

It is reasonable to ask at this point what we can anticipate learning from low- and medium-energy galactic γ-ray observations within the next few years. The graph shown in figure 11 attempts to answer this question for the continuum emission > 1 MeV. The shaded area shows the range of current measurements made in the direction of the galactic center (including limits) as depicted in figure 4. The points give estimates of the 3σ sensitivities of current instruments as adapted from publications or communications. No limits are given on figure 11 for the large-area multiplate chambers, but I'd estimate their sensitivities to be somewhat better than those plotted for the emulsion spark chambers. For purposes of comparison, I've included an estimate of the sensitivity of the conceptual heavy-gas spark chamber. It is also important to keep in mind that due to the rapidly changing background environment, systematic uncertainties in the HEAO-A measurements can significantly degrade the plotted sensitivities.

Even with these reservations, it is clear that much will be learned about diffuse galactic emission in the 1- to 100-MeV region in the next few years. The relative contribution of electron-initiated processes, such as bremsstrahlung and Compton interactions, to the total galactic

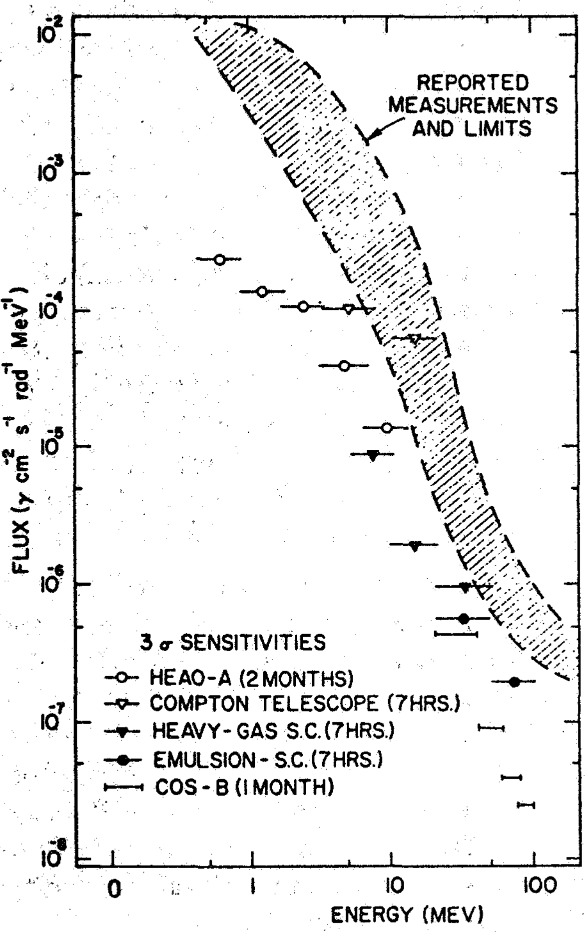

Figure 11. Comparison of galactic γ-ray sensitivities achievable in the next few years with current measurements.

γ-ray emission will be well known. In addition, initial mapping of these low-energy components will enable the spatial distribution to be determined to a level approaching that obtained from SAS-2 for higher-energy photons.

A similar comparison can be made between the reported nuclear-line intensities and sensitivities attainable within the next few years. This comparison is shown in table 2. The observed intensities are adapted from the work of Haymes et al. (1975) on the assumption that these features are emitted on a galactic scale. The limits have been adapted from sensitivities estimated by the different experimenters. The advantage that comes from extended observations, such as those available with the HEAO-A detector, is again clear. The sensitivity obtainable with the large-area Compton telescopes is also worthy of note; however, their limited energy resolution may be a significant liability for future line observations.

The sensitivities available during a single day's exposure with the current generation of germanium detectors are just sufficient to detect the reported line features. The increased exposure

Table 2
Estimated Sensitivities To Galactic γ-ray Lines
($\times 10^{-3}$ cm^{-2} s^{-1} rad^{-1})

Experiment	0.5 Mev	0.9 MeV	1.2-2 MeV	4.5 MeV
1. Double Compton telescope (7 hr)				
a. Riverside (Herzo et al., 1975)	–	–	–	0.4
b. Munich (Schönfelder, private comm.)	–	–	–	0.1
2. HEAO-A Scintillator (2 months) (Matteson et al., 1974)	0.04	0.03	0.09	0.03
3. Shielded Ge(Li)				
a. Balloon (7 hr) (Jacobson et al., 1975)	1.0	2.0	–	2.0
b. HEAO-C (Hicks and Jacobson, 1974)	0.02	0.05	–	0.15
Observed intensity (Haymes et al., 1975)	3.5±1.0	1.6±1.4	11.5±2.6	4.2±1.2

available with long-duration balloon flights and satellites improves their capabilities significantly as can be seen in table 2. However, we must remember that these sensitivities are estimated under the assumption that the intrinsic line width of the radiation is less than the detector's resolution (~ 2.5 keV). This is not the case with many of the lines (e.g., Doppler-broadening of the 4.43-MeV ^{12}C line is expected to be ~ 80 keV).

REFERENCES

Bennett, K., J. J. Burger, M. Gorisse, H. A. Mayer-Hasselwander, J. Paul, E. Pfeffermann, P. G. Shukla, R. Stiglitz, B. N. Swanenburg, B. G. Taylor and R. D. Wills, 1974, (Proc. 9th ESLAB Symp., ESRO SP-106), p. 323.

Bonfand, E., B. Parlier, M. Forichon, B. Mougin, A. Leconte, J. C. Courtois, B. Agrinier, J. Andrejo, M. Niel, M. Lavigne, and G. Vedrenne, 1975, (Proc. 14th Intl. Cosmic Ray Conf., No. 9, Munich), p. 3141.

Cowsik, R., and W. Voges, 1975, (Proc. 14th Intl. Cosmic Ray Conf., No. 1, Munich), p. 74.

Dodds, D., A. W. Strong, A. W. Wolfendale, and J. Wdowczyk, 1975, *J. Phys. A.*, **8**, p. 624.

Fichtel, C. E., R. C. Hartman, D. A. Kniffen, D. J. Thompson, G. F. Bignami, H. Ögelman, M. F. Özel, and T. Tümer, 1975a, *Ap. J.*, **198**, p. 163.

Fichtel, C. E., D. A. Kniffen, D. J. Thompson, G. F. Bignami, and C. Y. Cheung, 1975b, NASA TM X-70988.

Fishman, G. J., and D. D. Clayton, 1972, *Ap. J.*, **178**, p. 337.

Galper, A. M., V. A. Grigoryev, V. G. Kirillov-Ugryumov, Yu. D. Kotov, Ye. V. Kulakov, Yu. V. Smirnov, and V. N. Yurov, 1975, (Proc. 14th Intl. Cosmic Ray Conf., No. 9, Munich), p. 3143.

Graml, F., E. Mitchell, D. Zasche, J. Daugherty, V. Schönfelder, and M. R. Maier, 1975, (Proc. 14th Intl. Cosmic Ray Conf., No. 9, Munich), p. 3129.

Haymes, R. C., G. D. Walraven, C. A. Meegan, R. D. Hall, F. T. Djuth, and D. H. Shelton, 1975, *Ap. J.*, **201**, p. 593.

Helmken, H., and J. Hoffman, 1970, *Nucl. Inst. Meth.*, **80**, p. 125.

Helmken, H. F., and J. A. Hoffman, 1973, *Nature Phys. Sci.*, **243**, p. 6.

Herzo, D., R. Koga, W. A. Millard, S. Moon, J. Ryan, R. Wilson, A. D. Zych, and R. S. White, 1975, *Nucl. Inst. and Meth.*, **123**, p. 583.

Hicks, D. B., and A. A. Jacobson, 1974, (IEFE Trans. Nucl. Sci., NS-21), p. 169.

Jacobson, A. S., R. J. Bishop, G. W. Culp, L. Jung, W. A. Mahoney, and J. B. Willett, 1975, *Nucl. Inst. and Meth.*, **127**, p. 115.

Jenkins, T., P. Albats, G. Frye, R. Kolman, S. Schindler, R. Schreiner, G. Thomson, and O. Mace, 1974, (Proc. 9th ESLAB Symp., ESRO SP-106), p. 171.

Johnson, W. N., III, and R. C. Haymes, 1973, *Ap. J.*, **184**, p. 103.

Kinzer, R. L., R. C. Noggle, N. Seeman, and G. H. Share, 1970, *Bull. Amer. Phys. Soc.*, **15**, p. 613.

Kniffen, D., 1971, In: *Cosmic Gamma Rays,* F. W. Stecker, U.S. Government Printing Office, Washington, D.C., p. 237.

Maccagni, D., C. Paizis, F. Perotti, G. Piccinotti, R. Stiglitz, A. J. Dean, S. J. Martin, and D. Ramsden, 1975, (Proc. 14th Intl. Cosmic Ray Conf., No. 9), p. 3135.

Mandrou, P., M. Niel, J. Nrabonne, and C. Sabaud, 1975, preprint to be published in *Nucl. Inst. and Meth.*

Matteson, J. L., R. M. Pelling, and L. E. Peterson, 1974, (Proc. 9th ESLAB Symp., ESRO SP-106), p. 177.

Meneguzzi, M., and H. Reeves, 1975, Preprint to be published in *Ast. and Ap.*

Nakano, G. H., W. L. Imhof, and R. G. Johnson, 1974, (IEEE Trans. Nucl. Sci., NS-21), p. 159.

Ramaty, R., and N. J. Westergaard, 1976, NASA TM X-71052.

Rygg, T. A., and G. J. Fishman, 1973, (Proc. 13th Intl. Cosmic Ray Conf., No. 1), p. 472.

Samimi, J., G. H. Share, and R. L. Kinzer, 1974, (Proc. 9th ESLAB Symp., ESRO SP-106), p. 211.

Schönfelder, V., A. Hirner, and K. Schneider, 1973, *Nucl. Inst. and Meth.*, **107**, p. 385.

Share, G. H., R. L. Kinzer, and N. Seeman, 1974, *Ap. J.*, **187**, p. 45.

Shukla, P. G., and J. Paul, 1976, Preprint submitted to *Ap. J.*

Sood, R. K., K. Bennett, P. G. Clayton, and G. K. Rochester, 1975, (Proc. 14th Intl. Cosmic Ray Conf., No. 1, Munich), p. 35.

Walraven, G. D., R. D. Hall, C. A. Meegan, P. L. Coleman, D. H. Shelton, and R. C. Haymes, 1975, *Ap. J.*, **202**, p. 502.

VERY HIGH-ENERGY GAMMA-RAY ASTRONOMY

Jonathan E. Grindlay
Center for Astrophysics, Harvard College Observatory
and Smithsonian Astrophysical Observatory
Cambridge, Massachusetts 02138

ABSTRACT

Recent results in ground-based very high-energy ($> 10^{11}$ eV) γ-ray astronomy are reviewed. The various modes of the atmospheric Cerenkov technique are described, and the importance of cosmic-ray rejection methods is stressed. The positive detections (at $\gtrsim 10^{12}$ eV) of the Crab pulsar that suggest a very flat spectrum and time-variable pulse phase are discussed. Observations of other pulsars (particularly Vela) suggest that these features may be general. The "steady" flux upper limits for the Crab Nebula are thus reconsidered, and a new value of the implied (Compton-synchrotron) magnetic field in the Nebula is reported. Evidence that a 4.8-hour modulated effect was detected at $E_\gamma > 10^{12}$ eV from Cyg X-3 is strengthened in that the exact period originally proposed agrees well with a recent determination of the X-ray period. The southern sky observations are reviewed, and the significance of the detection of an active galaxy (NGC 5128) is considered for source models and future observations.

INTRODUCTION

Gamma-ray astronomy at very high energies ($\gtrsim 10^{11}$ eV) was last reviewed by Fazio (1973). Accordingly, the present review will be confined largely to results reported since that time. These results have been particularly exciting in that the first sources of very high-energy γ-rays have now been detected by several groups using different techniques. The detection of point sources and not diffuse emission from the galactic plane is significant for galactic structure in that the primary cosmic-ray sources may be identified.

The spectrum of observable electromagnetic radiation from cosmic sources outside the solar system now extends all the way through photon energies of $\gtrsim 10^{12}$ eV. This is approximately three orders of magnitude above the γ-ray energies accessible to current satellite detectors. Thus, for a source like the Crab pulsar NP0532, the integral photon flux is more than three orders of magnitude lower, and detection systems with extremely large area-time factors are required. In fact, for NP0532, the pulsed flux we shall summarize is only about 1 photon/hour if it were recorded by a detector measuring 100 by 100 m square. Such incredibly low fluxes at these highest energies are possible to detect with systems that detect the extensive air showers (EAS) that are produced in the Earth's atmosphere by single primary γ-rays with energies $> 10^8$ eV. For primary energies $\gtrsim 10^{11}$ eV, there are enough ($\sim$ 300) electrons in the shower with energies above the threshold for Cerenkov radiation in the atmosphere that the EAS initiated by a single γ-ray may be detected entirely by optical techniques (Jelley, 1958). The disk of optical Cerenkov photons ($\sim$ 150-m radius, $\sim$ 2-m thickness) produced in such a shower is sufficiently dense ($\sim$ 5 photons m^2) that it may be detected as a $\sim$ 10-ms light flash with a photomultiplier at the focus of a large optical light collector such as the 10-m reflector at Mt. Hopkins Observatory.

The atmospheric Cerenkov technique has been further developed recently by several groups seeking to improve the sensitivity of the early searches for very high energy γ-ray sources. We shall briefly review these experiments and the recent modifications of the Cerenkov technique. These experiments have finally yielded rather convincing evidence for the detection of at least two γ-ray sources above 10^{12} eV. In reviewing these results, it will be clear that the astrophysical implications of these very high-energy γ-ray sources for models of several classes of objects are already quite profound. It is especially interesting, for example, that one of these sources (Cen A) is an active radio galaxy. If nuclei of active galaxies are generally very high-energy γ-ray sources, then perhaps QSO's will be detectable with further increases in sensitivity. Detection of quasars, in turn, would permit testing the cosmological interpretation of QSO red shifts because objects more distant than 3C273 ($z \cong 0.16$) could be attenuated by (γ - ν) pair production of the γ-rays on the optical photon background. Alternatively, it should be pointed out that, because at $E_\gamma < 10^{14}$ eV, the γ-ray mean-free path for attenuation by either γ - ν or γ - p interactions is so long, essentially all objects but the most distant quasars are potentially observable unless there is significant self-absorption in the source.

OBSERVATIONAL TECHNIQUES

The simplest type of Cerenkov receiver, consisting of one or more (in coincidence) optical reflectors pointed directly at a suspected source, has been used in most of the searches for very high-energy γ-rays (e.g., Chudakov et al., 1965; Long et al., 1965; Fazio et al., 1968; Weekes et al., 1972; Porter et al., 1974; Stepanian et al., 1975; and Erickson et al., 1976). These "single-beam" detectors were pointed directly at the suspected sources because the optical Cerenkov radiation expected in the γ-ray-initiated EAS (γ-EAS) is calculated to be (Rieke, 1969) collimated about the primary direction within $\sim 1°$. In fact, most of the searches mentioned above employed the drift-scan technique where the detectors were pointed so that the Earth's rotation caused the object to transit through the (typically $\sim 1°$) detector field of view. In many of the observations of Weekes et al. (1972), as well as others we shall describe below, the candidate source (as well as background) was tracked for maximum exposure. In none of these observations was there active rejection of the background of cosmic-ray-initiated EAS (p-EAS); γ-rays from the source direction were sought as an increase in the total detected rate.

The absolute sensitivity of these various experiments is based on calculations of the Cerenkov light pool expected for γ-EAS. However, even the most complete calculations of the electromagnetic cascade and light distributions (Rieke, 1969), as well as the effects of the geomagnetic field (Weekes and Rieke, 1974), are uncertain to within a factor of ~ 2. Since the results are quite strongly dependent on the exact detector configuration (i.e., atmospheric depth, field of view, etc.), it is also difficult to make relative comparisons of the sensitivity of the various systems. In general, since the detector is operated at a threshold such that the background is entirely due to the flux $F_p \sim K\, E_p^{-1.6}$ of cosmic rays (p-EAS) above energy threshold $E_o \sim E_p$, the detectability of a γ-ray flux or S/N will vary as

$$\sim E^{-\alpha}/\sqrt{F_p} \sim E^{-\alpha + 0.8}$$

where α is the integral spectral index of the γ-ray source. Thus, for $\alpha > 0.8$, the maximum sensitivity should be possible for the lowest γ-ray energy thresholds or the largest optical collector area (directly proportional to E_o). This was, of course, the philosophy behind the single 10-m reflector at Mt. Hopkins with $E_o \sim 1 \times 10^{11}$ eV. It is interesting, however, that the sources detected so far have turned out to (probably) have flat spectra with $\alpha < 0.8$, and thus maximum detectability at the highest energies in the 10^{11} - 10^{13} eV range. Apart from the 10-m reflector results (Weekes et al., 1972), the energy threshold for all the other single-beam searches mentioned above was ~ 10^{12} eV. In all cases, the effective collection area was ~ 2×10^8 cm^2. In addition to the several uncertainties mentioned, the actual values of these parameters are also strongly dependent on zenith angle, sky brightness, and atmospheric transparency. A recent discussion of the sensitivity of atmospheric Cerenkov detection systems is given by Weekes (1976).

When the first single beam-observations (e.g., Chudakov et al., 1965; and Fazio et al., 1968) yielded γ-ray upper limits of $\lesssim$ 1 percent of the detected cosmic-ray flux (typically ~ 10 to 100 min^{-1}), it became clear that some degree of background rejection was needed. O'Mongain et al. (1968) attempted to select γ-EAS by using a fast (~ 3-nsec) coincidence system to favor detection of Cerenkov light from the first few interaction lengths of the shower because the γ-EAS develop faster than p-EAS. The light from this portion of the shower is "focused" (due to increasing index of refraction) in an annulus of radius ~ 120 m and duration < 3 nsec. Although this technique preferentially selects γ-EAS and, in fact, positive effects were reported (e.g., O'Mongain et al., 1968; and Jennings et al., 1974), the gackground p-EAS were still not actively rejected. Apart from the "fast annulus" mentioned, γ-EAS are expected (Zatsepin and Chudakov, 1962) to have a flatter lateral photon distribution than p-EAS, which will be more strongly peaked at the core. Tornabene (1976) has set up an array of Cerenkov detectors and by multicoincidence fast timing (Tornabene and Cusimano, 1968), the EAS core location, arrival direction, and Cerenkov front curvature may be determined, as well as the photon lateral distribution. EAS with peaked distributions at the core may therefore be rejected from the analysis for γ-ray events. This "multiple-beam" technique has the advantage that the individual detectors may have large (~ 5°) fields of view, and a source may be "tracked" with a series of drift scans. It suffers, however, from the systematic difficulty that, in a single

EAS, the lateral distribution can be quite different from the average due to the effects of fluctuations (i.e., the Cerenkov disk can be "spotty"), and thus the core density and location are uncertain. For observations of steady-source fluxes, the technique also requires (as usual) scans on background so that the response to a point source may be determined. Nevertheless, this technique is promising and could be further improved in its cosmic-ray rejection by also incorporating the double-beam technique described below.

Other multiple-beam techniques have been described by Grindlay et al. (1974 and 1976). These have employed multiple photomultiplier detectors at the focus of the Mt. Hopkins 10-m reflector. Because the angular distribution of γ-EAS (especially) will be broadened by geomagnetic effects, a class of EAS were selected by a three-fold coincidence of a 1° triangle of phototubes. Another configuration of six phototubes surrounding a central detector (all with $\sim 1^\circ$ beams) on the reflector optical axis was used to isolate a class of roughly circular shower spots by an anticoincidence of the center with the surrounding channels. Cosmic-ray showers would generally be incident off-axis and would produce elongated Cerenkov images. Both of these techniques were limited, however, since the effective detection area must be smaller (than for single-beam detection) because γ-rays must be incident within $\sim$ 50 m of the reflector for their Cerenkov image to appear circular (within $\sim 1^\circ$).

We conclude our discussion of Cerenkov detection techniques with the so-called "double-beam" technique for actively rejecting p-EAS (Grindlay, 1971a and 1972; and Grindlay et al., 1976 and references therein). This method embodies several of the distinguishing features of γ-EAS already mentioned—the fast timing and relatively broad versus peaked lateral distributions. However, the main feature (originally suggested by experiment (Grindlay, 1971b)), is the detection of the penetrating cores in p-EAS by identifying structure in the angular distribution of the Cerenkov light. The angular structure shows up as follows. Whereas the peak detection of background Cerenkov flashes by two reflectors (with $\sim 1^\circ$ beams), separated by, say, $\sim$ 70 m, occurs when the reflectors are inclined towards each other by $\sim 0.3^\circ$, an enhanced (over the optical beam response) rate is observed as the angle is increased, but not decreased. Furthermore, this relative increase is greatest in the ultraviolet, suggesting that the radiating particles are comparatively close to the detector and that the $1/\lambda^2$ Cerenkov spectrum suffers less atmospheric absorption than at the primary peak of the angular distribution. The natural interpretation of these data was (Grindlay, 1971a) that the primary peak is due to the large number of electrons at the p-EAS maximum and the UV component due to penetrating particles, primarily muons, on axis near the core and detected at the characteristic Cerenkov opening angle of $\sim 1^\circ$. This hypothesis was supported by detailed Monte Carlo calculations of p-EAS (proton through iron primaries) and the Cerenkov production of the penetrating particles. The calculated angular distribution shown in figure 1 (Grindlay, 1974) agrees well with the observations.

Thus, p-EAS may be actively rejected by detection of the penetrating muon cores which are not expected in the (nearly) pure electromagnetic cascades of γ-EAS. This requires an array of at least three spaced Cerenkov detectors: two originally detect the EAS at its maximum, and the third, through an appropriately delayed coincidence, searches for emission from the muon core. Such a system can be pointed at a suspected source either in the drift-scan mode (Grindlay, 1972) or by continuously tracking (Grindlay et al., 1975a and 1976). The double-beam technique is restricted to γ-ray energy thresholds $> 3 \times 10^{11}$ eV (or p-EAS thresholds of $> 6 \times 10^{11}$ eV) for sufficient muon numbers and to minimize the importance of fluctuations. In general, the other multiple-beam techniques mentioned are also restricted to threshold energies above the minimum values because of the importance of fluctuations.

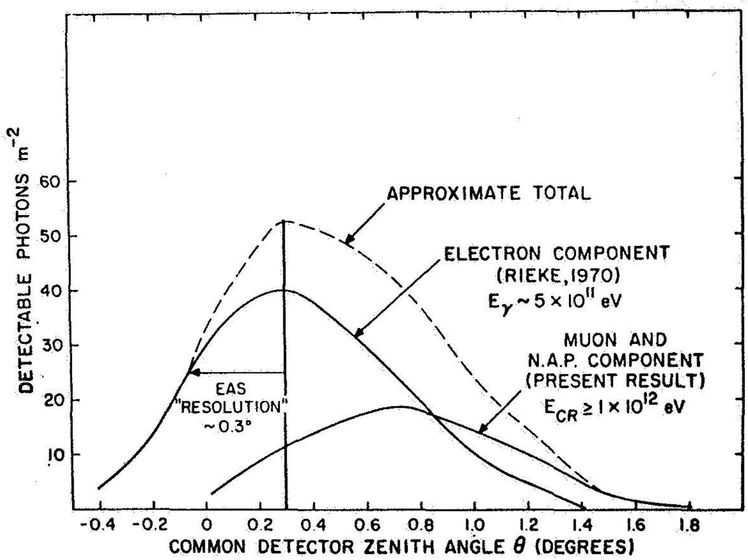

Figure 1. Calculated Cerenkov angular distributions at $R \simeq 40$ m from EAS axis at 2300 m as detected by $\sim 1°$ light receivers.

Finally, we note that all the coincidence techniques described here usually employed random coincidence controls. A number of the single-beam observations (Frazio et al., 1968; Charman et al., 1969; and Weekes et al., 1972) have also used servo systems such that the phototube current or pulse rate remained constant as sky brightness changed. Although this introduces additional noise, it is advisable for noncoincidence experiments (e.g., Weekes et al., 1972).

OBSERVATIONAL RESULTS

Crab Nebula and Pulsar NP0532

We begin with the Crab in our discussion of results since this object has been observed by all groups, and the pulsar NP0532 has now been detected in several of these observations. Since the review by Fazio (1973), the principal results have been obtained on the Crab pulsar at Mt. Hopkins by the SAO group, using the multibeam and double-beam techniques

(Grindlay et al., 1974 and 1976; and Helmken et al., 1975). These observations were all conducted with the 10-m reflector alone (multiple beam) or in coincidence with a remote 1.5-m reflector (double beam). All observations were done in a tracking mode on NP0532 in an effort to observe a pulsed flux; background was not measured off source to determine a steady flux. The final results have been described by Grindlay et al. (1976), and only a summary will be given here. In figure 2, the phase histograms of selected γ-EAS show the Crab pulsations at about the 5σ level. The phase of each EAS arrival time (recorded within 100 μs of absolute UT) was computed by interpolation between phases calculated for the optical pulse every 30 minutes. The accuracy of both the data recording and analysis systems was again verified by recording the optical pulsations of NP0532 with the 1.5-m Tillinghast telescope at Mt. Hopkins (adjacent to the 10-m reflector) and the γ-ray data recording system. The optical-phase histogram is also given in figure 2 (lower section), and the predicted versus observed phases of both the main and secondary pulses are in close agreement.

The most striking feature of these results is that the γ-ray pulsations at $E_0 \gtrsim 8 \times 10^{11}$ eV are time-variable. In December 1973, the pulsar was detected at $\sim 5\sigma$ by double-beam observations (figure 2, middle) in $\sim$ 24 hours of exposure on $\sim$ five nights. The phase of the pulsations is about 6 ms after the main pulse phase and is in a region of the light curve that is increasingly "filled-in" with increasing photon energy. Pulse features at this phase have also been detected occasionally at radio and X-ray energies. (See Grindlay et al., 1976, for references.) In January 1974, however, the pulsations were detected (figure 2, top) again in just a single peak but at a phase $\sim$ 2 ms before the phase of the optical secondary pulse. The effect was present only in the highest pulse-height data or for $E_0 > 10^{12}$ eV, whereas the double-beam pulses were evident over the entire (factor of $\sim$ 10) pulse-height range above the threshold $\sim 8 \times 10^{11}$ eV. Thus, these results provide strong evidence for a very flat spectral component (consistent with $F(> E) \sim A\,E^{\circ}$) of the NP0532 spectrum at the highest energies that is almost certainly not (by virtue of its shape and time variability) an extrapolation of the "low-energy" spectrum through $\sim$ 100 MeV. We return to further discussion of this spectrum below.

Several other groups have also reported phase shifts in positive effects from NP0532. Jennings et al. (1974) reported a $\sim 3\sigma$ pulsed effect at $\gtrsim 10^{12}$ eV that was peculiar in that two peaks (with the $\sim$ 13-ms separation of the optical pulses) were detected at a phase $\sim$ 14 msec before the optical phase. It should be noted that these observations were all conducted after the major Crab glitch of September 1969. In January 1972, Porter et al. (1974) reported a $\sim 4\sigma$ pulsed effect ($E_0 \gtrsim 5 \times 10^{12}$ eV) at the phase of the optical secondary pulse. The effect appeared to be variable on time scales of several days and was, in fact, only detected on the first two of three nights in January and not in February 1972. The observations were conducted with a coincidence wide-angle single-beam Cerenkov system at Mt. Hopkins, and it is interesting to note that the phase is in good agreement with the double-beam observations (Grindlay, 1972; and Grindlay et al., 1976) obtained in November and December 1971. It is also interesting to note that these observations all were within several months of a minor glitch of the pulsar in early October 1971.

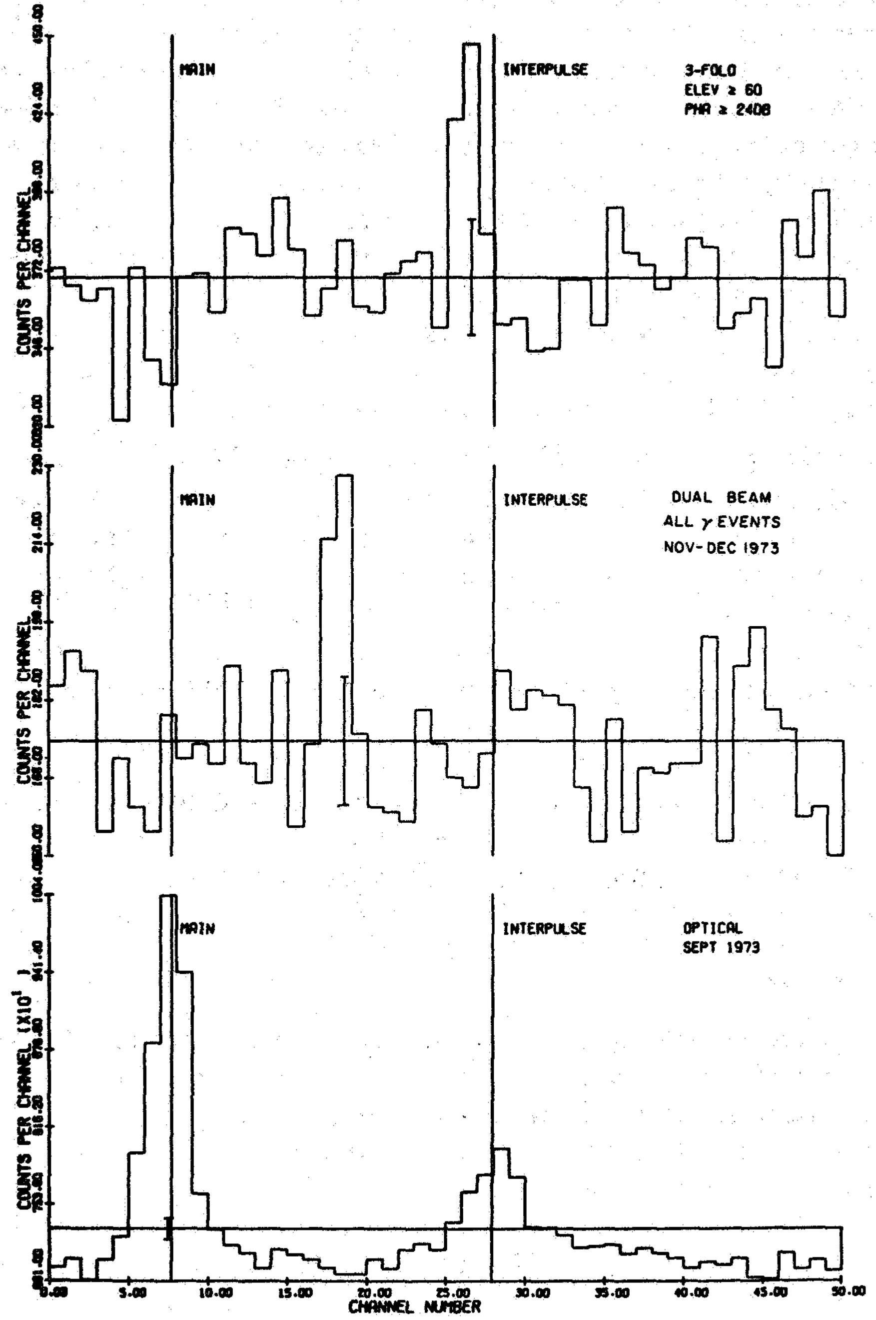

Figure 2. NP0532 phase histograms: multibeam three fold coincidence events in January 1974 (top); nonrejected double-beam events in December 1973 (middle); and optical pulses recorded with 1.5-m Tillinghast telescope and γ-ray data recording system in September 1973 (bottom).

In December 1973, on some of the same nights (e.g., December 1) as the Mt. Hopkins observations, Tornabene (1976) was recording on the Crab with his multidetector Cerenkov system for locating EAS cores and lateral distributions as described above. Analysis of these data is awaited. Because the detection threshold was $\gtrsim 10^{13}$ eV, a careful phase analysis of the selected EAS arrival times could establish or limit the highest energy end of the pulsed spectrum detected at Mt. Hopkins. Since the threshold energy is well above the expected (Grindlay and Hoffman, 1971) break at $\sim 10^{12}$ eV for any steady flux from the Nebula and since apparently no "sky" background scans were made, positive d.c. effects may be unlikely.

Finally, in February and March 1975, Erickson et al. (1976) have also recently found evidence for the detection of NP0532 at $E \gtrsim 10^{13}$ eV. They used a coincidence single-beam system in which two multimirror reflectors were coaligned on the Crab in a tracking mode. Events were defined by requiring the equivalent of four fold (out of 16) coincidences, but no active cosmic-ray rejection was available in the analysis. A phase analysis of the detected events on five nights yielded peaks either just before the optical secondary pulse (March 15) or at ~ 5 ms after the optical main pulse (March 14 and 17). These positive effects were again delayed after another major Crab pulsar glitch on February 4, 1975 (Lohsen, 1975); observations just after the glitch on February 10 and March 4 did not indicate pulsations.

We have plotted most of these Cerenkov results on the Crab pulsar in the spectral plot of figure 3, which also shows the extrapolation of the NP0532 spectrum through ~ 1 GeV (McBreen et al., 1973). Although probably only the double-beam results and the wide-angle results of Porter et al. (1974) are statistically very significant, all of the results taken together present an almost certain detection of NP0532 at energies $\gtrsim 10^{12}$ eV. If this detection is accepted (as the many independent observations require), it is also very likely that the pulsar spectrum at these energies is either flat or conceivably even has a positive slope above 10^{11} eV! It is also necessary to accept the fact that this spectral component of the pulsar is time-variable in both amplitude and phase.

There is evidence, of course, for changes in the pulsar emission that may directly relate to this high-energy γ-ray variability. The possible association of detection at the several phases with glitches has been mentioned above. The detections of December 1973 followed a period of enhanced (on a broad decline) radio emission (Rankin et al., 1974). This possible association of detectable pulsations and general pulsar variability suggests that the enhanced positive d.c. effects reported by Fazio et al. (1972) following the September 1969 and August and October 1971 glitches could, in fact, have been pulsed with variable phase. However, for this not to have been evident in the pulsation analysis, the phase variability must be on a time scale of several days such that pulsations were smoothed out in the less-sensitive single-beam data. Although time scales of days are, in fact, indicated for the phase variations described above, the apparently flat pulsed spectrum could tend to argue against a largely pulsed origin for the short-term enhancements at $\sim 10^{11}$ eV.

In any case, these lowest energy Cerenkov results are most significant for the d.c. flux limits that limit the minimum value of the average magnetic field in the Crab Nebula to

$B_\perp \gtrsim 5 \times 10^{-4}$ gauss. This value was recently calculated by the author using: (a) the Compton-synchrotron model of Grindlay and Hoffman (1971), (b) the "recalibration" of the Cerenkov sensitivities of Weekes (1976), and (c) the most recent X-ray data summarized by Wolfe and Novick (1976), who also derived an upper limit of $B_\perp \leqslant 8 \times 10^{-4}$ gauss from the variation of the size of the Nebula with X-ray energy. Thus, the high-energy γ-ray observations of extended objects like the Crab Nebula (in which Compton synchrotron processes may occur) can limit or establish the source magnetic fields. In the Crab, the best value appears to be $\sim 6 \times 10^{-4}$ gauss, or near the equipartition value.

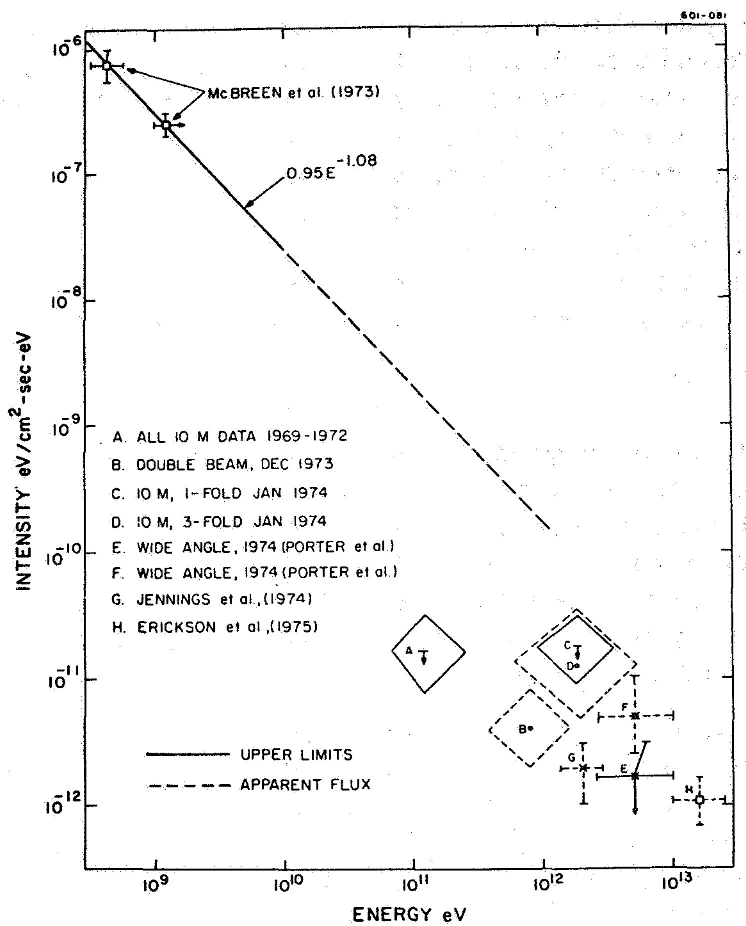

Figure 3. Spectral distribution of recent Cerenkov results on NP0532 pulsations. The extrapolation of the low-energy spectrum is also shown.

Results of Northern Sky Observations

We have emphasized the Crab results because these are the most significant detections of the northern sky observations. A large number of other candidate sources have also been observed, although for none has the exposure been more than a fraction of that on the Crab. Results on a list of 27 objects (primarily supernova remnants, radio galaxies, and quasars) have been reported by Weekes et al. (1972). Most of these were surveyed with the drift-scan technique although several were tracked with the 10-m reflector. All observations were done with the single-beam technique, and no significant positive effects were found, although useful limits on magnetic fields were obtained for several in addition to the Crab.

A total of 41 objects have been observed by the group at the Crimean Observatory (Stepanian et al., 1975) using a drift-scan technique. Although these observations were "single-beam" in that no cosmic-ray rejection was employed and the detectors were pointed directly at the position through which the source would transit, two separate two fold coincidence detectors (1.5-m reflectors) were used. These were offset in right ascension by 2.5° so that the candidate source would transit through the two systems sequentially, thus allowing a check on sky transparency independent of sky brightness or source contributions. These authors have derived the actual distribution of rate fluctuations and have found that the data are well-described (within a few percent) by normal statistics near the zenith. Such checks are especially important for all Cerenkov observations in which source and background are compared. In general, coincidence experiments—even without servoing the phototube singles rate or current on sky brightness—give experimental fluctuations within a few percent of Poisson values (see also discussion of southern-sky results below and Grindlay et al. (1975a)), whereas single-channel systems (e.g., Weekes et al. (1972)) yield $\sigma_{exp}/\sigma_{theor} \simeq 1.15$.

Three possible sources ($\geqslant 3\sigma$) at $E_0 \geqslant 2 \times 10^{12}$ eV were reported by the Crimean group. These are unidentified regions near $\alpha = 05^h\ 15^m$, $\delta = +1°$ and $\alpha = 01^h\ 11^m$, $\delta = +62°$. The first of these may be associated with a source at ~ 100 MeV reported by Frye (1973). The second of these is claimed by the authors to be time-variable as it was not detected by Mt. Hopkins observations (Weekes, 1973) between two periods of possible detection. Clearly further observations are needed. The third source reported is Cyg X-3, an X-ray source with a 4.8-hour period that has been detected up to hard X-ray energies (Pietsch et al., 1976). The drift scans in 1972 and 1973 on this object yielded ~ 3.5σ evidence for emission from Cyg X-3 at the X-ray phases, 0.3 and 0.9. The sum of several drift scans obtained at these phases is shown in figure 4. These data are from just the one of the two offset (in right ascension) detector systems which was at the lowest energy threshold. No effect was seen in the other system at a factor of ~ 2 higher energy, suggesting that, if the source was actually detected, its spectrum (unlike the Crab) must be very steep (with integral spectral index $\geqslant$ 3.2). This would imply detection at the high-energy cutoff of the spectrum. Unfortunately, Stepanian et al. (1975) do not give an estimate of the flux to which the effect in figure 4 corresponds so that comparison with other measurements is difficult. It is curious, though, that the detection of Cyg X-3 claimed by the same group (Vladimirsky et al., 1973) at the time of the September 1972 radio outburst was also only detected in the low-energy system, and yet the flux (given as 2×10^{-10} photons/cm^2 s) is significantly above an extrapolation of the X-ray spectrum. Apparently, during the outbursts, at least a two-component spectrum is required if these effects are confirmed.

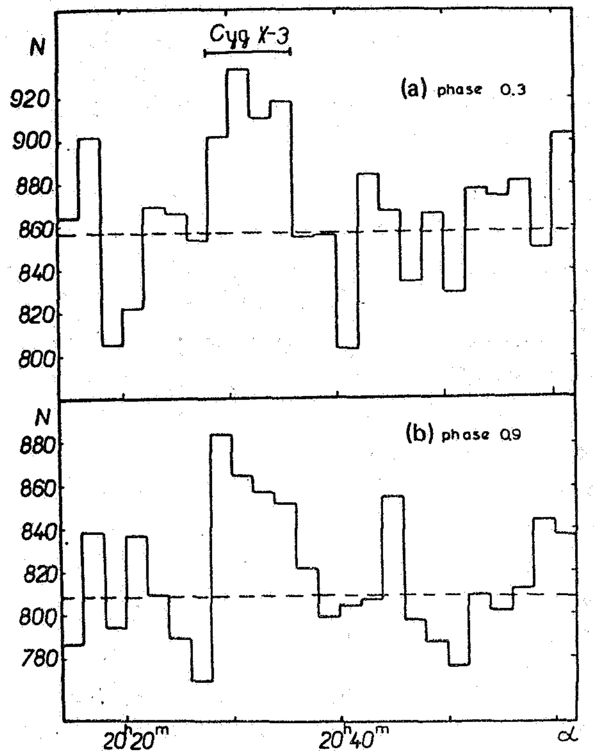

Figure 4. Drift-scan count rates obtained on Cyg X-3 with the first section or lowest energy threshold detection system: (a) for X-ray source phase is 0.300 ± 0.025, and (b) for X-ray source phase is 0.900 ± 0.025; α denotes the right ascension.

Tracking observations of Cyg X-3, with fields of view increased to 2° were conducted from July to November 1974 (Vladimirsky et al., 1975). In August (only) a significant effect ($\sim 4.4\sigma$) was detected, which was primarily at phase 0.35 of the 4.8-hour period and which was also apparently detected by both the low- and high-energy threshold systems. It is especially significant that the authors find the phase of the 1972 to 1973 effect would agree with that for 1974 if a period of 0.199682 day is used, because that is very close to the current best determination (Parsignault et al., 1976) of the X-ray period. This object deserves much further study by other Cerenkov detection groups as well, since there now (this conference) evidence that Cyg X-3 has also been detected at ~ 100 MeV.

A systematic sky survey of a large area of sky is needed to search for previously unsuspected sources of very high-energy γ-rays. Such a program was described by Weekes et al. (1975), and a survey of the entire sky north of declination 0° is in progress. A large fraction has now been covered, with some areas scanned several times. Preliminary analysis of some of the data has not revealed evidence for strong sources. One important addition to the system described by Weekes et al. (1975) was made: a double-beam system has been included. Two 1.5-m reflectors at 188-m separation from the 10-m reflector were operated in twofold coincidence with two pairs of detectors at the focus of the 10-m reflector. The reflectors were pointed towards each other so that EAS were originally detected at their electron maxima. Then, as in all the double-beam observations, a third reflector (in this case, located near the center of the baseline) was operated in coincidence with each of the original twofold coincidence outputs. This channel, biased to detect the penetrating muon component in the UV, then provided the cosmic-ray rejection with an efficiency of ~ 70 percent. In addition to completing the planned survey, a number of observations of the Cyg X-3 region will be conducted.

Results of Southern Sky Observations

Because the center of the galaxy passes directly overhead at southern latitudes (-30°), ground-based Cerenkov observations of the galactic center source region identified at ~ 100 MeV (e.g., Fichtel et al., 1975) are particularly attractive. An opportunity to conduct such observations, as well as a number of other potential very high-energy sources for the first time, became available in 1972. A group at the University of Sydney, Australia, had conducted Cerenkov observations (including an upper limit on the Crab steady flux) in 1968 using the two 7-m-aperture optical reflectors of the stellar intensity interferometer at Narrabri NSW (Hanbury-Brown et al., 1969). A collaborative observation program between this group and SAO was arranged in 1971 since it was recognized that the computer-controlled Narrabri reflectors were ideally suited for tracking-mode double-beam observations. The reflectors and data recording system were thus converted to accomodate the double-beam observations, and a program of observations of 11 candidate sources was carried out during April to July 1972, April to June 1973, and March to April 1974. A complete description of this program and the results have been given by Grindlay et al. (1975b), and we shall give only a brief summary here.

All the observations were conducted with the reflectors separated by 120 m and tracking the source under computer control while maintaining the double-beam pointing geometry as shown in figure 5. The rejection efficiency against p-EAS achieved by the off-axis photomultipliers was ~ 60 percent and the total EAS detection rate was ~ 1 sec^{-1}. Candidate source objects were tracked in between observations of ~ one-half the duration in which comparison sky regions ($\geqslant 2°$ in right ascension to either side of the source) were tracked over the identical ranges of track and elevation angle as the source. The comparison regions were selected for identical sky brightness and, hence, singles rate as the source, and thus no servo of photomultiplier voltages was required.

No significant effects were detected from the galactic center or from possible point sources reported at ~ 100 MeV (Frye et al., 1971). The upper limit for emission from within ~ 1° of the galactic center was $F (\geqslant 3 \times 10^{11}\ eV) < 8 \times 10^{-11}$ photons $cm^{-2}\ sec^{-1}$ and is a factor of ~ 3 above an extrapolation of a π^0 spectrum from the ~ 100 MeV results. This result also requires that any flat inverse Compton component of the galactic center (or plane) flux not extend to $> 10^{11}$ eV without a break in the spectrum. Interesting results were obtained on the three pulsars observed. All showed a "steady-source" excess of $> 2\sigma$ above background, with MP1451-68 actually ~ 3σ positive. However, upon analyzing the data for pulsations at the predicted periods and summing all the data in phase, only the Vela pulsar yielded evidence for pulsed emission, and this only in 1972. A ~ 4σ (single) peak was evident in

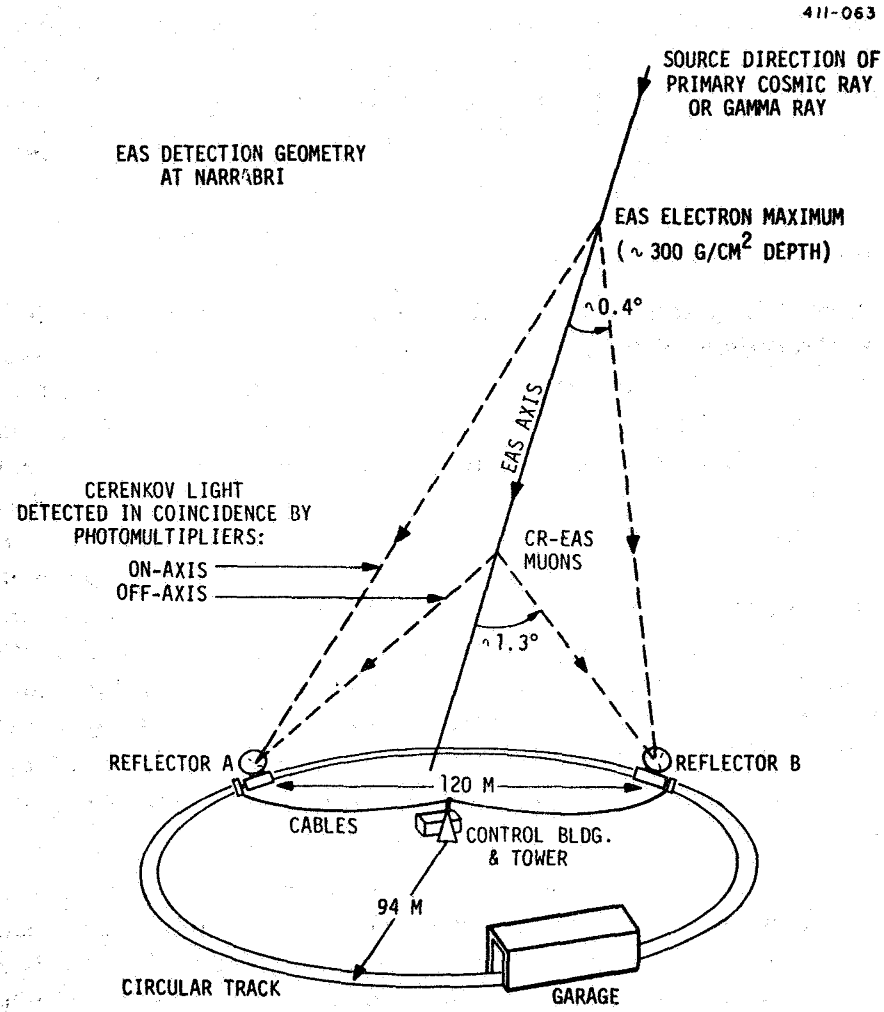

Figure 5. Geometry of Cerenkov detection of EAS by double-beam technique. Application shown is for 7-m optical reflectors of Narrabri Observatory, NSW, Australia.

these data at a phase within 3 ms before the (de-dispersed) radio pulse phase (Grindlay et al., 1975b). This single peak contrasts with the double-peaked pulse structure found at ~ 100 MeV (Thompson et al., 1975) although it is similar to the Crab pulsar results at comparable energies (figure 2). Thus, it is striking that just as the Crab and Vela pulsars show almost identical double-pulsed light curves at ~ 100 MeV, they may also be very similar (single pulse) at very high energies. Because a very much smaller effect, and only at the highest Cerenkov pulse heights (or primary energies), was detected in the 1973 observations, the

Vela spectrum may be like the Crab pulsar also in being very flat and time-variable. Unfortunately, the single 4σ detection (1972) of Vela renders these results much less certain statistically than for the Crab. However, one may speculate that, if pulsars produce very high-energy γ-ray sources with variable phase, perhaps the "steady" effects on MP1451-68 (and, although only $\sim 2\sigma$, also on PSR1749-28) are actually pulsed with phase variations occurring within a few days or less.

The final result we shall summarize was obtained on the radio galaxy Cen A (NGC5128). This is the closest ($\sim$ 5 Mpc) of three active galaxies (including the QSO 3C273) observed and is especially interesting for its compact source structure in the nucleus detected through hard X-ray energies. The source was detected at 2 to 3σ in each of the three observing periods for a total detection at the $\sim 4.6\sigma$ level of an average flux

$$F(\geqslant 3 \times 10^{11} \text{ eV}) \simeq 4.4 \times 10^{11} \text{ photons cm}^{-2} \text{ sec}^{-1}$$

Complete details are given by Grindlay et al. (1975a). About one-half of the data were recorded with pulse-height (spectral) information, and the spectrum of the observed γ-ray flux is consistent with a spectrum that is flatter than the background cosmic-ray spectrum up to a break at $\sim 3 \times 10^{12}$ eV. Such a spectrum and, indeed, the entire detected flux can be understood in terms of a Compton-synchrotron model of the nucleus of NGC5128 (Grindlay, 1975) in which the $\sim 10^{12}$ eV γ-rays are produced by inverse Compton scattering of an X-ray synchrotron electron spectrum (through electron energies $\sim 10^{13}$ eV) on the optical/X-ray synchrotron photons. The synchrotron spectra were calculated assuming that the compact sources are self-absorbed in the radio regime. The very high-energy γ-ray flux then provides the additional constraint necessary to solve for both the source angular diameter and the magnetic field. The complete source spectrum model requires a two-component source whose diameters are then calculated to be $\sim$ 0.01 and 0.2 pc and magnetic fields $\sim$ 2 and $\sim$ 0.01 gauss, respectively. The high-energy γ-rays are produced in the larger component, which may be a cosmic-ray source surrounding the smaller source in the nucleus of NGC5128.

CONCLUSIONS

After a long beginning, it now seems that ground-based γ-ray astronomy has begun to yield positive results of great astrophysical interest. The early upper limits on steady emission from objects such as the Crab Nebula were themselves of fundamental importance for establishing limits to pion production and to the necessity of continuing acceleration of electrons (Chudakov et al., 1965) and for important limits on the magnetic field (Weekes et al., 1972) in the Crab. With solid evidence for pulsed emission from NP0532 at $\geqslant 10^{12}$ eV (that is, variable in phase and amplitude), pulsar emission and particle acceleration theories are additionally constrained. Consideration of these theories suggests, for example, (Grindlay et al., 1976) that the very high-energy pulsed spectrum may arise from bremsstrahlung of a cosmic-ray beam (accelerated off the neutron star) as it traverses relatively dense matter accumulated at the "force-balance" radius (Roberts and Sturrock, 1973) relatively far from the star (thereby also escaping pair conversion in the magnetic field). The possible association of NP0532 emission (at $> 10^{11}$ eV) and pulsar glitch activity might then be understood, because glitches may arise when matter from this force balance shell is released into the Nebula. Alternatively, Cheng et al. (1976) have demonstrated that the observed ($\sim 90°$) phase shift suggests that the very high-energy pulsed flux can arise from a spark-gap region near the light cylinder where a phase shift is expected from the relativistic velocity of the magnetosphere.

The results obtained by the Crimean group, particularly on Cyg X-3, are of great interest. If the Cyg X-3 variable emission, primarily at X-ray phase ~ 0.3, can be confirmed, it is of major significance for theories of this very unusual X-ray source. None of the currently proposed theories for this object would directly predict 10^{12} eV γ-rays. A γ-ray flux could arise from (presumably, by inverse Compton or bremsstrahlung processes) production of $> 10^{12}$ eV cosmic rays in this type of source. The evidence for the reality of the periodic $\gtrsim 10^{12}$ eV emission from Cyg X-3 reported by Vladimirsky et al. (1975) is greatly strengthened by the fact that the trial best-fit period they proposed ($0^d.199682$) now turns out to be the best-fit X-ray period (Parsignault et al., 1976).

The most important result of the southern-sky observations is the detection of $> 10^{11}$ eV γ-rays from the first extragalactic source, Cen A. This result and the model (Grindlay, 1975), which accounts for the flux and entire NGC5128 spectrum by inverse Compton scattering in compact synchrotron sources in the nucleus, provides new insight into the physics of active galaxies. The results suggest that other objects of this type may also be detected. The other key results of the Australian observations were the possible detection of pulsed emission from the Vela pulsar PSR0833-45, with pulse profile and variability similar to that of the Crab pulsar, and the lack of detectable emission from the galactic center or galactic plane.

It is useful to summarize the major conclusions reached by very high-energy γ-ray astronomy to date:

1. Gamma-ray sources above 10^{11} eV appear to be point sources or compact objects which may usually be time-variable and are accelerating cosmic rays. The physical conditions (i.e., magnetic fields, energy densities, etc.) in these objects are revealed by the very high-energy γ-ray fluxes or upper limits.

2. Pulsars, at least the Crab and possibly Vela and others, produce very high-energy spectra of pulsed γ-rays that are variable in phase and amplitudes. These spectra are almost certainly not an extrapolation of the low-energy pulsar spectrum and may arise from the primary particles (rather than their cascades) accelerated by the pulsar.

3. All of the possible source fluxes or upper limits reported are $\lesssim 5$ percent (usually < 1 percent) of the background cosmic-ray rate detected. While the strongest classes of sources may not yet have been detected, the high background problem and results to date point out the necessity that future observations be either double-beam or multibeam or in some way actively reject the cosmic-ray background.

The final point should be reemphasized. Despite the very promising progress achieved in ground-based γ-ray astronomy, a major increase in sensitivity is needed. It is very likely that an extension of the double-beam technique to a multireflector EAS array could achieve this.

REFERENCES

Charman, W. N., J. V. Jelley, and R. W. P. Drever, 1969, (Proc. 11th Intl. Cosmic Ray Conf., OG-11), Budapest.

Cheng, A., M. Ruderman, and P. Sutherland, 1976, *Ap. J.*, **203**, p. 209.

Chudakov, A. E., V. L. Dadykin, V. I. Zatsepin, and N. M. Nesterova, 1965, *Cosmic Rays*, (Proc. P. N. Lebedev Inst., No. 26), p. 99.

Erickson, R. A., R. K. Fickel, and R. C. Lamb, 1976, *Ap. J.*, in press.

Fazio, G. G., H. F. Helmken, E. O'Mongain, and T. C. Weekes, 1972, *Ap. J. Letters*, **175**, p. L117.

Fazio, G. G., H. F. Helmken, G. H. Rieke, and T. C. Weekes, 1968, *Nature*, **220**, p. 892.

Fazio, G. G., 1973, *Gamma Ray Astrophysics*, NASA, SP-339, p. 153.

Fichtel, C. E., R. C. Hartman, D. A. Kniffen, D. J. Thompson, G. F. Bignami, H. Ögelman, M. F. Özel, and T. Tümer, 1975, (Proc. 14th Intl. Cosmic Ray Conf., No. 1, Munich), p. 29.

Frye, G. M., P. A. Albats, A. D. Zych, J. A. Staib, V. D. Hopper, W. R. Rawlinson, and J. A. Thomas, 1971, *Nature*, **233**, p. 466.

Frye, G., 1973, IAU Symp. No. 55, Madrid.

Grindlay, J. E., 1971a, *Smithsonian Astro. Obs. Special Report*, No. 334.

Grindlay, J. E., 1971b, *Nuovo Cimento*, **2B**, p. 119.

Grindlay, J. E., 1972, *Ap. J. Letters*, **174**, p. L9.

Grindlay, J. E., 1974, *Phys. Rev. D.*, **11**, p. 517.

Grindlay, J. E., 1975, *Ap. J.*, **199**, p. 49.

Grindlay, J. E. and J. A. Hoffman, 1971, *Ap. J. Letters*, **8**, p. 209.

Grindlay, J. E., H. F. Helmken, and T. C. Weekes, 1974, (ESLAB Symposium on Gamma Ray Astronomy, Frascati, Italy), p. 301.

Grindlay, J. E., 1976, *Ap. J.*, **209**, p. 592.

Grindlay, J. E., H. F. Helmken, R. H. Brown, J. Davis, and L. R. Allen, 1975a, *Ap. J. Letters*, **197**, p. L9.

Grindlay, J. E., 1975b, *Ap. J.*, **201**, p. 82.

Hanbury-Brown, R., J. Davis, and L. R. Allen, 1969, *M. N. R. A. S.*, **146**, p. 399.

Helmken, H. F., J. E. Grindlay, and T. C. Weekes, 1975, (Proc. 14th Intl. Cosmic Ray Conf., No. 1, Munich), p. 123.

Jelley, J. V., 1958, *Cerenkov Radiation and Its Applications*, New York, Pergamon Press.

Jennings, D. M., G. White, N. A. Porter, E. O'Mongain, D. J. Fegan, and J. White, 1974, *Nuovo Cimento*, **20B**, p. 71.

Lohsen, E., 1975, *Nature*, **258**, p. 689.

Long, C. D., B. McBreen, N. A. Porter, and T. C. Weekes, 1965, (Proc. 9th Intl. Cosmic Ray Conf., No. 1), London, p. 318.

McBreen, B., S. E. Ball, Jr., M. Campbell, K. Greisen, and D. Koch, 1973, *Ap. J.*, **184**, p. 571.

O'Mongain, E. P., N. A. Porter, J. White, D. J. Fegan, D. M. Jennings, and B. G. Lawless, 1968, *Nature*, **219**, p. 1348.

Parsignault, D. R., E. Schreier, J. Grindlay, and H. Gursky, 1976, *Ap. J. Letters*, in press.

Pietsch, W., E. Kendiziorra, R. Stanbert, and J. Trumper, 1976, *Ap. J. Letters*, **203**, p. L67.

Porter, N. A., T. Delaney, and T. C. Weekes, (ESLAB Symposium on Gamma Ray Astronomy, Frascati, Italy), p. 295.

Rankin, J. M., R. R. Payne, and D. B. Campbell, 1974, *Ap. J. Letters*, **193**, p. L71.

Rieke, G. H., 1969, *Smithsonian Astro. Obs. Special Report*, No. 301.

Roberts, D. H. and P. A. Sturrock, 1973, *Ap. J.*, **181**, p. 161.

Stepanian, A. A., B. M. Vladimirsky, Yu.I. Neshpor, and V. P. Fomin, 1975, *Astrophys. and Space Sci.*, **38**, p. 267.

Thompson, D. J., C. E. Fichtel, D. A. Kniffen, and H. Ögelman, 1975, *Ap. J. Letters*, **200**, p. L79.

Tornabene, H. S., 1976, contributed paper, this conference.

Tornabene, H. S. and F. J. Cusimano, 1968, *Can. J. Phys.*, **46**, p. S81.

Vladimirsky, B. M., A. A. Stepanian, and V. P. Fomin, 1973, (Proc. 13th Intl. Cosmic Ray Conf., No. 1, Denver), p. 456.

Vladimirsky, B. M., Yu. I. Neshpor, A. A. Stepanian, and V. P. Fomin, 1975, (Proc. 14th Intl. Cosmic Ray Conf., No. 1, Munich), p. 118.

Weekes, T. C., G. G. Fazio, H. F. Helmken, E. P. O'Mongain, and G. H. Rieke, 1972, *Ap. J.*, **174**, p. 165.

Weekes, T. C., 1973, (Proc. 13th Intl. Cosmic Ray Conf., No. 1, Denver), p. 456.

Weekes, T. C., 1976, submitted to *II. Nuovo Cimento.*

Weekes, T. C. and G. H. Rieke, 1974, (ESLAB Symposium on Gamma Ray Astronomy, Frascati, Italy), p. 287.

Weekes, T. C., H. F. Helmken, and E. Horine, 1975, (Proc. 14th Intl. Cosmic Ray Conf., No. 1, Munich), p. 133.

Wolfe, R. S. and R. Novick, 1976, *Nature*, in press.

Zatsepin, V. I. and A. E. Chudakov, 1962, *Soviet Phys. -JETP*, **15**, p. 1126.

RADIATION MECHANISMS AND MAGNETOSPHERIC STRUCTURE OF PULSARS*

P. A. Sturrock and K. B. Baker
Institute for Plasma Research
Stanford University, Stanford, California 94305

ABSTRACT

This article outlines the chain of thought which has led to a model of pulsars now being investigated at Stanford University. Key early considerations were those which led to the identification of pulsars with neutron stars and the Goldreich-Julian (1969) model of pulsar magnetospheres. Another important step was the recognition that, in a pulsar magnetosphere, a high-energy γ-ray may annihilate to produce an electron-positron pair. Arguments advanced by Scargle and Pacini (1971) suggest that pulsar magnetospheres may contain large masses of plasma, a suggestion which has important implications concerning the structure of the magnetosphere.

Observational data seems to support a magnetosphere model based on the Scargle-Pacini idea rather than the Goldreich-Julian (1969) model. The cascade process resulting from pair creation enables one to interpret the X-ray emission from the Crab and Vela pulsars as synchrotron radiation. On the other hand, the optical radiation from the Crab pulsar is best understood as coherent curvature radiation. Radio emission is interpreted as curvature radiation produced by charge bunches moving along magnetic-field lines. Certain tests of this model are proposed.

INTRODUCTION

I am very sorry that Franco Pacini could not be here today to give this talk. Franco would no doubt have had much to say about the origin of cosmic rays. By contrast, I have very little to say on this topic, and I shall be concerned primarily with the problem of the magnetospheric structure of pulsars and of radiation mechanisms.

*Presented by P. A. Sturrock

I think that virtually all scientists now believe that pulsars are rotating neutron stars, but, in the early days, there was a competing hypothesis that they were pulsing white dwarfs. Some of you may be curious to ask, "What ever happened to white dwarfs?." Table 1 shows why white dwarfs were ousted in favor of neutron stars.

Table 1
Is a Pulsar a Neutron Star or a White Dwarf?

	NS	WD
1. Period in range 0.03 to 3.7 s	√	X
2. Period stable to one part in 10^9	√	?
3. Period increases	√	X?
4. No optical photospheric radiation	√	X
5. Two pulsars in supernova remnants	√	X

It is believed that white dwarfs could not vibrate as rapidly as 0.03 seconds and that white dwarfs would not have a stability of the oscillation as good as one part in 10^9. If pulsars were pulsing white dwarfs, we would expect their period to decrease because stars become denser with age just as we all do. One would expect to be able to observe the objects (or some of them) by their photospheric emission. One would not expect to find pulsars in supernova remnants if they were white dwarfs. Now, of course, one fact will not destroy a theory or a theorist, but an array of five facts as good as these will bring any theorist into line.

Once that argument was settled and it was accepted that pulsars are neutron stars, the next question was where the radiation is produced. There were, and perhaps still are, two schools of thought. One school proposes that the radiation is produced at the light cylinder. T. Gold, one of the first, published a paper in 1969 (Gold, 1969) developing the idea of streams of plasma flowing out along field lines (figure 1). When they get to the light cylinder where $\omega r = c$, they must be moving at the speed of light, and they will beam radiation in the forward direction. In 1971, an improved model was developed by Professor Smith, who is now the director of the Royal Greenwich Observatory (Smith, 1971 and 1973). However, I have not seen much published from this school in recent years. Some of my colleagues feel that this particular question is now settled: that radiation is not produced at the light cylinder, it is actually produced near the polar cap. This school of thought began with two radio observers, Radhakrishnan and Cooke (1969), who also published in 1969. The diagram in their first paper is shown in figure 2. It is assumed that radiation is produced at two cones at the magnetic polar caps. Thus, there are, in fact, two lighthouse beams which swing around with the star.

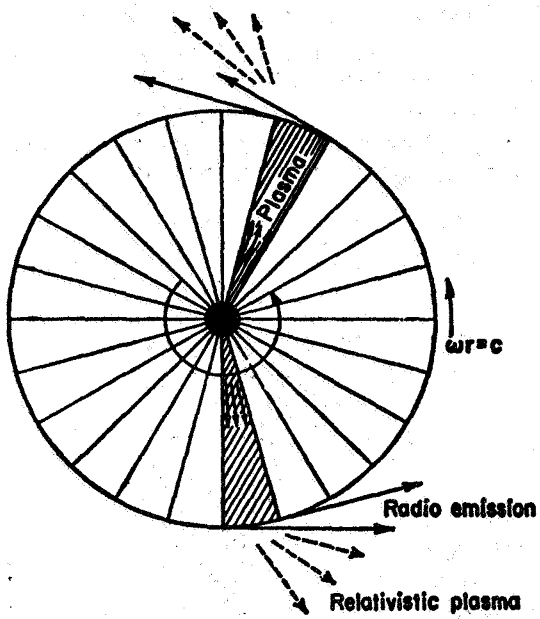

Figure 1. Light-cylinder model for emission of radio energy and relativistic gas. The neutron star has a corotating magnetosphere reaching out to the circle at which ωr, the peripheral speed, is close to the speed of light. Plasma emitted on the surface by nonthermal processes will be accelerated to relativistic speeds and will be flung out of the magnetosphere (Gold, 1969).

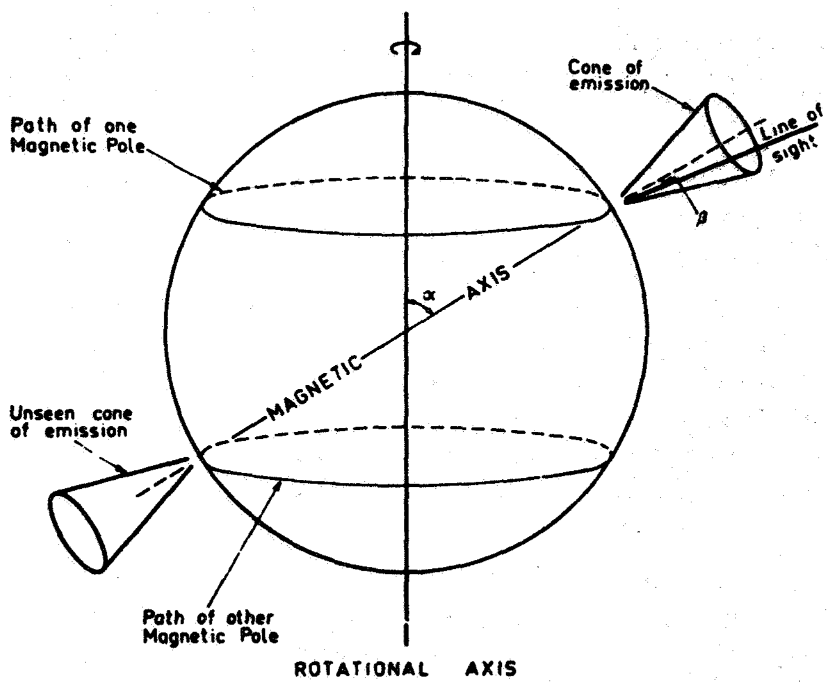

Figure 2. The geometry of polar-cap model: closeup view of neutron star with emission regions near the surface at the magnetic poles. The dipole-field lines give a preferred direction to each part of the emission region producing the linear sweep of polarization observed in a radio pulse (Radakrishnan and Cooke, 1969).

If an observer is lucky, he may be in the line of fire of one of these beams and see one pulse per rotation. If he is extremely lucky, so that the rotation axis is almost orthogonal to the magnetic axis, he may see two pulses. There are, in fact, a few pulsars which do show both the pulse and what is called an "interpulse."

Also in 1969, a very important paper was published by Goldreich and Julian (1969). (It is a rare theoretical paper which leads to an editorial in the New York Times.) This paper outlined a model for the structure of a pulsar magnetosphere. The authors showed that the electric fields produced by induction are so strong that there must be plasma in the vicinity of the star drawn off by field emission. They concluded that the magnetic-field lines could be closed only out to the light cylinder and must be open beyond that point. The plasma flow constitutes a "pulsar wind," similar to the solar wind.

MAGNETOSPHERIC STRUCTURE

Thus, there were two excellent ideas: that of Radhakrishnan and Cooke (1969) and that of Goldreich and Julian (1969), which together led to a prediction. One could calculate the expected pulse width of the beam produced at the polar cap of a pulsar and compare it with the observational data. However, when this is done, there is no fit between the mean pulse width expected for a given period on the basis of that model and what is actually observed (figure 3). This seems to imply that one of the two ideas is incorrect. Either radiation is not produced as proposed by Radhakrishnan and Cooke (1969) or the magnetosphere does not have the structure proposed by Goldreich and Julian (1969). I think the answer to that question comes from considering the braking index of a pulsar. The torque exerted on a pulsar will, we expect, vary as a power of the rotation frequency:

$$\Theta = - I \frac{d\omega}{dt} \propto \omega^n \tag{1}$$

We can, in fact, determine n from observational data if we know the period, the derivative of the period, and the second derivative of the period, which we do for the Crab:

$$n = \frac{\omega \ddot{\omega}}{\dot{\omega}^2} \tag{2}$$

Goldreich and Julian (1969) made the definite prediction that $n = 3$. Data for the Crab is still not certain, but it seems to be in the range 2.2 to 2.6 (Boynton et al., 1972).

In any case, it appears that there is a clear-cut discrepancy between prediction and observational data, suggesting that the idea of Radhakrishnan and Cooke (1969) may be correct but that of Goldreich and Julian (1969) is somehow probably incorrect. Where did it go wrong? A possible suggestion arose from a paper published by Scargle and Pacini (1971). They noted that the 1969 glitch of the Crab pulsar was apparently associated both with the disturbance of a wisp in the Crab Nebula and with a change in the dispersion measure. They proposed, therefore (contrary to most current thoughts), that a glitch is a magnetospheric phenomenon

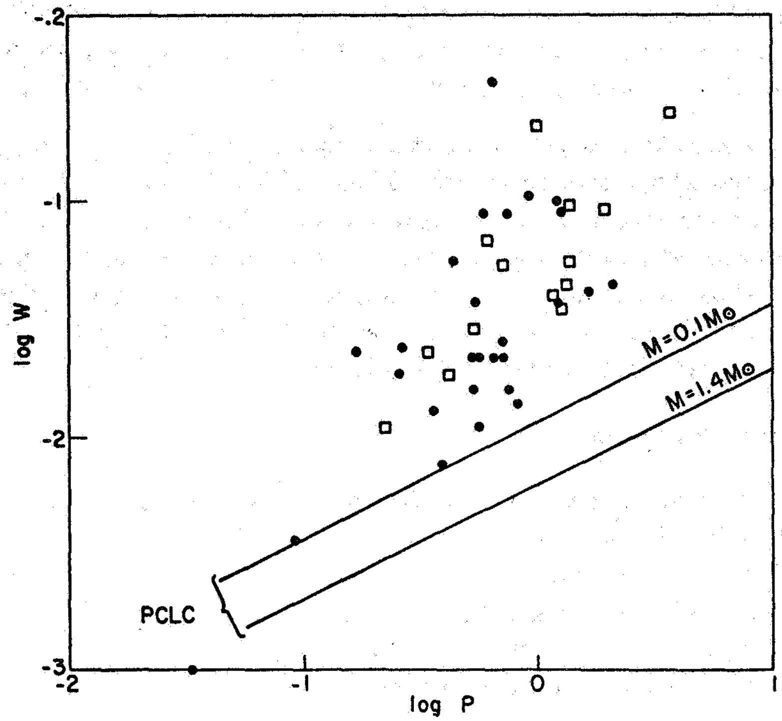

Figure 3. Pulse width, W, versus period, P, distribution of pulsars. The curves show the mean expected relationship for the PCLC model (polar-cap radiation, lines opening at the light cylinder) for the star masses indicated (● = S type; □ = C, D type).

involving an instability which itself involves a large mass of plasma trapped in a pulsar magnetic field. Their estimate was that mass must be about 10^{21} grams. Dave Roberts and I looked into this possibility, and we found that such a large mass could probably not be contained in the pulsar magnetosphere. Either gravitational force or centrifugal force would disrupt the equilibrium situation unless there was a singular situation with the gas collecting at the "force-balance" or "corotation" position where gravitational and centrifugal forces just balance. Suppose that gas were to be ejected into the magnetic field either by evaporation from the star or by ionization of neutral gas being accreted by the star. If a lot of gas collects and cools down at small radii, it will fall to the surface. If, on the other hand, it collects at large radii, it will pull open the field lines, the end result being that the largest closed-field line comes at the force-balance radius rather than at the light cylinder.

We can express this radius (of the Y-type neutral point) in terms of the mass of the star and the period of the star:

$$\omega^2 R_{FB} = \frac{GM}{R_{FB}^2} \tag{3}$$

which leads to

$$R_{FB} = 10^{-2.9} M^{1/3} P^{2/3} \qquad (4)$$

In the inner region, the magnetic field is approximately dipolar and drops off as r^{-3}, but, once the field lines open up, the field will drop off as r^{-2}. This change in the magnetospheric structure also produces a change in the braking index (Roberts and Sturrock, 1972), which we calculated to be $n = 2.33$. This value is in reasonable agreement with the known data. The opening of the field lines at R_{FB} also means a larger polar cap, and, hence, a different dependence of the pulse width on the period (Roberts and Sturrock, 1972):

$$W = 10^{1.1} M^{-1/6} R^{1/2} P^{2/3} \qquad (5)$$

This expression involves the mass of the star, but for masses in the range 0.1 to 1.4 M⊙, there is a reasonable fit with the data (figure 4). We note that different orientations of the spin axis and magnetic axis can give rise to values of the pulse period either larger or smaller than the value given by equation 5.

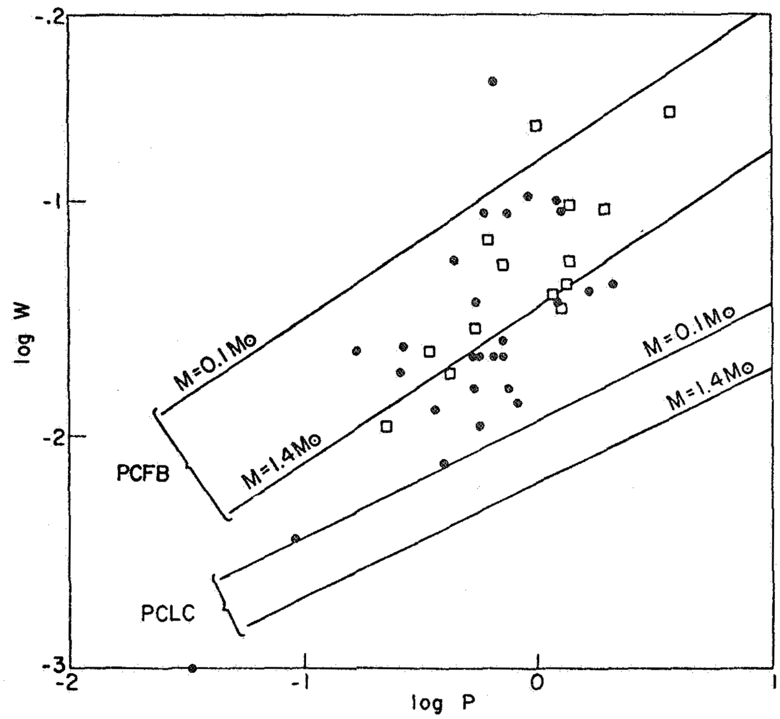

Figure 4. Pulse width, W, versus period, P, distribution of pulsars. The curves repeat those of figure 3 and also show the mean expected relationship for the PCFB model (polar-cap radiation, lines opening at the force-balance radius) for the star masses indicated (● = S type; □ = C, D type).

RADIATION

Now, I want to turn to the more important questions: Where and how is the radiation produced, and how intense is it? First, I would draw your attention to the fact that a wind such as the solar wind will cause magnetic-field lines to spiral in the equatorial plane. A field pattern such as this has nonzero curl, so that there must be currents flowing to maintain this field pattern. If these currents are flowing along field lines, they must originate in, or flow into, the polar caps. For the simple case that the dipole axis is parallel to the spin axis, at each polar cap, there will be an inflow of current at the center and an outflow at the edges, or vice versa. If intense currents are leaving the polar caps, one expects that electric fields somehow develop in that region to draw off the currents. We can estimate the current and the charge density and, hence, estimate the voltage required; for the Crab pulsar, which probably has a field strength of order 10^{12} gauss and a rotation period of about 33 ms, we find that the voltage must be of order 10^{16} volts. If any ions leave part of the polar cap, they may accelerate to that enormously high voltage, and, if they escape into interstellar space, they might contribute significantly to the cosmic-ray intensity. On the other hand, electrons will radiate, because they are moving along curved magnetic-field lines and have a smaller mass, and the radiation reaction becomes so intense that it limits the electron energy to about 10^{14} volts. Hence, if half the rotational power goes to driving the ion flow and the other half goes to driving the electron flow, almost all the power that goes into driving electrons will go into an intense flux of γ-rays of energy about 10^{12} eV.

Our model has now advanced to the point that we have a structure for the magnetosphere, and we have an elementary picture of where the acceleration occurs. But, what we now find is that we have produced an intense source of very high-energy γ-rays. Perhaps participants in this conference may be happy about that, but radio astronomers are not really satisfied because they assert that all pulsars produce radio emission. In addition, one pulsar produces optical emission and perhaps two produce X-rays, whereas the only radiation produced by the model at this stage is a flux of γ-rays.

The missing link (Sturrock, 1971) is believed to be the following: If a high-energy γ-ray is moving transverse to an intense magnetic field, it will annihilate to produce an electron-positron pair. The γ-ray energies in the Crab, for example, are so high and the field strength is so high that this annihilation will occur very rapidly. When it occurs, there are two important consequences. One is the production of secondary particles—electrons and positrons—moving with nonzero pitch angles which therefore will emit by the synchrotron process. This may give rise to the optical or X-ray or γ-ray part of the spectrum. The important point is that, whereas we began with a stream of charge of just one sign (electrons), we now have a stream with particles of opposite sign—positrons. Some of these will tend to move back toward the surface of the star under the action of the electric field, and this will create a two-stream situation which plasma physicists know is potentially unstable. If the instability should occur, it will give rise to bunching of the charges. It is precisely this bunching that one needs to give rise to radio emission, because single particles flowing along curved field lines will give negligible radio emission, but bunches of charge will give significant radio emission.

One may estimate the spectrum to be expected from this model (Roberts et al., 1973). With quite a reasonable assumption about the degree of bunching of the electron beam, one can fit the radio data. The simplest estimate of the X-ray spectrum gives a $\nu^{-1/2}$ law, but, when one takes full account of the cascade process, this becomes modified to a ν^{-1} law, which is a better fit to the observed data. The estimates are fairly sensitive to the mass of the star. However, an important point is that the model does not allow γ-rays of energy 10^{12} eV to escape from the polar-cap regions. Hence, the observations by Grindlay (1972) are hard to understand. Second, the emission is self-absorbed at 2- or 3-keV energy so that there is no way to explain the optical emission on the basis of this model. In fact, the optical pulse shape has such a sharp cusp that it must be produced by particles of energy 10^8 eV or more. This means that the magnetic-field strength must be less than 10^6 gauss if the radiation is being produced by the synchrotron mechanism. But, the field has this low a value only near the light cylinder. The difficulty with assuming the radiation to be produced near the light cylinder is again that the cusp is so sharp that it would require emission in a very small region of the light cylinder. I am not saying that these requirements cannot be met, but there is no current model that satisfactorily meets them.

One way out of this difficulty was proposed by Steve Turk, a student who worked with me and who, unfortunately, died 3 years ago. His suggestion was that each primary electron gives rise to a stream of γ-rays, each γ-ray producing an electron-positron pair, so that a string of secondary particles form near each primary electron. A very small separation of these particles, due to a quite small electric field, will mean that the electrons and positrons will behave independently so that one can obtain coherent radiation in this model even in the optical part of the spectrum. Hence, we propose that the optical radiation from the Crab may be coherent curvature radiation. The observational data yield a spectrum which peaks at little less than 10^{15} Hz at a luminosity of about 10^{18} ergs per Hz per second. One can fit this data approximately with a star of mass 0.4 solar masses, which is also the mass indicated by the power budget of the Crab Nebula (Sturrock et al., 1975).

DISCUSSION

To conclude, we shall review the properties which we attribute to pair creation:

1. We believe that pair creation explains the period-age distribution. The point is that, as a star slows down, it eventually reaches a period (for a given field strength and mass) for which pair creation will no longer occur. In that case, we believe that bunching will no longer occur so that there will no longer be radio emission (Sturrock et al., 1976).

2. We attribute the coherent RF radiation to pair creation, as discussed earlier.

3. We believe that the optical radiation from the Crab is coherent and is due essentially to the pair-creation process.

4. We believe that X-ray emission from the Crab and Vela pulsars is due to pair creation. [I would add that, if the new observations of radiation from 1747 and 1818 are correct, this γ-ray emission (which is of fairly low energy) may be due to pair creation.]

5. Based on analysis of the radio data (which is not unambiguous), there appears to be a large flux of low-energy particles into the Crab Nebula. The current model does lead to a large particle flux (mainly of positrons and electrons) into the Nebula.

6. The precursor of the Crab may be due to the possibility that radio emission occurs not only where electrons leave the polar cap (EPZ), but also where ions leave the polar cap (IPZ). Because the Crab is the only pulsar spinning rapidly enough for pair creation to occur in the IPZ, it is the only pulsar for which this process would occur. This interpretation suggests an explanation of the curious fact that the Crab is the only pulsar with a precursor.

There are still some observations to be made that I think would help to resolve some of the remaining outstanding equations. I think that it is most desirable to try to determine whether the optical and the X-ray parts of the spectra of the Crab pulsar are continuous or whether they are quite distinct. This can be determined by trying to extend the optical spectrum into the UV or by trying to extend the X-ray spectrum to lower energies. It would also be valuable to try to determine the polarization of the X-ray emission from the Crab pulsar because the model I am proposing suggests that the E-vector of the X-ray emission should be orthogonal to the E-vector of the optical emission. On the other hand, if they are both produced by the same process (e.g., if they are both synchrotron radiation), they should both have electric vectors in the same direction.

REFERENCES

Boynton, P. E., E. J. Groth, D. P. Hutchinson, G. P. Nanos, Jr., R. B. Partridge, and D. T. Wilkinson, 1972, *Ap. J.*, **175**, p. 217.

Gold, T., 1969, *Nature*, **221**, p. 25.

Goldreich, P., and W. H. Julian, 1969, *Ap. J.*, **157**, p. 869.

Grindlay, J. E., 1972, *Ap. J. Letters*, **174**, p. L9.

Radhakrishnan, V., and D. J. Cooke, 1969, *Astrophys. Letters*, **3**, p. 225.

Roberts, D. H., and P. A. Sturrock, 1972, *Ap. J. Letters*, **173**, p. L33.

Roberts, D. H., P. A. Sturrock, and J. S. Turk, 1973, *Ann. N.Y. Acad. Sci.*, **224**, p. 206.

Scargle, J. D., and F. Pacini, 1971, *Nature Phys. Sci.*, **232**, p. 144.

Smith, F. G., 1971, *Nature Phys. Sci.*, **231**, p. 191.

Smith, F. G., 1973, *Nature*, **243**, p. 207.

Sturrock, P. A., V. Petrosian, and J. S. Turk, 1975, *Ap. J.*, **196**, p. 73.

Sturrock, P. A., K. Baker, and J. S. Turk, 1976, *Ap. J.*, **206**, p. 273.

GAMMA-RAY PULSARS

H. Ögelman, S. Ayasli, and A. Hacinliyan
Middle East Technical University
Ankara, Turkey

ABSTRACT

Recent data from the high-energy γ-ray experiment have revealed the existence of four pulsars emitting photons above 35 MeV. An attempt is made to explain the γ-ray emission from these pulsars in terms of an electron-photon cascade that develops in the magnetosphere of the pulsar. Although there is very little material above the surface of the pulsar, the very intense magnetic fields (10^{12} gauss) correspond to many radiation lengths which cause electrons to emit photons by magnetic bremsstrahlung and which cause these photons to pair-produce. The cascade develops until the mean photon energy drops below the pair-production threshold which is in the γ-ray range; at this stage, the photons break out from the source.

INTRODUCTION

Initial results of the SAS-2 γ-ray telescope have shown that two of the outstanding γ-ray sources in the galactic plane survey were the pulsar, PSR 0531+21 (Crab) and PSR 0833-45 (Vela) (Kniffen et al., 1974; and Thompson et al., 1975). Subsequently, a more extensive search of the SAS-2 data for pulsed emission from 75 more radio pulsars has yielded positive fluxes with chance occurrences less than 10^{-4} for PSR 1747-46 and PSR 1818-04 (Ögelman et al., 1976).

Among these four γ-ray emitting pulsars that cover an age span of 10^3 to 10^6 years, only the youngest one, Crab-Nebula pulsar, exhibits emission in other parts of the electromagnetic spectrum in addition to the radio and γ-ray region. Thus, it appears that γ-ray emission around the 35 MeV region is a fundamental emission feature of pulsars. In this paper, we attempt to show that this feature is a consequence of the coexistence of intense magnetic and electric fields that can produce energetic electrons near the pulsar surface.

Because γ-rays in the energy range under discussion are commonly considered to be the signature of high-energy protons interacting with the ambient medium and producing π^0 mesons which, in turn, decay into γ-rays, we may consider the applicability of this process to the pulsars for the production of γ-rays. There are two strong objections to this alternate explanation. One is the fact that, above the surface of the pulsar, there is very little material to cause interactions of the high-energy protons that may be accelerated in the electric fields near the surface. The density of current-producing charges is estimated to be near 10^{13} cm^{-3} even for the fastest pulsars. This magnitude of density, integrated to the speed of light cylinder, only yields about 10 micrograms cm^{-2} of material above the surface, which is of the order of 10^{-6} to 10^{-7} interaction mean-free paths for protons. The second objection lies in the fact that, even if sufficient material was found for protons to interact, such as the surface of the neutron star, the efficiency of the π^oproduction process requires 10^{39} to 10^{40} protons s^{-1} to account for the γ-ray flux of an object such as Crab-Nebula pulsar. This is about a factor of 10^6 larger than the estimated primary electron flux.

Turning back to the material-starved, electromagnetically rich pulsar magnetosphere, we can speculate on how one may get special emphasis in the emission around γ-rays below the Earth's atmosphere. If we perform such an experiment, we may notice a preference of γ-rays around the 10- to 100-MeV region. Although the details of the interactions are complex, we can guess the reasons behind the energy preference. Initially, we start on top of the atmosphere with energetic particles. The atmosphere is many interacting mean-free-paths thick to the cosmic rays. The high-energy protons quickly interact, producing mesons which then decay immediately into electrons, positrons, and γ-rays, thereby initiating an electromagnetic cascade. The electrons predomimantly lose their energy by bremsstrahlung to photons of comparable energy and create electrons with about one-half their energy; the electromagnetic cascade thus multiplies and grows. When the average electron energy drops below 80 MeV, the electrons predominantly start losing their energy by ionization, and, at around 20 MeV, the photons lose energy through the Compton process. At this stage, the electron and photon components can no longer sustain each other, and the shower stops growing. Furthermore, around the 10- to 50-MeV region, the photons have a minimum in their absorption curve which allows them to penetrate deeper into the atmosphere.

A similar situation exists in the pulsar magnetosphere with the source and observer reversed. Energetic electrons accelerated near the surface have to emerge out of the intense magnetic fields of the magnetosphere. In doing so, they create an electromagnetic shower, the photons of which eventually break out of the surface. To understand more about the shower, let us review the electromagnetic processes that take place in intense magnetic fields.

HIGH ENERGY ELECTROMAGNETIC PROCESSES IN INTENSE MAGNETIC FIELDS

Typical parameters of electrons and magnetic fields in the astrophysical setting put the encountered electromagnetic conversion processes into the classical relativistic regime. However, the surface fields of 10^{12} gauss of pulsars and electric fields that can yield electrons with energies greater than 10^9 eV force us to treat this phenomenon with the proper quantum electrodynamical considerations. Following Erber (1966), we define the dimensionless parameter, Υ, that characterizes the transition probabilities:

$$\Upsilon = \left(\frac{E}{mc^2}\right)\left(\frac{B_\perp}{B_{cr}}\right) \tag{1}$$

where E is the energy of the electron or the photon, $B_\perp$ is the perpendicular component of the field to the direction of the particle, and B_{cr} is the natural quantum measure of the field strength:

$$B_{cr} \equiv \frac{m^2c^3}{e\hbar} = 4.414 \times 10^{13} \text{ gauss} \tag{2}$$

The measure of the dominance region of the electromagnetic process is also characterized by this parameter. For the case $\Upsilon \ll 1$, we are in the classical relativistic regime, and, for the $\Upsilon \gg 1$ region, we are in the quantum electrodynamic regime. In the $\Upsilon \gtrsim 1$ region, we can have pair-production of photons which eventually disappears as $\Upsilon \ll 1$. Furthermore, the peak of the emitted photon spectrum for an electron of energy E is given by:

$$\epsilon_{\gamma max} = E\left(\frac{3\Upsilon}{2 + 3\Upsilon}\right) \tag{3}$$

For $\Upsilon \gg 1$, $\epsilon_\gamma \sim E$, and, for $\Upsilon \ll 1$, $\epsilon_\gamma \sim 3E\Upsilon/2$.

With some simplifying assumptions that will alter the high-energy portion of the spectrum, the magnetic bremsstrahlung spectral distribution of an electron with energy E is given by:

$$I(E, \epsilon_\gamma, B) = \frac{\sqrt{3}\alpha}{2\pi}\left(\frac{mc}{\lambda\!\!\!^{-}_c}\right)\left(\frac{\Upsilon}{E}\right)\left(1 - \frac{\epsilon_\gamma}{E}\right) K(2\zeta) \tag{4}$$

where

$$\zeta = \frac{\epsilon_\gamma}{(E - \epsilon_\gamma)\, 3\Upsilon} \tag{5}$$

and K's are the incomplete Bessel function integrals that also appear in classical relativistic synchrotron radiation.

We may notice that the intrinsic rate of magnetic bremsstrahlung is measured by $mc^2/\lambda\!\!\!^{-}_c$, which is of the order of 10^{14} eV/cm. The total energy-loss rates integrated over the photon spectrum can be expressed as (Erber, 1966):

$$\frac{d\epsilon}{dx} = 6.43 \times 10^{13}\, g(\Upsilon)\, \text{eV cm}^{-1} \tag{6}$$

$$g(r) \simeq \begin{cases} 0.556\, \Upsilon^{2/3} & \Upsilon \gg 1 \\ \Upsilon^2(1 - 5.95\, \Upsilon) & \Upsilon \ll 1 \end{cases} \tag{7}$$

To get a feeling for this process we may notice that an electron of energy E in the $\Upsilon \gg 1$ regime will lose one-half of its energy in a distance of $0.11\, E^{1/3}$ (eV) $H^{-2/3}$ (gauss) cm, and, in doing so, it will typically radiate one photon with one-half of its energy. The situation is reminiscent of an energetic electron radiating bremsstrahlung photons in the coulomb field of the nucleus.

If we examine pair-production by energetic photons in magnetic fields, we again see the important effect of Υ parameter. The photon attenuation coefficient, $\alpha(\Upsilon)$, can be expressed as:

$$\alpha(\Upsilon) = \frac{1}{2}\left(\frac{\alpha}{\lambda_c}\right)\left(\frac{B_\perp}{B_{cr}}\right) T(\Upsilon) \tag{8}$$

where T (Υ) can be approximated by:

$$T(\Upsilon) \simeq \begin{cases} 0.76\,\Upsilon^{+1/3} & \Upsilon \gg 1 \\ 0.46 \exp\left(-\frac{8}{3\Upsilon}\right) & \Upsilon \ll 1 \end{cases} \tag{9}$$

The maximum of $\alpha(\Upsilon)$ occurs at $\Upsilon = 12$, or $\epsilon_\gamma = 12\, mc^2\, B_{cr}/B$

For a typical pulsar field of 10^{12} gauss, this maximum corresponds to 270 MeV. At this energy, the pulsar magnetosphere corresponds to approximately 10^{11} radiation lengths of material, or the equivalent of 5×10^5 kilometers of lead. Although the attenuation length grows exponentially as Υ decreases, the pulsar magnetosphere is so "thick" that, along the equatorial plane, it will cause all photons above a few MeV to pair-produce before emerging out. Near the poles, this threshold energy is increased by about a factor of csc θ due to the reduction of the perpendicular component of the magnetic field, thereby allowing higher-energy photons to emerge.

PRODUCTION OF ELECTROMAGNETIC CASCADES IN PULSAR MAGNETOSPHERES

Various authors have realized the importance of the above-mentioned electromagnetic processes in the pulsar magnetospheres and have invoked them to produce coherent bunches of electrons and photons to explain the microwave and optical radiation from these objects (Sturrock, 1971; Ruderman and Sutherland, 1975; and Sturrock et al., 1975).

In general, the complicated relationship and geometry between the rotation axis, $\vec{\Omega}$, the magnetic field, $\bar{B}$, and the resulting $\bar{E}$ field in a pulsar differ extensively between different models. In this paper, we ignore the details and assume that energetic electrons are produced near the pulsar surface and try to estimate the subsequent radiation produced by these electrons and the propagation of this radiation through the pulsar magnetosphere. In particular, we would like to trace the outlines of the cascade shower process that will develop as the energetic electrons radiate photons that, in turn, produce electron-positron pairs.

In the electromagnetic conversion processes discussed above, the relevant component of B for the radiation process is perpendicular to the direction of motion; therefore, it seems important to know what the $\bar{E}.\bar{B}$ term is that accelerates the electrons. If electrons are going along field lines, they emit curvature radiation instead of magnetic bremsstrahlung. However, even electrons accelerated in a typical pulsar can lose their energy by curvature radiation to photons around 10^9 - eV energy (Ruderman and Sutherland, 1975). These photons that travel in straight lines subsequently encounter the perpendicular component of B as they travel in the curved lines of force. Once they pair-produce, the electron-positron pair also feels this component of B in their radiation process. Henceforth, in our discussion, as a first approximation, we shall ignore the geometry of the field lines and assume that the component of B perpendicular to the direction of motion is comparable to B. We can then perturb our general conclusions for the polar region by decreasing the effective value of B.

Qualitatively, we can describe the cascade in the following manner: An energetic electron in $\Upsilon \gg 1$ regime ($E \gg 20$ MeV for $H = 10^{12}$ gauss) will lose one-half of its energy in a distance:

$$\Delta x_{1/2} \simeq 10^{-6} \left(\frac{B}{10^{12}}\right)^{-2/3} \left(\frac{E}{10^9}\right)^{1/3} \quad \text{cm} \tag{11}$$

where B is in gauss and E is in eV. It loses this energy by typically emitting one photon with energy E/2. The radiated photon, if still in the pair-production regime, will create an electron-positron pair with each particle containing one-half of the photon's energy. For a photon of 10^9 - eV energy in a 10^{12}-gauss field, the mean-free path against pair-production is about 5×10^{-6} cm. Subsequently, these electrons and positrons will again radiate one-half of their energy as a single photon and so forth. When the mean energy of the electron drops down to a value that corresponds to $\Upsilon \sim 1$ ($E \sim 22$ MeV for $B \sim 10^{12}$ gauss), it starts losing its energy mainly by radiating photons of $\Upsilon \sim 0.6$ which pair-produce electron-positrons with $\Upsilon \sim 0.3$. The next generation of photons has Υ around 0.1, and they can easily break out of the surface even if this energy is greater than the pair-production threshold of $2\ M_e C^2$.

Effectively, then, the maximum of the shower occurs when the mean energy of the electromagnetic component is degraded $\Upsilon = 0.1$ to 0.3 range. Because the photon component of the shower is attenuated at larger distances as compared to the electrons, this maximum will not be a strict spatial maximum, but, in the steady state, implies a concentration of electrons in the above energy range, that radiates photons in the corresponding energy range. The extent in height of this cascade is small compared with the distance over which B changes appreciably; hence, we can treat the problem as occurring at a constant B value.

We have carried out numerical calculations of the resulting photon spectrum when we let a monoenergetic beam of electrons with $E = 10^9$ eV pass through a uniform magnetic field of 10^{12} gauss. The results are shown in figure 1. The ordinate gives the resulting photon spectrum in units of energy per unit photon-energy interval produced by a single electron. The three different curves, labeled 1, 10, and 30, reflect the spectra after the corresponding number of iterations in which each iteration is a distance step of 10^{-6} cm. If we continue this iteration process and follow the photons out to large distances, the portion above 5 MeV should decrease more, and the cascade photons that are produced should increase uniformly the intensity level below this energy. We would approximate the resulting photon spectra by:

$$\frac{d\epsilon}{d\epsilon_\gamma} \sim \begin{cases} \dfrac{E_o}{\epsilon_{cr}} & \epsilon_\gamma < \epsilon_{cr} \\ 0 & \epsilon_\gamma > \epsilon_{cr} \end{cases} \tag{12}$$

where the critical energy, ϵ_{cr}, is given by:

$$\epsilon_{cr} \sim 0.2\, M_e c^2 \left(\frac{B_{cr}}{B_\perp}\right) \tag{13}$$

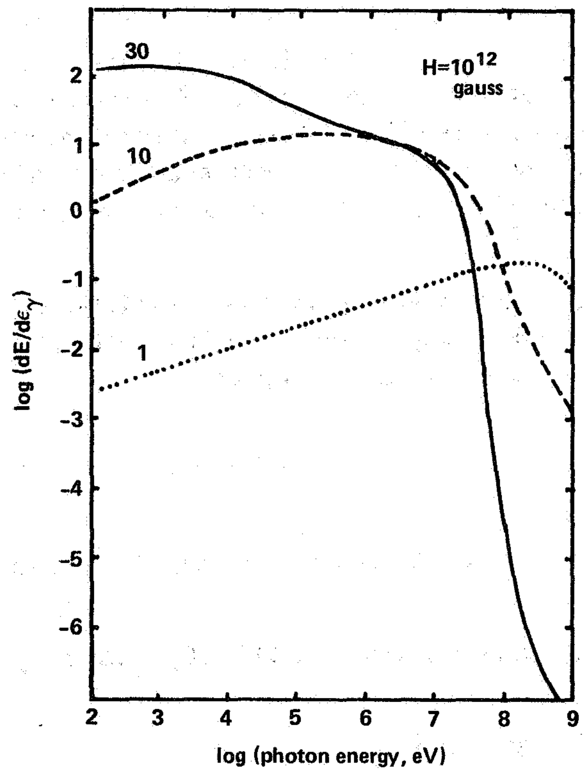

Figure 1. Numerical calculations on the photon spectrum of a shower initiated by a 10^9-eV electron in a 10^{12}-gauss field. The curves labeled 1, 10, and 30 are the number of iteration steps in units of 10^{-6} cm.

DISCUSSION

There are several factors that will change the idealized calculations of the previous sections. One factor is assumption of the monoenergetic electron beam. In reality, there will be a spectrum of electrons accelerated by the pulsar. However, as long as this spectrum implies the existence of electrons above ϵ_{cr}, the conclusions of the previous sections do not change. The second factor is the possibility of the reacceleration of the electrons as they lose energy. A third factor is the geometry of the field lines. We can include this effect approximately by considering the fact that ϵ_{cr} will increase as csc θ, where θ is the angle of propagation with respect to the poles. For example, in the case of the canonical pulsar with $B = 10^{12}$ gauss,

ϵ_{cr} is about 5 MeV, but within a cone of 6° from the poles. Gamma-rays above 50 MeV will be able to break through the pulsar. For the case of B = 10^{11} gauss, $\epsilon_{cr} \sim 50$ MeV, and 500-MeV photons can emerge from the poles within the 6° cone.

In short, γ-rays in the 10^6- to 10^9-eV region are the photons that can break out of the pulsar magnetic fields, as well as being photons that correspond to the shower maximum produced by an energetic electron.

The shape of the photon spectrum implies that most of the energy will be radiated away by the γ-rays near the critical energy. Experimentally, this fact is certainly supported by PSR 0833-45, PSR 1747-46, and PSR 1818-04, which radiate a factor of 3.5×10^5, 2.2×10^5 and 3.5×10^5 more, respectively, in γ-rays above 35 MeV than in the radio region, the only other region in which emission has been detected. In the case of the Crab-Nebula pulsar, PSR 0532 + 21, the ratio of the γ-ray to radio luminosity is again 3.1×10^5; however, the Crab pulsar shows additional emission in the optical and X-ray regions which must be explained by some other mechanism. Although the radio luminosity itself needs other coherent processes, it is interesting to note that in all the observed γ-ray pulsars, the ratio of γ-ray luminosity to radio luminosity is around 3×10^5.

In conclusion, if the general results of this work are correct, pulsars radiate predominantly in the 10^6- to 10^9-eV range. Although the radio emission is only a trivial part of the energy loss, in understanding pulsars it has received an unfair share of the effort.

REFERENCES

Erber, T., 1966, *Rev. Mod. Phys.*, **38**, p. 626.

Kniffen, D. A., R. C. Hartman, D. J. Thompson, G. F. Bignami, C. E. Fichtel, H. Ögelman, and T. Tümer, 1974, *Nature* **251**, p. 397.

Ögelman, H. B., C. E. Fichtel, D. A. Kniffen, and D. J. Thompson, 1976, *Ap. J.*, to be published.

Ruderman, M. A. and P. G. Sutherland, 1975, *Ap. J.* **196**, p. 51.

Sturrock, P. A., 1971, *Ap. J.* **164**, p. 529.

Sturrock, P. A., V. Petrosian, and J. S. Turk, 1975, *Ap. J.* **196**, p. 73.

Thompson, D. J., C. E. Fichtel, D. A. Kniffen, and H. B. Ögelman, 1975, *Ap. J. Letters*, **200**, p. L79.

CONTRIBUTED PAPERS
June 2, 1976, p. m.
(Listed by Title, Author, and Reference)

1. 3-30 MeV Gamma Rays From the Crab, Stephen White, Physics Department, University of California, Riverside, California 92502.

   Reference: 3- to 30-MeV Gamma Rays From the Crab, IGPP-UCR-76-7, Preprint of Institute of Geophysics and Planetary Physics, University of California, Riverside, 1976.

2. Ultra High Energy Gamma Rays from the Crab Nebula, Hugh Tornabene, Bowie State College, Bowie, Maryland 20715.

   No preprint is available.

3. Gamma Rays from Pulsars, Arnold Wolfendale, Physics Department, University of Durham, South Road, Durham, U.K.

   Preprint: Gamma Rays From Pulsars, C. Dahanayake, D. Dodds, and A. W. Wolfendale, Physics Department, University of Durham, England

4. Geminga, Giovanni Bignami, Universita di Milano, Instituto di Science Fisiche, Aldo Pontromeli, via Celoria 16, Milano, Italy 20133.

   Reference: Search for a Correlation Between the New Satellite Galaxy and an Unidentified Gamma Ray Source, G. F. Bignami, T. Macaccaro, C. Paizis, to be published in Astron. and Astrophys.

5. Search for Nuclear Gamma Ray Lines from Nova Cygni, Marvin Leventhal, Bell Telephone Labs., Murray Hill, New Jersey 07974

   Reference: D. D. Clayton and F. Hoyle, *Astrophysical Journal Letters*, **187**, 1974, pp. L101-L103.

6. OSO-7 Hard X-Ray Observations of Diffuse Galactic X-Ray Emission, William Wheaton, Center for Space Research, M.I.T., Cambridge, Massachusetts 02139

   Reference: William A. Wheaton, Thesis UCSD, 1976.

7. Preliminary Results on Background Gamma-Ray Lines Observed at Balloon Altitudes, A. S. Jacobson, J. C. Ling, W. A. Mahoney and J. B. Willett, 183-901 Jet Propulsion Laboratory, California Inst. of Technology, Pasadena, California 91103.

   Reference: Measurement of the Terrestrial and Extraterrestrial 0.511 MeV Gamma Rays With a High Energy Resolution Instrument at Balloon Altitude over Palestine, Texas,

J. C. Ling, W. A. Mahoney, J. B. Willett, and A. S. Jacobson, to be submitted to the *J. Geophys. Res.*, 1976.

Reference: Measurement of the Terrestrial and Extraterrestrial 0.511 MeV Gamma Rays With a High Energy Resolution Instrument at Balloon Altitude over Palestine, Texas, J. C. Ling, W. A. Mahoney, J. B. Willett, and A. S. Jacobson, to be submitted to the *J. Geophys. Res.*, 1976.

DENSITY WAVE THEORY

W. W. Roberts, Jr.
Department of Applied Mathematics and Computer Science
University of Virginia, Charlottesville, Virginia 22901

ABSTRACT

The prospect that density waves and galactic shock waves are present on the large scale in disk-shaped galaxies has received support in recent years from both theoretical and observational studies. Large-scale galactic shock waves in the interstellar gas are suggested to play an important governing role in star formation, molecule formation, and the degree of development of spiral structure. Through the dynamics of the interstellar gas and the galactic shock-wave phenomenon, a new insight into the physical basis underlying the morphological classification system of galaxies is suggested.

INTRODUCTION

In this symposium, a primary focus is the structure, content, and dynamics of our galaxy as revealed by various galactic constituents and tracers—HI, CO, OH, H_2, young stars, HII regions, supernova remnants, pulsars, γ-radiation, synchrotron radiation, and others. Some of these constituents help to make up the overall gaseous component of our galaxy, whereas the formation and large-scale distribution of others is directly related to the large-scale dynamics of the gaseous component. In this review on Density Wave Theory, strong emphasis will therefore be directed toward the gaseous component and the important role it can play. Our galaxy is not thought to be greatly different from external spiral galaxies we see, and this review will focus from time to time on external spirals to help us theoretically view our own galaxy.

In many external galaxies, the optical appearance of the disk reveals the presence of luminous spiral arms. If the spiral arms were material arms and were composed of the same material for a substantial portion of the lifetime of the galaxy, the differential rotation inherent in the disk would tend to overwind the arms into nearly circular forms instead of the spirals observed. Partly because of this winding dilemma associated with material arms, a wave interpretation of large-scale spiral structure seems necessary. In the wave interpretation, the enhanced luminosity of a spiral arm is believed to originate in the very young, newly formed stars whose births from interstellar clouds have been triggered by the passage of the crest of a spiral density wave.

STELLAR DENSITY WAVES

The density-wave viewpoint originated with Bertil Lindblad (1963; see also Lindblad and Langebartel, 1953) and has been developed toward a coherent density-wave theory by C. C. Lin and his associates and others (Lin, 1971). Gravitational forces are considered as dominant forces, with magnetic forces also playing a role, but of secondary importance. The fundamental spatial coherence of the wave pattern is provided by the orderly underlying spiral gravitational field of the collective distribution of old to moderately old disk stars participating in the wave pattern. Lin and Shu (1964 and 1966) find that this self-gravitation of the material participating in the wave pattern can go a long way toward helping to sustain it. On the other hand, Toomre (1969) shows that a group of spiral waves would still propagate in the radial direction and eventually disappear in several rotations of the galaxy. Thus, one of the intriguing problems at the present time is how to account for the origin and permanence of spiral structure. Fortunately, this problem is now receiving the attention of a number of researchers, and a variety of promising sources have already been found for the generation of spiral structure (Lin, 1970; Toomre and Toomre, 1972; Lynden-Bell and Kalnajs, 1972; van der Kruit et al., 1972; Feldman and Lin, 1973; Mark, 1974, 1976 a,b,c,d,; Lin and Lau, 1975; and Lau et al., 1976).

The mass concentration in a density wave is believed to constitute only a small perturbation on an otherwise rather smooth stellar disk. For this reason, the theory for stellar density waves has evolved primarily as a small-amplitude linear theory. Figure 1 provides a photographic simulation of a stellar density wave of 5-percent amplitude superposed on a stellar disk whose axisymmetric distribution is computed from the mass model of Vandervoort (1970) for our galaxy. Here, the resulting background wave pattern of old to moderately old stars is hardly visible, and such background patterns would most certainly be difficult to detect in real galaxies.

GALACTIC SHOCK WAVES

On the other hand, the response of the interstellar gas to the small-background spiral-gravitational field associated with such a stellar density-wave pattern is, in fact, found to be a rather large response in which shock waves form along the arms of the background pattern (Roberts, 1969; see also Fujimoto, 1966). Figure 2 illustrates the location of the shock formed along the background arms. Undergoing rapid basic rotation about the galactic center, the gas flows along the arrowed streamlines through the slower rotating wave pattern from one shock to the next. It is mainly the spiral-gravitational field of the background pattern, coupled with rotation along with the effect of pressure and the variation in streamtube cross section that drives the gaseous response and forms the shock. The galactic magnetic field and the cosmic-ray particles which interact with the magnetic field also constrain the gas motion. In the model here, a galactic magnetic field is embedded in the gas (Roberts and Yuan, 1970), and the shock that forms is a hydromagnetic shock wave. Because of the enormous size of the galaxy, the magnetic field is essentially "frozen into" the gas, and the arrowed streamlines represent the gas streamlines, as well as the magnetic lines of force.

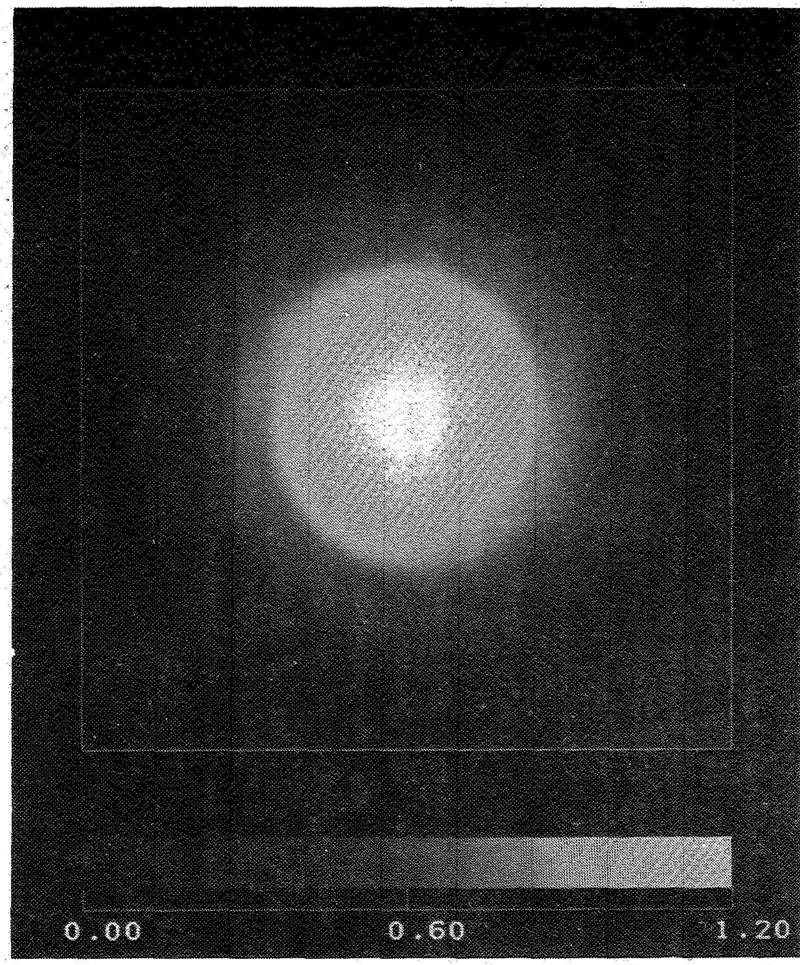

Figure 1. Photographic simulation of a background stellar density-wave pattern of 5-percent amplitude. (prepared by James M. Huntley).

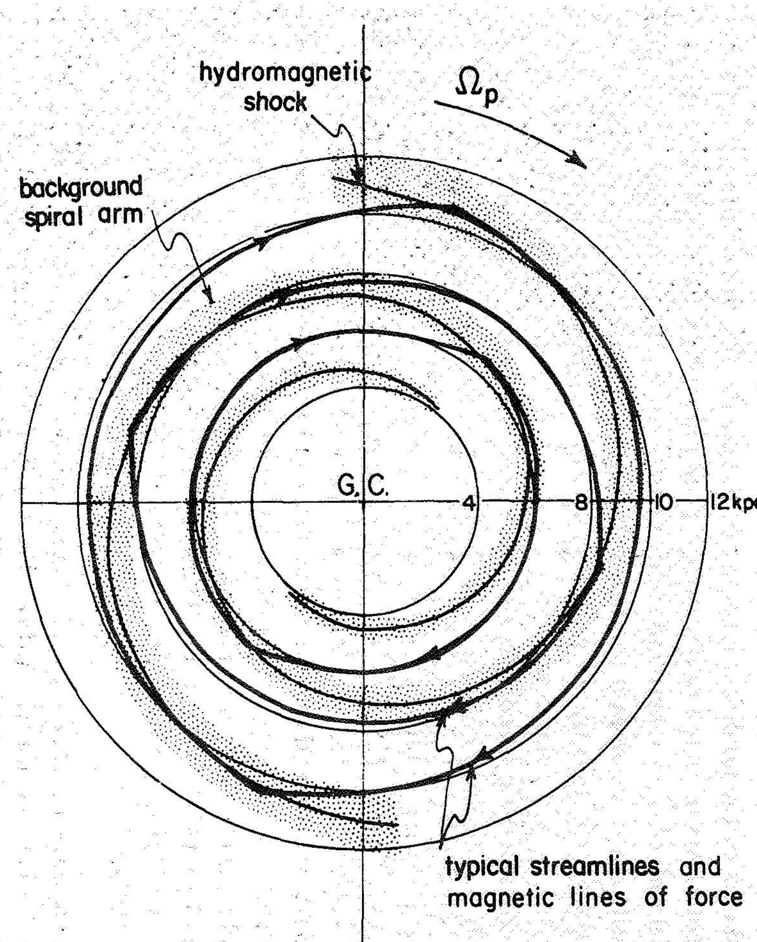

Figure 2. Sketch of the background spiral pattern and the gas response in the density-wave model. A shock forms in the background spiral arm. Each gas streamline appears as a sharp-pointed oval with a sharp turning point at each shock (from Roberts, 1969).

Figure 3 is a sketch of the nonlinear response of the gas-density distribution along a streamline. The gaseous response has a rather narrow peak induced by the shock wave which forms in the potential well of the background stellar density-wave arm. A photographic simulation of the gas-density distribution over the face of the model disk is provided in figure 4. The ridge of the light distribution traces out the shock and the gas-density ridge. The surface-density response of a particular component in a galaxy is roughly proportional to the inverse square of the characteristic speed. Because the effective acoustic speed of the interstellar gas is typically only one-third to one-fourth of the root-mean-square random velocity of the disk stars, it is not difficult to see how the same mild spiral gravitational field which induces only a small fractional variation of the disk stars (figure 1) can drive a very large density response in the interstellar gas toward the formation of shock waves (figure 4).

The formation of such large-amplitude spiral waves in the gas is not greatly sensitive to the form of the background forcing field adopted to drive the gas. For example, in a time-dependent study of the gas response to a bar-like oval distortion, Sanders and Huntley (1976) find a large-amplitude wave pattern of a character rather similar to that in figures 2 through 4, but with rather open spiral arms. Figure 5 shows a photographic simulation of the gas-density distribution in two different cases of mild bar-like forcing.

GAS-CLOUD COLLAPSE AND STAR FORMATION

Galactic shock waves may well form a possible triggering mechanism for the gravitational collapse of gas clouds, leading to star formation and the formation of other tracers along spiral arms. Figure 3 illustrates this possible star-formation mechanism. Gas flows into this shock and compression region from left to right. Before reaching the shock, some of the large clouds and cloud complexes may be on the verge of gravitational collapse. A sudden compression of the clouds in the shock could conceivably trigger the gravitational collapse of some of the largest gas clouds. As the gas leaves the shock region, it is rather quickly decompressed, and star formation ceases.

On the small scale, the main obstacle to star formation is that most of the interstellar gas clouds would not be even remotely bound by their self-gravitation if the clouds were isolated entities placed in a vacuum. Random motion can act as a "pressure" in that it provides support against the gravitational field of the galaxy; however, there are difficulties in visualizing how the "effective pressure" is transmitted on a small scale to trigger the gravitational collapse of clouds. This obstacle is now largely removed through recent work by a number of researchers who show that the nearly neutral component of the interstellar medium may consist of two gaseous phases in rough pressure equilibrium with one another. These two phases are identified with the observed cold, dense clouds at temperatures of 20 to 200 K and with an unobserved hot, rarefied intercloud medium at temperatures of perhaps 10^4 K.

In a study of gas flow based on the two-phase concept (Shu, et al., 1972) galactic shocks are found to be initiated by the "hot" intercloud medium. For the case of 5-percent spiral field, it is found that the total variation of pressure along a streamline at the solar circle exceeds

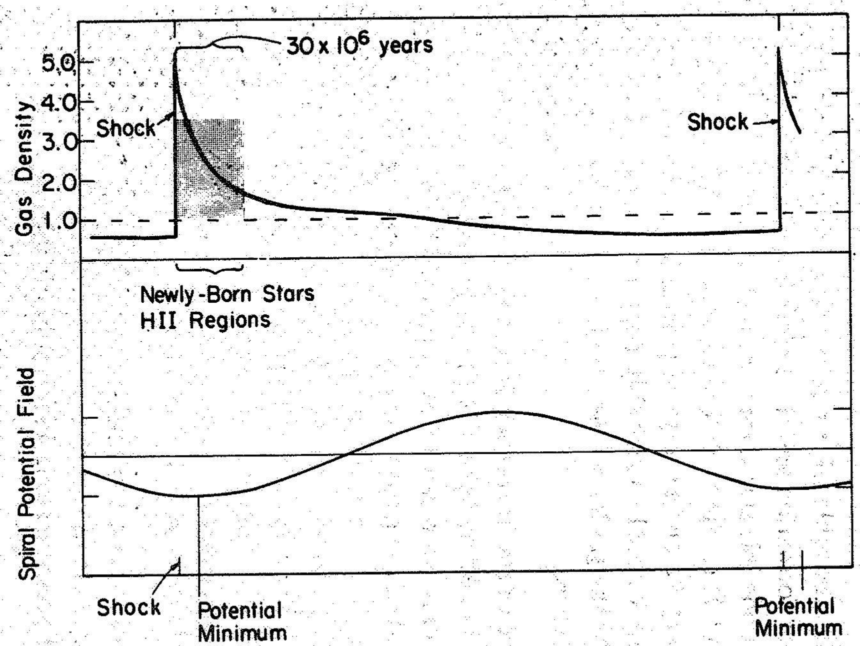

Figure 3. Gas-density distribution along a typical streamline in the density-wave model. The potential minimum corresponds to the center of the background spiral arm. Allowing a typical time of 30 million years for the formation and evolution of the relatively massive stars, the region of newly born stars and HII regions lie just outside the shock and sharp HI peak (from Roberts, 1969).

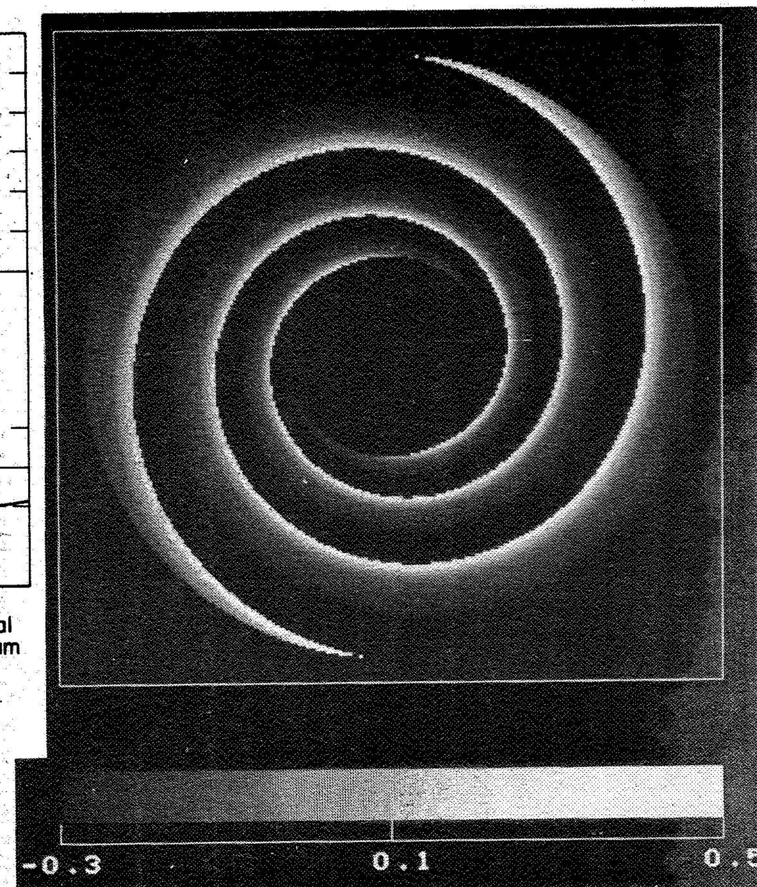

Figure 4. Photographic simulation of the gas-density distribution with the formation of a galactic shock wave in the density-wave model (from Roberts, 1969) (prepared by James M. Huntley).

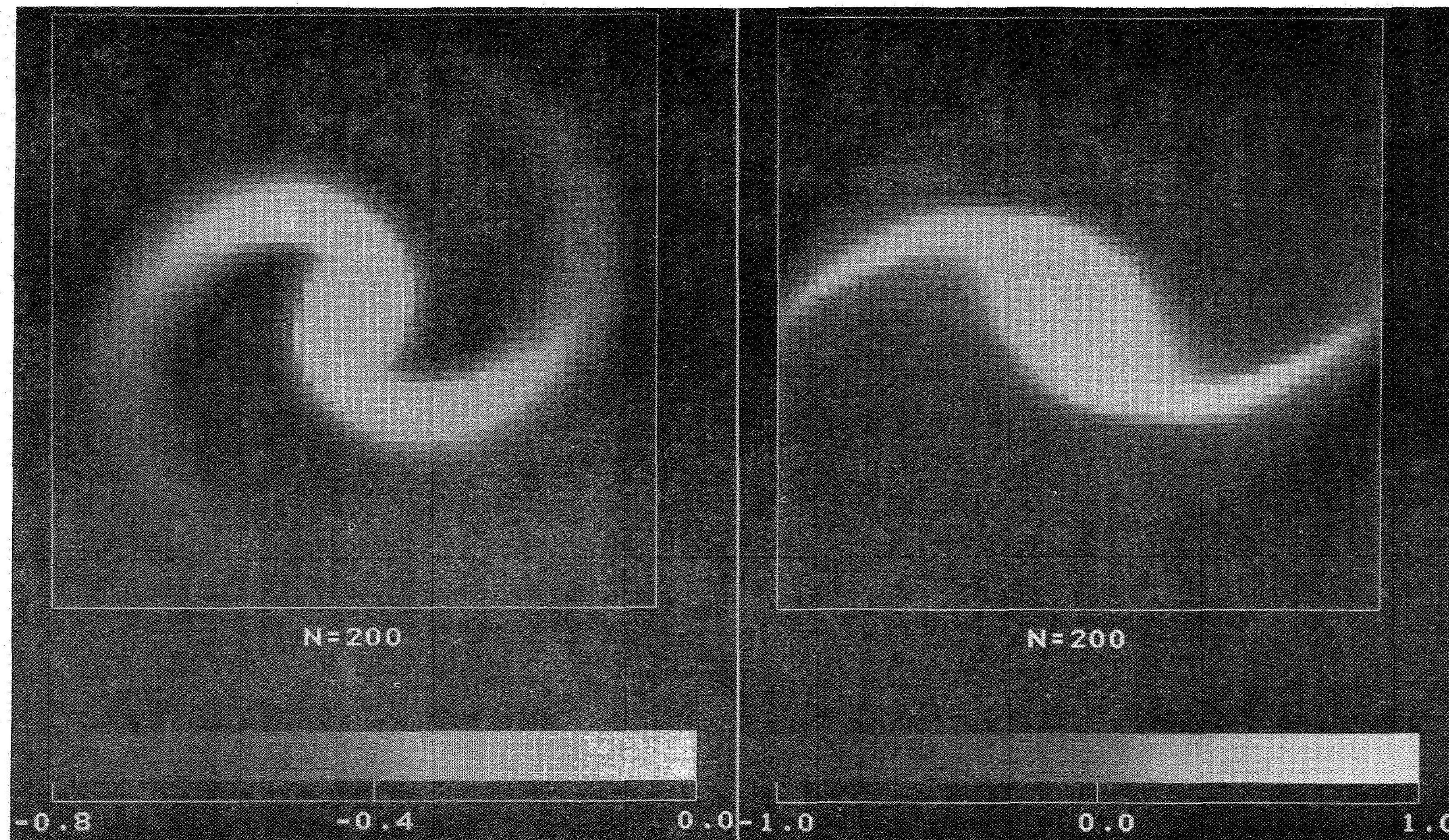

(a) (b)

Figure 5. Photographic simulation of the gas-density distribution in response to a mild bar-like oval distortion: (a) inner and outer Lindblad resonance and corotation are contained within the model gaseous disk; (b) only inner Lindblad resonance is contained within the gaseous disk (from Sanders and Huntley, 1976).

the range of pressures consistent with the thermal stability of both cloud and intercloud phases, and phase transitions occur in the flow. Inside the shock layer, the transient pressure tends to achieve a value higher than the maximum pressure p_{max}, consistent with thermal stability of the intercloud medium, and this forces a transition of some of the "hot" intercloud gas into the "cold" cloud phase. On the other hand, in the interarm region, the pressure tends to drop to a value lower than the minimum pressure, p_{min}, consistent with the thermal stability of the cloud medium, and this forces a reverse transition of some of the cold cloud gas into the hot intercloud phase. As the pressure tends to drop below p_{min} in the interarm region, the evaporation of cloud material to the intercloud phase helps to maintain a constant pressure environment for the remaining clouds.

In this picture, the clouds are viewed as embedded bodies which expand or contract to adjust to changes of the ambient pressure of the intercloud medium, and the increase in pressure across the galactic shock occurring in the hot intercloud phase is, in turn, transmitted to the cold clouds, leading to star formation. Due to the greater compressibility of the gas in the two-phase model and the nonlinear nature of self-gravity, the critical mass for the gravitational collapse of a gas cloud is substantially reduced from that estimated for an isothermal gas by a factor greater than 10. This decrease of the threshold for gravitational collapse, coupled with the effect of the galactic shock as a possible triggering mechanism, helps to explain why the regions of active star formation can be delineated so sharply in certain external galaxies.

In a study of the time scales relevant to cloud formation and star formation, Biermann et al (1972) follow the phase transition process by a simple numerical model of thermal evolution in cases for different strengths of compression and magnetic field and for different rates of heavy element depletion onto grains (see also Mufson, 1974 and 1975). Through this work, they reconfirm that the transition to the cool stable-cloud phase may occur within 10^6 years and that stars may form within approximately 5×10^6 years in agreement with the time estimates for M51 by Mathewson et al. (1972) and for M81 by Rots (1975). Woodward (1976) further enhances the theoretical picture through studies of shock-driven implosions of interstellar clouds toward star formation (see also Sawa, 1975). Shu (1974) considers the Parker (magnetic Rayleigh-Taylor) instability for an interstellar medium composed of thermal gas, magnetic field, and cosmic-ray particles and investigates the tendency of the gas to drain down magnetic field lines into dense pockets of concentration. Mouschovias et al. (1974) suggest further that the initiation of this instability in the interstellar medium by the passage of a galactic shock may play a strong role in the formation of large cloud complexes, OB associations, and giant HII regions.

STRONG SHOCKS WITH NARROW REGIONS OF HIGH-GAS COMPRESSION AND WEAK SHOCKS WITH BROAD REGIONS OF LOW-GAS COMPRESSION

For a wave of given amplitude, the strength of the shock and the degree of compression of the gas vary as the square of the ratio, $w_{\perp}/a$, where $w_{\perp}$ is the total (unperturbed plus perturbed) velocity component of the gas normal to a spiral arm, and a is the effective acoustic speed of the interstellar gas. If the two-component model of the interstellar medium is adopted, a is unlikely to be very different from the sound speed associated with the intercloud medium ~ 7 to 12 km s^{-1} and a mean value of a in this range might be dictated by the atomic physics of all spiral galaxies. On the other hand, $w_{\perp}$ oscillates along a streamline about its unperturbed value, $w_{\perp 0}$, because of the forcing of the spiral gravitational field of fractional amplitude, F. Shocks form if F is sufficiently large as to force, $w_{\perp}$, to achieve transonic values. There are actually two regimes: (1) $w_{\perp 0} > a$ and (2) $w_{\perp 0} < a$. For (1) $w_{\perp 0} > a$, most of the gas on the streamline is moving at supersonic speeds, and only a small portion is moving subsonically. The shocks which form in this ($w_{\perp 0} > a$) situation tend to be *strong* and give rise to *narrow* regions of *high* gas compression. For regime (2), $w_{\perp 0} < a$, most of the gas on the streamline is moving subsonically, and only a small portion travels supersonically. In this ($w_{\perp 0} < a$) situation, the shocks tend to be *weak* and yield rather *broad* regions of relatively *low* gas compression (Shu et al., 1973). Therefore, the strength of the shock and the compression of the gas and the consequent theoretical differentiation between spiral structure with *narrow* "filamentary" arms and *broad* "massive" arms seem to be critically dependent on the quantity:

$$w_{\perp 0} = (\Omega - \Omega_p)\,\widetilde{\omega} \cdot \sin i \tag{1}$$

where i is the pitch angle of the wave pattern which is determinable from the dispersion relation of the linear density-wave theory once the pattern speed, Ω_p, is specified.

INSIGHT INTO THE PHYSICAL BASIS UNDERLYING THE MORPHOLOGICAL CLASSIFICATION SYSTEM OF GALAXIES

A semiempirical study of the density-wave patterns predicted in the models of 24 external galaxies is made by Roberts et al. (1974 and 1975; see also Shu et al., 1971). Figure 6 provides the theoretical curves of $w_{\perp 0}$, i, and F, characterizing the density-wave pattern calculated for one sample galaxy, NGC3031-M81. The superposition of three sets of curves for three possible choices of the corotation radius illustrates that the magnitude of $w_{\perp 0}$ over its extent, and particularly at half-corotation, is not overly sensitive to the location of corotation. For NGC3031, the characteristically high levels reached by $w_{\perp 0}$ signify that potentially strong galactic shocks are possible, together with a high degree of development of spiral structure with narrow "filamentary" arms.

A photograph of the sample galaxy, NGC3031-M81, with its typically filamentary spiral arms taken from the Hubble Atlas (Sandage, 1961) is shown in figure 7. This well-developed spiral structure with narrow, filamentary spiral arms is thought to be a consequence of the rather strong shocks possible in this galaxy. Superposed is the computed wave pattern, based on the curve of theoretical pitch angle, i, for Ω_p = 26 km/s/kpc in figure 6.

The theoretical curves of $w_{\perp 0}$, i, and F for another sample galaxy, NGC598-M33, are provided in figure 8. The characteristically low levels of $w_{\perp 0}$ signify that only weak shocks, if any at all, would be possible. Consequently, the corresponding spiral structure would be expected to be poorly developed, perhaps with broad "massive" spiral arms of a fuzzy and patchy nature.

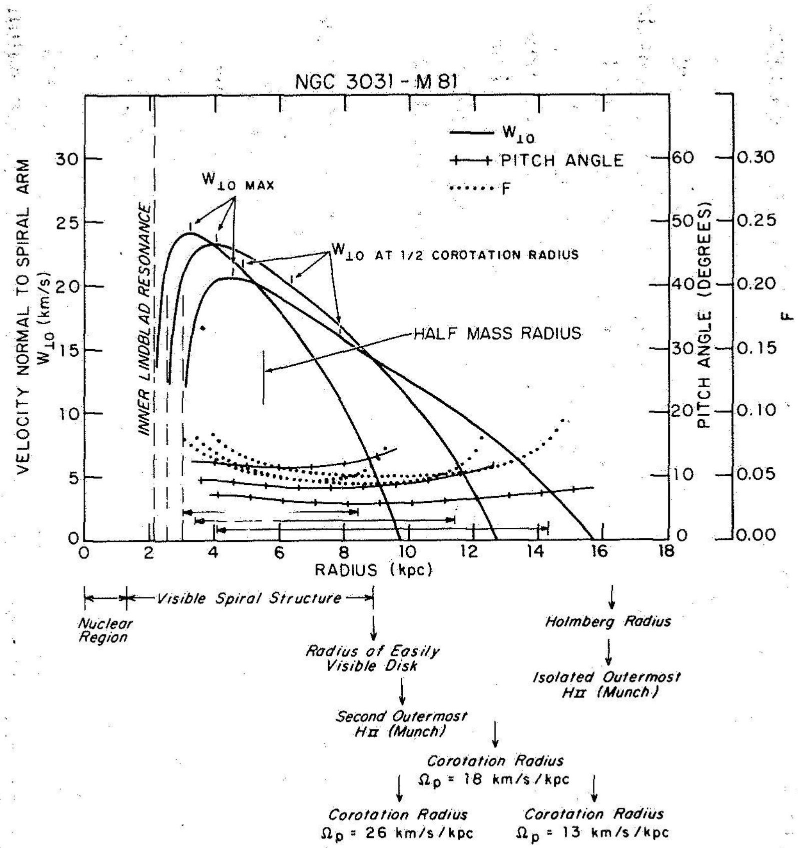

Figure 6. Characteristics of the density-wave model for the sample galaxy, NGC3031-M81. $w_{\perp 0}$, i, and F are sketched for each of three choices of the corotation radius. Because $w_{\perp 0}$ is so large, potentially strong shocks and correspondingly well-developed spiral arms are possible (from Roberts et al., 1975).

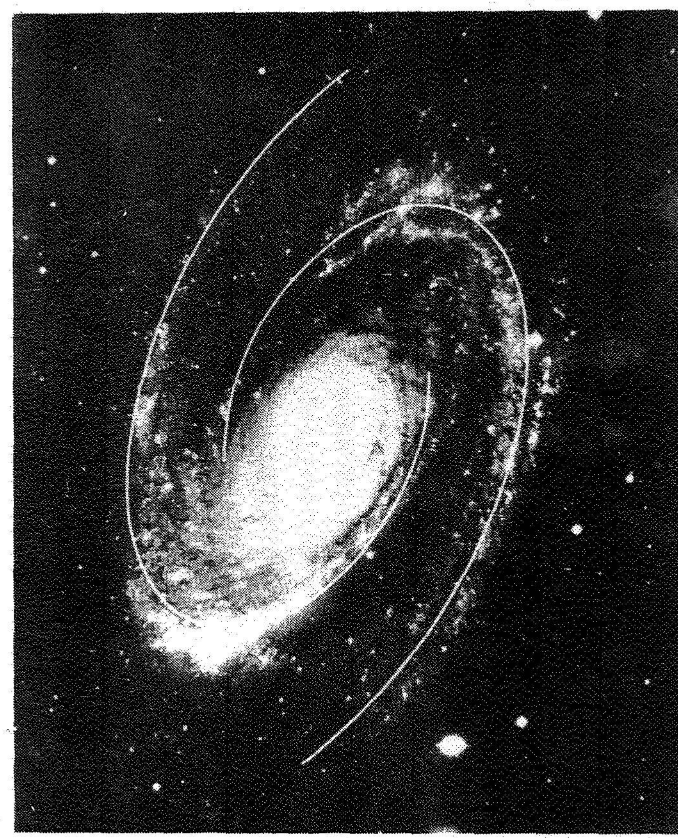

Figure 7. Photograph of the sample galaxy, NGC3031-M81, taken from the Hubble Atlas. The well-developed filamentary spiral arms are thought to be a consequence of the strong shocks possible in this galaxy (from Roberts et al., 1975).

A photograph of the sample galaxy, NGC598-M33, with its characteristically massive spiral arms taken from the Hubble Atlas is shown in figure 9. This poorly developed spiral structure with rather broad, massive spiral arms is thought to be a consequence of the result that only very weak shocks, if any at all, are possible in this galaxy. Superposed is the computed wave pattern, based on the curve of theoretical pitch angle, i, for Ω_p = 32 km/s/kpc in figure 8.

The results for the two sample galaxies in figures 6 through 9 suggest that the two parameters, $w_{\perp 0}$ and i, may play a major role in determining the degree of development of spiral structure in a galaxy, as well as its Hubble type. This role is illustrated in figures 10 and 11 where, for the computed density-wave patterns in the theoretical models of 24 external galaxies, $w_{\perp 0}$ (and potential shock strength) and the theoretical pitch angle of the wave pattern are well correlated with luminosity class and Hubble type, respectively. In figure 10, high $w_{\perp 0}$ and potentially strong shocks with narrow regions of high gas compression are found to correspond to galaxies with long, well-developed filamentary spiral arms; low $w_{\perp 0}$ and weak shocks with broad regions of relatively low gas compression are associated with galaxies with short, patchy, massive spiral arms. In figure 11, the computed wave patterns with small theoretical pitch angle, i, correspond to relatively early Hubble types, SO/a - Sbc; whereas the wave patterns with large theoretical pitch angle, i, correspond to relatively late Hubble types, Sc - Im. Because the theoretical pitch angle, i, is dependent on the choice of corotation radius in a galaxy, the correlation in figure 11 is equivalent to saying that the theoretical wave pattern obtained by choosing the corotation radius according to the criteria in Roberts et al. (1975) agrees reasonably well with the observed spiral pattern for each galaxy in the sample.

Through the correlations in figures 10 and 11, a new insight is suggested into the physical basis for the morphological classification system of galaxies. By showing that typical values of $w_{\perp 0}$ and i (say at one-half the corotation radius) can be expressed as:

$$w_{\perp 0} = (GM/\tilde{\omega}_c)^{1/2} f(\tilde{\omega}_{0.5M}/\tilde{\omega}_c) \tag{2}$$

$$\sin i = g(\tilde{\omega}_{0.5M}/\omega_c) \tag{3}$$

where f and g are functions whose forms are specified once the equilibrium disk has been specified except for scale factors. Roberts et al. (1975) identify what they believe to be the two fundamental physical parameters which underlie the accepted type-luminosity classification system of galaxies (van den Bergh, 1960a and 1960b): namely, (1) the total mass of the galaxy, divided by a characteristic dimension, $GM/\tilde{\omega}_c$, and (2) the concentration of mass toward the galactic center, $\tilde{\omega}_{0.5M}/\tilde{\omega}_c$. These two fundamental parameters govern $w_{\perp 0}$ and the potential strength of galactic shocks in the interstellar gas, as well as the geometry of the spiral wave pattern.

Figure 12 shows, for example, the dependence of $w_{\perp 0}$ and the potential shock strength on these two fundamental parameters. The black dots indicate the locations of the 24 galaxies of the sample, plus our own galaxy, with respect to the $w_{\perp 0}$ surface. A galaxy with a mass

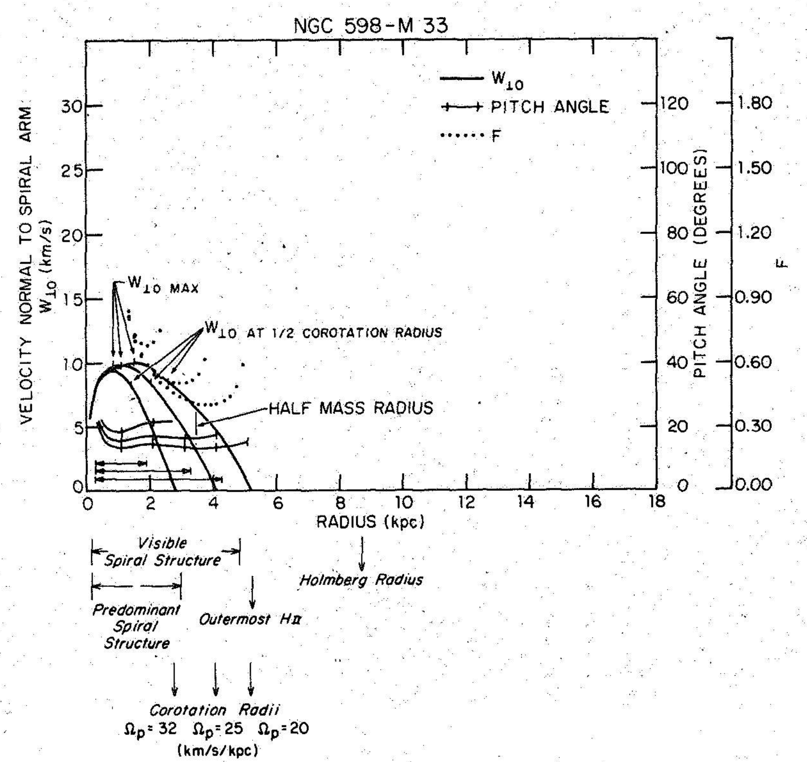

Figure 8. Characteristics of the density-wave model for the sample galaxy, NGC598-M33. $w_{\perp o}$, i, and F are sketched for each of three choices of the corotation radius. Because $w_{\perp o}$ is so small, only weak shocks, if any at all, could exist (from Roberts et al., 1975).

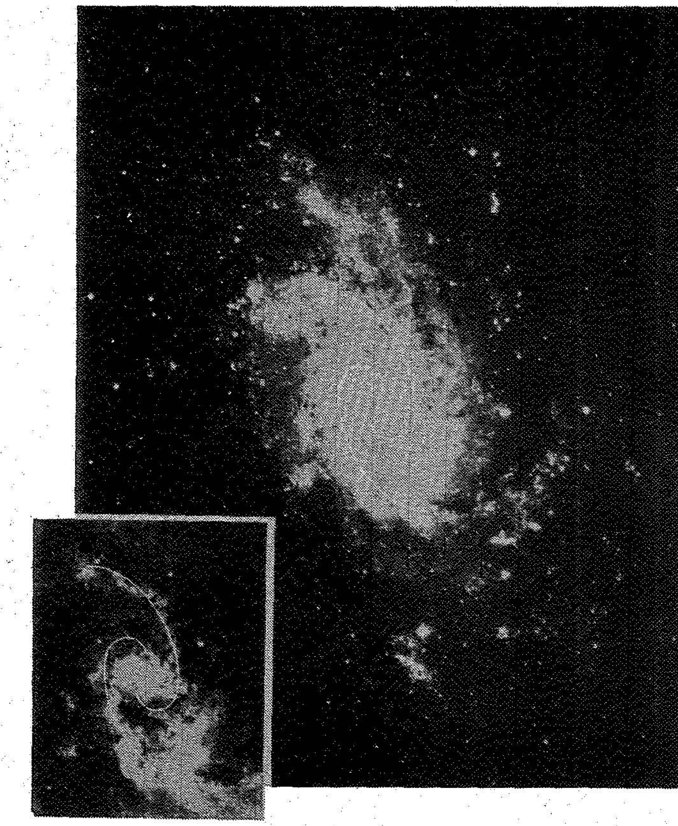

Figure 9. Photograph of the sample galaxy, NGC598-M33, taken from the Hubble Atlas. The poorly developed spiral structure is thought to be a consequence of the result that only weak shocks, if any at all, are possible in this galaxy (from Roberts et al., 1975).

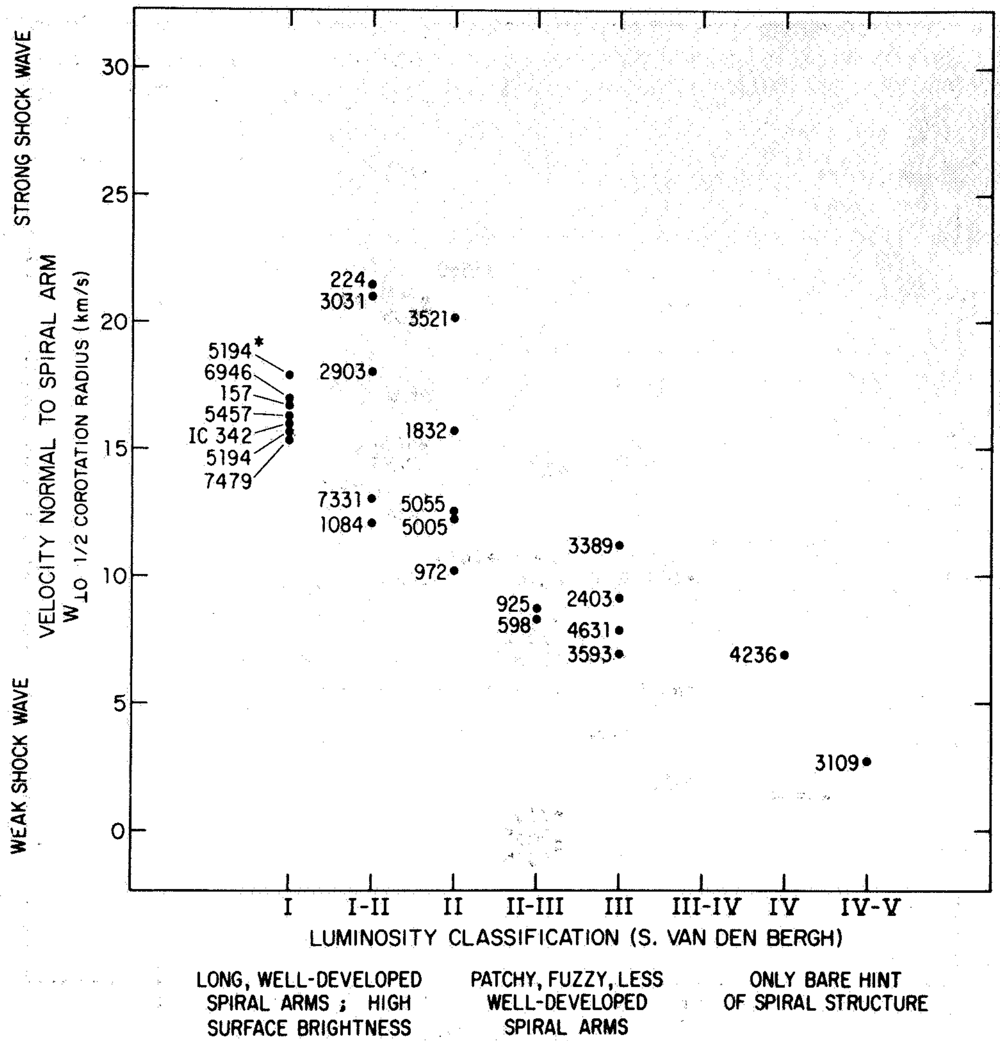

Figure 10. $w_{\perp 0}$ and luminosity class. Trend for a sample of 24 external galaxies indicative of a possible correlation between $w_{\perp 0}$—the velocity component of basic rotation normal to a spiral arm—and shock strength on the one hand, and luminosity classification and degree of development of spiral structure on the other. Those galaxies in which potentially strong shock waves are possible are found to exhibit long, well-developed spiral arms. Those galaxies in which weak shock waves are predicted are found to exhibit poorly developed spiral structure (from Roberts et al., 1975).

distribution of moderate central concentration, as evidenced by the parameter $\tilde{\omega}_{0.5M}/\tilde{\omega}_c$ being near the value of 0.5, is found to lie near the ridge of the $w_{\perp 0}$ surface. Such a galaxy is capable of forming rather strong shock waves (even with small-to-moderate forcing, F) and is therefore capable of exhibiting well developed filamentary spiral structure. The larger the mass of the galaxy, the higher along the ridge it can manifest itself, and the stronger the shocks

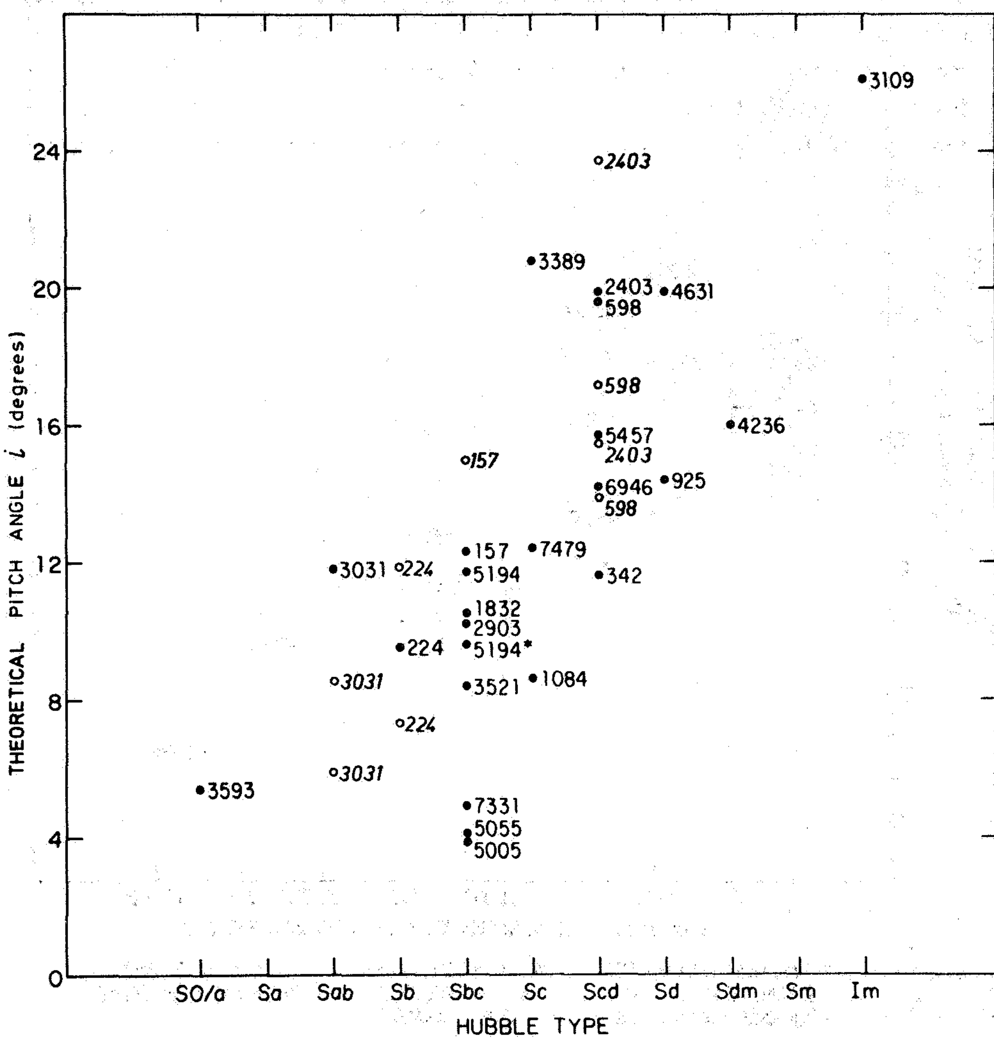

Figure 11. Theoretical pitch angle, i, and Hubble type. Those galaxies whose models predict wave patterns with very tightly wound spiral arms of small pitch angle, i, are the galaxies observed to be of relatively early Hubble type, SO/a - Sbc. Those galaxies whose models predict more open and loosely wound spiral arms with large pitch angle, i, are the galaxies observed to be of relatively late Hubble type, Sc - Im (from Roberts et al., 1975).

possible. On the other hand, a galaxy with a mass distribution of very low central concentration, as evidenced by the parameter, $\tilde{\omega}_{0.5M}/\tilde{\omega}_c$, being substantially larger than 0.5, would lie along the surface at a level well below the ridge. A galaxy in this range is capable of forming only weak shocks, if any at all (even with large forcing F); and the corresponding spiral structure is expected to be poorly developed and more massive. The three coordinates in this representation are ideal in the sense that they are distance independent parameters, and any uncertainty that may be present in the estimate of distance of a galaxy does not enter here.

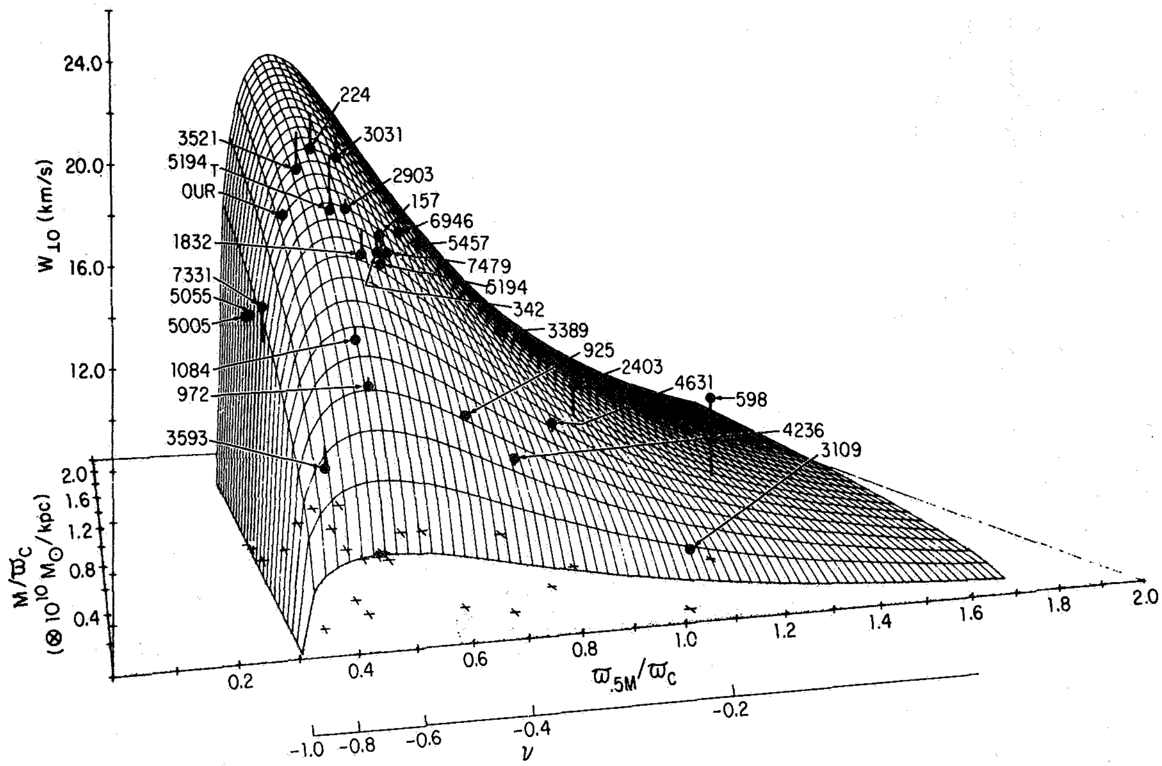

Figure 12. Theoretical categorization of disk-shaped galaxies—a representation of an ensemble ot cases spanning the two-dimensional parameter space of the two-fundamental parameters: $M/\tilde{\omega}_c$, $\tilde{\omega}_{0.5M}/\tilde{\omega}_c$. $w_{\perp 0}$ evaluated at half-corotation generates a $w_{\perp 0}$ surface which measures the strength of the galactic shock possible over all cases of the ensemble. Superposed are 24 external galaxies, plus our own. Those galaxies with a moderate concentration of central mass lie near the ridge of the $w_{\perp 0}$ surface; these galaxies can have the strongest shocks (e.g., NGC3031-M81). Those galaxies with a low central mass concentration lie well below the ridge and are predicted to have only weak shocks, if any at all (e.g., NGC598-M33) (from Roberts et al., 1975).

Some attention should be directed to the forcing amplitude, F, which, in the density-wave theory, measures the amplitude of the background stellar density wave driving the gas. In those galaxies with high levels of $w_{\perp 0}$, the potentially strong shocks and high gas compressions can be attained even for rather small (e.g., 5 percent) to moderate forcing amplitudes, F. The larger F is, the stronger the shocks and gas compressions which can be attained. However, with zero or negligible forcing, such potentially strong shocks and compressions could not be realized even for galaxies with high levels of $w_{\perp 0}$. Unfortunately within the present framework of the theory, the amplitude of the background driving wave, F, can be calculated only to within an arbitrary multiplicative scale factor. Of course, the real forcing of the gas in galaxies could be much more complex and even more difficult to calculate if various other driving and excitation mechanisms should enter to help drive the gas.

Empirical estimates of mean compression strengths reached in the spiral arms of eleven of the galaxies in the above sample are inferred observationally by van der Kruit (1973) from high spatial resolution 21-cm continuum studies with the Westerbork Radio Synthesis Telescope. What is indeed interesting is that F and other possible complexities do not seem to play an overwhelming role because a comparison of the $w_{\perp 0}$ levels in figures 10 and 12 with van der Kruit's mean compression strengths shows general agreement. Through observations of emission line strengths in the disks of twelve late-type galaxies, Jensen et al. (1976) find that radial changes in disk-gas composition across the face of a galaxy can largely be understood in terms of this density-wave picture and can be directly related to variations in the strength of the gas compression (and $w_{\perp 0}$) and the frequency of compression with each passage through a spiral wave crest $2(\Omega - \Omega_p)$.

INTERNAL STRUCTURE AND TEMPORAL SEQUENCE ACROSS A SPIRAL ARM

In Figure 12 our galaxy is located near the ridge of the $w_{\perp 0}$ surface. Unfortunately, from our vantage point within the Milky Way System, it is extremely difficult to view clearly and decipher the large-scale structure of our own galaxy. Consequently, before focusing on our galaxy, it might be instructive to view in some depth one or two external spirals which are located on the $w_{\perp 0}$ surface near our own galaxy in figure 12 and for which detailed observational studies are available.

One important feature to focus on is the predicted internal structure of a spiral arm. This is illustrated by the sketch in figure 13. With the formation of a galactic shock, the gas-density peaks along a narrow front and the magnetic field frozen into the gas, and possibly the dust particles as well, share in this compression. Therefore, a shock, a sharp HI peak, a narrow dust lane, and the strongest magnetic fields are all expected to lie in a narrow lane on the inside edge of the bright optical arm of young stars and HII regions triggered by the shock. Figure 14 provides a photographic simulation of the lane of young stars distributed in a Poisson distribution outside the shock. To be sure, complexities most certainly arise from a number of sources ranging from local processes within the shock region governing the interaction of clouds with the intercloud medium; e.g., through turbulent viscosity (Sawa, 1975) and governing the post-triggered collapse of gas clouds (Woodward, 1976) to the effects of spiral arm drift and age-dependent spreading of the newly formed stars (Biermann and Tinsley, 1974; and Wielen, 1975). Therefore, figures 13 and 14 are meant to provide only a qualitative overview of the temporal sequence of physical phenomena expected in the density-wave theory across a spiral arm in the region interior to corotation.

THE SAMPLE GALAXY, NGC5194-M51—OBSERVATIONAL STUDIES

Recent observational results from the Westerbork telescope in the Netherlands indicate that NGC5194-M51—a galaxy located on the $w_{\perp 0}$ surface near our own galaxy in figure 12—is one striking example which exhibits features suggested in this wave picture. Figure 15a shows a map of M51 and its companion, NGC5195, presented as a series of intensity profiles from

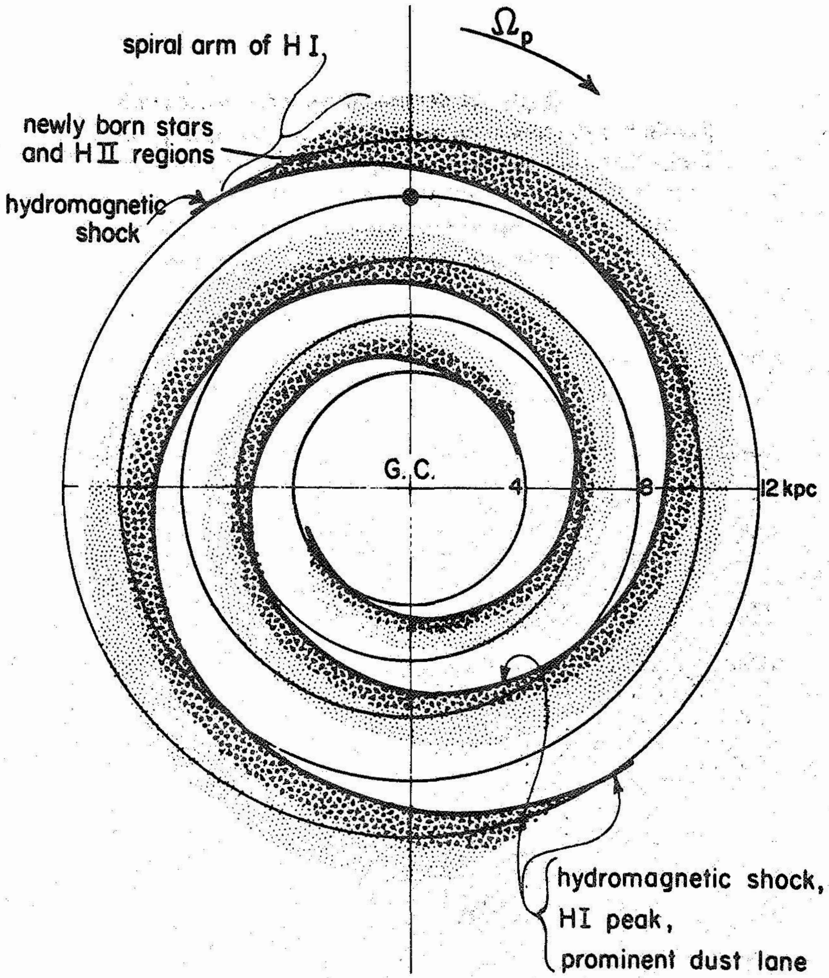

Figure 13. Internal structure and temporal sequence across a spiral arm triggered by the formation of a strong shock wave in the density-wave picture (from Roberts, 1969; and Roberts and Yuan, 1970).

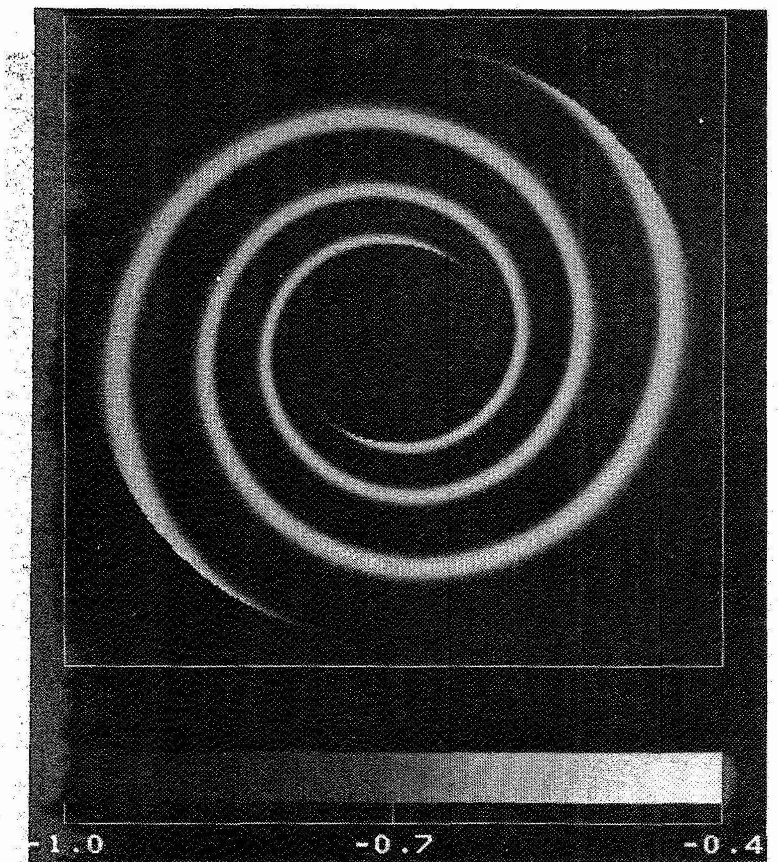

Figure 14. Photographic simulation of the lane of newly formed stars just outside the trailing spiral shock wave (from Roberts, 1969; and Roberts and Yuan, 1970) (prepared by James M. Huntley).

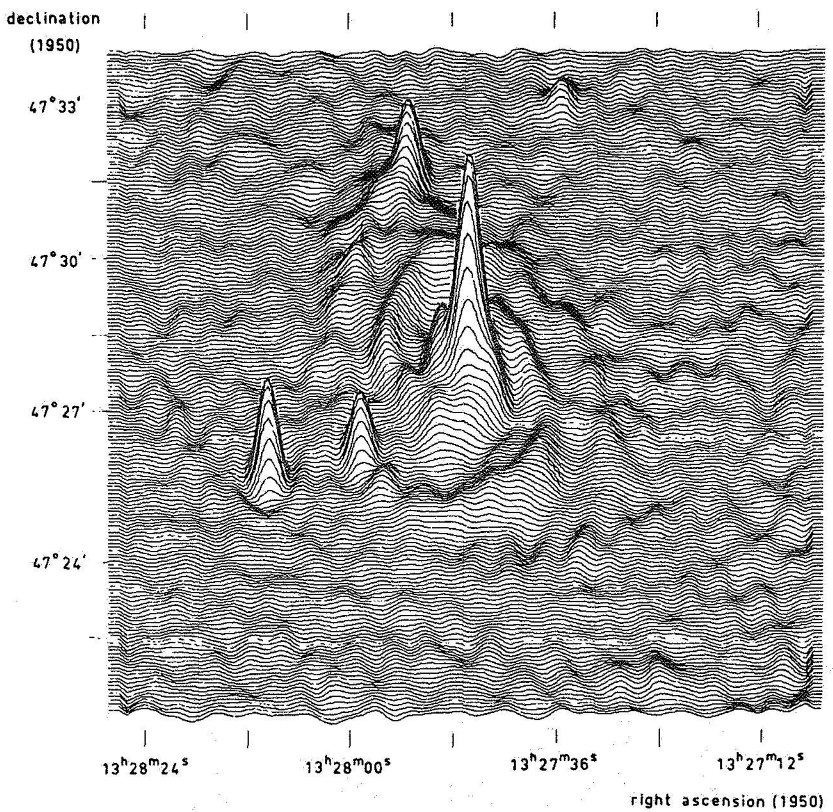

(a)

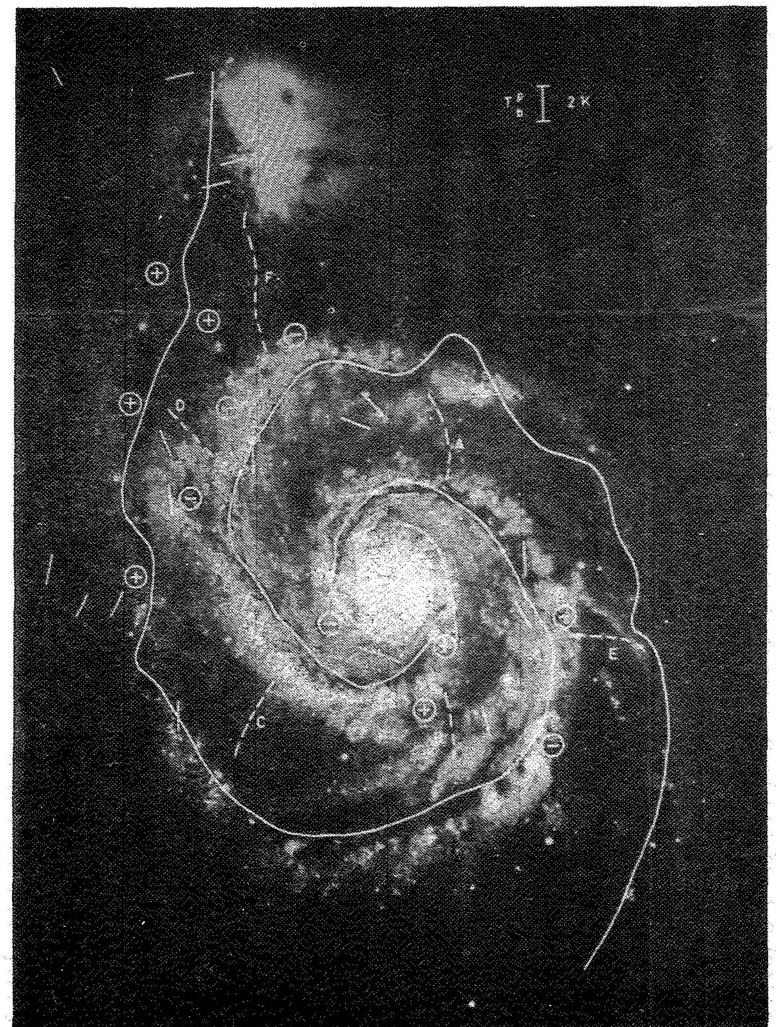

(b)

Figure 15. (a) Map of the 1415-MHz emission in M51 presented as a series of intensity profiles. Two rather striking radio-spiral arms stand out; (b) the ridge of the radio-spiral arms in synchrotron emission lies well along the dust lanes, generally on the inner sides of the optical spiral arms (from Mathewson et al., 1972).

the survey at 1415 MHz by Mathewson et al. (1972). The most striking feature of the radio map is the clear delineation of two radio spiral arms. Most of the spiral-arm emission does not arise in supernova remnants that lie in the bright optical arms, but rather more than half of the total emission of M51 is contained in the narrow radio-spiral arms. The inner portions of the radio arms are unresolved by the aerial beam, and this implies that they are less than 250 pc in width. Linear polarization is detected in their emission, which indicates that their origin is due to the synchrotron mechanism. Connected with this phenomenon of synchrotron emission is the strong dependence of the radio emissivity on the strength of the magnetic field which, in the density-wave theory, is predicted to be strongest in the compression region at the shock and dust lane.

The ridge line of the 1415-MHz emission from the radio-spiral arms is determined by Mathewson et al. (1972), and this ridge line is shown in figure 15b superposed on an optical photograph of NGC5195-M51. Here, it is apparent that the ridge of the radio-spiral arms in synchrotron emission and the strongest magnetic fields lie well along the dust lanes, generally on the inner sides of the optical-spiral arms.

Through a study of the detailed surface photometry of six galaxies, including M51, Schweizer (1976) detects background spiral patterns in the old stellar disk population. He identifies the arms of these broad patterns as background stellar density-wave arms. Figure 16 shows his surface brightness and color index maps for M51. The red arms which stand out in the O passband (lower left panel) are composed mainly of old giants underlying the old stellar disk, and these are the arms in M51 identified by Schweizer for the first time as background stellar density-wave arms. The blue arms which stand out in the B3 passband (upper left panel) are representative of the young population I stars.

In his identification of the background density-wave arms, Schweizer (1976) makes use of a sequence of azimuthal surface-brightness profiles at different radii, shown for M51 in figure 17. It is interesting to note that most of the strong dust lanes (marked by arrows) are not only located on the inside edge of the arm profiles, but are also often shifted a little onto the rising inside slope of the profiles. In fact, in the outer parts of M51, some appear even right on top of the arm profiles. Schweizer (1976) argues that the rise of surface brightness of the arm profiles inside the dust lanes must be largely due to the old disk stars which participate in the background density-wave arms.

In another view, figure 18 shows two projections of a three-dimensional map of the surface brightness of M51 and its companion, NGC5195, computed by Burkhead (1976) from a combination of photographic plates weighted toward yellow-green (centered about 5300 (Å)). Here, the spiral arms of M51 might well be characterized as narrow roadways slowly winding up the sides of the steep mountain of total surface brightness (not unlike the wave arms in figure 1).

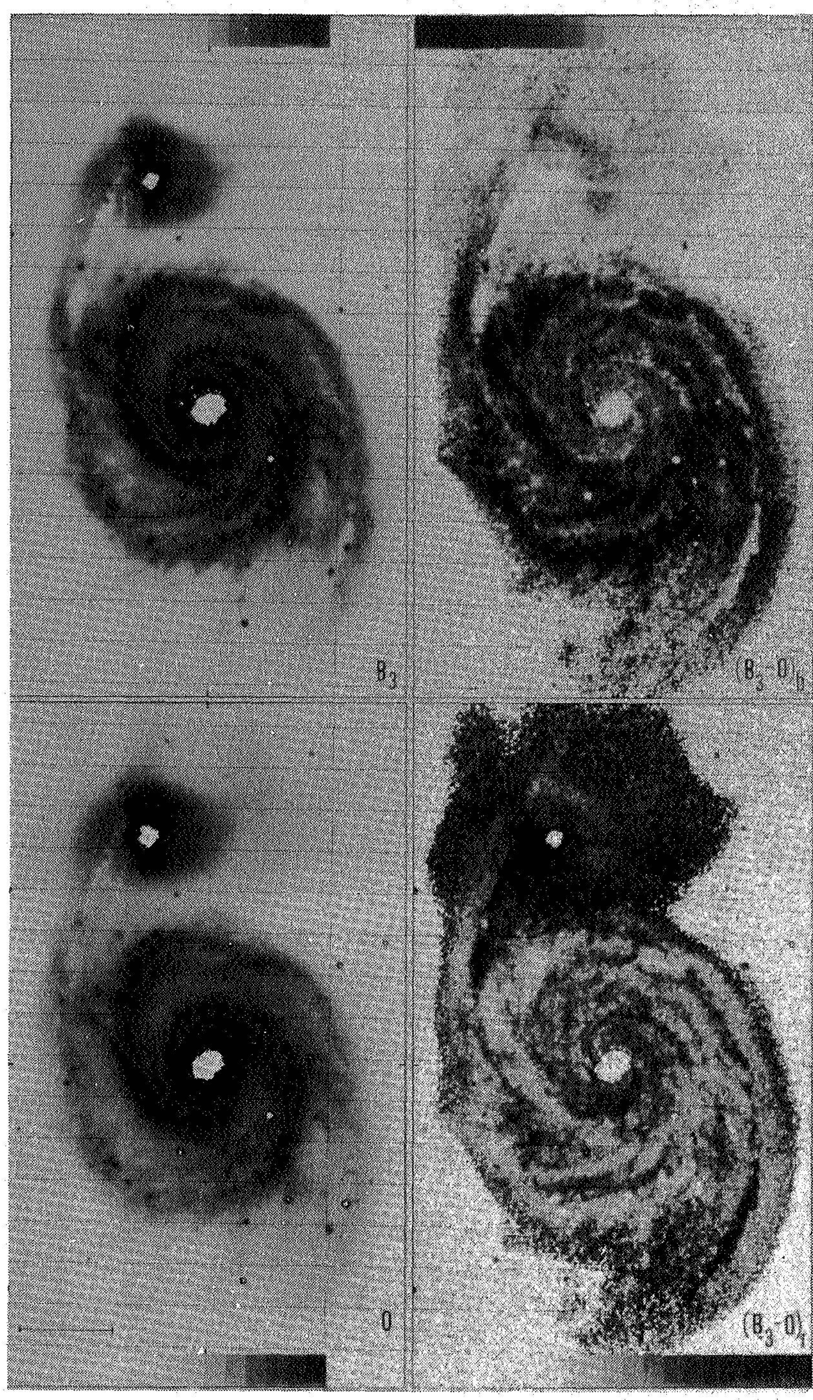

Figure 16. Surface brightness and color index maps of M51: in the lower left panel, the spiral pattern is interpreted as an azimuthal density variation in the old stellar disk population, as identifiable in a background stellar density wave (from Schweizer, 1976).

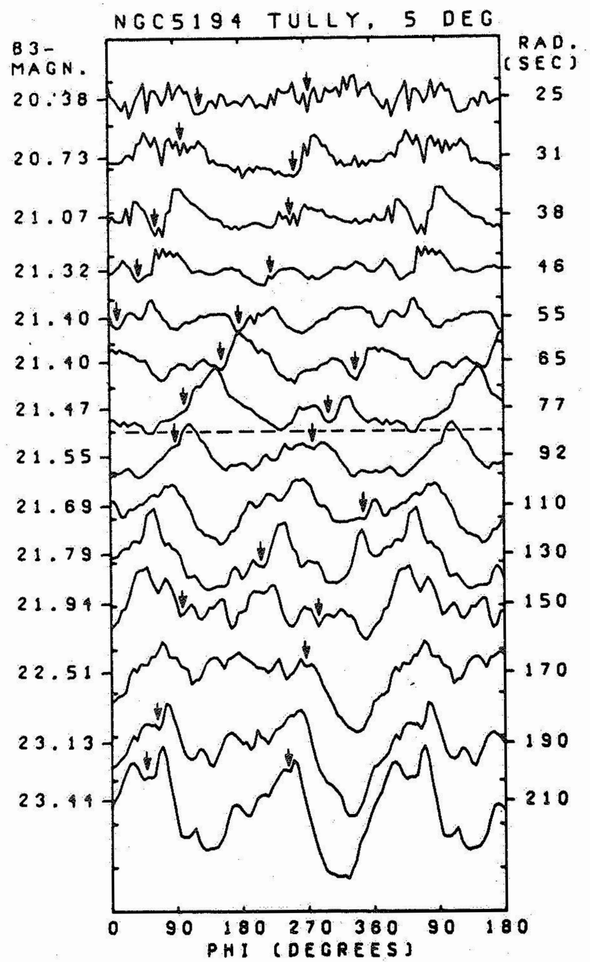

Figure 17. Azimuthal surface brightness profiles of M51 in the B3 passband: the strong dust lanes (arrows) often found on the inside edge of the arm profiles are actually shifted a little onto the rising inside slope (from Schweizer, 1976).

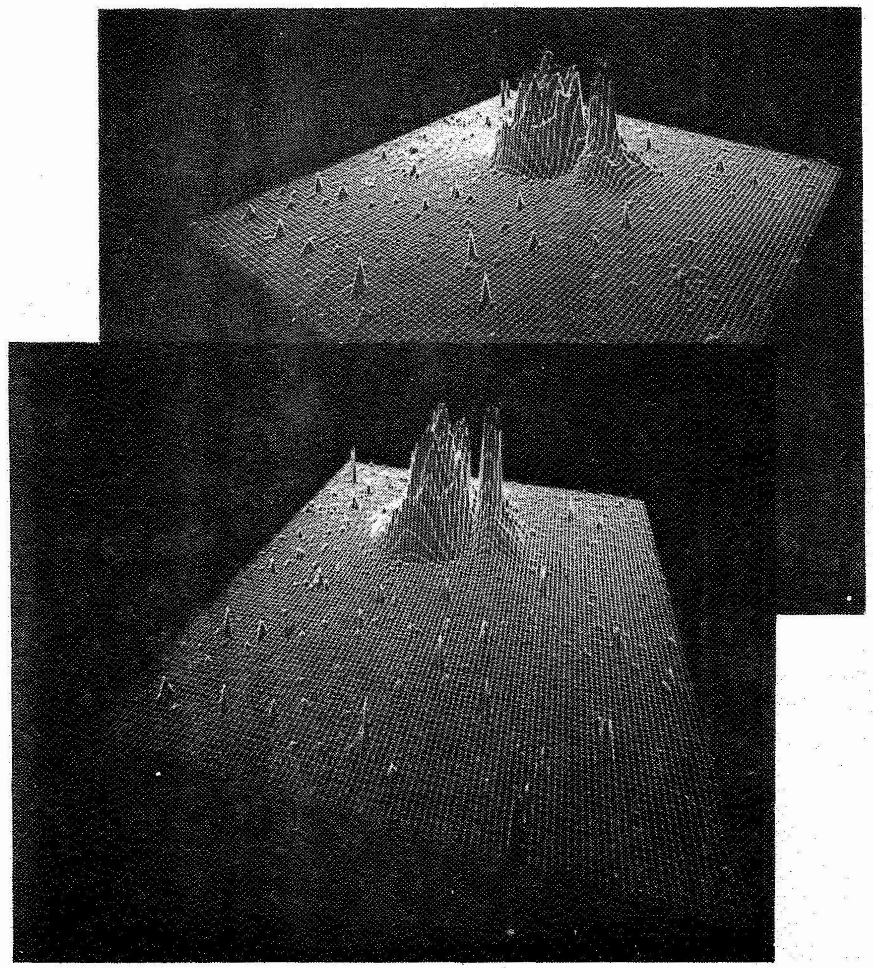

Figure 18. Two projections of a three-dimensional map of the surface brightness of M51 and its companion NGC5195 in a yellow-green passband: the spiral arms are visible winding up the slopes of the mountain of total surface brightness (from Burkhead, 1976).

THE SAMPLE GALAXY, NGC3031-M81—OBSERVATIONAL STUDIES

Another rather striking galaxy—on the $w_{\perp 0}$ surface near our own galaxy in figure 12—for which high-resolution 21-cm line observations have been possible is the galaxy NGC3031-M81. Figure 19 contains a radio photograph from Rots and Shane (1975) of the observed density distribution of neutral hydrogen in M81. Although there is a great deal of detailed structure, two major arms of neutral hydrogen seem to stand out as rather prominent spiral features. These HI arms are also closely coincident with the optical arms and the dust. Figure 20 shows the observed velocity field, determined by Rots (1975), superposed on the radio photograph.

Figure 21 from Rots (1975) shows the HI surface-density distribution as a function of the spiral phase around three circular bands in M81, each 2-kpc wide. The concentration of neutral hydrogen in the spiral arms is clearly visible, with the eastern arm around 0° in spiral phase and the western arm around 180°. Moreover, the density distribution appears to be of such a nature that the arm peaks are substantially narrower than the interarm troughs, altogether indicative of nonlinear wave phenomena.

Rots (1975) also plots the average B-V color in the circular band between 4 and 6 kpc as a function of spiral phase, and this is shown in figure 22. In view of the HI distribution in the upper panel of figure 21, a correlation seems to exist between HI and color in the sense that the higher the surface density of HI is, the bluer the color. Indeed the blue regions delineated by the troughs here appear even narrower than the corresponding arm peaks of HI (in the 4- to 6-kpc band) in figure 21. If these regions of bluer color are interpreted to represent relative increases in the number of young stars forming from the HI, then it would appear that star formation is occurring with prominence only in the limited regions of the HI spiral arms. Rots (1975) finds that there is actually a time lag between the highest density of very young stars and the maximum HI surface density of the order of 10 to 15°, which corresponds to an order of 10 million years, in the sense that the stars are forming with most prominence just outside the ridge of the HI arm from gas that has already just entered and been compressed within this ridge region. This observed time lag between the HI peak and the concentration of young stars across the spiral arms of M81 is just the temporal sequence expected in the theory between the shock and HI peak and the region of highest concentration of young stars and HII regions. Consequently, these observational results on M81 suggest that this galaxy is another example that exhibits features predicted in the wave picture.

Visser (1975a) applies the theoretical picture to simulate the nonlinear large-scale gas flow in M81. Figure 23 illustrates the theoretically calculated field of line-of-sight velocities superposed on a 200-inch photograph of M81. The overall trend of loci of equal heliocentric velocities indicates the general rotation of M81, whereas the crests and troughs of the contours reflect the systematic motions predicted along the wave arms. With the inclusion of the effect of beam smearing as shown in figure 24 (Visser, 1975b) (which is an unavoidable effect inherent in observations), substantial progress toward a deeper understanding of M81 is possible through a comparison of the smoothed theoretical velocity field (figure 24) and the observed velocity field (figure 20).

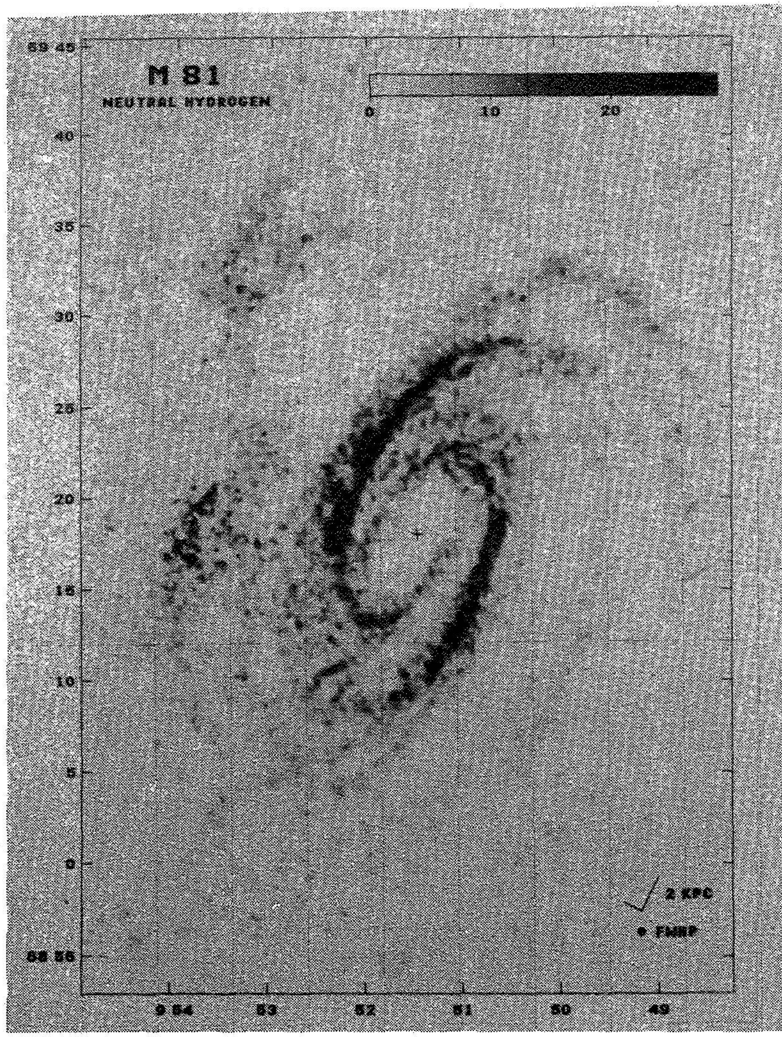

Figure 19. Radiograph of the density distribution of neutral hydrogen in NGC3031-M81: two major arms of HI stand out as rather prominent features (from Rots and Shane, 1975).

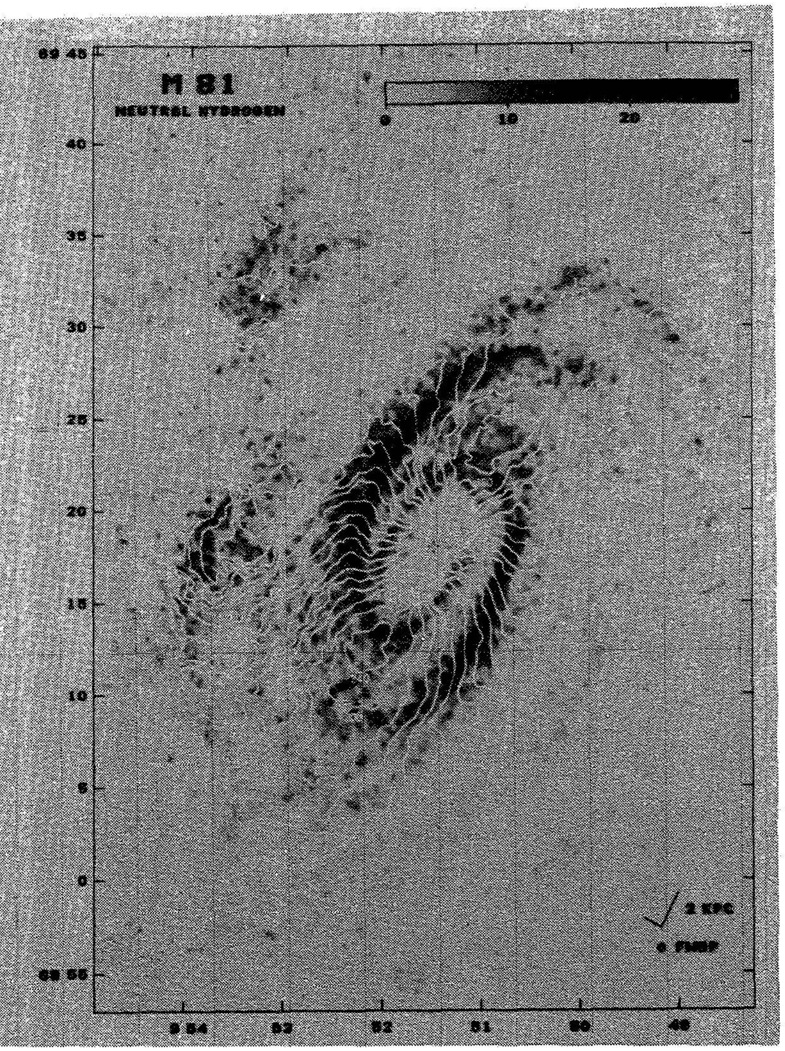

Figure 20. Observed velocity field of M81: a sequence of crests and troughs in the velocity contours is apparent near the arms, particularly the eastern arm (from Rots, 1975).

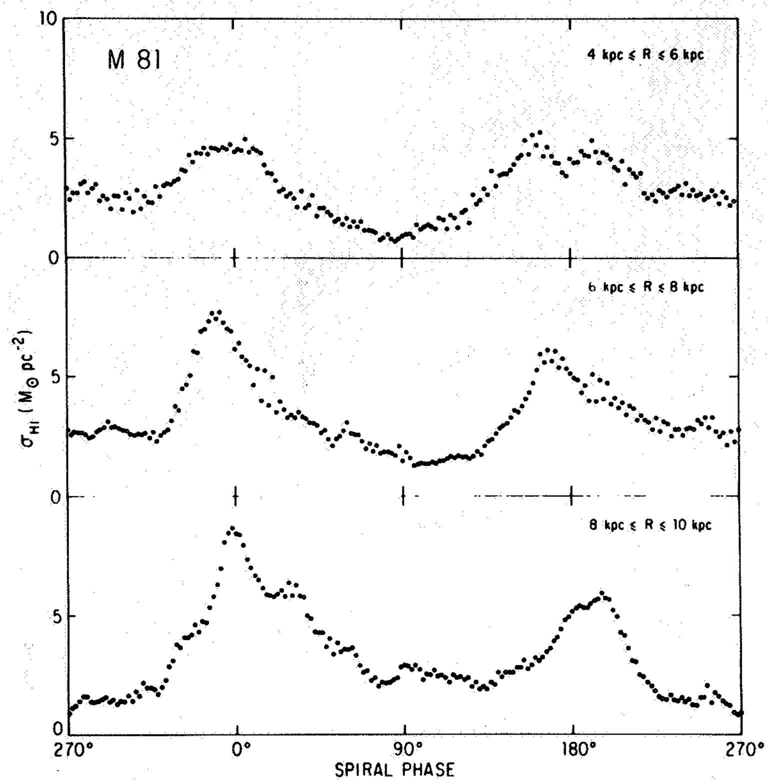

Figure 21. HI surface density as a function of spiral phase about the disk of M81: the three panels show different radius ranges. The concentration of neutral hydrogen into spiral arms is quite clear with the arm peaks substantially narrower than the interam troughs (from Rots, 1975).

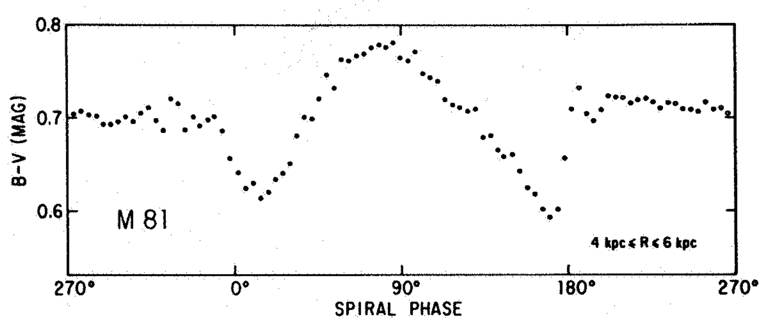

Figure 22. B-V color as a function of spiral phase about the disk of M81: this plot can be directly compared with the upper panel in figure 21. The arm ridges where the HI is most compressed (figure 21) correspond to the bluer regions (troughs in figure 22) where young stars may be forming with prominence (from Rots, 1975).

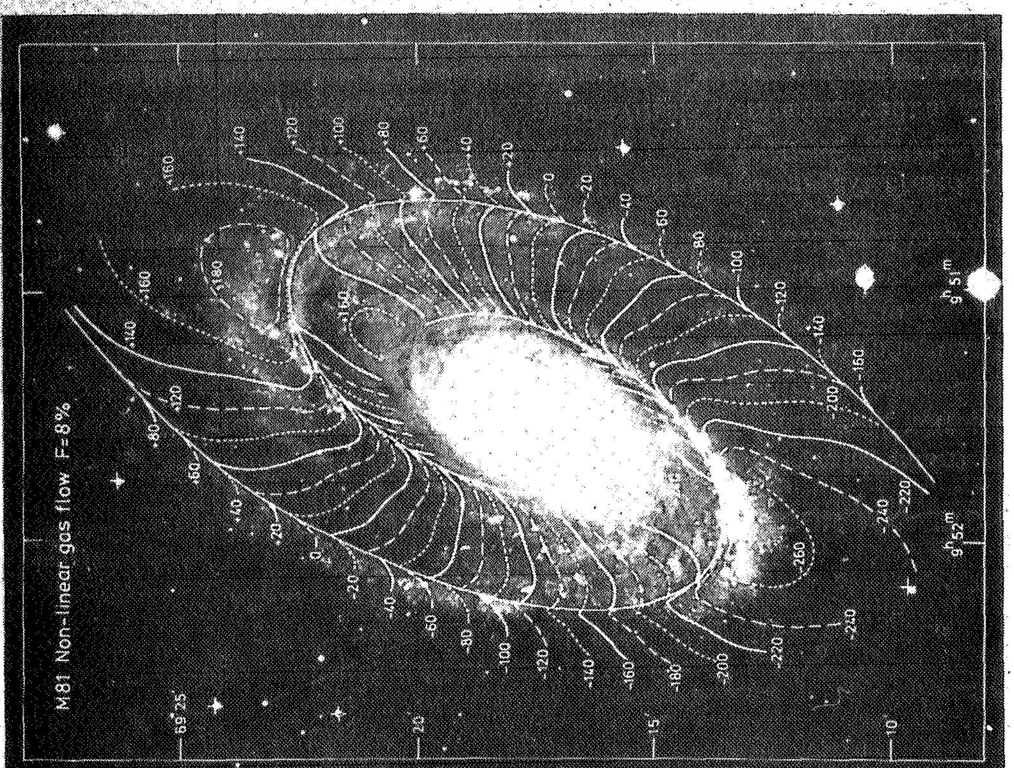

Figure 23. Theoretical velocity field of M81 with the presence of shock waves superposed on a 200-inch photograph (from Visser, 1975a).

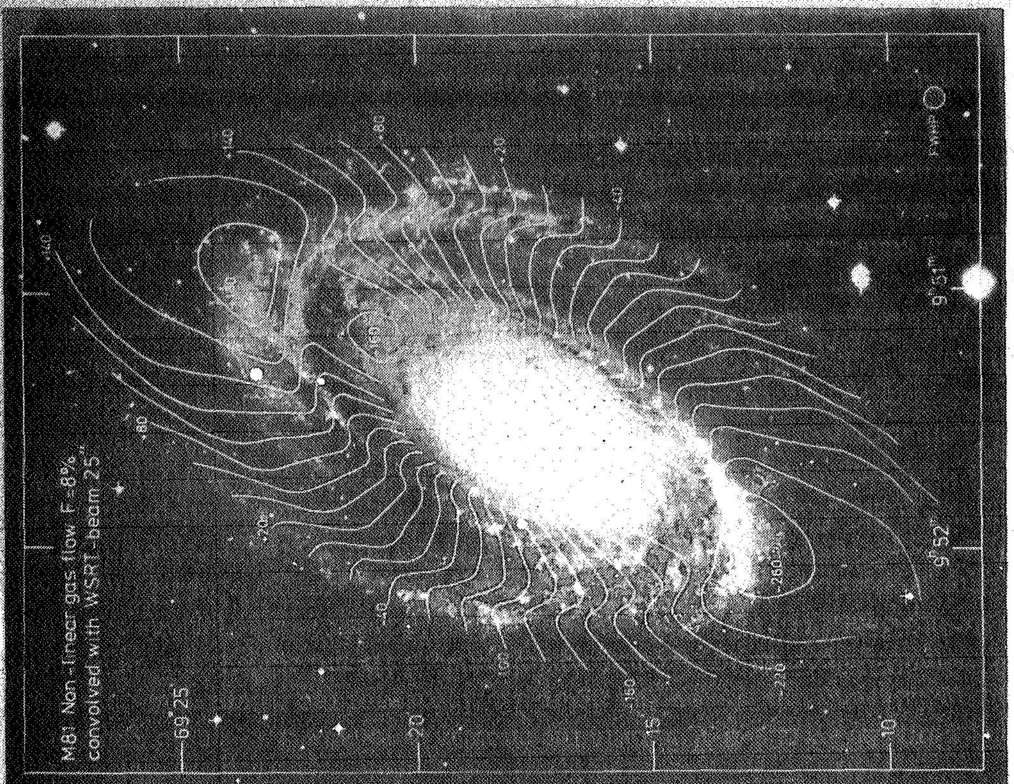

Figure 24. Smoothed theoretical velocity field of M81 after the effect of beam smearing is taken into account (from Visser, 1975b).

OUR GALAXY

We now turn to focus on our own Milky Way System. Hopefully, these concepts of density wave theory which seem to be playing an important role in M51 and M81—two extragalactic systems for which we enjoy a bird's-eye view—can be borrowed and applied to help us better understand our own galaxy.

Figure 25 provides curves of $w_{\perp 0}$ for two possible choices of corotation radius in our galaxy (see Burton, 1976). Because of the high levels attained by $w_{\perp 0}$, potentially strong shocks and high gas compressions are possible in the inner parts of the galaxy, and these have been calculated even for small-to-moderate forcing, F (Roberts, 1969; and Shu et al., 1972). Simultaneously, the frequency of compression, $2(\Omega\text{-}\Omega_p)$, with each passage through a spiral-wave crest is also substantially higher in the inner parts due to the differential rotation inherent in the galactic disk. Both these effects—the potential strength of gas compression and the frequency of compression—tend to make the conditions for star formation and molecule formation rather favorable in the inner parts of the galaxy, perhaps inwards as far as inner Lindblad resonance about 4 kpc where the spiral wave is thought to terminate (see Shu 1975; Oort, 1973; and Segalovitz, 1975, for application to M81).

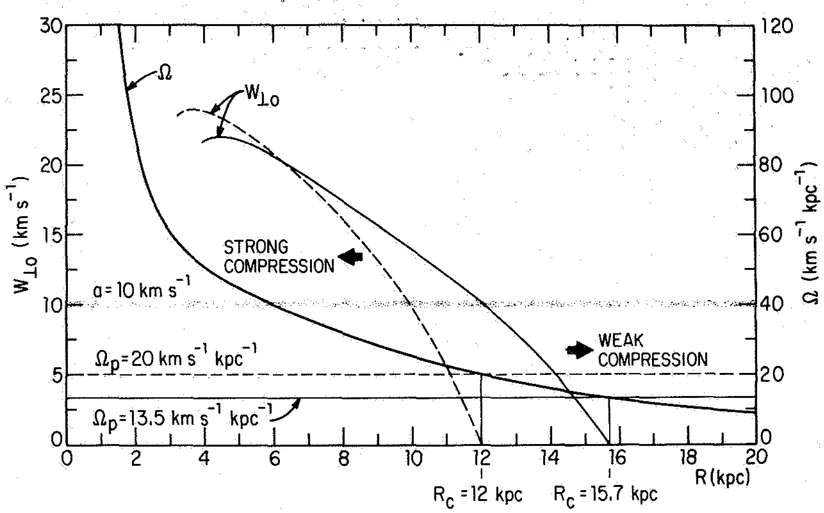

Figure 25. Characteristics of the density-wave picture for our galaxy: strong shocks and high gas compressions are possible (and have been calculated) in the inner parts where $w_{\perp 0} > a$. The frequency of gas compression in shocks is also high in the inner parts. These factors suggest that the conditions for shock-triggered star formation and molecule formation may be favorable in the inner parts of our galaxy (Burton, 1976).

Both $w_{\perp 0}$ (and potential shock strength) and the frequency of compression, $2(\Omega\text{-}\Omega_p)$, decrease with increasing radius in the galaxy. Moreover, in the outer regions over the range of radii near the solar circle where the intrinsic frequency, ν, of the density wave satisfies the relation

$$\nu^2 - \alpha^2 = n^{-2} \tag{4}$$

ultraharmonic resonances can occur in the gas (Shu et al., 1973). Here, α is the intrinsic acoustic speed of the gas, and $n = \pm 2, \pm 3, \pm 4, \ldots$. Such ultraharmonic resonances tend to produce secondary compressions and secondary arm structures in the gas. These secondary features bear some resemblance to the secondary arms, spurs, and feathers often observed (with a bird's-eye view) in the outer parts of many external spirals. However, their presence, more than anything else, probably confuses any coherence that the overall spiral structure might otherwise have in these outer regions. For larger radii outside the solar circle toward corotation where $w_{\perp 0} < a$, only very weak shocks, if any at all, are possible, together with broad regions of relatively low gas compression. Therefore, in these outer regions where there may be a lack of coherence, as well as a lack of sufficient gas compression, the conditions for efficient and coherent star formation and molecule formation may be rather unfavorable except in unusual local environments.

Figure 26 shows the radial abundance distribution of the carbon-monoxide molecule in our galaxy found by Gordon and Burton (1976). By relating the CO densities to those of molecular hydrogen on the basis of solar abundances, Gordon and Burton (1976) further derive the radial abundance distribution of H_2 in the galaxy. This is shown in figure 27, together with their deduced distribution for total interstellar nucleons. Stecker, et al. (1975) find that the abundance distributions for CO and H_2 are more concentrated than that of the HI toward the inner parts of our galaxy, as well as more concentrated than that of the HI toward the galactic plane. This separation of the peak concentrations of CO and H_2 from that of the HI suggests that there exists a factor other than the average neutral hydrogen-gas density which controls the present-day formation of molecules (and perhaps young stars) in the galaxy. If we adopt the density-wave picture in which the present-day formation of molecules (as well as young stars) occurs, in part, as a result of compression in a galactic shock wave, it is possible to account for this striking separation as a consequence of: (1) the inward increase of the gas-density compression (and $w_{\perp 0}$), and (2) the inward increase of the frequency, $2(\Omega\text{-}\Omega_p)$, at which the interstellar gas is periodically compressed. Because stellar density waves are absorbed at inner Lindblad resonance and cannot propagate inside this region, substantial molecule formation by the wave mechanism is not expected inside 4 kpc.

Similar morphological characteristics also seem to distinguish the distributions of a number of other constituents and tracers—HII regions, supernova remnants, pulsars, γ-radiation, synchrotron radiation, and other molecules—from that of the neutral hydrogen (Burton, 1976). It is intriguing to consider the prospect that the compression-wave mechanism, if strong enough, might play an important role in the formation and large-scale distribution of many of these constituents and tracers as well.

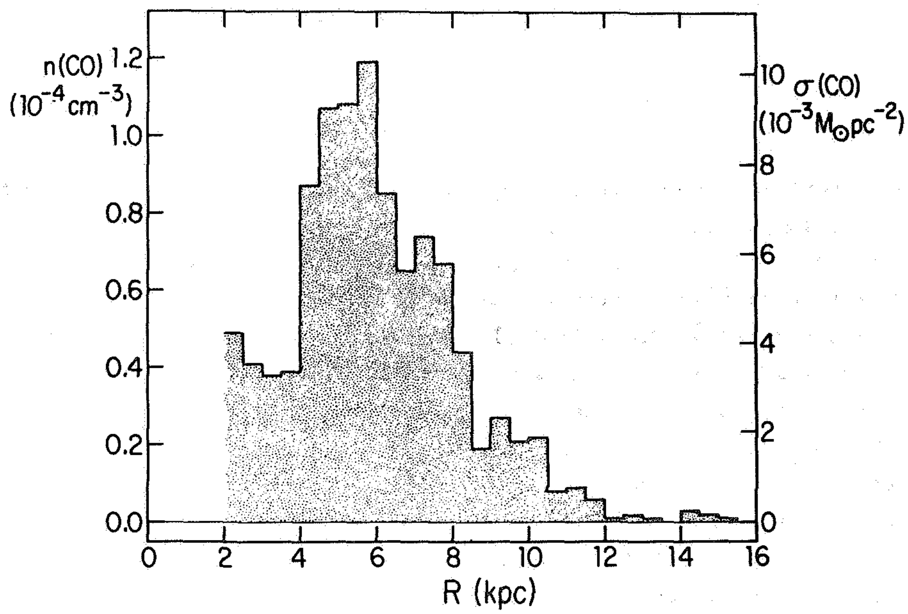

Figure 26. Radial distribution in the galaxy of $^{12}C^{16}O$ volume densities at b = 0° (left-hand ordinate) and of the projected $^{12}C^{16}O$ surface densities (right-hand ordinate) (from Gordon and Burton, 1976).

Optical observations of the spiral structure of our galaxy are confined to the realm of a few kiloparsecs in radius about the Sun. For this reason, the current picture of the large-scale spiral structure rests primarily on radio observations of the 21-cm line of neutral hydrogen. Unfortunately, from our vantage point within our Milky Way System, we have difficulty in seeing the forest because of the trees.

As Burton (1972) has demonstrated, it is extremely difficult, if not impossible, to interpret a profile of the 21-cm line of neutral hydrogen unambiguously, particularly with both the gas density and the gas velocity varying along the line of sight. Of course, in the density-wave theory, a relation between density and velocity does exist. However, because of the uncertainty in the choice of specific values for the parameters of the model and because of uncertainties in the physical properties and state of the HI gas and the interstellar medium (with multiphases, multicomponents, turbulence, complicated cloud structures, etc.), the interpretation of line profiles is still very difficult.

Despite these uncertainties, Simonson (1976) works toward a simulation of large-scale spiral structure by constructing a model based on density-wave kinematics that reproduces many of the main features of the 21-cm HI observations. Figure 28 provides a synthetic optical photograph of Simonson's (1976) simulated model of our galaxy as revealed through the 21-cm line profiles. A basically two-armed spiral pattern with a pitch angle of 6 to 8° is apparent

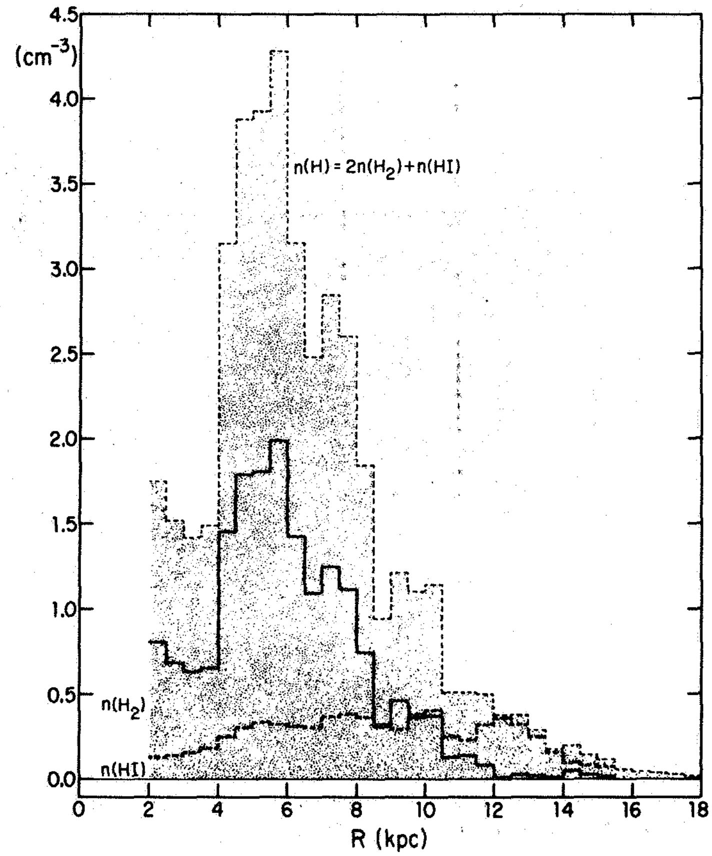

Figure 27. Radial distribution in the plane of the galaxy of volume densities of atomic and molecular hydrogen: the distribution of the sum, 2 n(H_2) + n(HI), indicates the overall distribution of interstellar nucleons (from Gordon and Burton, 1976).

between the 4-kpc dispersion ring and the solar circle. Near the solar circle, two additional arms originate, and the pattern outside is multiple-armed.

PERSPECTIVE TOWARD THE FUTURE

Toward the future, the outlook is optimistic. Definitive scientific research generally motivates further scientific research, no matter what the discipline. Most certainly of great benefit will be current and future observational studies and theoretical work on the various constituents and tracers delineating the structure, content, and dynamics of our galaxy, as well as extragalactic systems—HI, CO, OH, and H_2 and young stars, HII regions, supernova remnants, pulsars, γ-radiation, synchrotron radiation, and others.

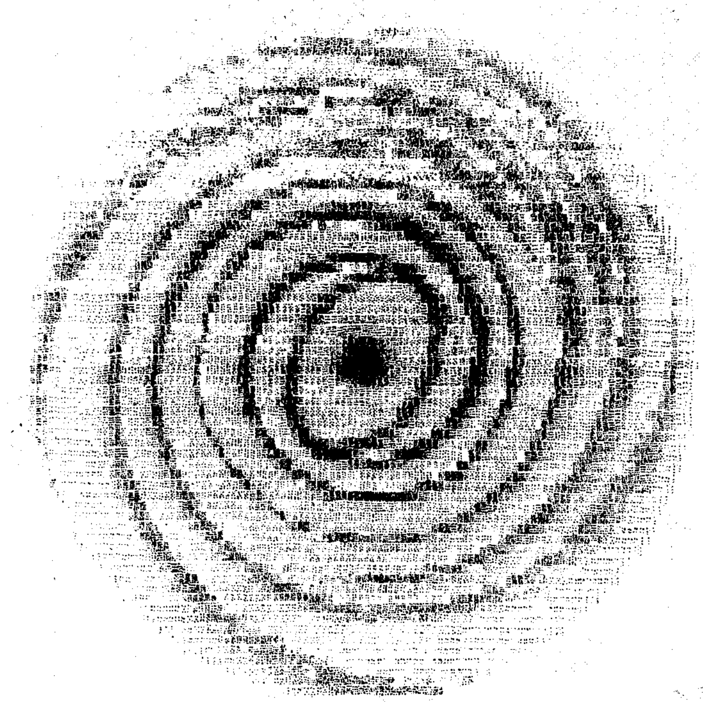

Figure 28. Synthetic optical photograph of a simulated model of our galaxy using density wave kinematics as deduced from 21-cm line profiles of neutral hydrogen (from Simonson, 1976).

Already, there are many exciting problems ripe for the challenge of future investigations. Answers are needed to such questions as: Does our galaxy indeed possess spiral structure, which many extragalactic systems seem to be capable of exhibiting for our bird's-eye viewing? If so, how coherent is it, and why do the present CO observations, for example, not show a better delineation of spiral structure in our galaxy? From our vantage point, how severely do we suffer from not seeing the forest because of the trees? Although the abundance distribution of CO does drop off within the inner 4 kpc in our galaxy in qualitative agreement with the compression-wave mechanism, why does the CO not drop off more abruptly there? Might the compression-wave mechanism be capable of penetrating to a sufficient distance inside 4 kpc to account for this low level of CO present, or need there be other sources? Indeed, these are only a few of the intriguing questions and problems that could be mentioned; there are many others.

At the present time, theoretical results and developments are progressing well on many fronts; exciting new observational results are springing forth; and theoreticians and observationalists alike have the opportunity to learn a great deal more and broaden our present understanding. The interaction between theory and observations is extremely important for the purpose of providing new challenges to current theory and to current observational techniques toward their better and better refinement.

ACKNOWLEDGMENTS

I would like to thank Martin Burkhead, Butler Burton, Jim Huntley, Arnold Rots, Francois Schweizer, Chris Simonson, and Herman Visser for supplying a number of the photographs included in this review, in many cases prior to publication. I would also like to thank Jim Huntley for preparing the photographic simulations. This work was supported in part by the National Science Foundation under grant AST72-05124 AO3.

REFERENCES

Biermann, P., R. Kippenhahn, W. Tscharnuter, and H. Yorke, 1972, *Astron. & Astrophys.*, **19**, p. 113.

Biermann, P., and B. M. Tinsley, 1974, *Publ. Astron. Soc. Pacific*, **86**, p. 791.

Burkhead, M., 1976, private communication.

Burton, W. B., 1972, *Astron. & Astrophys.*, **19**, p. 51.

Burton, W. B., 1976, *Ann. Rev. Astron. & Astrophys.*, **14**.

Feldman, S. I., and C. C. Lin, 1973, *Stud. Appl. Math.*, **52**, p. 1.

Fujimoto, M., 1966, (IAU Symp. No. 29), p. 453.

Gordon, M. A., and W. B. Burton, 1976, *Ap. J.*, in preparation.

Jensen, E. B., K. M. Strom, and S. E. Strom, 1976, in preparation.

Lau, Y. Y., C. C. Lin, and J. W.-K. Mark, 1976, in preparation.

Lin, C. C., 1970, (Proc. IAU Symp., No. 38), p. 377.

Lin, C. C., 1971, *Highlights of Astr.*, **2**, D. Reidel Publishing Co., Dordrecht, Holland, p. 88.

Lin, C. C., and F. H. Shu, 1964, *Ap. J.*, **140**, p. 646.

Lin, C. C., and F. H. Shu, 1966, (Proc. Nat. Acad. Sci.), **55**, p. 229.

Lin, C. C., and Y. Y. Lau, 1975, *Siam J. Appl. Math.*, **29**, pp. 2, 352.

Lindblad, B., 1963, *Stockholm Obs. Ann.*, **22**, p. 3.

Lindblad, B., R. G. Langebartel, 1953, *Stockholm Obs. Ann.*, **17**, p. 6.

Lynden-Bell, D., and A. J. Kalnajs, 1972, *MNRAS*, **157**, p. 1.

Mark, J. W.-K., 1974, *Ap. J.*, **193**, p. 539.

Mark, J. W. -K., 1976a, *Ap. J.*, **203**, p. 81.

Mark, J. W. -K., 1976b, *Ap. J.*, May issue.

Mark, J. W. -K., 1976c, *Ap. J.*, June issue.

Mark, J. W. -K., 1976d, *Ap. J.*, in preparation.

Mathewson, D. S., P. C. van der Kruit, and W. N. Brouw, 1972, *Astron. & Astrophys.*, **17**, p. 468.

Mouschovias, T. Ch., F. H. Shu, and P. R. Woodward, 1974, *Astron. & Astrophys.*, **33**, p. 73.

Mufson, S. L., 1974, *Ap. J.*, **193**, p. 561.

Mufson, S. L., 1975, *Ap. J.*, **202**, p. 372.

Oort, J. H., 1973, (IAU Symp. No. 58).

Roberts, W. W., 1969, *Ap. J.*, **158**, p. 123.

Roberts, W. W., M. S. Roberts, and F. H. Shu, 1974, (IAU Symp. No. 58), p. 439.

Roberts, W. W., M. S. Roberts, and F. H. Shu, 1975, *Ap. J.*, **196**, p. 381.

Roberts, W. W., and C. Yuan, 1970, *Ap. J.*, **161**, p. 877.

Rots, A. H., 1975, *Astron. & Astrophys.*, **45**, p. 43.

Rots, A. H., and W. W. Shane, 1975, *Astron. & Astrophys.*, **45**, p. 25.

Sandage, A. R., 1961, *The Hubble Atlas of Galaxies*, Carnegie Institution of Washington Washington, D.C.

Sanders, R. H., and J. M. Huntley, 1976, *Ap. J.*, in preparation.

Sawa, T., 1975, Sci. Reports Tohoku Univ. Series I, No. LVIII, p. 13.

Schweizer, F., 1976, *Ap. J.*, in preparation.

Segalovitz, A., 1975, *Astron. & Astrophys.*, **40**, p. 401.

Shu, F. H., 1974, *Astron. & Astrophys.*, **33**, p. 55.

Shu, F. H., 1975 (Proc. Colloquim on Spiral Galaxies, Bures Sur Yvette), p. 309.

Shu, F. H., V. Milione, W. Gebel, C. Yuan, D. W. Goldsmith, and W. W. Roberts, 1972, *Ap. J.*, **173**, p. 557.

Shu, F. H., V. Milione, and W. W. Roberts, 1973, *Ap. J.*, **183**, p. 819.

Shu, F. H., R. V. Stachnik, and J. C. Yost, 1971, *Ap. J.*, **166**, p. 465.

Simonson, S. C., III, 1976, *Astron. & Astrophys.*, **46**, p. 261.

Stecker, F. W., P. M. Solomon, N. Z. Scoville, and C. E. Ryter, 1975, *Ap. J.*, **201**, p. 90.

Toomre, A., 1969, *Ap. J.*, **158**, p. 899.

Toomre, A., and J. Toomre, 1972, *Ap. J.*, **178**, p. 623.

van den Bergh, S., 1960a, *Ap. J.*, **131**, p. 215.

van den Bergh, S., 1960b, *Ap. J.*, **131**, p. 558.

van der Kruit, P. C., 1973, *Astron. & Astrophys.*, **29**, p. 263.

van der Kruit, P. C., J. H. Oort, and D. S. Mathewson, 1972, *Astron. & Astrophys.*, **21**, p. 169.

Vandervoort, P. O., 1970, *Ap. J.*, **161**, p. 67.

Visser, H. C. D., 1975a, (Symp. on Galactic Dynamics, Bures-sur-Yvette, France), p. 211.

Visser, H. C. D., 1975b, private communication.

Wielen, R., 1975 (Conf. Optical Observing Programs, Bochum, German), p. 59.

Woodward, P. R., 1976, *Ap. J.*, in preparation.

THE GALACTIC DISTRIBUTION (IN RADIUS AND Z) OF INTERSTELLAR MOLECULAR HYDROGEN*

N. Z. Scoville
Department of Physics and Astronomy
University of Massachusetts
Amherst, Massachusetts 01002

P. M. Solomon and D. B. Sanders
Department of Earth and Space Sciences
State University of New York
Stony Brook, New York 11794

ABSTRACT

New observations of the galactic longitude and latitude distributions of $\lambda = 2.6$ mm CO emission are presented. Analysis of these spectral-line data yields the large-scale distribution of molecular clouds in the galactic disk and their z-distribution out of the disk. Strong maxima in the number of molecular clouds occur in the galactic nucleus and at galactic radii 4 to 8 kpc. The peak at 4 to 8 kpc correlates well with a region of enhanced 100-MeV γ-ray emissivity. This correlation strongly supports the conclusion of Stecker et al. (1975) that the γ-rays are produced as a result of cosmic-ray interactions in molecular H_2 clouds rather than in HI. One important implication of this is that the interstellar magnetic-field lines to which cosmic rays are confined must therefore not be exluded from these dense clouds.

The width of the cloud layer perpendicular to the galactic plane between half-density points is 105 ± 15 pc near the 5.5-kpc peak. The total mass of molecular gas in the interior of the galaxy exceeds that of atomic hydrogen and is $3 \cdot 10^9$ $M_\odot$ based on these observations.

INTRODUCTION

Until just the last year, there was little appreciation of the possibility that clouds of molecular H_2 rather than atomic hydrogen might constitute the dominant contribution to the

*This paper is Contribution 232 of the Five College Observatories. The research of Nicholas Scoville is partially supported by NSF Grant MPS73-D4949.

interstellar mass. The importance of the H_2 gas on a galactic scale was overlooked, essentially because it was impossible to detect from the ground. The rotational and vibrational transitions of H_2 are weak infrared quadruple lines, and observations of the ultraviolet resonance lines are limited to clouds of low visual extinction (< 1 mag) in front of nearby O and B stars (e.g., Spitzer et al., 1973). Our knowledge of H_2 in selected more opaque and more distant gas clouds has instead been deduced from observations of relatively rare trace molecules like CO, CS, and HCN which have fundamental rotation lines at $\lambda = 1 \rightarrow 6$ mm.

Recently, observations of the CO $J = 1 \rightarrow O$ line at 2.6 mm have been extended to surveys of this emission throughout the galactic plane (Scoville and Solomon 1975; and Burton et al., 1975). Scoville and Solomon (1975) used their CO observations to deduce the overall distribution and mass of molecular hydrogen in the galaxy. The relevance of these studies to observations of galactic γ-rays (Fichtel et al., 1975) rests on our early conclusion that "within the region of the galaxy interior to the solar circle, molecular hydrogen, not HI, is the dominant constituent of the interstellar medium." Stecker et al. (1975) have pointed out that the distribution of molecular hydrogen derived from the CO observations is very similar to the "missing" interstellar matter distribution required to account for the observed rise in γ-ray emission at galactic radii 4 to 8 kpc. The consistent conclusion of both analyses is that, at the peak in the molecular cloud distribution ($\bar{\omega} = 5.5$ kpc), perhaps 90 percent of the interstellar gas is H_2, and, as one moves outward in the galaxy, the ratio H_2/HI decreases until, at the solar circle, the two abundances are about equal.

In the following, we first review CO data obtained in the galactic plane ($b = 0$) from which one derives the radial distribution of CO (and H_2) outside the galactic nucleus. Then, some of our most recent observations pertaining to the z-distribution of molecular clouds are discussed. Because the CO emission from the galactic center shows quite different characteristics from that seen elsewhere in the galactic plane, we have devoted a separate section to analysis of the emission seen at $\ell \leq 3°$. Finally, in the last section, we are then able to estimate the mass and surface density contained in interstellar molecular hydrogen by integrating the radial distribution function over galactic radius and z.

CONSIDERATIONS FOR INTERPRETATION OF CO OBSERVATIONS

It is in no way obvious that the CO intensities we have observed at different positions in the galaxy should be a proportional indicator of gas column densities. Very generally, the line is found to be optically thick, and, in clouds having high gas density, the intensities will correlate with gas temperatures, not with gas densities. On the basis of ^{12}CO data alone, it is impossible to tell in what fraction of the clouds observed in the plane the CO is thermalized. Our limited ^{13}CO data obtained at three positions indicates that the CO is probably not thermalized in roughly one-half of the clouds.

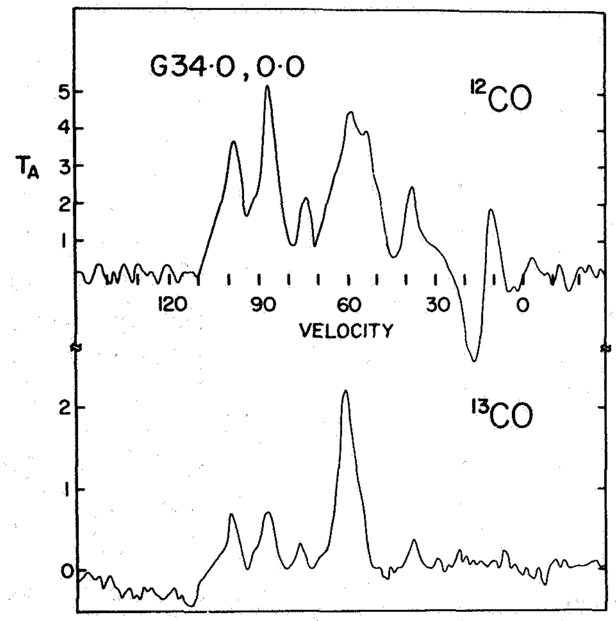

Figure 1. CO and ^{13}CO spectra are shown for the direction $\ell = 34°$, $b = 0°$. Note that there are at least five discrete features in the CO spectra, each of which has a counterpart in ^{13}CO. The negative dip at $v = 20$ km/s in the CO spectra is caused by the presence of CO emission at that velocity in the reference position 3° above the galactic plane. The intensity units are Rayleigh-Jeans antenna temperatures, K.

Figure 1 shows emission of $^{12}C\,^{16}O$ and the rarer isotope, $^{13}C\,^{16}O$, obtained at the position $\ell = 34°$, $b = 0°$. The closest approach of this line of sight to the galactic center occurs at galactic radius 5.5 kpc near the molecular cloud maximum. The discrepancy between the observed intensity ratios $^{13}CO/^{12}CO$ (ranging from 1/2 to 1/6 among the five features seen in figure 1) and the much lower value of the interstellar abundance ratio $[^{13}CO/^{12}CO] = 1/40$ (Wannier et al., 1976) imply that these ^{12}CO lines are optically thick with $\tau > 6$. It must be an important consideration that the CO lines are optically thick, and the observed brightness temperatures are therefore equal to the excitation temperature characterizing the relative $J = 1$ and $J = 0$ level populations.

This excitation temperature is determined by the rate of collisions of H_2 with CO, by spontaneous radiative decay ($A_{10} = 6 \cdot 10^{-8}$ sec^{-1}), and by stimulated radiative absorption and emission. In the event that a cloud has $n_{H_2} < 3000$ cm^{-3}, the collisions by themselves would not be sufficient to thermalize the CO levels. However, if in this same region, the CO lines are optically thick, a line photon will be absorbed and scattered approximately τ times before it escapes the cloud. Thus, one may visualize that, when this "radiation trapping" occurs, each collisional excitation is replicated approximately τ times, and the observed excitation temperature will be in some manner proportional to τ. In a more technical treatment of the excitation which solves the full equations of statistical equilibrium for CO (Scoville and Solomon, 1974), we have found that, for a large regime giving subthermal excitation of optically thick CO,

$$T_B \simeq T_{\text{excitation}} \propto (n_{H_2} \cdot n_{CO})^{0.4} \tag{1}$$

Therefore, if the abundance ratio, n_{CO}/n_{H_2} from cloud to cloud is constant,

$$T_B \propto n_{H_2}{}^{0 \cdot 8} \tag{2}$$

As the densities increase and $T_{excitation} = T_K$, then T_B gradually loses its dependence on n_{H_2} altogether and develops a linear dependence on T_K.

In most of the clouds outside the galactic nucleus (see "Galactic Center" section), we feel that the densities are insufficient for complete thermalization, and, therefore, an intuition which associates increased CO intensity with increased gas density seems reasonable although it is hardly proven.

RADIAL DISTRIBUTION OF MOLECULAR GAS

The entire run of data from our earlier observations in the galactic plane (ℓ = - 10 to +90° sampled once every degree with a 1-arcmin beam) can be displayed in a single longitude-velocity diagram (figure 2). In this representation, a single spectrum observation constitutes a horizontal line of shading. One sees both intense high-velocity emission arising from molecular clouds in the galactic center ($\omega \leqslant 300$ pc; see Scoville et al., 1974) and many individual less-intense features which were sampled in the galactic plane outside the center.

A more useful representation of the CO emission for comparison with γ-ray observations is obtained by using the Schmidt (1965) rotation law to transform from the ℓ, v coordinates of figure 2 to galactic radius (figure 3). This figure provides our best indication of the molecular gas distribution in the galactic plane outside ω = 3 kpc. The vertical scale of figure 3 may be approximately transformed from $\langle T_A \rangle$ to n_{H_2} by setting $n_{H_2} = 4\ cm^{-3}$ at the 5.5-kpc peak (Scoville and Solomon, 1975). This H_2 distribution matches well that of other population I components except for atomic hydrogen (figure 4). It is very similar to the distribution of discrete HII regions (Mezger, 1970), diffuse ionized gas (Westerhout, 1958; and Lockman, 1976), and is consistent with the pulsar distribution (Seiradakis, this symposium; and Taylor and Hulse, 1976). And, most important for the discussion at hand, the H_2 distribution is identical to the γ-ray emissivity (Stecker et al., 1975) within observational errors and the uncertainty involved in unfolding the γ-ray longitude distribution. All of these results have been confirmed by the finer spaced, higher sensitivity CO observations of Gordon and Burton (1976) at b = 0 and our most recent, higher sensitivity observations in 1 and b (Solomon et al., 1976).

THICKNESS OF THE MOLECULAR GAS DISK

When making a comparison with γ-ray data, a major shortcoming of the published CO observations is that the 1-arcmin CO beam observed only the galactic plane, whereas the γ-ray data have a much lower angular resolution, including contributions from over 5° of latitude. Our newest observations and those of Cohen (1976) are therefore especially addressed to estimating the thickness of the molecular cloud layer. We have observed along strips perpendicular to the galactic plane from b = - 1 to + 1° every even degree of longitude in the

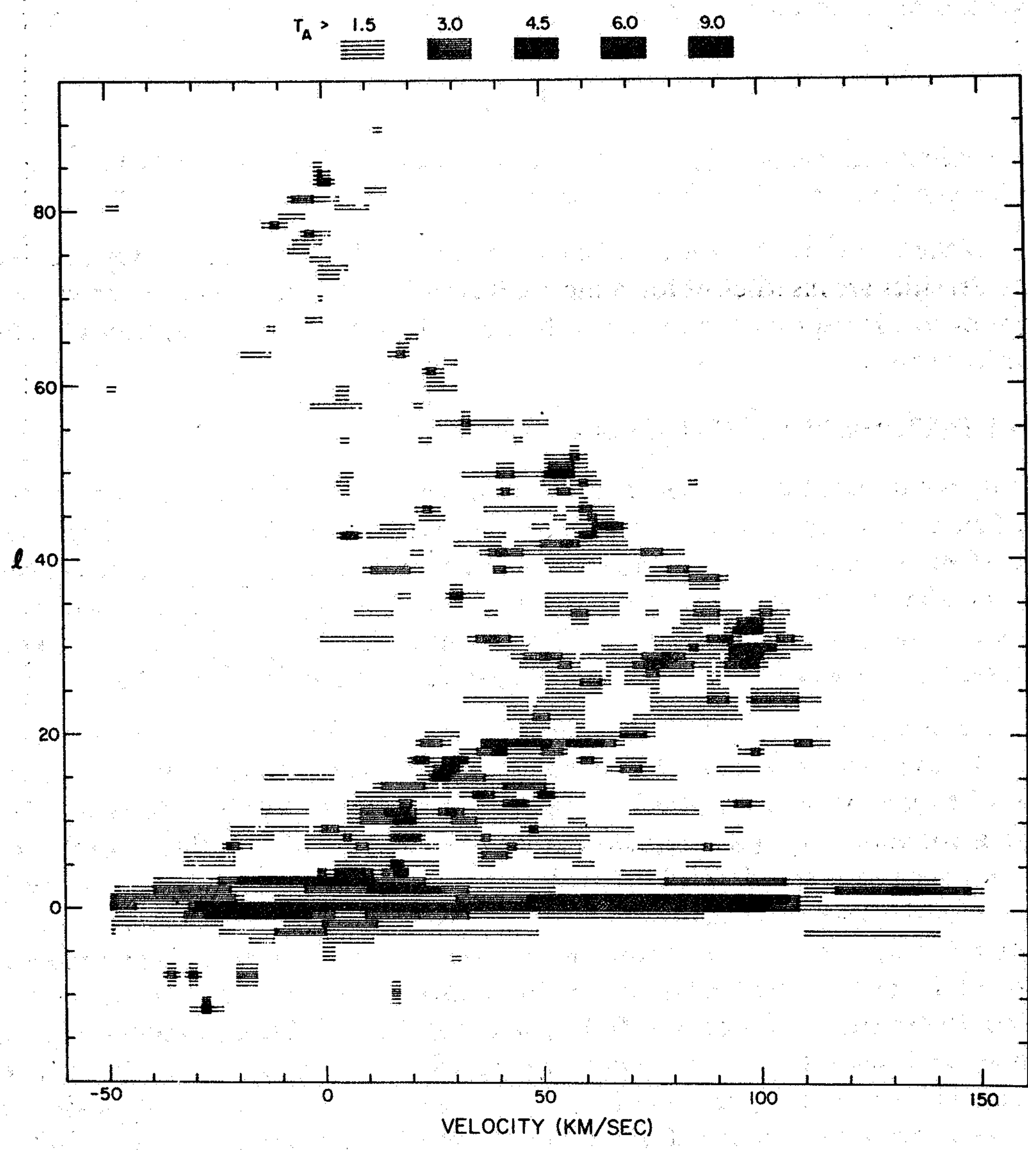

Figure 2. The intensity of CO emission along the galactic equator is shown as a function of longitude and velocity. Molecular emission tends toward lower longitudes and more positive radial velocities as compared with 21 cm (see Kerr, 1969), indicating that the molecules are concentrated toward the center of the galaxy. A version of this figure, spanning more velocities (±300 km s^{-1}) and therefore containing the full range found in the galactic center, may be found in Scoville (1975).

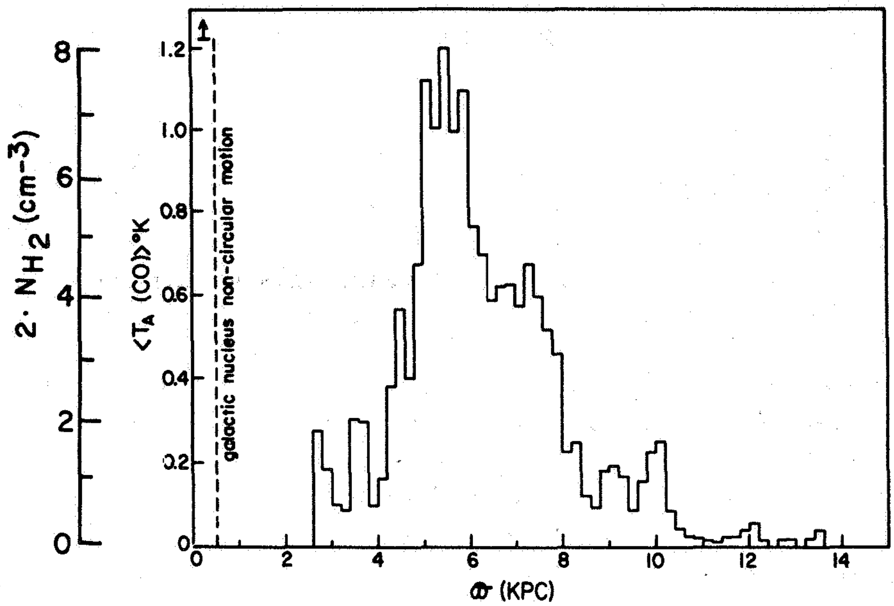

Figure 3. The mean CO antenna temperature as a function of radius in the galaxy ω, was calculated using the Schmidt (1965) rotation law to transform ℓ, v in figure 2 to ω. We use only data at $\ell \geqslant 10°$ in order to exclude the galactic center where much of the gas clearly is not in pure rotation. Note the sharp peak in CO at a radius of 5.5 kpc and the dramatic falloff toward the Sun and beyond. The vertical scale may also be converted to H_2 surface density through a normalization to 25 $M_\odot$ pc^{-2} at the 5.5-kpc peak. (See the last section of this paper.)

Figure 4. The surface density in giant HII regions (shaded area; Mezger, 1970) and free-free continuum radiation (figure 16 in Westerhout, 1958) show a remarkable similarity to the radial distribution of CO (figure 3). In contrast, the HI surface density varies little with galactic radius (Van Woerden, 1965).

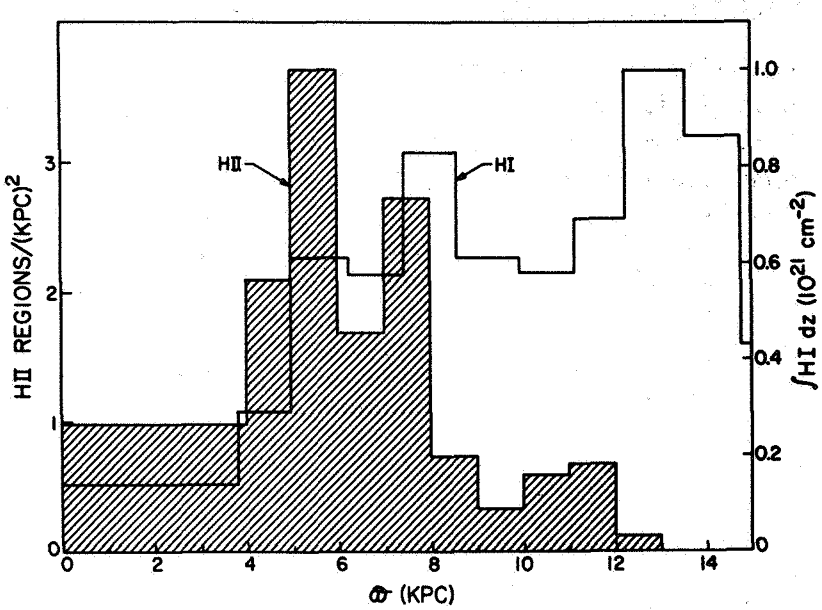

range $\ell = 0$ to $50°$. Although we have yet to fully analyze these new observations, samples in the form of integrated line intensities are shown in figures 5 and 6 and are tabulated in table 1.

Interpreting the intensity integral as a proportional indicator of the molecular column densities, we may use these data for estimating both the thickness and the central latitude of the clouds. The full width in latitude to half-intensity varies from $0\overset{\circ}{.}7$ to $1\overset{\circ}{.}0$ (excluding $\ell = 0°$). The mean latitude of this emission significantly deviates from the galactic plane in the 20 to 40° longitude range where $\langle b \rangle \simeq -0\overset{\circ}{.}2$, and most of the emission integral is contributed by gas in the 4- to 8-kpc ring. This amounts to a displacement $\langle Z \rangle$ of 40 pc below the plane. From the latitude thickness of the emission observed near the terminal velocity* at many longitudes $\ell = 10$ to $50°$, we have estimated that half-density points on either side of the plane are separated by 105 ± 15 pc at radii $4 \rightarrow 8$ kpc. This is in agreement with the crude value of 130 pc found in our earlier survey (Scoville and Solomon, 1975) and the estimate of 118 pc found by Burton and Gordon (1976) from data at $\ell = 21°$. A more sophisticated analysis of the data at all longitudes is planned in order to search for systematic variations of the scale height with galactic radius (Solomon et al., 1976).

Perhaps a most relevant quantity against which one should compare the γ-ray observations is the double integral of the line intensity over all velocities and over galactic latitude (last column of table 1). That the longitude dependence of this double integral is similar to the longitude distribution of 100-MeV γ-ray emission argues most persuasively in favor of the γ-rays being produced within molecular clouds. Indeed, this is perhaps the most straightforward comparison one can make. The alternative of comparing the radial distributions of γ-ray and CO emissivities which we have used in the past requires an assumption of azimuthal symmetry about the galactic origin. For a mere comparison of the two observations, the unfolding of both sets of data (in different ways) does not gain anything.

THE GALACTIC CENTER

One enigma in the comparison of CO and γ-ray emissions still remains. Within the inner 3° of longitude about $\ell = 0°$, there is a system of very dense, massive clouds. Here, the integrated CO emission is therefore 2 to 3 times the value at $\ell = 10$ to $30°$ (figures 5 and 7), yet the γ-ray emission varies less than 50 percent over the same longitudes. In interpreting the CO emission elsewhere in the galactic plane, it was convenient to imagine that all clouds had a similar kinetic temperature which was slightly above the observed brightness temperatures. One could justify this assumption observationally on the basis that all lines observed were weak (most had $T_A < 4$ K). However, in the galactic center clouds, the assumption is clearly not valid inasmuch as several of the CO features have $T_A \gtrsim 20$ K. In this region, there are also several infrared sources (e.g., Hoffman et al., 1971) of sufficiently high luminosity to

*Emission at the highest positive velocity in each line-of-sight with $\ell < 90°$ is produced at the point of closest approach to the galactic center. Therefore, the distance to gas-producing emission at these "terminal" velocities is unambiguous.

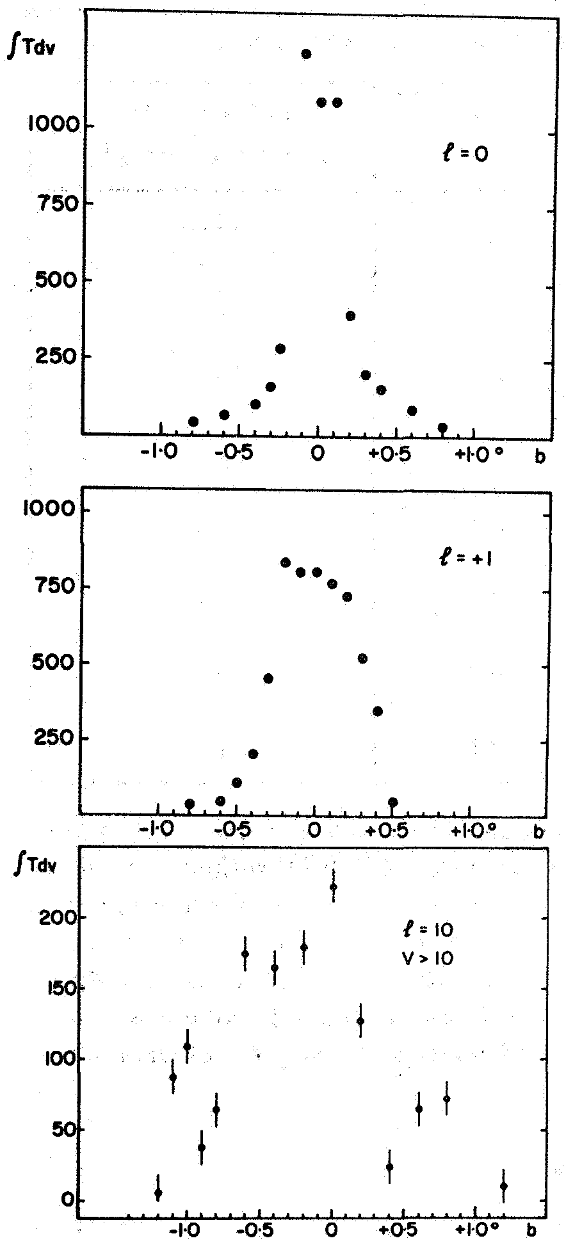

Figure 5. The distribution of integrated CO intensity $\int T_A\, dV$ in K·Km s^{-1} is shown perpendicular to the galactic plane at $\ell = 0, 1,$ and 10°.

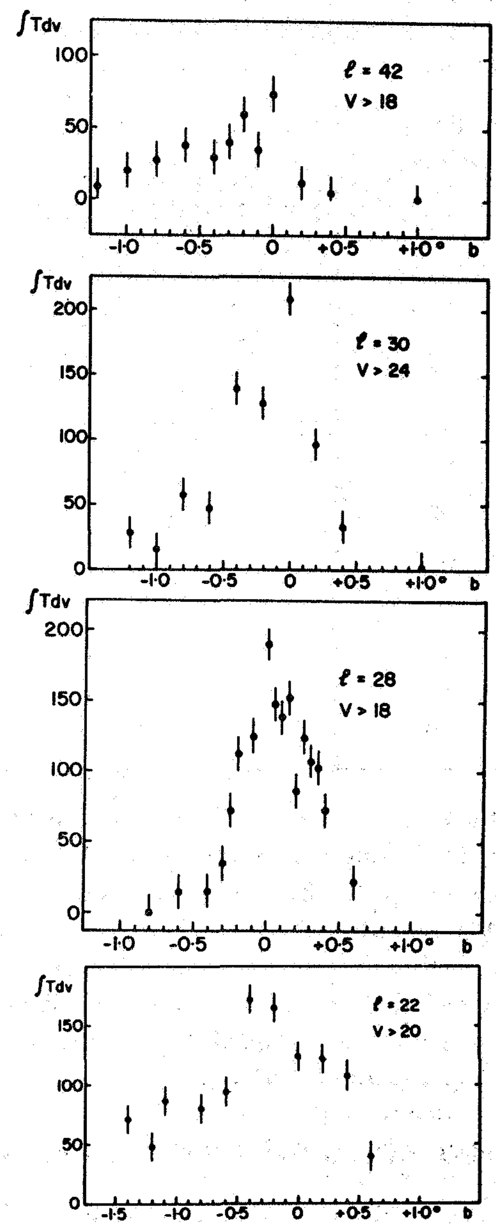

Figure 6. The distribution of integrated CO intensity $\int T_A\, dV$ in K·Km s^{-1} is shown perpendicular to the galactic plane at $\ell = 22,$ 28, 30, and 42°.

Table 1
Sample Data on the Latitude Distribution of CO Emission

ℓ (°)	$\int T_A\, dV$ at b = 0° (K·km s^{-1})	<b> (°)	$\int db \int T_A\, dV$ (10^{3} ° · K · km s^{-1})
0	1200	0	29
1	775	0	31
10	200	-0.2	15
22	170	-0.3	13
30	200	-0.1	7.4
36	110	-0.2	4.4
42	70	-0.3	3
50	37	-0.1	1

heat the dust and gas to $\gtrsim 30$ K. And, if the CO transition is close to thermalization, a change in T_K can bring about an equal change in the observed T_A (CO) without any change required in n_{H_2}. (See the second section of this paper, "Considerations for Interpretation of CO Observations.") We therefore judge that the increase in CO emission going from $\ell > 3°$ to $\ell < 3°$ does not accurately reflect column-density variation, but instead is due largely to kinetic temperature changes. We have previously obtained the total mass, $4 \cdot 10^7$ - $10^8 M_\odot$ of H_2, inside $\ell = 3°$ from analysis of detailed CO and ^{13}CO observations there (Scoville et al., 1974).

MOLECULAR CLOUD DENSITIES AND MASS

An important feature of the molecular hydrogen distribution, as deduced from the CO observations, is the extreme concentration of gas into clouds. The fraction of space filled by clouds is approximately 0.007 near the peak in the 4- to 8-kpc region with a mean molecular hydrogen density within the clouds of 670 cm^{-3}, corresponding to a smoothed-out density of 2 to 5 cm^{-3} (see figure 3 and Scoville and Solomon, 1975). The corresponding number derived by Gordon and Burton (1976) is 2 cm^{-3}.

The relative abundance of CO within clouds is $[CO/H_2] \approx 3 \cdot 10^{-5}$. This abundance ratio must itself depend on the density and opacity of the cloud. Low-density or low-opacity clouds of the type observed by the Copernicus satellite (Jenkins, this symposium) have a much lower $[CO/H_2] \sim 10^{-8}$ and therefore have much weaker CO emission per H_2 molecule. The mass of H_2 in these low-opacity clouds is an additional component to that determined through millimeter wave CO surveys.

Combination of the measured width and density estimate (4 H_2 cm^{-3}) yields a mass density of 25 $M_\odot$ pc^{-2} at 5.5 kpc (figure 3). Integrating this surface density function over the galactic disk, we find a total mass of $3 \cdot 10^9$ $M_\odot$ in interstellar H_2 interior to the solar circle.

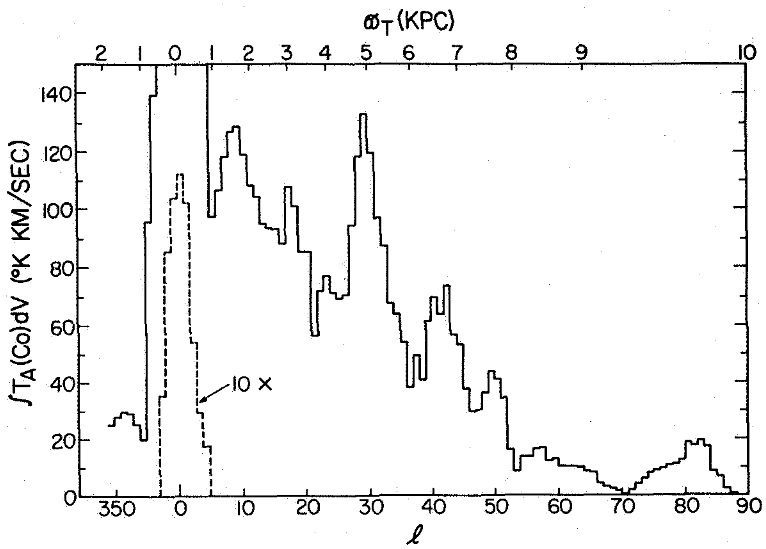

Figure 7. The very strong emission from the galactic center may be appreciated in this graph of integrated intensity as a function of galactic longitude at b = 0.

REFERENCES

Burton, W. B., M. A. Gordon, T. M. Bania, and F. J. Lockman, 1975, *Ap. J.*, **202**, p. 10.

Burton, W. B. and M. A. Gordon, 1976, preprint.

Cohen, R., 1976, Ph. D. Thesis, Columbia University.

Fichtel, C. E., R. C. Hartman, D. A. Kniffen, D. J. Thompson, G. F. Bignami, H. Ögelman, M. F. Özel, and T. Tümer, 1975, *Ap. J.*, **198**, p. 163.

Gordon, M. A. and W. B. Burton, 1976, preprint.

Hoffman, W. F., C. L. Frederick, and F. J. Emery, 1971, *Ap. J. Letters*, **164**, p. L23.

Kerr, F. J., 1969, *Ann. Rev. Astr. and Ap.*, **7**, p. 39.

Lockman, F. J., October 15, 1976, *Ap. J.*, in press.

Mezger, P. G., 1970, (IAU Symposium, No. 38, The Spiral Structure of Our Galaxy), ed. W. Becker and G. Contopoulos, Dordrecht: Reidel, p. 107.

Schmidt, M., 1965, *Galactic Structure*, eds. A. Blaauw and M. Schmidt, University of Chicago Press, Chicago, p. 513.

Scoville, N. Z., 1975, (Symposium on HII Regions), ed. D. Downs and T. L. Wilson, Kleinwalsertal, p. 513.

Scoville, N. Z. and P. M. Solomon, 1974, *Ap. J. Letters*, **187**, p. L67.

Scoville, N. Z. and P. M. Solomon, 1975, *Ap. J. Letters*, **199**, p. L105.

Scoville, N. Z., P. M. Solomon, and K. B. Jefferts, 1974, *Ap. J. Letters*, **187**, p. L63.

Solomon, P. M., N. Z. Scoville, and D. B. Sanders, 1976, in preparation.

Spitzer, L., J. F. Drake, E. B. Jenkins, D. C. Morton, J. B. Rogerson, and D. G. York, 1973, *Ap. J. Letters*, **181**, p. L116.

Stecker, F. W., P. M. Solomon, N. Z. Scoville, and C. E. Ryter, 1975, *Ap. J.*, **201**, p. 90.

Taylor, J. H. and R. A. Hulse, 1976, *Ap. J.*, in press.

Van Woerden, H., 1965, (Trans. IAU, No. 12A), p. 789.

Wannier, P. G., A. A. Penzias, R. A. Linke, and R. W. Wilson, 1976, *Ap. J.*, **204**, p. 26.

Westerhout, G., 1958, *B. A. N.*, **14**, p. 215.

REMARKS ON THE OVERALL DISTRIBUTION OF HYDROGEN IN THE GALACTIC DISK

W. B. Burton
*National Radio Astronomy Observatory**
Green Bank, West Virginia 24944

ABSTRACT

Several current problems concerning the overall distribution of hydrogen in the galaxy are discussed in general terms. These problems include the degree of saturation characterizing low-latitude emission observations of HI and the optical-depth corrections to the derived column and volume densities; the amount of fine-scale velocity and spatial structure diluted by the instrumental limitations of the presently available surveys; and the general problem of detailed mapping of HI in the galaxy. Comparison is made between the distribution of HI and that of CO and several other galactic tracers. Atomic hydrogen is unique in its distribution, instead of being typical of many Population I constituents. As defined by atomic hydrogen, the galactic disk has a diameter fully twice as large as that defined by the ionized and molecular states of hydrogen, as well as by other molecules, supernova remnants, pulsars, γ-radiation, synchroton radiation, and the youngest stars. It is also less confined to the galactic equator than most of the other constituents. The degree of small-scale structure apparent in the molecular observations is much greater than that in the HI observations. Parameters describing the small-scale structure have been determined using Monte Carlo techniques to simulate the observations.

OBSERVATIONS OF THE λ21-CM LINE OF ATOMIC HYDROGEN

A spectral line of wavelength 21 cm is produced by the well-known hyperfine transition of neutral atomic hydrogen (HI). Observations of this line give intensity (usually expressed as either antenna or brightness temperature) as a function of frequency Doppler-shifted from the line's natural frequency of 1420.406 MHz. The measured frequency shifts are converted to radial velocities (1 km s^{-1} = -4.74 kHz at λ21 cm), usually expressed in Milky Way studies with respect to the local standard of rest. Observational parameters of the major low-latitude HI surveys have been tabulated by Kerr (1968) and Burton (1974a and 1974b), and, for the central region of the galaxy, by Simonson (1974).

*Operated by Associated Universities, Inc., under contract with the National Science Foundation.

Observations from Westerhout's (1973) high-resolution survey of the galactic disk are represented in figure 1 and show HI emission from the portion of the galactic equator accessible to the NRAO 91-m telescope. These observations illustrate the ubiquitous distribution of atomic hydrogen in the galaxy. HI emission can be observed easily in any direction of the sky, and, although transformation from the observed velocity distribution to a spatial arrangement is very difficult, no region in the galactic disk has been identified as empty of HI.

MOTIONS AFFECTING THE λ21-CM LINE

A number of mechanisms broaden the 21-cm line from its negligibly small natural width of 10^{-16} km s^{-1}. The overall width of the HI line is determined at low latitudes by differential galactic rotation and is typically 150 km s^{-1}. To an approximation valid to first order over most of the galaxy, the motions of material are such that the linear rotational velocity, $\Theta(R)$, depends only on distance, R, from the galactic center. The rotation curve for $R < R_o$ was derived from 21-cm observations. The method (reviewed by Burton, 1974a) involves measuring the terminal velocities, v_t, contributed by material on the locus of subcentral points, where $R = R_{min} = R_o |\sin \ell|$, and where the linear rotational velocity is directed entirely along the line of sight. The observationally derived rotation curve is $\Theta(R_o |\sin \ell|) = |v_t| + \Theta_o |\sin \ell|$, where Θ_o and R_o refer to the observer's location.

Terminal velocities derived from 21-cm measurements at $b = 0°$, $\Delta\ell = 0.^\circ2$, are plotted in figure 2. The line in the figure represents the terminal velocities predicted by the smooth rotation curve tabulated by Gordon and Burton (1976). Deviations of the observed terminal velocities from this line should be attributed to deviations from circular rotation (see Shane and Bieger-Smith, 1966). The deviations which are not systematic over more than a degree or two of longitude can usually be associated with known HII regions. The deviations which show a systematic trend over more than several degrees are apparently streaming motions induced by the gravitational torque of large-scale density fluctuations in the overall galactic mass distribution (Barbanis and Woltjer, 1967; Yuan, 1969, Burton and Shane, 1970; and Burton, 1971). Indeed, these irregularities provide the most convincing direct evidence for the validity in our galaxy of the density-wave theory. Other arguments motivated by the 21-cm observations are less direct. The density-wave itself has not been directly studied because the expected 5-percent mass variation (Lin et al., 1969) in the old to moderately old disk stars is not detectable with present techniques. Some of the observational consequences of this theory for our galaxy have been reviewed recently by Burton (1973, 1974a, 1974b, and 1976), Wielen (1974), Roberts (1975), and Kaplan and Pikel'ner (1974).

If it is correct that the two major perturbations in the v_t longitude variation are due to motions induced by spiral arms, then the locations of these perturbations at $\ell \approx 52°$ and $\ell \approx 35°$ provide the tangent directions to two spiral arms. This quite circumstantial evidence seems to be the best from 21-cm observations for the existence of spiral arms in our galaxy, at least in the portion of it at $R < R_o$.

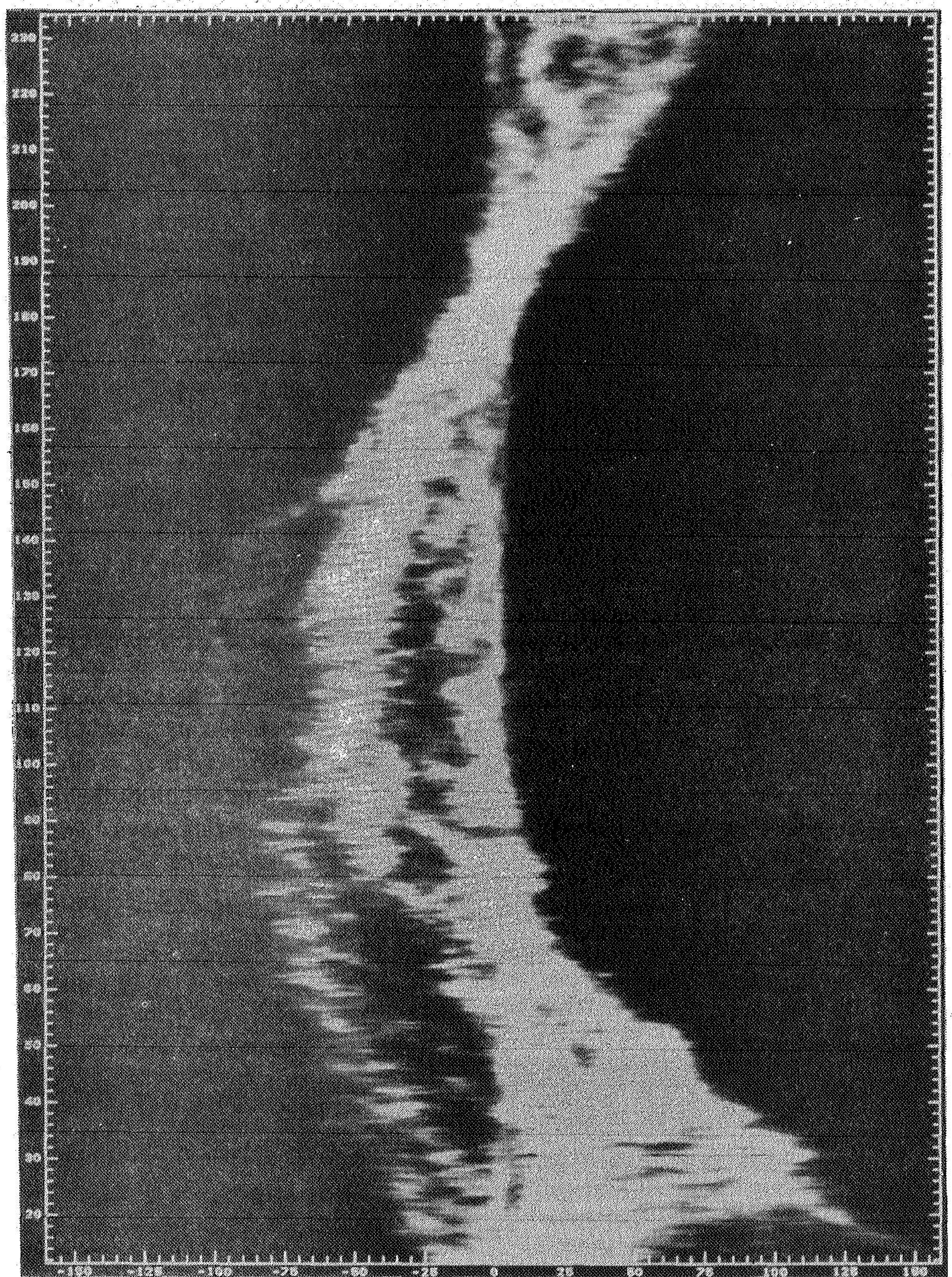

Figure 1. Gray-scale representation of HI emission intensities in longitude-velocity coordinates at $b = 0°$, $11° < \ell < 234°$, constructed from Westerhout's (1973) observations.

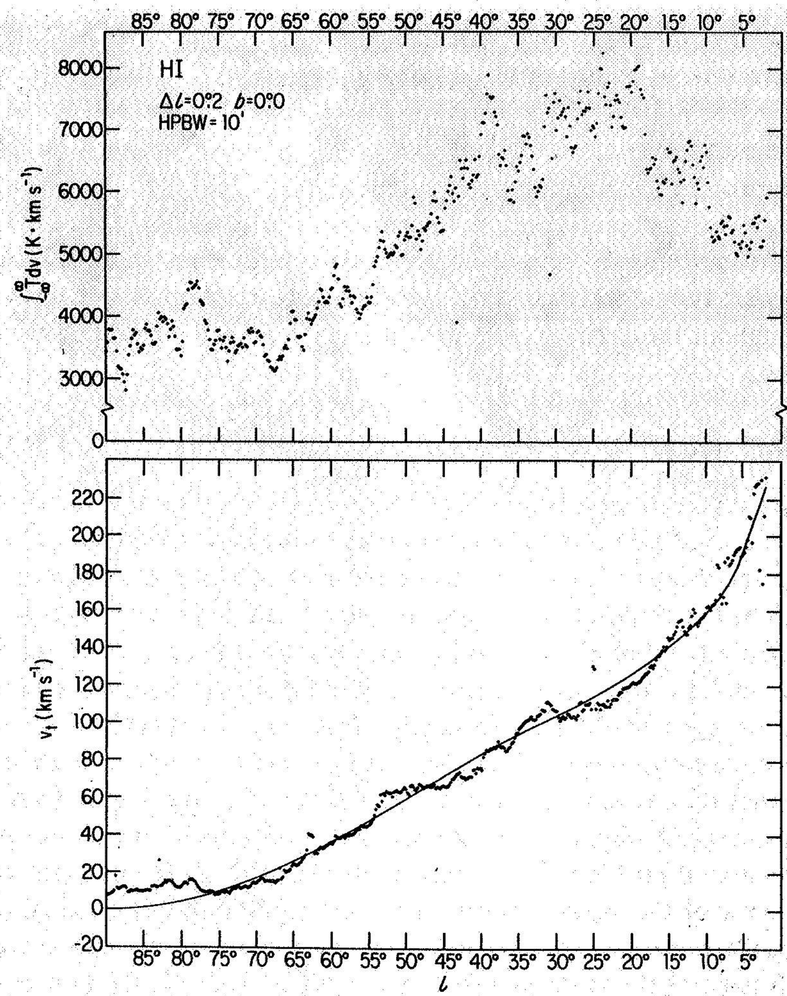

Figure 2. Upper panel: Variation with longitude of the total-velocity integrals ∫Tdv calculated from the HI observations of Westerhout (1976). Lower panel: Variation with longitude of the terminal velocities, representing material along the locus $R_0 \sin \ell$. The full-drawn line corresponds to the perturbation-free rotation curve tabulated by Gordon and Burton (1976).

The terminal velocities derived from observations in the longitude quadrant $270° < \ell < 360°$ show irregularities placed somewhat differently, although of about the same amplitude, from those found from the northern-hemisphere observations. There is also a well-known systematic difference between the two sides of the galaxy of about 7 km s^{-1} over the subcentral-point region between R = 5 and 8 kpc (Kerr, 1969). Manake and Miyamoto (1975) discuss attempts to find a dynamical explanation of this kinematic asymmetry.

Streaming motions of the sort which influence the terminal velocities are known from a wide variety of observations to be common throughout the galaxy. Although the amplitude of these motions, $\sim$ 5 to 8 km s^{-1}, is only about 2 or 3 percent of the rotational velocity of the galaxy, their occurrence nevertheless has a profound influence on the appearance of the observed 21-cm profiles. Thus, the shape of any observed HI profile can be modeled, with no fluctuations in the hydrogen density, by suitable, and plausible, adjustments to the galactic velocity field (Burton, 1971 and 1972; and Tuve and Lundrager, 1972). Although density fluctuations are bound to be present, the kinematic irregularities of the sort known to be present throughout the galaxy play a predominant role in determining the shape of the observed profiles.

DETAILED MAPPING OF THE HI SPATIAL DISTRIBUTION

One of the major results sought from observations of HI emission is a transformation of features in the observed intensity-velocity profiles to the corresponding spatial distribution of HI density in the galaxy. The procedures involved in making this transformation require that the profiles be decomposed into physically significant individual features, that these features are contributed directly by density concentrations in space, and that the velocity field is well enough known in advance that accurate kinematic distances can be derived. These requirements are very difficult to satisfy. Isolation of individual features in the heavily blended low-latitude profiles is itself usually a tedious chore, producing results which in many cases are somewhat tentative. Even after the separation is accomplished (obviously a necessary first step to detailed mapping), the relative contributions of the various physical parameters to the separated profile features remain problematic. If the motions are gravitationally-induced in the sense of the linear density-wave theory, the resulting spectral feature will furthermore usually occur at a velocity in the profile different from that corresponding to the center of HI mass of the structural feature (Burton, 1972). If the motions are those predicted by the nonlinear density-wave theory, one structural feature can contribute multiple peaks to the intensity-velocity profile (Roberts, 1972). Variations in the effective HI temperature can also influence the appearance of the line profiles; structural features could even appear as minima instead of as peaks in the profiles in some directions in the not implausible situation that cold clouds are concentrated near minima of the gravitational potential. Line profiles also show some features which result simply from the geometry of the transformation from space to velocity coordinates (Burton, 1971). Examples of such model-independent features apparent in figure 1 include the intensity-ridge near $v = 0$ km s^{-1} at $\ell < 90°$, the persistently enhanced intensities near the maximum velocities at $\ell < 90°$, the pseudo-feature centered on $\ell \sim 75°$, and the enhanced intensities near $\ell = 180°$.

These procedural difficulties do not mean that the structural characteristics of low-latitude HI are inaccessible, although it does seem important that the definiteness of the 21-cm derived picture of our galaxy's spiral structure not be overrated. In general, a grand design of a spiral nature in the overall HI distribution is not yet established. In particular, there is little comprehensive evidence for a spiral structure of HI concentrations at $R < R_o$, where, because of the double-valued nature of the velocity-distance relationship, the procedural difficulties become more important. Values applicable on a galactic scale for the spiral-arm tilt angle, radial separation, and arm-interarm density contrast are indirectly available from 21-cm observations, although the specific values depend on the validity of working hypotheses, on extrapolation over large portions of the galaxy, or on theoretical justifications. It is also not clear how representative the solar region ($r \lesssim 1$ kpc) is of the galaxy as a whole. Thus, there is no consensus (but many opinions) on the location of the Sun with respect to the nearest spiral arms; specification of our location in the overall galactic design is important if, as seems plausible, the parameters of the interstellar medium are regulated by passage of a spiral density wave and the associated compression zone. It is worth noting, however, that the mapping difficulties are primarily procedural. The kinematic irregularities characteristic of our galaxy are remarkably less severe than those commonly found in other spiral galaxies (see, e.g., Bottinelli, 1971). Similarly, the galaxy is found to be quite symmetric on a large scale (relative to the situation pertaining to many other spiral galaxies) when comparison of the total velocity extent, or of the total integrated emission, is made between data measured at $b > 0°$ with that at $b < 0°$, or when data at $0° < \ell < 180°$ is compared with that at $180° < \ell < 360°$.

HI-COLUMN AND VOLUME DENSITIES NEAR THE GALACTIC PLANE

The HI-column density is given by $N_{HI} = 1.823 \times 10^{18} \int T_k \; \tau(v)\, dv\ cm^{-2}$ and is usually not a measured quantity because the kinetic gas temperature, T_k, and the optical-depth profile, $\tau(v)$, are usually not measurable. Only in the case of a profile optically thin at all velocities does N_{HI} become directly measurable through the profile integral, $\int T_B(v)\, dv$, because, in this case, the observed brightness temperature profile, $T_B(v) = T_k \; (1\text{-exp}\,(-\tau(v))$, is $\approx T_k \; \tau(v)$. The volume density smoothed over a path of length Δr is derived from $\int T_B(v)\, dv/\Delta r$. Densities derived under the assumption of spectral thinness will underestimate the true amount of HI. The degree of saturation depends strongly on the characteristics of the space-to-velocity transformation inherent in the observations, and, thus, on longitude and latitude. In the limiting case of complete saturation, $T_B(v) = T_k$, and $\int T_B(v)\, dv/\Delta r = T_k \; |\Delta v/\Delta r|$, where Δv is the velocity extent of the portion of the profile considered. The arrangement of the geometrical parameter, $|dv/dr|$, in the galactic disk is what determines, through "velocity-crowding," the model-independent profile features mentioned in the preceding section. For example, as $\ell \rightarrow 0°$, $dv/dr \rightarrow 0°$ over most of the line of sight; the increasing saturation results in the decreasing values of the total profile integrals plotted in figures 2 and 3 at low ℓ. The condition of optical thinness is probably encountered for only certain velocity segments of most 21-cm profiles observed near the galactic plane, although at higher latitudes, $\tau(v) < 1$ is a realistic first approximation.

The spatial distribution at $|b| \leq 10°$ of the profile integrals derived from observations made by Weaver and Williams (1973) is plotted in figure 3. At these latitudes, $\tau(v) \sim 1$ is not

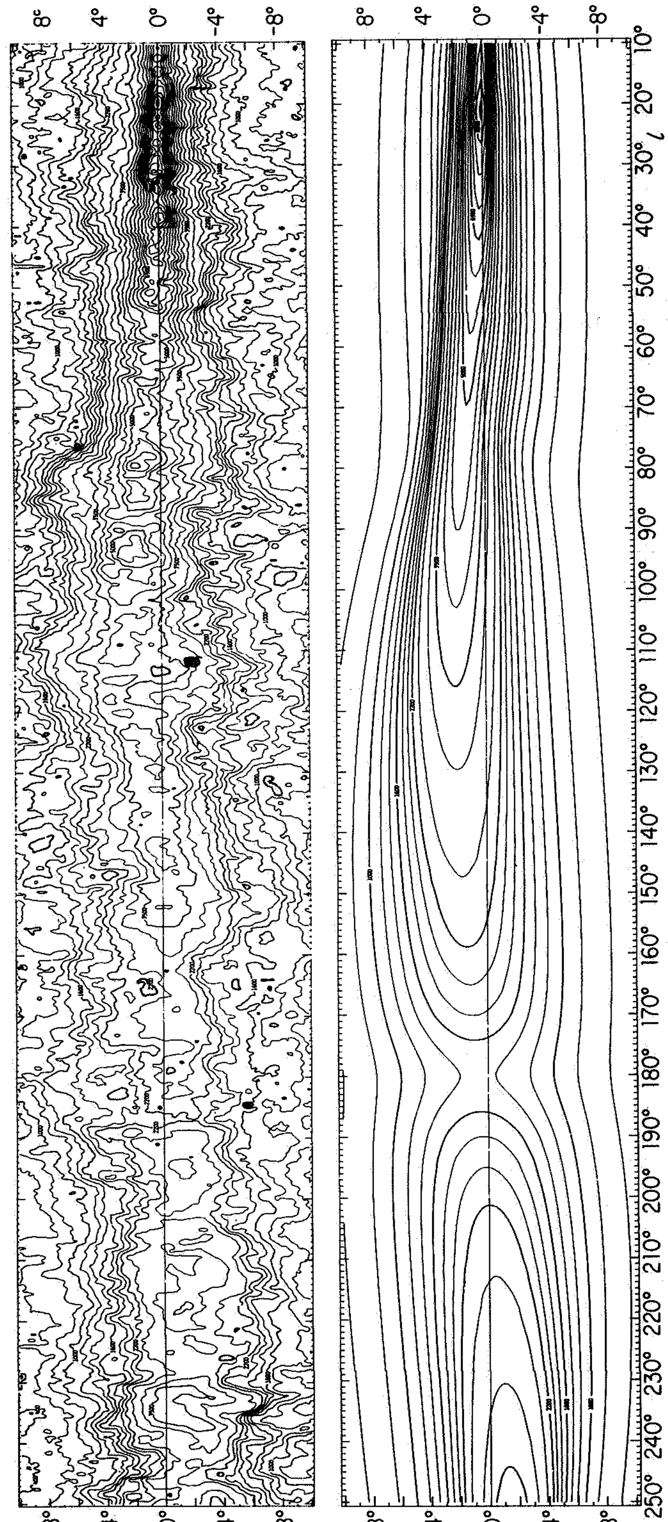

Figure 3. Upper panel: Arrangement on the plane of the sky of the total-velocity integrals, $\int T dv$, calculated from the HI observations of Weaver and Williams (1973). Lower panel: Arrangement on the plane of the sky of the total-velocity integrals, $\int T dv$, calculated from synthetic HI profiles. The parameters describing the model HI gas and its distribution are those given by Baker and Burton (1975).

uncommon, so that effects of optical depth become important. In fact, an estimate of the degree of saturation characterizing the low-latitude HI profiles can be found from the controlled conditions inherent in synthetic profiles. Many aspects of the projection on the plane of the sky of HI emission observed at low latitudes are approximately reproduced by synthetic profiles accounting for the radiative transfer effect of a smooth distribution of gas with T_k = 120 K, a peak density $n_{HI} = 0.33$ cm^{-3}, rotating according to a basic rotation curve corresponding to the smooth line in figure 2, with the z-distribution given by Baker and Burton (1975). The total-velocity integrals from such synthetic profiles are shown in the lower panel of figure 3. The overall distribution of the synthetic-profile integrals is approximately the same as the observed overall distribution of the total-velocity integrals plotted in figure 3. Thus, the saturation characteristics known for the model profiles can be used to determine corrections which should be applied to the observed profile integrals to give volume and column densities.

The volume density, $n_{HI}(R)$, and the line-of-sight column density, $N_{HI}(\ell)$, corrected for the effects of partial saturation, are plotted in figure 4. These quantities refer to the locus of latitudes where the total profile integral in the figure 3 observations is largest. The correction for partial saturation is greater at $R < R_o$ because of the double-valued nature of the velocity-space relationship there. The (beam-smoothed) density of the neutral hydrogen gas remains roughly constant over the major part of the galactic disk. This is in marked contrast to the distribution of total mass density, which increases strongly toward the galactic center. The HI decrease in the inner parts is a characteristic the galaxy shares in common with all other spiral galaxies for which projected HI surface densities have been measured (Roberts, 1974). In particular, the corrected $n_{HI}(R)$ distribution for our galaxy has quite the same form as that observed in the nearby spirals, M31 (Roberts, 1974) and M81 (Rots, 1975).

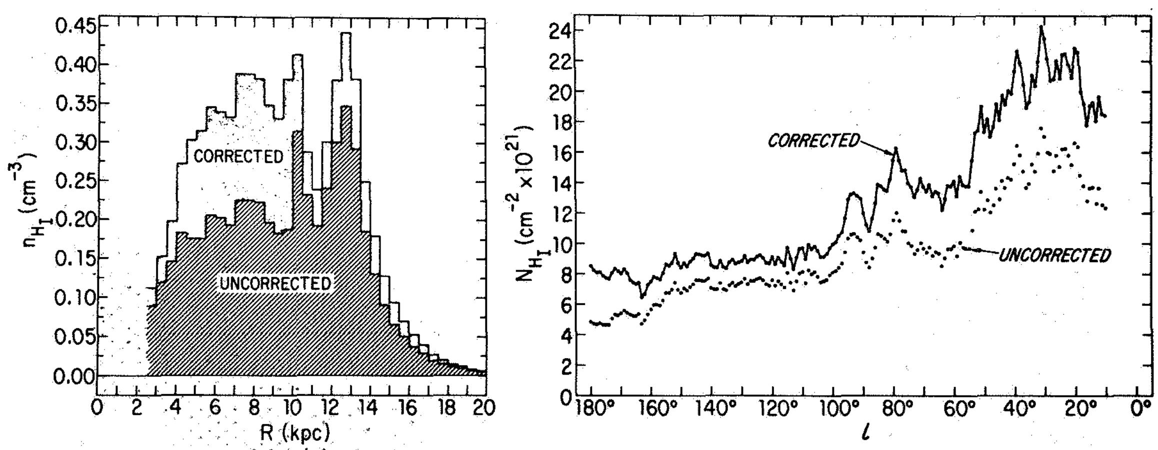

Figure 4. Large-scale distribution of HI-volume and -column densities in the galaxy. The densities labeled "corrected" contain an adjustment for optical-depth effects determined from the controlled conditions inherent in model-fitting. The values refer to the latitudes of maximum $\int T dv$ of the observations in figure 3. Substantial densities of HI exist at R > 10 kpc and at $\ell > 90°$, contrary to the situation pertaining for many other disk-population constituents.

BEAM DILUTION IN LOW-LATITUDE HI PROFILES

Although HI-emission measurements sample long lengths of path through the galactic layer, the heavily blended nature of the profiles is such that individual small-scale structure is evident at low latitudes only in special cases. The bulk of the information on the details of the interstellar medium is derived from observations of the solar neighborhood. This limitation is arbitrary, being imposed on most optical measurements by extinction and, at $\lambda 21$ cm, by the relative simplicity of high-latitude profiles. Analyses of high-latitude profiles routinely allow for a wide range of temperatures, densities, and sizes of emitting HI regions (see reviews by Heiles, 1974; and Verschuur, 1974).

All major surveys of HI galactic disk emission have been made with beamwidths varying from about 12′ (300-foot telescope) to $\sim 1°$ (60-foot telescope) and with velocity resolutions generally about 2 km s^{-1}. These beamwidths correspond at a distance of 5 kpc to lengths of 17 pc and 87 pc, respectively. It is not yet completely clear to what extent the limitations of angular and spectral resolution have affected the analyses of these surveys. The limitations imposed by the angular resolution seem to be more important. Thus, very little additional structure appears in a conventional beam if the spectral resolution is increased beyond 2 km s^{-1}. This practical limitation on the necessary spectral resolution is illustrated by figure 5, in which profiles are plotted that were measured with a velocity resolution of 0.17 km s^{-1} (Lockman and Burton, 1976). No fine-scale structure is revealed by these measurements. Indeed, HI spectral features observed at low latitudes rarely have dispersions less than ~ 3 km s^{-1}; thus, as is generally the case in radio spectroscopy, the widths of individual features are greater than those expected solely from thermal broadening. Unresolved turbulent elements would contribute to the broadening of apparently isolated features.

Substantial additional structure is revealed by measurements made with angular resolution higher than that used in the previously available surveys of HI emission. The newly resurfaced Arecibo 1000-foot telescope offers a 3′.5 beamwidth at $\lambda 21$ cm. A comparison is made in figure 6 between observations made with a 37′ beam (Weaver and Williams, 1973) and ones made of the same region of the sky, and with the same resolution in velocity, with the Arecibo telescope (Baker and Burton, 1976). Although there are many low-latitude structures with angular scales greater than 1° (see also figure 1 and the upper panel of figure 2), these structures show much fine-scale internal structure. An extensive series of Arecibo observations will provide direct measures (or at least limits) of length-scales of HI-emission regions and complexes (Baker and Burton, 1976).*

Aspects of this problem have been considered in a less direct way by Baker and Burton (1975). They emphasized that the cold opaque HI regions revealed in large numbers by absorption measurements (see, e.g., Radhakrishnan, 1974), which are made against distant continuum

*The National Astronomy and Ionosphere Center is operated by Cornell University under contract with the National Science Foundation. The observations in figures 5 and 6 represent a preliminary reduction; in particular, the intensity scale is uncalibrated.

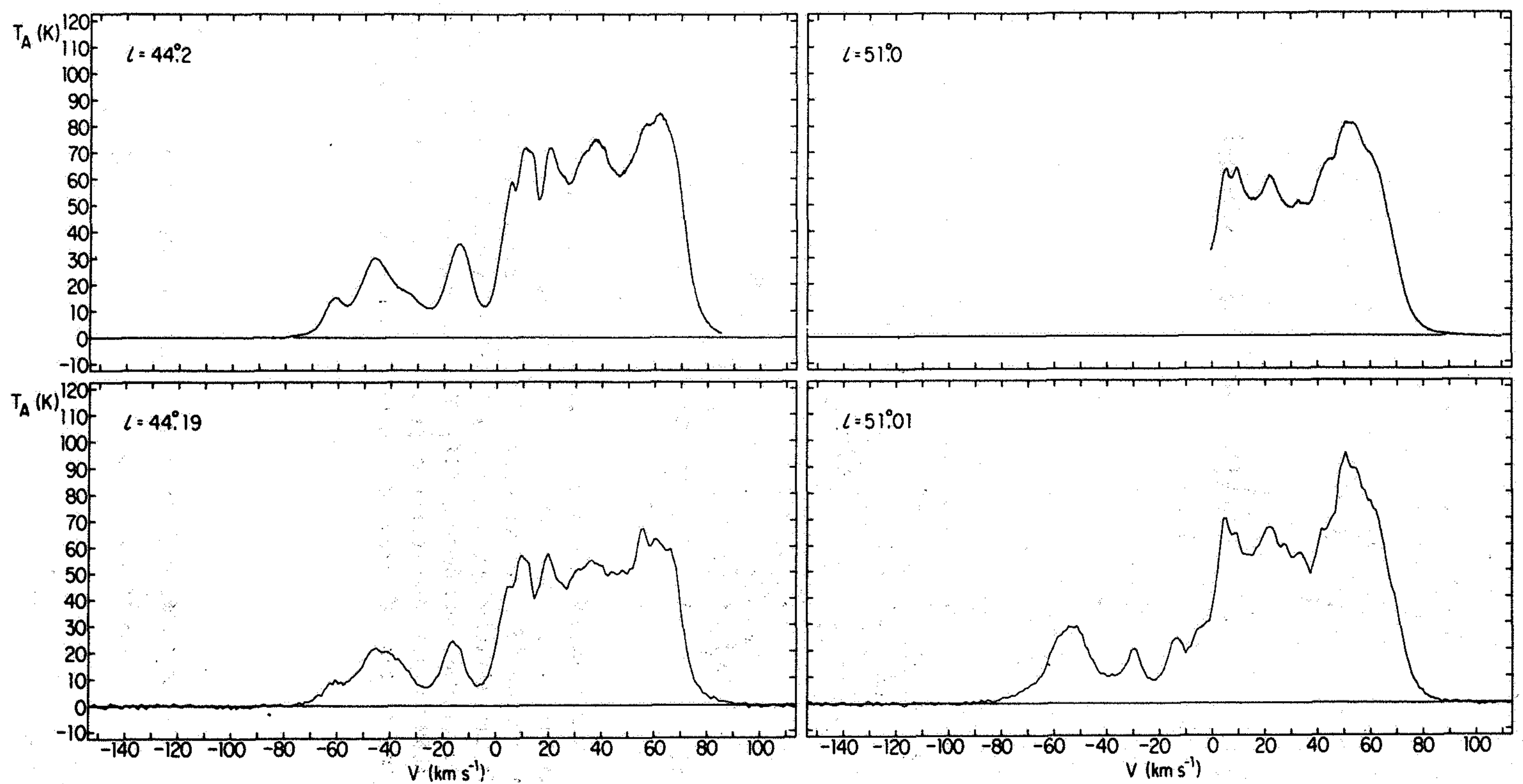

Figure 5. Upper panel: HI profiles observed in the galactic plane at the indicated longitudes with the very high spectral resolution of 0.17 km s^{-1}, using the NRAO 43-m telescope characterized at λ21 cm by a 20′ beamwidth (Lockman and Burton, 1976). These profiles show no more detail than corresponding ones observed with the same beamwidth and a spectral resolution of ~ 2 km s^{-1}.
Lower panel: HI profiles observed with 1-km s^{-1} spectral resolution but with the 3′5 beamwidth of the Arecibo 1000-foot telescope (Baker and Burton, 1976).

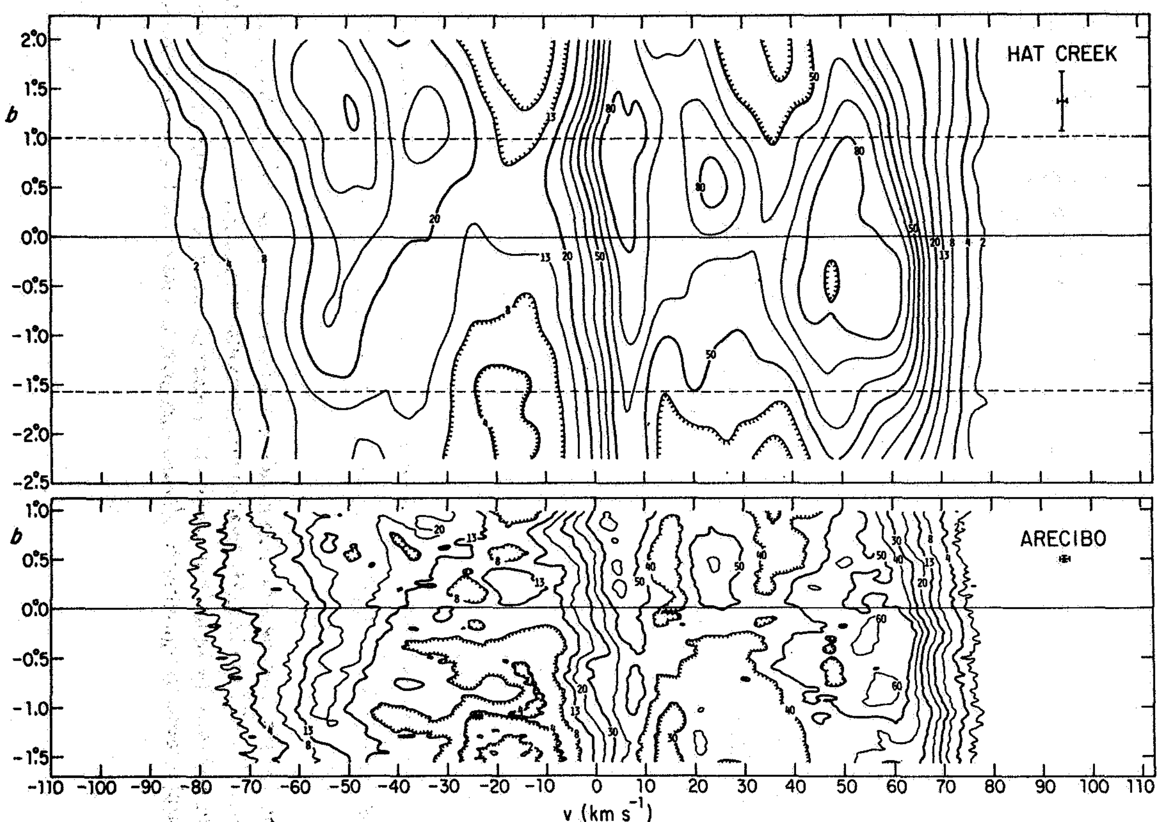

Figure 6. Comparison showing the widespread occurrence of small-scale HI structures. Upper panel: Latitude-velocity distribution at ℓ 52° constructed from the 21-cm observations of the Hat Creek survey of Weaver and Williams (1973). The 37′ beamwidth and 2.1 km s^{-1} velocity resolution are indicated by the cross in the upper right-hand corner. Lower panel: Latitude-velocity distribution at ℓ = 52° constructed from observations made with the Arecibo 1000-foot telescope (Baker and Burton, 1976). The profiles entering the lower panel were smoothed to the same spectral resolution as those in the upper panel. The 3′.5 beamwidth reveals substantial additional structure. At a distance of 5 kpc, representative for low-latitude investigations, 3′.5 subtends a length of 5 pc.

sources of vanishingly small angular size, must be strongly beam-diluted in the emission profiles. Otherwise, the emission profiles would be saturated; they are observed to be (effectively) optically thin.

GALACTIC DISTRIBUTION OF CARBON MONOXIDE AND, BY IMPLICATION, OF MOLECULAR HYDROGEN

Although 21-cm observations of atomic hydrogen show HI to be an ubiquitous tracer of a number of galactic characteristics, they cannot give the true amount and distribution of interstellar hydrogen. This is partly because cool HI is under-represented in the 21-cm observations, but it is much more important that large amounts of molecular hydrogen do not contribute at all to the 21-cm line. H_2 is the most stable low-temperature form of the most abundant element in the interstellar medium, and undoubtedly predominates over all other material in optically cool, opaque, compressed regions in which the molecule is shielded against photo-dissociation after formation on grain surfaces (Solomon and Wickramasinghe, 1969; Hollenbach et al., 1971). H_2 has no observable transition in the radio or in the optical windows. Direct observations of H_2 Lyman absorption bands in the ultraviolet spectra of reddened stars have been made first from rockets (Carruthers, 1970) and extensively from the Copernicus satellite (Spitzer et al., 1973; and Spitzer and Jenkins, 1975). Ultraviolet extinction due to interstellar dust limits such observations to material within 1 kpc or so of the Sun. The next most abundant interstellar molecule, CO, is also concentrated to cool, dense regions in which it is self-shielded against radiative dissociation. The most important source of excitation of the CO line involves collisions with H_2 (Goldreich and Kwan, 1974; and Scoville and Solomon, 1974). Thus, the observable abundance distribution of CO provides, by implication, some aspects of the distribution of H_2.

Observations made along the galactic equator of the $J = 1 \rightarrow 0$ rotational transition of ^{12}CO at $\sim$ 2.6 mm (115 GHz) are shown in figure 7. At this wavelength, the NRAO 11-m telescope has a beamwidth of 65″; however, the effective resolution of figure 7 is set by the $\sim$ 12″ longitude interval between spectra, which is the same as the 12′ beamwidth of the 91-m telescope at $\sim$ 21 cm characterizing figure 1. Certain salient characteristics of the CO distribution which distinguish it from the HI distribution are apparent from these observations (see Scoville and Solomon, 1975; Burton et al., 1975; and Burton and Gordon, 1976a).

The most striking difference between the overall HI distribution and that of CO is that the CO flux is much more confined to the inner galaxy. The relative radial abundance of CO is shown in figures 8 and 10. The mean radius of the distribution is $\bar{R} = 5.9$ kpc; 66 percent of the accumulated emission originates between 4 and 8 kpc, where the abundance has fallen to its half-maximum level. The abundance distribution is skew, falling off less sharply at $R > 7$ kpc than at $R < 5$ kpc. At $R > 10$ kpc, generally corresponding to the portion of figure 7 at $\ell > 0°$, $v < 0$ km s^{-1}, very little CO is observed outside the galactic nucleus. In addition, the CO disk is substantially thinner in the z-direction than the HI disk (figure 9).

The radial distributions of several other galactic tracers which can be observed along trans-galactic paths are also plotted in figure 8. Within the uncertainties of the observations, the galactic radial distribution of molecules, distributed ionized hydrogen, giant HII regions, supernova remnants, pulsars, γ-radiation, and synchrotron radiation are roughly equivalent. The extent of the galctic disk is for HI approximately twice as large as the extent measured for these other tracers. It is clear that the chemical composition and physical state of the interstellar medium show great variations, even on a galactic scale. It is necessary to distinguish between compressed material, confined to the inner galaxy and representing recent or current phenomena, and atomic hydrogen, whose fundamental distribution extends to much larger distances. Instead of being the prototype for the distribution of the constituents of extreme Population I, the distribution of atomic hydrogen seems unique (see Burton et al., 1975; Burton, 1976; Stecker, 1976). The general picture emerging for our galaxy is, in these respects, consistent with the morphological information available for external galaxies.

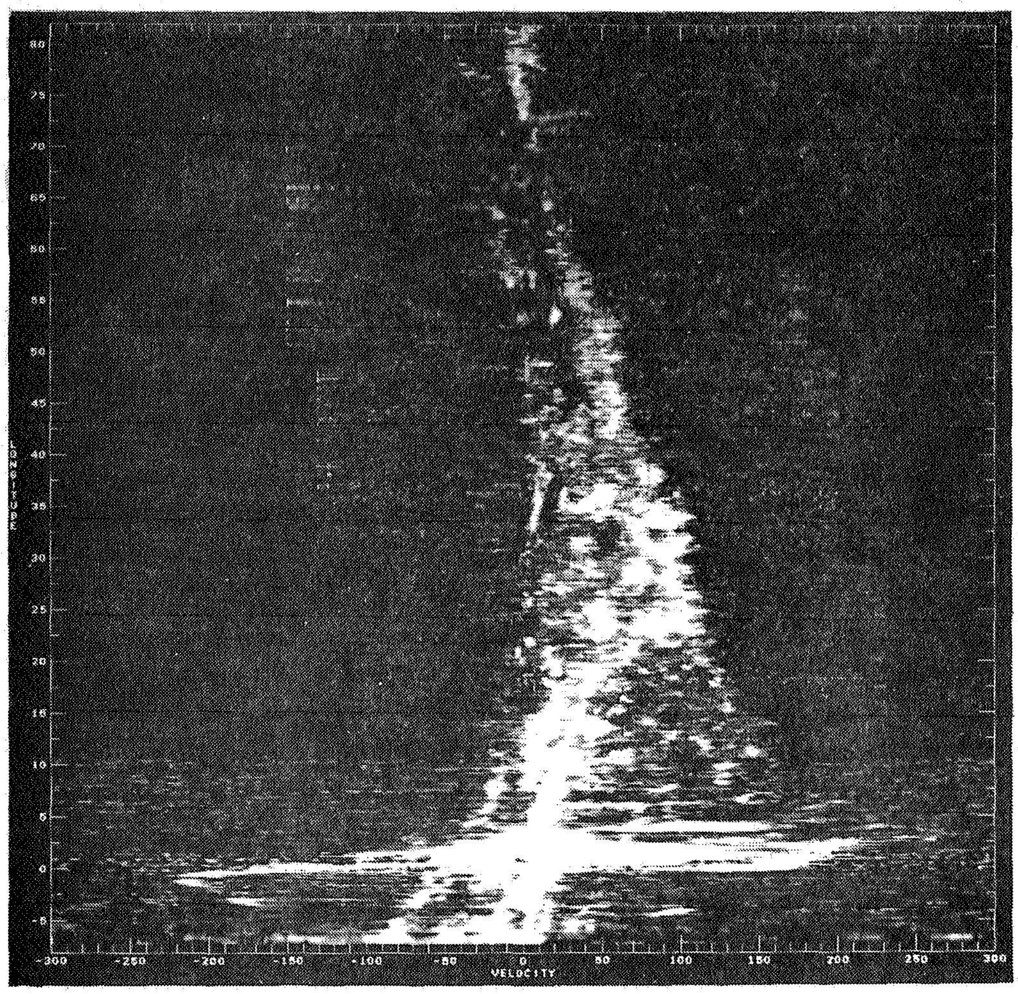

Figure 7. Longitude-velocity arrangement of $^{12}C^{16}O$ emission observed along the galactic equator. Little CO emission is seen in the portions of this figure corresponding to R > 9 kpc (except for the exceptional Cygnus region) and to R <4 kpc (except for the exceptional 3-kpc arm and the intense nuclear sources). The observations at $\ell < 10°$ are due to Bania (1976), those at $10° < \ell < 36°$, to Gordon and Burton (1976), and those at $\ell > 36°$, to Burton and Gordon (1976b).

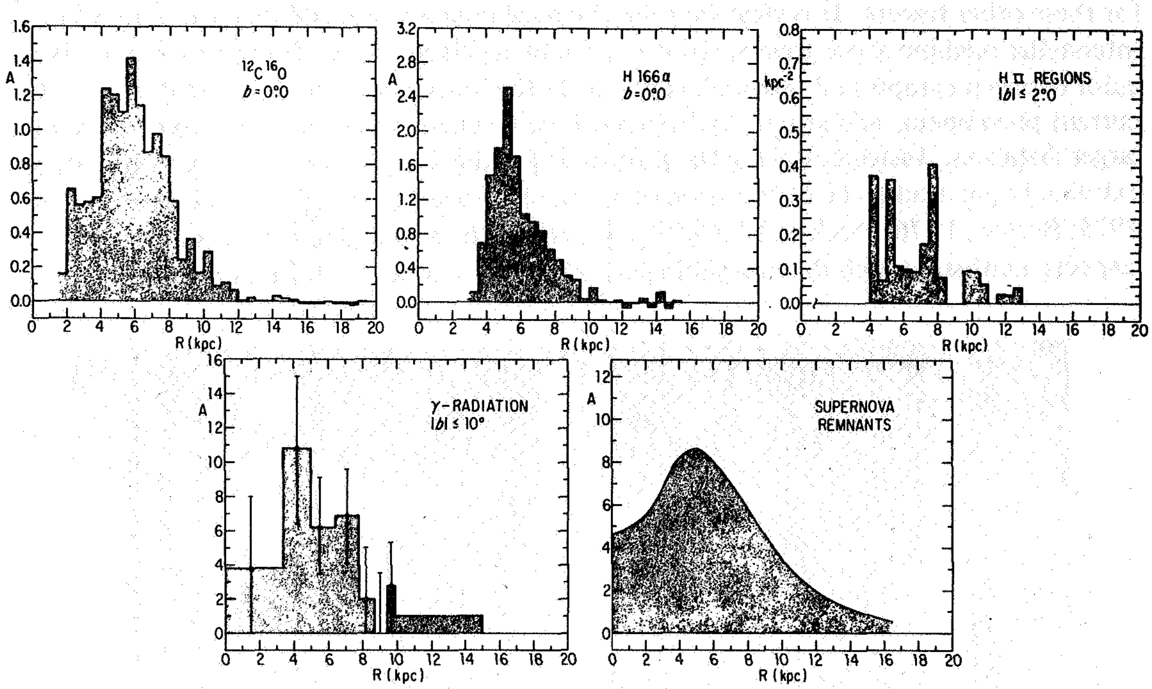

Figure 8. Radial distributions of several constituents of the galactic disk. The CO distribution is from Gordon and Burton (1976); the H166α distribution is from Lockman (1976), and that for the giant HII regions is from a compilation by Burton et al. (1975); only data at $\ell > 0°$ enter these distributions. The γ-ray distribution (Strong, 1975) and that for supernova remnants (Kodaira, 1974) utilize data from both sides of the Sun-center line and from a wider latitude range; these distributions are probably less accurate than the upper three, especially in view of the lack of direct kinematic information. The vertical axes labeled "A" refer to abundances on an arbitrary relative scale.

There is so far no straightforward, comprehensive, or conclusive evidence for spirality on a galactic scale of any of the inner-galaxy tracers. Of the distributions considered, probably that of CO is the most basic representative of the compressed Population I. Extensive and detailed observational material should become available for CO within the next few years. If the inner galaxy is characterized by a grand design of a spiral form, it is reasonable to expect that this would be demonstrated by observations of CO because of the high angular resolution at 2.6 mm, the relatively low characteristic velocity dispersion, the abundance of CO, the accessibility of long lengths of path, and the expected confinement to rather narrow zones of high compression. Figures 8 and 11 show that the CO apparently is not confined to the narrow zones which are predicted to trace the compression due to the passage of a galactic density wave. It is particularly puzzling that the run with longitude of terminal velocities, calculated from the CO observations and plotted in the lower panel of figure 11,

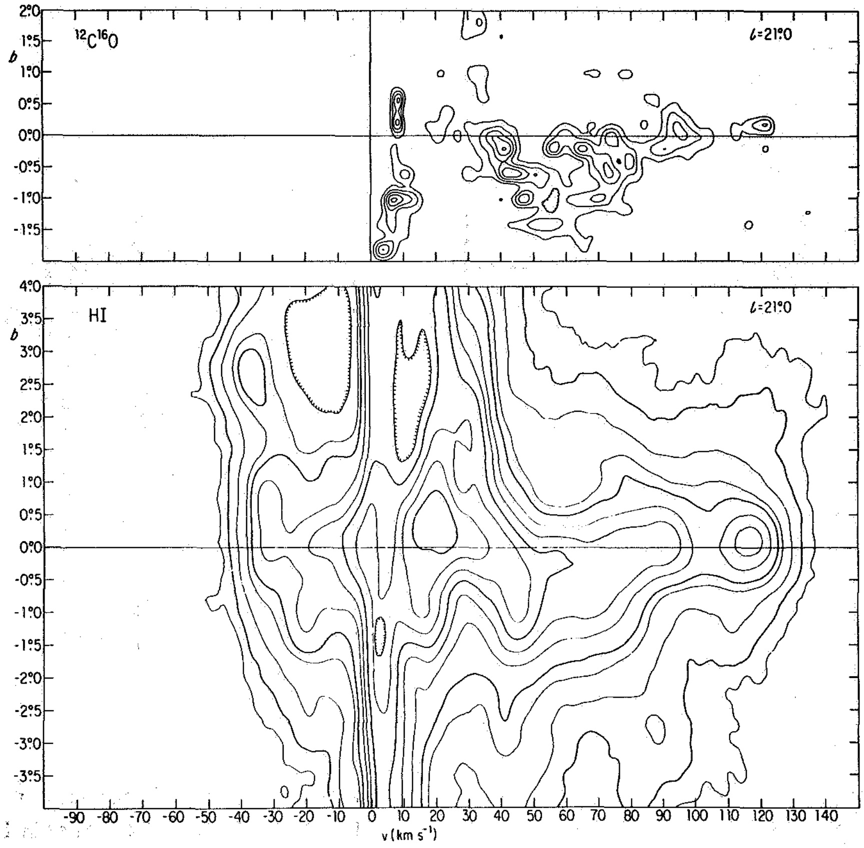

Figure 9. Comparison of CO and HI latitude-velocity distributions in the direction ℓ = 21°, showing that the z-thickness of the neutral hydrogen layer is about twice that of the carbon-monoxide layer (Burton and Gordon, 1976 a). The HI observations are from the survey of Weaver and Williams (1973).

shows large-scale irregularities of the same form as those found for HI and plotted in figure 2. If the CO kinematics were governed by a galactic shock, it seems reasonable to expect that this would be indicated by terminal-velocity perturbations of larger amplitude and narrower extent in longitude than those found for the neutral gas. Bash and Peters (1976) have recently considered several consequences of the CO terminal velocity variation.

Another important difference between the figure 1 HI observations and the figure 7 CO observations concerns the amount of apparent small-scale structure. Although much detail may be unresolved in the HI observations, features extending over many beamwidths are nevertheless common. The CO observations show few extended features. The small-scale irregularities in figure 11 mainly represent characteristics of the CO distribution, not measurement errors. The characteristic appearance in the CO spectra of isolated features allows estimates to be made of the characteristic size and separation of the emitting clumps.

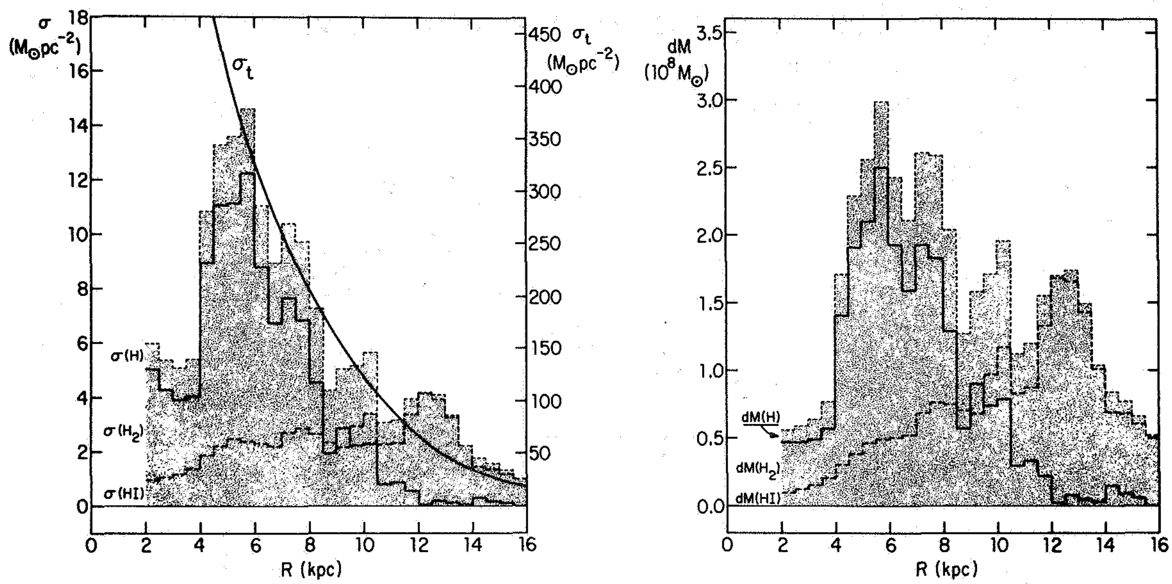

Figure 10. Radial distribution of projected surface densities and differential masses of atomic and molecular hydrogen. This figure is from Burton and Gordon (1976a), who summarize the several important uncertainties inherent in the derivation of H_2 densities from observations of CO. Also shown is the total-mass surface density, σ_t, predicted dynamically by Innanen (1973).

Burton and Gordon (1976a and 1976b) have modeled the CO observations by generating synthetic profiles corresponding to a stochastic assemblage of dark clouds (see Baker and Burton, 1975). The stochastic distribution is governed by the probability of finding a cloud in a particular interval, of length Δr, along the line of sight:

$$P_i = \frac{\Delta r}{<d>} \frac{1}{f(r)} A_{CO}(R)$$

Here, $A_{CO}(R)$ is the (normalized) radial distribution of CO plotted in figure 8, f (r) is the telescope beam-filling factor, and <d> is the average separation between clouds at the mode of the $A_{CO}(R)$ distribution. The kinematics of the clouds are governed by circular galactic rotation and a motion of one cloud with respect to another characterized by a dispersion $\sigma_{c\longleftrightarrow c}$. Each cloud has an internal velocity dispersion of σ_c. Using preliminary determinations of these parameters, Burton and Gordon (1976a) have modeled several characteristics of the CO observations. Figure 12 shows that the small-scale irregularities in the synthetic-profile integrals and the modeled terminal velocities are approximately the same as those observed. The model assemblage consists of clouds that each have a diameter of 5 pc, an excitation temperature of 16 K, a representative optical depth of 5, an internal dispersion of 2.5 km s^{-1}, a cloud-to-cloud motion of 4 km s^{-1}, and a cloud-to-cloud separation of 800 pc at the peak of the $A_{CO}(R)$ distribution.

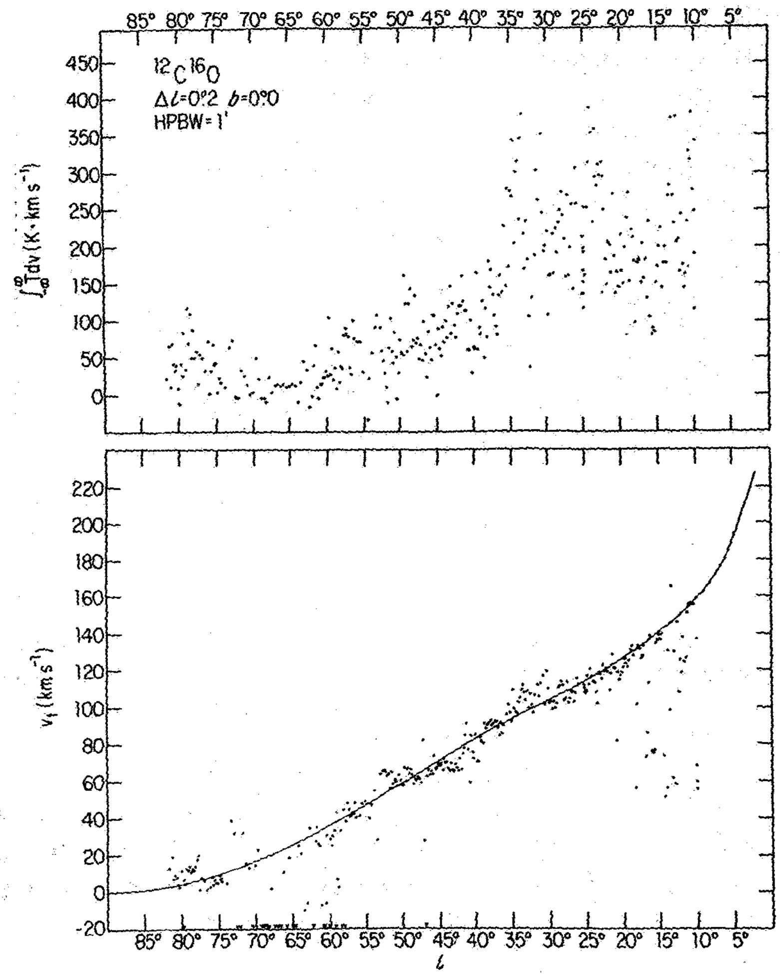

Figure 11. Upper panel: Variation with longitude of the total-velocity integrals, ∫Tdv, calculated from the CO observations of figure 7. Lower panel: Variation with longitude of the CO terminal velocities. Comparison with the HI terminal velocities plotted in figure 2 shows that the compressed molecular material is characterized by the same overall kinematics that characterize the much more ubiquitous atomic hydrogen.

DISTRIBUTION OF CARBON MONOXIDE WITHIN 10° OF THE GALACTIC CENTER FROM BANIA'S (1976) OBSERVATIONS

The $J = 1 \rightarrow 0$ rotational transition of the $^{12}C^{16}O$ isotope of carbon monoxide has been surveyed at $\ell = 0°$ in the inner region of the galaxy by Bania (1976). The observations, which extend over the range $10° \geq \ell \geq 352°$, are shown in figure 13 in the form of a velocity-longitude contour diagram. Also shown in figure 13 is the observed velocity-longitude behavior of 21-cm neutral hydrogen emission for the same region of the galaxy. Although the telescope beamwidths for the CO and HI observations are quite different (1′ and 20′ of arc, respectively) the angular sampling resolution of both sets of observations, $\Delta \ell = 0\overset{\circ}{.}2$, is the same. The similarity of the distribution and kinematics of the CO and HI emission is striking. Apparently, the regions in which atomic hydrogen is converted to molecular hydrogen do not possess large velocity anomalies. The overall velocity-longitude behavior of both CO and HI is dominated by differential galactic rotation because the major portion of the emission observed occurs at positive velocities for $10° \geq \ell \geq 0°$ and at negative velocities for $352° \leq \ell \leq 360°$.

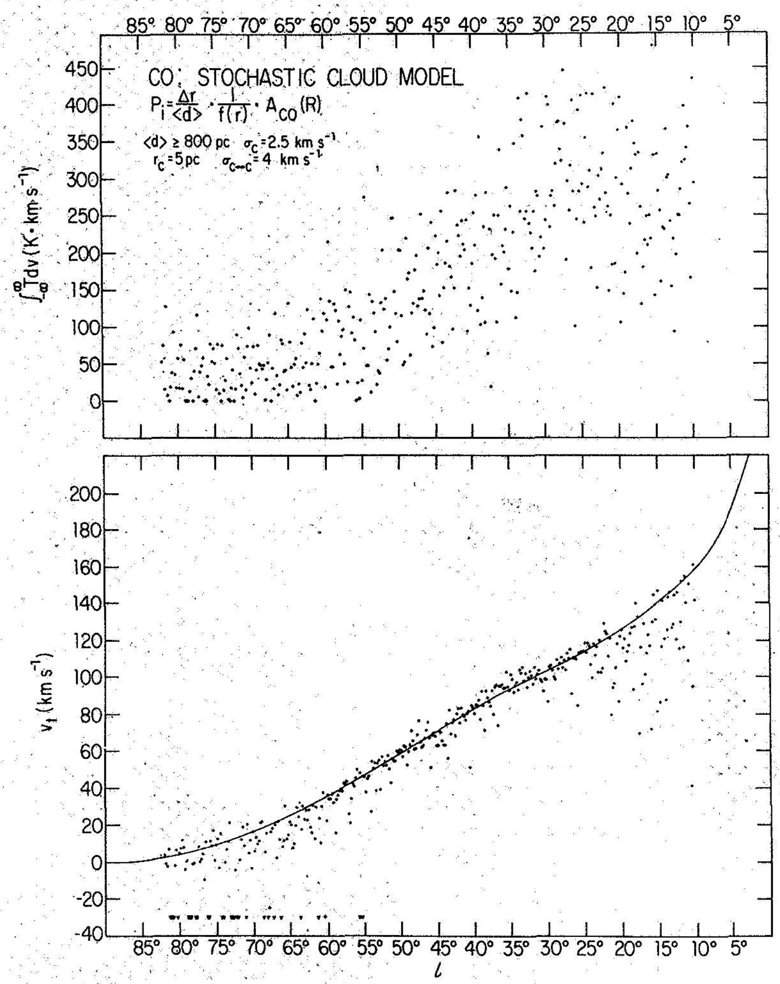

Figure 12. Longitude variations of the total-velocity integrals and of the terminal velocities calculated from synthetic line profiles constructed to mimic the CO observations. The model CO distribution consists of discrete clouds distributed stochastically as discussed in the text (see Burton and Gordon, 1976a). The symbols v in figures 11 and 12 refer to profiles for which no terminal velocity was determined because of the lack of an emission feature more intense than 1.2 K.

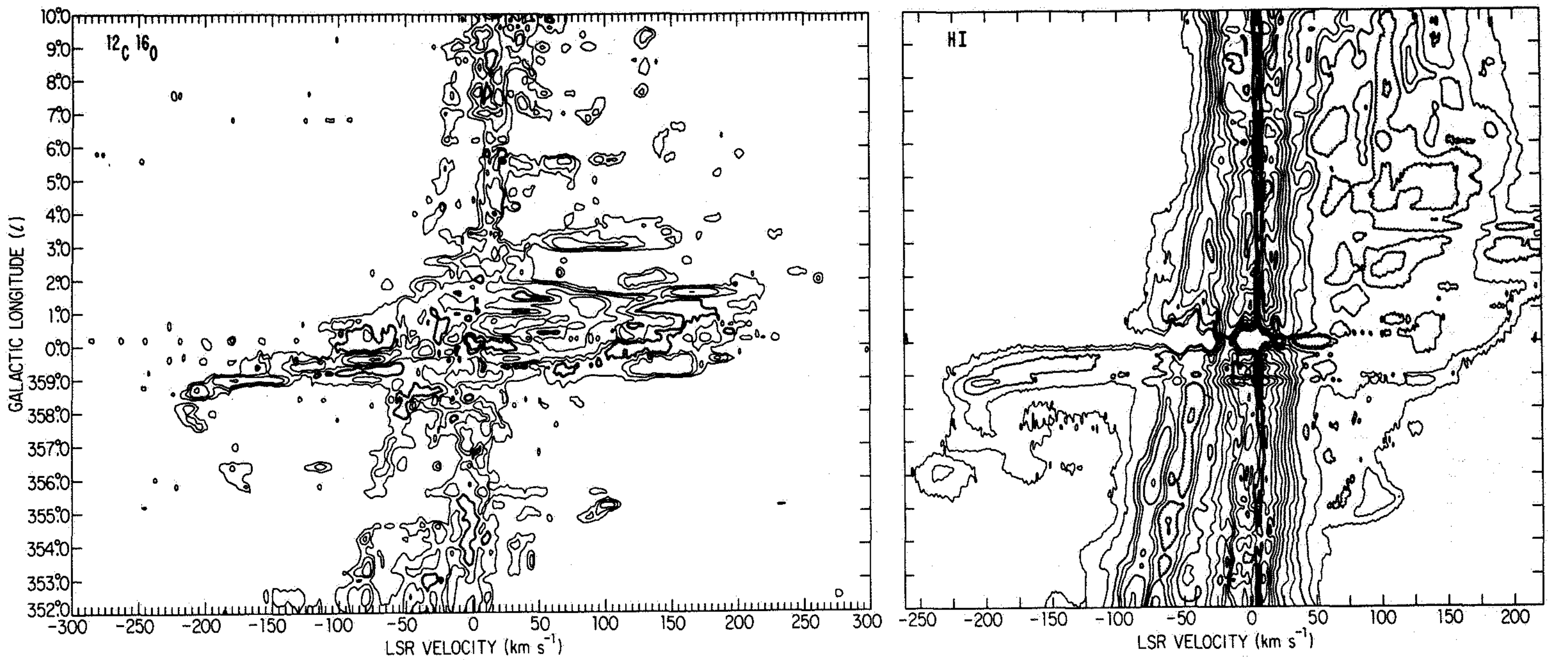

Figure 13. Longitude-velocity contour maps of carbon monoxide ($^{12}C^{16}O$) and neutral hydrogen (HI) in the inner galaxy (Bania, 1976). The data in both maps were taken at b = 0°. Although the beamwidths of the CO and HI observations are 1′ and 20′ of arc, respectively, the data were both taken with the same angular sampling resolution ($\Delta\ell = 0\overset{\circ}{.}2$). CO contour intervals correspond to antenna temperatures of 1.4, 3, 4, 10, 15, . . . K; HI contours are drawn at antenna temperatures of 2, 3, 10, 15, 20, 30, 40, . . .K. Because the CO emission is collisionally excited by molecular hydrogen, the striking similarity of the CO and HI observations implies that the kinematics of atomic and molecular hydrogen are generally similar in the inner regions of the galaxy. The CO observations in the region $|\ell| < 1°$ are from Liszt et al. (1976).

Some extended kinematic features which are common to both the CO- and HI-emission data and which are discussed in detail by Bania (1976) include (1) the 3-kpc arm; (2) an anomalous cloud at $\ell = 355°$, v = 100 km s^{-1}, moving at a velocity forbidden by circular rotation; and (3) the well-known nuclear disk feature.

The longitude dependence of the integrated intensity of $^{12}C^{16}O$ emission in the inner galaxy is plotted in figure 14 (Bania, 1976). The intense peak near $\ell = 0°$, with a half-width of about 1°5, probably arises from CO lying within 350 pc of the galactic center (see Liszt et al., 1976). The background integrated intensity at the level indicated by the line in figure 14 at 200 K km s^{-1} is consistent with the accumulation along the line of sight of the annular disk of CO (figure 8), with no additional contribution from the region, R ≲ 2 kpc.

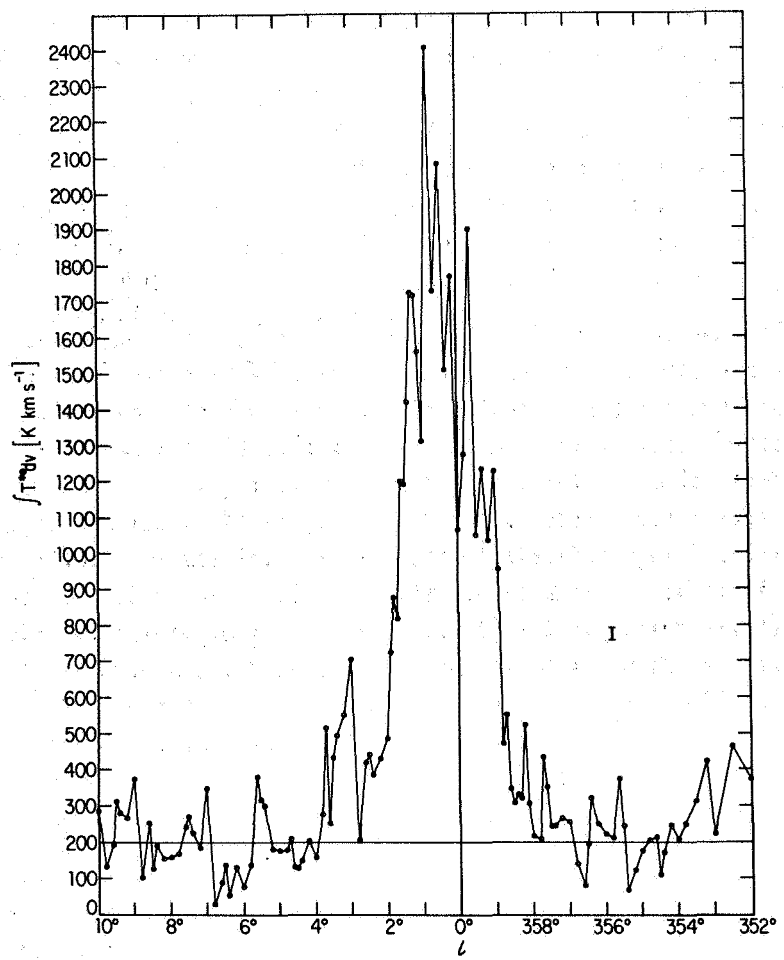

Figure 14. Observed longitude dependence of the integrated intensity of $^{12}C^{16}O$ emission in the inner galaxy (Bania, 1976). The symbol indicates the magnitude of a one-standard-deviation measurement error.

GALACTIC DISTRIBUTION OF IONIZED HYDROGEN FROM LOCKMAN'S (1976) OBSERVATIONS OF THE H166α RECOMBINATION LINE

Ionized hydrogen, in concentrations sufficiently dense to produce measurable radio recombination lines, is associated with very young, hot stars, and thus identifies sites of recent star formation in the galaxy. In addition to the rather dense, compact HII regions which have been studied in radio surveys of, for example, the H109α recombination line, the interior part of the galaxy contains larger regions of more moderate-density ionized hydrogen. This lower-density material is most easily observed in recombination lines at frequencies near 1 GHz, and, although the emission is quite weak, it is seen at enough locations to be a useful tracer of both the velocity field and the overall level of star formation in the galaxy. A survey of part of the galactic plane in the H166α recombination line near 1.4 GHz has recently been completed (Lockman, 1976), and the gross distribution of this gas is reasonably well known.

Figure 15 shows the observed H166α emission from a portion of the northern galactic plane, plotted in velocity-longitude coordinates. The lines from moderate-density gas are detected at every observed position $4° \leq \ell \lesssim 44°$. The power in the line, averaged over 3° intervals, is plotted against longitude in figure 16. Although these observations do not cover longitudes greater than 51°, a survey by Hart and Pedlar (1976) at Jodrell Bank indicates that there is virtually no H166α emission between longitudes 52 and 70°. When considered with the absence of emission at small velocities (corresponding to locations near the Sun) and the low level of emission at high positive velocity for low longitudes, this indicates that most H166α emission originates between galactocentric radii $4 < R < 8$ kpc.

A quantitative description of the radial distribution of H166α emission is shown in figure 17, in which the power in the line per kiloparsec derived under the assumption of pure circular galactic rotation is plotted against galactocentric radius, R. The apparent emission at $R > 8$ kpc can be attributed to the broad nature of the features in the profiles because emission at each velocity has been separately assigned to the corresponding radius, and does not necessarily imply significant ionized gas at these radii. In contrast, it is quite likely that the apparent emission at $R < 4$ kpc is real, although the limited observations of this region cause large uncertainties in the analysis. A comparison with the radial distribution of neutral hydrogen (figure 4) shows no strong correlation between the HI and the H166α distributions, implying that the source of ionization must be distributed somewhat like the H166α emission. Qualitatively, the radial distribution of H166α resembles that of CO (figure 8) much more than that of HI. Although the exact nature of the regions giving rise to this recombination line emission is unclear, the ionized gas is so prevalent in the interior parts of the galaxy that stars must be forming at a rate much greater than would be implied from observations made in the solar neighborhood.

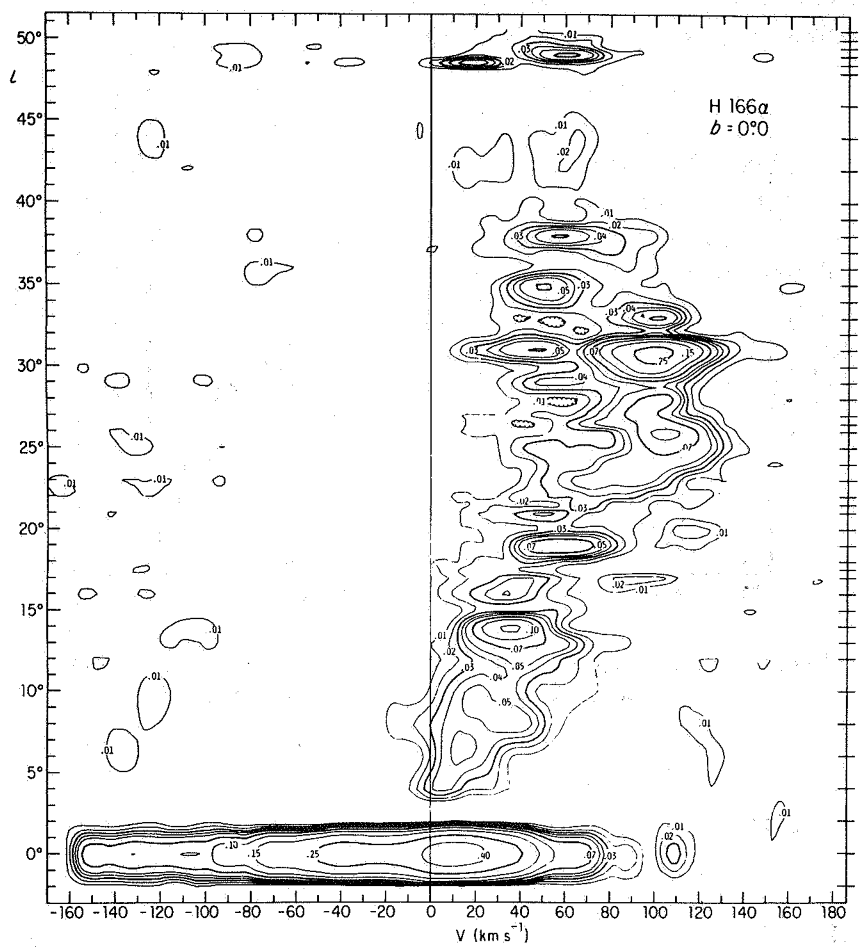

Figure 15. Distribution of H166α antenna temperature in velocity-longitude coordinates (Lockman, 1976). Marks through the right-hand border show the observed longitudes. Some of the weak emission at $v < 0$ km s^{-1} can be attributed to the C166α recombination line of ionized carbon.

ACKNOWLEDGEMENTS

Several of the topics discussed briefly in the first six sections of this paper are dealt with in more detail in a chapter in Volume 14 of the *Annual Review of Astronomy and Astrophysics*. I am indebted to T. M. Bania and F. J. Lockman for providing the material, the last two sections.

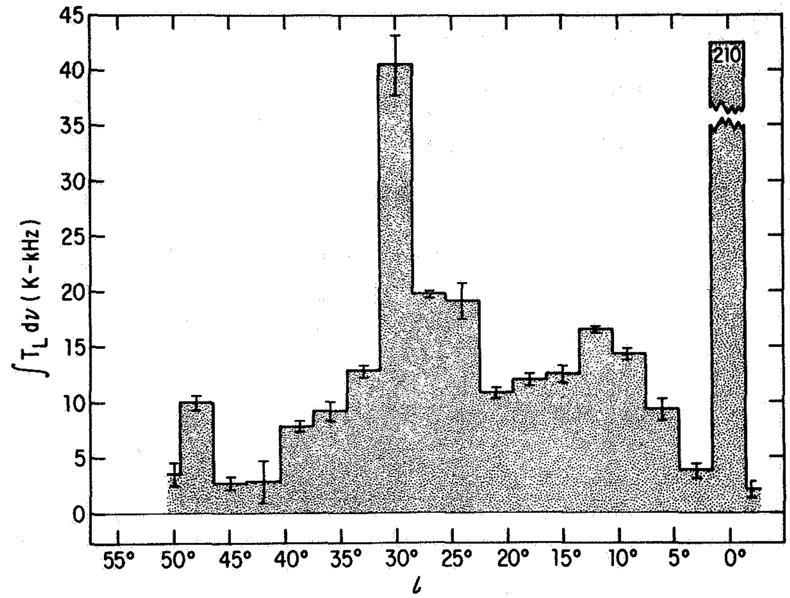

Figure 16. Total power in the H166α line averaged over 3° intervals as a function of longitude (Lockman, 1976).

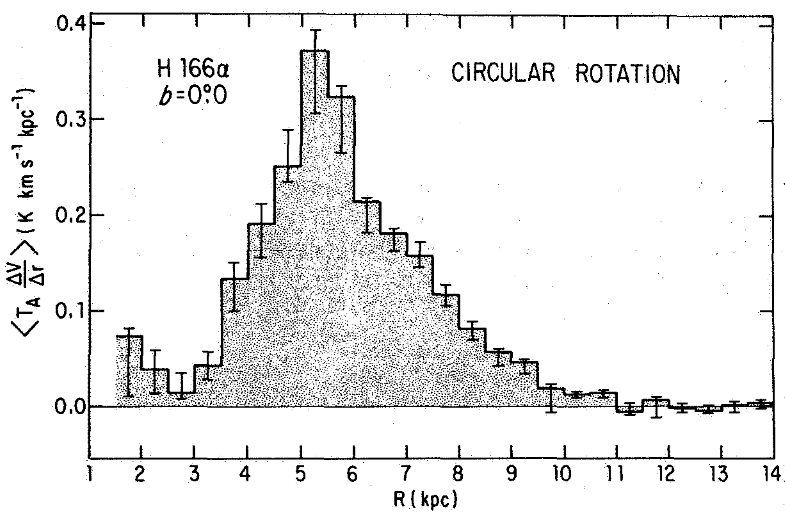

Figure 17. Power in the H166α line, per kiloparsec, derived under the assumption of pure circular galactic rotation, and plotted against the galactocentric radius (Lockman, 1976).

REFERENCES

Baker, P. L., and W. B. Burton, 1975, *Ap. J.*, **198**, p. 281.

Baker, P. L., and W. B. Burton, 1976, in preparation.

Bania, T. M., 1976, in preparation.

Barbanis, B., and L. Woltjer, 1967, *Ap. J.*, **150**, p. 461.

Bash, F. N., and W. L. Peters, 1976, *Ap. J.*, **205**, p. 786.

Bottinelli, L., 1971, *Astr. and Ap.*, **10**, p. 437.

Burton, W. B., 1971, *Astr. and Ap.*, **10**, p. 76.

Burton, W. B., 1972, *Astr. and Ap.*, **19**, p. 51.

Burton, W. B., 1973, *Publ. Astr. Soc. Pac.*, **85**, p. 679.

Burton, W. B., 1974a, *Galactic and Extragalactic Radio Astronomy*, Springer-Verlag, New York, p. 82.

Burton, W. B., 1974b, (Proc. I.A.U. Symp., No. 60), p. 551.

Burton, W. B., 1976, *Ann. Rev. Astr. and Ap.*, **14**, in press.

Burton, W. B., and M. A. Gordon, 1976a, *Ap. J. Letters*, in press.

Burton, W. B., and M. A. Gordon, 1976b, in preparation.

Burton, W. B., M. A. Gordon, T. M. Bania, and F. J. Lockman, 1975, *Ap. J.*, **202**, p. 30.

Burton, W. B., and W. W. Shane, 1970, (Proc. I.A.U. Symp., No. 38), p. 397.

Carruthers, G. R., 1970, *Ap. J. Letters*, **161**, p. L81.

Goldreich, P., and J. Kwan, 1974, *Ap. J.*, **189**, p. 441.

Gordon, M. A., and W. B. Burton, Sept. 1, 1976, *Ap. J.*, in press.

Hart, L., and A. Pedlar, 1976, in press.

Heiles, C., 1974, (Proc. I.A.U. Symp., No. 60), pp. 13-44.

Hollenbach, D. J., M. W. Werner, and E. E. Salpeter, 1971, *Ap. J.*, **163**, p. 165.

Innanen, K. A., 1973, *Ap. Space Sci.*, **22**, p. 393.

Kaplan, S. A., and S. B. Pikel'ner, 1975, *Ann. Rev. Astr. and Ap.*, **12**, p. 113.

Kerr, F. J., 1968, *Stars and Stellar Systems VII*, University of Chicago Press, Chicago, p. 575.

Kerr, F. J., 1969, *Ann. Rev. Astr. and Ap.*, **7**, p. 39.

Kodaira, K., 1974, *Publ. Astr. Soc. Japan*, **26**, p. 255.

Lin, C. C., C. Yuan, and F. H. Shu, 1969, *Ap. J.*, **155**, p. 721.

Liszt, H. S., W. B. Burton, R. H. Sanders, and N. Z. Scoville, 1976, submitted to *Ap. J.*

Lockman, F. J., 1976, Oct. 15, *Ap. J.*, in press.

Lockman, F. J., W. B. Burton, 1976, in preparation.

Manake, S., and M. Miyamoto, 1975, *Publ. Astr. Soc. Japan*, **27**, p. 35.

Radhakrishnan, V., 1974, (Proc. I.A.U. Symp., No. 60), p. 3.

Roberts, M. S., 1974, *Science*, **183**, p. 371.

Roberts, W. W., 1972, *Ap. J.*, **173**, p. 259.

Roberts, W. W., 1975, *Vistas in Astr.*, **19**, p. 91.

Rots, A. H., 1975, *Astr. and Ap.*, **45**, p. 43.

Scoville, N. Z., and P. M. Solomon, 1974, *Ap. J. Letters*, **187**, p. L67.

Scoville, N. Z., and P. M. Solomon, 1975, *Ap. J. Letters*, **199**, p. L105.

Shane, W. W., and G. P. Bieger-Smith, 1966, *Bull. Astr. Inst. Netherlands*, **18**, p. 263.

Simonson, S. C., 1974, (Proc. I.A.U. Symp., No. 50), p. 511.

Solomon, P. M., and N. C. Wichramasinghe, 1969, *Ap. J.*, **158**, p. 511.

Solomon, P. M., and N. C. Wichramasinghe, 1969, *Ap. J.*, **158**, p. 449.

Spitzer, L., et al., 1973, *Ap. J. Letters*, **181**, p. L116.

Spitzer, L., and E. B. Jenkins, 1975, *Ann. Rev. Astr. and Ap.*, **13**, p. 133.

Stecker, F. W., 1976, *Nature*, **260**, p. 412.

Strong, A. W., 1975, *J. Phys. A.*, **8**, p. 617.

Tuve, M. A., and S. Lundrager, 1972, *Astr. J.*, **77**, p. 652.

Verschuur, G. L., 1974, *Galactic and Extragalactic Radio Astronomy*, eds. G. L. Verschuur and K. I. Kellerman, Springer, New York, pp. 27-50.

Weaver, H., and D. R. W. Williams, *Astr. and Ap. Suppl*, **8**, p. 1.

Westerhout, G., 1973, *Maryland-Green Bank Galactic 21-cm Line Survey*, 3rd ed. University of Maryland.

Westerhout G., 1976, *Maryland-Bonn Galactic 21-cm Line Survey*, University of Maryland.

Wielen, R., 1974, *Publ. Astr. Soc. Pac.*, **86**, p. 341.

Yuan, C., 1969, *Ap. J.*, **158**, p. 871.

THE NONTHERMAL RADIATION IN THE GALAXY

J. E. Baldwin
Cavendish Laboratory
Cambridge, England

ABSTRACT

This paper does not attempt to review all aspects of the nonthermal continuum radiation in the galaxy, but concentrates on two topics of particular interest for γ-ray studies:

1. The distribution of nonthermal emissivity with height z above the galactic plane. The main result here is that recent observations of the distribution of brightness at intermediate latitudes in the galaxy and of the edge-on spiral galaxy, NGC 891, indicate that the emissivity extends to heights of several kpc perpendicular to the plane.

2. The relationship between the nonthermal emissivity and the neutral gas. In several galaxies, the angular distributions of neutral hydrogen and nonthermal emission are roughly coextensive and show similar features, such as spiral structure. If radio galaxies and normal galaxies with strong nuclear radio sources are excluded, there appears to be a proportionality between their total HI content and their nonthermal radio luminosity.

INTRODUCTION

In the last few years there have been notable advances in observations of the nonthermal radiation from the galaxy, but almost no corresponding progress in our understanding of the phenomena in terms of physical processes taking place in the galaxy. The observational advances can be summarized as:

> Improved angular resolution. There are now several surveys with angular resolutions better than 10 arcmin at frequencies above 1 GHz, notably those initiated by Beard and Kerr (1969) at 2.7 GHz and continued by others. The highest angular resolution used has been 3 arc-min by Green (1974) at 408 MHz, where the galactic radiation appears to be fully resolved except for details of individual sources.

- Improved sensitivity. Surveys now extend to higher latitudes then previously at high frequencies. Good examples are the surveys by Hirabayashi et al. (1969) and Altenhoff et al. (1970).
- Observations at very high frequencies. The upper limit of frequency has now been extended to 15 GHz by Hirabayashi et al. (1972). This is extremely important for distinguishing the thermal component of the galactic background radiation.
- Surveys with identical angular resolutions have been made over a range of frequencies by Altenhoff et al. (1970).
- The spectrum of the nonthermal radiation has been studied over a wide frequency range at low latitudes by many authors and with high accuracy at high galactic latitudes at frequencies up to 1.4 GHz by Sironi (1974) and Webster (1974).
- Whole sky surveys have been completed at lower frequencies (Landecker and Wielebinski, 1970) and are partially complete at 408 MHz (Haslam et al., 1974).
- Low frequency observations at 30 MHz by Jones and Finlay (1974) with an angular resolution of $0\overset{\circ}{.}8$ provide important measures of the absorption coefficient due to ionized hydrogen close to the galactic equator.
- Observations of nearby spiral galaxies with high resolution and good sensitivity have revealed their disks and spiral structure in the nonthermal continuum (Pooley, 1969; Mathewson et al., 1972; and van der Kruit, 1973) and have made possible the study of edge-on systems for measuring of the thickness of their disks and for searching for galactic halos.

Of these advances, the one which has changed our viewpoint most is the extension of studies to nearby galaxies. It is still true that the actual properties of our galaxy and no other are of the greatest importance for understanding the cosmic-ray and γ-ray data. But, the freedom we gain by not being tied to model-making from a viewpoint inside one system is of crucial importance. Particularly so, because we can examine what relationship exists between the nonthermal emission and other constituents of galaxies in a way which is impossible with a sample of only one system.

In spite of these advances, the questions being asked 20 years ago are still with us. Do the radio observations provide evidence for a region of containment of cosmic rays in the galaxy? What are the sources from which the cosmic-ray electrons originate? What processes determine the shape of the radio spectrum and the corresponding shape of the electron energy spectrum? Of course, there are answers to these questions, but which are we to believe?

In the following, I shall ignore many problems of importance and concentrate on two aspects of the nonthermal radiation which seem particularly important for this meeting. They are:

1. The distribution of emission perpendicular to the galactic plane
2. The relationship between the nonthermal radiation and the neutral gas

First, we must review briefly the main properties of the distribution of nonthermal emission which are generally accepted.

THE NONTHERMAL DISK

The distribution of brightness temperature, T (ℓ), in longitude, ℓ, at $b = 0°$ has been well-known for many years. Improvements in angular resolution have revealed the presence of many HII regions and supernova remnants but have not changed the basic picture. The symmetry about the galactic center is sufficiently good (figure 1a) that it is reasonable to make a circularly symmetric model of the radiation in the equatorial plane. I emphasize here, as in the past, that model-making is a reputable technique if one is good at guessing the correct model and that the model is a simple one. The procedure adopted in deriving the variation of the emissivity, J (R), as a function of radius, R, from the galactic center is straightforward. It differs slightly from many similar derivations in astronomy in that the Sun is situated in the disk itself and therefore $\{T(\ell) + T(\ell + 180°)\}$ is the brightness temperature which would be observed from a point outside the galaxy along a line of sight passing a distance $R_0 \sin \ell$ from the galactic center. Note that, in this case, we have no knowledge about the distribution of emission outside the Sun's radius R_0 and are subject to appreciable uncertainties even just inside R_0. The distribution of emissivity with radius, derived from the brightness temperatures in figure 1a, is shown in figure 1b. It is fairly similar to that derived, for instance, by Ilovaisky and Lequeux (1972) and by Baldwin and Pooley (1973). The most important features of the curve are the fairly uniform value of the emissivity within R = 8 kpc and the rapid falloff with radius near the Sun. The increase of emissivity with radius beyond R_0 is not shown by this technique, but models of the local spiral arm (using data at high latitudes as well as at $b = 0°$) strongly suggest that there is an increased emissivity in this arm.

The contours of brightness close to the galactic equator correspond very closely with those expected for a uniform thin disk of emission. The width in latitude between half-intensity points is only 2°, very much smaller than the width in longitude, and the contours run remarkably parallel to the galactic Equator for altitudes up to about 5°.

A long-standing problem is how much of this disk radiation is truly nonthermal. There is, beyond doubt, a thermal component from individual HII regions and also perhaps a smooth distribution of ionized hydrogen. Its magnitude has fluctuated from observer to observer. The reasons for this are simple. The extraction of a thermal component from several surveys at different frequencies depends on having observations with identical

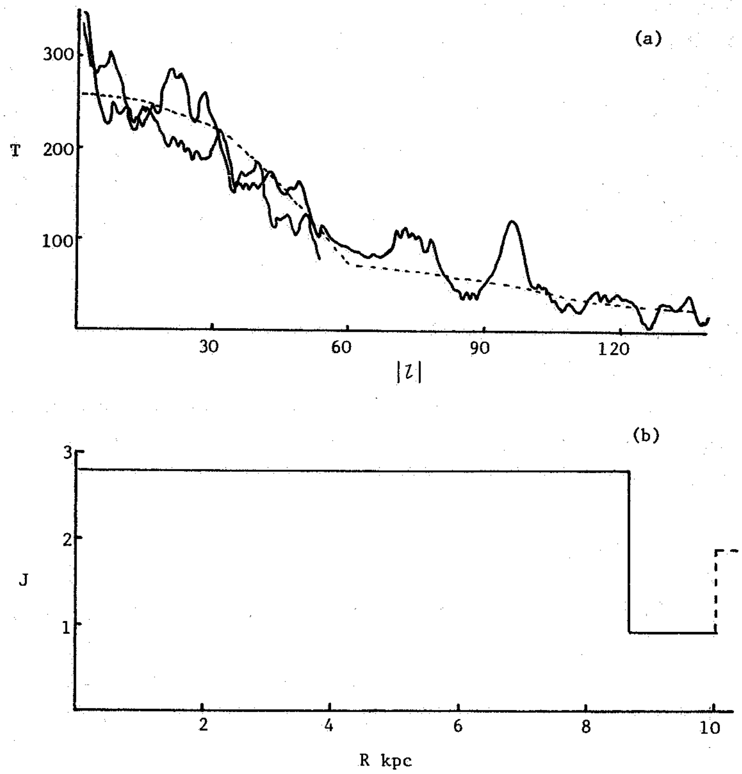

Figure 1. (a) The distribution of brightness temperature with longitude at 408 MHz at b = 0° from Green (1974). The two halves of the curve have been reflected about ℓ = 0° to show the departures from symmetry. The dotted line corresponds to the smooth model adopted. (b) The variation of emissivity at 408 MHz with radius in the galaxy derived from figure 1a. The units are 10^{-40} W m^{-3} Hz^{-1}.

beam shapes and accurately determined zero levels. The zero levels, in particular, can be a potent source of error because they give rise to systematic variations of spectral index with latitude which mimic the behavior expected from a narrow distribution of thermal emission along the galactic Equator. In the first analysis of this kind, Westerhout (1958) found that, at 1420 MHz, about 50% of the radiation at b = 0° was thermal. From the surveys by Altenhoff et al. (1970) at 1.4, 2.7, and 5.0 GHz, all with a resolution of 11 arcmin, Downes (Ph. D. thesis) concluded reluctantly that it was not possible to make the separation into thermal and nonthermal components because of uncertainties in one of the beam shapes. Jackson and Kerr (1971), who needed this result, were bolder using the same data and obtained a thermal component of 50 ±25 percent of the total brightness at b = 0° at 5 GHz. This value refers to a smooth distribution of thermal emission which has a total flux density far greater than that due to individual sources. The sources listed by Altenhoff et al. (1970) and by Reifenstein et al. (1970) have a combined flux density only about 5 percent of the total flux density of the disk. Measurements of the galactic radiation at 15 GHz by Hirabayashi et al. (1974) are an important addition to our knowledge. For a number of points along the galactic Equator, selected to be free of HII regions, they show spectra containing a very significant thermal component–about 80 percent of the total at 15 GHz. Taking a nonthermal temperature spectral index of -3 at high frequencies, this value would correspond to a 60-percent contribution at 5 GHz, well within the errors in Jackson and Kerr's (1971) determination, and 30 percent at 1.4 GHz, which is only a small reduction on Westerhout's (1958) value. But a number of other authors have found a negligible contribution from thermal radiation even at 5 GHz. The resolution of this problem needs more serious measurements. At 408 MHz, the effects of the thermal radiation can be neglected for most purposes. The distribution in latitutde of the thermal component is narrower than that for the nonthermal, and it does not influence a discussion of the distribution of emission outside the plane of the disk.

THE VARIATION OF EMISSIVITY WITH z

The evidence presented in the previous section suggests that the distribution of the nonthermal radiation is well represented by a plane stratified disk in which the emissivity is independent of R but may, however, have some dependence on z. If such a disk were of infinite extent and the Sun lay in its meridian plane, the brightness temperature observed at any latitude b would be

$$T(b) = \int_0^\infty J(z) \operatorname{cosec} b \, dz$$

$$= \text{constant x cosec b}$$

Baldwin (1967) found that the best available data, which were at 400 MHz, fitted this law very closely for $20° > b > 2°$. Departures from the relation showed at lower latitudes but were perhaps affected by the angular resolution of the observations (about 50 arcmin). Under these circumstances, it was only possible to derive a value of the equivalent thickness of the disk, $2 \int_0^\infty J(z)dz/J(o)$, of about 750 pc. The 150-MHz contour map of the entire sky assembled by Landecker and Wielebinski (1970) was used by Ilovaisky and Lequeux (1972) as the basis for fitting model disks as mentioned in the previous section. They found it necessary to use two disks, both having the same radius of about 10 kpc. The first had a thickness of 500 pc and an emissivity at 150 MHz of 200 K kpc^{-1} and the second, a thickness of 2000 pc and an emissivity of 100 K kpc^{-1}. The method of fitting model contours to those observed is not described, and it is hard to see which features in the observations led to the choice of disks used. The equivalent thickness of their disk, which would be 1500 pc, is in clear disagreement with Baldwin's (1967) value unless either it is due to the low resolution of the 150-MHz survey or there is a very rapid variation with frequency. An alternative explanation is that the old 400-MHz data were in error. Examination of modern data suggests that this may be so.

Improved angular resolution in the observations make it useful to reexamine the question of the z dependence of the emissivity. Jones and Finlay (1974) noted that, in the observations of Altenhoff et al. (1970), departures from the cosec b law occurred at $|b| \sim 1^\circ\!.5$, a much larger value than the resolution of 11 arcmin. Evidently this tells us something about the z distribution of emission. Consider now a disk of finite radius, R, which is, in fact, slightly less than R_o. The situation is shown in figure 2. Then, taking $\ell = 0°$ for simplicity, the brightness at latitude b will be

$$T(b) = \int_{(R_o - R)\tan b}^{(R_o + R)\tan b} J(z) \operatorname{cosec} b \, dz$$

for low latitudes tan b ~ b. The change in T(b) due to change in the lower limit of integration is, to a good approximation, $-(R_o - R)J(o)$. This is just the emission lying very close to z = o, present in the infinite disk and now missing in the case of the finite disk.

Therefore,

$$b\left\{T(b) + (R_o - R)J(o)\right\} = \int_o^{(R_o + R)b} J(z)dz$$

and

$$\frac{d}{db}\, b\left\{T(b) + (R_o - R)J(o)\right\} = (R_o + R)J((R_o + R)b)$$

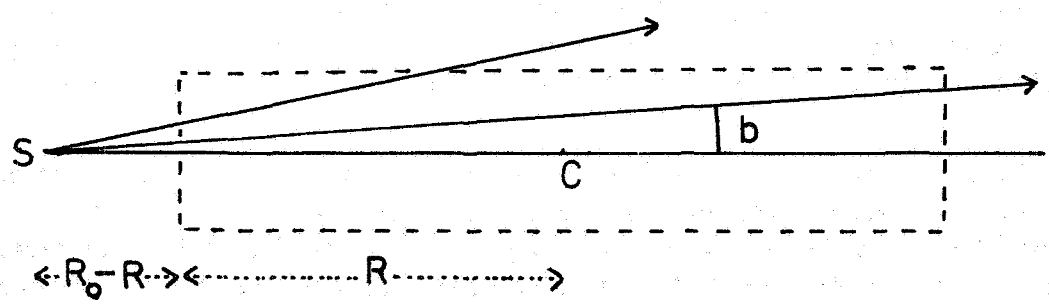

Figure 2. Geometry of a thick disk with radius $R < R_o$.

Thus, in this model, the departures of the brightness from the cosec b variation provide direct measurements of the emissivity at different heights. The behavior is easily seen from figure 2. If the line of sight at latitude b emerges from the top face of the disk into a region of zero emissivity before reaching the distant edge of the disk, the variation of brightness with latitude will vary as cosec b (or 1/b for small latitudes). If the line of sight reaches the far edge of the disk while still in a region of finite emissivity, the variation of brightness with latitude is slower than cosec b. In plotting the observational data, the constant term $(R_o$-R)J(o) on the left-hand side must be allowed for. It is about 7 to 8 percent of the brightness temperature at $b = 0°$, and, at 408 MHz, is roughly 25 K. The emissivity outside radius, R, is probably not zero, but I think it likely that the value of the term must be at least 15 K. In practice, there is a further constant term to be allowed for, because the observed value of T(b) already includes a constant contribution from extragalactic sources and perhaps an almost constant term from any large extended radio halo of the galaxy, neither of which have been mentioned in the model analysis. My best guesses of their combined value range from 6 to 20 K at 408 MHz. Values from the 408-MHz survey of Haslam et al. (1974) are plotted directly in figure 3a, making no allowance for either of these terms, on the basis that they exactly cancel. I adopted this as the most conservative view (i.e., that will lead to the lowest values of emissivity at large values of z). In fact, it is probable that the term, $(R_o - R)J(o)$, will be the larger and will lead to larger emissivities at high z.

Also plotted in figure 3a are data from the 1.4-GHz survey at Altenhoff et al. (1970). An allowance of 1 K has been made for the constant term, $(R_o - R)J(o)$. The zero level of their brightness temperature scale corresponded to the sky brightness at latitudes of ±25°, which is certainly higher than the sum of extragalactic and possible halo contributions. Thus, again the values plotted represent a conservative view of the emissivity at large z. The shape of the curve fits that of the 408-MHz data very closely. The variation of emissivity with z derived from the 408-MHz data is shown in figure 3b, together with the model of Ilovaisky and Lequeux (1972) adjusted to 408 MHz with a temperature spectral index of -2.6.

The most interesting features of the curve are the extensions to at least 3 kpc from the galactic plane. Because the constant terms in the brightness temperatures were chosen conservatively, the extensions are probably larger yet. The correctness of the result obviously depends on whether the model is correct. Tests which might justify it would be an analysis at all longitudes, including those where the edge of the disk is seen tangentially, but I have not yet completed these.

In the discussion so far, I have avoided the use of the phrase "radio halo." It arouses antagonism in otherwise placid astronomers, and many, including Burke (1967), Wielebinski and Peterson (1968), Yates (1966), Ilovaisky and Lequeux (1972), and Price (1974), have sought to deny its existence. The main feature of all these analyses is that features formerly associated with the presence of a halo can be explained in terms of features in the disk but at the expense of leaving an embarrassingly large isotropic component which is presumed to be of extragalactic origin. The only recent supporter of halos has been Webster (1975), who showed that the distribution of the spectral index of the radiation at high latitudes was consistent with a model in which a spherical halo has a steeper spectrum than the disk radiation. The question of its existence seems to me to be still quite open, but hard to resolve. The main point to establish is the existence of emission at large values of z. The shape of the distribution seems to me to be a subsidiary refinement. Perhaps the compromise which would satisfy everyone would be if the galaxy has a very thick disk as indicated by the preceding discussion. An independent line of evidence which suggests that it may be so comes from the study of other galaxies.

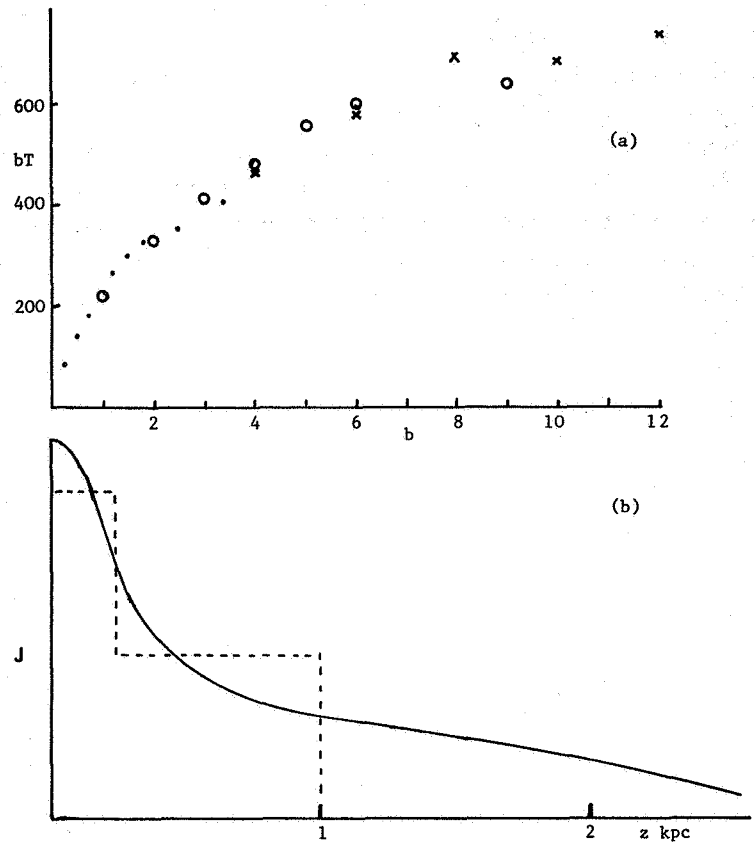

Figure 3. (a) The variation of bT(b) with galactic latitude. Dots are 1.4 GHz (Altenhoff et al., 1970) for $12^\circ < \ell < 17^\circ$. Crosses are 408 MHz (Haslam et al., 1974) for $30^\circ < \ell < 40^\circ$, $b > 0^\circ$. Circles $b < 0^\circ$. (b) The variation of emissivity, J(z), with height, z, above the galactic plane for a plane-stratified disk model derived from the 408-MHz data in (a). The dotted line is Ilovaisky and Lequeux's (1972) emissivity adjusted to 408 MHz.

THE EDGE-ON SPIRAL GALAXY, NGC891

Studies of an edge-on spiral might settle unambiguously whether radio halos exist or not. Many negative searches made in the past did not, in fact, have sensitivities adequate to detect them. For several years, M31 has been thought to possess one, but Wielebinski (1976) has recently argued that it does not. The next best candidate we know is NGC891. It is very close to edge-on. It is an Sb galaxy, probably of slightly earlier type than the galaxy but looking very similar optically to the wide-angle infrared photographs of the Milky Way showing the central bulge of the galaxy. It has slightly larger dimensions than the galaxy; it is rather more massive; and its intrinsic radio luminosity is a few times larger. Observations by Baldwin and Pooley (1973) at Cambridge indicated that the equivalent thickness of the disk was larger than that in the galaxy (4.8 kpc at the present distance of 14 Mpc), although in retrospect, that determination was certain to err on the large side by an uncertain amount. More recent observations at Westerbork (Sancisi et al., 1974; Allen and van der Kruit, 1976; Allen and Baldwin and Sancisi, in preparation) have provided a study at higher resolution and greater sensitivity over a range of frequencies from 610 MHz to 5 GHz. In these observations, extensions of the emission above and below the galactic Equator were detected to heights of 8 kpc at 21 cm. The most detailed profile of the emission normal to the plane was obtained at 5 GHz and is shown in figure 4. The width of the narrow component to half-intensity points after correction for beam smoothing is 9.6 arcsec or 700 pc, rather similar to that in the galaxy. The extensions seen out to ± 1 arcmin (4 kpc) in z also resemble those seen in the galaxy.

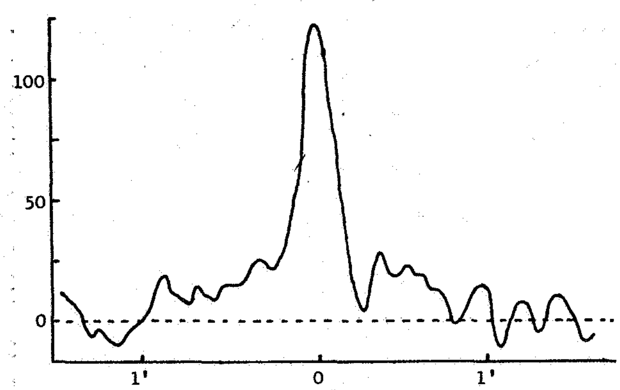

Figure 4. The distribution of emission with z in NGC891 at 5 GHz.

One of the most interesting aspects of the results concerns the spectral variations over the galaxy. In the equatorial plane, the spectral index, α, is uniformly -0.65, but the spectrum steepens with increasing z, reaching values of α of -1 at heights of 4 kpc above the disk. Whether the steepening is associated with energy losses by the electrons contained for periods of about 10^8 years or is merely due to lower magnetic fields at large z is not yet known. The uniformity of the spectrum in the disk suggests that either the sources of the electrons are spread throughout the disk or diffusion in the disk is relatively rapid.

The evidence discussed in the previous section makes it probable that the radio emission in the galaxy resembles that in NGC891 quite closely. It is of great interest to examine the variations in spectral index at high latitudes discussed by Webster (1975) in terms of a thick disk model rather than the spherical halo which he adopted for analysis, but work on this has not yet started.

RELATIONSHIP BETWEEN NONTHERMAL RADIATION AND NEUTRAL GAS

There are many reasons for expecting that there should be some correlation between the nonthermal emission and the gas in galaxies. For instance:

1. If magnetic flux is frozen into neutral gas clouds, then $B \propto n_H^{0.67}$. Because the nonthermal emissivity $J \propto B^{1-\alpha}$ and $\alpha \simeq -0.7$, then $J \propto n_H^{1.1}$ if the cosmic-ray electron density is uniform.

2. Regions of high n_H give rise to star formation, leading perhaps rather quickly to supernovas which might provide a high flux of cosmic-ray particles.

3. Galaxies having a high gas content and rate of star formation should also have a high supernova rate and a generally high flux of cosmic-ray particles not solely in the neighborhood of a single supernova. At the other extreme, dwarf elliptical galaxies with almost no gas may be very weak sources of cosmic-ray electrons, and they are also unlikely to have large-scale magnetic fields which could trap particles for a long period.

If correlations do exist, they are evidently very important for our interpretation of the γ-ray data. Correlations are hard to substantiate in the galaxy because of the distance problems for both the HI and the continuum emission, except close to the Sun at high latitudes. There have been a number of discussions of this region, notably of the nonthermal spurs and loops (Berkhuijsen et al., 1971). Heiles (1974) has also drawn attention to some local features in the neutral hydrogen which are correlated with continuum features.

It must be clear that we are not seeking a one-to-one correlation of HI with nonthermal radiation. HI in the galaxy extends radially well beyond the Sun, but the nonthermal emission probably dies away quite rapidly beyond the local spiral arm; the z distribution of HI well may not be as wide as that of the continuum. It must also be clear that we are talking about the disk radiation associated with normal spiral galaxies, not radio galaxies or the nuclei of spirals. Finally, we must recognize that any correlations we find may not imply a direct physical connection.

Similarities in the features of the distribution of HI and nonthermal radiation have been commented on for individual galaxies for a long time (for instance, the LMC and SMC (Mathewson and Healey, 1964), M31 (Pooley, 1969; and Emerson, 1974); M101 (Allen and van der Kruit, 1976)). Thermal radiation, which might well correlate with HI, is not the dominant in the continuum distributions, even in the LMC. In most cases, the nonthermal continuum is more centrally condensed in the galaxy than the HI.

A direct comparison of the total HI content and the nonthermal radio luminosity is now possible for a large number of nearby galaxies. The data are presented in figure 5. They cover a wide range from the most massive spirals rich in gas, such as M101, to the lowest mass of HI detected (3×10^5 $M_\odot$) in recent measurements we have made of NGC205, one of the dwarf companions of M31. The radio luminosities are based on flux densities measured at a wide range of frequencies but converted to 1420 MHz assuming a spectral index of -0.6. Where possible, the flux densities refer only to the disk component and have had any nuclear component subtracted. They are all small corrections for the values plotted. There is a very

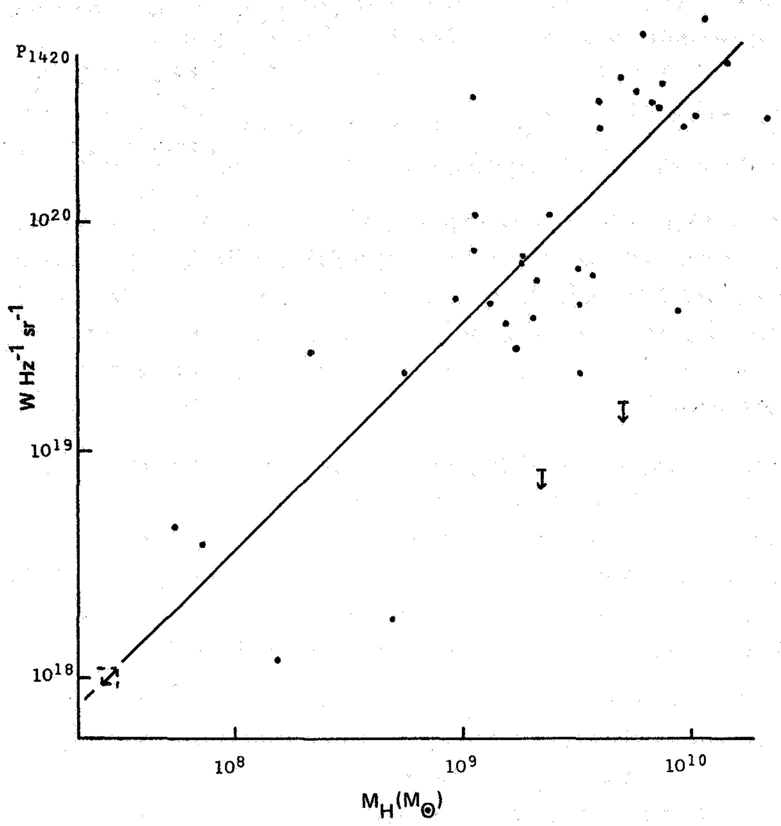

Figure 5. The relationship between radio luminosity at 1420 MHz and the neutral hydrogen content of galaxies.

clear correlation in the diagram with a scatter of only about X 2 about a line of unit slope. Errors in distances merely slide points in a direction parallel to this line. The absence of points well above the line is very significant. Below the line we must beware. The data suffer from rather unknown selection effects. Values are plotted only when there are published measurements of both HI and continuum flux densities. Astronomers are notorious for not publishing negative results so that some genuinely interesting points which lie away from the line may be missing. The line drawn corresponds to a constant ratio of column density of HI to nonthermal brightness temperature at 1420 MHz, N_H/T_{1420} of 2.5×10^{25} atoms m^{-2} K^{-1} (2.5×10^{21} atoms cm^{-2} K^{-1}). It is clearly consistent with what we know for nearby galaxies which have been mapped—that the surface densities of HI are typically 10^{25} atoms m^{-2} (10^{21} atoms cm^{-2}) and that they have brightness temperatures of about 0.4 K. If observed from outside, our galaxy would lie well on the line.

It would be easy, but perhaps idle, to speculate on the significance of the correlation until one understands why some galaxies lie off the line with abnormally low values of continuum emission. Prominent examples are NGC3109 and NGC4244, both late-type, perhaps Sc or

Irr I galaxies. It seems to me that, if we understood what is peculiar about such objects, we might gain some important clues about the origin of cosmic rays.

OBSERVATIONAL NEEDS

In the fields I have discussed, there are two very clear opportunities for improved observations:

1. Measurements of continuum flux densities of galaxies with high sensitivity. We are now engaged in a survey which is sensitive to sources of low surface brightness at 150 MHz, which we hope will cover most of the northern sky. I hope other surveys are undertaken at higher frequencies.

2. Measurements of the galactic nonthermal continuum at high frequencies (> 1 GHz) with the aim of extending the surveys to higher galactic latitudes. Such observations would be important in establishing any systematic variation of spectral index with z.

REFERENCES

Allen, R. J., and P. C. van der Kruit, 1976, *Ann. Rev. Astr. and Ap.,* **14**, p. 417.

Altenhoff, W. J., D. Downes, L. Goad, A. Maxwell, and R. Rinehort, 1970, *Astr. and App. Suppl.,* **1**, p. 319.

Baldwin, J. E., 1967, (IAU Symposium No. 31., Radio Astronomy and the Galactic System), p. 337.

Baldwin, J. E., and G. Pooley, 1973, *M.N.R.A.S.,* **161**, p. 127.

Beard, M., and F. J. Kerr, 1969, *Australian J. Phys. Suppl,* **11**.

Berkhuijsen, E. M., C. G. T. Haslam, and C. J. Salter, 1971, *Astr. and Ap.,* **14**, p. 252.

Burke, B. F., 1967, (IAU Symposium No. 31, Radio Astronomy and the Galactic System), p. 361.

Emerson, D. T., 1974, *M.N.R.A.S.,* **169**, p. 607.

Green, A. J., 1974, *Astr. and Ap. Suppl.,* **18**, p. 267.

Haslam, C. G. T., W. E. Wilson, D. A. Graham, and G. C. Hunt, 1974, *Astr. and Ap. Suppl.,* **13**, p. 359.

Heiles, C. E., 1974, (IAU Symposium No. 60, Galactic Radio Astronomy), p. 625.

Hirabayashi, H., T. Ojina, and M. Morimoto, 1969, *Nature,* **223**, p. 49.

Hirabayashi, H., H. Yokoi, and M. Morimoto, 1972, *Nature Phys. Sci.,* **237**, p. 54.

Ilovaisky, S. A., and J. Lequeux, 1972, *Astr. and Ap.,* **20**, p. 347.

Jackson, P. D., and F. J. Kerr, 1971, *Ap. J.*, **168**, p. 29.

Jones, B. B., and E. A. Finlay, 1974, *Australian J. Phys.*, **27**, p. 687.

Landecker, T. L., and R. Wielebinski, 1970, *Australian J. Phys. Ap. Suppl.*, **16**.

Mathewson, D. S., and J. R. Healey, 1964, (IAU/URSI Symposium No. 20, The Galaxy and the Magellanic Clouds), p. 283.

Mathewson, D. S., P. C. van der Kruit, and W. N. Brouw, 1972, *Astr. and Ap.*, **17**, p. 468.

Pooley, G. G., 1969, *M.N.R.A.S.*, **144**, p. 101.

Pooley, G. G., 1969, *M.N.R.A.S.*, **144**, p. 143.

Price, R. M., 1974, (IAU Symposium No. 60, Galactic Radio Astronomy), p. 637.

Reifenstein, E. C., T. L. Wilson, B. F. Burke, P. G. Mezger, and W. J. Altenhoff, 1970, *Astr. and Ap.*, **4**, p. 357.

Sancisi, R., R. J. Allen, and T. S. van Albada, 1974, (Colloques Internationaux du Centre National de la Recherche Scientifique No. 241, La Dynamique des Galaxies Spirales), p. 295.

Sironi, G., 1974, *M.N.R.A.S.*, **166**, p. 345.

van der Kruit, P. C., 1973, *Astr. and Ap.*, **29**, p. 231.

Webster, A. S., 1974, *M.N.R.A.S.*, **166**, p. 355.

Webster, A. S., 1975, *M.N.R.A.S.*, **171**, p. 243.

Westerhout, G., 1958, *Bull. Astr. Ned.*, **14**, p. 215.

Wielebinski, R., 1976, *Astr. and Ap.*, **48**, p. 155.

Wielebinski, R., and C. E. Peterson, 1968, *Observatory*, **88**, p. 219.

Yates, K. W., 1968, *Australian J. Phys.*, **21**, p. 147.

INFRARED ASTRONOMY AND HIGH-ENERGY ASTROPHYSICS

Giovanni G. Fazio
Center for Astrophysics
Cambridge, Massachusetts 02138

F. W. Stecker
Theoretical Studies Group
Goddard Space Flight Center
Greenbelt, Maryland 20771

ABSTRACT

Observations of the diffuse far-infrared flux from the galactic plane, as well as far-infrared measurements of the properties of dense molecular clouds, when combined with recent high-energy γ-ray measurements and radio observations of carbon monoxide, can yield new information about the total mass of molecular clouds, the large-scale structure of the inner galaxy, and the density of cosmic rays.

INTRODUCTION

Our picture of the distribution of interstellar gas in the galaxy has been changing rapidly, with important implications for galactic-structure theory (Burton, 1976; and Stecker, 1976).

Earlier studies of the interstellar gas distribution depended on studies of diffuse optical light, radio continuum and 21-cm radiation. Recently, observations of absorption lines in the ultraviolet spectra of reddened stars have yielded information on the density of molecular hydrogen, but only within a distance of about 1 kpc of the Sun. However, recent changes in our knowledge of large-scale galactic structure have come about as a consequence of two new and important observations: (1) the detection, at millimeter wavelengths, of carbon monoxide in molecular clouds; in particular, the ground-based observations of the 2.6-mm line associated with the rotational transition ($J = 1 \rightarrow 0$) in CO (Scoville and Solomon, 1975; Burton et al., 1975; and Gordon and Burton, 1976), and (2) the satellite observations of γ-radiation from the galactic plane (in particular, the SAS-2 and COS-B results for γ-rays greater than MeV) Fichtel et al., 1975.

The CO measurements yield the molecular cloud abundance in the galaxy, which can then be indirectly related to the molecular hydrogen density (Scoville and Solomon, 1975; and Gordon and Burton, 1976). Emission of the 2.6-mm rotation line of CO ultimately results from collisions of H_2 and CO. Hence, the CO observations can yield information on the H_2 density and temperature.

Assuming the radiation arises either from electron bremsstrahlung of π°-meson decay, the γ-ray measurements yield information on the product of the interstellar gas density and the cosmic-ray intensity.

The CO surveys show that the molecular cloud abundance in the galaxy exhibits a strong radial dependence with a broad maximum in the 5- to 6-kpc region. A strong increase in the γ-ray emissivity, peaking in the 5- to 6-kpc region (Stecker, et al., 1974), has now been associated with the increase in molecular cloud concentration (Solomon and Stecker, 1974; and Stecker et al., 1975). The consequence of these observations and their interpretation is that molecular hydrogen is by far the most abundant form of gas in the inner galaxy.

Thus, observations of the millimeter CO line and the galactic γ-ray flux are related in that they both give similar distribution of radiation and both lead to a determination of the molecular hydrogen density in the galaxy. Although they complement each other, both require independent analysis in obtaining the molecular hydrogen density, each with different uncertainties.

With this in mind, I would like to suggest an alternative technique—far-infrared observations—for exploring the physics and galactic distribution of interstellar gas, particularly cold molecular clouds, and molecular hydrogen.

Specifically, in connection with high-energy astrophysics, I would like to suggest two explicit observations that could yield new and important information on the gas density and cosmic-ray density in the galaxy: (1) measurement of the diffuse far-infrared flux and spectrum from the galactic plane (Fazio and Stecker, 1976), and (2) measurement of the γ-ray flux from dense molecular clouds in the galaxy (Black and Fazio, 1973).

DIFFUSE FAR-INFRARED FLUX

The basic source of far-infrared radiation in a molecular cloud or HII region is the reradiation of dust heated by light from early-type stars or young stellar associations. Judging from measurements of CO excitation temperatures in the molecular clouds (Scoville and Solomon, 1975, for example), the dust temperature in them is expected to be of the order of 10 to 25 K, so that they are expected to radiate most of their energy in the $\gtrsim$ 100-μm wavelength range in distinct contrast to the hotter, strong infrared sources at shorter wavelengths (<100 μm), which are primarily associated with HII regions. Stein (1966), Pipher (1973), and Andriesse (1974) have previously proposed the existence of a diffuse infrared flux from the galactic plane due to thermal radiation by dust grains, but the recent CO observations now permit a more detailed prediction of the properties of this radiation.

For this discussion, we will assume that the ratio of total gas to dust is roughly the same as that in more diffuse atomic clouds (Ryter et al., 1975) and that the physical properties of the dust are roughly uniform throughout the galaxy. We will then propose a framework for future far-infrared surveys by suggesting some basic numerical relations for predicting flux distributions and emissivities. Using dust temperatures derived from CO and other measurements, we can then predict the diffuse far-infrared flux distribution in the galactic plane as a function of galactic longitude, ℓ, in the $4° \leqslant \ell \leqslant 90°$ range and the far-infrared emissivity distribution as a function of galactocentric distance.

Galactic Plane Emission

If we assume that the dust is at an equilibrium temperature, T_d, and radiates with an absorbtivity, Q_{IR}, then the energy emitted in the wavelength interval $d\lambda$ per unit volume of the dust cloud per second is given by

$$J_{IR}(\lambda)d\lambda = 4\pi^2 a^2 n_d Q_{IR}(\lambda) B_\lambda(T_d) d\lambda \tag{1}$$

where a is the radius of the dust grain, n_d is the density of dust particles, and $B_\lambda(T)$ is the Planck function.

The value of n_d is related to the total hydrogen density by

$$n_d = (3m_H/4\pi\rho a^3)(M_d/M_H)\, n_H \tag{2}$$

where m_H is the mass of the hydrogen atom, n_H is the total hydrogen density ($n_H = 2n_{H_2} + n_{HI}$); ρ is the grain density, and M_d/M_H is the dust-to-gas mass ratio. The column density $N_H = \int n_H ds$ in any direction can be related to the CO emission in that direction as follows:

$$N_H = 4.6 \times 10^{20}\, I_{CO}\ \mathrm{cm^{-2}} \tag{3}$$

where $I_{CO} = \int T_A dv$ is the integrated CO intensity in units of K km s^{-1} (Solomon, 1973; Scoville and Solomon, 1975; and Gordon and Burton, 1976 preprint).*

The dust parameters are ρ, a, and Q_{IR}. The value of ρa can be determined using a hydrogen column density at $\ell = 0°$ (excluding the galactic nucleus) of 7×10^{22} cm^{-2} (Stecker et al., 1975) and an optical depth in that direction $\tau_v = 28$, (Becklin and Neugebauer, 1968; and Spinrad et al., 1971). Then

$$\tau_v = 0.92\, A_v = \pi a^2 Q_v N_d \tag{4}$$

where A_v is the visual extinction in magnitudes, Q_v is the extinction efficiency at visible wavelengths, and N_d is the column density of the dust. If we assume the canonical values, $(M_d/M_H) = 10^{-2}$ and $Q_v = 1$, we find

$$\rho a = 3.1 \times 10^{-5}\ \mathrm{g\ cm^{-2}} \tag{5}$$

*Based on the CO measurements alone, equation 3 is uncertain by a factor of 5 (Scoville and Solomon, 1975). However, arguments taking into account infrared and X-ray absorption measurements reduce this uncertainty to within a factor of 2 (Stecker et al., 1975).

This is consistent with the values given by Allen (1973) of $\rho = 1$ g cm^{-3} and a = 3×10^{-5} cm estimated from Q_v and which we now adopt. We then obtain from equation 2

$$N_d = 1.4 \times 10^{-13} N_H \tag{6}$$

The value of Q_{IR} is assumed to be of the form $A_1 \lambda^{-1}$ with $A_1 = 4.5 \times 10^{-5}$ cm (Pottasch, 1973).* The optical depth of the dust is then

$$\tau_{IR} = Q_{IR} \pi a^2 N_d = 8.2 \times 10^{-6} \lambda_{cm}^{-1} I_{CO} \tag{7}$$

For the range of values for I_{CO} given by Scoville and Solomon (1975) and taking $\lambda = 300\ \mu$m, it is found that the galaxy is optically thin at far-infrared wavelengths.

From equations 1 and 3, the infrared brightness can be computed as a function of galactic longitude, ℓ,

$$\iota_{IR}\, d\lambda = \frac{d\lambda}{4\pi} \int J_{IR} ds = 0.97 \times 10^{-10}$$

$$\times \left\{ I_{CO}(\ell)\, d\lambda\, \lambda^{-6} (\exp(1.44/\lambda T) - 1)^{-1} \right\} \tag{8}$$

$$\text{erg cm}^{-2}\ \text{s}^{-1}\ \text{Sr}^{-1}$$

with λ in cm. The total infrared brightness is

$$I_{IR} = \int_0^\infty \iota_{IR} d\lambda = 3.8 \times 10^{-13} T_d^5\, I_{CO}(\ell) \quad \text{wm}^{-2}\ \text{Sr}^{-1} \tag{9}$$

The total emission per grain is

$$\epsilon_g = n_d^{-1} \int J_{IR}\, d\lambda = 7.7 \times 10^{-24} T_d^5 \quad \text{w} \tag{10}$$

The temperature of the dust can be derived by relating it to the CO kinetic temperature, T_{CO}. Goldreich and Kwan (1974) and Scoville and Kwan (1975) have investigated the thermal coupling between radiatively heated dust and ambient molecular gas (H_2) and indicate that the gas will approach thermal equilibrium with the dust ($T_{H_2} \rightarrow T_d$) via collisions of H_2 with grains for $n_{H_2} > 10^4$ cm^{-3}. However, at $n_{H_2} = 10^4$ cm^{-3}, the collision rate is sufficient to give only $T_{H_2} = 1/2\ T_d$. Observational evidence, however, suggests that the coupling may be stronger. Scoville and Solomon (1975) derive an average value of T_{CO} of 6.6 K. We shall assume that a lower limit to T_d is 7 K.

---

*The dependence $Q_{IR} \propto \lambda^{-n}$ with n = 1 is somewhat uncertain at long wavelengths. Pottasch (1973) and Soifer et al., (1972) find evidence in favor of an overall dependence given by $n \simeq 1$. Scoville and Kwan (1975) and Leung (1975) suggest that the dependence may be better represented by $n \sim 1.5$ for $\lambda \gtrsim 30\ \mu$m, although Leung (1975) also gives several examples of grains for which $n \simeq 1$. Andriesse (1974) suggests that n = 2 for $\lambda > \lambda_c$ with λ_c between 50 and 200 μm.

An upper limit to the dust temperature can be derived by assuming that the dust particle absorbs all the incident visible and ultraviolet radiation and reradiates it in the infrared. At equilibrium,

$$4\pi^2 a^2 \int_0^\infty Q_{IR} B_\lambda (T_d)\, d_\lambda = \pi a^2 c u_\gamma \tag{11}$$

where u_γ is the density of radiation in interstellar space $\simeq 7 \times 10^{-13}$ erg/cm^3 (Allen, 1973). Solving for T_d, we get T_d = 15 K. Kaplan and Pikelner (1970) and Greenberg (1971) obtain similar estimates. Although u_γ may vary somewhat throughout the galaxy, equation 11 gives only a $u_\gamma^{0.2}$ dependence for T_d.

In presenting our results in graphical form, we shall assume a value T_d = 10 K. In figure 1, we have plotted the total infrared brightness, I_{IR}, as a function of galactic longitude derived from equation 9, using the data of Scoville and Solomon (1975) for I_{CO} and excluding the galactic center. Of particular importance is the predicted large peak at $\ell = 30°$ tangent to the maximum interstellar gas density near 5 kpc.

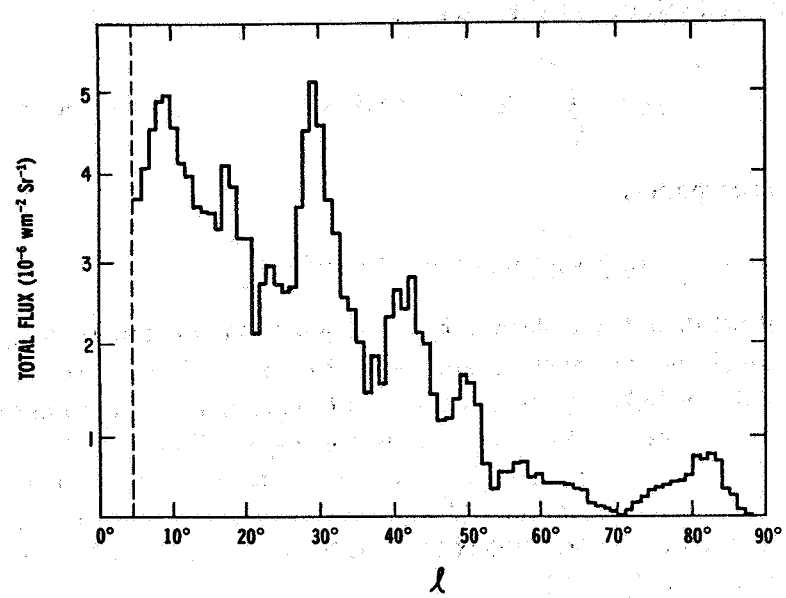

Figure 1. Predicted longitude dependence of the galactic far-infrared flux based on the model in equation 9, using the CO data of Scoville and Solomon (1975) and a temperature of 10 K.

A further consequence of our model, which can be used as an experimental test, is the prediction that the width of the galactic far-infrared disk should be comparable to that of the molecular cloud disk. The full width of the cloud disk is given by Scoville and Solomon (1975) to be ~ 130 pc, corresponding to a full width in galactic latitude of ~ 1° at $\ell \sim 30°$.

The infrared spectrum can be obtained from equation 8. The maximum in the spectral curve is given by

$$\lambda_m \simeq (hc/5.98kT_d) \simeq 0.24\, T_d^{-1} \text{ cm} \tag{12}$$

where for $T_d = 10$ K, $\lambda_m = 240\ \mu$m. In general, with Q_{IR} of the form $A_n \lambda^{-n}$ $(n \geqslant 0)$,

$$\lambda_m = hc/\left\{(n + 5)kT_d\right\} \simeq \frac{1.44}{(n + 5)T_d} \text{ cm} \tag{13}$$

In the Rayleigh-Jeans approximation, $hc \ll \lambda kT$, the far-infrared spectrum takes the power-law form

$$\iota_{IR}\, d\lambda \propto \lambda^{-(4+n)}\, d\lambda \tag{14}$$

It follows from equation 11 (also from Andriesse (1974)) that assuming $n > 1$ would result in higher T_d estimates and smaller differential fluxes at long wavelengths, although the total infrared flux integrated over all λ, as shown in the figures, remains unchanged (Greenberg, 1971). For example, Andriesse (1974), with n = 2, obtains $T_d \sim 24$ K with $\lambda_m \sim 85\ \mu$m. For the intermediate case, n = 1.5, $\lambda_m \sim 150$ to 200 μm. Future spectral measurements over the galactic plane in the far-infrared could therefore help to determine the wavelength dependence of Q_{IR}.

Using the relations derived by Stecker et al. (1975) in conjunction with equations 6 and 10 and employing the data of Scoville and Solomon (1975) on the molecular cloud distribution in the galaxy, the total far-infrared emissivity from molecular clouds as a function of galactocentric distance was calculated. The results are given in figure 2.

Galactic Center Region

In the galactic center region $|\ell| \leqslant 3°$, Scoville et al. (1974) have already shown that a correlation exists, as a function of galactic longitude, between the 100-μm flux and the maximum CO brightness temperature at each longitude. These authors conclude that the CO and dust coexist in nearly thermal equilibrium.

The CO measurements indicate that the molecular cloud disk surrounding the galactic nucleus has a radius of ~ 250 pc and that the total mass of molecular gas, mostly H_2, within the cloud is $\sim 5 \times 10^7\ M_\odot$.

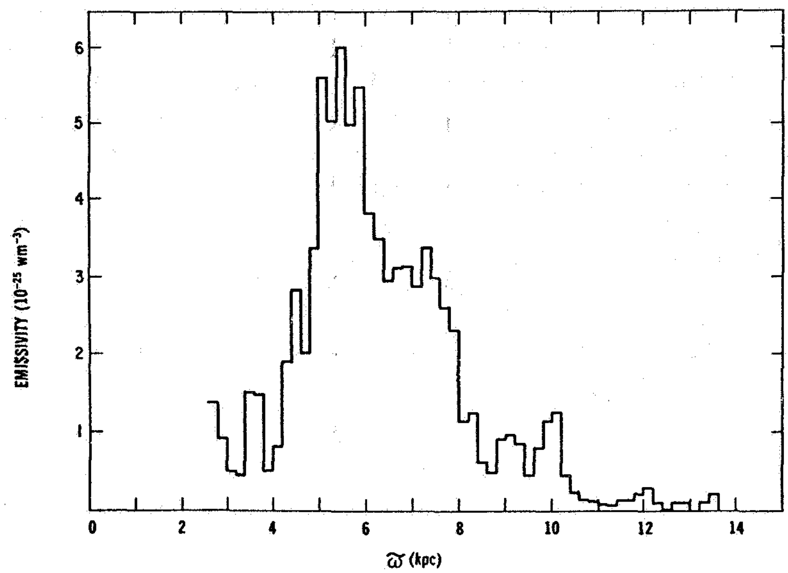

Figure 2. Predicted galactic far-infrared emissivity distribution using equations 6 and 10, together with the data of Scoville and Solomon (1975) and the values for n_{H_2} derived by Stecker et al. (1975). Again, a cloud of T = 10 K has been assumed.

In accordance with our assumed gas-to-dust ratio, the implied dust mass is then $M_d \sim 5 \times 10^5$ $M_\odot$ or about 10^{39} g. The total number of grains is then

$$N_g = (3M_d/4\pi a^3 \rho) \simeq 10^{52} \tag{15}$$

and, from equation 10, the total luminosity of the galactic-center source is estimated to be

$$L_{G.C.} = N_g \epsilon_g \simeq 8 \times 10^{28}\, T_d^5 \text{ w} \tag{16}$$

which, using the data given by Hoffman, et al. (1971), yields an estimated temperature $T_{d,G.C.}$ of the order of 25 K. The mean temperature of the CO gas, expected to be somewhat cooler, is of the order of 20 K (Scoville et al., 1974), so that our model gives reasonable results for the galactic-center source.

CONCLUSIONS

Our results indicate that much can be learned about the physics and conditions of interstellar dust and molecular clouds, as well as of the galactic dust and cloud distribution, by making far-infrared studies of the galactic plane. In the inner galaxy, most of the interstellar medium is in the form of the cold clouds. Far-infrared surveys, in conjunction with other observations, will enable us to get better estimates of quantities like N_H, N_d, and T_d. We have predicted the intensity, angular distribution, and spectrum of the diffuse far-infrared radiation over that region of the galactic plane about which sufficient CO data are available ($4° \leqslant \ell \leqslant 90°$), using the data of Scoville and Solomon (1975). Comparison of our model with 100-μm observations of the galactic-center source, which is expected to be about three times hotter than the average galactic molecular cloud, gives us confidence in the basic relations given in this paper. We believe the flux estimates calculated here to be reasonable predictions; however, one should bear in mind the assumptions made (in particular the wavelength dependence of Q_{IR}, the uncertainty in the relationship between I_{CO} and n_H, and the assumption of a uniform value of T_d = 10 K since the predicted flux has a steep temperature sensitivity).

Other Infrared Experiments

Recently other infrared experiments have been proposed for studying galactic structure. Ito et al. (1976, preprint) have observed the diffuse near-infrared radiation (2.4 microns) from the galactic plane and observed a correlation with the longitude distributions of CO molecular clouds, thermal radio emission, neutral hydrogen, and γ-ray emission. The authors predict that models of the galactic mass distribution should be improved by these observations.

Puget et al (1975) have discussed the general distribution of interstellar reddening within ~ 1 kpc of the Sun and find a correlation with the distribution and column density of nearby dense molecular clouds. From this mass distribution, the nearby cosmic γ-ray flux can be predicted and subtracted from the measured flux to obtain the true γ-ray flux from the inner galaxy. This true flux then yields the large-scale cosmic-ray distribution in the galaxy.

GAMMA-RAY FLUX FROM DENSE INTERSTELLAR CLOUDS

In 1973, John Black and I (Black and Fazio, 1973) predicted that dense interstellar clouds could be detectable discrete sources of γ-rays (> 100 MeV), produced by cosmic-ray interactions with the gas in the cloud, particularly molecular hydrogen. The γ-ray flux from a discrete cloud of mass, M, at a distance, R_{pc}, is given by the simple expression:

$$F_\gamma(> 100\ \mathrm{MeV}) \approx 1.3 \times 10^{-6} \left(\frac{1}{R_{pc}}\right)^2 \left(\frac{M}{M_\odot}\right) \mathrm{photons/cm^2\ sec}$$

This formula assumes that the cosmic-ray intensity is uniform in the galaxy with the same intensity as observed at the Earth.

Recently, near- and far-infrared observations, as well as radio molecular line emission, of dense, dark clouds have yielded new information on the density, extent, and central position of these clouds. Hence, better estimates of the cosmic γ-ray fluxes can now be predicted. Also, the SAS-2 has now provided the most extensive and highest sensitivity survey of γ-rays from these clouds. It is necessary, therefore, to reinvestigate this problem.

The dark cloud south of the star, ρ Oph, is perhaps the largest and most dense of the nearby molecular clouds. It is also one of the best-observed clouds at infrared wavelengths (Vrba et al., 1975; and Fazio et al., 1976) and in microwave line emission (Encrenaz et al., 1975). Using a gas density of $\sim 10^4$ cm^{-3} in the cloud and D $\sim$ 3 pc gives a total mass of 4×10^3 $M_\odot$. The distance to the cloud is about 190 pc. Hence, the predicted γ-ray flux is 1.4×10^{-7} photons/cm^2 s. The SAS-2 observations of this source yield only an upper limit (95-percent confidence level) to the γ-ray flux above 100 MeV of 2×10^{-6} cm^{-2} s (Kniffen et al., private communication, 1976). Thus, the present sensitivity is about a factor of 10 above the predicted flux. Other possible sources have also been investigated with negative results. These results are summarized in table 1.

As Black and Fazio (1973) pointed out earlier, the molecular cloud ring around the galactic center, which is at a radius of 250 pc and moving radially outward, should be a detectable γ-ray source. For a total mass of $\sim 10^8$ $M_\odot$ and a distance of 10 kpc, the predicted flux is $\sim 1.3 \times 10^{-6}$ photons/cm s, and the predicted size is $\sim 3°$ along the plane and $\sim 0.5°$ perpendicular to the plane. However, this source is presently obscured by the more intense radiation from the 5-kpc ring and the lack of sufficient angular resolution.

Further high-energy γ-ray experiments with increased angular resolution and sensitivity are obviously needed before important new information can be obtained on the discrete molecular cloud sources and the density of cosmic rays in the galaxy.

It is interesting to note that, although no discrete sources were observed, a plot of the positions of the center of mass of dark clouds along the plane, as given by B. T. Lynds (1962), shows an inclination to the plane above it in the 0° to 150° region and below it in the 150° to 250° region. This inclination is the same as bright B stars and indicates that these clouds are associated with Gould's Belt. The SAS-2 γ-ray flux measurements exhibit a similar asymmetry to the plane, and, although no discrete dark cloud was observed, the cumulative effect of many smaller clouds could be important.

ACKNOWLEDGMENTS

I am particularly indebted to the SAS-2 group of D. A. Kniffen, R. C. Lamb, C. E. Fichtel, and D. J. Thompson for their rapid analysis of the γ-ray observations of discrete molecular clouds.

Table 1
Upper Limits to the Gamma-Ray
Flux from Dense Molecular Clouds

Molecular Cloud Source	Gamma-Ray Flux (> 100 MeV) Upper Limit (photons/cm^2 s)*
Oph dark cloud	2.0×10^{-6}
R Cor A dark cloud	6.7×10^{-7}
Taurus dark cloud	3.1×10^{-6}
IC 1848-1	2.0×10^{-6}
Orion A	1.1×10^{-6}
Orion I-2	1.3×10^{-6}
B 227	5.0×10^{-6}†
L 134	5.4×10^{-7}
L 121	1.1×10^{-6}
B 335	2.1×10^{-6}
B 163	2.0×10^{-6}
NGC1333	2.0×10^{-6}
M78	1.1×10^{-6}

*Upper limits to the flux are at the 95-percent confidence limit; results are from SAS-2 observations (Kniffen et al., private communication, 1976).

†This flux limit is high due to confusion with the γ-ray sources NP0532 and γ (195+5). Whether this cloud could be the latter source should be investigated further.

REFERENCES

Allen, G. W., 1973, *Astrophysical Quantities,* 3rd ed., Athlone Press, London.

Andriesse, C. D., 1974, *Astr. and Ap.,* **37**, p. 257.

Becklin, E. E., and C. Neugebauer, 1968, *Ap. J.,* **151**, p. 145.

Black, J. H., and G. G. Fazio, 1973, *Ap. J. Letters,* **185**, p. L7.

Burton, W. B., 1976, *Ann. Rev. Astr. and Ap.,* **14**, p. 275.

Burton, W. B., M. A. Gordon, T. M. Bania, and F. J. Lockman, 1975, *Ap. J.,* **202**, p. 30.

Encrenaz, P. J., E. Falgarone, and R. Lucas, 1975, *Astron. and Ap.*, **44**, p. 73.

Fazio, G. G., and F. W. Stecker, 1976, *Ap. J. Letters,* **207**, p. L49.

Fazio, G. G., E. L. Wright, M. Zeilik II, and F. J. Low, 1976, *Ap. J. Letters,* to be published.

Fichtel, C. E., R. C. Hartman, D. A. Kniffen, D. J. Thompson, G. F. Bignami, H. Ögelman, M. E. Özel, and T. Tümer, 1975, *Ap. J.*, **198**, p. 163.

Greenberg, J. M., 1971, *Astr. and Ap.,* **12**, p. 240.

Goldreich, P., and J. Kwan, 1974, *Ap. J.,* **187**, p. 243.

Gordon, M. A., and W. B. Burton, 1976, *Ap. J.,* **208**, p. 346.

Hoffman, W. F., C. L. Frederick, and F. J. Emery, 1971, *Ap. J. Letters,* **164**, p. L23.

Kaplan, S. A., and S. B. Pikelner, 1970, *The Interstellar Medium,* Harvard U. Press, Cambridge, Massachusetts, 1970.

Leung, C. M., 1975, *Ap. J.,* **199**, p. 340.

Lynds, B. T., 1962, *Ap. J. Suppl.,* **7**, p. 1.

Pipher, J. L., 1973, (IAU Symp. No. 52, *Interstellar Dust and Related Topics*), ed. J. M. Greenberg and H. C. van de Hulst, Reidel Publishing Co., Holland, p. 559.

Pottasch, S. R., 1974, *Astr. and Ap.,* **30**, p. 371.

Puget, J. L., C. E. Ryter, G. Serra, and G. Bignami, 1976, *Astron. and Ap.,* in press.

Ryter, C. E., C. J. Cesarsky, and J. Audouze, 1975, *Ap. J.,* **198**, p. 103.

Scoville, N. Z., and J. Kwan, 1975, *Ap. J.,* in press.

Scoville, N. Z., and P. M. Solomon, 1975, *Ap. J. Letters,* **199**, p. L105.

Scoville, N. Z., P. M. Solomon, and K. B. Jefferts, 1974, *Ap. J. Letters,* **187**, p. L63.

Soifer, B. T., J. L. Pipher, and J. R. Houck, 1972, *Ap. J.,* **177**, p. 315.

Solomon, P. M., 1973, *Physics Today,* **26**, p. 32.

Solomon, P. M., and F. W. Stecker, 1974, (Proc. ESLAB Symp. on the Context and Status of γ-ray Astronomy, Frascati, ESRO SP-106), p. 253.

Spinrad, H., J. Liebert, H. E. Smith, F. Schweizer, and L. Kuhi, 1971, *Ap. J.*, **165**, p. 17.

Stecker, F. W., 1976, *Nature,* **260**, p. 412.

Stecker, F. W., J. L. Puget, A. W. Strong, and J. H. Bredekamp, 1974, *Ap. J. Letters,* **188**, p. L59.

Stecker, F. W., P. M. Solomon, N. Z. Scoville, and C. E. Ryter, 1975, *Ap. J.*, **201**, p. 90.

Stein, W., 1966, *Ap. J.,* **144**, p. 318.

Vrba, F. J., K. M. Strom, S. E. Strom, and G. L. Grasdalen, 1975, *Ap. J.*, **197**, p. 77.

ULTRAVIOLET OBSERVATIONS OF LOCAL GAS

E. B. Jenkins
Princeton University Observatory
Princeton, New Jersey 08540

ABSTRACT

From satellite measurements of ultraviolet spectra of stars, an average density of approximately 1.1 cm^{-3} for hydrogen atoms, in both atomic and molecular form, is estimated for regions of space along the galactic plane within about 1 kpc of the Sun. About 20 percent of the atoms are bound in molecular form, although this figure is uncertain because the ultraviolet measurements avoid the very dense interstellar clouds. Discrete values for this percentage are observed to vary markedly; regions with less than average density appear to have fractional abundances of H_2 several orders of magnitude lower than average. A ratio of CO/H which ranges from 10^{-9} to 10^{-6} is observed for regions in front of stars observed by the Copernicus satellite.

INTRODUCTION

A basic theme which underlies many of the contributions to the study of galactic structure is the complementarity of information derived from such diverse observables as diffuse γ-ray emission, radio continuum fluxes, 21-cm and CO line emissions, and counts of pulsars and supernova remnants. Against the backdrop of these methods, studies on the distribution and properties of interstellar matter from observations in the ultraviolet appear to be relatively myopic, since only about 1 percent of the volume of the galactic disk can be surveyed by present-day orbiting telescopes. The primary factor which limits ultraviolet studies to regions within a few kpc of the Sun is the strong attenuation of ultraviolet radiation by the intervening interstellar dust. In spite of this restriction of range, we shall see in the discussion which follows the special contributions which arise from viewing interstellar absorption features in the ultraviolet. In particular, one obtains unique information on the general behavior of atoms and molecules in space, which is of value in the interpretations of data from other areas of research. Also, we can ascertain average densities of various gaseous constituents in the local part of our galaxy, and such measurements serve as a benchmark for calibrating the broader scale mappings of interstellar matter which are quantitatively uncertain.

BACKGROUND

Just over 10 years ago, the development of attitude control systems for Aerobee sounding rockets triggered the beginning of the age of ultraviolet stellar spectroscopy, because the spectrographs could be stabilized with enough precision to record exposures of bright stars during the vehicle's coasting trajectory above the atmosphere. Owing to the moderate wavelength resolutions of the early observations (typically a few angstroms), much of the research concentrated on the properties of stellar features, rather than on absorption features produced by the intervening gas in space. However, these early rocket flights were able to provide two important contributions which furthered our understanding of the local interstellar gas. First, a number of observations of Lα absorption by interstellar HI established that the average densities toward most of the stars observed were substantially lower than expected in our region of the galaxy from studies of 21-cm emission, suggesting that a good fraction of the volume of space within several hundred pc of the Sun had densities lower than the overall mean density (Jenkins, 1970). The second main achievement in the study of the interstellar medium was the discovery of absorption by molecular hydrogen (Carruthers, 1970; and Smith, 1973), a form of matter long suspected to be an important constituent of the gas, but one which until then had been tantalizingly elusive to detect.

The spectrometer aboard the first Orbiting Astronomical Observatory, OAO-2, permitted us to survey at 12-A resolution the Lα absorption for a substantial number of stars (Savage and Jenkins, 1972). Although 21-cm radio-line observations provide a rich backlog of information on the distribution and kinematics of interstellar gas, several important differences in the way the gas is measured establish a unique value to the Lα data. First, the volume sampled toward a star has a definite length and virtually infinitesimal width, whereas the radio beam samples a cone-shaped space of unlimited extent. Also, corrections for saturation are unnecessary for the Lα line, because it is already heavily saturated so much that the damping wings are the principal contributors to the absorption. Hence, the line strength is governed purely by the column density of the gas rather than a complex interrelationship between the amount, velocities, and spin temperatures of atoms along a line of sight. Finally, the Lα measurements permit one to compare directly the abundances of HI to other species observed toward the same stars, such as interstellar Na I, Ca II, and K I (seen by absorptions in the visible spectrum) and also interstellar dust grains (revealed by continuous absorption).

In the discussions which follow, we will draw heavily upon the inference from the OAO-2 Lα survey that hydrogen-gas column densities and obscuration by dust (as revealed by B-V color excesses) are well correlated with each other, and that measurements of E (B-V) toward a star can be used with reasonable accuracy to predict the total amount of gas present (Jenkins and Savage, 1974). The collocation of gas and dust has also been demonstrated in analyses of radio data (e.g., see references cited in Jenkins (1970) and also recent work by Grayzeck and Kerr, 1974; Heiles, 1976; and Heiles and Jenkins, 1976).

Over the past 4 years, the successful operation of the Copernicus satellite (the last of the OAO's) has brought about a climax in the study of the interstellar gas, because absorption by strong resonance lines from the ground states of important constituents could be studied in detail. Much has been learned about the composition and physical state of interstellar gases from the Copernicus observations; however, it is out of place to summarize the broad spectrum of conclusions here, especially since much of the material has already been reviewed in the literature (Spitzer and Jenkins, 1975; and Snow, 1976). Instead, we shall focus on two topics which have a special relevance to the study of cosmic γ-rays and galactic structure. First, the ultraviolet observations can give an independent determination of the average density of both atomic and molecular hydrogen, against which we can compare the representative densities derived from larger-scale observations at a galactocentric distance, R = 10 kpc. The second area of interest is a study of the relative abundances of CO and H_2 in the interstellar medium, because it enables us to calibrate the H_2 densities in terms of CO radio measurements for gas outside the dense molecular clouds.

AVERAGE DENSITY OF HI AND H_2

Observational Selection

Our objective in analyzing the surveys of HI and H_2 column densities (which we denote as N(HI) and N(H_2)) is to arrive at a representative average for the space densities within the overall sampling volume. If the stars chosen for the survey are widely enough distributed and represent a truly random sample of directions in the sky, one can total all the column densities and divide by the sum of the distances, r, to give a measure of average space density along all of the lines of sight. If we draw upon the Lα results of Savage and Jenkins (1972), Jenkins and Savage (1974),* Bohlin (1975), and preliminary results from Bohlin, Drake, and Savage (private communication), we find for 130 stars an average value

$$\frac{\Sigma\, N(HI)}{\Sigma r} = 0.32\ cm^{-3}$$

From the work of Spitzer et al. (1973 and 1974) and Bohlin, Drake, and Savage (private communication), we find for 70 stars

$$\frac{\Sigma\, N(H_2)}{\Sigma r} = 0.043\ cm^{-3}$$

We must immediately realize, however, that these figures are far from representative, because the choice of stars is not random. A strong bias against reddened stars exists in all of the surveys. That such selection is a dominant effect follows from two main factors: (1) the distribution of gas in space is highly irregular, and (2) the extinction of star light is very strong at short wavelengths (York et al., 1973). Another contributing factor is that some of

*In all of our use of the data of Savage and Jenkins (1972) and Jenkins and Savage (1974), we have rejected the type B1.5 and B2 stars for which Savage and Panek (1974) estimated the stellar Lα feature to be a significant part of the measured absorption.

the stars are at large distances from the plane of the galaxy: 21 percent of the total sample path length has z > 100 pc, and 10 percent is more than 200 pc away from the plane. Figure 1 shows a plot of color excess per unit distance, E(B-V)/r, against distance, r, for all of the stars studied for Lα or H_2 absorption.

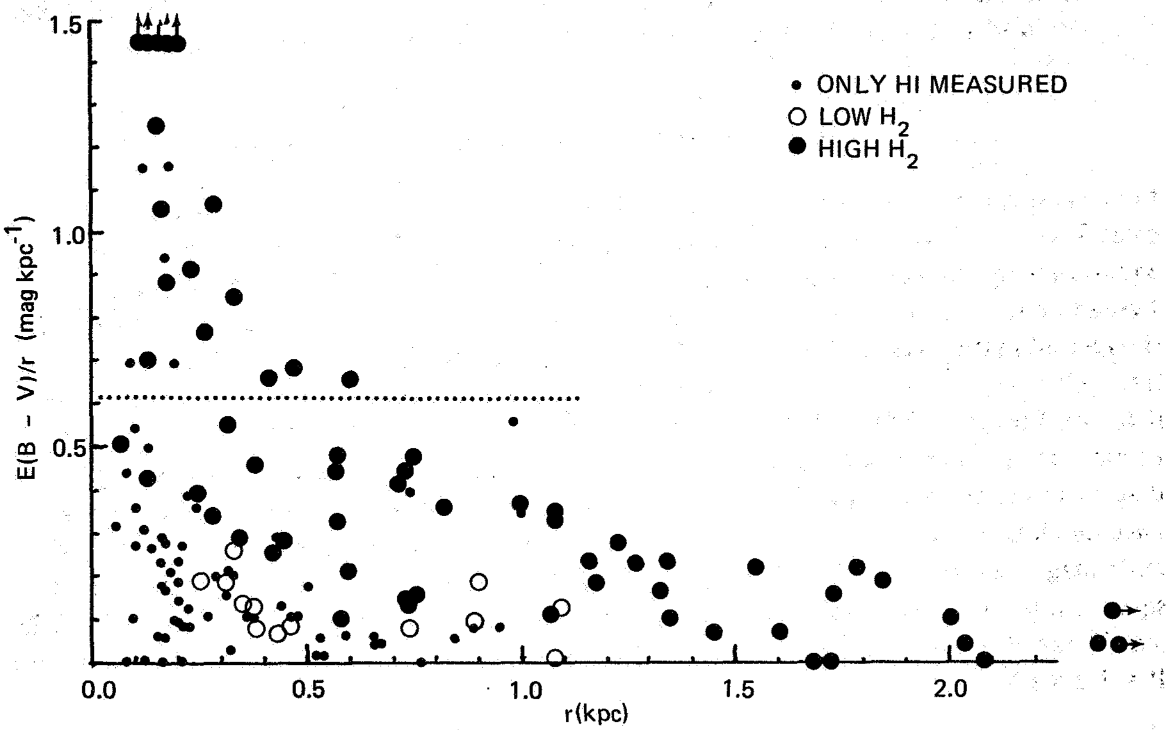

Figure 1. Color excess per kpc, E(B-V)/r, against distance, r, for all stars studied for Lα or H_2 absorption.

If one samples truly random regions of space in the plane of the galaxy within 1 kpc of the Sun, one should have an average E(B-V)/r of 0.61 mag kpc^{-1} (Spitzer, 1968), shown by the dotted line in the diagram (about one-half this value is obtained if stars are selected to a given magnitude limit in the visible). In the immediate vicinity of the Sun (a few hundred pc or so), the actual reddening per unit distance is somewhat less than normal (Fitzgerald, 1968). Figure 1 shows us that, for stars more distant than about 300 pc, the sample represents lines of sight which avoid areas with normal reddening, and this bias becomes worse with increasing distance. For all of the stars shown on the diagram, Σ E(B-V)/Σr = 0.23 mag kpc^{-1}. Thus, an interpretation of the HI and H_2 data must contain some compensation which overcomes the effects of this selection.

IONIZATION

Another effect which must be considered is the fact that every measurement is toward a star which is hot enough to photoionize a region of space around it. Thus, to varying degrees, some of the gas will be removed from sight in a systematic manner, in addition to our having lines of sight which intersect by chance the ionization zones around other stars. One can assess how important ionization of the observed stars is to an overall result by the following analysis: under ideal circumstances we expect for each observation the equation

$$N(HI) + 2N(H_2) + (3N_L n_e/4\pi\alpha)^{1/3} = R\,E(B\text{-}V)$$

to be valid, where R is the ratio of the total gas column density to the color excess (we treat R as an unknown, but whose value is constant everywhere). The third term in the equation is the expected column density of ionized hydrogen around a star emitting N_L Lyman limit photons per second in a region with a uniform electron density, n_e. At 10^4 K, the recombination coefficient, α, to all levels of hydrogen except n = 1 is estimated to be 2.6×10^{-13} cm^3 s^{-1} (Spitzer, 1968), and values of N_L for stars of various spectral types are listed by Panagia (1973). We have no direct knowledge about values for n_e in the vicinity of most of the stars, but Hα and radio continuum emission measurements indicate typical densities ranging from 1 to 10 cm^{-3}, although some of the more conspicuous HII regions have much higher densities. For these two values of n_e, best solutions for R give 5.7×10^{21} cm^{-2} mag^{-1} and 6.3×10^{21} cm^{-2} mag^{-1}, respectively, for all of the stars surveyed. A least-squares solution which allows both R and $n_e^{1/3}$ to vary as free parameters yields $n_e^{1/3} = 0.33$ cm$^{-2/3}$ and $R = 5.4 \times 10^{21}$ cm^{-2} mag^{-1}.* If ionization were neglected, we would have found $R = 5.2 \times 10^{21}$.

To summarize, the least-squares solution suggests that ionization by the target stars reduces the amount of gas seen by only about 4 percent, but this fraction could be as large as 17 percent if n_e were typically 10 cm^{-3}. The fact that the least-squares solution for a representative $n_e^{1/3}$ is small may be an indication that the actual values for R inside the ionization zones are somewhat larger than those in the general gas regions.

Evaluation of Overall Densities

In analyzing the behavior of the average volume density, n, along various lines of sight, it is instructive to study the relationship for different values of E(B-V)/r. For the 70 stars for

*The expression

$$\Sigma\epsilon^2 = \Sigma\left\{[N_t + 8720\,N_L^{1/3} n_e^{1/3} - R\,E(B\text{-}V)]^2/(N_t + R^2\,E(B\text{-}V)^2)^{1/2}\right\},$$

where $N_t = N(HI) + 2N(H_2)$, was minimized by varying the parameters, R and $n_e^{1/3}$. The error matrix terms, $\partial^2\Sigma\,\epsilon^2/\partial R^2$, $\partial^2\Sigma\,\epsilon^2/\partial R\,\partial(n_e^{1/3})$, and $\partial^2\Sigma\epsilon^2/\partial(n_e^{1/3})^2$ are 0.35, -1.7×10^{20} and 3.2×10^{41}, respectively.

which both N(HI) and $N(H_2)$ have been measured (see references cited in the "Observational Selection" section), we see from figure 2* that the average total hydrogen densities, $n(HI) + 2n(H_2)$, are linearly related to E(B-V)/r, although the points show some scatter. This scatter is worse if one plots just n(HI) versus E(B-V)/r, because of the large variability in the fraction of hydrogen in molecular form (see the following section, "Behavior of H_2").

The lack of any gross irregularities in the relationship of total gas density to dust density suggests that a derivation of an average density, with a compensation for the selection discussed in "Observational Selection," is relatively straightforward. We may take the observed $\Sigma[N(HI) + 2N(H_2)]/\Sigma r$, multiply it by the true average reddening per unit distance, and divide by the observed $\Sigma E(B-V)/\Sigma r$. The resulting estimate for the overall density of hydrogen atoms, in both atomic and molecular form, is approximately 1.1 cm^{-3}, a figure which one might consider raising to 1.2 or 1.3 to compensate for the systematic losses from ionization discussed in the "Ionization" section.

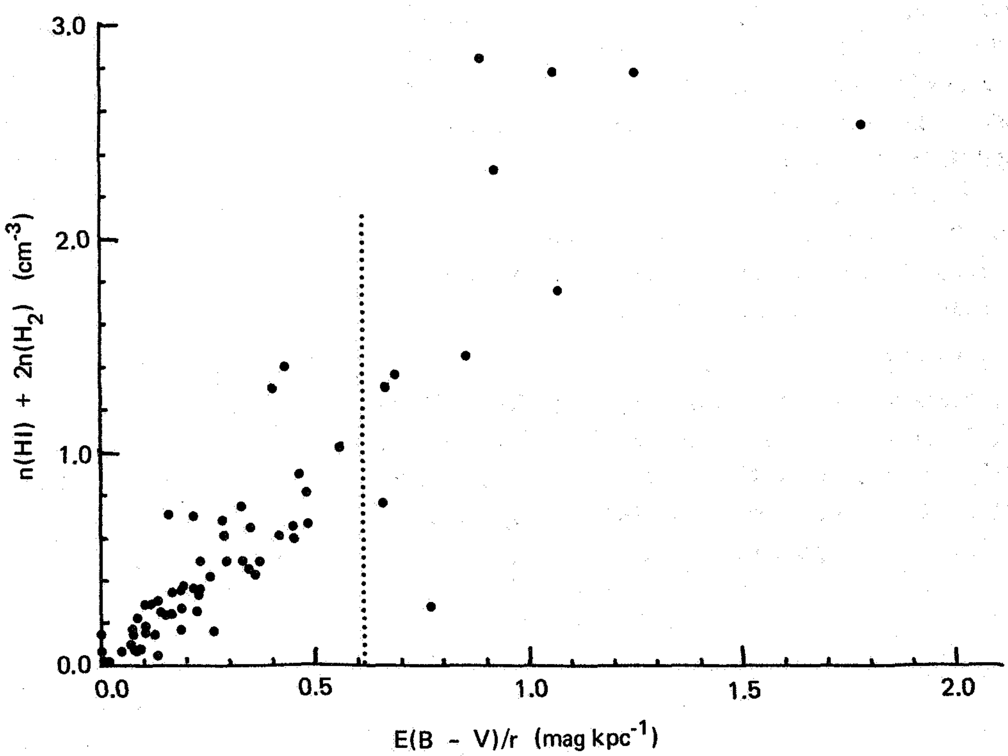

Figure 2. Average total hydrogen density versus color excess per kpc.

*The points for a few of the 70 stars are outside of the range of figure 2; they are reasonably in line with the average tendency, but off beyond the upper right corner of the diagram.

Behavior of H_2

If we concentrate on the distribution of H_2, we find considerably more variability in the measurements. Early data from Copernicus suggested a bimodal distribution in H_2 column densities (see figure 4 of Spitzer and Jenkins, 1975); the more recent, extensive survey by Bohlin, Drake and Savage, private communication, (1976) confirms that values for $n(H_2)$ are either around 10^{-6} cm^{-3} or are in the range 10^{-3} to 10^{-1} cm^{-3} for various lines of sight. (Cases with low and high molecular abundances are shown as different symbols in figure 1.)

This phenomenon may be qualitatively understood if one considers the formation and destruction of H_2 in space (Hollenbach et al., 1971). Because H_2 is probably formed as the atoms collide with dust grains and combine on the grain surfaces, the rate of H_2 production scales with the square of the density. The destruction of the molecules is primarily from photodissociation by starlight, and, for reasonable densities and starlight fluxes, the expected abundances are in accord with the very low values for $n(H_2)$ quoted above. An important feature of the photodissociation, however, is that it occurs by absorption in discrete, strong lines, rather than by a continuum. This process, originally proposed by Solomon (see Field et al., 1966), involves the absorption of an ultraviolet photon which raises the molecule to a higher level of electronic excitation, which is then followed by a spontaneous decay to the ground electronic level. Occasionally (about 11 percent of the time), the decays are to the vibrational dissociative continuum of the ground state, resulting in the destruction of the molecule. For moderate column densities of H_2 ($\sim 10^{17}$ cm^{-2}), the lines become optically thick, and thus, for increasing interstellar cloud thicknesses, self-shielding becomes important. As a result, an abrupt transition to high molecular density occurs, because photodestruction rates are markedly reduced in the cloud's interior.

For a given line of sight, we are unable to ascertain the details of cloud geometry, incident starlight fluxes, or other factors which govern the equilibrium between atoms and molecules. However, the measured E(B-V)/r is a crude indicator of whether dense clouds are present. Figure 3 shows a plot of $2n(H_2)$ versus E(B-V)/r for the stars shown in figure 2. Instead of the direct proportionality we saw for the total hydrogen density, the observed relationship of molecules to dust suggests that, for E(B-V)/r $\lesssim 0.1$, molecules have difficulty in accumulating, but, as E(B-V)/r exceeds this value, the shielding becomes important and the average molecular densities begin to grow with increasing amounts of material present. We note that the scatter of points is larger here than in figure 2; this is also probably a consequence of the unusual evolution for molecular regions.

Because of the nonlinearity in the growth of molecules, it is harder for us to derive an overall average for $n(H_2)$ that has the compensation for observational selection. In essence, we must know a frequency distribution for the true E(B-V)/r for small volumes of space in our part of the galaxy, rather than just a mean value. A crude estimate for the best value of $n(H_2)$ can be made by assuming the intersection of the dotted line (0.61 mag kpc^{-1}) with the trend of points in figure 3 gives an indication of the average conditions, under the assumption that, when we observe this amount of reddening per unit distance, the distribution of material is

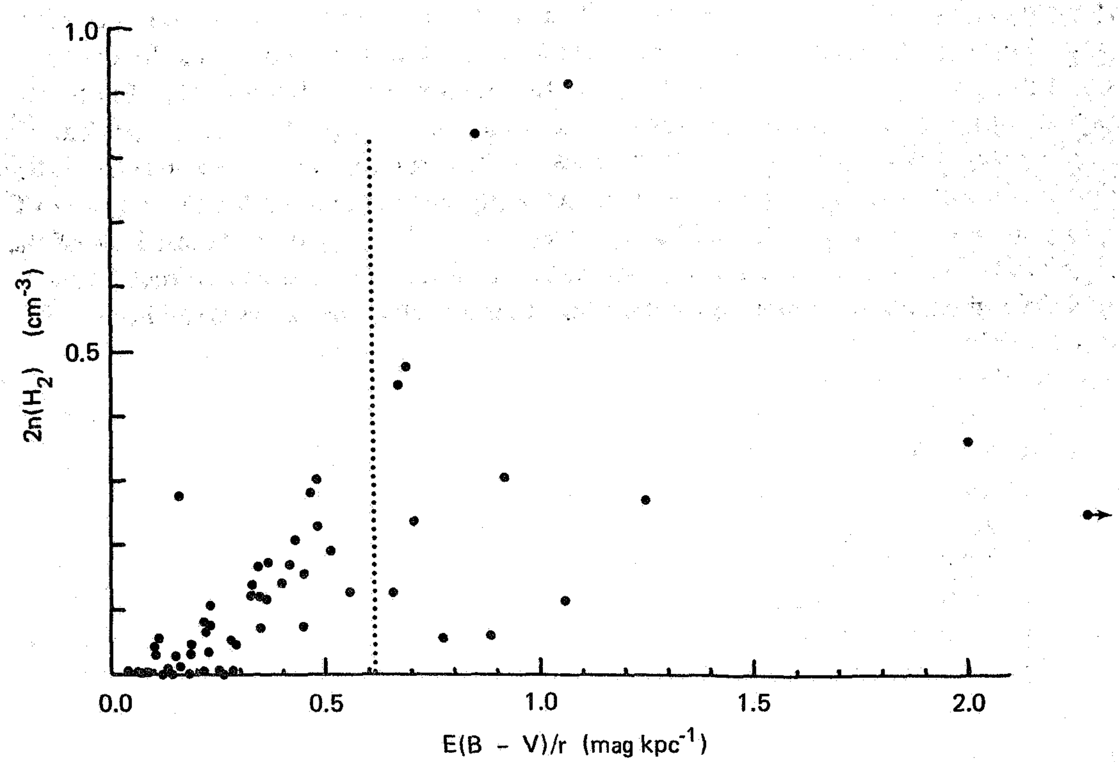

Figure 3. A plot of $2n(H_2)$ versus E(B-V)/r for the stars shown in figure 2.

typical of more general regions of space. A value of 0.1 cm^{-3} seems to be a good estimate for a representative H_2 density; from the spread of points, we see that this number could easily be in error by a factor of two. Combining this result with the total density derived in "Evaluation of Overall Densities," we find that roughly 20 percent of the neutral atoms are bound in molecular form.

RATIO OF CO TO H_2

In addition to measuring column densities of HI and H_2, the Copernicus satellite can scan absorptions by CO molecules in front of a star. Although this offers us some insight into the formation of CO in space, measurements of the ratio of CO to HI and H_2 are also of interest for comparing with the adopted ratios used to derive H_2 densities from radio measures of CO. The radio observations are of prime importance in mapping the distribution of molecular regions in our galaxy.

Figure 4 shows CO/H_2 density ratios, plotted against our familiar scale of E(B-V)/r, for 21 stars which were analyzed for CO by Jenkins and Shaya (1976) and for H_2 by Spitzer et al. (1973 and 1975) and Bohlin, Drake and Savage (private communication, 1976). The uncertainties in some of the ratios are as large as 50 percent, although many of the values are better defined than this. The sharp change in the abundance ratio shown here is reminiscent of the contrasts in H_2 abundances discussed in "Behavior of H_2." In fact, if we examine the ratio of CO to total hydrogen, as shown in figure 5, we see that the variation of the CO to H_2 ratio is simply a result of the large changes in the fractional abundance of H_2. In other words, the density of CO is governed more by the total density of gas than by the presence of H_2. This conclusion is of relevance to theories on the formation of CO, because ion-molecule reaction chains initiated by the presence of H_2 are a popular explanation for the origin of CO in interstellar clouds (e.g., see Glassgold and Langer, 1975). The apparent insensitivity of the presence of CO to the amount of H_2 suggests that other mechanisms, such as direct formation of CO on grains, may be more important for the interstellar clouds observed here.

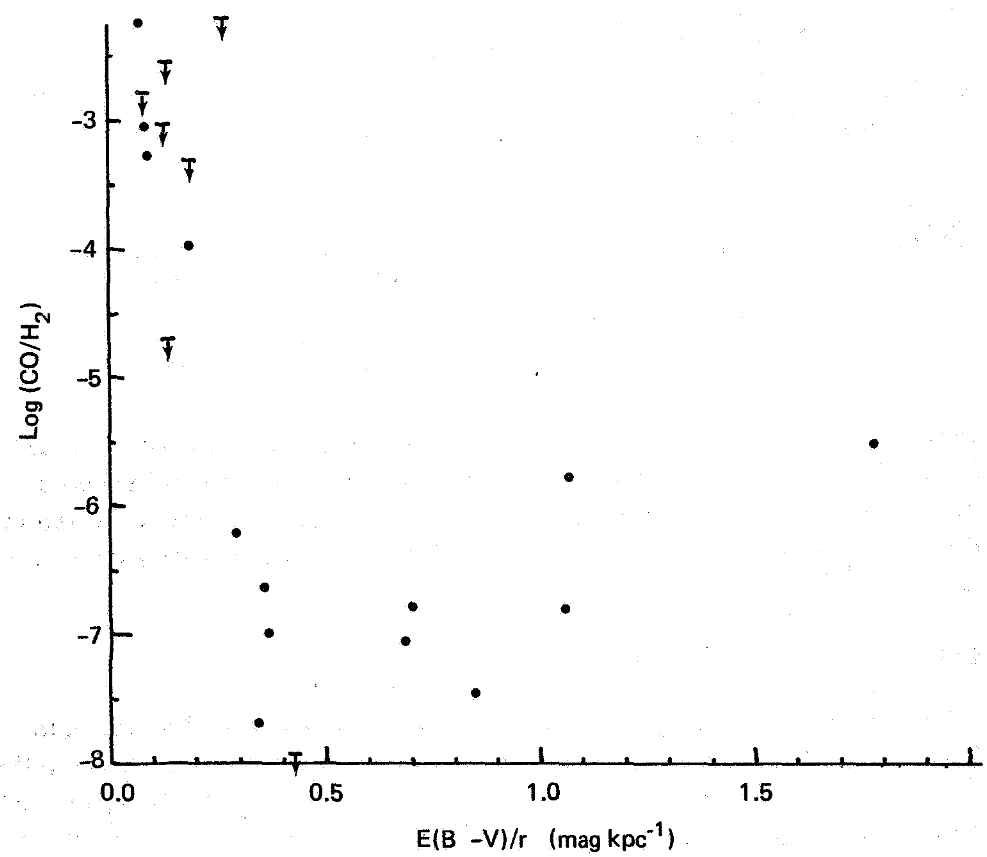

Figure 4. CO/H_2 density ratios versus E(B-V)/r for 21 stars that were analyzed by Jenkins and Shaya (1976).

When relating the observed values of CO/H shown in figure 5 to the radio observations, it is important to emphasize that the Copernicus results refer to interstellar material of much lower density than the classical "molecular clouds" identified by most radio observers. As suggested by the trend of points as E(B-V)/r increases, the relative amount of CO increases as larger densities are reached. However, it is interesting to note that the ratios shown here are substantially lower than the estimate of log (CO/H) = -4.2 sometimes adopted for the dense clouds (e.g., see Gordon and Burton, 1976, and references cited therein), the latter being equivalent to roughly 10 percent of the available cosmic abundance of carbon being bound in the form of CO.

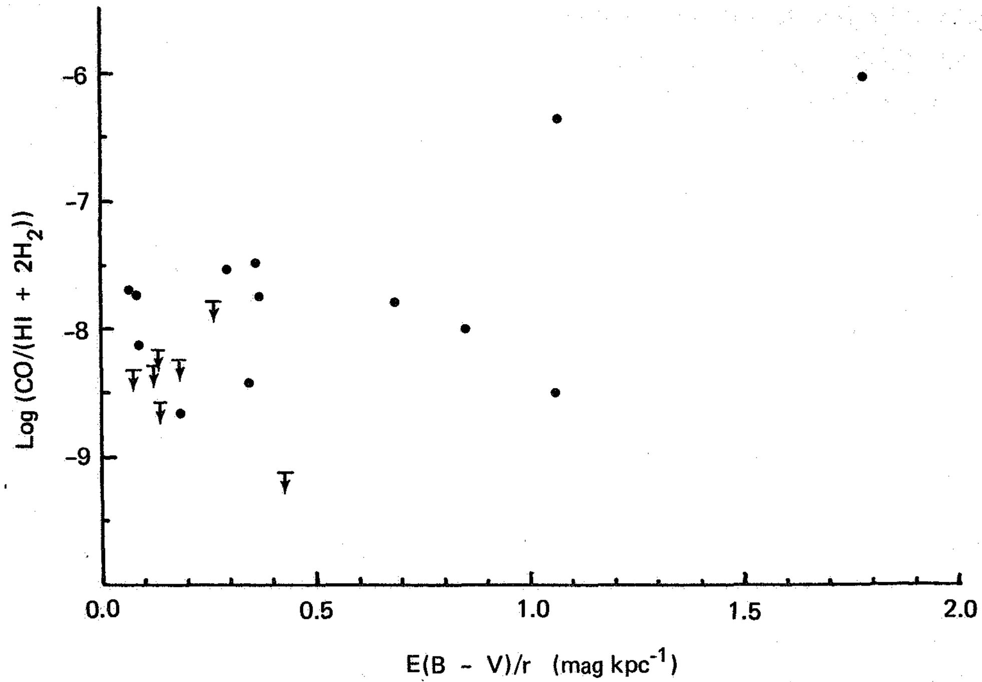

Figure 5. CO/HI + 2H_2 density ratios versus E(B-V)/r.

CONCLUSIONS

From the preceding discussion, we have seen that information gathered from ultraviolet telescopes covers several topics that are helpful in synthesizing our concepts of galactic structure. We have learned about some general properties of interstellar material (i.e., ratios of dust extinction and CO to HI and H_2), and we have evaluated the density of gas in our local part of the galaxy. Each of these studies help to place quantitative constraints on the interpretations of those observations that provide a more global outlook on the distribution of material in the galaxy.

From a survey of galactic 21-cm and CO line emission, Gordon and Burton (1976) mapped the distributions of n(HI) and n(H_2) as a function of distance from the center of the galaxy. For a galactocentric distance, R = 10 kpc, they estimate both n(HI) and n(H_2) to be about 0.4 cm^{-3}. On the other hand, the ultraviolet data suggest that n(HI) $\approx$ 0.9 cm^{-3} and n(H_2) $\approx$ 0.1 cm^{-3} within approximately 1 kpc of the Sun. Some of the discrepancy can be attributed to systematic errors or unrealistic assumptions inherent in the interpretations of these two quite different modes of measurements. However, even without these inaccuracies, the differences would be understandable: How could we possibly expect the local density of gas to closely match the density found for a ring covering a wide azimuth at the same distance from the galactic center? In fact, we should expect reasonably strong density contrasts across arms of the galaxy. Hence, although there is some disagreement, it does not seem too unreasonable in view of the uncertainties in both evaluations and the variability we expect to have in the actual distribution of material.

When Gordon and Burton (1976) defined an absolute scale for $N(H_2)$ to accompany their molecular density distribution function, they assumed a ratio, $\log (CO/H_2) = -4.2$, a value considerably above the ratio we observe for clouds having up to one magnitude of visual extinction. It should be immediately apparent, however, that, if they had assumed $\log (CO/H_2) \sim -6$ or -7, as suggested in figure 4, they would have derived inordinantly high molecular densities toward the inner region of the galaxy. We should recall from the preceding discussion that their measurement of $n(H_2)$, 0.4 cm^{-3}, already seems a bit high for R = 10 kpc. One can therefore surmise that, unless there is some large and systematic error resulting from their assumptions used to convert antenna temperatures to CO densities, practically all (i.e., at least 99 percent) of the CO emission must come from clouds which are characteristically much more dense than we can observe in the ultraviolet. The marked irregularity in the distribution of CO emission in itself suggests that dense clouds are primary sources of the radiation; we can presume that the more diffuse emission that fills in the spaces between the obvious clouds originates from smaller clouds which, while still very dense, are unresolved by the radiotelescope.

Finally, we have distilled from the Copernicus data a relation, which seems to be fairly universal under a variety of conditions, for the amount of gas associated with given amount of extinction by dust. The value quoted here, $[N(HI) + 2N(H_2)]/E(B-V) = 5.4 \times 10^{21}$ cm^{-2} mag^{-1}, is somewhat lower than an earlier determination from OAO-2 data by Jenkins and Savage (1974) of 7.5×10^{21} cm^{-2} mag^{-1}. As shown by Savage and Panek (1974) and Bohlin (1975), some of the stars observed by OAO-2 had more than the expected contamination by stellar lines, and, also, Jenkins and Savage (1974) applied what appears to be too large a correction for ionization by the target stars.

We must bear in mind, of course, that the observed gas-to-dust ratio may vary from place to place in the galaxy if there are abundance gradients (i.e., an enhancement of the relative CNO abundances toward the galactic center; see the discussion by Stecker et al. (1975)). In addition, the character and, hence, extinction properties of the dust grains may change as the interior densities of clouds increase.

ACKNOWLEDGEMENTS

The author is grateful to R. C. Bohlin, J. F. Drake, and B. D. Savage for communicating preliminary results from their survey of HI and H_2 from data taken by the Copernicus satellite. Their results constituted the largest fraction of the data base from which the conclusions in this paper were derived. This research was supported by the National Aeronautics and Space Administration under contract NAS5-1810.

REFERENCES

Bohlin, R. C., 1975, *Ap. J.*, **200**, p. 402.

Carruthers, G. R., 1970, *Ap. J. Letters*, **161**, p. L81.

Field, G. B., W. B. Somerville, and K. Dressler, 1966, *Ann. Rev. Astr. and Ap.*, **4**, p. 207.

Fitzgerald, M. P., 1968, *A. J.*, **73**, p. 983.

Glassgold, A. E., and W. D. Langer, 1975, *Ap. J.*, **197**, p. 347.

Gordon, M. A., and W. B. Burton, 1976, *Ap. J.*, in press.

Grayzeck, E. J., and F. J. Kerr, 1974, *A. J.*, **79**, p. 368.

Heiles, C., 1976, *Ap. J.*, **204**, p. 379.

Heiles, C., and E. B. Jenkins, 1976, *Astr. and Ap.*, **46**, p. 333.

Hollenbach, D. J., M. W. Werner, and E. E. Salpeter, 1971, *Ap. J.*, **163**, p. 165.

Jenkins, E. B., 1970, *Ultraviolet Stellar Spectra and Related Ground-Based Observations*, ed. L. Houziaux and H. E. Butler (IAU Symp., No. 36), Reidel Publishing Co., Dordrecht, Holland, p. 281.

Jenkins, E. B., and B. D. Savage, 1974, *Ap. J.*, **187**, p. 243.

Jenkins, E. B., and E. Shaya, 1976, in preparation.

Panagia, N., 1973, *A. J.*, **78**, p. 929.

Savage, B. D., and E. B. Jenkins, 1972, *Ap. J.*, **172**, p. 491.

Savage, B. D., and R. J. Panek, 1974, *Ap. J.*, **191**, p. 659.

Smith, A. M., 1973, *Ap. J. Letters*, **179**, p. L11.

Snow, T. P., 1976, *Earth and Extraterrestrial Sciences,* in press.

Spitzer, L., 1969, *Diffuse Matter in Space,* Wiley Interscience, New York.

Spitzer, L., W. D. Cochran, and A. Hirshfeld, 1975, *Ap. J. Suppl.*, **28** (266), p. 373.

Spitzer, L., J. F. Drake, E. B. Jenkins, D. C. Morton, J. B. Rogerson, and D. G. York, 1973, *Ap. J. Letters*, **181**, p. L116.

Spitzer, L., and E. B. Jenkins, 1975, *Ann. Rev. Astr. and Ap.*, **13**, p. 133.

Stecker, F. W., P. M. Solomon, N. Z. Scoville, and C. E. Ryter, 1975, *Ap. J.*, **201**, p. 90.

York, D. G., J. F. Drake, E. B. Jenkins, D. C. Morton, J. B. Rogerson, and L. Spitzer, 1973, *Ap. J. Letters*, **182**, p. L1.

SMALL-SCALE LOCAL GAMMA-RAY FEATURES

J. L. Puget
Département d'Astrophysique Fondamentale
Observatoire de Meudon, 92190 Meudon, France

C. Ryter
Centre d'Etude Nucléaire de Saclay
B.P. No. 2, 91190 Gif-sur-Yvette, France

G. Serra
Centre d'Etude Spatiale des Rayonnements
31100 Toulouse, France

ABSTRACT

In order to draw implications from nearby γ-ray emission, the different ways that can be used to obtain an estimate of the amount of matter on each line of sight are investigated. Then, it is shown that, within present uncertainties, the cosmic-ray intensity inside molecular clouds within 1 kpc from the Sun is the same as the cosmic-ray intensity measured at the Sun. In the last part, what can be learned from a comparison of far infrared and γ-ray data is discussed.

IMPORTANCE OF LOCAL FEATURES

Because the galactic plane is transparent to γ-rays produced in the interaction of cosmic rays with interstellar matter, they are a good probe for the large-scale structure of our galaxy. It has been shown that longitude profiles of γ-ray intensity along the galactic plane can be unfolded, assuming cylindrical symmetry, to obtain the γ-ray production rate as a function of galactocentric distance (Puget and Stecker, 1974). Nevertheless, due to poor resolution of γ-ray detectors, such profiles are averaged over several degrees in latitude, and this gives relatively more importance to local features than distant ones for similar contributions to the column density. In consequence, it is important to substract the local contribution, which is very patchy due to the structure of the interstellar medium in which most of the mass is gathered in dense clouds, in order to unfold meaningfully the longitude profile.

Solomon and Stecker (1974) pointed out the importance of molecular clouds and their large-scale distribution in the galaxy for the understanding of γ-ray production. This has since been confirmed by papers using different approaches (Stecker et al., 1975; and Paul et al., 1976). The molecular clouds which contain most of the mass of the interstellar medium in the inner galaxy have been shown to be $10^{4\text{-}5}$ $M_\odot$ clouds with radii of a few parsecs and typical column densities of 10^{22} cm^{-2}, except for a dense core for which the column density can be up to 10^{23} cm^{-2} but which contains only a small fraction of the total mass. The question of the density of cosmic rays in such clouds compared to the density of cosmic rays in the surrounding interstellar medium is important for the interpretation of the large-scale variations of the matter density versus cosmic-ray density and the implication on the hydrostatic equilibrium of the gas disk (Wentzel et al., 1975; and Mouschovias, 1975).

MATTER COLUMN DENSITY—THE GAS-TO-DUST RATIO

In recent years, it has become apparent that a substantial fraction of the interstellar hydrogen is in molecular form, and that, consequently, 21-cm observations are not necessarily faithful tracers of the total amount of interstellar gas. Here, we propose that interstellar reddening and absorption permits quantitative estimates of column densities to be made, at least within 1 kpc of the Sun. This requires a prior knowledge of the gas-to-dust ratio.

Numerous studies of the gas-to-dust ratio can be found in published literature, but the question does not appear to be understood in any detail (see, for instance, Heiles, 1974). Puget et al. (1976) discussed the different estimates of this ratio made recently and showed that, if all forms of hydrogen (atomic, molecular, and ionized) are included, it appears that the gas-to-dust ratio is constant in a wide range of densities, from a very tenous, partly ionized medium to obscured regions with $E_{B\text{-}V} \approx 2$ magnitudes, or $A_v \approx 6.5$ magnitudes. Up to this value at least, one is able to assess the total matter column density by using interstellar reddening data and the gas-to-dust ratio; we adopt here the relation

$$N_H = 7 \times 10^{21} E_{B\text{-}V} \text{ H atoms cm}^{-2} \tag{1}$$

However, some care should be exercised when using equation 1 along with large-scale reddening surveys. As is well-known, obscured regions frequently accommodate dense gas and dust clouds, with extinction in excess of 10 magnitudes which practically escape detection in low angular resolution maps, as obtained by star counts. In other words, the very strong extinction in the clouds, which reaches 50 magnitudes or more, does not contribute to the extinction when averaged in picture elements of a few tens of square degrees. In such cases, equation 1 provides only a lower limit to the true average column density. One should then rely on radio and far-infrared observations (radiations for which the cores can be optically thin) to estimate the core contribution to the total mass. This contribution is negligible (within a 10-percent uncertainty limit) for a few molecular clouds for which a detailed comparison of molecular column densities and reddening have been made.

Star counts can be used to get the visual absorption on part of the line of sight for regions with up to 6 magnitudes of extinction. This method was used by Encrenaz et al. (1975) to show that the ratio, N_{CO}/A_v is constant throughout the ρ-Ophiucus cloud.

When one wants the extinction integrated over the entire line of sight, the only way to get data covering completely large areas of the sky is to use galaxy counts. For directions around the galactic center, data can be obtained for only latitudes, b, such that $|b| > 5°$. In the anticenter direction, if averages are taken on wide enough longitude ranges, meaningful values can be obtained down to even b = 0.

Another question one must ask is how good is the gas-to-dust ratio when one looks at regions far away from the Sun. This can be investigated by comparing latitude distributions for HI (Daltabuit and Meyer, 1972), reddening (Fitzgerald, 1968), and visual absorption from galaxy counts (Shane and Wirtanen, 1967; and Kiang, 1969). Four such profiles are shown in figure 1 for different longitude ranges around the anticenter direction. For $|b| \gtrsim 5°$, the column densities deduced from reddening or absorption (in good agreement within uncertainties) are larger than the column densities deduced from 21-cm data. On the other hand, at b = 0, they are significantly smaller. Puget et al. (1976) have argued that, because gas-to-dust ratio is a well-defined quantity only when all forms of hydrogen are included, we should take into account molecular hydrogen (HII is negligible). Gordon and Burton (1976) give 48 percent of hydrogen in molecular form for the interstellar gas at 10 kpc from the center and 34 percent on the line of sight at b = 0 in the anticenter direction. So, once again, it is found that, near the Sun ($b \gtrsim 7°$) with $N_H \sim 2\, N_{HI}$ on the average, equation 1 gives the right column density. At b = 0, we find $< E_{B-V} > = 0.95$, $< N_{HI} > = 9.8\ 10^{21}$ cm^{-2}. Assuming $< N_H > = 1.34$, $< N_{HI} > \simeq 1.3\ 10^{22}$ cm^{-2}. This implies a gas-to-dust ratio twice as large on the average as the value adopted in equation 1 or a 20-percent decrease per kiloparsec of the relative amount of dust.

Such a gradient compares well with the metal abundance gradients deduced from observations of HII regions in external galaxies (Searle, 1971) and in our galaxy (Peimbert and Sivan, private communication).

GAMMA-RAY EMISSION

Most of the γ-ray emission above 100 MeV from the galactic plane is attributed to the decay of neutral pions formed in the interaction of cosmic rays with interstellar matter.

The γ-ray intensity, I_γ, associated with a line of sight is given by

$$I_\gamma = 1.3 \times 10^{-25}\, N_H/4\pi \text{ photon cm}^{-2}\text{ s}^{-1}\text{ sr}^{-1} \tag{2}$$

using the production rate per hydrogen atom for a cosmic-ray density equal to that observed in the solar vicinity (Stecker, 1973). With equation 1, this relation becomes

$$I_\gamma = 7.25\ 10^{-5}\, E_{B-V}\, (n_{CR}/n_{CR\odot}) \text{ photon cm}^{-2}\text{ s}^{-1}\text{ sr}^{-1} \tag{3}$$

where n_{CR} is the density of cosmic rays, and $n_{CR\odot}$ the value of this density in the solar neighborhood. Their ratio is not expected to be very different from 1 when averaged over lines of sight at $|b| > 5°$.

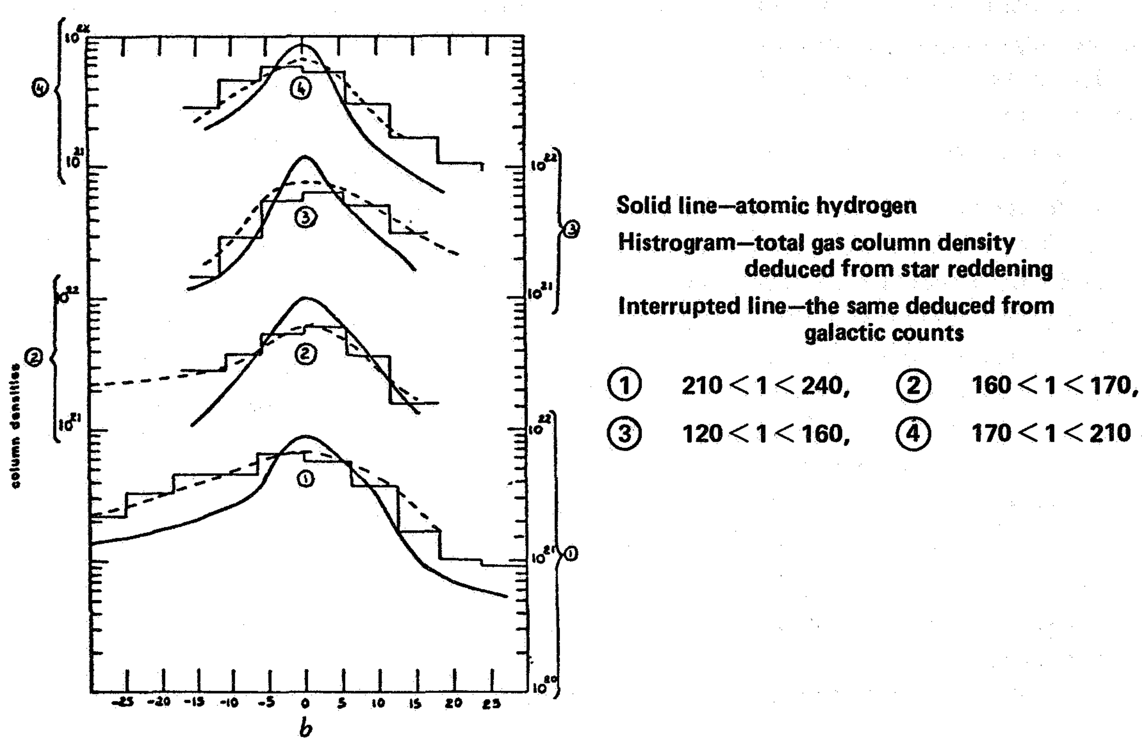

Figure 1. Evidence for gas-to-dust gradient in the outer region of the galactic disk.

The latitude distribution of the intensity I_γ averaged between $\ell^{II} = 350°$ and $\ell^{II} = 20°$ is given by the COS-B Caravane Collaboration (these proceedings). For $|b| > 5°$, visual absorption deduced from galaxy counts is expected to give the best estimates of the total column densities as shown above. For $b > 5°$, Shane and Wirtanen (1967) and Kiang (1969) have been used; for $b < 10°$, we used the fine galaxies per square degree contour from Harvard counts as quoted by Shane and Wirtanen (1967). The γ-ray fluxes are computed using equation 3 and

$$E_{B\text{-}V} = 0.4 \log (65/N) \tag{4}$$

where N is the number of galaxies per square degree. Considering the uncertainties in relation 4 and the statistical errors in the counts of galaxies, $E_{B\text{-}V}$ is obtained with uncertainties of the order of 20 percent, and we conclude from the fair agreement obtained in figure 2 that, within this precision range, cosmic-ray intensity in these regions is, on the average, equal to the solar-vicinity intensity. Mouschovias (1975) suggests that, for the production of γ-rays in molecular clouds, there will be a tradeoff between increased gas density and decreased cosmic-ray intensity. Because about one-half the gas on the line of sight is in molecular form, we can conclude that there is no strong depletion of cosmic rays in molecular clouds. This

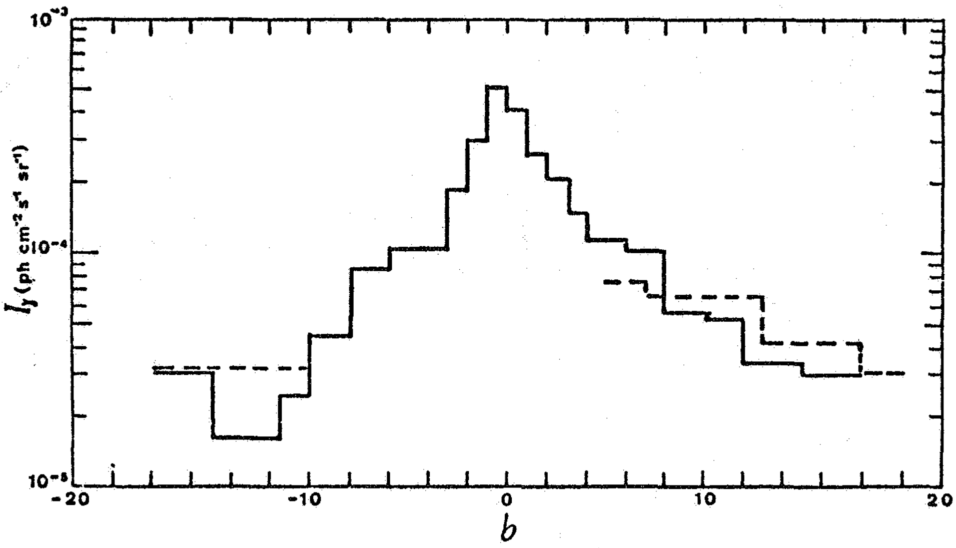

Figure 2. Latitude distribution of the γ-ray emission in the galactic center region as measured by the COS-B satellite (solid line) and γ-ray emission predicted from the total column density deduced from galaxy counts (interrupted line).

question can be investigated in more detail by comparing γ-ray isophotes and galaxy-count contours. The only published map of γ-ray isophotes is the one given by Kniffen et al. (1975) for the anticenter direction. In figure 3, we compare the outermost isophote of this map with contours at 1 and 10 galaxies per square degree corresponding to $E_{B-V} = 0.7$ and 0.3 magnitudes, respectively.

We estimate the γ-ray intensity associated with this isophote by normalization of the total flux of the Crab pulsar above 35 MeV which shows very clearly on this map. We assumed the flux to be 60 percent pulsed from variation of the pulsed fraction with energy, and the pulsed flux is 6.2 10^{-6} photons cm^{-2} s^{-1} (Kniffen et al., 1975). This leads to an intensity of 3.2 10^{-5} γ cm^{-2} s^{-1} sr^{-1}, which would be associated with lines of sight with $E_{B-V} = 0.44$. From the relative positions of the γ isophote, the $E_{B-V} = 0.3$ and $E_{B-V} = 0.7$ contours, one can say that there is no evidence for depletion of cosmic rays in molecular clouds as far as the envelopes are concerned. (Nothing can be said about cores.)

In figure 4, the same galaxy-count contours are shown for the whole galactic plane and should compare well with γ-ray isophotes at 5 10^{-5} and 2 10^{-5} γ s^{-1} sr^{-1} cm^{-2}.

GALACTIC FAR-INFRARED EMISSION

Another probe for large-scale structure in the galaxy is far-infrared radiation emitted by dust. Here, again, the study of individual clouds and comparison of infrared emission and γ-rays

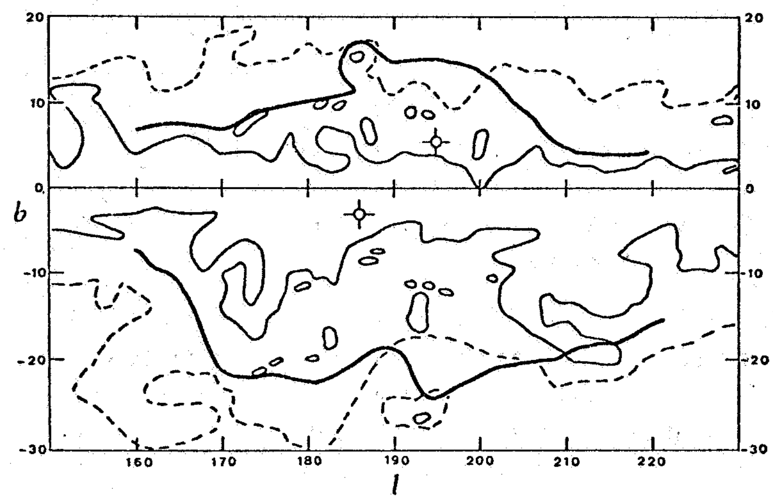

Figure 3. Gamma-ray emission and interstellar matter in the galactic anti-center region: heavy line—outer contour of the γ-ray map obtained from SAS-2 satellite; light solid line—contour of the $E_{B-V} \gtrsim 0.7$ magnitude region; interrupted line—contour of the $E_{B-V} \approx 0.3$ magnitude region; crosses—the two γ-ray sources Tau γ - 1 and 195 + 5.

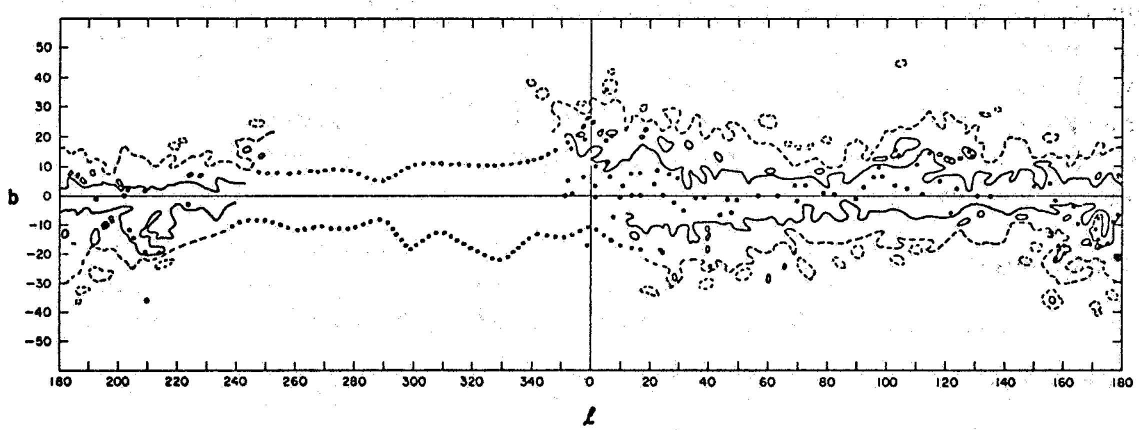

Figure 4. Contours of the interstellar extinction deduced from galaxy counts (Kiang, 1969): solid line—$E_{B-V} \gtrsim 0.7$ magnitude (i.e., zero to one galaxy per square degree); interrupted line—$E_{B-V} \approx 0.3$ magnitude (i.e.,10 galaxies per square degree); dotted line—$E_{B-V} \approx 0.45$ magnitude (i.e., five galaxies per square degree) (Harvard counts as quoted by Shane and Wirtanen (1967); filled circles—molecular clouds observed.

can help to disentangle matter distribution and cosmic-ray distribution. Assuming that the gas-to-dust ratio is known, the infrared intensity might be a tracer of interstellar matter. For any realistic dust model and for $\lambda > 70$ μm, the galaxy is optically thin. The integrated far-infrared intensity relies also on the energy density of the exciting field. Ryter and Puget (1976) have shown that the power radiated by the dust mixed to the gas in clouds is about a factor of 20 larger than the power that can be accounted for by the usual starlight density $u \simeq 0.5$ eV cm^{-3}. This implies that strong power sources are imbedded in the clouds and are obviously attributed to newborn stars.

The amount of dust and the source of the power (related to the star formation rate) can be separated if sufficient spectral information is obtained. The total power radiated by the dust can be evaluated and expressed as a radiated power normalized per hydrogen atom L_{IR}^{H}. On the other hand, the temperature can be deduced from multicolor photometry. Based on a realistic dust model (a mixture of ice and silicates), Ryter and Puget (1976) find the approximate relation

$$L_{IR}^{H}(T) = 5 \times 10^{-39}\, T^{5.8}\, \mathrm{W(H\ atom)^{-1}} \tag{5}$$

where T is the dust temperature. The general result is that, for a sample of clouds located between the Sun and the 5-kpc ring, the temperatures needed to explain the total power radiated (through equation 5) are in good agreement with the color temperatures. We can then use those results in the following way: The temperature can be obtained precisely from equation 5 if the total power is measured and can be used to infer the column density of dust from the infrared intensity at wavelengths such that the Rayleigh-Jeans approximation is valid. The different physical parameters n_{HI}, n_{H_2}, n_{dust}, n_{CR}, dust, and gas temperatures are all physically related, and the understanding of the physics implies the confrontation of γ-ray, far-infrared, and radio data for which dense molecular clouds and the entire galactic plane are optically thin.

REFERENCES

Daltabuit, E., and S. Meyer, 1972, *Astron. and Astrophys.*, **20**, p. 415.

Encrenaz, P. J., E. Falgarone, and R. Lucas, 1975, *Astron. and Astrophys.*

Fitzgerald, M. P., 1968, *Astron. J.*, **73**, p. 983.

Gordon, M. A. and W. B. Burton, 1976, preprint.

Heiles, C., 1974, In *Galactic Radio Astronomy*, (IAU Symp. No. 60), ed. F. J. Kerr and S. C. Simonson, III, Reidel Publishing Co., Dordrecht, Holland, p. 625.

Kiang, T., 1969, Dunsink Observatory Publications, 1, No. 5.

Kniffen, D. A., G. F. Bignami, C. E. Fichtel, R. C. Hartman, H. Ögelman, D. J. Thompson, M. E. Özel, and T. Tümer, 1975, (14th Intl. Conf. on Cosmic Rays, Munich).

Mouschovias, T. C., 1975, *Ap. J. Letters,* **202**, p. L1.

Paul, J., M. Cassé, and C. J. Cesarsky, 1975, (14th Intl. Conf. on Cosmic Rays, Munich).

Puget, J. L., and F. W. Stecker, 1974, *Ap. J.,* **191**, p. 323.

Puget, J. L., C. Ryter, G. Serra, and G. Bignami, 1976, *Astron. and Astrophys.,* in press.

Ryter, C. and J. L. Puget, 1976, preprint.

Searle, L., 1971, *Ap. J.,* **168**, p. 327.

Shane, C. D., and C. A. Wirtanen, 1967, *Pub. of the Lick Obs.,* **22**, p. 1.

Solomon, P. M. and F. W. Stecker, 1974, (ESRO Symp. Context and Status of Gamma-Ray Astronomy), Reidel Publishing Co., Dordrecht, Holland, in press.

Stecker, F. W., 1973, *Ap. J.,* **185**, p. 499.

Stecker, F. W., P. M. Solomon, N. Z. Scoville, and C. E. Ryter, 1975, *Ap. J.,* **201**, p. 90.

Wentzel, D. G., P. D. Jackson, W. K. Rose, and R. P. Sinha, 1975, *Ap. J. Letters,* **201**, p. L5.

DIFFUSE GALACTIC GAMMA-RAY LINES

R. E. Lingenfelter
*Department of Astronomy and Department of Geophysics and Space Physics, University of California Los Angeles, California 90024**

R. Ramaty
NASA/Goddard Space Flight Center Laboratory for High Energy Astrophysics Greenbelt, Maryland 20771

ABSTRACT

We have studied the origin and observability of diffuse γ-ray line emission from our galaxy. We find that such lines could be formed by nuclear excitation interactions of low-energy cosmic rays with both interstellar gas and dust grains. The γ-ray emission lines from deexcitation of grain nuclei are sharp with Doppler widths of the order of 10 keV or less; the lines from gas nuclei are also relatively sharp with widths of the order of ~ 100 keV for the most intense line $^{12}C^{*4.439}$, and of the order of a few keV for the $^{56}Fe^{*0.847}$ line; and the lines from cosmic-ray nuclei are broad with widths of the order of several hundred keV.

We present here a detailed evaluation of the production rate of the 4.44-MeV line for a variety of assumed cosmic-ray spectra. We compare these results with reported galactic γ-ray line intensities and conclude that the measurements are consistent with a low-energy cosmic-ray density which increases toward the galactic center in proportion to the molecular gas density.

An exciting possibility for the future would be the detection of nuclear γ-ray lines from interstellar dust-grain nuclei, using a solid-state detector with energy resolution of a few keV or better.

*This research was supported in part by National Science Foundation grant AST67-08178.

INTRODUCTION

We have calculated the γ-ray line emission expected to result from cosmic-ray nuclear interactions with interstellar gas and dust in the galaxy. This emission consists of a sharp line component from deexcitation of interstellar grain nuclei, a relatively narrow line component from deexcitation of gas nuclei, and a broad line component from deexcitation of cosmic-ray nuclei. These three components can in principle be separated in measured spectra permitting study of both the interstellar medium and the cosmic rays.

In the study of galactic structure, the sharp-line component of nuclear γ-ray emission offers the first opportunity to determine the composition and spacial distribution of interstellar grains. The narrow line component also appears to offer a better opportunity than either atomic or molecular line emission for determining the spacial distribution and composition of interstellar gas because of the high transparency of even very dense interstellar clouds to γ-radiation, and the lack of dependence of the γ-ray emissivity on the chemical state of the matter.

In addition, the broader γ-ray line component provides the best opportunity available so far for studying the low-energy cosmic rays which are important not only in conjunction with understanding the origin and propagation of cosmic rays, but also in the study of galactic structure where the role of low-energy cosmic rays in heating of the interstellar gas and in nucleosynthesis of the light elements is not yet understood.

At present, galactic γ-ray line astronomy is only in a rudimentary stage, but it has already produced surprising results. Emission in several γ-ray lines from the direction of the galactic center have been reported for balloon experiments by Haymes et al. (1975) and possibly confirmed at least for the 4.4-MeV line in a preliminary analysis of Apollo experiments by Trombka (private communication, 1976). The intensities of these lines are roughly two orders of magnitude higher than would be predicted assuming uniform density and composition of the interstellar gas and cosmic rays throughout the galaxy. If these observations are correct, these intensities suggest strong spacial variations in both the density and composition of interstellar gas and cosmic rays.

Very little systematic study has been made of γ-ray line production by low-energy cosmic rays in the galaxy, although there have been extensive theoretical studies (e.g., Ramaty et al., 1975) of γ-ray line production by solar flare particles at the Sun.

Fowler et al. (1970) first estimated the combined line emission of γ-rays of energy greater than 1 MeV as a possible limitation on the production of LiBeB in the interstellar medium by low-energy cosmic rays. Meneguzzi and Reeves (1975), pursuing this problem further, have calculated some individual line emissivities, but only for a very limited class of low-energy cosmic-ray spectra.

Ramaty and Boldt (1971) also estimated the γ-ray line emission at 4.4 and ~ 6.2 MeV as a possible limit on their model of heating the Gum Nebula by low-energy cosmic rays from the Vela supernova.

The first measurements of broad line emission at slightly less than 0.5 MeV from the direction of the galactic center by Johnson et al. (1972) and Johnson and Haymes (1973) led Fishman and Clayton (1972) to suggest the possibility of γ-ray emission at 0.478 and 0.431 MeV resulting from excitation and spallation of low-energy cosmic-ray ^{7}Li nuclei. Kozlovsky and Ramaty (1974) also considered the contribution to this emission from production of excited ^{7}Li and ^{7}Be in low-energy alpha-particle interactions with helium.

The most general study of the problem of γ-ray line emission resulting from low-energy cosmic-ray interactions with the interstellar gas was made by Rygg and Fishman (1973). They considered a larger number of nuclear-excitation processes and a wider range of possible low-energy cosmic-ray spectra than were previously considered. They predicted significant emission in the 1- to 2-MeV range, which appears to have been observed by Haymes et al. (1975). But they calculated only direct excitation of low-energy cosmic-ray nuclei by interstellar hydrogen, ignoring the broadening of excited cosmic-ray emission lines and the production of excited nuclei by spallation reactions. They also apparently only estimated the contribution from the excitation of cosmic-ray nuclei by interstellar helium and the excitation of the interstellar-gas nuclei by cosmic-ray protons and alpha particles. The production by these processes is very sensitive to the assumed energy spectrum and should be calculated explicitly.

In the present study, all of these processes are considered, as well as additional direct-excitation processes. We also explore a much wider range of possible low-energy cosmic-ray spectra and possible galactic spatial variations in both cosmic-ray and interstellar-gas compositions in the hope of better assessing the usefulness of γ-ray line observations for studies of galactic structure and composition, the role of cosmic-ray heating and light element nucleosynthesis in the interstellar medium, and the nature, origin, and propagation of the low-energy cosmic rays.

The full results of these calculations will be given in a forthcoming paper. Here, we will present only a sampling of these calculations relating to the strongest single line (that is, the line at 4.44 MeV resulting from deexcitation of the first excited nuclear level in ^{12}C). This is also currently the best measured line, and we will discuss the implications of these measurements in the light of our calculations.

GAMMA-RAY LINE EMISSION

There is an enormous variety of nuclear interactions between cosmic rays and the interstellar gas and dust which lead to γ-ray line emission. The relative intensities of different lines depend on the excitation cross sections, the cosmic-ray energy spectrum and composition, and the interstellar gas and dust composition. The various γ-ray deexcitation lines that we consider, together with their nuclear excitation interactions, are listed in table 1.

Table 1
Gamma-Ray Lines

GAMMA RAY ENERGY (Mev)	DEEXCITATION PROCESS	EXCITATION REACTION
0.431	$^{7}Be^{*0.431} \rightarrow g.s.$	$^{4}He(^{3}He,\gamma)^{7}Bo^{*0.431}$ $^{4}He(\alpha,n)^{7}Bo^{*0.431}$ $^{6}Li(p,\alpha)^{7}Be^{*0.431}$ $^{7}Li(p,n)^{7}Be^{*0.431}$ $^{10}B(p,\alpha)^{7}Be^{*0.431}$
0.477	$^{55}Fe^{*1.408} \rightarrow ^{55}Fe^{*0.931}$	$^{56}Fe(p,2n)^{55}Co(e^{+})^{55}Fe^{*1.408}(12\%)$ $^{56}Fe(p,pn)^{55}Fe^{*1.408}$
0.478	$^{7}Li^{*0.478} \rightarrow g.s.$	$^{3}He(\alpha,\gamma)^{7}Be(\epsilon)^{7}Li^{*0.478}(12\%)+$ $^{4}He(\alpha,p)^{7}Li^{*0.478}$ $^{4}He(\alpha,n)^{7}Be(\epsilon)^{7}Li^{*0.478}(12\%)+$ $^{7}Li(p,p')^{7}Li^{*0.478}$ $^{7}Li(p,n)^{7}Be(\epsilon)^{7}Li^{*0.478}(12\%)+$ $^{7}Li(\alpha,\alpha')^{7}Li^{*0.478}$ $^{14}N(p,x)^{7}Be(\epsilon)^{7}Li^{*0.478}(12\%)+$ $^{12}C(p,x)^{7}Be(\epsilon)^{7}Li^{*0.478}(12\%)+$ $^{12}C(p,x)^{7}Li^{*0.478}$
0.511	$e^{+}+e^{-} \rightarrow 2\gamma$ (annihilation)	$^{10}B(p,n)^{10}C(e^{+})$ $^{12}C(p,pn)^{11}C(e^{+})$ $^{12}C(p,x)^{10}C(e^{+})$ $^{12}C(\alpha,\alpha n)^{11}C(e^{+})$ $^{14}N(p,x)^{11}C(e^{+})$ $^{16}O(p,pn)^{15}O(e^{+})$ $^{16}O(p,x)^{13}N(e^{+})$ $^{16}O(p,x)^{11}C(e^{+})$ $^{16}O(\alpha,\alpha n)^{15}O(e^{+})$ $^{19}F(p,\alpha)^{16}O^{*6.05}(e^{+}e^{-})$ $^{24}Mg(p,x)^{22}Na(e^{+})$ $^{28}Si(p,x)^{22}Na(e^{+})$ $^{56}Fe(p,n)^{56}Co(e^{+})$ $^{56}(Fe(p,2n)^{55}Co(e^{+})$ $^{56}Fe(p,x)^{52}Mn(e^{+})$
0.717	$^{10}B^{*0.717} \rightarrow g.s$	$^{10}B(p,p')^{10}B^{*0.717}$ $^{10}B(p,n)^{10}C(e^{+})^{10}B^{*0.717}$ $^{10}B(\alpha,\alpha')^{10}B^{*0.717}$ $^{11}B(p,pn)^{10}B^{*0.717}$ $^{12}C(p,x)^{10}B^{*0.717}$ $^{12}C(p,x)^{10}C(e^{+})^{10}B^{*0.717}$ $^{16}O(p,x)^{10}B^{*0.717}$
0.744	$^{52}Cr^{*3.119} \rightarrow ^{52}Cr^{*2.370}$	$^{56}Fe(p,x)^{52}Mn(e^{+})\ ^{2}Cr^{*3.114}(85\%)$
0.811	$^{58}Fe^{*0.811} \rightarrow g.s$	$^{56}Fe(\alpha,pn)^{58}Co(e^{+})^{58}Fe^{*0.811}$
0.835	$^{54}Cr^{*0.835} \rightarrow g.s$	$^{56}Fe(p,x)^{54}Mn(\epsilon)^{54}Cr^{*0.835}+$
0.847	$^{56}Fe^{*0.847} \rightarrow g.s$	$^{56}Fe(p,p')^{56}Fe^{*0.847}$ $^{56}Fe(p,n)^{56}Co(e^{+})^{56}Fe^{*0.847}$ $^{56}Fe(\alpha,\alpha')^{56}Fe^{*0.847}$ $^{56}Fe(\alpha,p3n)^{56}Co(e^{+})^{56}Fe^{*0.847}$
0.889	$^{46}Ti^{*0.889} \rightarrow g.s$	$^{56}Fe(p,x)^{46}Sc(e)^{46}Ti^{*0.889}$
0.931	$^{55}Fe^{*0.931} \rightarrow g.s.$	$^{56}Fe(p,pn)^{55}Fe^{*0.931}$ $^{56}Fe(p2n)^{55}Co(e^{+})^{55}Fe^{*0.931}(76\%)$
0.936	$^{52}Cr^{*2.370} \rightarrow ^{52}Cr^{*1.434}$	$^{56}Fe(p,x)^{52}Mn(e^{+})^{52}Cr^{*2.370}$
0.937	$^{18}F^{*0.937} \rightarrow g.s.$	$^{18}O(p,n)^{18}F^{*0.937}$
0.983	$^{48}Ti^{*0.983} \rightarrow g.s$	$^{56}Fe(px)^{48}V(e^{+})^{48}Ti^{*0.983}$
1.023	$^{10}B^{*1.740} \rightarrow ^{10}B^{*0.717}$	$^{10}B(pp')^{10}B^{*1.740}$
1.042	$^{18}F^{*1.042} \rightarrow g.s.$	$^{18}O(p,n)^{18}F^{*1.042}$
1.121	$^{46}Ti^{*2.010} \rightarrow ^{46}Ti^{*0.889}$	$^{56}Fe(p,x)^{46}Sc(e^{-})^{46}Ti^{*2.010}$
1.238	$^{56}Fe^{*2.085} \rightarrow ^{56}Fe^{*0.847}$	$^{56}Fe(p,p')^{56}Fe^{*2.085}$ $^{56}Fe)p,n)^{56}Co(e^{+})^{56}Fe^{*2.085}$ $^{56}Fe(\alpha,\alpha')^{56}Fe^{*2.085}$
1.266	$^{31}P^{*1.266}$	$^{31}P(p,p')^{31}P^{*1.266}$ $^{32}S(p,2p)^{31}P^{*1.266}$ $^{32}S(p,pn)^{31}S(e^{-})^{31}P^{*1.266}$
1.273	$^{29}Si^{*1.273} \rightarrow g.s.$	$^{32}S(p,\alpha)^{29}P(e^{+})^{29}Si^{*1.273}$
1.275	$^{22}Ne^{*1.275} \rightarrow g.s.$	$^{22}Ne(p,p,)^{22}Ne^{*1.275}$ $^{23}Na(p,pn)^{22}Na(e^{+})^{22}Ne^{*1:275}$ $^{24}Mg(p,x)^{22}Na(e^{+})^{22}Ne^{*1.275}$ $^{28}Si(p,x)^{22}Na(e^{+})^{22}Ne^{*1.275}$
1.312	$^{48}Ti^{*2.295} \rightarrow ^{48}Ti^{*0.983}$	$^{56}Fe(p,x)^{48}V(e^{+})^{48}Ti^{*2.295}$
1.369	$^{24}Mg^{*1.369} \rightarrow g.s.$	$^{24}Mg(p,p')^{24}Mg^{*1.369}$ $^{24}Mg(p,x)^{24}Na(e^{-})^{24}Mg^{*1.369}$ $^{24}Mg(\alpha,\alpha')^{24}Mg^{*1.369}$ $^{27}Al(p,x)^{24}Mg^{*1.369}$ $^{27}Al(p,x)^{24}Na(e^{-})^{24}Mg^{*1.369}$ $^{27}Al(\alpha,x)^{24}Na(e^{-})^{24}Mg^{*1.369}$ $^{28}Si(p,x)^{24}Mg^{*1.369}$ $^{28}Si(p,x)^{24}Na(e^{-})^{24}Mg^{*1.369}$
1.395	$^{21}Ne^{*1.746} \rightarrow ^{21}Ne^{*0.351}$	$^{23}Na(p,2pn)^{21}Ne^{*1.746}$
1.408	$^{54}Fe^{*1.408} \rightarrow g.s.$	$^{54}Fe(p,p')^{54}Fe^{*1.408}$ $^{54}Fe(\alpha,\alpha')^{54}Fe^{*1.408}$
1.408	$^{55}Fe^{*1.408} \rightarrow g.s.$	$^{56}Fe(p,pn)^{56}Fe^{*1.408}$ $^{56}Fe(p,2n)^{55}Co(e^{+})^{55}Fe^{*1.408}(17\%)$
1.434	$^{52}Cr^{*1.434} \rightarrow g.s.$	$^{56}Fe(p,x)^{52}Mn(e^{+})^{52}Cr^{*1.434}$
1.571	$^{18}O^{*3.55} \rightarrow ^{18}O^{*1.982}$	$^{18}O(p,p')^{18}O^{*3.55}$
1.632	$^{14}N^{*3.945} \rightarrow ^{14}N^{*2.313}$	$^{14}N(p,p')^{14}N^{*3.945}$ $^{16}O(p,x)^{14}N^{*3.945}$
1.634	$^{20}Ne^{*1.634} \rightarrow g.s.$	$^{20}Ne(p,p')^{20}Ne^{*1.634}$ $^{20}Ne(\alpha,\alpha')^{20}Ne^{*1.634}$ $^{24}Mg(p,x)^{20}Ne^{*1.634}$ $^{27}Al(p,x)^{20}Ne^{*1.634}$ $^{28}Si(p,x)^{20}Ne^{*1.634}$
1.636	$^{23}Na^{*2.076} \rightarrow ^{23}Na^{*0.440}$	$^{23}Na(p,p')^{23}Na^{*2.076}$ $^{24}Mg(p,2p)^{23}Na^{*2.076}$
1.772	$^{56}Fe^{*3.857} \rightarrow ^{56}Fe^{*2.085}$	$^{56}Fe(p,p')^{56}Fe^{*3.857}$ $^{56}Fe(p,n)^{56}Co(e^{+})^{56}Fe^{*3.857}$

Table 1 (Continued)

GAMMA RAY ENERGY (Mev)	DEEXCITATION PROCESS	EXCITATION REACTION
1.779	$^{28}Si^{*1.779}$	$^{28}Si(p,p')^{28}Si^{*1.779}$ $^{28}Si(\alpha,\alpha')^{28}Si^{*1.779}$ $^{32}S(p,p\alpha)^{28}Si^{*1.779}$
1.809	$^{26}Mg^{*1.809} \to g.s.$	$^{26}Mg(p,p')^{26}Mg^{*1.809}$ $^{26}Mg(p,n)^{26}Al(e^+)^{26}Mg^{*1.809}$ $^{27}Al(p,2p)^{26}Mg^{*1.809}$ $^{27}Al(p,pn)^{26}Al(e^+)^{26}Mg^{*1.80}$ $^{28}Si(p,x)^{26}Al(e^+)^{26}Mg^{*1.809}$
1.982	$^{18}O^{*1.982} \to g.s.$	$^{18}O(p,p')^{18}O^{*1.982}$ $^{18}O(\alpha,\alpha')^{18}O^{*1.982}$
1.995	$^{11}C^{*1.995} \to g.s.$	$^{11}B(p,n)^{11}C^{*1.995}$ $^{12}C(p,pn)^{11}C^{*1.995}$ $^{12}C(\alpha,\alpha n)^{11}C^{*1.995}$ $^{14}N(p,x)^{11}C^{*1.995}$ $^{16}O(p,x)^{11}C^{*1.995}$
2.124	$^{11}B^{*2.124} \to g.s.$	$^{11}B(p,p')^{11}B^{*2.124}$ $^{11}B(\alpha,\alpha')^{11}B^{*2.124}$ $^{12}C(p,2p)^{11}B^{*2.124}$ $^{12}C(\alpha,x)^{11}B^{*2.124}$
2.184	$^{17}O^{*3.055} \to {}^{17}O^{*0.871}$	$^{17}O(p,p')^{17}O^{*3.055}$
2.313	$^{14}N^{*2.313} \to g.s.$	$^{12}C(He^3,n)^{14}O \to {}^{14}N^{*2.313}$ $^{13}C(p,\gamma)^{14}N^{*2.313}$ $^{14}N(p,p')^{14}N^{*2.313}$ $^{14}N(p,n)^{14}O(e^+)^{14}N^{*2.313}$ $^{14}N(\alpha,\alpha')^{14}N^{*2.313}$ $^{16}O(p,x)^{14}N^{*2.313}$ $^{16}O(p,x)^{14}O(e^+)^{14}N^{*2.313}$
2.365	$^{13}N^{*2.365} \to g.s.$	$^{10}B(\alpha,n)^{13}N^{*2.365}$ $^{12}C(p,\gamma)^{13}N^{*2.365}$ $^{13}C(pn)^{13}N^{*2.365}$
2.741	$^{16}O^{*8.872} \to {}^{16}O^{*6.131}$	$^{16}O(p,p')^{16}O^{*8.872}$
3.086	$^{13}C^{*3.086} \to g.s.$	$^{13}C(p,p')^{13}C^{*3.086}$
3.365	$^{10}Be^{*3.366} \to g.s.$	$^{10}Be(p,p')^{10}Be^{*3.366}$ $^{11}B(p,2p)^{10}Be^{*3.366}$
3.561	$^{6}Li^{*3.562}$	$^{4}He(^{3}He,p)^{6}Li^{*3.562}$ $^{4}He(\alpha,pn)^{6}Li^{*3.562}$ $^{6}Li(p,p')^{6}Li^{*3.562}$ $^{6}Li(\alpha,\alpha')^{6}Li^{*3.562}$ $^{7}Li(p,pn)^{6}Li^{*3.562}$ $^{9}Be(p,\alpha)^{6}Li^{*3.562}$ $^{12}C(p,x)^{6}Li^{*3.562}$
3:684	$^{13}C^{*3.684}$	$^{12}C(\alpha,x)^{13}C^{*3.684}$ $^{13}C(p,p')^{13}C^{*3.684}$ $^{13}C(\alpha,\alpha')^{13}C^{*3.684}$ $^{16}O(p,x)^{13}C^{*3.684}$
3.853	$^{13}C^{*3.854}$	$^{12}C(\alpha,x)^{13}C^{*3.854}$ $^{13}C(p,p')^{13}C^{*3.854}$ $^{13}C(\alpha,\alpha')^{13}C^{*3.854}$ $^{16}O(p,x)^{13}C^{*3.854}$
4.438	$^{12}C^{*4.439} \to g.s.$	$^{9}Be(\alpha,n)^{12}C^{*4.439}$ $^{11}B(p,\gamma)^{12}C^{*4.439}$ $^{12}C(p,p')^{12}C^{*4.439}$ $^{12}C(\alpha,\alpha')^{12}C^{*4.439}$ $^{14}N(p,x)^{12}C^{*4.439}$ $^{15}N(p,\alpha)^{12}C^{*4.439}$ $^{16}O(p,p\alpha)^{12}C^{*4.439}$ $^{16}O(\alpha,2\alpha)^{12}C^{*4.439}$
4.443	$^{11}B^{*4.444} \to g.s.$	$^{7}Li(\alpha,\gamma)^{11}B^{*4.444}$ $^{11}B(p,p')^{11}B^{*4.444}$ $^{11}B(\alpha,\alpha')^{11}B^{*4.444}$ $^{12}C(p,2p)^{11}B^{*4.444}$ $^{12}C(\alpha,p\alpha)^{11}B^{*4.444}$
4.741	$^{11}B^{*9.186} \to {}^{11}B^{*4.444}$	$^{7}Li(\alpha,\gamma)^{11}B^{9.186}$
4.830	$^{11}B^{*9.275} \to {}^{11}B^{*4.444}$	$^{7}Li(\alpha,\gamma)^{11}B^{*9.275}$
5.180 and 5.241	$^{15}O^{*5.181} \to g.s.$ $^{13}O^{*5.242} \to g.s.$	$^{12}C(\alpha,n)^{15}O^{*5.181}$ & 5.242 $^{16}O(p,pn)^{15}O^{*5.101}$ & 5.242 $^{16}O(\alpha,\alpha n)^{15}O^{*5.101}$ & 5.242
5.270 and 5.298	$^{15}N^{*5.271} \to g.s.$ $^{15}N^{*5.299} \to g.s.$	$^{12}C(\alpha,p)^{15}N^{*5.271}$ & 5.299 $^{15}N(p,p')^{15}N^{*5.271}$ & 5.299 $^{16}O(p,2p)^{15}N^{*5.271}$ & 5.299 $^{16}O(\alpha,\alpha p)^{15}N^{*5.271}$ & 5.299 $^{18}O(p,\alpha)^{15}N^{*5.271}$ & 5.299
6.129	$^{16}O^{*6.131} \to g.s.$	$^{16}O(p,p')^{16}O^{*6.131}$ $^{16}O(\alpha,\alpha)^{16}O^{*6.131}$ $^{20}Ne(p,p\alpha)^{16}O^{*6.131}$ $^{20}Ne(\alpha,2\alpha)^{16}O^{*6.131}$
6.176	$^{15}O^{*6.177} \to g.s.$	$^{12}C(\alpha,n)^{15}O^{*6.177}$ $^{15}N(p,n)^{15}O^{*6.177}$ $^{16}O(p,pn)^{15}O^{*6.177}$ $^{16}O(\alpha,\alpha n)^{15}O^{*6.177}$
6.322	$^{15}N^{*6.324} \to g.s.$	$^{12}C(\alpha,p)^{15}N^{*6.324}$ $^{15}N(p,p')^{15}N^{*6.324}$ $^{16}O(p,2p)^{15}N^{*6.324}$ $^{16}O(\alpha,\alpha p)^{15}N^{*6.324}$
6.478	$^{11}C^{*6.480}$ (89%)	$^{12}C(p,pn)^{11}C^{*6.5}$
6.741 and 6.791	$^{11}B^{*6.743} \to g.s.$ (70%) $^{11}B^{*6.793} \to g.s.$ (71%)	$^{11}B(p,p')^{11}B^{*6.743}$ & 6.793 $^{11}B(\alpha,\alpha')^{11}B^{*6.743}$ & 6.793 $^{12}C(p,2p)^{11}B^{*6.743}$ & 6.793
6.786	$^{15}O^{*6.780} \to g.s.$	$^{16}O(p,pn)^{15}O^{*6.792}$ & 6.788
6.917	$^{16}O^{*6.919} \to g.s.$	$^{16}O(p,p')^{16}O^{*6.919}$ $^{16}O(\alpha,\alpha')^{16}O^{*6.919}$
7.117	$^{16}O^{*7.119} \to g.s.$	$^{16}O(p,p')^{16}O^{*7.119}$ $^{16}O(\alpha,\alpha')^{16}O^{*7.119}$

For each of these lines, we calculate a γ-ray emission rate or emissivity. In general, the production rate of excited nuclei, which will emit deexcitation γ-rays of energy ϵ_k, produced by cosmic-ray interactions with the interstellar gas may be simply written:

$$q_k = \sum_i \sum_j \int_0^\infty dE n_i \phi_j(E) \sigma_{ijk}(E) \tag{1}$$

where E is the cosmic-ray kinetic energy per nucleon, n_i is the density of interstellar-gas nuclei of isotope i, $\phi_j(E)$ is the flux of cosmic-ray nuclei of isotope, j, as a function of energy, $\sigma_{ijk}(E)$ is the cross section for the interaction of nuclei, i and j, producing an excited nucleus which at rest emits a γ-ray of energy ϵ_k.

If the excited nuclei were at rest with respect to the observer, the energy spectrum of the γ-ray emission would be essentially a series of delta functions at energies, ϵ_k. But, because the excited nuclei have either some residual or recoil velocity after the nuclear interaction, the observed γ-ray emission will be Doppler-shifted. This Doppler-shifted energy, ϵ, is given by the transformation

$$\epsilon = \epsilon_k \left[\gamma - (\gamma^2 - 1)^{1/2} \cos\theta\right]^{-1} \tag{2}$$

where γ is the Lorentz factor of the excited nucleus in the rest frame of the observer, and θ is the angle between the direction of motion of the excited nucleus and the line of sight between it and the observer. Then, given a distribution of the Lorentz factor of the excited nuclei, $P(\gamma)d\gamma$, and assuming that the distribution of directions is isotropic, the observed distribution of γ-ray energies

$$P(\epsilon) = \int_{\gamma^*}^\infty d\gamma P(\gamma) \frac{1}{2\epsilon_k (\gamma^2 - 1)^{1/2}} \tag{3}$$

where $\gamma^* = (\epsilon_k^2 + \epsilon^2)/(2\epsilon\epsilon_k)$ is the minimum Lorentz factor which the excited nucleus must have in order to Doppler-shift the γ-ray of energy, ϵ_k, to energy, ϵ.

The observed γ-ray emissivity, as a function of energy, including all lines k, is then

$$q(\epsilon) = \sum_i \sum_j \sum_k \int_0^\infty dE n_i \phi_j(E) \sigma_{ijk}(E) \int_{\gamma^*}^\infty d\gamma' \frac{P_{ijk}(E, \gamma')}{2\epsilon_k (\gamma'^2 - 1)^{1/2}} \tag{4}$$

noting that $P_{ijk}(E, \gamma')$ is the probability that the excited nucleus, resulting from the interaction of nuclei, i and j, and energy, E, will have a Lorentz factor, γ', at the time of deexcitation.

The γ-ray line emission resulting from these interactions tends to fall into three components: sharp line emission by excitated interstellar dust-grain nuclei; narrow line emission by excited interstellar gas nuclei; and broad line emission by excited cosmic-ray nuclei. Excited nuclei of dust grains lose most, if not all, of their recoil kinetic energy before deexcitation so that their emission-line widths primarily reflect the bulk motions of the grains in the galaxy leading to Doppler widths of the order of 10 keV or less. The small recoil energies of the excited interstellar gas nuclei cause the γ-ray lines emitted by them to have a typical Doppler broadening of only ~ 100 keV, and the γ-ray lines emitted by the excited cosmic-ray nuclei, which lose little kinetic energy in these interactions, have a typical Doppler broadening of several hundred keV. A typical γ-ray line profile from deexcitation of interstellar gas and cosmic-ray nuclei is shown in figure 1.

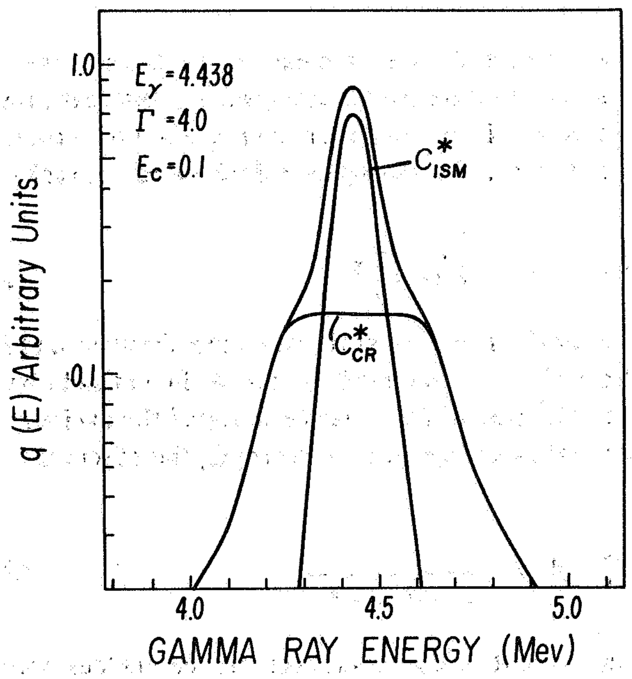

Figure 1. A typical γ-ray line profile showing the narrow line emission spectrum of excited interstellar gas nuclei and the broad line emission of cosmic-ray nuclei.

Measurements of the integral intensity of individual lines have much better statistical significance, and a comparison of these with calculated integral intensities provides the greatest information on the density, composition, and energy spectra of the cosmic rays and interstellar gas.

The integral emissivity for a particular γ-ray line, k, can be obtained by integrating the emissivity (equation 4) over a γ-ray energy range of $\pm\Delta\epsilon$ around ϵ_k. If $\Delta\epsilon$ is larger than the broadening of the line emission from the excited interstellar gas and dust nuclei, then the integral emissivity $q(\epsilon_k \pm \Delta\epsilon)$ becomes,

$$q(\epsilon_k \pm \Delta\epsilon) = \sum_{i^*} \sum_{j} \int_0^\infty dEn_i\phi_j(E)\sigma_{ijk}(E) +$$

$$\sum_{i} \sum_{j^*} \int_0^{E'} dEn_i\phi_j(E)\sigma_{ijk}(E) + \tag{5}$$

$$\sum_{i} \sum_{j^*} \int_{E'}^\infty dEn_i\phi_j(E)\sigma_{ijk}(E) \quad \frac{\Delta\epsilon}{\epsilon_k (\gamma^2 - 1)^2}$$

where

$$E' = mc^2 \left[\left\{ 1 + \left(\frac{\Delta\epsilon}{\epsilon_k} \right)^2 \right\}^{1/2} - 1 \right] \tag{6}$$

is the incident cosmic-ray energy per nucleon at which the width of the broadened line emission from the excited cosmic-ray nucleus equals $2\Delta\epsilon$.

Because either the energy density of the cosmic rays or the instantaneous energy-loss rate of the cosmic rays can be more easily related to other properties of the interstellar medium than to the intensity, $\phi_j(E)$, we normalize the γ-ray line emissivity to these parameters. Thus, we calculate the emissivity per unit cosmic-ray energy density, $q(\epsilon)/w$, in photons s^{-1} eV^{-1} and the emissivity per unit energy loss, $q(\epsilon)/\dot{w}$, in photons erg^{-1}. The cosmic-ray energy density, in eV cm^{-3}, is

$$w = 10^6 \sum_{j} \int_0^\infty dEA_j\phi_j(E)E/c\beta \tag{7}$$

where A_j is the atomic number of cosmic-ray nuclei, j, and the instantaneous cosmic-ray energy loss rate,

$$\dot{w} = \sum_{i} \sum_{j} \int_0^\infty dE\phi_j(E) \left(\frac{dE}{dx} \right)_i \tag{8}$$

where the energy loss rate dE/dx is taken from Barkas and Berger (1964).

From the above equations, we can thus calculate γ-ray line emissivities for the interstellar medium based on measured, or in some cases calculated, cross sections, an assumed cosmic-ray energy spectrum, and cosmic-ray and interstellar-gas abundances.

The energy-dependent excitation cross sections used in these calculations for the various interactions listed in table 1 will be published in a forthcoming paper. Most of the measurements on which they are based are summarized in the extensive review papers on charged particle reactions by McGowan and Milner (1972, 1973a, 1973b, and 1975). The energy-dependent excitation cross sections for some of these interactions have also been presented and discussed in Ramaty et al. (1975) and Meneguzzi and Reeves (1975).

The cosmic-ray energy spectrum in interstellar space is not known below about 500 MeV/nucleon because the interplanetary magnetic field and solar wind exclude lower energy particles from the inner part of the solar system. Thus, we must consider a range of different energy spectra and then try to place some bounds on the spectral shape from a comparison of the relative emissivisites of various lines calculated for each spectrum with the observations of relative line intensities.

For these calculations, we have assumed that the cosmic-ray intensity is a power law in energy per nucleon with a spectral index $-\Gamma$ down to some cutoff energy, E_c, below which the intensity is constant; i.e., the intensity of cosmic-ray particles, j, has the form

$$\phi_j(E) = \phi_{o_j} \text{ for } E < E_c \tag{9}$$

and

$$\phi_j(E) = \phi_{o_j}(E/E_c)^{-\Gamma} \text{ for } E_c < E < E_s \tag{10}$$

where

$$E_s = \Gamma mc^2/(2.7 - \Gamma) \text{ for } \Gamma < 2.7 \text{ and } E_s = \infty \text{ for } \Gamma \geqslant 2.7$$

so that the flatter spectra join smoothly at high energies into a power law in total energy with the observed spectral index of -2.7, giving

$$\phi_j(E) = 14.61\phi_{o_j}(2.7 - \Gamma)^{\Gamma-2.7}\left(\frac{E_c}{\Gamma mc^2}\right)^{\Gamma}\left(\frac{mc^2}{E + mc^2}\right)^{2.7} \tag{11}$$

for $E > E_s$.

For the relative elemental and isotopic abundances in the combined interstellar gas and dust, we have used the solar-system abundances compiled by Cameron (1973). Although these may be representative of the local interstellar medium, the recent work of Searle (1971), Shields (1974), Smith (1975), and D'Odorico et al. (1976), studying abundances in galactic Nebulae suggest large radial gradients in the abundances of He, N, and O relative to H across our galaxy. Such gradients in these and other elements, such as C, are expected from galactic evolutionary models (e.g., Talbot and Arnett, 1975). The present observations allow only very preliminary modeling of the spatial dependence of the relative abundances, but γ-ray line observations may be able to contribute significantly to our understanding of this problem.

For the relative elemental and isotopic abundances of the cosmic rays, we have used the measurements of elemental abundances of Smith et al. (1973) at energies > 1.5 GeV/nucleon, except for the more recent iron abundance measurement of Garcia-Munoz et al. (1975) and the relative isotopic abundance measurements summarized by Meyer (1975). For the initial calculations, we have assumed that these abundances are energy-independent. There is, however, a significant energy dependence in the relative abundance of some nuclei, especially those elements and isotopes which are mainly of secondary origin. If the composition of cosmic rays reflects in any way the gross composition of matter in the region of their source, we must also consider the possibility of cosmic-ray abundance gradients related to those in the interstellar gas and dust.

CALCULATED EMISSIVITY

With these relative abundances, we have calculated the γ-ray line emissivities for a variety of possible cosmic-ray energy spectra (equations 9 to 11) characterized by a spectral index, $-\Gamma$, and a cutoff energy, E_c.

The emissivity per unit cosmic-ray energy density, q/w, for the combined γ-ray line emission from the nuclear excited states, $^{12}C^{*4.439}$ and $^{11}B^{*4.444}$, at energies of 4.44 ±0.44 MeV is shown in figure 2, calculated from equations 5 and 7 for the interactions listed from those lines in table 1. This is then the emissivity in the local interstellar medium for an average hydrogen density of 1 atom cm^{-3} and assuming a total cosmic-ray energy density of 1 eV cm^{-3}. The emissivity, q/w, for this line is roughly linear in the C/H ratio for changes of an order of magnitude or less, if C/O is constant.

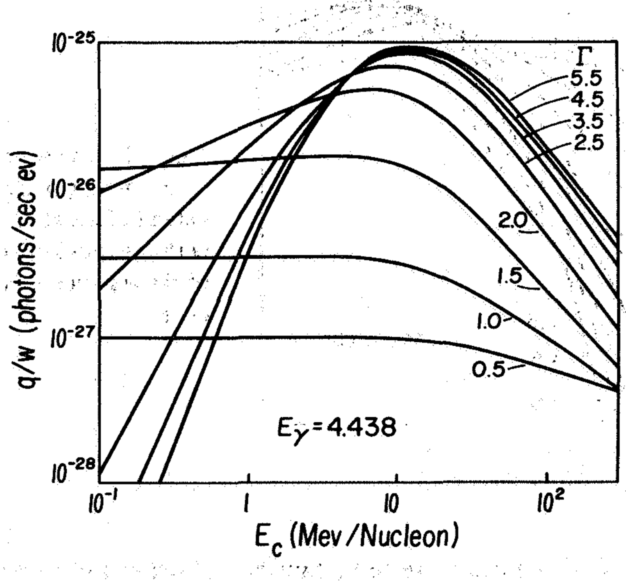

Figure 2. The 4.44 ±0.44-MeV γ-ray emissivity per unit cosmic-ray energy density as a function of the assumed cosmic-ray energy spectral index, $-\Gamma$, and the cutoff energy, E_c, defined in equations 9 to 11.

The peak in emissivity for essentially all spectra at a cutoff, E_c, of ~ 10 MeV/nucleon reflects a peak in the excitation cross sections at roughly that energy. Thus, spectra which carry most of their energy in particles of around 10 MeV/nucleon are most efficient in producing $^{12}C^{*4.439}$. The fraction of the emissivity in the narrow line component of excited interstellar gas and dust depends strongly on the spectral shape, but for cases with E_c of ~ 10 MeV/nucleon, which give the maximum emissivity, roughly one-half is in the narrow line component within 4.44 ± 0.05 MeV. Note also that, for E_c > 3 MeV/nucleon, the emissivity per unit energy density is rather insensitive to the spectral index, Γ, so long as it is greater than about 2.5.

These emissivities for the 4.44-MeV line are between 1.4 and 20 times larger than those calculated for that line by Rygg and Fishman (1973), depending on spectral index, and are the same to two times higher than those of Meneguzzi and Reeves (1975). Both differences result primarily from our inclusion of additional excitation interactions.

The emissivity per unit cosmic-ray energy loss rate, $q/\dot{w}$, for the same line is shown in figure 3, calculated from equations 5 and 8. This is the yield of 4.44-MeV γ-rays per erg of energy dissipated by ionization and nuclear interactions in an ambient medium of solar composition. This emissivity is also roughly linear in C/H for constant C/O. As can be seen, the yield is greatest for cutoff energies, $E_c \gtrsim 10$ MeV/nucleon, and it is not strongly dependent on the spectral index for these cases.

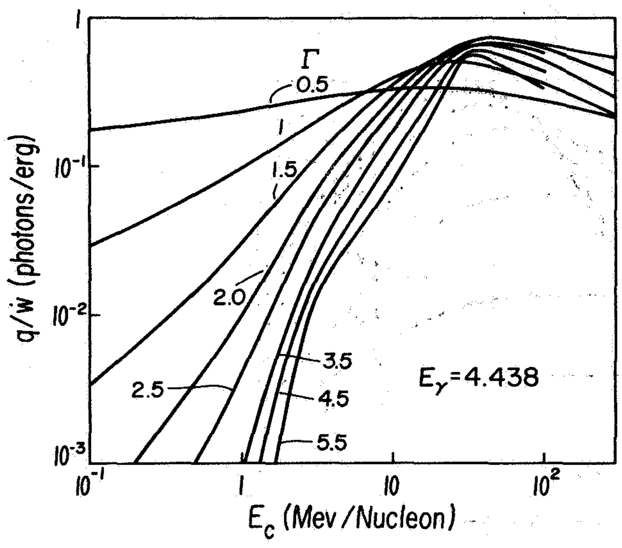

Figure 3. The yield of 4.44 ± 0.44-MeV γ-rays per erg of cosmic-ray energy dissipated in ionization and nuclear interactions with the interstellar medium as a function of the assumed cosmic-ray spectral parameters.

In addition to the 4.44-MeV line, there are a number of other lines which, depending on the assumed cosmic-ray spectral shape and composition, can have comparable emissivity. The combined emissivity per unit cosmic-ray energy density of all γ-ray lines listed in table 1 with γ-ray energies > 0.8 MeV is shown in figure 4, for the same conditions as above.

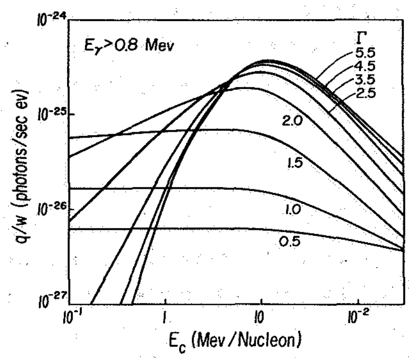

Figure 4. The combined γ-ray line emissivity per unit cosmic-ray energy density of all of the γ-ray lines of energy > 0.8 MeV listed in table 1, as a function of the assumed cosmic-ray energy spectral parameters.

As can be seen by comparison with figure 2, the combined γ-ray line emissivity is roughly four times that of the 4.44-MeV line alone. This ratio is essentially independent of the assumed shape of the cosmic-ray energy spectrum. Haymes et al. (1975), in fact, report a total γ-ray line intensity above 0.8 MeV that is about 4.1 ± 0.8 times that of the 4.4-MeV γ-rays.

If the reported γ-ray flux at about 4.4 MeV (Haymes et al., 1975; and Trombka, private communication, 1976) is of galactic origin, then unresolved line emission at energies > 0.8 MeV may make a significant contribution to the apparent flattening of the diffuse γ-ray background at these energies.

GALACTIC GAMMA-RAY LINE INTENSITY

From these emissivities, we can estimate the expected galactic γ-ray line intensity, assuming some distribution of the interstellar gas, dust, and cosmic rays. If the density and composition of the cosmic rays, gas, and dust were uniform throughout the galaxy with n_H = 1 atom cm^{-3} and w = 1 eV cm^{-3} and solar composition, then the expected local galactic intensity of even the narrow line component of 4.44 ± 0.05-MeV γ-rays would be $\lesssim 3 \times 10^{-5}$ photons $cm^{-2}\ s^{-1}$. This intensity, as was previously noted by Meneguzzi and Reeves (1975), could not be detected above the diffuse γ-ray background of $\sim 10^{-3}$ photons $cm^{-2}\ s^{-1}$ in that energy interval.

But this is not the case, because the density and composition of the interstellar gas and dust are now known to vary significantly across the galaxy. The details of these spatial dependences, however, are not yet fully understood. The neutral hydrogen distribution in the galaxy is fairly well-determined from 21-cm observations recently reevaluated by Burton et al. (1975). But estimates of the molecular hydrogen distribution based on the observed CO distribution (Scoville and Solomon, 1975; Burton et al., 1975; and Gordon and Burton, 1976) necessarily reflect the uncertainties in possible C/H and O/H abundance variations. However, for the purpose of calculating the narrow line component of 4.44-MeV γ-ray emission from deexcitation of carbon in the interstellar gas and dust, we shall assume that the spatial distribution of the carbon and oxygen density in the galaxy is directly proportional to that deduced for

CO molecules at galactic radii $>$ 2 kpc (Gordon and Burton, 1976), ignoring for the moment any contribution from the galactic nucleus. Then, if the cosmic-ray energy density were uniform throughout the galaxy with $w = 1$ eV cm^{-3}, the local galactic γ-ray intensity of the narrow line component at 4.44 ± 0.05 MeV could be as much as 10^{-4} photons cm^{-2} s^{-1}, which is still only 10 percent of the diffuse background.

However, we might also expect the cosmic-ray energy density in the galaxy to vary because of a nonuniform distribution of cosmic-ray sources. Observations of the spatial distribution of likely cosmic-ray sources, such as supernovae (Ilovaisky and Lequeux, 1972) and pulsars (Hulse and Taylor, 1974 and 1975), show a strong dependence on galactic radius. These distributions are qualitatively similar (Burton et al., 1975) to that of CO molecules. If we thus assume that the cosmic-ray energy density is also proportional to the CO distribution of Gordon and Burton (1976) with a local value of 1 eV cm^{-3}, then the expected galactic γ-ray intensity in the narrow line component at 4.44 ± 0.05 MeV could be as large as $\sim 0.6 \times 10^{-3}$ photons cm^{-2} s^{-1}, which should be resolvable above the background. In a preliminary analysis of measurements with an omnidirectional detector on Apollo 16, Trombka (private communication, 1976) reports seeing a 4.4-MeV γ-ray line intensity of $\sim 1.5 \pm 0.75 \times 10^{-3}$ photons cm^{-2} s^{-1}, although part of this flux is background due to neutron activation of the detector. Further analysis of the background is required before it can be established that diffuse γ-ray line emission has been observed.

GAMMA-RAY LINE EMISSION FROM THE GALACTIC NUCLEAR RING

A significant fraction of the intensity reported by Trombka (private communication, 1976) may also come from the direction of the galactic center from which Haymes et al. (1975) report a spectral feature at about 4.4 MeV with an intensity of $(0.95 \pm 0.27) \times 10^{-3}$ photons cm^{-2} s^{-1}. This emission could also result from cosmic-ray interactions in a dense ring of interstellar gas, deduced from molecular line observations to lie in the nuclear disk of the galaxy at a radius of about 270 pc from the center (Kaifu et al., 1972; Scoville, 1972; and Robinson, 1974). The hydrogen density in this ring must be $> 10^3$ cm^{-3} in order to excite the observed CO and NH_3 emission lines, and the total mass of the ring is estimated to be between 10^8 and 10^9 $M_\odot$, corresponding to a volume of $\sim 10^{62}$ cm^3. This should be compared to estimates of the total mass of gas in the galaxy of $\sim 4 \times 10^9$ $M_\odot$ (Gordon and Burton, 1976).

The local γ-ray line intensity coming from such a ring is simply

$$\phi = \frac{q n_H V}{4\pi r^2} \tag{12}$$

where q is the emissivity, $n_H V$ is the total number of hydrogen atoms in the ring, equal to 10^{65} to 10^{66} for a ring mass of 10^8 to 10^9 $M_\odot$, and r is 10 kpc, the distance of the Sun from the galactic center. With these values, the reported 4.4-MeV γ-ray intensity ϕ of 10^{-3} photon cm^{-2} s^{-1} would require an emissivity q of 10^{-22} to 10^{-23} photons cm^{-3} s^{-1}. Assuming, as discussed above, that the C/H and O/H ratios in the galactic nuclear ring are an order of magnitude greater than solar values, then we could expect q/w to be as much as 10^{-24} photons s^{-1} eV^{-1}. The reported emission could therefore be produced by cosmic-ray interactions with the gas in the nuclear ring if the cosmic-ray energy density were between 10 and 10^2 eV cm^{-3}. This is comparable to cosmic-ray energy densities already suggested for a nuclear region by Sanders and Wrixon (1973), who estimated that either a magnetic field or a cosmic-ray pressure, or energy density, of the order of 10 eV cm^{-3} was required to keep the gas from collapsing into the galactic equatorial plane. It is also much less than might be expected if the cosmic-ray energy density were assumed to be roughly proportional to the C and O density which is at least $\sim 10^4$ times larger in the nuclear ring than locally. The total energy in such low-energy cosmic rays in the ring is only 10^{51} to 10^{52} ergs which could, in principle, be produced by a single supernova.

From the calculated $q/\dot{w}$ for the 4.44-MeV line shown on figure 3, we also see that the maximum γ-ray photon yield per erg of cosmic-ray energy lost in ionization and nuclear interactions is on the order of unity for the local C/H ratio. Hence, it could be as much as 10 in the gas in the nuclear ring, if the C/H ratio there is ten times higher. The reported intensity ϕ of 10^{-3} photons cm^{-2} s^{-1} implies 4.4-MeV γ-ray luminosity of $4\pi r^2 \phi = 10^{43}$ photons s^{-1} for the nuclear ring. The above $q/\dot{w}$ further implies a total energy loss rate for the cosmic rays in the ring of 10^{42} ergs s^{-1}. This is comparable to the infrared luminosity of the galactic nucleus (Hoffman et al., 1971). If the total cosmic-ray energy is between 10^{51} and 10^{52} ergs, then the mean life of such cosmic rays $w/\dot{w}$ is between 30 and 300 years. Because the estimated mass of molecular gas in the ring is between 3 and 30 percent of the molecular gas in the galaxy (Gordon and Burton, 1976), we might expect the relative frequency of occurrence of supernovae in the ring and in the galaxy to be similar. A galactic supernova rate of one every 25 years (Tammann, 1974) could therefore give a supernova rate of one every 75 to 750 years in the nuclear ring. If each supernova produced a few times 10^{51} ergs in low-energy cosmic rays, this rate could supply the required cosmic-ray energy a substantial fraction of the time, producing a variable γ-ray source on time scales of the order of the cosmic-ray energy loss time.

SUMMARY

We have evaluated the production rate of the most significant nuclear γ-ray lines from 0.4 to 7 MeV, produced in cosmic-ray interactions with the interstellar material. Each of these lines consists of three components with different line widths. There is a sharp line component with a Doppler width of the order of 10 keV or less emitted on deexcitation of interstellar grain nuclei which should be easily observed by solid-state detectors with energy resolution of a few keV or less. Studies of this component can give the first measurement of the composition and spatial distribution of interstellar grains throughout the galaxy. There is also a relatively narrow γ-ray line component with a width of the order of 100 keV for the most intense line, $^{12}C^{*4.439}$, and of the order of a few keV for the $^{56}Fe^{*0.847}$ line,

emitted on deexcitation of interstellar-gas nuclei, and lastly a broad line component with a width of several hundred keV, emitted on deexcitation of low-energy cosmic-ray nuclei.

Here we have presented a detailed evaluation of the production rate of the 4.44-MeV line for a variety of assumed cosmic-ray spectra. Comparing these results with reported (Haymes et al., 1975; Trombka, private communcation, 1976) galactic γ-ray line intensities, we conclude that the measurements are consistent with a low-energy cosmic-ray density which increases toward the galactic center in proportion to the molecular-gas density.

ACKNOWLEDGMENTS

We particularly wish to thank Helen Lee for her aid with the machine computations.

REFERENCES

Barkas, W. H., and J. J. Berger, 1964, *Tables of Energy and Ranges of Heavy Charged Particles,* NASA SP 3013.

Burton, W. B., M. A. Gordon, T. M. Banis, and F. J. Lockman, 1975, *Ap. J.*, **202**, p. 30.

Cameron, A. G. W., 1973, In *Explosive Nucleosynthesis,* ed. D. N. Schramm and W. D. Arnett, Univ. of Texas Press, Austin, p. 3.

D'Odorico, S., M. Peimbert, and F. Sabbadin, 1976, *Astron. Astrophys.*, **47**, p. 341.

Fishman, G. J., and D. D. Clayton, 1972, *Ap. J.*, **178**, p. 337.

Fowler, W. A., H. Reeves, and J. Silk, 1970, *Ap. J.*, **162**, p. 49.

Garcia-Munoz, M., E. Juliusson, G. M. Mason, P. Meyer, and J. A. Simpson, 1975, *Ap. J.*, **197**, p. 489.

Gordon, M. A., and W. B. Burton, 1976, *Ap. J.*, in press.

Haymes, R. C., G. D. Walraven, C. A. Meegan, R. D. Hall, F. T. Djuth, and D. H. Shelton, 1975, *Ap. J.*, **201**, p. 593.

Hoffman, W. F., C. K. Frederick, and R. J. Emery, 1971, *Ap. J. Letters,* **164**, p. L23.

Hulse, R. A., and J. H. Taylor, 1974, *Ap. J.*, **191**, p. L59.

Hulse, R. A., and J. H. Taylor, 1975, *Ap. J.*, **201**, p. L55.

Ilovaisky, S. A., and J. Lequeux, 1972, *Astron. Astrophys.*, **18**, p. 169.

Johnson, W. N., III, F. R. Harnden, Jr., and R. C. Haymes, 1972, *Ap. J. Letters,* **172**, p. L1.

Johnson, W. N., III, and R. C. Haymes, 1973, *Ap. J.*, **184**, p. 103.

Kaifu, N., T. Kato, and T. Iguchi, 1972, *Nature,* **286**, p. 105.

Kozlovsky, B., and R. Ramaty, 1974, *Ap. J. Letters,* **191**, p. L43.

Meneguzzi, M., and H. Reeves, 1975, *Astron. Astrophys.,* **40**, p. 91.

Meyer, J. P., 1975, (14th Intl. Cosmic Ray Conf. Papers), **11**, p. 3698.

McGowan, F. K., and W. T. Milner, 1972, *Nuclear Data Tables,* **11**, p. 1.

McGowan, F. K., and W. T. Milner, 1973a, *Charged Particle Reaction List 1948-1971,* Academic Press, New York, p. 547.

McGowan, F. K., and W. T. Milner, 1973b, *Atomic Data and Nuclear Data Tables,* **12**, p. 499.

McGowan, F. K., and W. T. Milner, 1975, *Atomic Data and Nuclear Data Tables,* **15**, p. 189.

Ramaty, R., and E. A. Boldt, 1971, "The Gum Nebula and Related Problems," NASA TM X-65749, p. 97.

Ramaty, R., B. Kozlovsky, and R. E. Lingenfelter, 1975, *Space Sci. Rev.,* **18**, p. 341.

Robinson, B. J., 1974, (Proc. IAU Symposium No. 60., Galactic Radio Astronomy), ed. F. J. Kerr and S. C. Simonson, Reidel Publishing Co., Dordrecht, Holland, p. 521.

Rygg, T. A., and G. J. Fishman, 1973, (Proc. 13th Intl. Cosmic Ray Conf., Denver), **1**, p. 472.

Sanders, R. H., and G. T. Wrixon, 1973, *Astron. Astrophys.,* **26**, p. 365.

Scoville, N. Z., 1972, *Ap. J.,* **175**, p. L127.

Scoville, N. Z., and P. M. Solomon, 1975, *Ap. J. Letters,* **199**, p. L105.

Searle, L., 1971, *Ap. J.,* **168**, p. 327.

Shields, G. A., 1974, *Ap. J.,* **193**, p. 335.

Smith, H. E., 1975, *Ap. J.,* **199**, p. 591.

Smith, L. H., A. Buffington, G. F. Smoot, and L. W. Alvarez, 1973, *Ap. J.,* **180**, p. 987.

Talbot, R. J., Jr., and W. D. Arnett, 1975, *Ap. J.,* **197**, p. 551.

Tammann, G. A., 1974, In *Supernovae and Supernova Remnants,* ed. C. B. Cosmovici, Reidel Publishing Co., Dordrecht, Holland, p. 155.

CONTRIBUTED PAPERS
June 3, 1976, p.m.
(Listed by Title, Author, and Reference)

1. Steepening of the γ-Ray Background Spectrum From Local γ-Ray Production, K. Thielheim, Institute für Reine and Angewandte Kernphysik, Universitat Kiel, W. Germany

   Reference: R. Schlickheiser and K. O. Thielheim, 1976, *Nature*, **261**, p. 478.

2. Production Spectrum of π°-Mesons in the Galaxy, S. A. Stephens, NASA/Johnson Space Flight Center, Houston, Texas 77058.

   Reference: No preprint available.

3. Carbon Monoxide Kinematics in the Inner Galaxy, T. M. Bania, National Radio Astronomy Observatory, Edgemont Road, Charlottesville, Virginia 22901.

   Reference: T. M. Bania, 1976, Carbon Monoxide Kinematics in the Inner Galaxy, *Bull. AAS*, **8**, p. 334.

4. CO Observation of the Scale Height and Distribution of Molecular Clouds in the Galactic Plane, Richard Cohen, Columbia University and Goddard Institute for Space Studies, 2880 Broadway, New York, New York 10025.

   Reference: No preprint available.

5. A Survey of Ionized Hydrogen in the Plane of the Galaxy, F. J. Lockman, National Radio Observatory, Edgemont Rd., Charlottesville, Virginia 22901.

   Reference: F. J. Lockman, A Survey of Ionized Hydrogen in the Plane of the Galaxy, 1976, *Ap. J.*, **209**, p. 429.

6. Angular Distribution of Low Energy γ-Ray Flux as Observed on Apollo 16, David Gilman, Dept. of Astronomy, Cornell University, Ithaca, New York.

   Reference: No preprint available.

7. 0.3-10 MeV Diffuse γ-Ray Spectrum From Measurements Obtained During the Apollo 15, 16, and 17 missions, Jacob Trombka, Goddard Space Flight Center.

   Reference: J. Trombka, C. W. Dyer, L. G. Evans, M. J. Bielfeld, S. M. Seltzer, and A. E. Metzger, 1976, *Bull. Am. Phys. Soc.*, **21**, p. 562.
   Also: Reanalysis of the Apollo Cosmic γ-Ray Spectrum in the 0.3-10 MeV Region, J. Trombka, C. W. Dyer, L. G. Evans, M. J. Bielfeld, S. M. Seltzer, and A. E. Metzger, 1976, NASA TM X71150.

3. Cosmic Diffuse γ-Ray Angle and Energy Distributions from 2 to 30 MeV, R. S. White, S. Moon, J. Ryan, R. Wilson, A. D. Zych, and B. Dayton, Physics Dept., U. of California, Riverside, California 92502.

Reference: Cosmic Diffuse γ-Ray Angle and Energy Distributions From 2 to 30 MeV, R. S. White, S. Moon, J. Ryan, R. Wilson, A. D. Zych and B. Dayton, 1976, *Bull. Am. Phys. Soc.*, 21, p. 56a.

CONTRIBUTED PAPERS
June 4, 1976, a.m.
(Listed by Title, Author, and Reference)

1. Cosmic Ray Propagation in a Closed Galaxy, Bernard Peters, Danish Space Research Institute, Lyngby, Denmark.

   Preprint: Cosmic Ray Propagation in a Closed Galaxy, B. Peters and N. J. Westergaard, Danish Space Research Institute, Lyngby, Denmark.

2. Distribution of Cosmic Ray Nuclei in the Galaxy, Arnold Wolfendale, Physics Department, University of Durham, England.

   Preprint: Distribution of Cosmic Ray Nuclei in the Galaxy, D. Dodds and A. W. Wolfendale, Physics Department, University of Durham, England.

3. The Source Function for the Inverse Compton Process in the Solar Vicinity, Giovanni Bignami, Instituto di Science Fisiche, Aldo Pontromeli, Via Celoria 16, Milano, Italy 20133.

   Reference: The Source Function for the Inverse Compton Process in the Solar Vicinity, G. Piccinotti and G. F. Bignami, to be published in *Astron. and Astrophysics*.

GAMMA RAYS AND SUPERNOVA EXPLOSIONS

W. D. Arnett
Department of Astronomy
University of Illinois
Urbana, Illinois 61801

ABSTRACT

The detection of γ-rays from supernovae will provide interesting tests of current theory. This discussion will review some current ideas on the expected γ-ray flux, as modified by recent theoretical results.

CONTINUUM EMISSION

After the explosion, high-energy electromagnetic radiation may be produced by an uncovered pulsar or by the interaction of the ejected debris with the interstellar medium. Here, we will consider instead the radiation associated with the explosion itself, especially with high temperatures.

It appears that most of the radiation from type II supernovae is thermal radiation. To produce copious γ-radiation of this sort requires high temperature. The observational data is well-represented by low temperatures ($T \lesssim 20000$ K). Thus, $kT \lesssim 10$ eV, which certainly is not favorable for γ-emission. A detailed discussion for SN 1969ℓ is given by Falk and Arnett (1976). Most of the luminosity seems to be due to the diffusive release of imprisoned radiation by an expanding plasma. There is a "first burst" due to the arrival of the supernova shock at the stellar surface. It is not clear just how high the temperatures get in this brief stage ($\Delta t \lesssim 1$ day). The calculations give $T_{max} \simeq 40000$ K; it is unlikely that this is off by orders of magnitude. Consequently, it appears that type II supernovae do not release very much of their energy as γ-ray continuum radiation.

There is a simple reason for this result. A massive star of, say, $10\ M_\odot$ develops a large radius, $r \simeq 5 \times 10^{13}$ cm after helium burning. The observed luminosity at peak, which looks like a blackbody, has $L \simeq 10^{43}$ erg, so, if we allow for some expansion,

$$\sigma T_e^4 = L/4\pi r^2 \lesssim 10^{43}/\pi \times 10^{28}$$

or $T_e \lesssim 50000$ K. Doppler shifts in absorption lines of up to about 10^9 cm/s are observed.

The radius doubles in a time

$$t \simeq r/v \simeq 5 \times 10^{13}/10^9 \simeq 5 \times 10^4 \text{ s} \simeq 1/2 \text{ day}$$

and, in two days, $r \simeq 2 \times 10^{14}$ cm, so $T_e \simeq 25000$ K, and it continues to cool. When the photospheric temperature drops below about 6000 K, the opacity decreases due to recombination, and one sees in to deeper, hotter regions. Thus, T_e decreases below 6000 K only slowly.

When will the temperature throughout the envelope drop low enough to cause transparency? First, the initial (post-shock) temperature must be estimated. Using a value of 10 $M_\odot$ and an average velocity of 6000 km/s yields a kinetic energy of 3.6×10^{51} ergs, a value in accord with that estimated as necessary to explain the nature of galactic supernova remnants. This energy can fill a sphere of radius $r = 5 \times 10^{13}$ cm with blackbody radiation at a temperature $T \simeq 1.0 \times 10^6$ K.

Is the expansion approximately adiabatic? It appears to be possible; observed supernova luminosities, integrated over the outburst, give energies of order 10^{50} ergs. The diffusion time is

$$\tau \simeq 3r^2/\lambda c \simeq 3r^2 \rho\eta/c.$$

Now most of the stellar mass is in an extended, almost constant, density envelope; therefore,

$$\rho \simeq 3M/4\pi r^3$$

and the diffusion time is

$$\tau \simeq 2 \times 10^8 \text{ s} \left(\frac{10^{14}\text{ cm}}{r}\right)\left(\frac{\eta}{0.4 \text{ cm}^2/\text{g}}\right)\frac{M}{M_\odot}$$

Because this equals $t \sim r/v$ for only $r \simeq 10^{16}$, the dominant effect is expansion.

For quasi-adiabatic expansion, $\rho \sim T^3$, so we have

$$T/10^6 \text{ K} \simeq 5 \times 10^{13} \text{ cm}/(10^9 \text{ cm/s } t)$$

therefore, for $T \simeq 6000$ K,

$$t \simeq 80 \text{ days}$$

After this time, a significant fraction of the envelope becomes transparent. (This is sufficiently long to hide many γ-lines; see table 1.) More complex calculations support these simple arguments.

It is not clear how high the energy densities associated with the "burst" in type I supernovae become. They may be similar to SN II. The Morrison-Sartori (1969) model requires fairly hard (UV) radiation in large amounts (energies $> 10^{52}$ ergs). Although Lasher (1975) has explained the shape of the visual light peak of SN I, his models do not yet explain the hard

Table 1
Gamma-Line Prospects (after Clayton, 1973)

Nucleus	$X_{\odot}$	Progenitor	$\tau_{1/2}$	Atoms/SN	Process and Comments
^{56}Fe	1.3×10^{-3}	^{56}Co	77 d	3.0×10^{54}	e-process; Si burning; good prospect
^{56}Co	1.3×10^{-3}	^{56}Ni	6.1 d	3.0×10^{54}	e-process; Si burning; good prospect
^{48}Ti	2.3×10^{-6}	$(^{48}Cr)\,^{48}V$	16 d	6.2×10^{51}	e-process; Si burning; good prospect
^{44}Ca	1.9×10^{-6}	$(^{44}Ti)\,^{44}Sc$	48 yr	5.6×10^{51}	Not produced at solar value in any network calculation to date (?!)
^{60}Ni	2.0×10^{-5}	^{60}Fe	3×10^{5} yr	4.4×10^{52} (?)	Hypothetical result of neutron capture during explosive carbon burning
		^{60}Co	5.26 yr		
^{22}Ne	1.2×10^{-4}	^{22}Na	2.6 yr	(?!)	Rapid $^{14}N(\alpha, \gamma)\,^{18}F(\alpha, \gamma)\,^{22}Na$ in exploding He zone; most ^{22}Ne not formed this way
^{238}U (example)	1.3×10^{-10}	(r-process)	4.5×10^{9} yr	1.3×10^{47}	r-process; relatively little matter is processed this way

*Clayton's estimate.

UV pulse. It is not at all obvious that a hard UV pulse, even if it exists, means that significant γ-radiation will result. Such radiation is difficult to rule out entirely for all (as yet unspecified) models.

Colgate (1975) assumes that the supernova shock has a high temperature precursor. If, instead, the matter is accelerated by radiation pressure (Falk and Arnett, 1976), then the reason for expecting a strong γ-ray burst disappears. Until the physics of the "peak" in SN I is well understood and agreed upon, it seems wise to regard the theoretical situation as unclear.

Because of many underlying similarities, it is beginning to appear that both SN I and SN II may be the result of explosions in extended stars. More condensed objects may explode and give rise to higher effective temperatures and γ-radiation. Such events would not correspond to those events astronomers term supernovae.

LINE EMISSION

The last stable nucleus with Z = N is ^{40}Ca. In stars, the thermonuclear synthesis of heavier nuclei tends to form Z = N nuclei which are unstable toward electron capture or positron emission. Radiative decay from excited states of the daughter nucleus gives rise to γ-ray lines. This process is particularly important because a lot of mass—the iron group—is formed this way. Similarly, nuclear processing in proton-rich or neutron-rich environments can also produce unstable nuclei whose decay may give γ-lines.

The Typical-Zone Approach

To be useful for the experimenter a theory of such processes should be able to predict γ-line emission. To date, most predictions have relied on detailed analysis of thermonuclear processing in "typical zones." One specifies a set of initial conditions (temperature, density, and composition) and an expansion time scale and then solves the coupled nonlinear equations (reaction network) for the evolution of the abundances. For a clear review of the γ-line problem from this viewpoint, see Clayton (1973).

Table 1 summarizes these results and gives a few comments on the problems with some of the proposed sources.

The astrophysical aspects of a single zone approximation are clearly oversimplified. Stars are not homogeneous; they have structure. Further, stars of different mass behave in very different ways. The net result of all this complexity may be different in some important details from a set of typical zones which reproduce some of the dominant features.

The Stellar Model Approach

Some preliminary work which attempts to go beyond the one-zone approach has just been completed. The evolution of the cores of stars of mass $10 \leq M_{\odot} \lesssim 95$ have been evolved to dynamical instability. They all develop a nickel-iron core which exceeds the Chandrasekhar mass and contracts toward the neutron star state (or beyond). The remaining matter is loosely bound in a surrounding mantle. It is assumed that this mantle is explosively ejected from the star and that this process corresponds to at least some observed supernovae (see Arnett, 1975a). The circumstantial evidence for this point of view is fairly strong. The precise mechanism for the explosion is unclear (see papers by Wilson et al., Colgate, Arnett, Schramm, and Brueen in the Seventh Texas Symposium; 1975).

Nucleosynthesis Yield per Star

The evolutionary calculations dealt with helium cores of mass M_α. To correlate these with the masses, M, of main sequence stars (with which the initial mass function, the IMF, deals), the carbon-burning cores were compared with carbon-burning models of Paczynski (1970) and Lamb, Iben, and Howard (in preparation). These models were more complete and consistent than those of the other authors which were examined. The first two columns in table 2 give the derived transformation for M_α and M.

The other columns give the fractions by mass of the star in the form of ^{4}He (α), ^{12}C, ^{16}O, ^{20}Ne, ^{24}Mg and "Si + Fe." The latter entry is the matter which has been processed through oxygen burning but not silicon burning. It is expected that this matter, which lies just outside the collapsing core, will undergo silicon burning upon ejection, hence the notation Si + Fe. For a given mass, these entries do not sum to unity; the "missing mass" is the collapsing core. The values shown were taken when γ became less than 4/3; that is, when dynamical collapse began. Some nuclear rearrangement may yet occur during the explosion, especially among the inner regions (higher Z nuclei).

Nucleosynthesis Yield per Generation

To get the net yield, we must weight the results in table 2 by the (number × mass) of stars having a given mass, M. This weighting is discussed in detail in Talbot and Arnett (1973) and references therein. If X_i (m) is the fraction by mass of a star of mass, m, that is ejected (see table 2), then the yields are

$$q_i = \int_1^{max} \psi(m)\ X_i(m)\ dm$$

where we use a Salpeter IMF,

$$\psi(m) = \zeta(\mu - 1)\, m^{-\mu}$$

for m ⩾ 1 $M_\odot$, where $\mu = 4/3$, and the lower end of the IMF has been corrected for Weistrop's dwarfs ($\zeta = 0.25$; see Talbot and Arnett, 1973). This choice is probably the most straightforward at present. Table 3 gives these yields per generation.

Table 2
Yield Per Star

Masses		Abundances by Mass					
M_α	M	α	C	O	Ne	Mg	Si + Fe
3	10	5.08 (-1)	1.59 (-2)	1.30 (-3)	- -	- -	- -
4	12	5.11 (-1)	4.80 (-2)	4.18 (-2)	1.01 (-2)	1.64 (-2)	2.53 (-2)
6	16	4.30 (-1)	4.80 (-2)	1.29 (-1)	7.10 (-2)	4.23 (-2)	4.42 (-2)
8	22	3.87 (-1)	7.10 (-2)	2.07 (-1)	9.61 (-2)	3.38 (-2)	4.24 (-2)
12	28	2.99 (-1)	1.02 (-1)	3.20 (-1)	8.67 (-2)	2.59 (-2)	3.53 (-2)
16	35	2.54 (-1)	1.01 (-1)	3.85 (-1)	8.90 (-2)	2.52 (-2)	6.12 (-2)
24	50	2.09 (-1)	9.57 (-2)	4.88 (-1)	8.22 (-2)	2.60 (-2)	3.89 (-2)
32	75	2.07 (-1)	6.40 (-2)	5.19 (-1)	7.33 (-2)	3.03 (-2)	3.73 (-2)
48	95	1.70 (-1)	5.84 (-2)	6.32 (-1)	7.01 (-2)	3.26 (-2)	7.09 (-3)

Table 3
Yield Per Generation

Z	q_z	$q_z/1\text{-}f$	$X_\odot$
α	2.2 (-2)	2.5 (-2)	2.4 (-1)
C	4.4 (-3)	5.3 (-3)	4.5 (-3)
O	1.7 (-2)	2.0 (-2)	1.1 (-2)
Ne	4.2 (-3)	4.9 (-3)	1.2 (-3)
Mg	1.7 (-3)	2.0 (-3)	5.6 (-4)
Si + Fe	1.9 (-3)	2.2 (-3)	2.0 (-3)

Galactic evolutionary models must be consistent with the paucity of metal-poor, low-mass stars. The identification of Pu^{244}, I^{129}, and ^{26}Al as extinct radioactivities demands that nucleosynthesis be an ongoing process in our galaxy. Those currently interesting models which can satisfy these constraints predict that the abundance of a species, i, approaches

$$X_i \rightarrow q_i/(1 - f)$$

where f is the fraction of matter returned to the interstellar medium by stars of $M \geq 1\ M_\odot$ ($f \simeq 0.15$). This is true for infall models, inhomogeneous models, or metal-enchanced star-formation models. It is not true for initial burst models.

These predicted abudances are compared with the solar-system abundances in table 3. Except for ^4He (which is thought to be produced cosmologically anyway) the agreement is good. Uncertainties due to further processing in the explosion, to errors in the IMF, and to errors in the input physics will give rise to variations of factors of 2 in these numbers. Larger variations are possible. Still, it is encouraging that the most straightforward prediction of the absolute yield of stellar nucleosynthesis comes out so well.

Implications for Gamma Lines

These results have several important implications for γ-line astronomy:

1. Our ideas of explosive nucleosynthesis, and, hence, our predictions of γ-line luminosities, can be put on a firmer foundation.
2. By filling in the gaps between "typical zones," the production of important nuclei like ^{44}Ti and ^{44}Sc can be understood (see table 1).
3. By pinning down the explosive conditions, we can see how much of nuclei such as ^{60}Fe, ^{60}Co, and ^{22}Na are produced (see table 1).

4. We will be able to predict luminosities from particular events, rather than be forced to consider a "typical supernova."

5. The more realistic approach to the problem may give rise to some surprises.

This research has been supported in part by the National Science Foundation.

REFERENCES

Arnett, W. D., 1975a, *Ap. J.*, **195**, p. 727.

Arnett, W. D., 1975b, *Ann. N. Y. Acad. Sci.*, **262**, p. 47.

Bruenn, S. W., 1975, *Ann. N. Y. Acad. Sci.*, **262**, p. 80.

Clayton, D. D., 1973, *Explosive Nucleosynthesis*, (ed. D. N. Schramm and W. D. Arnett), Univ. Texas Press, Austin, p. 264.

Colgate, S. A., 1975, *Ann. N. Y. Acad. Sci.*, **262**, p. 34.

Falk, S. W. and W. D. Arnett, 1976, *submitted*., preprint.

Lasher, G., 1975, *Ap. J.*,

Morrison, P. and L. Sartori, 1969, *Ap. J.*, **158**, p. 541.

Paczynski, B., 1970, *Acta Astr.*, **20**, p. 47.

Schramm, D. N., 1975, *Ann. N. Y. Acad. Sci.*, **262**, p. 65.

Talbot, R. J., Jr., and W. D. Arnett, 1973, *Ap. J.*, **186**, p. 51.

Wilson, J. R., R. Couch, S. Cochran, J. Le Blanc, and Z. Barkat, 1975, *Ann. N. Y. Acad. Sci.*, **262**, p. 54.

GALACTIC DISTRIBUTION OF PULSARS

J. H. Seiradakis
Max Planck Institut für Radioastronomie
Auf dem Hügel 69
5300 Bonn 1, West Germany

ABSTRACT

The density distributions of pulsars in luminosity, period, Z-distance, and galactocentric distance have been derived, using a uniform sample of pulsars detected during a 408-MHz pulsar survey at Jodrell Bank. There are indications of a "fine-scale" structure in the spatial distribution and evidence that there is a general correlation with other galactic populations and the overall spiral structure. The electron layer in our galaxy is shown to be wider than the pulsar layer and uniform on a large scale. The number of pulsars in the galaxy has been estimated and used to derive the pulsar birthrate.

INTRODUCTION

This paper attempts to establish the distribution of pulsars in luminosity, period, and position within the galaxy. Obviously, any such attempt is limited not only by the small number of pulsars (149) so far discovered, but also by the fact that these have been discovered by many observatories, at many different frequencies, and using widely different techniques. Table 1 summarizes the observatories and the means by which pulsars have so far been discovered.

It is obvious that any attempt to statistically analyze pulsar data should take into account the uncertainties of the search techniques and thus try to concentrate on a smaller sample with well-defined selection effects.

Large (1971) studied the distribution of 29 pulsars observed at Molonglo and was able to deduce the period, luminosity, and galactic Z-distance distributions from his data. Using this information, it became clear that a considerably more sensitive search confined to a limited region close to the galactic plane would reveal a large number of pulsars. In fact, such a survey carried out at Jodrell Bank at 408 MHz has yielded 51 pulsars, 31 of which were new discoveries (Davies et al., 1972 and 1973). Because of the greater sensitivity of the survey, these pulsars are generally rather more distant than those obtained at Molonglo and show the distribution on a larger galactic scale. The results of a statistical analysis of these pulsars

Table 1
Observatories and Techniques by Which Pulsars Have Been Discovered

Observatory	Pulsars Discovered	Technique
Arecibo (Puerto Rico)	45	Periodicity searches, dedispersion
Bologna (Italy)	5	Paper charts
Cambridge (U.K.)	6	Paper charts
Jodrell Bank (U.K.)	42	Dispersion and periodicity technique
Molonglo (Australia)	32	Paper charts, dedispersion
NRAO (U.S.A.)	6	Dispersion and periodicity technique
Ootacamund (India)	3	Paper charts?
Parkes (Australia)	9	Periodicity searches
Puschino (U.S.S.R.)	1	Paper charts

show a number of features which had not been previously detected. The galactocentric distribution has been derived, which, combined with the Z-distribution, gives a good view of the distribution of pulsars in the galaxy.

OBSERVATIONS

The observing system employed during the survey was similar to that described by Davies et al. (1970). The observations were made at 408 MHz, using the 76-m MkIA radiotelescope at Jodrell Bank. The total intensity of radiation from each beam area in the sky was obtained by adding the outputs of two receivers, each sensitive to one hand of circular polarization. The receivers had excess noise temperature of 110 K and bandwidths of 4 MHz. The overall system gave 1.2 K per Jy for a source at the beam center. The half-power beamwidth of the telescope was $0\overset{\circ}{.}7$ at this frequency.

The detected receiver output was sampled in an on-line Ferranti Argus 400 computer over 16 384 intervals of 40 ms (a total of about 11 minutes) and stored for further analysis. While one such observation was in progress, the computer processed previously acquired data, the analysis time for one observation taking about 10 minutes.

The main properties of the search system are summarized in table 2.

Periodic signals having periodicities in the range $0.16 < P < 4$ seconds were detected, using a fast-folding algorithm (FFA) specially adapted for a pulsar search. The basic algorithm has been described by Staelin (1969). It amounts to cross correlating the data with pulse trains of varying period and phase, having duty cycles between 12.5 and 25 percent. The system was therefore equally sensitive to all pulsars within a large range of dispersion measures which

Table 2
The Jodrell Bank Pulsar Search System

Telescope	MK1A
Frequency	408 MHz
Bandwidth	4 MHz
Beamwidth	0.75°
Sensitivity	1.2 K/Jy
Technique	Periodicity search
Integration time	$10^m 55^s$
Sampling interval	40 ms
Method of analysis	Fast-folding algorithm
Period range	0.16 to 4 s
Other characteristics	On-line analysis, gave about two pages of output per integration

would be expected to lengthen the pulses in the receiver bandwidth. For pulsars having dispersion measures up to about 500 × P pc cm^{-3}, where P is the period in seconds; the minimum detectable mean flux near the center of the beam was about 0.010 Jy for regions away from the galactic plane where the total system temperature was at a minimum. Figure 1 shows how the sensitivity of the system varied as a function of pulsar period and dispersion measure.

The area of the sky surveyed was systematically observed by setting the telescope to track each position for 11 minutes and then moving it to another. This area was chosen in order to study both the galactic longitude and latitude distribution of pulsars.

Figure 2 indicates the region of the galaxy surveyed. It covers the areas with longitude extending from the galactic center to $\ell^{II} = 240°$ and latitude $|b^{II}| < 5°$. The latitude coverage for areas with low longitude ($\ell^{II} < 115°$) was extended to $|b^{II}| < 10°$. The survey was made in two sessions. In the first, the whole area was surveyed on a primary grid of points having 1° spacing and centered on the half degrees of both longitude and latitude. Because the beamwidth was only 0°.7, the observed region was considerably undersampled (~40-percent coverage). In order to improve the statistics for the interesting regions (at longitudes below 115°), in the second session, observations were made at the interstices of the grid (i.e., at the integral degree points in longitude and latitude). These observations were essentially independent of those at the primary grid points. About 80 percent of the area where the two sessions overlap was covered. This area is shaded in figure 2.

If, during the search procedure, there were any indications of the presence of a periodicity in the data or if the observation was spoiled by interference, a further observation was made at the same position, and the new observation was checked for periodicities close to any obtained in the first observation. If no coincidence was found, a negative observation was recorded. About 15 percent of the observations were repeated in this way. If there was a coincidence, a pulsar was likely to be in the beam, and the area was then searched by scanning across the grid point, using a simple pulsar observing program which folded the data, using the periodicity determined from the search observations. This generally confirmed the presence of a pulsar and allowed a more precise determination of the period and the position of the pulsar.

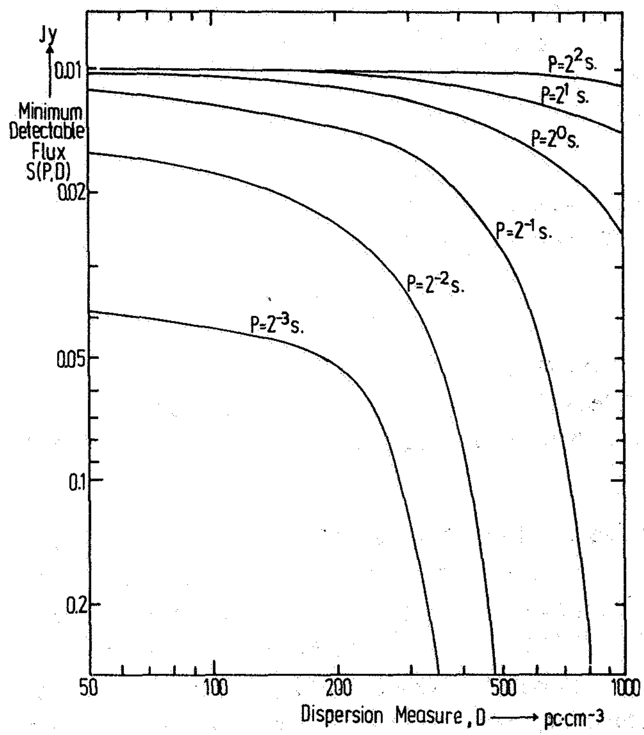

Figure 1. The system sensitivity as a function of pulsar period and dispersion measure.

During the survey, 51 pulsars were detected, of which 31 were previously unknown. Only one previously known pulsar which lay within the survey area, PSR 1915 + 13, was not detected using the procedure described above.

Table 3 presents the data on the 51 pulsars which were detected. The first seven columns give the observed parameters. The integrated equivalent width quoted in this table is the ratio between the area beneath the pulse profile and the peak of the profile. The last three columns give derived parameters which will be discussed later.

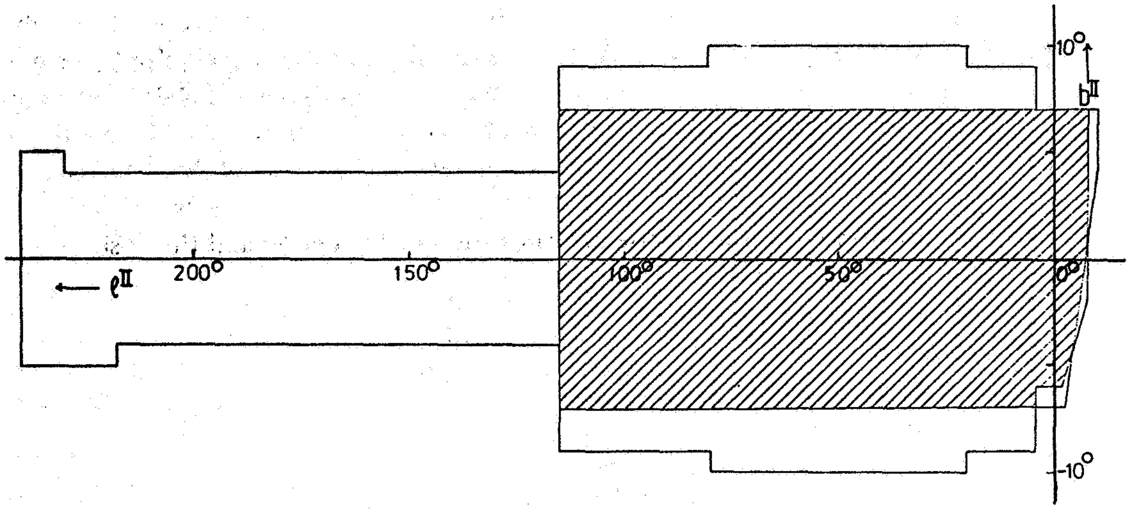

Figure 2. The area searched: the coverage in the shaded area was 80 percent, and in the rest, it was 40 percent.

ANALYSIS

When the survey was completed, about 5000 beam areas along the galactic plane had been investigated in which 51 pulsars had been detected. The sky background temperature in each beam could be found from the literature (e.g., Seeger et al. (1965)), and the sensitivity of the search system, S(P, D), was also available.

Assuming that the spatial distribution of pulsars in the galaxy is cylindrically symmetrical, each of the 51 pulsars occupies a point in a four-dimensional space of luminosity ($L = SD^2$), period (P), galactic Z-distance ($Z = D \sin b^{II}$) and galactocentric distance projected on the plane of the galaxy ($R = (D^2 \cos^2 b^{II} + D_{GC}^2 - 2\,D\,D_{GC} \cos b^{II} \cos \ell^{II})^{1/2}$). Here, the dispersion measure, D, has been used directly as a measure of distance, and D_{GC} is the dispersion measure corresponding to the distance of the center of the galaxy. This use of the dispersion measure implies a uniform electron density throughout the region of interest. If the electron density is averaged over long path lengths, this assumption has been shown to be satisfied in the local neighborhood of the Sun (Prentice and ter Haar, 1969), and there are strong indications that over greater distances, and throughout the volume containing the observed pulsars, the same assumption is true (Guélin, 1974; and Lyne, 1974).

The aim of this work is to obtain, from the observed distribution of pulsars in L, P, Z, and R, which contain a number of selection effects, an estimate of their true density distribution.

The number of pulsars observed, having luminosity, L, period, P, lying at a distance, Z, away from the galactic plane and at a distance, R, from the galactic center can be written

Table 3
Data on the 51 Detected Pulsars

PSR	ℓ^{II} deg.	b^{II} deg.	P sec.	DM pc. cm^{-3}	S_{408} Jy	W_E deg.	R pc. cm^{-3}	Z pc. cm^{-3}	L_{408} Jy (pc. $cm^{-3})^2$
0105+65	124.6	3.3	1.284	30	0.025	7.8	268	1.73	23
0153+63	130.5	0.2	2.352	60	0.013	5.0	293	0.21	47
0329+54	145.0	-1.2	0.715	27	2.27	4.5	273	-0.56	1655
0355+54	148.2	0.8	0.156	57	0.056	8.1	300	0.90	182
0540+23	184.4	-3.3	0.246	72	0.030	13.7	322	-4.14	156
0611+22	188.8	2.4	0.335	97	0.048	11.0	346	4.06	452
1700-32	351.7	5.4	1.212	103	0.092	12.5	149	9.69	976
1717-29	356.5	4.3	0.620	45	0.030	15.7	205	3.37	61
1718-32	354.5	2.5	0.477	120	0.095	12.1	131	5.23	1368
1730-22	4.0	5.8	0.872	45	0.031	16.0	205	4.55	63
1749-28	1.5	-1.0	0.563	51	1.07	4.5	199	-0.89	2783
1813-26	5.2	-4.8	0.593	90	0.026	26.6	161	-7.53	211
1818-04	25.5	4.7	0.598	85	0.15	7.5	178	6.96	1084
1819-22	9.4	-4.3	1.874	140	0.022	10.0	115	-10.50	431
1822-09	21.5	1.4	0.769	21	0.025	6.5	231	0.48	11
1826-17	14.5	-3.3	0.307	210	0.085	20.8	71	-12.09	3748
1831-04	27.0	1.8	0.290	68	0.081	54.0	192	2.14	375
1831-03	27.7	2.3	0.687	230	0.067	8.5	117	9.23	3544
1845-04	28.9	-1.0	0.598	142	0.055	16.0	143	-2.48	1109
1845-01	31.3	0.1	0.659	163	0.057	20.6	139	0.57	1514
1846-06	26.7	-2.4	1.451	152	0.031	4.9	133	-6.37	716
1859+03	37.2	-0.6	0.655	402	0.074	11.0	253	-4.21	11959
1900-06	28.5	-5.6	0.432	180	0.016	13.8	126	-17.56	518
1900+01	35.8	-1.9	0.729	228	0.103	7.5	148	-7.56	5354
1906+00	35.1	-3.9	1.017	111	0.026	2.7	171	-7.55	320
1907+02	37.6	-2.7	0.495	190	0.015	13.9	153	-8.95	542
1907+10	44.8	1.0	0.284	144	0.061	16.0	179	2.51	1265
1910+20	54.0	5.0	2.233	84	0.010	2.9	212	7.32	71

Table 3 (Continued)

PSR	ℓ^{II} deg.	b^{II} deg.	P sec.	DM pc. cm^{-3}	S_{408} Jy	W_E deg.	R pc. cm^{-3}	Z pc. cm^{-3}	L_{408} Jy (pc. $cm^{-3})^2$
1911-04	31.3	-7.1	0.826	89	0.074	3.2	180	-11.00	586
1917+00	36.5	-6.2	1.272	85	0.034	5.2	189	-9.03	246
1918+19	53.9	2.7	0.821	135	0.038	28.6	202	6.36	693
1919+21	55.8	3.5	1.337	12	0.056	6.8	244	0.73	8
1920+21	55.3	3.0	1.078	220	0.048	6.9	220	11.51	2323
1929+10	47.4	-3.9	0.227	3	0.61	9.1	248	-0.20	6
1933+16	52.4	-2.1	0.359	158	0.36	6.1	198	-5.79	8987
1944+17	55.3	-3.5	0.441	16	0.033	19.0	241	-0.98	8
1946+35	70.7	5.1	0.717	129	0.12	5.7	240	11.24	1997
1952+29	65.9	0.8	0.427	8	0.020	17.0	247	0.10	1
2002+31	69.0	0.0	2.111	225	0.014	3.6	270	0.18	709
2016+28	68.1	-4.0	0.558	14	0.29	9.6	245	0.98	57
2020+28	68.9	-4.7	0.343	25	0.25	7.0	242	-2.05	156
2021+51	87.9	8.4	0.529	23	0.31	12.0	250	3.36	164
2106+44	86.9	-2.0	0.415	129	0.038	20.0	275	4.50	632
2111+46	89.0	-1.3	1.015	142	0.19	10.0	285	-2.97	3831
2148+63	104.3	7.4	0.380	125	0.025	20.5	305	16.10	391
2217+47	98.4	-7.6	0.538	44	0.063	6.0	260	-5.82	122
2223+65	108.6	6.9	0.683	100	0.038	18.0	298	12.18	380
2255+58	108.8	-0.5	0.368	148	0.042	12.2	329	-1.81	920
2305+55	108.6	-4.2	0.475	45	0.023	18.3	268	-3.30	47
2319+60	112.1	-0.6	2.256	96	0.07	10.4	299	-1.01	645
2324+60	112.9	0.0	0.234	120	0.041	21.9	317	0.06	590

$$N(L, P, Z, R)\, dL\, dP\, dZ\, dR = V(L, P, Z, R)\, \rho(L, P, Z, R)\, dL\, dP\, dZ\, dR \tag{1}$$

where $V(L, P, Z, R)$ is the volume of the galaxy explored, $\rho(L, P, Z, R)$ is the true pulsar density, and dL, dP, dZ, and dR are intervals in L, P, Z, and R. Thus, in principle, it is possible to deduce an estimate of $\rho(L, P, Z, R)$ from the observed distribution of pulsars, $N(L, P, Z, R)$, and a knowledge of the volume searched.

Unfortunately, $N(L, P, Z, R)$ is not a continuous function and is zero everywhere except for 51 delta functions corresponding to the positions of the pulsars, and it is clear that equation 1 cannot be solved without some simplifying assumptions. In this, we follow Large (1971) and assume that the variables are independent in density, and we write:

$$\rho(L, P, Z, R) = \rho(L)\, \rho(P)\, \rho(Z)\, \rho(R) \tag{2}$$

This separation of the variables would not be justified if there were any correlation between them. Later, however, it is shown that no significant correlation exists, and the variables can therefore be treated as completely separable.

Combining equations 1 and 2, one gets:

$$\rho(L) = \frac{\iiiint N(L, P, Z, R)\, dL\, dP\, dZ\, dR}{\iiint \rho(P)\, \rho(Z)\, \rho(R)\, V(L, P, Z, R)\, dP\, dZ\, dR} \tag{3}$$

and three similar equations for $\rho(P)$, $\rho(Z)$, and $\rho(R)$. If $V(L, P, Z, R)$ is known, the four equations can be solved iteratively, using the observed distribution of pulsars, $N(L, P, Z, R)$.

The calculations for the volume, $V(L, P, Z, R)$, are illustrated in figure 3.

Each of the 5000 beams that were observed explored a region of the (L, P, Z, R) space. The volume of the galaxy searched for each element in this space was obtained by considering the telescope beam, which occupies a conical volume of width, θ, to consist of a number of segments at distance, D (dispersion measure), of length, δD, and diameter, θD, so that the volume for each segment searched is:

$$\delta V(L, P, Z, R) = \frac{\pi}{4}\theta^2 D^2\, \delta D$$

Knowing the sky background temperature and the sensitivity of our system, it was possible to calculate the minimum luminosity, L_{min}, that a pulsar with period, P, and dispersion measure, D, would need to be detectable.

$$L_{min} = D^2 \frac{0.01}{S(P, D)} \frac{T_s}{140\ K}$$

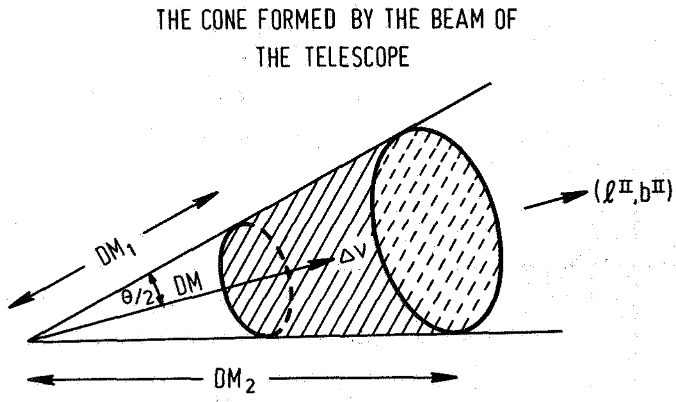

$$\Delta V = \frac{\pi}{12}\theta^2\,(DM_2^3 - DM_1^3)$$

$$L_{min} = \left(\frac{T_{BG}+120}{30+120}\right)\cdot(DM)^2\cdot 0.01\cdot\frac{B(p)}{1-A(p)\cdot DM}$$

Figure 3. The explored volume calculations.

T_s consists of the sum of the receiver excess noise temperature (110 K) and the sky background temperature, which varied over the sky between about 30 K and several hundred K.

Thus, for this survey, P and L were incremented by small steps in the range $2^{-3} \leq P \leq 2^2$ s and $10° \leq L \leq 10^5$ Jy (pc cm^{-3})^2, and we set $\Delta V = 0$ for $L < L_{min}$ or $\Delta V = \int_{DM_1}^{DM_2} \delta V = \frac{\pi}{12}\theta^2\,(DM_2^3 - DM_1^3)$ for $L \geq L_{min}$ (see figure 3).

By carrying out this procedure on all conical segments which form the telescope beam for D incremented by small steps in the range $0 < D < 1000$ pc cm^{-3} and for all the beam positions observed during the survey, it was possible to estimate the volume of the galaxy searched for each point in the (L, P, Z, R) space.

RESULTS

The four distributions shown in figures 4, 5, 6, and 7 are the density distributions of pulsars in luminosity, period, Z-distance, and galactocentric distance. The units employed are arbitrary and are as follows:

$\rho(R)$ and $\rho(Z)$ are chosen to be unity in the solar neighborhood.

$\rho(P)$ is unity for periods in the range $2^{-3/4} < P < 2^{1/4}$ (i.e., at $P = P_{max}$).

$\rho(L)$ is the number of pulsars per cubic dispersion measure unit, per semidecade in luminosity, having period $P = P_{max}$, in the solar neighborhood.

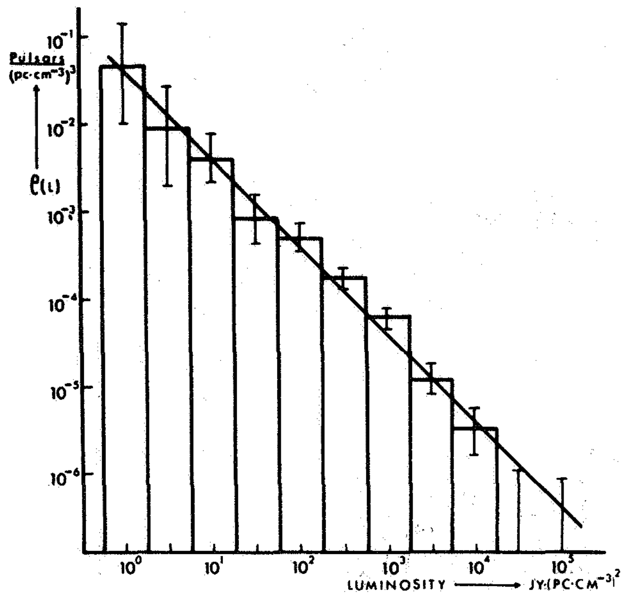

Figure 4. The luminosity distribution of pulsars.

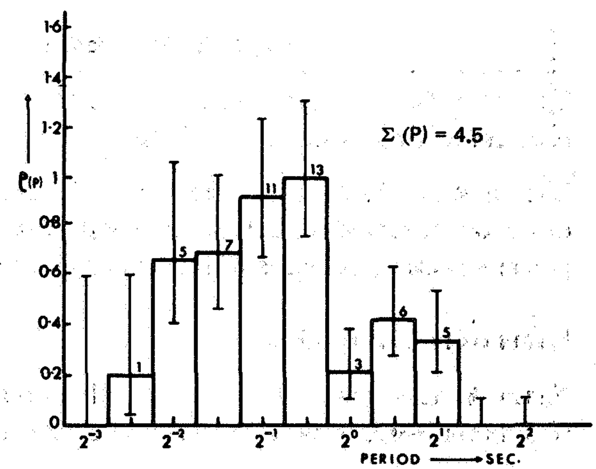

Figure 5. The period distribution of pulsars.

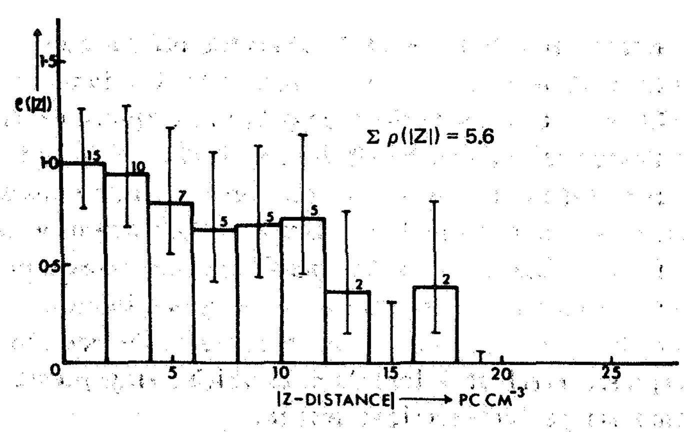

Figure 6. The Z-distance distribution of pulsars.

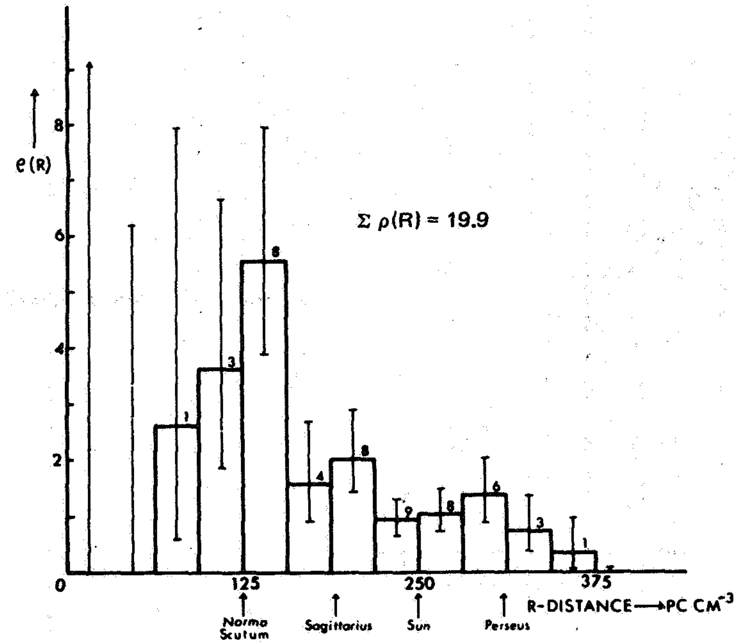

Figure 7. The galactocentric distribution of pulsars.

This choice of units is convenient for estimating the true pulsar density in any volume of the four-dimensional space (L, P, Z, R).

The error bars in the above-mentioned figures have been calculated assuming that the number of pulsars observed in each interval is small-samples Poisson-distributed. They give the 20-percent confidence limits of the presented distributions.

Luminosity Distribution

Figure 4 shows that the number of pulsars per unit volume in the galaxy decreases rapidly with luminosity. A best-fit to the data gives a power law

$$\rho(L) = \rho(L_0)\ L^{-b}$$

with b = 2 ± 0.2. This is in excellent agreement with Large's (1971) results and the most recent analysis of the Arecibo survey data (Roberts, 1976). The errors of the less luminous classes are quite large, and the possibility of a turnover at the faint pulsar end cannot be excluded. In fact, the high-sensitivity pulsar search in Arecibo (Hulse and Taylor, 1974 and 1975), in which a boundary to the spatial distribution of pulsars was detected, didn't discover pulsars that were intrinsically less luminous than the ones in our sample. Their pulsars were fainter only because they were more distant. The fact that they didn't discover many more intrinsically faint nearby pulsars indicates that a turnover in the luminosity distribution should be placed at about 1 Jy (pc cm^{-3})^2. This statement is corroborated by the negative results of a low-frequency (151-MHz) pulsar search at Jodrell Bank in which a large portion of the northern hemisphere was covered using a fairly sensitive system.

Period Distribution

The median of the period distribution of pulsars is at 0.55 ± 0.09 seconds with a standard deviation of about 1.0 in $\log_2 P$. The distribution shows a marked decrease in pulsar density for either short or long period pulsars. This is not due to any instrumental effects but is a genuine property of pulsars. The decrease of the density of pulsars at periods of around 1 second is independent of the period interval chosen and has been confirmed by the Arecibo search (J. H. Taylor, private communication). This is a result that needs further investigation.

Z-Distance Distribution

The pulsar Z-distance distribution can be adequately described by a gaussian function:

$$\rho(Z) = \rho(Z_o)\, e^{-\frac{(Z - 0.5)}{134.2}}$$

where Z is in dispersion measure units, and $\rho(Z_o)$ is the pulsar density on the galactic plane. Figure 6 shows this distribution. It was found to be convenient to describe our spatial distributions in dispersion measure units (pc cm^{-3}). These are the units used in the horizontal scale. The scale height is $\sigma = 8.2$ pc cm^{-3}. Assuming a uniform electron density of 0.025 electrons/cm^3 extending beyond the pulsar layer, the full width of the pulsar Z-distance distribution to half-power points can be calculated to be 660 pc. The pulsar layer seems to be considerably wider than that of any other class of young population objects. In particular, it is much wider than the supernova remnants layer (Ilovaisky and Lequeux, 1972; and Kodaira, 1974), but one should bear in mind that this may simply reflect the effect of pulsar high velocities as reported by several authors.

Recent observations (Falgarone and Lequeux, 1973) suggest that the full width of the electron layer is of the order of 1 kpc or greater. This is much wider than the pulsar layer. In fact, a careful inspection of table 3 shows that no pulsar at such high Z-distance was detected (assuming an electron density of 0.025 electrons/cm^3, 1 kpc corresponds to 25 pc cm^{-3}). Some futher comments on the electron layer are made later.

Our results, although heavily affected by statistical ambiguities, give evidence that the median of the Z-distribution occurs at -0.5 pc cm^{-3} (with a standard error of 1.5 pc cm^{-3}). Assuming a mean electron density of 0.025 electrons/cm^3, this corresponds to -20 pc from the plane. In other words, the suggestion that the Sun lies 20 pc north of the galactic plane (e.g., Elvis, 1965) has also been revealed by our pulsar observations.

Galactocentric Distribution

Figure 7 illustrates our best estimate for pulsar galactocentric distribution. The horizontal scale is, as explained in the previous section, in dispersion measure units (to convert into pc, divide by the electron density, i.e., 0.025 electrons/cm^3).

The distribution of pulsars in galactocentric distance shows a marked decrease away from the galactic center. The median of the distribution is at 161 ± 13 pc cm^{-3} (6.4 ± 0.5 kpc). No pulsar with R < 70 pc cm^{-3} (~ 3 kpc) was detected, but the errors of the invervals in the inner region are so large that the possibility that the pulsar density may still be quite high near the galactic center cannot be excluded. On the other side, towards the anticenter, there is a genuine decrease of the number of pulsars. The density distribution becomes practically zero after the Perseus arm (~ 13 kpc), in excellent agreement with the spatial boundary found by the Arecibo search.

Among the pulsars which were detected, PSR 1826-17 was the closest to the galactic center (~ 3 kpc), and PSR 0611+22–the IC 443 pulsar–was the furthest away (~ 14 kpc).

In the distribution shown in figure 7, there are indications of spiral structure. The tangential points of the Norma-Scutum, the Sagittarius, and the Perseus arms are shown, and it is obvious that the pulsar density follows this pattern quite closely. The large statistical errors of the present distribution do not allow any conclusive statement to be made.

In order to investigate the significance of the spiral structure found, we scaled our galaxy differently and, using the same procedure, tried to fit the observations to the new model. If the spiral structure originally found was due to periodicities created by the analysis procedure, they should show up again. Figure 8 shows the results of such an exercise. The galactic center distance has been taken to be 400 pc cm^{-3} (16 kpc). No other change to our data or analysis procedure was made. It is obvious that any trace of spiral structure has disappeared. The other distributions (luminosity, period, and Z-distance) did not change by more than 0.1 percent. This was expected unless there was some significant degree of correlation among them.

The existence of a definite cutoff in pulsar density and the indications of (a) the offset of the Sun's position by 20 pc, and (b) the spiral structure revealed, suggest that pulsars may prove to be a very powerful tool in studying the spiral structure of our galaxy. Their built-in measure of distance (the dispersion measure), the independent measure of distance that can be obtained by hydrogen absorption measurements and the fact that they can be observed at much greater distances than optical observations allow make them unique in this field. A more sensitive survey than the one presented here should reveal many more pulsars, as indicated by their luminosity distribution (figure 4) and confirmed by the Arecibo search.

DISCUSSION

Throughout the analysis, the dispersion measure of pulsars has been taken as a measure of distance. This assumption is justified only if the electron layer is: (a) wider than the pulsar layer and (b) uniform on a scale comparable to the interval scale used during the analysis.

Many authors have contributed to the understanding of these problems. Falgarone and Lequeux (1973) give a comprehensive review of the relevant arguments. They show that the width of the ionized layer is ~ 1000 pc (i.e., wider than the pulsar layer). This result is further corroborated by the pulsar Z-distance distribution shown in figure 6. This shows a monotonic decrease in density with Z-distance. If the ionized layer was substantially thinner than the pulsar layer, this would have been indicated by a peak at nonzero Z-distance. (For more detals, see Gould, 1971.) Such an effect has not been found.

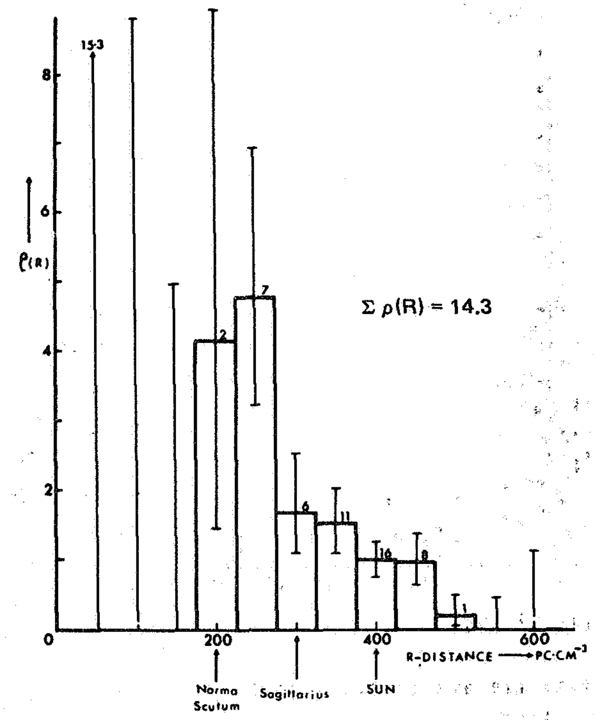

Figure 8. The hypothetical galactocentric distribution of pulsars assuming that the distance to the galactic center is 16 kpc.

Inhomogeneities in the distribution of thermal electrons are expected to occur in the interstellar medium. Not only is a correlation with the spiral structure expected, but also local variations of the electron density due to the different components of the interstellar gas will inevitably upset a uniform distribution. However, Gomez-Gonzales and Guélin (1974), Lyne (1974), and other authors have shown that the electron density near the galactic plane may be regarded as uniform when averaged over a pathlength of a few kiloparsecs. The mean electron density suggested is ~ 0.025 electrons/cm^3. Figure 9 illustrates the above arguments.

It shows the dispersion measure of 147 pulsars plotted as a function of galactic latitude. It indicates that if one uses the dispersion measure as a measure of distance, pulsars do follow the cosec b^{II} law predicted by a uniform disk-shaped distribution of sources having distances greater than a few hundred parsecs.

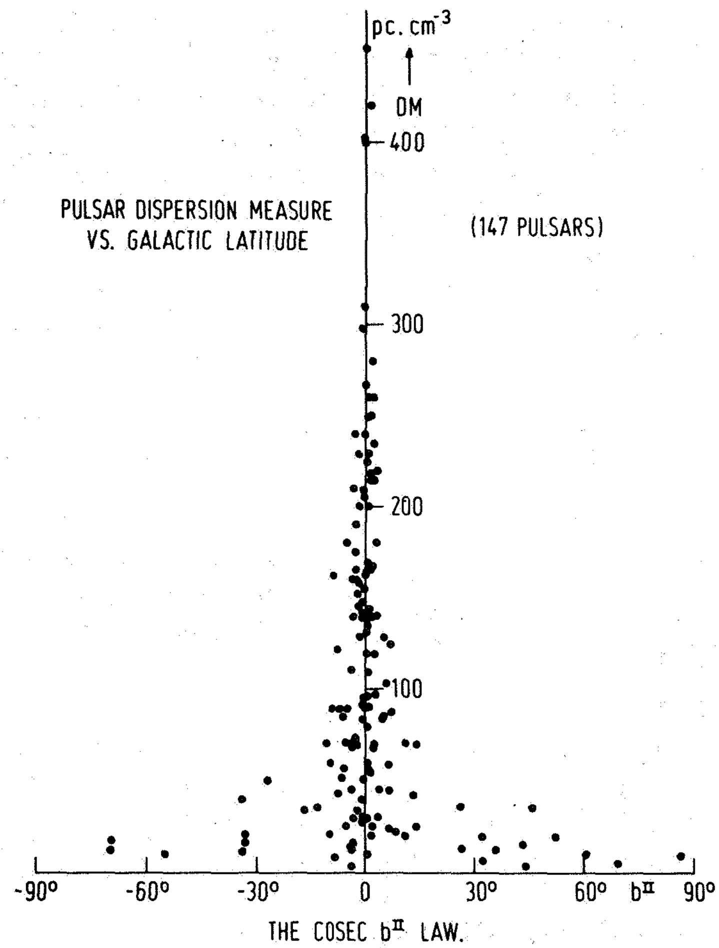

Figure 9. Pulsar dispersion measures as a function of galactic latitude.

A justification of the assumption of the independence of the examined distributions was mentioned in the preceding section. In order to further investigate this, another method was devised.

From the previously derived distribution of pulsars and a knowledge of our system sensitivity, it was possible to calculate the number of pulsars expected to be observed in each range of the four-dimensional space, (L, P, Z, R). Assuming that there were no digitization errors and no correlation between the examined distributions, this number should be very close to the observed number of pulsars. Any correlation between the distributions would upset this result. Table 4 presents χ^2-tests for the observed and expected two-dimensional distributions. The first two columns give the distribution to be tested and the number of classes into which

Table 4
χ^2-Tests for Observed and Expected
Two-Dimensional Distributions

Distribution	Classes (n)	χ^2	P (%)
R - Z	4	0.379	93.5
R - P	4	0.564	82.5
R - L	3	0.222	81.5
Z - P	4	0.305	95.8
Z - L	3	1.493	71.9
P - L	4	1.053	78.9

it was divided. The last two columns show the statistic (χ^2) and the result (P) of the test. It is obvious that no discrepancy between expected and observed numbers was found, which suggests that the assumption of no correlation between the examined distributions is correct.

Recombination line observations (e.g., Matthews et al. (1972)) indicate the existence of a dense ionized bulk of material in the inner region of the galaxy ($R < 5$ kpc). The effect of such a region on pulsar observations would be of great importance. Dispersion and scintillation broadening would make pulsars practically undetectable in such a region. The effect would be a kind of "brick wall" where the observed pulsars show first a sudden increase of their dispersion measure and then a sharp cutoff of their number density.

Our observations indeed show such a sharp cutoff at about 130 pc cm^{-3} ($\sim$ 5 kpc, figure 7). However, we claim that this is due to limitations in our sensitivity, and it is quite independent of any brick-wall effect. Only if the observed number of pulsars in a certain region was significantly different from the expected number (calculated by the method mentioned above) could it be said that an effect which had not been taken into account had been discovered. In this survey, no such region was found. The brick-wall effect was not detected.

However, what was detected is an enhancement of pulsar density in the 5- to 6-kpc region (figure 7). This is in excellent agreement with the distribution of many important constituents of our galaxy, such as molecular clouds, HII regions, supernova remnants, cosmic rays, and γ-rays (see Stecker, 1976). In particular, HII regions (a good indicator of the distribution of massive hot stars) appear to correlate very well with the distribution of pulsars. As explained earlier, pulsars that happen to lie in dense ionized regions would be practically undetectable. However, high-pulsar velocities would result in the bulk of pulsars escaping from their birthplaces. They would then surround their parent population, and thus still be detectable. All of the above-mentioned constituents are associated with the formation and destruction of young OB stars in our galaxy. As explained by Stecker (1976), the correlation of these components can be physically explained.

Of course, the mean Z-distance of pulsars is much wider than the mean Z-distance of any of these populations. However, one should bear in mind that this reflects only high-pulsar velocities. On the other hand, these high velocities, in conjunction with the indications of spiral structure found (figure 7), support other evidence that pulsar true ages do not exceed $\sim 5 \times 10^6$ years (Lyne et al., 1975). A mean age of $\sim 10^7$ years and a typical velocity of ~ 200 km/s would have resulted in the disappearance of any spiral structure.

CONCLUSIONS

The distributions illustrated in figures 4 through 7 are, to our best estimate, independent of selection effects due to either pulsar position or system sensitivity. They describe the density distribution of pulsars in luminosity, period, Z-distance, and galactocentric distance.

Using these distributions and equation 1, it is possible to calculate the total number of pulsars in the galaxy. It is reasonable to use a lower limit of 1 Jy $(\text{pc cm}^{-3})^2$ for the luminosity distribution (i.e., the luminosity of the least luminous pulsar observed). However, it must be pointed out that the error bars of the last two luminosity intervals in figure 4 indicate that the uncertainties are about one order of magnitude. These uncertainties become the largest source of error in the estimation of the total number of pulsars. The unknown distribution of pulsars in the inner region of the galaxy (figure 7) does not give rise to significant errors because the corresponding volume of space decreases rapidly at this region. The calculated number of pulsars does not vary by more than 20 percent if one assumes: (a) a uniform distribution with space density 5.6 units (see figure 7), and (b) a distribution extending to the maximum value indicated by the error bars in the range $0 < R < 70$ pc cm^{-3}.

The estimated number of pulsars in the galaxy with luminosity exceeding 1 Jy $(\text{pc cm}^{-3})^2$ and period in the range $2^{-3} < P < 2^2$ s is $(6 \pm 5) \times 10^4$. The errors are mainly due to uncertainties in the luminosity distribution. No beaming factor has been taken into account.

Assuming a two-beam model, the probability of a pulsar being observable is given by $f = \psi \sin\theta$, where θ is the angle between the rotation and the magnetic axes and ψ is the integrated pulse width. If the rotation and magnetic axes are randomly distributed, then $\langle \sin\theta \rangle = \pi/4$, and, taking a value of $\psi = 20°$, it is found that $f = 0.25$. Taking into account this beaming factor, we find that the number of pulsars in the galaxy is

$$N = 2 \times 10^5$$

in good agreement with Large's (1971) estimate of 5×10^5 pulsars.

Taking a mean age of 5×10^6 years for pulsars (Lyne et al., 1975; and Manchester et al., 1974), we find a pulsar birth rate of

1 pulsar every 25 years

This is in good agreement with previous publications and the rate of occurrence of supernovae (e.g., Tammann (1973)). However, supernovae and pulsar birth rates are subject to many assumptions (distances, lifetime, beaming factor, etc.), and, hence, they are not very reliable.

ACKNOWLEDGMENTS

It is my pleasure to thank Professor J. G. Davies and Dr. A. G. Lyne for their continuous help during this work.

REFERENCES

Davies, J. G., M. I. Large, and A. C. Pickwick, 1970, *Nature*, **227**, p. 1123.

Davies, J. G., A. G. Lyne, and J. H. Seiradakis, 1972, *Nature*, **240**, p. 229.

Davies, J. G., A. G. Lyne, and J. H. Seiradakis, 1973, *Nature Phys. Sci.*, **244**, p. 84.

Elvis, T., 1965, *Stars and Stellar Systems*, (ed. A. Blaauw and M. Schmidt), University of Chicago Press, **5**, chapter 3.

Falgarone, E., and J. Lequeux, 1973, *Astron. Astrophys.*, **25**, p. 253.

Gomez-Gonzales, J., and M. Guélin, 1974, *Astron. Astrophys.*, **32**, p. 441.

Gould, R. J., 1971, *Astrophys. and Space Sci.*, **10**, p. 265.

Guélin, M., 1974, (IAU Symposium No. 60), p. 51.

Hulse, R. A., and J. H. Taylor, 1974, *Ap. J. Letters*, **191**, p. L59.

Hulse, R. A., and J. H. Taylor, 1975, *Ap. J. Letters*, **201**, p. L55.

Ilovaisky, S. A., and J. Lequeux, 1972, *Astron. Astrophys.*, **18**, p. 169.

Kodaira, K., 1974, *Publ. Astr. Soc.*, Japan, **26**, p. 255.

Large, M. I., 1971, (IAU Symposium No. 46), p. 165.

Lyne, A. G., 1974, (IAU Symposium No. 60), p. 87.

Lyne, A. G., R. T. Ritchings, and F. G. Smith, 1975, *M.N.R.A.S.*, **171**, p. 579.

Matthews, H. E., A. Pedlar, and R. D. Davies, 1973, *M.N.R.A.S.*, **165**, p. 149.

Prentice, A. J., and D. ter Haar, 1969, *M.N.R.A.S.*, **146**, p. 423.

Roberts, D. H., 1976, *Ap. J. Letters*, **205**, p. L29.

Seeger, C. L., G. Westerhout, R. G. Conway, and T. Hoekama, 1965, *Bull. Astr. Inst.*, Netherlands, **18**, p. 11.

Stecker, F. W., 1976, *Nature*, **260**, p. 412.

Tammann, G. A., 1973, "Supernovae and Supernovae Remnants," *Astrophys. and Space Sci. Library*, **45**.

COSMIC-RAY PROPAGATION AND CONTAINMENT

E. N. Parker
Laboratory for Astrophysics and Space Research
933 East 56th Street
Chicago, Illinois 60637

ABSTRACT

The cosmic rays are an active gaseous component of the disk of the galaxy, and their propagation and containment is a part of the general dynamics of the disk. The sources of cosmic rays are a matter of speculation. The disk is inflated by the cosmic-ray gas pressure, P, comparable to the magnetic pressure $B^2/8\pi$, but the rate of inflation is unknown. The time spent by the individual cosmic-ray particles in the disk is inversely proportional to the cosmic-ray production rate and may be anything from 10^5 years to more than 10^7 years. It is evident from the decay of Be^{10} that the cosmic rays circulate through a volume of space perhaps ten times the thickness of the gaseous disk, suggesting a magnetic halo extending out $\sim$ 1 kpc from either face of the disk. The cosmic rays may be responsible for the halo by inflating the magnetic fields of the disk. Extension of the fields to 1 kpc would imply a high production rate and short life ($< 10^7$ years) of cosmic rays in the dense gaseous disk of the galaxy. But the dynamical questions, including the role of the tunnels of superhot gas produced by supernovae, cannot yet be answered in any unique way. The purpose of this review is to outline the problem as it faces us at the present time.

INTRODUCTION

There has accumulated in the last three decades a body of detailed information on the properties of the galactic cosmic rays as they show themselves at the present time in the solar system. From this information, we now believe, with some confidence, that cosmic rays are a permanent feature of the galactic environment, with an intensity that has not varied much over the last 10^4 to 10^9 years. Information is beginning to be available on the relative abundances and the energy spectra of the many isotopes that make up the cosmic rays. The abundances probably vary with time, reflecting the activity of nearby sources. Some cosmic-ray isotopes are collision products, some are synthesized in the neutron-rich environment before acceleration, and some are just the "natural" isotopes found in all matter. The measurements of relative abundances, and the variation of those abundances with energy, are our strongest tool for probing the origin of cosmic rays.

At the same time, there has become available considerable, but by no means complete, information on the gas and fields through which the cosmic rays move in the gaseous disk of the galaxy. The galactic nonthermal radio emission has been mapped, presumably giving a picture of the distribution of cosmic-ray electrons across the celestial sphere, and, finally, γ-ray observations are available, mapping the collisions of the cosmic-ray protons with the interstellar gas.

These observational facts and inferences have been explored with a multitude of theoretical models so that today we have an idea of the possibilities for the origin and behavior of cosmic rays in the galaxy. It is the task of the present review to sift from our heap of knowledge and interpretations those ideas and principles that seem to be basic for understanding the role played by cosmic rays in the galaxy.

Now, the complex observational and theoretical pictures of cosmic rays in the galaxy are far from complete and are therefore ambiguous. Hence, it is possible to form a summary opinion only by looking at the overall picture with a not unjaundiced eye. This review is, then, to be understood as a view of cosmic rays through tinted eyeglasses. Whenever confronted with alternatives, I choose what seems to be the simpler. The choice that I make will, therefore, not always be the most interesting choice. And I stand ready to amend an opinion whenever observational or theoretical facts suggest a simpler alternative.

I should emphasize that it is possible to put together a "plausible" picture of cosmic rays only because so many workers have had the patience, determination, and ingenuity to explore so many alternatives. It is not possible in the available time to give proper credit to all those whose efforts have made an opinion possible.

Consider, then, the circumstances in which we find cosmic rays in the galaxy. They appear to be a permanent fixture at about their present level in the solar neighborhood. Gamma-ray observations, on which others will speak at length, suggest somewhat greater and smaller cosmic-ray intensities elsewhere in the gaseous disk of the galaxy. The cosmic rays are trapped in the general galactic magnetic field, and the field is embedded in the gaseous disk. Without the weight of the interstellar gas to confine the field, the field and the cosmic rays would expand out of the galaxy and disappear. The basic point of departure for understanding cosmic rays in the galaxy is their role in the local dynamics of the galactic disk. The cosmic rays, the magnetic field, and the interstellar gas shape each other so that the propagation and containment of cosmic rays in the galaxy are inseparable from the dynamical theory of the disk.

Considering the individual cosmic-ray proton at the median energy of 10 GeV, we note that its cyclotron radius in the mean azimuthal field of 3 to 4 $\times 10^{-6}$ gauss (Hiltner, 1956; and Manchester, 1972) is 10^{13} cm. This is so small compared to the characteristic thickness 10^{21} cm (300 pc) of the gaseous disk and field that the particle may be considered tied to the local lines of force. Scattering across the field by any conceivable field irregularities (say, one scattering through a large angle every cyclotron period of 2×10^3 s) is negligible over the 10^6 to 10^8-year life of the particle in the galaxy, as are the gradient and curvature drifts of 10^3 cm/s in the observed large fluctuations in the field with scales of 30 to 150 pc (Jokipii and Lerche, 1969; and Jokipii et al., 1969). Therefore, a cosmic-ray particle is a permanent companion of the flux tube in which it is born, condemned to roam this one-dimensional space until it dies by collisions or until the tube is convected out of the galaxy.

As far as motion along the line of force is concerned, note that cosmic rays of 1 to 10 GeV are scattered principally by field variations with scales of 10^{12} to 10^{13} cm. These scales lie in the large and unknown interval between the strong fluctuations at 10^{11} cm, determined from pulsar scintillation studies, and the strong fluctuations at scales of 3×10^{18} cm and larger, observed directly with instruments on telescopes. Whether there are fluctuations in the range of 10^{12} to 10^{13} cm determines whether cosmic rays are significantly scattered back and forth along the magnetic lines of force, or whether they stream unhindered along the lines. Scattering is not necessary to understand the observed behavior of cosmic rays as far as we are able to tell. But, because it is a necessary condition for Fermi acceleration in interstellar space, the question must be settled if we are to decide the role of interstellar Fermi acceleration. The reader is referred to a recent paper by Lee and Jokipii (1976) where the problem of cosmic-ray propagation and interstellar density and field fluctuations is reviewed.

But we should not think of the propagation and containment of cosmic rays in terms of the individual particle. The individual particles do not interact directly with each other, but, nonetheless, they constitute a fluid constituent of the disk. They form a relativistic gas with a density of about $10^{-10}/\text{cm}^3$ (or $3 \times 10^{45}/\text{pc}^3$), and with a pressure, P (equal to one-third of their energy density), of about 0.5×10^{-12} dynes/cm^2. Their pressure is as large as the Reynolds stresses of the mean turbulent motion of the interstellar gas, as large as the magnetic pressure of the galactic field, and very much larger than the mean thermal pressure of the interstellar gas.

Observations of the gaseous disk of the galaxy show a mean gas density of approximately 2 hydrogen atoms/cm^3 over a thickness of 300 pc. The disk is thinner toward the center of the galaxy and considerably thicker farther out. The gas is distributed very inhomogeneously in cloud complexes separated by distances of the order of 500 pc. There is an irregular magnetic field embedded in the gas. The mean field is in the azimuthal direction around the disk (Hiltner, 1956) with a local strength of 3 to 4 $\times 10^{-6}$ gauss (Manchester, 1972). The fluctuations, ΔB, are as large as the mean field, B, with a characteristic correlation length of 10^2 pc (Jokipii and Lerche, 1969; and Jokipii et al., 1969).

The magnetic field is observed only within the dense gaseous disk of the galaxy where there is enough dust to polarize the passing starlight and enough free electrons to give a measurable Faraday rotation. Hence, we have no direct information on the lines of force as they extend outside the gaseous disk. We can say, however, that the external magnetic field of any astrophysical body tends toward the lowest energy state available to it and that is a closed configuration of the form of a dipole for a globular object like the Sun or the Earth. The closed configuration is rapidly achieved by dynamical line cutting (neutral-point annihilation). We therefore expect to find astrophysical fields to be largely closed on themselves (Parker, 1973a and 1975b; and Jokipii, 1973). In some cases, there is an active outflow of gas from the body that forces the field open. The solar wind extends the magnetic lines of force of the Sun out through the solar system; there may be a galactic wind from the nucleus of the galaxy (Burke, 1968; and Johnson and Axford, 1971) which forces open the magnetic field of the nucleus. But there is no evidence of an outflow of gas from the surface of the thin gaseous disk. We therefore suggest that the local galactic magnetic field is largely closed. Hence, most of the magnetic lines of force extending out of the disk in the local irregularities are reentrant nearby.

Altogether, then, the cosmic rays below approximately 10^{16} eV/nucleon are tied to the lines of force, and the lines have a closed topology. The cosmic rays are bottled up and are not free to escape individually from the surface of the galaxy. This view forces us to the conclusion that, if they escape at all, it must be as a consequence of the group pressure inflating the field and pushing outward from the galaxy. The 10-GeV particles escape along with the 10^4 GeV particles, etc. (Parker 1965, 1966, 1968b, 1969 and 1975.) The cosmic rays "bubble" out of the galaxy, if they escape at all (see below).

Other possibilities have been contemplated in which the lines of force of the galactic magnetic field are presumed open to the outside in some way. In that case, the cosmic rays are confined by scattering from the fluctuations in the field, their theoretical escape rate determined by whatever mean cosmic-ray age seems appropriate. Thus, for instance, if the distance to the exit is $L = 1$ kpc $= 3 \times 10^{21}$ cm and we believe that the cosmic-ray age is $t = 2 \times 10^6$ years, the scattering must reduce cosmic-ray transport along the magnetic field to the effective diffusion coefficient, $D_{\parallel} \cong L^2/t = 2 \times 10^{29}$ cm^2/s. The various options and possibilities have been thoroughly explored (see, for instance, Ramaty et al., 1970; Jokipii, 1973; and Ramaty, 1974). If cosmic rays are generated within the disk at a suitably high rate, then, there is also the possibility that the cosmic rays are scattered, and their escape limited, by the Alfven waves caused by their own rapid streaming (Wentzel, 1968 and 1969; and Kulsrud and Pearce, 1969).

The ideas invoking an open magnetic topology are faced with the problem of explaining the turbulent spectrum and the gas-density variations in just such a way that all energies from 1 to 10^7 GeV have about the same diffusion coefficient (Kulsrud and Cesarsky, 1971; Skilling, 1971; Cesarsky and Kulsrud, 1973; Skilling et al., 1974; Holmes, 1974; and Jokipii, 1976). We might expect that the more energetic particles, being fewer in number and having higher rigidity, would escape more freely along the magnetic lines of force, so that the cosmic-ray spectrum would cut off rather sharply above 10^2 or 10^3 GeV. The fact that the spectrum extends as $E^{-\alpha}$ with $\alpha \cong 2.6$ all the way to 10^7 GeV indicates that the very high energy particles are locked up in the same box as the particles at 10 GeV. Thus, we interpret the absence of a high-energy cutoff as direct evidence that the galactic magnetic field topology is closed. It remains to be seen, then, whether cosmic rays are significantly scattered as they move as individuals, or stream in bulk, along the galactic magnetic field. There is no evident theoretical need for scattering, nor are observations able to come to grips with the magnetic fluctuations over the scales 10^{12} to 10^{13} cm that are relevant for the median-energy (10 GeV) particles. It is the accumulated effects of the small-angle scattering of these magnetic fluctuations that may reduce the effective mean free path to 10^{18} to 10^{20} cm. Insofar as the individual cosmic rays are scattered as the cosmic-ray gas flows slowly along the lines of force, the theoretical treatment would presumably combine diffusion with the focusing effects of the large-scale field, as pointed out by Earl (1974a, 1974b, and 1975), to give a realistic treatment of the stochastic and ordered components of the particle motion in the stochastic lines of force of the general field.

If we are to think of cosmic rays as a hot gas inflating the gaseous disk, there are several obvious questions that come to mind, such as their source and their ultimate destination. Is the cosmic-ray gas streaming by the solar system on its way to escape from the galaxy? A relative bulk velocity, v, leads to an anisotropy in the frame of the solar system. The fractional intensity difference recorded by a detector with a fixed-energy window looking first upstream and then downstream is $\Delta I/I = 2(2 + \alpha)$ v/c for the differential energy spectrum $E^{-\alpha}$. This result can be applied to the protons (above about 500 GeV) that penetrate to the orbit of Earth without being too greatly deflected by the interplanetary magnetic field. A bulk streaming velocity of 10^2 km/s yields $\Delta I/I = 3 \times 10^{-3}$. The Earth and its daily rotation can be used to scan around the directions perpendicular to the axis of Earth. It is a difficult experimental task, but possible in principle, to detect such small intensity differences. One needs a suitably large, stable detector at a sufficient depth underground. There must be enough atmospheric information available to make suitable corrections for the height and density variations of the air overhead. It is a complicated undertaking with a long and troubled history, but there is some reason to think that the major pitfalls have been discovered and understood, so that efforts such as the Utah experiment (Bergeson et al., 1975) will soon have definite results. The work already done shows that the anisotropy is small, of the order of 10^{-3} or less. (See the summary of results in Osborne, 1975.)

There is no experiment of which I am aware that can look for $\Delta I/I$ in the direction parallel to the axis of Earth. Thus, a null result from the sidereal diurnal variation above 500 GeV proves nothing. Indeed, Jones (1970) has pointed out that whatever the variable streaming of cosmic rays in the galaxy, the single most probable result of a measurement of $\Delta I/I$ is zero. We have every right to expect that $\Delta I/I$ is not zero, however, and look forward to a positive answer.

Lacking a direct measurement of the local bulk streaming of the cosmic rays, what can we deduce about their origin and their ultimate fate? What is the source of the cosmic-ray gas that inflates the interstellar medium? The simplest assumption is that the cosmic rays are produced here in the galaxy, although it has been fashionable in some circles to argue other, more spectacular possibilities. Supernovae, flare stars, and the turbulence of the interstellar gas and field are among the obvious possible accelerators. The enormous energy (10^{51} to 10^{52} ergs) of the type II supernova, the copious supply of relativistic particles observed in the remnant after the explosion, and the large relative abundance of heavy elements within the exploding star are the circumstantial evidence on which the supernova is considered to be a major source (Ginzberg, 1958; and Ginzburg and Syrovatskii, 1964). The recent work of Schramm and Arnett (1975) on neutral current interactions indicates that enough of the heavy elements in the interior of the supernova can be blasted outward in the explosion to supply the observed heavy elements. The spinning neutron star (pulsar) left behind and the interstellar blast wave produced by the supernova may accelerate the individual nuclei to relativistic energies (Pacini, 1968; Gunn and Ostricker, 1969; Kulsrud et al., 1972; Mertz, 1974; Scott and Chevalier, 1975; and Jodogne, 1975). One of the outstanding theoretical obstacles, however, is the injection of the accelerated particles into the surrounding interstellar magnetic field. First of all, fast particles remaining for long within the expanding blast wave (the supernova remnant) are rapidly decelerated by the expansion. They must therefore leave quickly and enter the interstellar field outside the expanding remnant. But, on the other hand, it has been pointed out (Wentzel, 1968, 1969, and 1974; Kulsrud and Pearce, 1969; Tademaru, 1969; and Lee, 1972) that the bulk streaming of cosmic rays along a magnetic field is limited to a few times the Alfven speed computed in the ionized component of the thermal gas. Faster streaming generates transverse fluctuations in the magnetic field (Alfven waves) that scatter the individual cosmic-ray particles and strongly impede their flow. A single supernova must produce 10^{49} to 10^{51} ergs of relativistic particles at the time of the explosion and/or in the next thousand years or so in the active remnant (Woltjer, 1972) if one supernova every 50 years in the galaxy is to supply most of the cosmic rays. How can so many fast particles be absorbed quickly into the surrounding interstellar gas and field? It is not obvious that escape into the interstellar medium is possible (see, for instance, the discussion of Cowsik and Wilson, 1975). Hence, the possibility that there are other major sources of cosmic rays cannot be ignored. The flare stars are a popular alternative (Cowsik, 1975). They are cool subdwarfs of small mass, roughly one thousandth or less as bright as the Sun, commonly occurring throughout the galaxy. A few of them have been observed to flare every few hours with outbursts one thousand times larger than the big cosmic-ray flares on the Sun (see, for instance, Moffett, 1974). But, even if all red subdwarfs were as active as the more extreme cases, there would be barely enough total energy available. The local cosmic-ray energy density of 1.6×10^{-12} ergs/cm^3 with a nominal replacement time of 10^7 years requires an input of 0.5×10^{-26} ergs/cm^3. If there is one active flare star in each 4 pc^3 (10^{56} cm^3), then each such flare star must supply relativistic particles at a rate of 0.5×10^{30} ergs/s. This is 10^{-1} the total luminosity of the flare star. The acceleration mechanism on the flare star must be very efficient indeed. It would appear that the flare stars are a contributor, but not the major source.

The general feeling on the subject is that both flare stars and supernovae produce cosmic rays, but how much is an open question (see, for instance, Cowsik, 1975). By analogy to solar flares, we may guess that the flare star contributes heavily at the low energy end of the spectrum, below, say, 10^9 eV per nucleon. The study of isotopic abundances among cosmic rays is the principal tool for getting at these questions. The problem is complicated by the local solar modulation and by competition between the spallation and fragmentation of cosmic-ray nuclei within the source and while in transit in interstellar space. A number of authors have worked for many years conducting numerical experiments on parameterized hypothetical models of the cosmic rays and galactic field, exploring the consequences at Earth of a variety of cosmic-ray energy spectra and nuclear compositions at the sources, the distribution of sources in space, the mean cosmic-ray life or path length before arrival at Earth, the interstellar scattering mean free paths, the interstellar gas-density distributions, and, finally, the unknown modulation of the cosmic rays by the solar wind, necessary to account for the observed energy spectra and abundances of the nuclear species presently observed (see, for instance, Ramaty et al., 1970; Lingenfelter et al., 1971; and the review by Osborne, 1975). A number of preliminary suggestions are already available, but, to carry the task through to completion, the isotopic observations must be extended to more massive nuclei. Whatever the outcome of the isotopic studies, a host of possible sources, from young massive stars to old black holes, must be considered. Presumably, the sources are concentrated in the dense gaseous disk. The old idea—that there may be a strong contribution to cosmic-ray acceleration from the turbulence in the interstellar gas (Fermi, 1949 and 1954; Morrison et al., 1954; and Parker, 1955)—has surfaced again. As noted above, an interstellar energy input of the order of 10^{-26} ergs/cm^3 s to the cosmic rays is required, so that significant interstellar cosmic-ray acceleration would be a major sink of energy for the turbulence of the interstellar gas. And it would occur only if there were strong turbulence over scales of 10^{12} to 10^{13} cm.

The work on cosmic-ray propagation in the galaxy has come a long way from the early days when the concept was first pointed out (Fermi, 1949 and 1954). In those days, we thought of the field as entirely chaotic, with cosmic-ray transport a matter of random walk through space (Morrison, Olbert, and Rossi, 1954) to free escape at the "surface" of the disk. The general ordered pattern of the mean galactic field of some 3 to 4×10^{-6} gauss is now an observational fact of life (Hiltner, 1956; and Manchester, 1972). But, noting that the scattering of most cosmic-ray particles ($E \leqslant 10^{13}$ eV) across the magnetic field is completely negligible, the random walk of the magnetic lines of force (Getmantsev, 1963; Jokipii 1966; Jokipii and Parker, 1969a and 1969b; Parker, 1969; and Jones, 1971 and 1972) is the principal transport of cosmic-ray particles from the interior to the surface of the disk of the galaxy. It is the random walk of the lines of force, described by the mean-square transverse displacement, Δz, of the line per unit length, Δs, along the field that permits the cosmic rays to diffuse across the disk and escape. The correlation length, λ, for the field fluctuation, ΔB, is of the order of 100 pc and $\langle(\Delta B/B)^2\rangle^{1/2} \sim 0.5$ (Jokipii and Lerche, 1969; and Jokipii et al., 1969). Hence, in order of magnitude $\langle(\Delta Z)^2\rangle/\Delta S \sim 0.5\ \lambda$. The scale height of the disk is of the order of $\Lambda = 1.5\ \lambda$ so that a magnetic line of force wanders the distance, Λ, from the center to the "surface" of the disk in a distance, s, where

$$s\langle(\Delta z)^2\rangle/\Delta s = \Lambda^2$$

from which it follows that $s = 4.5\ \lambda = 500$ pc in order of magnitude. Thus escape follows in distances of 0.5 kpc = 1.5×10^{21} cm. A mean life of $t = 10^7$ years implies a mean streaming velocity of $u = s/t = 50$ km/s, or an anisotopy of $\Delta I/I \cong 1.5 \times 10^{-3}$.

The diffusion of cosmic-ray particles, scattered back and forth along the stochastic lines of force, has been explored in the literature under the name of "compound diffusion" (Lingenfelter et al., 1971; Allen, 1972).

It is possible to obtain information on the electron component of the cosmic rays as they progress out from their sources in the disk by looking at the nonthermal galactic radio emission (Ginzburg and Syrovatskii, 1964 and 1965).

Badhwar and Stephens (1975) have put together a self-consistent model, including hydrostatic equilibrium of the disk and the nonthermal radio emission (presumed to be from the cosmic-ray electrons in the galactic field, B). The requirement for mean hydrostatic equilibrium of the gas pressure, p, and density, ρ, the field pressure, $B^2/8\pi$, and the cosmic-ray pressure, P, in the local gravitational acceleration, g, of the galactic disk, is (Parker, 1966 and 1969)

$$\frac{d}{dz}\left(p + \frac{B^2}{8\pi} + P\right) = -\ \rho g,$$

while the nonthermal radio emission (synchroton emission) is proportional to the square of the energy of the individual electrons and to the energy density of the magnetic field (Ginzburg and Syrovatskii, 1964 and 1965). The calculations of Badhwar and Stephens (1975) lead to a model of broad extent, with the gas, field, and cosmic rays extending out 1 kpc on either side of the disk, in order to account for the observed radio emission from directions perpendicular to the plane of the disk. Webster (1975) has suggested a weaker broader halo of approximately 10-kpc extent, containing relativistic electrons with a steeper energy spectrum, based on radio data alone. The reconciliation, or the relation, of these halo models has yet to be determined.

The broad distribution of gas, field, and cosmic rays implied by this theoretical model is most interesting in view of the recent measurements of the low Be^{10} abundance and the implications for the existence of a cosmic-ray halo around the galaxy.

The recent observational determination (Garcia-Munoz et al., 1975a and 1975b) of the nearly complete absence of the spallation product, Be^{10}, has direct implications for the region of space occupied by the cosmic rays. Garcia-Munoz et al., 1975a and 1975b point out that, if interpreted in terms of the usual ideas of cosmic-ray production within the disk, followed by escape from the galaxy after penetrating 4 to 5 gm/cm^3, the very low abundance of Be^{10} indicates a low average spallation rate of the heavy nuclei. That is, the cosmic rays circulate through a volume of space in which the mean density is one-tenth or less of the mean value of 2 hydrogen atoms/cm^3 in the gaseous disk. Because the cosmic rays are observed here among the dense gases of the disk, they must spend ten times as long in some other region of much lower density ($N \lesssim 0.1$ atom/cm^3). Evidently the cosmic rays circulate freely through the disk and an extensive magnetic halo surrounding the disk to a distance of 1 kpc or more on either side. Presumably, the magnetic fields of the gaseous disk are inflated to form magnetic bubbles extending outward for 1 to 2 kpc from either surface of the disk so that the galaxy has a significant halo of magnetic field and cosmic rays (Parker, 1965, 1968b, and 1969). In view of the fundamental importance of the result, an independent direct determination in space is desirable (see, for instance, the balloon work of Preszler et al., 1975; Hagen et al., 1975; and Fisher, et al., 1976).

Now, we have learned from the development of the many parametrized models of cosmic-ray diffusion and spallation that the possibilities range all the way from the minimum cosmic-ray life of 10^5 to 10^6 years before escaping from the gaseous disk of the galaxy (just enough time to penetrate the 4 to 5 gm/cm^2 to account for the observed spallation in interstellar space and/or in the source (see, for instance, Ramaty et al., 1970; Silberberg and Tsao, 1973; Shapiro and Silberberg, 1975; and Shapiro et al., 1975) to the opposite extreme that cosmic-ray particles never escape but knock around in the disk for 10^7 to 10^8 years before losing their energy and becoming diluted with fresh particles (Rasmussen and Peters, 1975). These views have various fundamental consequences for the dynamics of the cosmic rays and the gaseous disk. First of all, the calculated production rate is profoundly affected. A life of only 10^6 years averages out to an energy input of 5×10^{-26} ergs/cm^3 s, or 1.5×10^{41} ergs/s over an estimated volume of 3×10^{66} cm^3 for the gaseous disk of the galaxy, whereas the production rate need be only 0.03 as large if the cosmic rays do not escape. Second, the high-production, short-life cosmic-ray model implies that the galactic magnetic field is rapidly inflated by the cosmic-ray gas produced in the disk, blowing magnetic bubbles out the sides of the disk at approximately 10^2 km/s (Parker, 1965, 1966, 1968b, and 1969). The cosmic rays are a major source of activity in the interstellar medium, and it would appear unlikely therefore that the interstellar turbulence could be the source of significant cosmic-ray acceleration. The tail cannot be expected to wag the dog. We would expect to find cosmic rays streaming at 1 to 2×10^2 km/s along the field in the disk, producing a local anisotropy possibly as large as $\Delta I/I = 3 \times 10^{-3}$. The dynamical limitations to cosmic-ray streaming pointed out by Wentzel and Kulsrud would come into play, so that the cosmic rays would often be strongly scattered as they move along the galactic field ($D_{\parallel} \cong 10^{29}$ cm^2/s).

On the other hand, the long-life model leads to little or no blowing of magnetic bubbles, to very little streaming of cosmic rays, to low anisotropy $\Delta I/I \sim 10^{-4}$, and to no large contribution from cosmic rays to interstellar turbulence. The activity of the interstellar gas and field would be largely a consequence of the formation, passage, and explosion of massive stars within the interstellar gas.* Significant Fermi acceleration in interstellar space (say, 0.3×10^{-26} ergs/cm^3 s) is then a real possibility in the long-life model. It needs only to be shown that the cosmic-ray particles are strongly scattered back and forth along the magnetic field by the local turbulent fluctuations.

From the purely theoretical point of view, the controlling effect is the production rate of cosmic rays within the disk of the galaxy. For a given cosmic-ray density, the life within the disk is inversely proportional to the production. So long as their strength is not negligible, the sources build up the cosmic-ray pressure until it becomes comparable to the magnetic pressure, $B^2/8\pi$. Thus, over a wide range of source strength, $P \cong B^2/8\pi$, and the cosmic-ray density is fixed by the strength of the field. Hence, we do not learn much from the observational fact that $P \cong B^2/8\pi$ (Parker, 1968b). Instead, we try to determine the age of the local cosmic rays, hoping that it represents the mean life of the cosmic rays in the disk. The age is inferred from the abundance of spallation products and the decay of those spallation products that are radioactive, such as Be^{10}. The source strength is then assumed to be inversely proportional to the estimated age.

These issues are the principal questions concerning the containment and propagation of cosmic rays in the galaxy: Are cosmic rays generated so rapidly in the disk of the galaxy that they escape in only a few times 10^6 years with considerable dynamical agitation of the magnetic fields of the disk, or are they generated slowly so that escape is negligible and they slowly die through collisions while remaining captive within the galaxy? It appears that cosmic rays circulate freely through a volume of space an order of magnitude thicker than the disk. Is that volume anything more than the magnetic bubbles extended out the side of the disk by the pressure of the cosmic rays? It should be noted that a large ($\sim 10^{-3}$) local cosmic-ray anisotropy would imply a high production rate and a short life. A measured small anisotropy (in a direction perpendicular to the axis of Earth) would imply nothing (Jones, 1970). As already noted, isotopic studies are the principal means for getting at the ages, and, hence, the source strengths. As a working hypothesis, we suppose that all abundances represent steady-state mean values when it comes to working out their implications. But it must be kept in mind that, although there is observational evidence that the mean overall cosmic-ray intensity (made up largely of protons) has not fluctuated much, we have no proof that the various spallation products do not vary (over periods of 10^4 to 10^6 years). The different energies and isotopes may be the transient products of different nearby sources.

*Incidentally, the recent observational work of Hobbs (1976) shows that, whatever the cosmic-ray life may be, the interstellar gas is heated principally by dissipation of turbulence and by the UV from hot stars (Oort and Spitzer, 1955; and Parker, 1968a), rather than by a high intensity of low-energy cosmic rays.

There is some possibility that the high-energy electrons may shed light on cosmic-ray life in the galaxy (with the usual assumption that the electrons have the same origin as the protons, of course). The point is that the very high energy electrons (10 to 10^3 GeV) lose energy rapidly by synchrotron emission, with the characteristic life diminishing with increasing particle energy. The power emitted is proportional to the square of the electron energy. Thus, the electron spectrum is depressed at high energies (relative to the source spectrum) by the synchroton losses. It has been hoped that a careful study of the spectrum might reveal the energy at which the losses become severe, giving an indication of the time the electrons have been in the galactic magnetic field since their acceleration to the energies of which they are observed. For a thorough review of the present state of knowledge of the electron component, the reader is referred to Ramaty (1974) and Meyer (1974 and 1975). The other side of this picture is the point of Ginzburg and Syrovatskii (1964 and 1965) already noted, that the synchrotron emission is observed as the principal component of the galactic nonthermal radio emission, giving us the product of the number of electrons per unit volume, their mean-square energy, and the magnetic-field energy density integrated along the line of sight. Unfortunately, from our position near the central plane of the gaseous disk, it is difficult to disentangle the contribution of relativistic electrons trapped in the strong fields of supernova remnants from the general background of the cosmic-ray electrons. The nonthermal emission from directions perpendicular to the plane of the disk is more reliably employed (see, for instance, Badhwar and Stephens, 1975) than the intense hodge-podge that is seen from the directions of low galactic latitude, along lines of sight that traverse long distances through the disk.

Finally, it should be mentioned that the most direct view of cosmic rays in the gaseous disk is provided by the γ-ray observations, which are thoroughly discussed by several other authors in this document. The γ-rays give the integral of the products of the gas density and the cosmic-ray intensity along the line of sight. Hence, unfortunately, their sensitivity falls off rapidly when we look to the galactic halo because of the small gas density there. It is difficult to separate the small halo contribution from the massive signal from the dense gaseous disk.

A lot of theoretical work remains to be done, based on the studies of magnetohydrostatic equilibrium of the cosmic rays and the gaseous disk already available (Parker, 1966, 1968a, and 1969; Lerche, 1967a and 1967b; Mouschovias, 1974; Mouschovias et al., 1974; and Badhwar and Stephens, 1975), showing the structure of the gas concentrations with the expanded field between. Appenzeller (1971) has observations of the compressed configuration of the field where it is weighed down in regions of dense gas. The full problem is not static, of course, but dynamical, because the equilibrium of the interstellar gas, field, and cosmic rays is unstable over dimensions of 500 pc along the magnetic field. The dynamical instability is the major factor in the formation of the large cloud complexes and the bulging magnetic bubbles in between. The bulges are inflated by the cosmic rays and the inflation, at whatever rate it may occur, provides the escape of cosmic rays from the disk of the galaxy. The inflated loops of field may extend 500 pc or more out from the disk, providing the halo indicated by the very low abundance of Be^{10} in the cosmic rays. Figure 1 shows a formal example of the inflated magnetic field, (Parker, 1968b) above the surface of the disk on

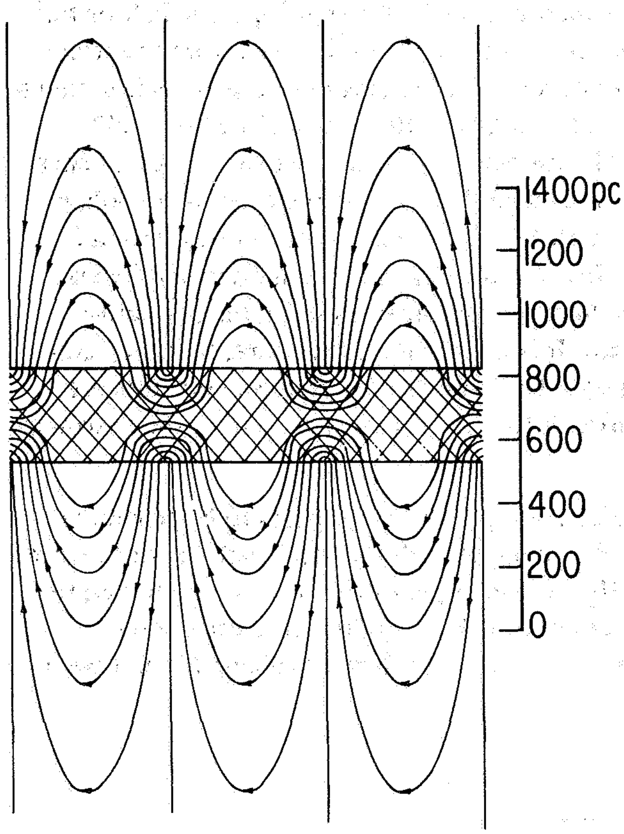

Figure 1. An idealized plot of the inflated magnetic lines of force outside the galactic disk. The gaseous disk is represented by the cross-hatched horizontal region with a thickness of 300 pc, indicated by the scale on the right-hand side. The normal component of the field is specified as $B_0 \sin k\chi$ at the surface of the disk, inflated by a cosmic-ray pressure $0.9\ (B_0^2/8\pi) \cos^2 k\chi$. The lines within the disk are drawn in a completely arbitrary form. Presumably, the massive interstellar cloud complexes are confined in the pockets of field sketched within the disk.

which the normal component of the field is specified as $B_0 \sin k\chi$ and the cosmic-ray pressure is $\epsilon (B_0^2/8\pi) \cos^2 k\chi$ with $\epsilon = 0.9$. The field outside the disk is extended by about a factor of three beyond the normal magnetostatic form in the absence of cosmic-ray pressure. Noting the neutral sheets between successive bulges and the possibility for rapid reconnection of the lines of force, it seems to us that, if the extensive (1-kpc) halo is to be accounted for by inflation by cosmic rays, then the inflation of the loops of field must proceed at a lively pace (~ 100 km/s) or the loops, with the dynamical instability (Parker, 1975) would not survive to such great distance. We suggest, then, that the simplest explanation of the absence of Be^{10} is a high cosmic-ray production rate, so that the mean dwell time in the disk is closer to 10^6 years than to 10^7. If the cosmic-ray life is, in fact, very long ($> 10^7$ years), then some other dynamical origin of an extended (1-kpc) magnetic halo must be imagined.

A variety of effects need yet to be fitted into the overall picture. The implications of extensive tunnels of very hot gas (Cox and Smith, 1975; Scott, 1975; and Jones, 1975) from supernova remnants are estimated to occupy fully one-half of interstellar space. Their properties and their consequences to the dynamics of the gaseous disk have not yet been fully explored. We should begin thinking about the problem because the enormous scale height of the hot gas (10^6 K) suggests that it plays a dynamic, rather than a static, role in the disk. The formation of the tunnels from supernova remnants to occupy one-half of the interstellar space must have a cooling effect on the cosmic rays inside and a warming effect on the cosmic rays in the interstellar medium outside. The superheated tunnel gas is tenuous ($\lesssim 10^{-2}/cm^3$) and buoyant, representing a bubble relative to the surrounding "normal" traditional two-phased interstellar medium. The tunnels rise out of the gaseous disk in characteristic times, 2×10^7 years or less, which are a little shorter than the estimated cooling time. Hence, the escaping tunnels of hot gas contribute a corona of gas and field around the gaseous disk of the galaxy. The magnetic fields in the expanded tunnels would be expected to be very weak, so that they are more likely to permit free escape than effective confinement of the cosmic-ray gas within them. It is not obvious, therefore, that they contribute to the cosmic-ray halo around the galaxy. The tunnels of supernova remnants present one more complex reason why it is so difficult to form a unique picture of the dynamical life of the cosmic-ray gas in the galaxy.

Finally, we should not fail to note that the galactic magnetic field appears to be generated by the nonuniform rotation of the gaseous disk in concert with the local cyclonic turbulence of the disk (Parker, 1971a; and Stix, 1975). Hence, the origin of the field is closely tied to the motions in the disk to which the cosmic rays may make a significant contribution. Apart from some very idealized examples (Parker, 1971b), this larger problem has not been explored at all.

REFERENCES

Allen, H. R., 1972, *Astrophys. Letters,* **12**, p. 237.

Appenzeller, I., 1971, *Astron. Astrophys.,* **12**, p. 313.

Badhwar, G. D., and S. A. Stephens, 1975, (Proc. 14th Intl. Conf. Cosmic Rays, Munich), **2**, p. 639.

Bergeson, H. E., D. E. Groom, and W. J. West, 1975, (Proc. 14th Intl. Conf. Cosmic Rays, Munich), **2**, p. 581.

Burke, J. A., 1968, *Mon. Not. Roy. Astron. Soc.,* **140**, p. 241.

Cesarsky, C. J., and R. M. Kulsrud, 1973, *Ap. J.,* **185**, p. 153.

Cowsik, R., 1975, (Proc. 14th Intl. Conf. Cosmic Rays, Munich), **11**, p. 3758.

Cowsik, R., and L. W. Wilson, 1975, (Proc. 14th Intl. Conf. Cosmic Rays, Munich), **2**, p. 475.

Cox, D. P., and B. W. Smith, 1975, *Ap. J. Letters,* **189**, p. L105.

Earl, J. A., 1974a, *Ap. J.,* **188**, p. 379.

Earl, J. A., 1974b, *Ap. J.,* **193**, p. 231.

Earl, J. A., 1975, (Proc. 14th Intl. Conf. Cosmic Rays, Munich), **5**, p. 1733.

Fermi, E., 1949, *Phys. Rev.,* **75**, p. 1169.

Fermi, E., 1954, *Ap. J.,* **119**, p. 1.

Fisher, A. J., F. A. Hagen, R. C. Maehl, J. F. Ormes, and J. F. Arens, 1976, *Ap. J.*

Garcia-Munoz, M., G. M. Mason, and J. A. Simpson, 1975a, (Proc. 14th Intl. Conf. Cosmic Rays, Munich), **1**, pp. 325, 331.

Garcia-Munoz, M., G. M. Mason, and J. A. Simpson, 1975b, *Ap. J. Letters,* **201**, p. L141.

Getmantsev, G. G., 1963, *Soviet Astron. A. J.,* **6**, p. 477.

Ginzburg, V., 1958, *Prog. in Elementary Particles and Cosmic Ray Physics,* **4**, Chap. 5., North Holland Publishing Co., Amsterdam.

Ginzburg, V. L., and S. I. Syrovatskii, 1964, *Origin of Cosmic Rays,* Pergamon Press, New York.

Ginzburg, V. L., and S. I. Syrovatskii, 1965, *Ann. Rev. Astron.,* **3**, p. 297.

Gunn, J., and J. Ostricker, 1969, *Phys. Rev. Letters,* **22**, p. 728.

Hagen, F. A., A. J. Fisher, J. F. Ormes, and J. F. Arens, 1975, (Proc. 14th Intl. Conf. Cosmic Rays, Munich), **1**, p. 361.

Hiltner, W. A., 1956, *Astrophys. J. Suppl.,* **2**, p. 389.

Hobbs, L. M., 1976, *Ap. J.,* **203**, p. 143.

Holmes, J. A., 1974, *Mon. Not. Roy. Astron. Soc.,* **166**, p. 155.

Jodogne, J. C., 1975, (Proc. 14th Intl. Cosmic Ray Conf., Munich), **2**, p. 435.

Johnson, H. E., and W. I. Axford, 1971, *Ap. J.,* **165**, p. 381.

Jokipii, J. R., 1966, *Ap. J.,* **146**, p. 480.

Jokipii, J. R., 1973, *Comments Astrophys. Space Sci.,* **5**, p. 125.

Jokipii, J. R., 1976, *Ap. J.,* in press.

Jokipii, J. R., and I. Lerche, 1969, *Ap. J.,* **157** p. 1137.

Jokipii, J. R., I. Lerche, and R. A. Schommer, 1969, *Ap. J. Letters,* **157**, p. L119.

Jokipii, J. R., and E. N. Parker, 1969a, *Ap. J.,* **155**, p. 777.

Jokipii, J. R., and E. N. Parker, 1969b, *Ap. J.,* **155**, p. 799.

Jones, E. M., 1975, *Ap. J.,* **201**, p. 377.

Jones, F. C., 1970, *Phys. Rev. Letters,* **25**, p. 1534.

Jones, F. C., 1971, *Ap. J.,* **169**, p. 477.

Jones, F. C., 1972, *Ap. J.,* **172**, p. 525.

Kulsrud, R. M., and C. Cesarsky, 1971, *Astrophys. Letters,* **8**, p. 189.

Kulsrud, R. M., J. P. Ostricker, and J. E. Gunn, 1972, *Phys. Rev. Letters,* **28**, p. 638.

Kulsrud, R., and W. Pearce, 1969, *Ap. J.,* **156**, p. 445.

Lee, M., 1972, *Ap. J.,* **178**, p. 837.

Lee, L. C., and J. R. Jokipii, 1976, *Ap. J.,* in press.

Lerche, I., 1967a, *Ap. J.,* **148**, p. 415.

Lerche, I., 1967b, *Ap. J.,* **149**, p. 553.

Lingenfelter, R. E., R. Ramaty, and L. A. Fisk, 1971, *Astrophys. Letters,* **8**, p. 93.

Manchester, R. N., 1972, *Ap. J.,* **172**, p. 43.

Mertz, L., 1974, *Astrophys. Space Sci.,* **30**, p. 43.

Meyer, P., 1974, *Phil. Trans. R. Soc. London A,* **277**, p. 349.

Meyer, P., 1975, In *Origin of Cosmic Rays*, ed. J. L. Osborne and A. W. Wolfendale, Reidel Publishing Co., Dordrecht, Holland, p. 233.

Moffett, T. J., 1974, *Ap. J. Suppl.,* **29** (273), p. 1.

Morrison, P., S. Olbert, and B. Rossi, 1954, *Phys. Rev.,* **94**, p. 440.

Mouschovias, T. Ch., 1974, *Ap. J.,* **192**, p. 37.

Mouschovias, T. Ch., F. H. Shu, and P. R. Woodward, 1974, *Astron. Astrophys.,* **33**, p. 37.

Oort, J. H., and L. Spitzer, 1955, *Ap. J.,* **121**, p. 6.

Osborne, J. L., 1975, In *Origin of Cosmic Rays,* ed. J. L. Osborne and A. W. Wolfendale, Reidel Publishing Co., Dordrecht, Holland, p. 203.

Pacini, F., 1968, *Nature,* **219**, p. 145.

Parker, E. N., 1955, *Phys. Rev.,* **99**, p. 241.

Parker, E. N., 1965, *Ap. J.,* **142**, p. 584.

Parker, E. N., 1966, *Ap. J.,* **145**, p. 811.

Parker, E. N., 1968a, *Ap. J.,* **154**, pp. 57, 875.

Parker, E. N., 1968b, *Stars and Stellar Systems,* **VII**, *Nebulae and Interstellar Matter,* ed. B. M. Middlehurst and L. H. Aller, University of Chicago Press, Chap. 14, Section 7.4.

Parker, E. N., 1969, *Space Sci. Rev.,* **9**, p. 651.

Parker, E. N., 1971a, *Ap. J.,* **163**, p. 255; **166**, p. 295.

Parker, E. N., 1971b, *Ap. J.,* **168**, p. 239.

Parker, E. N., 1973a, *Astrophys. Space Sci.,* **22**, p. 279.

Parker, E. N., 1973b, *Astrophys. Space Sci.,* **24**, p. 279.

Parker, E. N., 1975, *Ap. J.,* **202**, p. 523.

Preszler, A. M., J. C. Kish, J. A. Lezniak, G. Simpson, and W. R. Webber, 1975, (Proc. 14th Intl. Conf. Cosmic Rays, Munich), **12**, p. 4096.

Ramaty, R., 1974, In *High Energy Particles and Quanta in Astrophysics,* ed. F. B. McDonald and C. E. Fichtel, MIT Press, Cambridge, Massachusetts, Chap. III.

Ramaty, R., D. V. Reames, and R. E. Lingenfelter, 1970, *Phys. Rev. Letters,* **24**, p. 913.

Rasmussen, I. L., and B. Peters, 1975, (Proc. 14th Intl. Conf. Cosmic Rays, Munich), **12**, p. 4102.

Schramm, D. N., and W. D. Arnett, 1975, *Ap. J.,* **198**, p. 629.

Scott, J. S., 1975, *Nature,* **258**, p. 58.

Scott, J., and R. Chevalier, 1975, *Ap. J. Letters,* **197**, p. L5.

Shapiro, M. M., and R. Silberberg, 1975, *Phil. Trans. Roy. Soc. London A,* **277**, p. 317.

Shapiro, M. M., R. Silberberg, and C. H. Tsao, 1975, (Proc. 14th Intl. Conf. Cosmic Rays, Munich), **2**, p. 532.

Silberberg, R., and C. H. Tsao, 1973, *Ap. J. Suppl.*, **25**, p. 315.

Skilling, J., 1971, *Ap. J.*, **170**, p. 265.

Skilling, J., J. McIvor, and J. A. Holmes, 1974, *Mon. Not. R. Astron. Soc.*, **167**, p. 87.

Stix, M., 1975, *Astron. and Astrophys.*, **42**, p. 85.

Tademaru, E., 1969, *Ap. J.*, **158**, p. 959.

Webster, A., 1975, *Mon. Not. Roy. Astron. Soc.*, **171**, p. 243.

Wentzel, D. G., 1968, *Ap. J.*, **152**, p. 987.

Wentzel, D. G., 1969, *Ap. J.*, **157**, p. 545.

Wentzel, D. G., 1974, *Annual Rev. Astron. Astrophys.*, **12**, p. 71.

Woltjer, L., 1972, *Annual Rev. Astron. Astrophys.*, **10**, p. 129.

GAMMA RAYS AND LARGE-SCALE GALACTIC STRUCTURE

D. A. Kniffen, C. E. Fichtel, and D. J. Thompson
NASA/Goddard Space Flight Center
Greenbelt, Maryland 20771

ABSTRACT

Recent γ-ray observations have provided a new means of studying large-scale galactic structure. Many theoretical models have been developed in an attempt to explain the spatial structure in the observed emission that results from interactions of energetic cosmic rays with the interstellar gas. Bignami and Fichtel (1974) and Bignami et al. (1975) have pointed out that the peaks in the observed distribution are remarkably well-correlated with longitudes corresponding to tangential directions to known spiral-arm features. Based on theoretical and experimental arguments, they assumed that, on the scale of galactic arms, the cosmic rays are more intense where the mass of the gas to which they are coupled is greatest. Refining this model with the results of recent surveys of the interstellar gas (Gordon and Burton, 1976) as interpreted by the Simonson model (1976) of the galactic structure, a good fit to the observations is obtained whether the cosmic rays are confined to the spiral arms in the disk or are more evenly confined as in a flat halo model. A universal cosmic-ray distribution leads to a distribution that disagrees with the observations, but this interpretation is subject to the large uncertainties in the molecular hydrogen densities deduced from the observations of the 2.6-mm carbon-monoxide line.

INTRODUCTION

Gamma-ray astronomy is now emerging as an important observational technique for the study of the structure and content of our galaxy. The intensity of the radiation stands clearly above the diffuse celestial background, and the fluctuations in the spatial distribution provide important information on the dynamic conditions in the galaxy. Furthermore, the highly penetrating nature of the γ-radiation makes it a valuable probe across the most dense regions of interstellar space without the uncertainties introduced when absorption corrections are required.

The question of the origin of the galactic-plane emission has been the object of intensive study since the first clearly positive observation of galactic γ-rays by Kraushaar et al. (1972) which indicated a general galactic disk enhancement with a peak intensity toward the galactic center. It has been recognized for some time (Pollack and Fazio, 1963; and Stecker, 1971) that cosmic rays in the galaxy interact with the interstellar gas, leading to high energy γ-rays. Kraushaar et al. (1972) pointed out that the observations were not consistent with a uniform cosmic-ray distribution.

Strong et al. (1973) assumed that the cosmic-ray density has a distribution which increases smoothly toward the galactic center. Using the galactic magnetic field model of Thielheim and Langhoff (1968), they developed a model in which the cosmic rays were assumed to vary proportionally with the magnetic field to the first and second powers. Although the model failed to produce some of the detail in the distribution, it was the first to assume a variable cosmic-ray intensity, and it gave improved results over previous models. Many attempts have subsequently been made to develop models which yield the longitude distribution of γ-radiation above 100 MeV observed by SAS-2. With the greater sensitivity and the improved spectral and spatial resolutions available with the SAS-2 observations (Fichtel et al., 1975) and with the recent radio surveys of interstellar atomic and molecular hydrogen densities (Burton et al., 1975; and Gordon and Burton, 1976), it is possible to study the details of the conditions in the emission region.

DEVELOPMENT OF THEORETICAL MODELS

Kniffen et al. (1973) suggested that the large intensity increases in the longitude distribution of γ-radiation above 100 MeV over a broad 70 to 90° galactic interval toward the galactic center are possibly due predominantly to radiation from galactic features, especially from the spiral-arm segments.

Following the initial report of the SAS-2 galactic γ-ray observations, several theoretical models were developed in an attempt to explain the details of the spatial distribution. Bignami and Fichtel (1974) proposed that the cosmic rays were enhanced where the interstellar gas to which the cosmic rays are coupled is more dense. Because the production of γ-rays is proportional to the product of the cosmic-ray intensity and gas density, the resulting γ-ray emission tends to be higher within the galactic spiral arms, with the longitude distribution showing an overall enhancement toward the central galactic region with peaks in the directions tangential to the spiral arms.

An approach similar to that of Strong et al. (1973) has been taken by Schlickeiser and Thielheim (1974a and 1974b) and Thielheim (1975). They also note that the cosmic rays should be dynamically coupled to some portion of the matter through galactic fields. Assuming a power-law dependence of the cosmic-ray interstellar-gas density product on the magnetic-field strength, they determine the relationship that gives the best fit to the γ-ray distribution. Using the spiral shaped galactic magnetic-field model of Thielheim and Langhoff (1968), reasonable agreement with the observations is obtained by assuming a third- to fourth-power dependence of this product on the magnetic field.

Paul et al. (1974 and 1976) have used the high-energy γ-ray and nonthermal radio observations of M31 to deduce the cosmic-ray distribution and find it consistent with the assumption of proportionality with the interstellar-gas density. The magnetic-field strength and gas densities obtained are in agreement with other estimates of these parameters.

Stecker et al. (1975) have used the distribution of molecular hydrogen inferred from the carbon-monoxide observations of Scoville and Solomon (1975). They determine that the best agreement to the γ-ray distribution is obtained with cosmic rays proportional to the 0.3-power of the gas density. As an alternate approach, Stecker (1975) has assumed that the supernova distribution obtained by Kodaira (1974) is representative of the galactic cosmic-ray distribution, and, again, using the carbon-monoxide observations, obtains a good fit to the observations. However, this interpretation is subject to the experimental uncertainties in the observed interstellar-gas and γ-ray distributions and conversion of these observations to galactocentric radial distributions, as well as to the uncertainties in the determination of supernova remnant distributions (Ilovaisky and Lequeux, 1972; Kodaira, 1974; and Clark and Caswell, 1976). A significant contribution from the inverse Compton production of high-energy γ-rays on the enhanced starlight density at the galactic center is required to produce the observed intensities in the 0 to 30° galactic longitude range for both of these models. Because galactic-plane surveys do not yet exist for the southern hemisphere, this theory is developed only for the 0 to 180° longitude range and cannot yet speak to the 180 to 360° range where the evidence of spiral structure is most pronounced in the γ-ray distribution. Fuchs et al. (1975) have performed an analysis similar to that of Stecker et al. (1975) with different estimates of the atomic and molecular hydrogen and reach the conclusion that no power of the cosmic-ray/gas-density relationship gives a particularly good fit to the observations.

The resolution of the open questions on the distribution and relative influence of the interstellar hydrogen, especially the molecular component where the values are obtained from the rather uncertain interpretation of the 2.6-mm line of carbon monoxide, and the form of the coupling of the cosmic rays to the various gas components must await more and better observations both in radio and γ-ray astronomy. In addition, the resolution of the question of the contribution of discrete sources to the γ-ray distribution depends on γ-ray observations with better angular resolution.

This brief summary of some of the models currently being used to explain the observed distribution of high-energy γ-rays is not intended to be a complete review, but to set the background for a more complete discussion of the model of Bignami et al. (1975) and Fichtel et al. (1976) for explaining the observed distribution of high-energy galactic γ-rays and the importance of making observations in the medium-energy (8- to 50-MeV) γ-ray energy range.

THE MODEL

In this section, a model is developed for the emission of γ-radiation from the galactic disk. To introduce the model, the original work of Bignami and Fichtel (1974) and Bignami et al. (1975) for explaining the observed spatial distribution of galactic γ-radiation above 100 MeV is briefly discussed. The importance of making observations at medium γ-ray energies for studying the galactic cosmic-ray electron distribution and its relationship to these concepts will be discussed. Finally, the most recent survey of the interstellar gas densities is used to update the calculations.

As already discussed, Bignami and Fichtel (1974) proposed a model that assumed that the cosmic rays were proportional to the interstellar gas to which they are coupled. Assuming that the cosmic rays and magnetic fields are galactic in nature, this hypothesis is supported by the following considerations. Bierman and Davis (1960) and Parker (1966) have shown in more detail that the expansive pressures of the magnetic fields, the kinetic motion of matter, and the cosmic rays can be balanced only by the gravitational attraction of the matter. In particular, the only matter that is relevant to the portion of the expansive pressure due to the cosmic rays and magnetic fields is that through which the magnetic fields penetrate. Moreover, the galactic cosmic-ray energy density cannot substantially exceed that of the magnetic fields, or the cosmic-ray pressure will push a bulge into the fields, ultimately allowing the cosmic rays to escape. Locally, the energy density in each of the expansive pressures discussed above appears to be approximately the same, and the total of the three is about equal to that allowed by the gravitational attraction of the gas. This suggests that the cosmic-ray density may generally be as large as would be expected under quasi-equilibrium conditions. This concept is given some theoretical support by the calculated slow diffusion rate of cosmic rays (Parker, 1969; Lee, 1972; and Wentzel, 1974).

Based on these concepts and the trial assumption that cosmic rays are coupled to the interstellar gas on the scale of galactic arms, Bignami and Fichtel (1974) and Bignami et al. (1975) calculated the expected longitude distribution of the γ-rays with energies above 100 MeV principally from the production of γ-rays by the decay of neutral pions produced in cosmic-ray/gas collisions. Bignami et al. (1975) have pointed out that the enhancements in the γ-ray longitude distribution seen by SAS-2 at ℓ values of about 35°, 0°, 345°, 330°, and 315° (Fichtel et al., 1975) are remarkably well-correlated with the galactic longitude directions tangent to the major spiral-arm features in Simonson's model (1976) of galactic structure. Shown in figure 1, this model is based on the density-wave theory with an arm-to-interarm contrast of about 3 to 1. The enhanced γ-ray intensities seem to be correlated with the directions of the Scutum (35°), 4 kpc (345°), Norma (330°), and, again, the Scutum (315°) arm. The strong correlation with these features led Bignami et al. (1975) to adopt a model for the total galactic-gas distribution based on 21-cm observations of neutral atomic hydrogen as interpreted by the Simonson model (1976). The γ-ray intensity is then determined by the expression

$$\Phi(E_\gamma, \ell) = \frac{1}{4\pi}\int S(E_\gamma)\, g(r, \ell, b)\, N(r, \ell, b)\, dr db$$

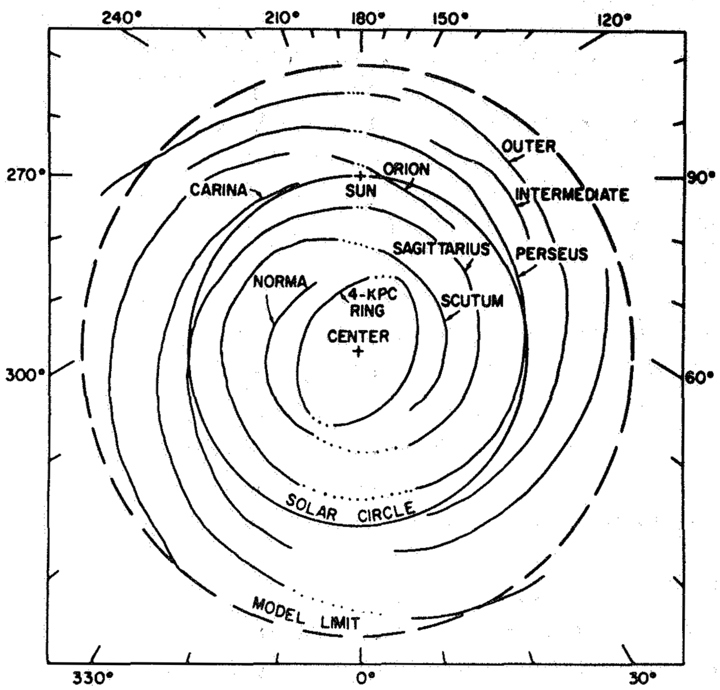

Figure 1. A smoothed spatial diagram of the ridges of the gas density deduced from 21-cm measurements of HI and the density wave theory (Simonson, 1976).

where $S(E_\gamma)$ is the local source function for the production of γ-rays of energy, E_γ. Above 100 MeV, $S(E_\gamma)$ is dominated by the decay of neutral pions formed in collisions of the cosmic rays with the interstellar gas whose total density is $N(r, \ell, b)$. The expression $g(r, \ell, b)$ takes into consideration the spatial dependence of the source function due to the variation of the cosmic-ray density. r is the radial distance from the Sun, and ℓ and b are galactic longitude and latitude. As a trial assumption, based on the arguments given above, a linear dependence on the gas density was assumed.

In the model of Bignami et al. (1975), it is assumed that the spiral structure is common to both the atomic and molecular hydrogen. Although the question of the degree of spiral structure in our galaxy is still an open question, recent studies (Georgelin and Georgelin, 1976; and Clark and Caswell, 1976) give strong new evidence for a spiral structure in the distribution of HI, HII, and supernova remnants; hence, the assumption of a common distribution for HI and H_2 seems reasonable. A density of molecular hydrogen equal to that of the atomic hydrogen (Spitzer et al., 1973; and Jenkins and Savage, 1974) as observed locally is assumed throughout the inner galaxy with a 40-percent contribution beyond the solar cycle. The resulting calculation reproduces the essential features of the distribution with a direct calculation involving no normalization.

The discussion to this point has been based on the production of galactic γ-rays above 100 MeV. Fichtel et al. (1976) have pointed out the significant new information obtainable from observations at somewhat lower energies. In the 10- to 30-MeV energy range, additional important production mechanisms include bremsstrahlung production by energetic cosmic-ray electrons traversing the interstellar gas, Compton emission of cosmic-ray electrons colliding with interstellar photons, and the synchrotron emission of electrons interacting with the galactic magnetic fields. "Local" source functions for each of these mechanisms for the production of medium (10- to 30-MeV) and high (> 100-MeV) γ-radiation are given in table 1. The bremsstrahlung source function is calculated, using the cross sections of Koch and Motz (1959) integrated over the interstellar spectrum deduced by Daugherty et al. (1975) and the secondary electron spectrum calculated by Ramaty (1974). The density of higher Z elements in the interstellar gas is more important in this case because of the Z(Z+1) dependence on charge. This increases the production rate by a factor of 0.55. The Compton and synchrotron cross sections are given by Ginzburg and Syrovatskii (1964). The pion decay source mechanism is taken from the work of Stecker (1971).

Table 1
Source Functions in Solar Vicinity

Source Mechanism	Value of Source Function ($cm^{-3}\ s^{-1}$)	
	10 to 30 MeV	> 100 MeV
Neutral pion decay*	6.5×10^{-27}	13.0×10^{-26}
Electron bremsstrahlung*	1.2×10^{-25}	3.5×10^{-26}
Compton scattering (starlight)	0.6×10^{-26}	0.2×10^{-26}
Compton scattering (3 K)	1.0×10^{-26}	0.2×10^{-26}
Synchrotron radiation	1.0×10^{-30}	0.2×10^{-30}

* Assuming 1.05 hydrogen nuclei/cm^3 locally in the galaxy, a helium-to-hydrogen ratio of 0.1, and heavy nuclei-to-hydrogen ratio of 0.01: Electron spectrum–$J(E_e) = (6.8 \times 10^{-3})\ E_e^{-1.8}$, $E_e \leq$ 2 GeV; $J(E_e) = (1.4 \times 10^{-3})\ E_e^{-2.8}$, $E_e > 2$ GeV. Photon energy densities–(starlight) $\simeq 0.45$ eV/cm^3, (3 K) $\simeq 0.25$ eV/cm^3.

Table 1 clearly shows the shift from a nucleonic mechanism at higher energies to an electron mechanism in the medium-energy range. However, the cosmic-ray/gas interactions dominate over other processes in all energy ranges for regions, except where the starlight photon/inter-interstellar-gas-density ratio, $N_{ph}(r, \ell, b)/N(r, \ell, b)$, is much larger than its local value. This condition is expected to exist throughout the galaxy, except possibly at the center. Because there is no direct evidence pertaining to the photon density in the region of the galactic center, this possibility remains an open question. The 3 K universal blackbody radiation is a source of Compton-produced γ-radiation, but this contribution is only a significant γ-ray producer where the interstellar-gas density is much lower than it is locally.

The γ-ray intensity applicable to this more general case is given by

$$\Phi(E_\gamma, \ell) = \frac{1}{4\pi}\int drdb \; [S_{\gamma n}(E_\gamma, r = 0) g(r, \ell, b) \frac{N(r,\ell,b)}{N(r=0)} + S_{\gamma e_p}(E_\gamma, r, \ell, b) + S_{\gamma e_s}(E_\gamma, r, \ell, b)] \; . \tag{1}$$

$S_{\gamma n}$ represents the γ-rays created per second by the decay of pions produced in interactions of nucleonic cosmic rays (with the intensity and spectral distribution in the solar vicinity) with the interstellar gas. $S_{\gamma_{e_p}}$ and $S_{\gamma_{e_s}}$ are similar functions for primary and secondary cosmic-ray electrons, respectively. Fichtel et al. (1976) have shown that the primary cosmic-ray electrons contribute to the γ-ray production in proportion to N^2 times a function which decreases the strength of the dependence to some degree. At the same time, the secondary cosmic-ray electrons contribute as N^3 times a term which somewhat decreases the strength of the dependence. Hence, the secondaries become somewhat more significant in high-density regions, but remain a minority contribution within the range of densities considered here.

As in the nuclear cosmic-ray case, the electron contribution to the γ-radiation from a specific direction can be calculated by performing the appropriate integral of the cosmic-ray/gas-density product for a given galactic longitude. The calculated 10 to 30 MeV emission gives a longitude distribution similar, although not exactly the same as, the high-energy distribution. The outstanding feature of the resulting emission can be seen from the spectral distribution for the direction $\ell = 335°$, $b = 0°$ shown in figure 2 taken from Fichtel et al. (1976). This calculation uses the model of Bignami et al. (1975), although the basic features of the spectrum are not very model-dependent. The dramatic shift from the bremsstrahlung mechanism at lower energies to the pion decay mechanism at higher energies is evident. Thus, comparing the longitude distribution of medium-energy γ-ray observations with those at higher energies provides a test of the hypothesis that cosmic-ray electrons are predominantly primary in origin and are produced in the same sources and in the same proportion as the nucleonic component.

There are very few experimental data with which to compare the medium- to high-energy γ-ray emission over the galaxy. A comparison of the Share et al. (1974) observations of the galactic center with those of SAS-2 (Fichtel et al., 1975) tend to confirm the spectral shape shown in figure 2. A comparison of high-energy γ-ray observations with radio observations of synchrotron emission are inconclusive because of the difficulty of interpretation due to the lack of a detailed knowledge of the interstellar fields.

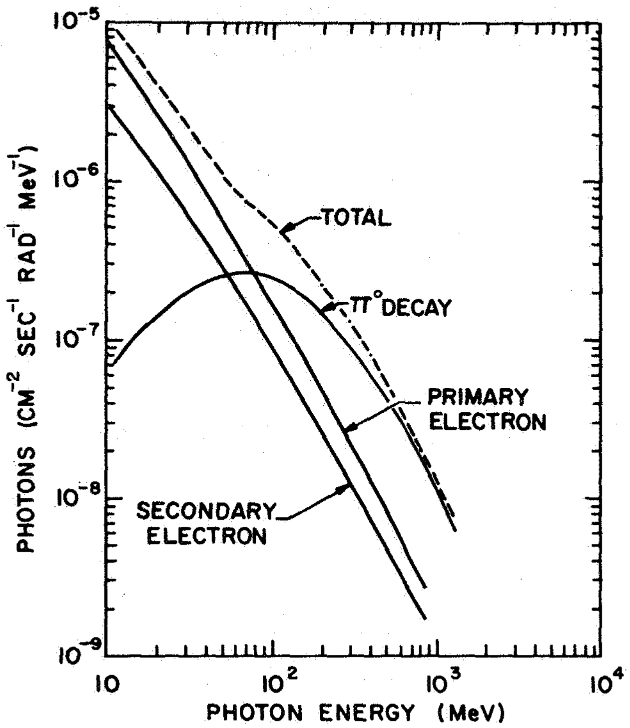

Figure 2. Expected γ-ray spectrum for $\ell = 335°$, $b = 0°$. Dashed line includes total of contributions from cosmic-ray/interstellar-gas interactions and bremsstrahlung emission from both primary and secondary electrons. This spectrum should be typical except near the galactic center where a substantial Compton component may be present.

Rasmussen and Peters (1975) have recently reexamined the closed-galaxy model for cosmic rays and shown that, under certain assumptions, it can explain the observed nuclear composition and flux of cosmic rays near the Earth. One interesting prediction of this model, as noted by Ramaty and Westergaard (1976), is that the cosmic-ray electron bremsstrahlung would be larger relative to the cosmic-ray nucleon π^{o} γ-ray flux than in the more currently popular model discussed here wherein there is significant cosmic-ray leakage from the galaxy. An accurately measured γ-ray energy spectrum can clearly help to resolve the question of whether this alternate theory is correct.

INTERSTELLAR GAS DISTRIBUTION

A crucial input to any model of galactic γ-ray production due to cosmic-ray interactions is the distribution of the interstellar gas. The most recent large-scale galactic survey of the 21-cm line of atomic hydrogen of which the authors are aware is the work of Burton (1976) and Gordon and Burton (1976). Recent surveys of the 2.6-mm line of carbon monoxide from which the densities of molecular hydrogen are inferred include those of Scoville and Solomon (1975), Burton et al. (1975), and Gordon and Burton (1976). The limited data on disk thicknesses indicate that the molecular hydrogen with a scale height of about 50 pc is apparently more closely confined to the disk (Burton and Gordon, 1976) than is the neutral atomic hydrogen which has a scale height of 120 pc inside the solar circle, increasing linearly beyond

Sun to about twice this value at about 15 kpc (Baker and Burton, 1975). These scale heights somewhat reduce the dominance of the molecular hydrogen at galactocentric radii observed in the surveys. Unfortunately, these surveys do not cover the entire galactic plane, because the observations were made from the northern hemisphere. Hence, any model attempting to explain the γ-ray emission over the entire plane from these data must necessarily infer the densities for the galactic longitude region from 180 to 360°. Furthermore, the densities of molecular hydrogen depend on a rather uncertain evaluation of the CO/H_2 ratio in interstellar space.

The model of Bignami et al. (1975) has been applied to these recent observations of the interstellar constituents. The data have been interpreted in terms of the Simonson model of galactic structure (1976). The arm densities are estimated by modulating the radial distribution of both atomic and molecular hydrogen given by Gordon and Burton (1976). The modulation provides a 3-to-1 arm-to-interarm contrast with a peak at the galactocentric radius of the arm and with an average value consistent with the radial distributions obtained from the surveys. For the portions of the plane where observations ($270 \leqslant \ell \leqslant 360$) do not exist, the densities in the extensions of a given arm were reduced by 20 percent to reflect the larger galactocentric distances. The height dependence of each constituent is taken to be a gaussian with the scale heights given by Baker and Burton (1975) and Burton and Gordon (1976). As before, the cosmic rays were assumed to be coupled linearly to the total gas density with a scale height similar to that of the atomic hydrogen. The contributions to the galactic γ-ray distribution were calculated in the same manner as described before.

Figure 3 indicates the γ-ray distribution calculated for this model. As in the previous model, most of the major features of the observed distribution are reproduced with an excellent intensity fit for most cases. The success of the model in reproducing the γ-ray distribution for the portion of the plane where the gas densities are observed indicates the validity of the reasonable assumption of a linear coupling between the cosmic rays and the interstellar gas. For comparison, figure 4 indicates the distribution expected for a thick, or fat, "disk" model of the galactic cosmic rays in which the cosmic rays are still confined by the galactic magnetic fields anchored in the spiral arms but have a scale height, 500 pc, much greater than that of the gas. Within the experimental uncertainties, an equally good fit is obtained to the observed γ-ray distribution.

Figure 5 indicates the γ-ray longitude distribution expected for a model in which the cosmic rays are constant throughout the galaxy with a value equal to that observed near the Sun. Clearly, this distribution is inconsistent with the SAS-2 observations, and would seem to offer evidence against the universality of cosmic rays. Unfortunately, the uncertainty in the measured interstellar molecular hydrogen densities weakens this interpretation.

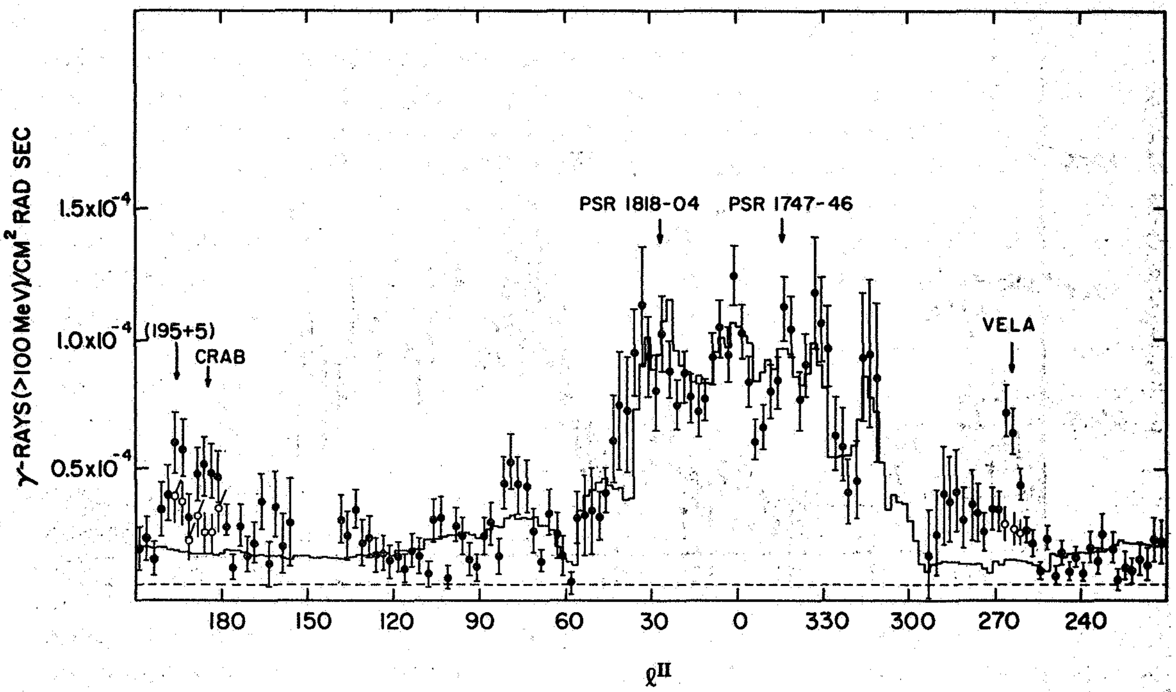

Figure 3. The solid line represents the longitude distribution of the calculated γ-ray emission above 100 MeV summed from -10 to +10° in galactic latitude. The distribution obtained by applying the model of Bignami et al. (1975) to the recent HI and H_2 distributions of Gordon and Burton (1976) as interpreted by the Simonson model (1976) of galactic structure. The cosmic rays are assumed to have the same scale heights as the HI. The SAS-2 data are shown for comparison. Open circles represent the residual intensities with known point-source contributions removed. The low predicted model intensities in the longitude range from 250 to 290° result from the gap in the Carina arm shown in figure 1.

CONCLUSION

Gamma-ray astronomy is now beginning to provide a new look at the galactic structure and the distribution of cosmic rays, both electrons and nucleons, within the galaxy. The observations are consistent with a galactic spiral-arm model in which the cosmic rays are linearly coupled to the interstellar gas on the scale of the spiral arms. The agreement between the predictions of the model and the observations for regions of the plane where both 21-cm and 2.6-mm CO surveys exist emphasizes the need to extend these observations to include the entire plane. Future γ-ray observations with more sensitivity and better angular resolutions, combined with these radio surveys, should shed new light on the distribution of cosmic rays, the nature of the galaxy, and the location and intensity of the spiral arms.

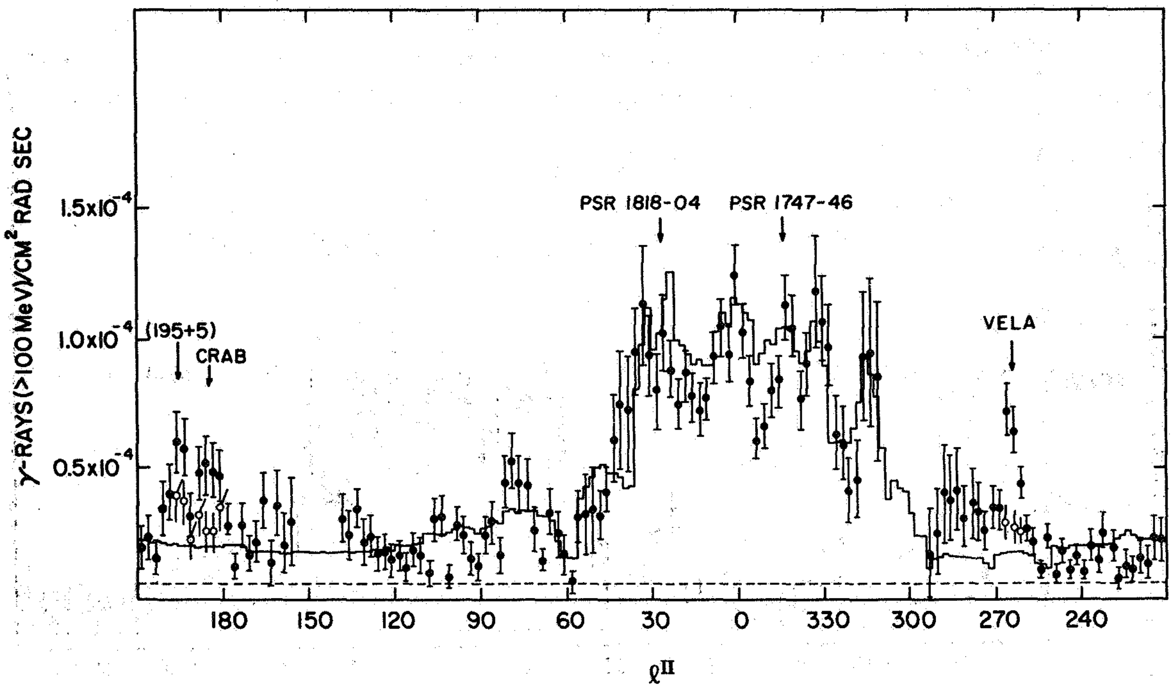

Figure 4. Same as figure 3 with a thick "disk" model for the cosmic rays. A scale height of 500 pc is assumed.

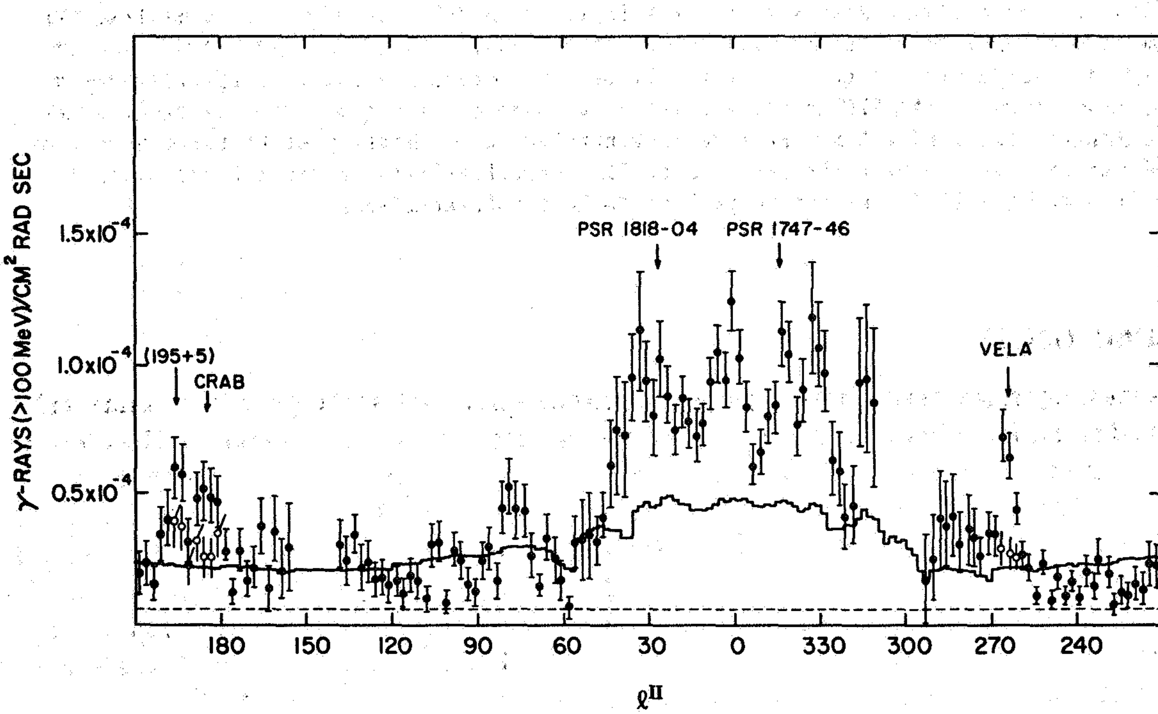

Figure 5. Same as figure 4 for a constant cosmic-ray model with an intensity as measured near the Sun.

REFERENCES

Baker, P. L., and W. B. Burton, 1975, *Ap. J.*, **198**, p. 281.

Biermann, L., and L. Davis, 1960, *Zs. F. Ap.*, **51**, p. 19.

Bignami, G. F., and C. E. Fichtel, 1974, *Ap. J. Letters*, **189**, p. L65.

Bignami, G. F., C. E. Fichtel, D. A. Kniffen, and D. J. Thompson, 1975, *Ap. J.*, **199**, p. 54.

Burton, W. B., 1976, to be published.

Burton, W. B., M. A. Gordon, T. M. Bania, and F. J. Lockman, 1975, *Ap. J.*, **202**, p. 30.

Burton, W. B., and M. A. Gordon, 1976, *Ap. J. Letters*, **207**, p. L185.

Clark, D. H., and J. L. Caswell, 1976, *Mon. Not. R. Astr. Soc.*, **174**, p. 267.

Daugherty, J. K., R. C. Hartman, and P. J. Schmidt, 1975, *Ap. J.*, **198**, p. 493.

Fichtel, C. E., R. C. Hartman, D. A. Kniffen, D. J. Thompson, G. F. Bignami, H. Ögelman, M. Özel, and T. Tümer, 1975, *Ap. J.*, **198**, p. 163.

Fichtel, C. E., D. A. Kniffen, D. J. Thompson, G. F. Bignami, and C. Y. Cheung, 1976, *Ap. J.*, in press.

Fuchs, B., R. Schlickeiser, and K. O. Theilheim, 1975, (Proc. 14th Intl. Cos. Ray Conf., Munich), **1**, p. 83.

Georgelin, Y. M., and Y. P. Georgelin, 1976, *Astron. and Astrophys.*, **49**, p. 57.

Ginzburg, V. L., and S. I. Syrovatskii, 1964, *The Origin of Cosmic Rays*, Pergaman Press, Oxford.

Gordon, M. A., and W. B. Burton, 1976, *Ap. J.*, to be published.

Ilovaisky, A., and J. Lequeux, 1972, *Astron. and Astrophys.*, **20**, p. 347.

Jenkins, E. B., and B. D. Savage, 1974, *Ap. J.*, **187**, p. 243.

Kniffen, D. A., R. C. Hartman, D. J. Thompson, and C. E. Fichtel, 1973, *Ap. J. Letters*, **186**, p. L105.

Koch, M. W., and J. W. Motz, 1959, *Rev. Mod. Phys.*, **31**, p. 920.

Kodaira, K., 1974, *Pub. Astr. Soc. Japan*, **26**, p. 255.

Kraushaar, W. L., G. W. Clark, G. P. Garmire, R. Borken, P. Higbie, V. Leong, and T. Thorsos, 1972, *Ap. J.*, **177**, p. 341.

Lee, M. A., 1972, *Ap. J.*, **183**, p. 837.

Parker, E. N., 1966, *Ap. J.*, **145**, p. 811.

Parker, E. N., 1969, *Space Science Revi.*, **9**, p. 654.

Paul, J., M. Cassé, and C. J. Césarsky, 1974, (Proc. 9th ESLAB Symp., ESRO SP-106), p. 246.

Paul, J., M. Cassé, and C. J. Césarsky, 1976, *Ap. J.*, **207**, p. 62.

Pollack, J. B., and G. G. Fazio, 1963, *Phys. Rev.*, **131**, p. 2684.

Ramaty, R., 1974, *High Energy Particles and Quanta in Astrophysics*, ed. F. B. McDonald and C. E. Fichtel, MIT Press, Cambridge, Chap. III.

Ramaty, R., and N. J. Westergaard, 1976, "Electrons in a Closed Galaxy Model of Cosmic Rays," *Astr. and Sp. Science*, in press.

Rasmussen, I. L., and B. Peters, 1975, *Nature*, **258**, p. 412.

Reames, D. V., 1974, *High Energy Particles and Quanta in Astrophysics*, ed. F. B. McDonald and C. E. Fichtel, MIT Press, Cambridge, Chap. II.

Schlickeiser, R., and K. O. Thielheim, 1974a, *Physics Letters*, **53B**, p. 369.

Schlickeiser, R., and K. O. Thielheim, 1974b, *Astron. and Astrophys.*, **34**, p. 167.

Scoville, N. Z., and P. M. Solomon, 1975, *Ap. J. Letters*, **199**, p. L105.

Share, G. H., R. L. Kinzer, and N. Seeman, 1974, *Ap. J.*, **187**, p. 45.

Simonson, S. C., III, 1976, *Astron. and Astrophys.*, **46**, p. 261.

Spitzer, L., J. F. Drake, E. B. Jenkins, D. C. Morton, J. B. Rogerson, and D. York, 1973, *Ap. J. Letters*, **181**, p. L116.

Stecker, F. W., 1971, *Cosmic Gamma Rays*, Mono, Baltimore.

Stecker, F. W., 1975, *Phys. Rev. Letters*, **35**, p. 188.

Stecker, F. W., P. M. Solomon, N. W. Scoville, and C. E. Ryter, 1975, *Ap. J.*, **201**, p. 90.

Strong, A. W., J. Wdowczyk, and A. W. Wolfendale, 1973, ed. F. W. Stecker and J. I. Trombka, U.S. Government Printing Office, Washington, p. 259.

Thielheim, K. O., 1975, *Origin of Cosmic Rays*, ed. J. L. Osborne and A. W. Wolfendale, (Dordrecht-Holland, Reidel Pub. Co.), p. 165.

Thielheim, K. O., and W. Langhoff, 1968, *J. Phys. A.*, (Proc. Phys. Soc.) Ser. 2, **1**, p. 694.

Wentzel, D. G., 1974, *Ann. Rev. of Ast. and Astr.*, **12**, p. 71.

GAMMA RAYS, COSMIC RAYS, AND GALACTIC STRUCTURE

F. W. Stecker
Theoretical Studies Group
Goddard Space Flight Center
Greenbelt, Maryland 20771

ABSTRACT

The relation of the recent SAS-2 observations of galactic γ-rays to the large-scale distribution of cosmic rays and interstellar gas in the galaxy is reviewed and reexamined. Beginning with a discussion of production rates, the case for π^o-decay being the predominant production mechanism in the galactic disk above 100 MeV is reestablished, and it is also pointed out that Compton γ-rays can be a significant source near $\ell = 0°$. To facilitate discussion, the concepts of four distinct galactic regions are defined; namely, the nebulodisk, the ectodisk, the radiodisk, and the exodisk. Bremsstrahlung and π^o-decay γ-rays are associated with the first two (primarily, the first) regions and Compton γ-rays and synchrotron radiation are associated with the latter two regions. On a large scale, the cosmic rays, interstellar gas (primarily, H_2 clouds in the inner galaxy), and γ-ray emissivity all peak in a region between 5 and 6 kpc from the galactic center. This correlation is related to correlation with other Population I phenomena and is discussed in terms of the density-wave concept of galactic structure. The singular nature of the HI distribution has led to the concept of Population 0. The deduced cosmic-ray distribution appears to follow the supernova remnant and pulsar distribution in the galaxy. This fact, together with the falloff of cosmic rays in the outer galaxy, favors a galactic origin theory for most cosmic rays.

Correlations with arm features do not appear to be evident at longitudes $0° \leqslant \ell \leqslant 180°$. Between 180 and 360°, some evidence for correlation with arm features may or may not exist but, arguments against confinement of cosmic rays in spiral arms (with $I_{CR} \propto n_{gas}$) are given on the basis of γ-ray evidence, lifetime of cosmic rays, isotropy, etc. The galactic γ-ray and nonthermal radio distribution are compared with similarities and differences noted. Finally, the contribution of high-latitude γ-rays to the observed cosmic background is discussed, and this contribution is shown to reasonably account for the observed spectrum of high-latitude γ-rays between 35 and 200 MeV.

INTRODUCTION

The pioneering work of Kraushaar, et al. (1972) with their OSO-3 satellite experiment showed that the Milky Way dominates the sky at γ-ray wavelengths and that the galactic γ-radiation is much more intense in directions toward the galactic center than away from it. With the advent of the successful SAS-2 satellite detector (Fichtel et al., 1975), we have our sharpest view yet of the galaxy in γ-rays. In addition, new data from the European COS-B satellite are now becoming available. Although we still do not have many of the answers we want regarding galactic γ-rays, we are now in a position to allow us to start asking questions about what γ-ray astronomy tells us about the galaxy and to begin to answer these questions in a cautious way. In order to find plausible answers, we must consider the new information provided by the γ-ray observations, together with related information from other branches of astronomy. I will attempt here a review and reexamination of some of these questions in order to basically clarify some of the answers.

DATA

We start with a summary of the general features of the SAS-2 observations, which are as follows:

1. On a large scale, the cosmic γ-ray radiation can be considered as consisting of two components; there is a general cosmic background radiation coming from all directions that may be cosmological in origin (Stecker, 1971 and 1975a; Stecker et al., 1971) and also a bright band of radiation coinciding with the galactic plane or Milky Way that is both much more intense and harder, relative to the background components.

2. The galactic γ-radiation is most intense in the region within ±40° from the galactic center where it is almost an order of magnitude stronger than in directions away from the galactic center.

3. Two young nearby pulsars; namely, the Vela pulsar and the Crab Nebula pulsar (NP0532) stand out strongly in the observations at galactic longitudes 264 and 185°, respectively. In addition, another γ-ray source, as yet unidentified, has been reported at 195° longitude (Kniffen et al., 1975).*

4. There are indications of more fine-scale structure in the observations, possibly due to such causes as: (a) more distant discrete sources such as pulsars, (b) "hot spots" due to supernova remnants and gas clouds, and (c) possible general correlations due to spiral structure.

*Evidence for γ-ray emission from Cygnus X-3 and two new pulsars, PSR 1747-46 and PSR 1818-04, has now been reported by the SAS-2 group (see Hartman, et al., these proceedings).

In order to arrive at an understanding of these observations, we must first plausibly establish what the predominant mechanism is that produces the observed galactic γ-rays. In addition to the production of γ-rays in discrete galactic objects such as pulsars, there are three main mechanisms by which high-energy (greater than 100 MeV) radiation is produced by high-energy interactions involving cosmic rays in interstellar space. These processes, which produce what may be called "diffuse galactic γ-rays," are: (a) the decay of π° mesons produced by interactions of cosmic-ray nucleons with interstellar-gas nuclei, (b) the bremsstrahlung radiation produced by cosmic-ray electrons interacting in the Coulomb fields of nuclei of interstellar-gas atoms, and (c) Compton interactions between cosmic-ray electrons and low-energy photons in interstellar space.

PRODUCTION MECHANISMS AND SPECTRA

For the γ-ray region above 100 MeV, it is easy to show that π°-decay γ-rays dominate over bremsstrahlung γ-rays in the galaxy because one knows the relevant cross sections, and the estimates of the cosmic-ray electron-nucleon ratio are good enough for this conclusion to be reached (Stecker, 1968, 1971, and 1975a). (Of course, the reverse is true for lower-energy γ-rays because the π°-decay differential spectrum turns over at $\sim$ 70 MeV.) The above conclusion is valid independent of the gas-density distribution in the galaxy if the cosmic-ray electrons and nucleons have similar distributions because both production processes are proportional to the total gas density. Thus, one would therefore expect similar γ-ray emissivity distributions in the galaxy in both cases.

Using recent estimates of the demodulated cosmic-ray electron spectrum in the solar vicinity of the galaxy (Goldstein et al., 1970; Daugherty et al., 1975; and Daniel and Stephens, 1975) and canonical total mean hydrogen density in the solar vicinity of $n_H = 1$ cm^{-3}, the integral and differential production rates of γ-rays at 10 kpc from the various processes have been calculated and are shown in figures 1 and 2. The π°-decay production rate is taken from Stecker (1970). The bremsstrahlung and Compton production rates have been calculated, using the formulas for a $KE^{-\Gamma}$ differential electron spectrum

$$q_B(E_\gamma) = \frac{4.33 \times 10^{-25}}{\Gamma - 1} n_H KE^{-\Gamma} \text{ cm}^{-3} \text{ s}^{-1} \text{ MeV}^{-1} \tag{1}$$

and

$$q_c(E_\gamma) = \frac{8\pi}{3} \sigma_T \rho_{ph} (m_e c^2)^{1-\Gamma} \left(\frac{4}{3}\langle\epsilon\rangle\right)^{(\Gamma-3)/2} KE_\gamma^{(\Gamma+1)/2} \tag{2}$$

(see, e.g., Ginzburg and Syrovatskii, 1964; and Stecker, 1971 and 1975a). The bremsstrahlung rate is given specifically for the cosmic mixture of H and He based on the cross sections for these elements given by Dovzhenko and Pomanskii (1964). In the equations, n_H is the hydrogen atomic density, σ_T is the Thomson cross section equal to 6.65×10^{-25} cm^2, ρ_{ph} is the photon energy density, and $\langle\epsilon\rangle$ is the mean photon energy so that

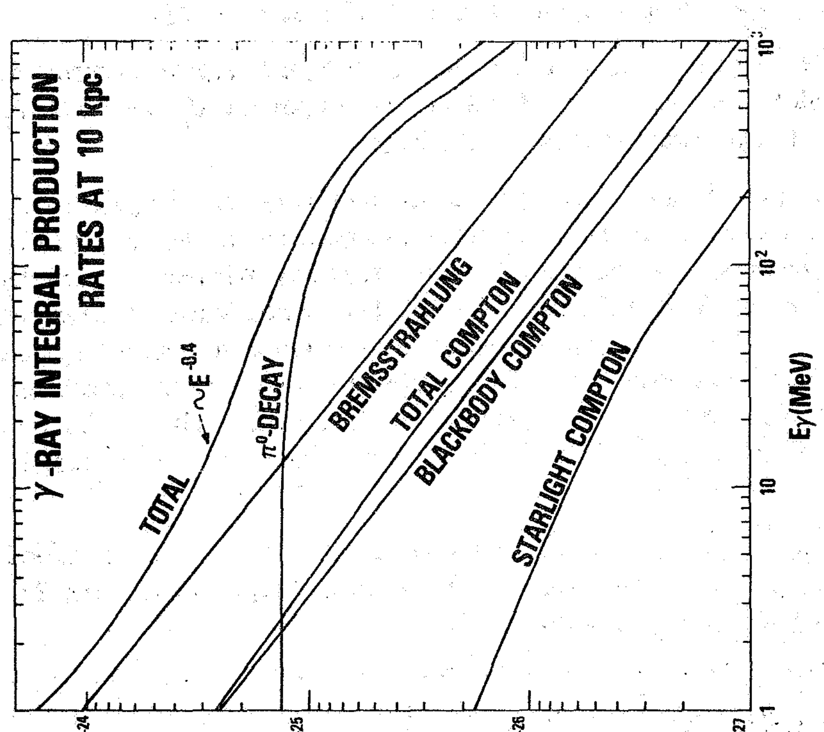

Figure 1: Local galactic γ-ray integral production for a local total gas density of 1 atom per cm^3 and starlight radiation density of 0.44 eV/cm^3. The π°-decay rate is from Stecker (1970).

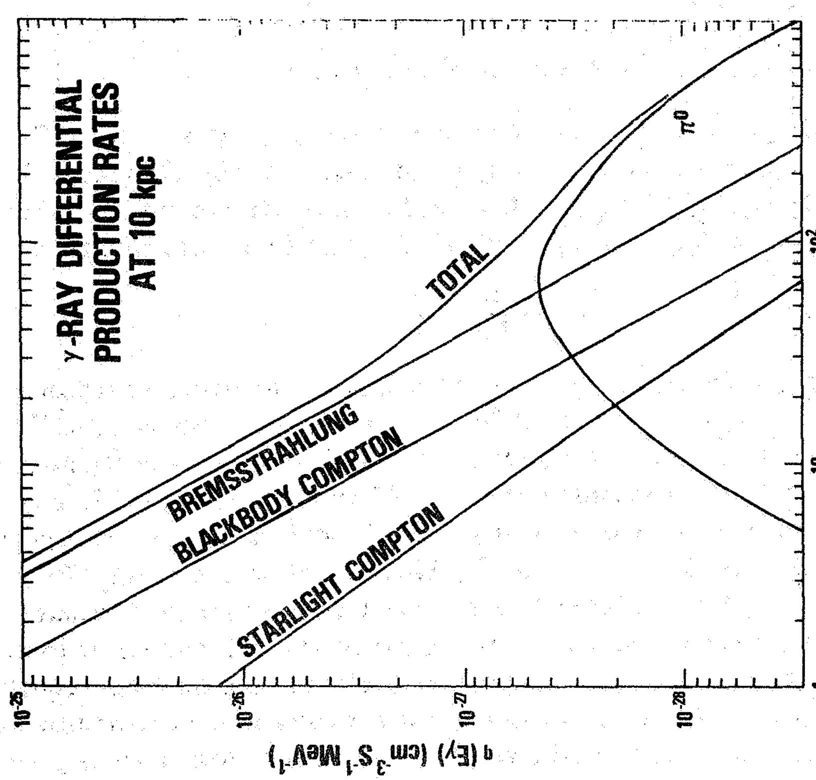

Figure 2. Local galactic γ-ray differential production rate for a total gas density of 1 atom per cm^3 and starlight radiation density of 0.44 eV/cm^3. The π°-decay rate is from Stecker (1970).

$$\frac{4}{3}\langle\epsilon\rangle = 3.1 \times 10^{-4}\,T(\mathrm{eV}) \tag{3}$$

Equations 1 and 2 are accurate to within a few percent. For the Compton process, Ginzburg and Syrovatskii (1964) give a correction factor, $f_c(\Gamma)$, dependent on the differential electron spectral index, Γ, so that $f_c(2) = 0.86$, $f_c(3) = 0.99$, and $f_c(4) = 1.4$. For bremsstrahlung, using the formulas given by Blumenthal and Gould (1970), I find the correction factor to be

$$f_B \simeq 1 - \frac{2}{3}\frac{(\Gamma - 2)}{\Gamma(\Gamma + 1)} \tag{4}$$

so that $f_B(2) = 1$, $f_B(2.5) = 0.96$, and $f_B(3) = 0.94$. (The local bremsstrahlung rate calculated here is similar to that given by Fichtel et al. (1976) and Ramaty and Westergaard (1976).) The Compton production rate was calculated for a 2.7 K blackbody background and a two-component starlight model of total radiation density, 0.44 eV cm^{-3} (Allen, 1973), consisting of a 10^4 K graybody component of energy density, 0.22 eV cm^{-3}, and a 5×10^3 K graybody component of equal energy density, 0.22 eV cm^{-3} (Lillie, quoted by Greenberg, 1971). The 10^4 K component will hereafter be referred to as the Population I component because it is due primarily to Population I stars, and the 5×10^3 K component will be referred to as the Population II component. Although these components contribute approximately equally at a galactocentric distance of 10 kpc, it is expected that the Population I component will be negligible at the galactic center region, which, we will see, is the only region where Compton interactions are expected to play a significant role (Stecker et al., 1975).

The Population I component produces a break in the starlight Compton spectrum at a critical energy, $E_{C,I} \simeq 60$ MeV, whereas, for the Population II component, $E_{C,II} \simeq 30$ MeV. The total starlight Compton spectrum is shown in the figures.

A comparison of the pion-decay and Compton processes throughout the galaxy is not as straightforward as the comparison with bremsstrahlung because, in this case, the Compton process scales like the low-energy photon density in the galaxy, whereas the pion-decay process scales like the gas-density distribution. There is also the possibility, pointed out by Cowsik and Voges (1974), that Compton production takes place throughout a greater volume of the galaxy since starlight is expected to exist at higher distances from the galactic plane than gas. Therefore, for the purposes of further discussion, I will introduce the useful concepts of various galactic-disk regions with different thicknesses as shown in figure 3. These disks are defined as follows:

1. The nebulodisk is defined as the region where most of the dust clouds and molecular clouds are found. Its thickness is of the order of 130 pc (Scoville and Solomon, 1975; and Burton and Gordon, 1976).

2. The ectodisk is the domain of the more diffuse atomic hydrogen (HI). Its thickness is of the order of 260 pc (Burton et al., 1975).

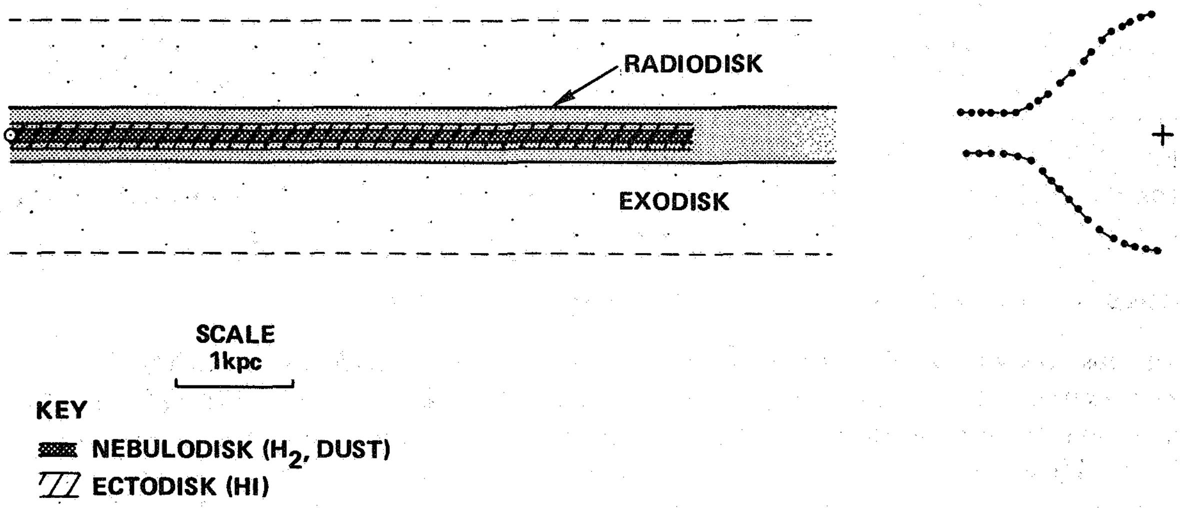

Figure 3. Regions of the galaxy as defined in the discussion given in the text.

3. The radiodisk, about 500-pc thick, is the region from which most of the synchrotron emission in the galaxy originates, according to the interpretation of Ilovaisky and Lequeux (1972) of the 150-MHz data of Landecker and Wielebinski (1970). For conceptual purposes, I will consider this as the diffusion-trapping region of most cosmic rays. Trapping in a more extensive "halo" will tend to wipe out radial gradients in the cosmic-ray intensity which are necessary to an explanation of the γ-ray measurements (Stecker, 1975b; Dodds et al., 1975; and Stecker et al., 1975), as will be discussed in more detail in a later section. In any case, recent observations appear to rule out significant trapping in a halo-type region (Webster, 1975).

4. The exodisk is tentatively identified here with a disk about 2-kpc thick from which some synchrotron emission is also occurring, according to the interpretation of Ilovaisky and Lequeux (1972). I call this the exodisk because cosmic rays may be escaping from the galaxy primarily from this region. (See the discussion of Jokipii, 1976.)

Using this language, γ-rays from bremsstrahlung and pion decay originate in the nebulodisk and ectodisk, whereas those from Compton scattering originate in the radiodisk and exodisk. Even so, the theoretical estimates shown in figures 1 and 2 indicate that in typical regions of the galactic disk (excluding the galactic nuclear region which we will be discussing separately), pion-decay dominates over Compton scattering even if the Compton-producing disk is an order of magnitude thicker than the gas disk. Furthermore, the latitude distribution of galactic γ-rays obtained by SAS-2 shows that the galactic γ-ray disk is thinner than the radiodisk, whereas dominant Compton production would imply that the γ-ray disk should be comparable in width to the radiodisk. Stronger evidence for the thinness of the γ-ray disk has been reported by Samimi et al. (1974) which places this width at 3°, whereas the SAS-2 resolution can only place an upper limit of about 6° on this width.* The asymmetry in the latitude distributions of γ-rays in the center and anticenter directions is further found to correlate well with the gas distribution, again arguing for the dominance of pion-bremsstrahlung processes (Fichtel et al., 1975; Stecker et al., 1975; and Puget et al., 1976).

COMPTON GAMMA-RAYS FROM THE GALACTIC CENTER

The observed angular distribution of galactic γ-rays does not exclude the possibility of a significant Compton component being produced near the galactic center, which is far enough away so that only a small angle is subtended by the galactic bulge. With a half-angle of 0.1 rad (~ 5°), a source of 2-kpc thickness will be consistent with the γ-ray observations at the galactic center. Assuming that the starlight radiation density varies as the total mass distribution of Perek (1962), as suggested by Cowsik and Voges (1974), but with the radiation density at 10 kpc taken to be 0.44 eV/cm^3 (Allen, 1973), I have recalculated the galactic Compton γ-ray flux as a function of galactic longitude, assuming a cosmic-ray electron flux equal to its value at 10 kpc. The results are shown in figure 4 for two different values of the γ-ray disk half-width, h, as indicated. For γ-ray production in the inner galaxy, where the detector beam covers the whole source, the line intensity is simply proportional to h and is given by

$$I_\gamma(\ell) = \frac{h \cos \ell}{2\pi} \int_{\sin^2 \ell}^{(R_m/10)^2} \frac{2x dx Q_\gamma(x)}{(1 - x^2)(x^2 - \sin^2 \ell)^{1/2}} \quad \text{where } x = R/10. \tag{5}$$

R is the galactic radius in kpc and R_m is taken to be ~ 9 kpc (Puget and Stecker, 1974).

It can be seen that, given an increased cosmic-ray electron intensity near the galactic center or a large enough value of h, it is possible for Compton scattering to provide a significant or even major portion of the γ-ray flux near the galactic center as suggested by Cowsik and coworkers, contrary to the conclusions of Shukla et al. (1975). However, at longitudes less than 10 or 15° from the galactic center, the Compton contribution to the galactic γ-ray flux becomes relatively unimportant. This calculation is essentially in agreement with that of Dodds et al. (1975) for h = 115 pc. Stecker et al. (1975) pointed out that, because of the relative lack of both HI and H_2 gas inside of 3 kpc (except at the galactic nucleus), not enough pion-decay and bremsstrahlung γ-rays could be produced to account for the flux at the galactic center, but pointed out that the inclusion of Compton γ-rays could adequately account for the observed flux distribution and intensity.

One may ask whether the observed spectrum of γ-rays coming from the galactic center region can tell us the production source. Using a 5 × 10^3 K (Population II) photon field in the

*The COS-B results in the 300- to 2000-MeV range reported here place an upper limit of 4° on this width.

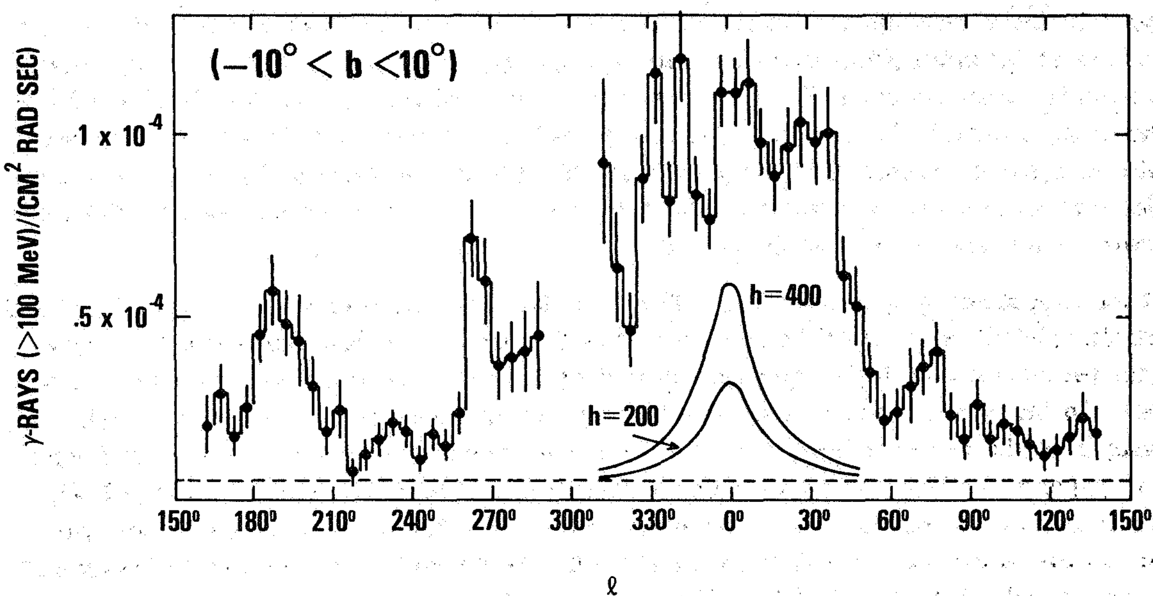

Figure 4. Compton production rate calculated using the method of Puget and Stecker (1974) for two values of half-thickness of the production disk h = 200 pc and 400 pc. These rates are shown together with the SAS-2 data reported by Fichtel et al. (1975).

central region of the galaxy, and based on the radio synchrotron data, one would expect a differential γ-ray spectral index of 1.8 from Compton-produced γ-rays in the 35- to 200-MeV energy range. The pion-bremsstrahlung spectrum shown in figures 1 and 2 has an average index of 1.4 in this energy range. The observations (Fichtel et al., 1975) yield a mean index of about 1.65 ± 0.25, which is, unfortunately, not accurate enough to tell us whether Compton or pion-bremsstrahlung γ-rays provide the dominant contribution.

GAMMA-RAYS IN THE GALACTIC DISK

As was discussed earlier, it is expected that cosmic-ray/gas interactions (pion-bremsstrahlung) are more important than Compton interactions in producing γ-rays in most of the galactic disk. There remains the question of whether most of the galactic γ-rays are produced by diffuse processes or point sources. Here, the lines are not clearly drawn, but two arguments seem to favor diffuse processes:

1. Only three significant point sources have been found by SAS-2, two of which are relatively nearby pulsars; moreover they have steeper spectra than the general galactic γ-radiation.
2. By analogy with the case of the nonthermal radio radiation from cosmic-ray electrons in the galaxy, one may argue that it is expected that the γ-rays also should be produced mainly by cosmic rays after they have left their sources and are in interstellar space rather than when they are still at the source (Lequeux, 1971).

Therefore, because it is likely that most galactic γ-rays with energy above 100 MeV result from the decay of π°-mesons which were produced in interstellar interactions of cosmic-ray nucleons with interstellar gas nuclei, it follows that, by studying the γ-ray emissivity distribution in the galaxy, one may learn about the distribution of cosmic-rays, mainly 1- to 10-GeV protons (Stecker, 1973) and gas in the galaxy. In the rest of this article, we thus turn our attention to a discussion of the implication of the SAS-2 observations of galactic γ-rays for determining new information about the distribution and origin of cosmic rays and about the structure and composition of the galaxy.

It was first deduced by Stecker et al. (1974) and later supported in calculations by Puget and Stecker (1974), Strong (1975), and Puget et al. (1976) that the SAS-2 observations imply that γ-ray emission is highly nonuniform in the galaxy and that the emissivity distribution peaks in the region of the galaxy about halfway between the Sun and the galactic center. My analysis of the latest version of the SAS-2 data with more events and smaller longitude bins (see paper of Kniffen, these proceedings), using the method of Puget and Stecker (1974), places this peak emissivity in the region between 5 and 6 kpc from the galactic center for the positive longitude side of the galaxy ($0° \leqslant \ell \leqslant 180°$), and at $\sim$ 5 kpc for the "negative" longitude side ($180° \leqslant \ell \leqslant 360°$). (See figures 5 and 6 and the section, "Spiral Features and Solid-Arm Models.") The correlation between the CO and γ-ray distribution is excellent for the range $0° \leqslant \ell \leqslant 180°$; unfortunately, there are presently no CO data yet available for the range, $180° \leqslant \ell \leqslant 360°$. The new γ-ray unfolding is in good agreement with that of Puget et al. (1976) for the range, $0° \leqslant \ell \leqslant 180°$; however, there are some differences in the range, $180° \leqslant \ell \leqslant 360°$, due mainly to differences in the data used and the subtraction of a contribution at 345° from PSR 1747-46.

It was noted by Solomon and Stecker (1974) that the γ-ray emissivity distribution bears a strong similarity to the distribution of molecular clouds in the galaxy which also peaks in the 5- to 6-kpc region (Scoville and Solomon, 1975; and Burton et al., 1976). This similarity, coupled with the lack of enough gas in atomic form to explain the γ-ray measurements led to the supposition that H_2 is far more abundant in the inner galaxy than HI and that H_2 plays the major role in producing galactic γ-rays (Solomon and Stecker, 1974; Burton et al., 1975; and Stecker et al., 1975). In fact, a γ-ray emissivity which scales like the more uniform HI distribution will not explain the observations. An alternative explanation for the γ-ray observations is to assume that the cosmic rays increase by more than an order of magnitude in intensity in the inner galaxy (Stecker et al., 1974), but this alternative encounters difficulties in producing instability in the galactic gas disk (Wentzel et al., 1975). The remaining problem has been to determine the absolute amount of H_2 in the galaxy, as well as its distribution. This can be estimated both by using the UV observations of H_2 in the local galactic neighborhood as typical of the H_2 at a galactocentric distance of 10 kpc and by using the infrared and X-ray absorption measurements in the direction of the galactic center to estimate the total column density of gas in that direction. Stecker et al. (1975) used the data shown in table 1 to estimate a total column density of $\sim 7 \times 10^{22}$ cm^{-2}.

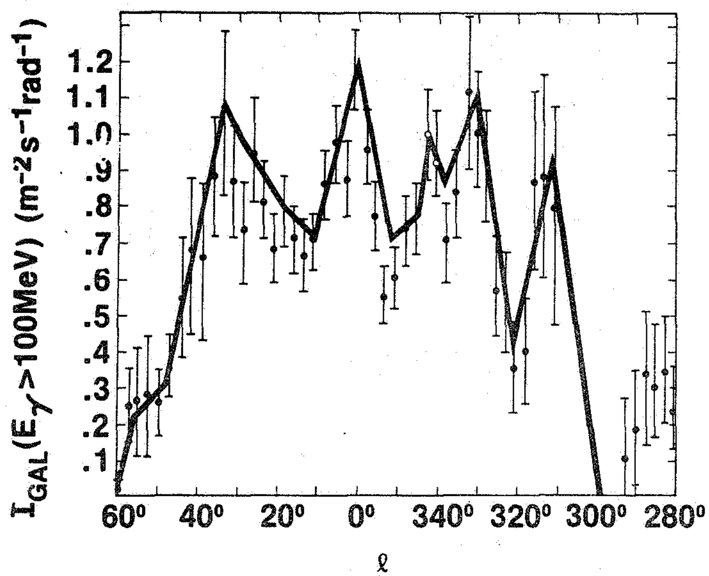

Figure 5. Most recent SAS-2 longitude data with more events reported in 2.5° longitude bins shown for the inner region of galactic longitude with the two points shown by the open circles having the contribution of pulsar PSR 1747-46 subtracted out (Kniffen, personal communication). The solid line shows the approximation to the distribution used in the unfolding calculation, the results of which are given in figure 6.

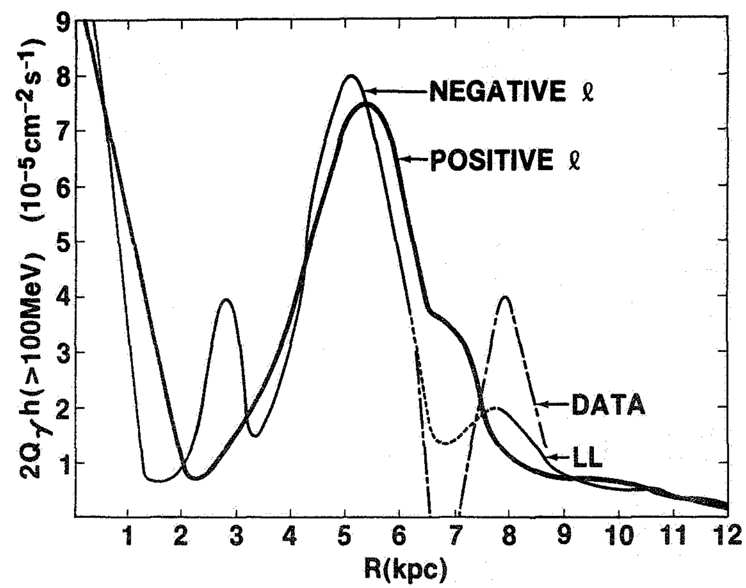

Figure 6. Radial distribution of galactic γ-ray emission obtained from unfolding the longitude distribution of figure 5 for the ranges $0° \leqslant \ell \leqslant 180°$ (positive longitudes) and $180° \leqslant \ell \leqslant 360°$ (negative longitudes). For negative ℓ, the unfolding using the data points in the range $310° \leqslant \ell \leqslant 317.5°$ is shown by the dot-dashed curve; that obtained using the lower limits to the statistical error bars is shown by the curve marked LL. The emissivity at the galactic center (R = 0) is approximately 1.5×10^{-4} cm^{-2} s^{-1}.

Table 1
Column Densities of Hydrogen at $\ell = 0°$, Excluding the Galactic Nucleus ($\times 10^{-22}$) (cm^{-2}) ($N_{G.C.,\odot}$) (from Stecker et al., 1975)

$\langle N_{HI} \rangle$ from 21-cm radio	$\gtrsim 0.6$ to 1.5	Daltabuit and Meyer (1972)
	~ 2	Kerr and Westerhout (1965)
	$\leqslant 1.2$	Clark (1965)
$\langle 2N_{H_2} \rangle$ from CO	3 to 10	Scoville and Solomon (1975)
$\langle 2N_{H_2} + N_{HI} \rangle$ from SAS-2 γ-ray flux	$\lesssim (11.5 \pm 2)$	this work ($I_{CR} \gtrsim I_{\odot}$)
$\langle 2N_{H_2} + N_{HI} \rangle$ from X-ray absorption	6.5 to 9	$\sigma_{H_2}/2\sigma_{HI} \leqslant 1.7$ (Kaplan and Markin, 1973) as verified by the measurements of Crasemann et al. (1974).
$\langle 2N_{H_2} + N_{HI} \rangle$ from IR absorption	5 to 7.5	Ryter et al. (1975)

Gordon and Burton (1976) worked directly from their CO data to determine the H_2 density. Both these methods yield consistent results and indicate that the volume averaged density of H_2 is of the order of two molecules per cm^3 in the 5- to 6-kpc region (Stecker et al., 1975; and Gordon and Burton, 1976) and drops off dramatically inside of 4 kpc and in the outer galaxy. At 10 kpc, at least half of the interstellar gas is probably in atomic form, and there is a negligible amount of H_2 in the outer regions of the galaxy (Scoville and Solomon, 1975; and Burton et al., 1976). The gas distributions obtained are shown in figures 7 and 9. A subsequent deduction of the implied cosmic-ray distribution indicates that the cosmic rays increase (relative to the local intensity) by about a factor of 2 (Stecker et al., 1975) or slightly more (Puget et al., 1976) at a maximum coincident with the maximum in the gas density in the 5- to 6-kpc region and that the cosmic rays drop off rather rapidly in the outer galaxy (Stecker et al., 1975; and Dodds et al., 1975). Dodds et al. (1975) have calculated the latitude distribution of γ-rays in detail under the "extragalactic" hypothesis (uniform cosmic-ray intensity) and "galactic" hypothesis (reduced cosmic-ray intensity in the outer galaxy) and have compared the results with the SAS-2 observations as shown in figure 8.

Stecker (1975b) has shown that the cosmic-ray distribution deduced using the γ-ray observations in conjunction with the deduced variation of total gas (HI + H_2) in the galaxy is, within experimental error, identical to the distribution of supernova remnants (Ilovaisky and Lequeux,

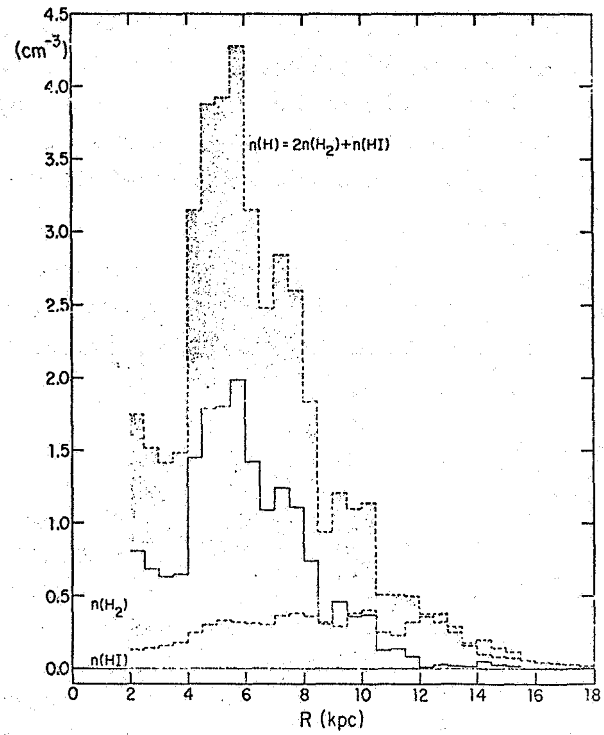

Figure 7. Volume density of interstellar hydrogen as a function of galactic radius given by Gordon and Burton (1976).

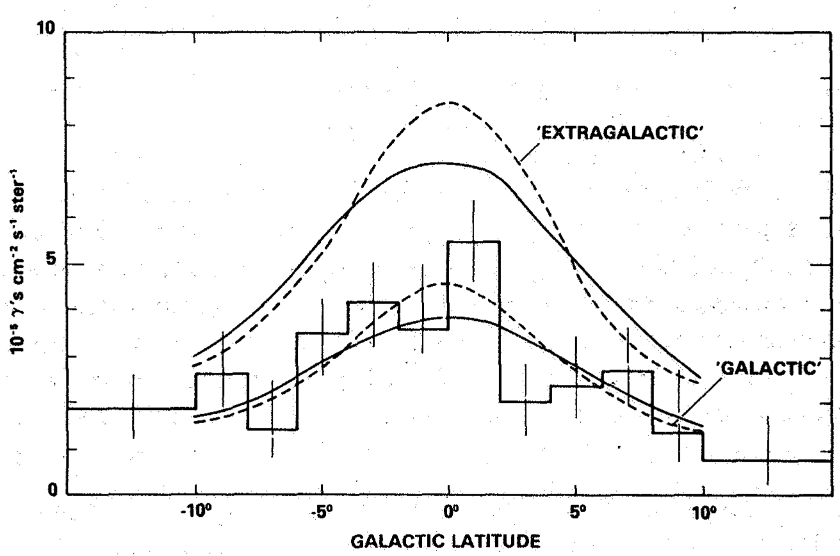

Figure 8. Calculated galactic latitude distributions of γ-rays for the "extragalactic" (uniform cosmic-ray flux) and "galactic" (falloff of cosmic rays in the outer galaxy) hypotheses as given by Dodds et al. (1975), together with SAS-2 data of Fichtel et al. (1975).

1972; and Kodaira, 1974) and pulsars (Lyne, 1974; Hulse and Taylor, 1975; and Seiradakis, these proceedings). The similarity of the deduced cosmic-ray distribution and the distribution of supernova remnants provides our strongest evidence to date that the observed cosmic-ray nucleons, which make up 99 percent of the cosmic rays, originate in galactic supernovae either in the explosion or the resulting pulsars. It supports other evidence from measurements of abundance ratios of heavy nuclides (see, e.g., Reeves, 1975).

Figure 9 shows the rough distributions of supernova remnants and total gas in the galaxy, and figure 10 shows the implied γ-ray longitude distribution calculated by Stecker (1975b) with Compton interactions included at the galactic center. Also shown is the observed longitude distribution (Fichtel et al., 1975).

IMPLICATION OF THE LARGE-SCALE GALACTIC DISTRIBUTIONS

On an overall large scale, there appears to be an excellent correlation between several important constituents of the galaxy in terms of their distributions as a function of galactocentric distance. These constituents are molecular clouds, HII regions (ionized hydrogen), cosmic rays, γ-rays, supernova remnants, and pulsars. All these constituents of the galaxy seem to be most dense in the 5- to 6-kpc region and appear to drop off sharply inside 4 kpc and in the outer galaxy. They can be associated with the formation and evolution of the so-called Population I stars in the galaxy and are known to have a Population I distribution. They are associated with the formation and destruction of hot young O and B stars in the galaxy which delineate arms in other spiral galaxies. That the correlation of these components is natural can be seen in figure 11. The gravitational collapse of molecular clouds is expected to lead to the formation of OB associations containing the massive, hot, short-lived O and B stars whose ultraviolet radiation causes the formation of zones of ionized gas around them (HII regions). After a few million years, the massive O and B stars terminate their existence as supernovae, which, in turn, leads to the generation of cosmic rays. It has also been suggested that the supernova explosions can trigger the formation of new OB associations in a feedback effect (Öpik, 1953; and Ögelman and Maran, 1975). The compound effect of cosmic rays and molecular clouds being enhanced in the same region of the galaxy then leads to an even stronger enhancement in the γ-ray emissivity in the enhanced region. In addition, an increase in the flux of subrelativistic cosmic rays may help lead to an additional increase in the amount of ionized gas in the region around 5 kpc as indicated in recent surveys (Mezger, 1970; and Lockman, 1976).

As a final note, Hayakawa et al. (1976) have recently reported a correlation between their observed 2.4-μm infrared flux and CO emission on a galactic scale. The shape of the longitude distribution given by Hayakawa et al. (see figure 12) implies a strong maximum near 5 kpc which, one can argue, points to the emission originality in very young Population I objects. Thus, one may speculate that a major contribution comes from circumstellar shells surrounding premain-sequence stars such as T Tauri stars or close surrounding Be stars (see, e.g., the review of Neugebauer et al., 1971). A similar galactic distribution of diffuse far-infrared

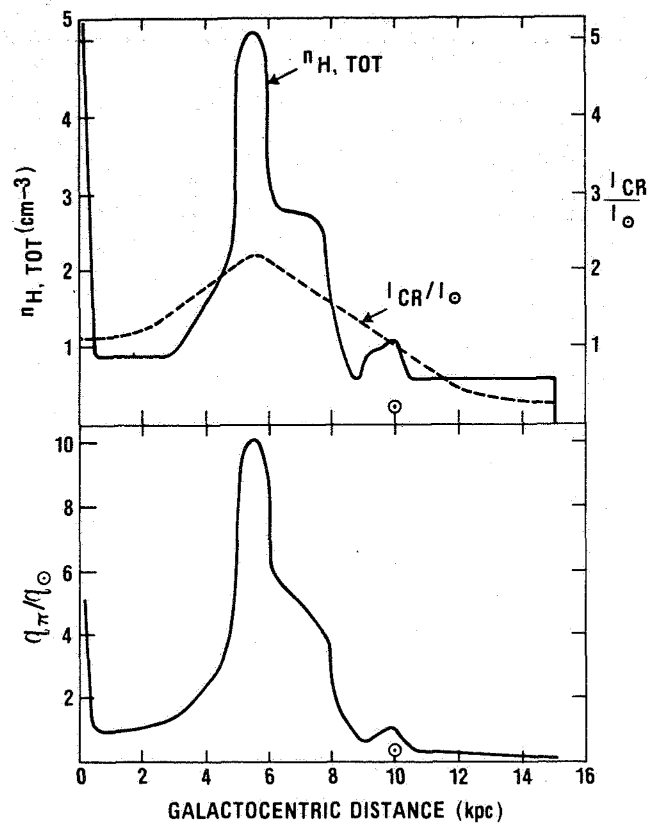

Figure 9. Volume density of interstellar hydrogen given by Stecker (1975b) as deduced using the CO data of Scoville and Solomon (1975) together with the relative large-scale galactic cosmic-ray distribution assumed proportional to the supernova remnant distribution deduced by Kodaira (1974) (top); the implied relative γ-ray emissivity from π°-decay is also shown (bottom).

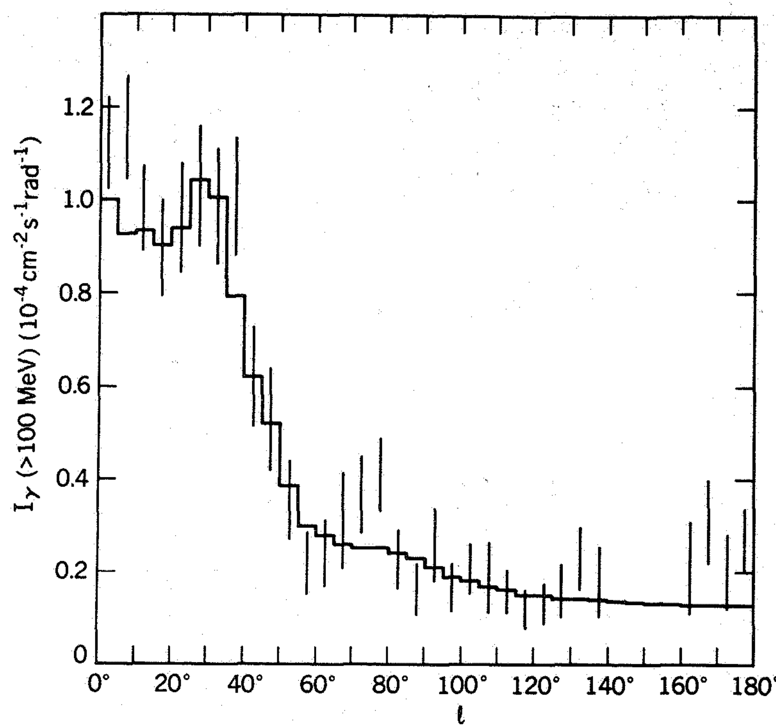

Figure 10. Longitude distribution of galactic γ-rays for $-10^\circ \leqslant b \leqslant 10^\circ$ averaged over 5° intervals calculated using the π°-decay emissivity distribution given in figure 9 and including effects of bremsstrahlung from secondary electrons and Compton γ-rays at the galactic center (Stecker, 1975b). The Compton contribution at the galactic center, calculated using a local electron flux and a value of h = 100 pc, may be underestimated. The calculations are only valid for $0^\circ \leqslant \ell \leqslant 180^\circ$ and are shown by the histogram together with the data given by Fichtel et al. (1975), shown by the vertical lines.

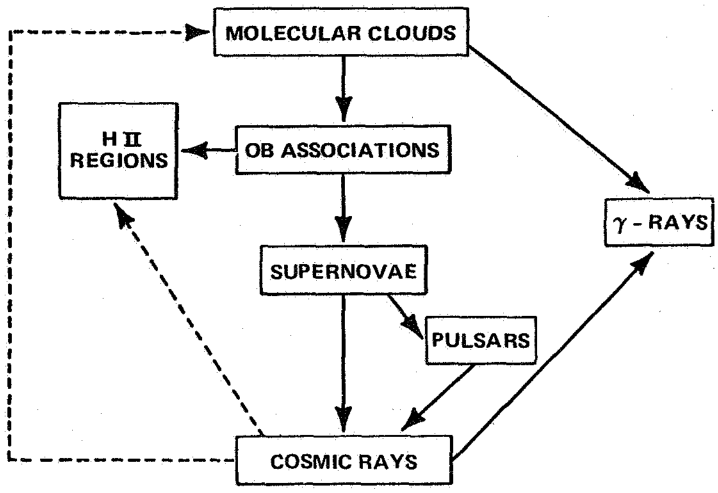

Figure 11. Plausible generic relations between various Population I galactic constituents (Stecker, 1976).

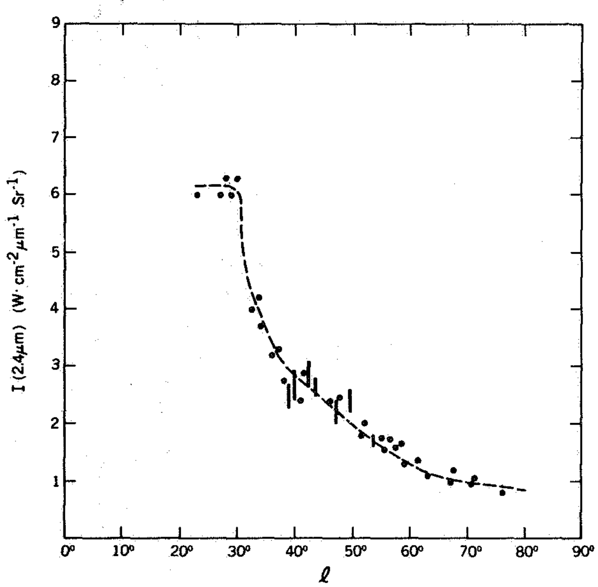

Figure 12. Galactic longitude distribution of 2.4-μm infrared mission reported by Hayakawa et al. (1976).

(100-μm to 300-μm) emission originating in dust in molecular clouds has been predicted by Fazio and Stecker (1976).

Whereas all of the components of the galaxy just discussed have correlated large-scale galactic distributions with maximum densities in the 5- to 6-kpc region, 21-cm radio observations of HI indicate a relatively constant overall density distribution of atomic hydrogen between 4 and 14 kpc from the galactic center with no evidence for a significant enhancement in the

5- to 6-kpc region (Kerr and Westerhout, 1965; and Burton et al., 1975). This implies that the H_2 distribution is much more sensitive to the compression effects expected in density-wave models of galactic structure than the more diffuse HI with the ratio H_2/HI having a radial galactic dependence somewhat similar to that of HII/HI as discussed by Shu (1973).

The density-wave models have the attractive feature of explaining the persistence of spiral arms in galaxies over time periods for which the differential rotation of these galaxies would destroy material arms. In these models, a spiral perturbation on the overall gravitational field of a galaxy results in excess gas accumulating in troughs of gravitational potential where star formation will then preferentially take place leading to the young OB associations and associated HII regions which stand out in optical surveys of external galaxies and delineate spiral arms. In this case, then, one is seeing only the wave of new star formation rather than the real bulk of existing stars (approximately 95 percent) as they move around the galactic center. The density-wave models provide a plausible framework in which to consider the structure of spiral galaxies, but they are not complete in that they do not explain the origin of the spiral-wave pattern itself or the energy input required to maintain it. In the context of the density-wave theories, however, a crowding of the wave pattern and an increase in the frequency of gas shocking in the region of the inner arms would naturally lead to an increased density of molecular clouds, young stars, supernovae, and HII regions in the 5- to 6-kpc region. However, the question of the details of spiral structure in the galaxy is more difficult. Our galaxy apparently shares with other spiral galaxies a lack of gas of all types in the inner-most region (radius less than 4 kpc with the exception of the galactic nucleus). Similar structural characteristics have been found in other spiral galaxies (Roberts, 1974).

However, there is a large variation in structural details among spiral galaxies. This range of detail, from those with long, thin, well-developed arms and high surface brightness (van den Bergh type I) to those with only a bare hint of arm structure (van den Bergh type V) has been incorporated into the general framework of density-wave theory by Roberts et al. (1975). The galaxies with well-developed arms and high surface brightness with an implied high star-formation rate are found to satisfy the condition $(W_{\perp 0}/a) > 1$ where $W_{\perp 0}$ is the velocity component of basic rotation normal to the spiral arms, and a is the effective acoustic speed of the interstellar gas. Within galaxies themselves there can exist in the inner regions, zones of strong nonlinear compression where $(W_{\perp 0}/a) > 1$, and in the outer regions, zones of weak linear compression where $(W_{\perp 0}/a) < 1$. Burton (1976) has estimated the interface between these two zones in our own galaxy to occur at a galactocentric radius $R \sim 10$ kpc (see Roberts' paper, these proceedings).

Figure 13 shows the smoothed radial distribution of mean surface density of the atomic and molecular components of interstellar gas in our galaxy based on recent data of Burton et al. (1975) where the H_2 density is normalized according to the methods of Stecker et al. (1975) with a scale height of ~ 65 pc for the molecular clouds (Scoville and Solomon, 1975; and Burton and Gordon, 1976). Also shown are the regions of weak and strong compression. It can be seen that the transition region near 10 kpc is one in which the total surface density

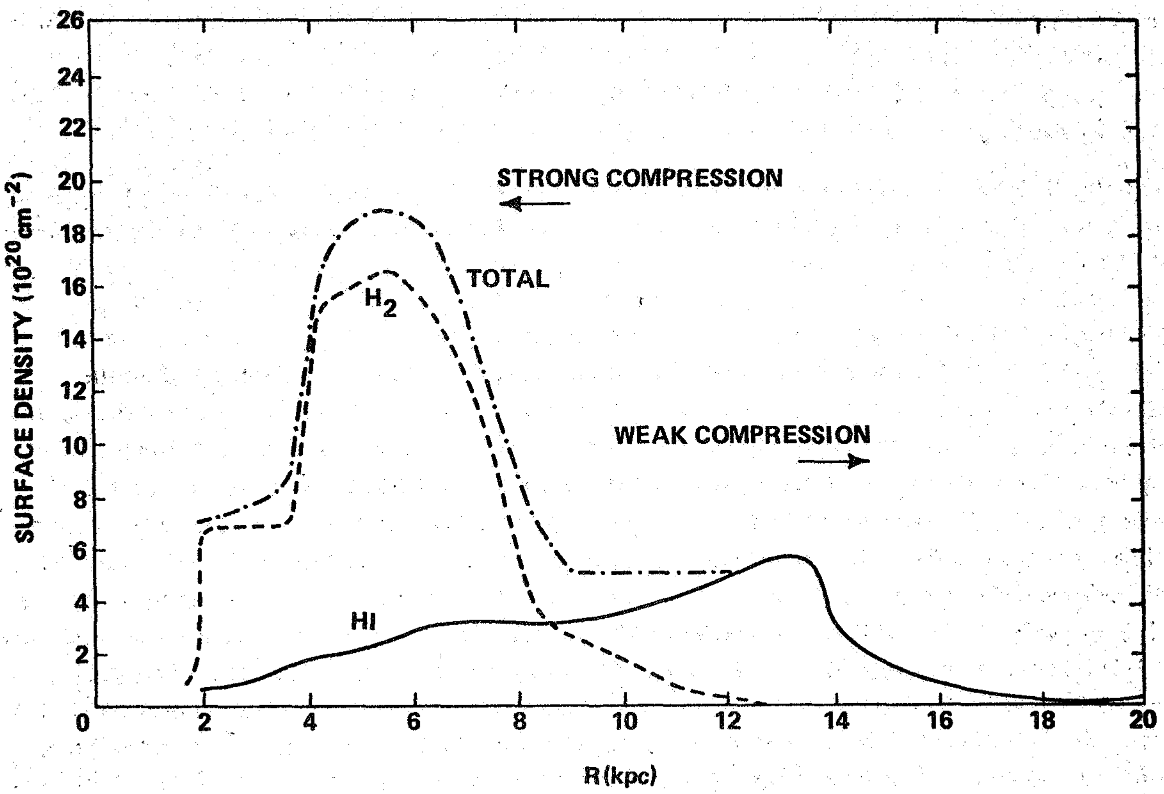

Figure 13. Surface density distribution of HI, H_2, and total gas derived as described in the text, shown with regions of weak (linear) and strong (nonlinear) density wave compression as determined by Burton (1976). The figure is from Stecker (1976).

is roughly constant, but where larger and larger amounts of gas are converted from HI to H_2 as R decreases.

All of these recent observational and theoretical developments regarding galactic structure* prompted Stecker (1976) to suggest the following changes in the Baade (1944) classification scheme for galactic objects:

1. The classification, Population II, which consists of old disk stars ("high-velocity" stars), nuclear bulge stars, halo stars, and globular cluster stars stays the same.

2. The classification, Population I, should be expanded to include all galactic objects narrowly confined to the galactic plane and associated with the formation of Population I stars. Thus, the set of galactic Population I objects will include molecular clouds, OB associations, HII regions, dark Nebulae, dust, supernovae, and even associated radiation fields such as infrared (Fazio and Stecker, 1976), synchrotron, and π°-decay γ-radiation from molecular clouds. This population is expected to predominate in regions of the galaxy where $(W_{\perp 0}/a) > 1$ (strong compression).

*See also the summary and discussion of Burton (1976).

3. I define a new population class, Population 0, consisting of the more diffuse atomic hydrogen, which is now considered not to play a primary role in star formation. (In the case of some of the denser HI clouds, there may be some blurring of definition.) This population will be important in regions where $(W_{10}/a) < 1$ (weak compression). The main distinction between Population 0 and I stems from the effects of compression and, with the higher compression, stemming from the nonlinear density waves. Two basic differenees between the galactic distributions of the Population I and Population 0 components are shown in table 2.

Table 2
Galactic Distribution of Population I and Population 0 Components

Population	Scale Height Perpendicular to Plane	Galactocentric Radius of Maximum Surface Density
Population I	$\sim$ 50 to 70 pc (nebulodisk)	5 to 6 kpc
Population 0	$\geqslant$ 110 pc (ectodisk)	12 to 13 kpc

The Population I component is therefore associated with the nebulodisk, and the Population 0 component with the ectodisk. It is found that in late-type spiral galaxies it is characteristic for the neutral hydrogen density to peak well outside the visible radius of the galaxy (Roberts, 1974). This is illustrated by figures 14 and 15 from the work of Rots and Shane (1975) which shows clearly that, for M81, the 21-cm emission peaks outside the optical disk of the galaxy. The above classification, with Population 0 removed from a primary role in the star-formation process, naturally accommodates this hitherto somewhat mysterious fact.

SPIRAL FEATURES AND SOLID-ARM MODELS

As has been discussed above, there is a large variation in structural details among spiral galaxies, ranging from a bright and well-defined arm structure (the so-called grand design) in galaxies such as M51 and M101, to the more crowded complex and nondescript features of galaxies such as M33 (Roberts et al., 1975; and Sandage, 1961). In the latter cases, ordered spiral features extending over distances of the order of several kpc would be difficult, if not impossible, to determine from a point within the galactic disk.

This brings us to the question of what can be learned about the "small-scale" structure of the galaxy (i.e., spiral density perturbations) from the recent γ-ray observations.

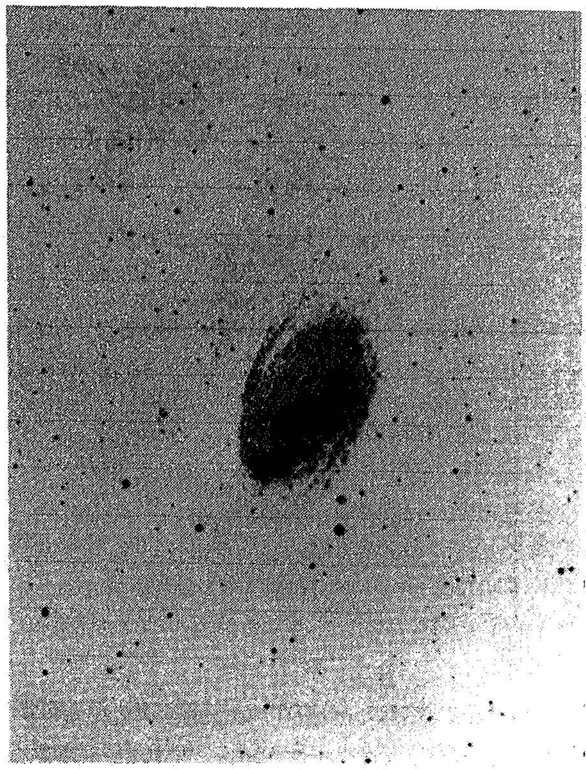

Figure 14. Optical image of M81, together with 21-cm contours (Rots and Shane, 1975).

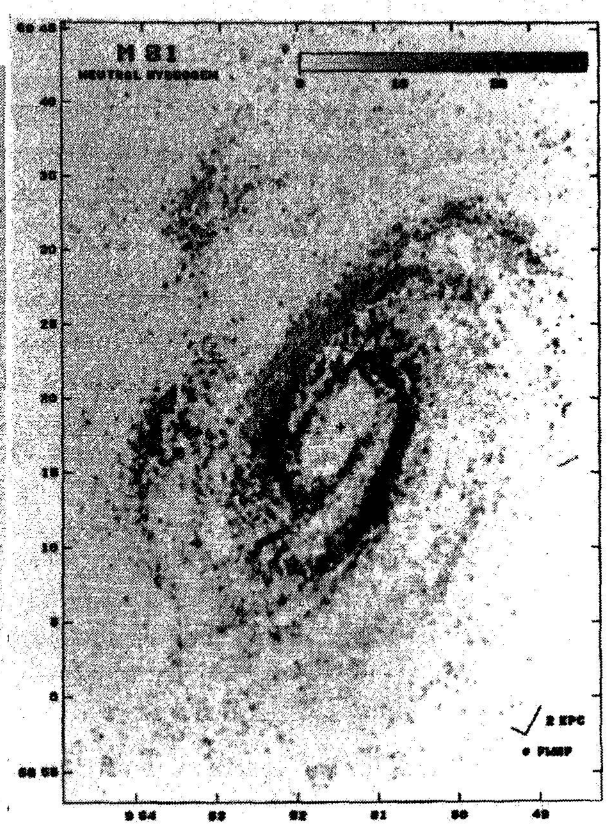

Figure 15. 21-cm radio map of M81, showing regions of neutral atomic hydrogen. The scale is the same as for figure 14. It can be seen that the peak HI density lies at the outside of the optical image of the galaxy (Rots and Shane, 1975).

In considering the question of looking for evidence of spiral structure in the γ-ray observations, two points must be kept in mind: the limited resolution of the SAS-2 telescope and the ambiguous interpretation of data from other types of astronomical observations as to the character of the spiral features of our galaxy (Simonson, 1970; and Burton, 1974). Burton (1974) has pointed out that 21-cm features associated with spiral arms could be due mainly or in part to kinematic effects. Therefore, while the overall distribution of Population I material can be understood in terms of density wave models of the galaxy, one is on much shakier ground when it comes to analyzing the detailed structural features, such as reconstructing spiral arms.

Attempts have been made to interpret the SAS-2 γ-ray data based on grand-design spiral models of the galaxy (Simonson, 1976) with large arm-interarm ratios of both gas and cosmic rays (Bignami and Fichtel, 1974; Bignami et al., 1975; and Paul et al., 1976).

Because of the lack of CO data at negative longitudes, Bignami et al. (1975) constructed models based on 21-cm studies of atomic hydrogen. These models did not fully utilize the emerging implications of recent molecular-cloud observations with regard to the galactic H_2 component in the inner galaxy. The models of Bignami et al. (1975) had therefore required unrealistically high amounts of HI at locations which have been attributed to arm features (figure 16) and proportionally large amounts of cosmic rays relative to the solar intensities ($I_{CR} \propto n_H$) in order to obtain fluxes of γ-rays to compare with the observations in the range $|\ell| \leqslant 40°$. These models also assumed that H_2 was proportional to HI everywhere in the galaxy so that $(n_{H_2} + n_{HI})/n_{HI} = K$ with (in the recent model of Bignami et al. (1975)) $K = 2$. Then, since the γ-ray emissivity is proportional to the product $I_{CR} n_H$ with I_{CR} assumed proportional to n_H, $I_\gamma \propto (Kn_{HI})^2 \propto 4n_{HI}^2$. Given this sensitive density dependence, the assumptions about n_{HI} shown in figure 16 with $\langle n_{HI} \rangle$ assumed to be considerably above the recently observed values take on critical importance. Therefore, Kniffen et al. (these proceedings) have reexamined this model, including the implications of the recent CO data. The model of Paul et al. (1976) has sought to relate the radio data to the γ-ray data by making the additional assumptions, $I_{CR} \propto I_e \propto n_H \propto B^2$. They themselves point out, however, that the b distribution of the radio-synchrotron and γ-ray emission are different (see figure 17). Also, there is only a rough relation between the longitude distributions of the two components, which mainly reflects the overall structural features discussed earlier. (See also "Comparison of Radio and Gamma-Ray Longitude Distributions.")

Passing on, then, from specific spiral-arm models, one may still consider the general question of whether the γ-ray observations provide evidence of spiral features. In this context, I previously noted that the expanding "3-kpc" arm, observed by its distinct separation on velocity-longitude plots of both HI and CO emission, has insufficient material either in atomic or molecular form to account for the largest peak in the observed galactic γ-ray distribution at $340° \leqslant \ell \leqslant 345°$ shown in figure 4 as proposed by Bignami et al. (1975). The new longitude distribution reported here no longer has such a prominent feature as shown in figure 5 with a ~ 5 percent contribution from PSR 1747-46 subtracted out (see Hartman, these proceedings). The unfolding of the new SAS-2 data shown in figure 6 is compatible with emission from the 3-kpc feature; however, the explanation of a superimposed nearby source, together with statistical fluctuations, cannot be ruled out.

The large peak in the data in the range $310° \leqslant \ell \leqslant 315°$ has been associated by the SAS-2 group (Fichtel et al., 1975) with the "Scutum arm" feature as interpreted by some 21-cm observers. However, the narrow profile of this feature is hard to reconcile with that expected from a spiral arm. An ideal uniform spiral arm will fill in at longitudes closer to the galactic center than the tangential longitude so that it traces out a characteristic longitude distribution shaped somewhat like a shallow letter M. The inside slope of this pattern as calculated by the SAS-2 group in this model should be shallower than that actually observed. Looking at it another way, if one tries to unfold the longitude data for $180° \leqslant \ell \leqslant 360°$, it requires a negative γ-ray emissivity for $R \simeq 7$ kpc (see the dot-dashed curve in figure 6) in order to obtain the steep slope inside of 315° on the longitude distribution. Because this is clearly

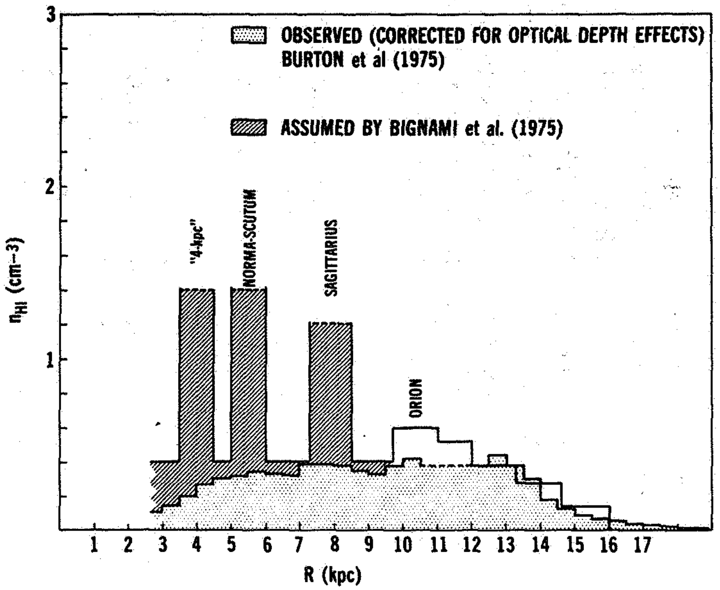

Figure 16. Mean HI density as a function of galactic radius as obtained from 21-cm surveys (Burton et al., 1975) and assumed in the recent spiral-arm model of Bignami et al. (1975). This model further assumes that H_2 has the same galactic distribution as HI (contrary to the observations of Scoville and Solomon (1975) and Burton et al. (1975)). It is assumed in the model that $n_{TOT} = KN_{HI}$ with K = 2 (Bignami et al. (1975)). Circular symmetry is not assumed in the model and the figure only represents typical positions for the arm features. The model appears to overestimate the volume averaged density of HI (regardless of structural details) as determined by the 21-cm observations (see Stecker et al. (1975) for further discussion).

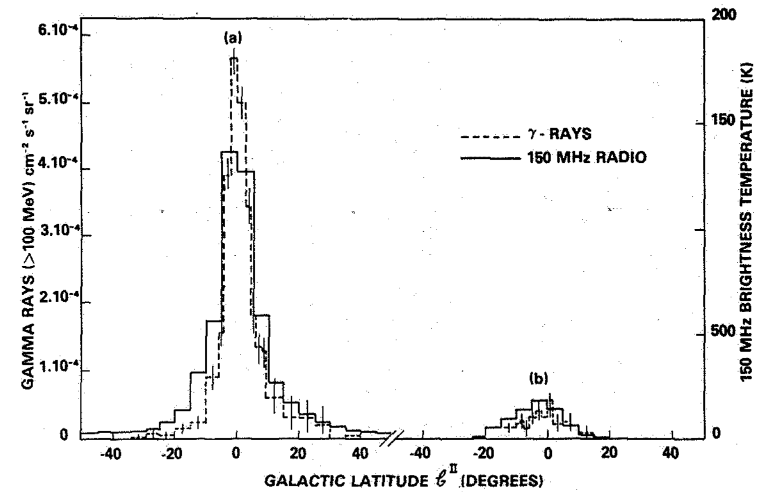

Figure 17. Comparison of latitude distribution of γ-rays (unresolved) and 150-MHz nonthermal emissions in the galaxy for the center (a) and anticenter (b) directions (Paul et al., 1976).

nonphysical, one must look for an alternate explanation. One such explanation is to assume that the true flux is near the low end of the statistical error bars. The unfolding then results in the solid line shown in figure 6 with a relatively small arm-type feature at $R \simeq 7.7$ kpc that may be associated with the "Scutum arm." Such a feature is compatible with the mean gas density falling outside of 6 kpc. Another possibility is point-source contamination. In order to truly resolve this problem and the entire problem of gas density on the "negative longitude" side of the galaxy, we must await further γ-ray observations with better statistics near 310° and fill in the data gap in the range $290° \leqslant \ell \leqslant 315°$. We also need CO observations from a millimeter wave facility in the southern hemisphere which will have access to this half of the galactic plane, and we also could make use of related far-infrared observations (Fazio and Stecker, 1976).

In summary, neither the γ-ray nor CO observations provide clear evidence of arm features at positive longitudes, but an overall larger scale structure, fairly symmetric vis-a-vis positive and negative longitudes, indicating a maximum emissivity in the 5- to 6-kpc region is seen (see figure 6). Possible evidence of arm features is found at negative longitudes (Fichtel et al., 1975) that may be associated with the complex distribution of HII regions at those longitudes (Puget et al., 1976) but that does not correspond to the flat $\langle n_{HI} \rangle$ distribution seen in 21-cm observations, even modulated with a large arm-interarm ratio. Such a model will not give the proper intensity or distribution of galactic γ-rays unless the H_2 cloud distribution is taken into account (Stecker et al., 1975). Further evidence for this may be seen in the lack of a "Sagittarius arm" feature at $\ell = 50°$, which is absent in both the CO observations (Scoville and Solomon, 1975; and Burton et al., 1975) and the SAS-2 γ-ray observations (Fichtel et al., 1975). A strong Sagittarius arm would also be inconsistent with the γ-ray latitude observations of Samimi et al. (1974). The small γ-ray enhancement in the Cygnus region ($65° \leqslant \ell \leqslant 80°$) has been identified with the Orion arm by the SAS-2 group; however, the existence of the Orion arm is in serious question from the kinematical evidence of HI gas in that region (Burton and Bania, 1974), and known clumpiness of gas with relatively large amounts of CO emission in that region, together with supernova remnants in that direction, may help account for the observed γ-ray enhancement.* Additional evidence against cosmic-ray confinement in a local ("Orion") arm comes from the lack of cosmic-ray anisotropy in this direction, as well as the long-term constancy of the cosmic-ray flux (Brecher and Burbidge, 1972). New evidence of a possible 2×10^7-year lifetime for cosmic rays in the solar neighborhood (Garcia-Munoz et al., 1975) would rule out strict cosmic-ray confinement in arms with a γ-ray production rate proportional to n_H^2 as suggested by Bignami and Fichtel (1974) and Paul et al. (1976). Such a lifetime, although still uncertain (O'Dell et al., 1973; and Hagen et al., 1975), would argue for diffusion of cosmic rays in a larger region of the galaxy (Jokipii, 1976), as will be discussed in more detail in the next section, and will support a weaker cosmic-ray correlation with larger-scale galactic features, as argued by Stecker et al. (1975) on the basis of the CO data.† These authors note that an approximate relation $I_{CR} \propto n_{TOT}^{a}$ holds in the inner

*Much of the Cygnus enhancement has now been associated with Cygnus X-3 (Hartman et al., these proceedings).

†Arm effects in the γ-ray longitude profile can be caused by density and source perturbations alone without invoking cosmic-ray confinement.

galaxy where $n_{TOT} \simeq n_{H_2}$ and $0.2 \leqslant a \lesssim 0.5$. Finally, in a recent study of galactic synchrotron emission, French and Osbrone (preprint) conclude that 1- to 10-GeV electrons cannot be confined to spiral arms.

IMPLICATIONS OF 20-MY LIFETIME FOR COSMIC-RAYS ON INTERPRETATION OF GAMMA-RAY DATA

It has been established earlier that there must be a positive overall correlation between cosmic-rays and matter in the galaxy in order to explain the γ-ray production rate. On the other hand, should it be established that cosmic rays have a mean lifetime of $\sim 2 \times 10^7$ years, as obtained by Garica-Munoz et al. (1975), this would imply a relatively small mean gas density seen by cosmic rays throughout their lifetime. Studies of cosmic-ray secondaries have revealed that cosmic rays travel through an average of 1.5 to 3×10^{24} atoms/cm^2 during their lifetime in the galaxy. Taking that lifetime to be 6×10^{14} s implies that over the cosmic-ray confinement region, $\langle n_H \rangle \simeq 0.1 - 0.2\ \mathrm{cm}^{-3}$. Jokipii (1976) has pointed out that the γ-ray evidence argues against their being trapped in "tunnels" in the galactic disk, as suggested by Scott (1975). The other alternative, arguing against confinement in spiral arms, is that the cosmic rays spend considerable time in regions where $n_H \lesssim 0.2\ \mathrm{cm}^{-3}$, as well as those where $n > 0.2\ \mathrm{cm}^{-3}$, and in a region thicker than the gas disk such as the radiodisk or exodisk (see figure 3). Confinement in a large halo would require a $\sim 10^8$-year trapping time (Ginsburg and Syrovatskii, 1974) and appears to be inconsistent with the radio evidence (Webster, 1975). In addition, confinement in such a large region would tend to wipe out any radial gradient in the cosmic-ray flux as suggested by the γ-ray observations (Stecker, 1975; and Dodds et al., 1975). Thus, one might presently favor an "exodisk" concept, as suggested by Jokipii (1976) and perhaps as illustrated by the radiodisk studies of some spiral galaxies in the observation of Ekers and Sancisi (1976). An example from these observations is NGC4631, shown in figure 18. As can be seen from figure 18, a fat disk or flat halo-type region of synchrotron emission surrounds NGC4631; such a region may also exist around our own galaxy. An even more apt example may be the spiral, NGC891, which shows a radiodisk of thickness ~ 4 kpc (van der Kruit and Allen, 1976) and a gas disk of $\lesssim 500$-pc thickness, seen in 21 cm (Sancisi, quoted by Ekers, 1975). (See Baldwin, these proceedings.)

COMPARISON OF RADIO AND GAMMA-RAY LONGITUDE DISTRIBUTIONS

Paul et al. (1976) have constructed a model of γ-ray emission in our galaxy, based in part on the assumption of the relation $I_e B^2 \propto I_{CR} n_H$, which implies $I_{sync} \propto I_\gamma$. It is my own philosophy that one should eliminate such a priori assumptions and work from the data as much as possible. One can learn from comparisons of the distributions of various galactic emissions from both their similarities and their differences. It has already been remarked that the 150-MHz radio and γ-ray emissions have different latitude distributions. Figure 19 shows that similarities and differences also exist in the longitude distributions. The SAS-2 γ-ray data are shown by the histogram, and the radio data are taken from Price (1974) with the positions of the tangents of 21-cm features shown by the arrows. Note that the γ-ray distribution is generally wider in the inner galaxy than the radio distribution. Both are enhanced in the Cygnus region ($\ell \approx 80°$) and in the longitude range near 310°. Note, however, that, in the later case, the reported γ-ray emission is relatively much more intense than the 150-MHz emission, supporting the suggestion made earlier in this paper regarding the 310° feature (see figure 6). The peak in the γ-ray distribution at ~260° can be attributed to the Vela pulsar, and the enhancement in the anticenter direction is due primarily to the Crab pulsar and another γ-ray source at $\ell \approx 195°$.

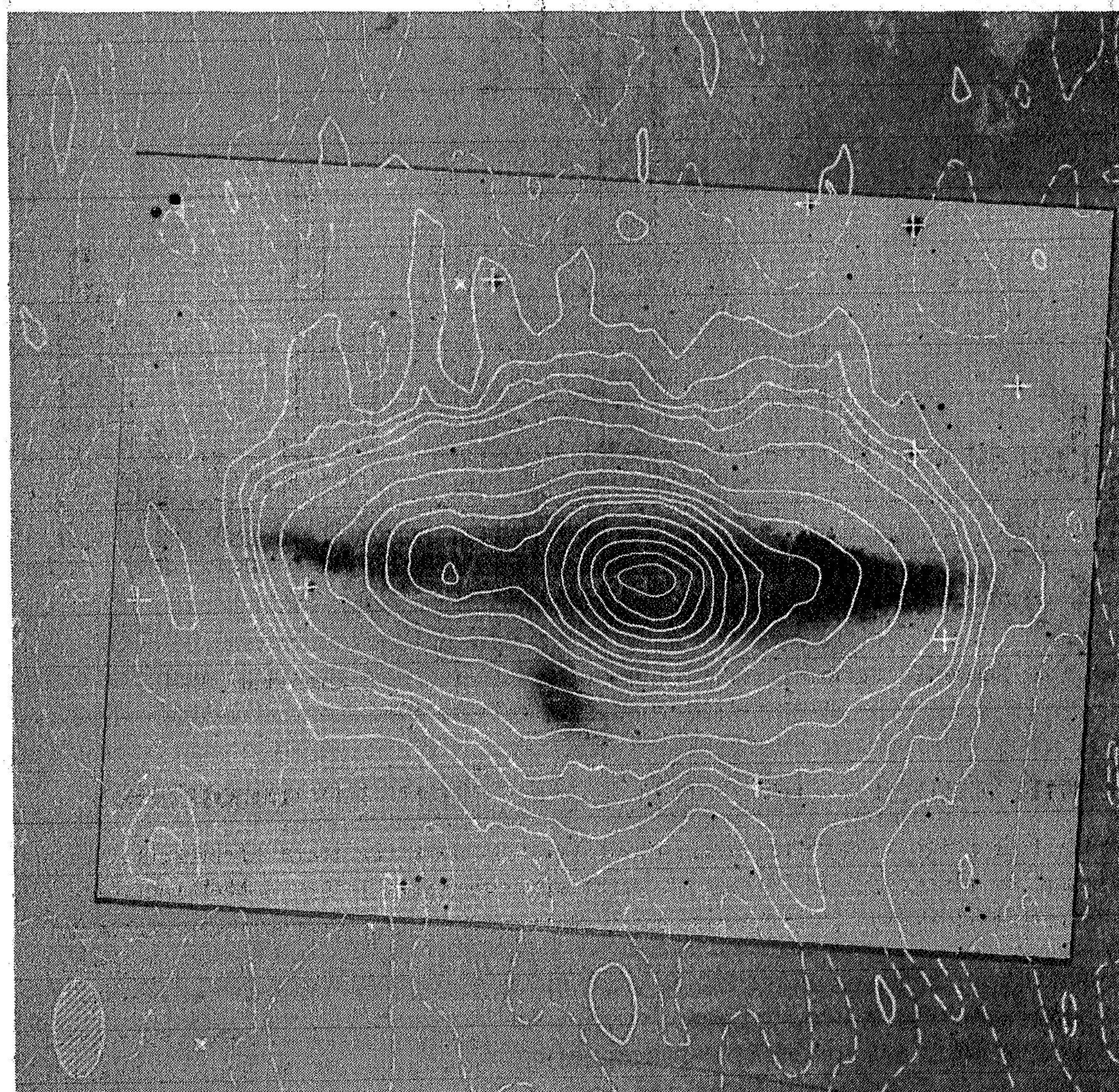

Figure 18. Optical image of the edge-on spiral galaxy, NGC 4631, together with preliminary 50-cm radio contours obtained with the aperture synthesis array at Westerbork by Ekers and Sancisi (personal communication).

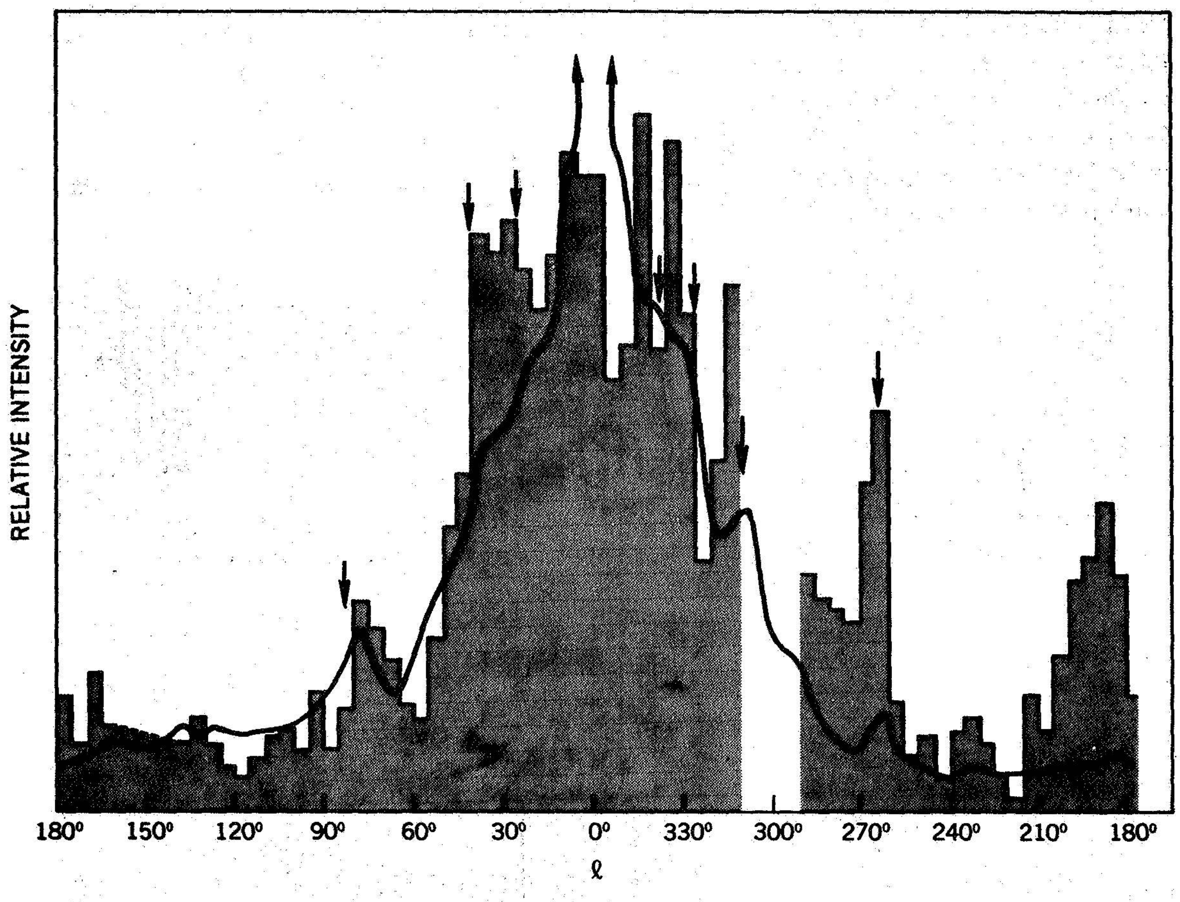

Figure 19. Comparison of longitude distributions of γ-rays (Fichtel et al., 1975) and 150-MHz radio emission (Price, 1974).

GALACTIC CONTRIBUTION TO HIGH-LATITUDE GAMMA-RAY BACKGROUND

Recent satellite data on the γ-ray background spectrum shown in figure 20 (Mazets et al., 1975; and Trombka et al., 1977) are consistent with other data in the ~1-MeV range and are consistent with cosmological redshifted π^o-decay processes proposed by the author in the past (Stecker, 1969; Stecker et al., 1971; and Stecker, 1974 and 1975a), which predict a shelf-like feature near ~1 MeV and a steep spectrum $\sim E^{-3}$ above 10 MeV. At energies between 35 and 200 MeV, the observed spectrum at high galactic latitudes (b > 30°) appears to be flatter than at lower energies, $\sim E^{-(2.4 \pm 0.2)}$ (Fichtel et al., 1975). This can be readily explained as high-latitude galactic background emission due to the finite thickness of the galactic γ-ray disk. Taking a typical SAS-2 path length of 3×10^{20} csc b cm^{-2} (Falgarone and Lequeux, 1973) with b = 40°, and using the differential production rate shown in figure 2, the galactic high-latitude component obtained is shown by curve G in figure 20. Also

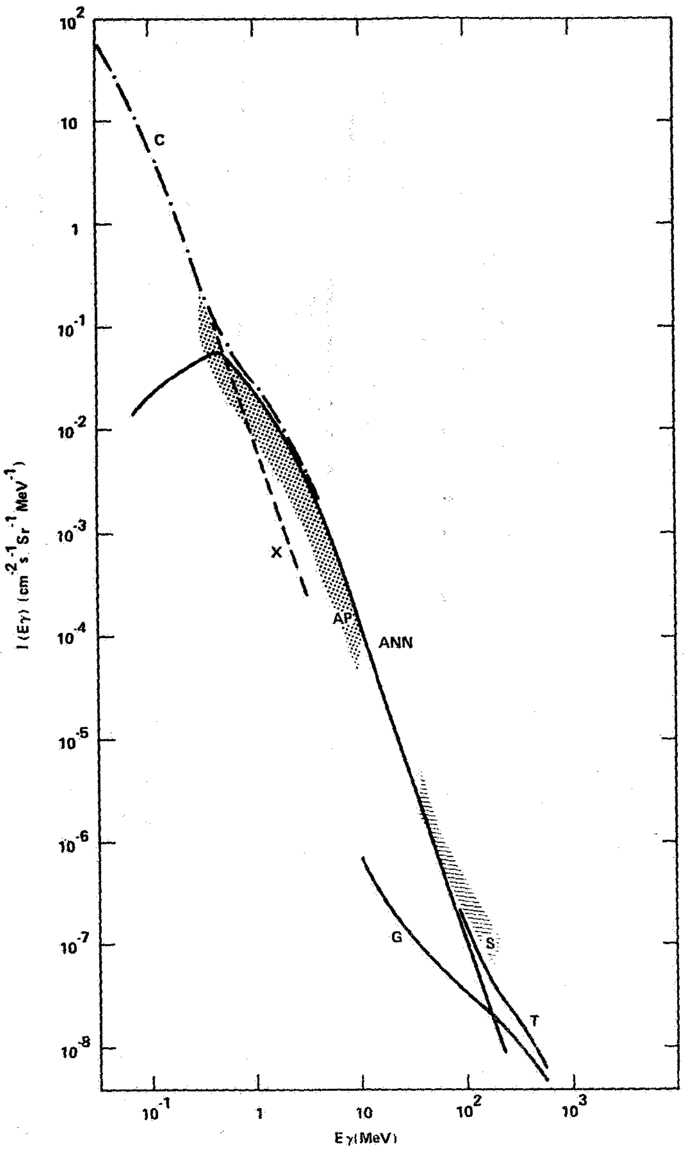

Figure 20. Revised background γ-ray observations from Apollo 15 (AP, Trombka et al., 1977) high-latitude SAS-2 observations (S, Fichtel et al., 1975) and observations from Cosmos 461 (C, Mazets et al., 1975). The cosmological background from the annihilation model of Stecker et al. (1971) with $n_0 = 3 \times 10^{-7}$ and $H_0 = 50$ km/s/Mpc is shown (ANN), as well as the X-ray extrapolation of Mazets et al. (X, 1975). The contribution from the high-latitude galactic flux, as calculated in this work (G), is sufficient to flatten the total spectrum (T) to the shape observed by SAS-2 with an approximate $E^{-2.4}$ form at energies between 35 and 200 MeV. The galactic Compton contribution at high latitudes used here may be underestimated (a larger scale height may be more appropriate). But this does not significantly change the total flux or shape of the spectrum calculated. For other data, see Stecker (1975a).

shown in figure 20 are the extragalactic background from annihilation γ-rays calculated by using the method of Stecker et al. (1971) for an open universe low-density model ($n_0 = 3 \times 10^{-7}$ cm^{-3}, H_0 = 50 km/s/Mpc), marked ANN, and satellite data. This can be seen to be flatter than the pure extragalactic background component and consistent with the SAS-2 data. The effect of the galactic contamination can be reduced ideally by ~33 percent by making observations at $b = 90°$. However, it should be noted that the galactic background can still be expected to dominate at energies above 300 MeV, making a proposed test (Stecker, 1974 and 1975) between the cosmological π°-decay models of the γ-ray background invalid.

GAMMA-RAYS AND GALACTIC STRUCTURE: AN APPROACH FOR THE FUTURE

The early optimistic hope of 21-cm observers to delineate the spiral structure of the galaxy has been dimmed by complications in the analysis of even the most thorough velocity-longitude plots due to kinematic (velocity streaming) effects, nonuniformities within arm features (fragmentation, branching, etc.), and strong noncircular gas velocities as evidenced at $\ell = 0°$. At the same time, high-resolution 21-cm surveys of external spirals, such as the Rots and Shane (1975) work on M81 shown in figure 14, have shown that large-scale spiral structure exists in the gas in spiral galaxies as we know it exists in other components, such as dust clouds, HII regions, and OB associations. The CO observations of our galaxy, which should reflect arm structure in young molecular clouds even more strongly than in the 21-cm observations, have not revealed such structure in the $0° \leqslant \ell \leqslant 180°$ range. However, they have excitingly revealed a larger-scale overall galactic structure which shows a broad maximum in the 5- to 6-kpc region. The existence of this structure is supported by the γ-ray observations. Strong correlations with other Population I phenomena in the galaxy suggest that a new picture of overall galactic structure is emerging and will lead to new understandings of the nature of the galaxy.

Some γ-ray observers have exhibited the optimism shown in the early 21-cm work in looking for spiral features. However, it should be remembered that γ-ray observations have some difficulties in their analysis, as do 21-cm observations. Three problems inherent to the interpretation of γ-ray observations and not the 21-cm observations are: (1) no velocity information to help determine from where in the galaxy emission at a specific longitude originates, (2) relatively poor angular resolution in the present data, which restricts fine-scale structure studies, and (3) the fact that the γ-ray emission is proportional to the product of gas density and cosmic-ray intensity integrated along the line-of-sight so that assumptions must be made to separate these two quantities or, preferably, other observations must also be used to determine the gas density.

Of course, the γ-ray observations have their advantages. Optical depth corrections are entirely unnecessary. And, to the extent that the gas-density distribution can be obtained by other means, using as much of the electromagnetic spectrum as possible (e.g., radio, microwave, and far-infrared observations (Fazio and Stecker, 1976)), the galactic cosmic-ray nucleon distribution can then be deduced. Indeed, 100-MeV γ-ray observations are unique in their potential for determining information about the large-scale distribution of galactic cosmic-ray nucleons. Using the above approach, large-scale structure in both interstellar gas and cosmic-ray distributions is now becoming apparent. Higher resolution γ-ray observations should enable us to study important unresolved questions about small-scale and spiral structure features. A concerted "synoptic" approach to galactic surveys by observers at all wavelengths should enable us to take advantage of complementary observations in the future and to improve our understanding of the structure and dynamics of the galaxy.

REFERENCES

Allen, C. W., 1973, *Astrophysical Quantities*, 3rd Ed., Athlone Press, London.

Baade, W., 1944, *Ap. J.*, **100**, p. 137.

Bignami, G. F., and C. E. Fichtel, 1974, *Ap. J. Letters*, **189**, *p. L65.*

Bignami, G. F., C. E. Fichtel, D. A. Kniffen, and D. J. Thompson, 1975, *Ap. J.*, **199**, p. 54.

Blumenthal, G. R., and R. J. Gould, 1970, *Rev. Mod. Phys.*, **42**, p. 237.

Brecher, K., and G. Burbidge, 1972, *Ap. J.*, **174**, p. 253.

Burton, W. B., 1974, *Galactic Radio Astronomy*, ed. F. J. Kerr and S. C. Simonson, III, Reidel Publishing Co., Dordrecht, Holland, p. 551.

Burton, W. B., 1976, *Ann. Rev. Astr. Ap.*, **14**, p. 275.

Burton, W. B., and T. M. Bania, 1974, *Astr. and Ap.*, **33**, p. 425.

Burton, W. B., and M. A. Gordon, 1976, *Ap. J. Letters*, **207**, p. L189.

Burton, W. B., M. A. Gordon, T. M. Bania, and F. J. Lockman, 1975, *Ap. J.*, **202**, p. 30.

Cowsik, R., and W. Voges, 1974, (Proc. ESLAB Gamma-Ray Symposium, Frascati, ESRO SP-106), p. 229.

Daniel, R. R., and S. A. Stephens, 1975, *Space Sci. Rev.*, **17**, p. 45.

Daugherty, J. K., R. C. Hartman, and P. J. A. Schmidt, 1975, *Ap. J.*, **198**, p. 493.

Dodds, D., A. W. Strong, and A. W. Wolfendale, 1975, *Mon. Nat. RAS.*, **171**, p. 569.

Dovzhenko, O. I., and A. A. Pomanskii, 1964, *Sov. Phys. JETP*, **18**, p. 187.

Ekers, R. D., 1975, *Structure and Evolution of Galaxies*, ed. G. Setti, Reidel Publishing Co., Dordrecht, Holland, 217.

Ekers, R. D., and R. Sancisi, 1976, in preparation.

Falgarone, E., and J. Lequeux, 1973, *Astron. and Astrophys.*, **25**, p. 253.

Fazio, G. G., and F. W. Stecker, 1976, *Ap. J. Letters*, **207**, p. L49.

Fichtel, C. E., R. C. Hartman, D. A. Kniffen, D. J. Thompson, G. F. Bignami, H. Ögelman, M. E. Özel, and T. Tümer, 1975, *Ap. J.*, **198**, p. 163.

Fichtel, C. E., D. A. Kniffen, D. J. Thompson, G. F. Bignami, and C. Y. Cheung, 1976, *Ap. J.*, in press.

Garcia-Munoz, M., G. M. Mason, and J. A. Simpson, 1975, (Proc. 14th Intl. Cosmic Ray Conf., Munich), **1**, p. 221.

Ginzburg, V. L., and S. I. Syrovatskii, 1964, *Origin of Cosmic Rays*, MacMillan Co., New York.

Goldstein, M. L., L. A. Fisk, and R. Ramaty, 1970, *Phys. Rev. Letters*, **25**, p. 732.

Gordon, M. A., and W. B. Burton, 1976, *Ap. J.*, **208**, p. 346.

Greenberg, J. M., 1971, *Astron. and Astrophys.*, **12**, p. 240.

Gunn, J. E., and B. M. Tinsley, 1975, *Nature*, **257**, p. 454.

Hagen, F. A., A. J. Fisher, J. F. Ormes, and J. F. Arens, 1975, (Proc. 14th Intl. Cosmic Ray Conf., Munich), **1**, p. 361.

Hayakawa, S., K. Ito, T. Matsuda, T. Ono, and K. Uyama, 1976, *Nature*, **261**, p. 29.

Hulse, R. A., and J. H. Taylor, 1975, *Ap. J. Letters*, **201**, p. L55.

Ilovaisky, A., and J. Lequeux, 1972, *Astron. and Astrophys.*, **20**, p. 347.

Jokipii, J. R., 1976, *Ap. J.*, **208**, p. 900.

Kerr, F. J., and G. Westerhout, 1975, In Galactic Structure; *Stars and Stellar Systems*, **5**, ed. A. Bluaaw and M. Schmidt, U. Chicago Press, Chicago, Illinois.

Kodaira, K., 1974, *Pub. Astr. Soc. Japan*, **26**, p. 255.

Kniffen, D. A., G. F. Bignami, C. E. Fichtel, R. C. Hartman, H. Ögelman, D. J. Thompson, M. E. Özel, and T. Tümer, 1975, (Proc. 14th Intl. Cosmic Ray Conf., Munich), **1**, p. 100.

Kraushaar, W. L., G. W. Clark, G. P. Garmire, R. Borken, P. Higbie, C. Leung, and T. Thorsos, 1972, *Ap. J.*, **177**, p. 341.

Landecker, T. L., and R. Weilebinski, 1970, *Australian J. Phys. Suppl.*, **16**, p. 1.

Lequeux, J., 1971, *Astron. and Astrophys.*, **15**, p. 42.

Lockman, F. J., 1976, *Ap. J.*, **209**, p. 429.

Lyne, A. G., 1974, In *Galactic Radio Astronomy*, ed. F. J. Kerr and S. C. Simonson, III, Reidel Publishing Co., Dordrecht, Holland, p. 87.

Mazets, E. P., S. V. Golenetskii, V. N. Il'inskii, Yu. A. Gur'yan, and T. V. Kharitonova, 1975, *Ap. and Space Sci.*, **33**, p. 347.

Mezger, P. G., 1970, (Proc. IAU Symp. No. 38, Basel, Switzerland), ed. W. Becker and G. Contopoulos, Reidel Publishing Co., Dordrecht, Holland, p. 107.

Neugebauer, G., E. Becklin, and A. R. Hyland, 1971, *Ann. Rev. Astr. Ap.*, **9**, p. 67.

O'Dell, F. W., M. M. Shapiro, R. Silberberg, and C. H. Tsao, 1973, (Proc. 13th Intl. Cosmic Ray Conf., Denver), **1**, p. 490.

Ögelman, H. B., and S. P. Maran, 1975, *Ap. J.*, **209**, p. 124.

Öpik, E., 1953, *Irish Astr. J.*, **2**, p. 219.

Paul, J., M. Cassé, and C. J. Cesarsky, 1976, *Ap. J.*, **207**, p. 620.

Perek, L., 1962, *Advances in Astron. and Ap.*, **1**, p. 165.

Price, R. M., 1974, *Galactic Radio Astronomy*, ed. F. J. Kerr and S. C. Simonson, III, Reidel Publishing Co., Dordrecht, Holland, p. 637.

Puget, J. L., and F. W. Stecker, 1974, *Ap. J.*, **191**, p. 323.

Puget, J. L., C. E. Ryter, G. Serra, and G. F. Bignami, 1976, *Astr. and Ap.*, in press.

Ramaty, R., and N. J. Westergaard, 1976, preprint.

Reeves, H., 1975, *Origin of Cosmic Rays*, ed. J. L. Osborne and A. W. Wolfendale, Reidel Publishing Co., Dordrecht, Holland, p. 135.

Roberts, M. S., 1974, *Science*, **183**, p. 371.

Roberts, W. W., Jr., M. S. Roberts, and F. H. Shu, 1975, *Ap. J.*, **196**, p. 381.

Rots, A. H., and W. W. Shane, 1973, *Astron. and Astrophys.*, **45**, p. 25.

Samimi, J., G. H. Share, and R. L. Kinzer, 1974, (Proc. ESLAB Gamma-Ray Symp., Frascati, ESRO SP-106), p. 211.

Sandage, A., 1961, *The Hubble Atlas of Galaxies*, Carnegie Institute, Washington, D.C.

Scott, J. S., 1975, *Nature*, **258**, p. 58.

Scoville, N. Z., and P. M. Solomon, 1975, *Ap. J. Letters*, **199**, p. L105.

Shu, F. J., 1973, *The Interstellar Medium*, ed. K. Pinkau, Reidel Publishing Co., Dordrecht, Holland, p. 219.

Shukla, P. G., M. Cassé, C. J. Ceasarsky, and J. Paul, 1975, (Proc. 14th Intl. Cosmic Ray Conf., Munich), **1**, p. 65.

Seiradakis, J., 1976, in preparation.

Simonson, S. C., III, 1970, *Astron. and Astrophys.*, **9**, p. 163.

Simonson, S. C., III, 1976, *Astron. and Astrophys.*, **46**, p. 261.

Solomon, P. M., and F. W. Stecker, 1974, (Proc. ESLAB Gamma-Ray Symp., Frascati, ESRO SP-106), p. 253.

Stecker, F. W., 1968, Thesis, Harvard University Library.

Stecker, F. W., 1969, *Ap. J.*, **157**, p. 507.

Stecker, F. W., 1970, *Astrophys. and Space Sci.*, **6**, p. 377.

Stecker, F. W., 1971, *Cosmic Gamma Rays,* Mono. Book Co., Baltimore.

Stecker, F. W., 1973, *Ap. J.*, **185**, p. 499.

Stecker, F. W., 1974, (Proc. ESLAB Gamma-Ray Symp., Frascati, ESRO SP-106).

Stecker, F. W., 1975a, *Origin of Cosmic Rays*, ed. J. L. Osborne and A. W. Wolfendale, Reidel Publishing Co., Dordrecht, Holland, p. 267.

Stecker, F. W., 1975b, *Phys. Rev. Letters*, **35**, p. 188.

Stecker, F. W., 1976, *Nature*, **260**, p. 412.

Stecker, F. W., D. L. Morgan, and J. H. Bredekamp, 1971, *Phys. Rev. Letters*, **27**, p. 1469.

Stecker, F. W., J. L. Puget, A. W. Strong, and J. H. Bredekamp, 1974, *Ap. J. Letters*, **188**, p. L59.

Stecker, F. W., P. M. Solomon, N. Z. Scoville, and C. E. Ryter, 1975, *Ap. J.*, **201**, p. 90.

Strong, A. W., 1975, *J. Phys.*, **A8**, p. 617.

Trombka, et al., 1977, *Ap. J.*, in press.

Van der Kruit, P. C., and R. J. Allen, 1976, *Ann. Rev. Astr. Ap.*, **14**, in press.

Webster, A., 1975, *Mon. Not. RAS*, **171**, p. 243.

Wentzel, D. G., P. D. Jackson, W. K. Rose, and R. P. Sinha, 1975, *Ap. J. Letters*, **201**, p. L5.

AGENDA FOR SYMPOSIUM ON THE STRUCTURE AND CONTENT OF THE GALAXY AND GALACTIC GAMMA RAYS

June 2, 1976
Morning Chairman: Raymond D. Wills
European Space Research and Technology Centre
Noordwijk, The Netherlands

Introductory Remarks—Floyd W. Stecker, NASA/Goddard Space Flight Center, Greenbelt, Maryland

Opening Remarks—John F. Clark, Director, NASA/Goddard Space Flight Center, Greenbelt, Maryland

SAS-2 Galactic Gamma-Ray Results—I. Diffuse Emission—David J. Thompson, Laboratory for High Energy Astrophysics, NASA/Goddard Space Flight Center, Greenbelt, Maryland

SAS-2 Galactic Gamma-Ray Results—II. Localized Sources—Robert C. Hartman, Laboratory for High Energy Astrophysics, NASA/Goddard Space Flight Center, Greenbelt, Maryland

Preliminary Results from the European Space Agency's COS-B Satellite for Gamma-Ray Astronomy—The Caravene Collaboration

The COS-B Experiment and Mission—Boudewijn Swanenburg, Cosmic-Ray Working Group, Huygens Laboratorium, Leiden, The Netherlands

COS-B Observations of the High-Energy Gamma Radiation from the Galactic Disk—Jacques Paul, Service d'Electronique Physique, Centre d'Etudes Nucleaires de Saclay, Gif-sur-Yvette, France

COS-B Observations of Localized Sources of Gamma-Ray Emission—Hans Mayer-Hasselwander, Max Planck Institut für Physik und Astrophysik, Institut für Extraterrestrische Physik, Garching bei München, Germany

The Time Structure of the Gamma-Ray Emission from the Crab and Vela Pulsars—Rosolino Buccheri, Instituto Fisica, Universita di Palermo, Italy

June 2, 1976
Afternoon Chairman: George F. Pieper
NASA/Goddard Space Flight Center, Greenbelt, Maryland

Low- and Medium-Energy Galactic Gamma-Ray Observations—Gerald H. Share, E. O. Hurlburt Center for Space Research, U.S. Naval Research Laboratory, Washington, D.C.

Very High-Energy Gamma-Ray Astronomy—Jonathan E. Grindlay, Center for Astrophysics, Harvard College Observatory and Smithsonian Astrophysical Observatory, Cambridge, Massachusetts

Radiation Mechanisms and Magnetospheric Structure of Pulsars—P. A. Sturrock, Institute for Plasma Research, Stanford University, Stanford, California

Gamma-Ray Pulsars—Hakki Ögelman, Middle East Technical University, Ankara, Turkey

Contributed Papers

June 3, 1976
Morning Chairman: Maurice Shapiro
U.S. Naval Research Laboratory, Washington, D.C.

Density Wave Theory—William W. Roberts, Jr., Department of Applied Mathematics and Computer Science, University of Virginia, Charlottesville, Virginia

The Galactic Distribution (in Radius and Z) of Interstellar Molecular Hydrogen—Nicholas Z. Scoville, Department of Physics and Astronomy, University of Massachusetts, Amherst, Massachusetts

Remarks on the Overall Distribution of Hydrogen in the Galactic Disk—W. B. Burton, National Radio Astronomy Observatory, Green Bank, West Virginia

The Nonthermal Radiation in the Galaxy—J. E. Baldwin, Cavendish Laboratory, Cambridge, England

Infrared Astronomy and High-Energy Astrophysics—Giovanni G. Fazio, Center for Astrophysics, Cambridge, Massachusetts

June 3, 1976
Afternoon Chairman: Arnold Wolfendale
University of Durham, England

Ultraviolet Observations of Local Gas—Edward B. Jenkins, Princeton University Observatory, Princeton, New Jersey

Small-Scale Local Gamma-Ray Features—Jean-Loup Puget, Département d'Astrophysique Fondamentale, Observatoire de Meudon, 92190 Meudon, France

Diffuse Galactic Gamma-Ray Lines—Richard E. Lingenfelter, Department of Astronomy and Department of Geophysics and Space Physics, University of California, Los Angeles, California

Contributed Papers

June 4, 1976
Morning Chairman: Bernard Peters
Danish Space Research Institute, Lyngby, Denmark

Contributed Papers (Continued)

Gamma Rays and Supernova Explosions—David Arnett, Department of Astronomy, University of Illinois, Urbana, Illinois

Galactic Distribution of Pulsars—John H. Seiradakis, Max Planck Institut für Radioastronomie, Auf dem Hügel 69, 5300 Bonn 1, West Germany

Cosmic-Ray Propagation and Containment—Eugene N. Parker, Laboratory for Astrophysics and Space Research, Chicago, Illinois

Gamma Rays and Large-Scale Galactic Structure—Donald A. Kniffen, NASA/Goddard Space Flight Center, Greenbelt, Maryland

June 4, 1976
Afternoon Chairman: Livio Scarsi
Universita di Palmero, Palmero, Italy

Gamma Rays, Cosmic Rays, and Galactic Structure—Floyd W. Stecker, Theoretical Studies Group, NASA/Goddard Space Flight Center, Greenbelt, Maryland

Summary and Panel Discussion—Giovanni F. Bignami, University of Milan, Italy; Edward L. Chupp, University of New Hampshire; Carl E. Fichtel, NASA/Goddard Space Flight Center; Kenneth Greisen, Cornell University; Eugene N. Parker, University of Chicago; Volkes Schönfelder, Max Planck Institut, West Germany; Evry Shatzman, Observatoire de Meudon, France; Jack I. Trombka, NASA/Goddard Space Flight Center; Raymond D. Wills, European Space Research and Technology Center, The Netherlands.

Concluding Remarks—Carl E. Fichtel

GSFC Colloquim: Gamma Rays and the Structure of Our Galaxy—Kenneth Greisen, Cornell University

REGISTERED PARTICIPANTS

Prof. W. David Arnett
Enrico Fermi Institute
University of Chicago
Chicago, IL 60637

Dr. C. Ayre
Harrison M. Randall Lab. of Physics
University of Michigan
Ann Arbor, MI 48109

Dr. T. Bai
Code 660
NASA/GSFC
Greenbelt, MD 20771

Dr. V. K. Balasubrahmanyan
Code 661
NASA/GSFC
Greenbelt, MD 20771

Dr. John E. Baldwin
Cavendish Laboratory
Madingley Road
Cambridge, England

Dr. W. Baldwin
Department of Astronomy
University of Virginia
Charlottesville, VA 22901

Dr. T. M. Bania
National Radio Astronomy Observatory
Edgemont Road
Charlottesville, VA 22901

Dr. B. Beron
High Energy Physics Laboratory
Stanford University
Stanford, CA 94305

Dr. David Bertsch
Code 662
NASA/GSFC
Greenbelt, MD 20771

Dr. G. F. Bignami
Instituto Di Science Fisiche
Universita Di Milano
Aldo Pontromeli
Via Veloria 16
Milano, Italy

Dr. Albert Boggess
Code 673
NASA/GSFC
Greenbelt, MD 20771

Dr. Ralph Bohlin
Code 672
NASA/GSFC
Greenbelt, MD 20771

Dr. E. Boldt
Code 661
NASA/GSFC
Greenbelt, MD 20771

Dr. R. Buccheri
Instituto Fisica Universita
Universita di Palermo
Via Archirafi 36
Palermo, Italy

Dr. W. B. Burton
National Radio Astronomy Observatory
Edgemont Road
Charlottesville, VA 22901

Dr. E. L. Chupp
Physics Department
University of New Hampshire
Durham, NH 03824

Dr. J. F. Clark
Code 100
NASA/GSFC
Greenbelt, MD 20771

Dr. Thomas L. Cline
Code 661
NASA/GSFC
Greenbelt, MD 20771

Dr. Richard Cohen
NASA/Goddard Institute for Space Studies
2880 Broadway
New York, NY 10025

Dr. John T. Cowan
Astronomy Program
University of Maryland
College Park, MD 20742

Dr. Carol Crannell
Code 682
NASA/GSFC
Greenbelt, MD 20771

Dr. Glen Dahlbacka
Code L-32
Lawrence Livermore Lab.
Livermore, CA 94550

Dr. Upendra Desai
Code 663
NASA/GSFC
Greenbelt, MD 20771

Dr. M. Dubin
Code 680
NASA/GSFC
Greenbelt, MD 20771

Dr. L. Dunkelman
Code 673
NASA/GSFC
Greenbelt, MD 20771

Dr. P. Durouchoux
CEA-CEN Saclay
DPH/EP, BP 2
Gif-sur-Yvette 31, France

Dr. C. Dyer
Code 682
NASA/GSFC
Greenbelt, MD 20771

Dr. Engel
Imperial College of Science and Technology
Prince Consort Road
London SW72AZ, England

Mr. Charles Ehrmann
Code 663
NASA/GSFC
Greenbelt, MD 20771

Dr. L. Evans
Code 682
NASA/GSFC
Greenbelt, MD 20771

Dr. G. G. Fazio
Smithsonian Astrophysical Observatory
60 Garden Street
Cambridge, MA 02138

Dr. Carl Fichtel
Code 660
NASA/GSFC
Greenbelt, MD 20771

Dr. Richard Fahey
Code 671
NASA/GSFC
Greenbelt, MD 20771

Mr. D. Galasso
Code 682
NASA/GSFC
Greenbelt, MD 20771

Dr. D. Gilman
Clark Hall
Cornell University
Ithaca, NY 14850

Dr. M. Goldstein
Code 692
NASA/GSFC
Greenbelt, MD 20771

Prof. K. Greisen
Dept. of Physics, Clark Hall
Cornell University
Ithaca, NY 14850

Dr. J. E. Grindlay
Harvard College Observatory
60 Garden Street
Cambridge, MA 02138

Dr. R. C. Hartman
Code 662
NASA/GSFC
Greenbelt, MD 20771

Dr. Michael Hauser
Code 661
NASA/GSFC
Greenbelt, MD 20771

Prof. R. C. Haymes
Space Science Department
Rice University
Houston, TX 77001

Dr. W. Hermsen
Cosmic-Ray Working Group
Huygens Laboratorium
Leiden, The Netherlands

Dr. E. B. Hughes
High Energy Physics Laboratory
Stanford University
Stanford, CA 94305

Dr. W. L. Imhof
Lockheed Palo Alto Research Laboratory
3251 Hanover Street
Palo Alto, CA 94304

Dr. A. Ito
Dept. of Physics and Astronomy
University of Maryland
College Park, MD 20771

Dr. Allen S. Jacobson
Code 183-901
Jet Propulsion Laboratory
California Institute of Technology
4800 Oak Grove Drive
Pasadena, CA 91103

Dr. E. B. Jenkins
Princeton University Observatory
Princeton, NJ 08540

Dr. W. N. Johnson
Code 7128
U.S. Naval Research Lab.
Washington, DC 20375

Dr. Frank Jones
Code 602
NASA/GSFC
Greenbelt, MD 20771

Dr. G. Kanbach
Max Planck Institut für Physik
und Astrophysik
Institut für Extraterrestrische Physik
8046 Garching bei München, Germany

Dr. F. J. Kerr
Astronomy Program
University of Maryland
College Park, MD 20742

Dr. R. Kinzer
Code 7120 13
U.S. Naval Research Lab.
Washington, DC 30475

Dr. A. Klimas
Code 692
NASA/GSFC
Greenbelt, MD 20771

Dr. Donald A. Kniffen
Code 662
NASA/GSFC
Greenbelt, MD 20771

Dr. Fred Knight
Code 011
Dept. of Physics
University of California
San Diego
La Jolla, CA 92093

Dr. David Koch
American Science and Engineering
955 Massachusetts Avenue
Cambridge, MA 02139

Dr. L. Koch
Service d'Electronique Physique
Centre D'Etudes Nucléaires de Saclay
Gif-sur-Yvette, France

Dr. J. Kurfess
Code 7122
U.S. Naval Research Lab.
Washington, DC 20375

Dr. Richard Lamb
Code 662
NASA/GSFC
Greenbelt, MD 20771

Dr. L. C. Lee
Code 602
NASA/GSFC
Greenbelt, MD 20771

Dr. Marvin Leventhal
Room 1C-302
Bell Telephone Lab., Inc.
Murray Hill, NJ 07974

Dr. James Ling
Jet Propulsion Laboratory
California Institute of Technology
Pasadena, CA 91103

Dr. R. E. Lingenfelter
Department of Astronomy
University of California
Los Angeles, CA 90024

Dr. F. J. Lockman
National Radio Astronomy Observatory
Edgemont Rd.
Charlottesville, VA 22901

Dr. Crawford MacCallum
Sandia Laboratories
Albuquerque, NM 87115

Dr. Glenn Mason
Fermi Institute for Nuclear Studies
University of Chicago
Chicago, IL 60637

Dr. Mather
Code 661
NASA/GSFC
Greenbelt, MD 20771

Dr. Christian Matzler
Code 660
NASA/GSFC
Greenbelt, MD 20771

Mr. G. Maurer
Code 682
NASA/GSFC
Greenbelt, MD 20771

Dr. H. A. Mayer-Hasselwander
Max Planck Institut für Extraterrestrische Physik
8046 Garching bei Munchen, Germany

Dr. Brian McBreen
Department of Physics
University College
Dublin, Ireland

Dr. F. McDonald
Code 660
NASA/GSFC
Greenbelt, MD 20771

Dr. Jaylee Mead
Code 671
NASA/GSFC
Greenbelt, MD 20771

Dr. Charles Meegan
Code ES-22
Marshall Space Flight Center
Huntsville, AL 35812

Dr. T. Montmerle
Division de la Physique Service d'Electronique Physique
Centre d'Etudes Nucléaires de Saclay
Boite Postal No. 2
91190 Gif-sur-Yvette, France

Prof. Philip Morrison
Massachusetts Institute of Technology 6 308
Cambridge MA 02139

Dr. G. Morfil
Max Planck Institut für Physik und Astrophysik
Institut fur Extraterrestriche Physik
8046 Garching bei München, West Germany

Dr. L. Moskaleva
Institute of Geochemistry and Analytical Chemistry
USSR Academy of Sciences
Moscow, USSR

Dr. M. Mustafa
Code 682
NASA/GSFC
Greenbelt, MD 20771

Dr. George H. Nakano
Organ 52-12, Bldg. 205
3251 Hanover Street
Palo Alto, CA 94304

Dr. Naraman
Tata Institute of Fundamental Research
Bombay 400-005, India

Dr. Hakki Ögelman
Faculty of Science
Dept. of Theoretical Physics
Middle East Technical University
Ankara, Turkey

Dr. K. Omidvar
Code 602
NASA/GSFC
Greenbelt, MD 20771

Dr. E. N. Parker
Fermi Institute for Nuclear Studies
University of Chicago
Chicago, IL 60637

Dr. J. Paul
Centre d'Etudes Nucléaires de Saclay
Boite Postal No. 2
91 Gif-sur-Yvette, France

Dr. Charles Pellerin
Code 662
NASA/GSFC
Greenbelt, MD 20771

Dr. George F. Peiper
NASA/GSFC Code 600
Greenbelt, MD 20771

Dr. Bernard Peters
Danish Space Research Institute
Lundloftevej 7
2800 Lyngby, Denmark

Dr. J. L. Puget
Department d'Astrophysique Fondamenrale
DAF Observatoire de Meudon
France

Dr. R. Ramaty
Code 660
NASA/GSFC
Greenbelt, MD 20771

Dr. William Roberts, Jr.
Dept. of Applied Math and Computer Science
University of Virginia
Charlottesville, VA 22901

Dr. Nancy Roman
Code SG
NASA Headquarters
Washington, DC 20546

Dr. Herman Rothermel
Code 662
NASA/GSFC
Greenbelt, MD 20771

Dr. Arnold Rots
National Radio Astronomy Observatory
Edgemont Road
Charlottesville, VA 22901

Dr. L. Scarsi
Instituto Fisica
Universita di Palermo
Via Archirafi 36
Palermo, Italy

Dr. E. Schatzman
Institute Dastrophysique
98 Bis Bldg. Arago
Paris 14, France

Dr. W. Schmidt
Code 660
NASA/GSFC
Greenbelt, MD 20771

Dr. V. Schonfelder
Max Planck Institut für Extraterrestrische Physik
8046 Garching bei München, Germany

Dr. N. Z. Scoville
Dept. of Physics and Astronomy
University of Massachusetts
Amherst, MA 01002

Dr. Nathan Seeman
Code 7025
U.S. Naval Research Lab.
Washington, DC 20375

Dr. John Seiradakis
Max Planck Institut für Radioastronomie
Auf dem Hügel 69
53 Bonn 1, West Germany

Dr. Maurice M. Shapiro
Code 7020
U.S. Naval Research Lab.
Washington, DC 20390

Dr. A. Schardt
Code 660
NASA/GSFC
Greenbelt, MD 20771

Dr. Gerald H. Share
Code 7120 14
U.S. Naval Research Lab.
Washington, DC 20375

Dr. P. Shukla
Service d'Electronique Physique
Centre d'Etudes Nucléaires de Saclay
Gif-sur-Yvette, France

Dr. R. Silberberg
Code 7028
U.S. Naval Research Lab.
Washington, DC 20375

Dr. G. Simpson
Space Science Center
University of New Hampshire
Durham, NH 03824

Dr. R. P. Sinha
Astronomy Program
University of Maryland
College Park, MD 20742

Dr. Barham Smith
Code 660.1
NASA/GSFC
Greenbelt, MD 20771

Dr. P. M. Solomon
Earth and Space Sciences Dept.
State University of New York
Stony Brook, NY 11714

Dr. Lyman Spitzer
Princeton University Observatory
Princeton, NJ 08540

Mr. T. Stecher
Code 672
NASA/GSFC
Greenbelt, MD 20771

Dr. Floyd Stecker
Code 602
NASA/GSFC
Greenbelt, MD 20771

Dr. Gary Steigman
Yale University Observatory
Box 2023, Yale Station
New Haven, CT 06520

Dr. S. A. Stephens
Code TN2
Johnson Space Flight Center
Houston, TX 77058

Dr. P. A. Sturrock
Institute for Plasma Research
Stanford University
Stanford, CA 94305

Dr. Yu. A. Surkov
Institute of Geochemistry and
Analytical Chemistry
USSR Academy of Sciences
Moscow, USSR

Dr. B. N. Swanenburg
Cosmic Ray Working Group
Huygens Laboratorium
Leiden, The Netherlands

Dr. Jean Swank
Code 661
NASA/GSFC
Greenbelt, MD 20771

Dr. B. Taylor
Space Science Dept. (ESLAB)
ESTEC
Noordwijk, The Netherlands

Dr. B. Teegarden
Code 661
NASA/GSFC
Greenbelt, MD 20771

Prof. K. Thielheim
Institut für Reine und Angewandte
Kernphysik der
Universitat Kiel
Kiel, West Germany

Dr. David Thompson
Code 662
NASA/GSFC
Greenbelt, MD 20771

Dr. Hugh S. Tornabene
6012 Westchester Park Dr., No. T1
College Park, MD 20740

Dr. J. Trainor
Code 663
NASA/GSFC
Greenbelt, MD 20771

Dr. J. Trombka
Code 682
NASA/GSFC
Greenbelt, MD 20771

Dr. Melville P. Ulmer
Smithsonian Astrophysical Observatory/
Harvard College Observatory
Center for Astrophysics
60 Garden Street
Cambridge, MA 02138

Dr. A. Underhill
Code 670
NASA/GSFC
Greenbelt, MD 20771

Dr. M. S. Vardya
Code 671
NASA/GSFC
Greenbelt, MD 20771

Larry Varnell
Code 183-401
Jet Propulsion Laboratory
Pasadena, CA 91106

Dr. G. Vedrenne
Centre d'Etude Spatiale
des Rayonnements
Complexe Aerospatialde Toulouse-Lespinet
31 Toulouse, France

Dr. C. Wende
Code 601
NASA/GSFC
Greenbelt, MD 20771

Dr. C. Wentz
Code 682
NASA/GSFC
Greenbelt, MD 20771

Dr. G. Westerhout
Astronomy Program
University of Maryland
College Park, MD 20742

Dr. William A. Wheaton
Center for Space Research
Massachusetts Institute of Technology
Cambridge, MA 02139

Dr. R. Stephen White
Department of Physics
University of California
Riverside, CA 92502

Dr. J. Willett
Code 183-901
Jet Propulsion Laboratory
California Institute of Technology
4800 Oak Grove Drive
Pasadena, CA 91103

Dr. R. D. Wills
Space Science Dept. (ESLAB)
ESTEC
Noordwijk, The Netherlands

Dr. Arnold W. Wolfendale
Dept. of Physics
University of Durham
Durham DH1-3LE, England

Mr. P. Yasskin
Code 602
NASA/GSFC
Greenbelt, MD 20771

Dr. A. Zych
Inst. Geophys/Planetary Science
California University at Riverside
Riverside, CA 92502

INDEX OF AUTHORS

*U.S. GOVERNMENT PRINTING OFFICE: 1977 - 735-004/41